ALLEGATO A

Al Direttore dell' Istituto di Ricerca sugli Ecosistemi Terrestri

La sottoscritta Valentino Anna

Codice Fiscale VLNNNA88C57F839U

Nata a Napoli Prov. Napoli il 17/03/1988

Attualmente residente ad Afragola Prov. Napoli

Indirizzo Via Messina n° 4

CAP 80021 Telefono : 3281152165

Indirizzo PEC. anna.valentino88@pec.it

chiede, ai sensi dell'art. 22 della L. 240 del 30/12/2010, di essere ammesso a sostenere la selezione pubblica, per titoli e colloquio, per il conferimento di n° 1 assegno per lo svolgimento di attività di ricerca nell'ambito del programma di ricerca: "MICROPOLI", per la seguente tematica: "Isolamento, caratterizzazione e validazione dell'attività biologica su opportuni modelli in vitro di patologie correlate all'invecchiamento dei principi e/o frazioni di più principi attivi isolati da scarti della filiera olivicola

sotto la responsabilità scientifica della Dott. dott.ssa Anna Calarco e della dott.ssa Anna Di Salle.

da svolgersi presso la sede di Napoli, dell'Istituto di Ricerca sugli Ecosistemi Terrestri (IRET). A tal fine, la sottoscritta dichiara sotto la propria responsabilità:

1) di essere cittadina italiana
2) di aver conseguito il diploma di laurea in Biotecnologie mediche (LM-9) il 29/03/2012 presso l'Università degli Studi di Napoli Federico II con votazione 110/110 e lode;
3) di aver conseguito il titolo di dottore di ricerca in Scienze Mediche Cliniche e Sperimentale il 15/12/2016 presso l'Università degli Studi della Campania Luigi Vanvitelli
4) di non aver riportato condanne penali e di non avere procedimenti penali pendenti a proprio carico
5) di non aver usufruito di altri assegni di ricerca dal 01/05/2011 al 01/02/2020 e di non aver usufruito delle tipologie di rapporti di lavoro di cui all'art. 2 dell'avviso di selezione.

Il sottoscritto allega alla presente domanda:

- dichiarazione sostitutiva di certificazione e dell'atto di notorietà ai sensi degli art. 46 e 47 del DPR 445/2000 e s.m.i. da compilarsi mediante l'utilizzo del modulo (allegato B) attestante la veridicità del contenuto del Curriculum vitae et studiorum;
- i lavori non reperibili attraverso rete (es, rapporti tecnici, monografie, capitoli di libro, brevetti) oppure, quelli reperibili attraverso la rete ma con accesso a pagamento;
- elenco dei lavori trasmessi dal candidato per via telematica di cui all'art. 4 del bando.
- informativa sul trattamento dei dati personali (allegato C), come richiesto all'art. 4 del bando.

Luogo e data
Napoli, 14/12/2021

FIRMA

* - **Qualora il titolo di studio sia stato conseguito all'estero, dovrà essere presentata idonea documentazione attestante l'equipollenza con un titolo rilasciato in Italia, secondo quanto previsto dall'art. 3, punto d) del presente avviso.**

FAC-SIMILE ALLEGATO B

DICHIARAZIONI SOSTITUTIVE DI CERTIFICAZIONI
(art. 46 D.P.R. n. 445/2000)

DICHIARAZIONI SOSTITUTIVE DELL'ATTO DI NOTORIETÀ
(art. 47 D.P.R. n. 445/2000)

La sottoscritta

COGNOME: VALENTINO

NOME: ANNA

NATA A: NAPOLI **PROV.** Napoli **IL** 17/03/1988

ATTUALMENTE RESIDENTE A: AFRAGOLA **PROV. Napoli INDIRIZZO** Via Messina n° 4

C.A.P. 80021

TELEFONO: 3281152165

Visto il D.P.R. 28 dicembre 2000, n. 445 concernente "T.U. delle disposizioni legislative e regolamentari in materia di documentazione amministrativa" e successive modifiche ed integrazioni;

Vista la Legge 12 novembre 2011, n. 183 ed in particolare l'art. 15 concernente le nuove disposizioni in materia di certificati e dichiarazioni sostitutive *(*)*;

Consapevole che, ai sensi dell'art.76 del DPR 445/2000, le dichiarazioni mendaci, la falsità negli atti e l'uso di atti falsi sono punite ai sensi del Codice penale e delle leggi speciali vigenti in materia, dichiara sotto la propria responsabilità:

che quanto dichiarato nel seguente curriculum vitae et studiorum
comprensivo delle informazioni sulla produzione scientifica
corrisponde a verità

(*) ai sensi dell'art. 15, comma 1 della Legge 12/11/2011, n. 183 le certificazioni rilasciate dalla P.A. in ordine a stati, qualità personali e fatti sono valide e utilizzabili solo nei rapporti tra privati; nei rapporti con gli Organi della Pubblica Amministrazione e i gestori di pubblici servizi, i certificati sono sempre sostituiti dalle dichiarazioni sostitutive di certificazione o dall'atto di notorietà di cui agli artt. 46 e 47 del DPR 445/2000

FIRMA(**)

14/12/2021

Curriculim vitae

INFORMAZIONI PERSONALI

Valentino Anna

Via Messina n.4, Afragola (NA), CAP 80021

3281152165

annavalentino88@gmail.com; anna.valentino88@pec.it

Data di nascita 17/03/1988 | Nazionalità Italiana

ESPERIENZA PROFESSIONALE

FEBBRAIO 2021 – AD OGGI — Assegno di ricerca

Università del Piemonte Orientale (UPO). Dipartimento Scienze del Farmaco, via Duomo, 6 - 13100 Vercelli.

Progetto Cariplo 2008-1001-Cup: C15J19000150007. Titolo: High added-value bioactive polyphenols recovered from waste of olive oil production. Realizzazione di scaffold bioattivi per la rigenerazione ossea e cartilaginea con l'uso di scarti di produzione alimentare.

Principali mansioni e responsabilità

- Studio in vitro su cellule umane primarie di prodotti di scarto della produzione alimentare (scarti della produzione di olio d'oliva) quali possibili principi bioattivi nella rigenerazione ossea e cartilaginea. I prodotti di interesse verranno utilizzati per arricchire scaffold 3D a rilascio controllato;
- Test in vitro di attività antiossidante e anti-infiammatoria;
- Test in vitro di attività pro ed anti-proliferativa.

APRILE 2018 – GENNAIO 2021 — Ricercatore tempo indeterminato

Elleva Pharma Srl - 5, Via S. Francesco D'Assisi – Marigliano (NA).

Principali mansioni e responsabilità

- Estrazione di molecole biologicamente attive mediante metodi convenzionali (uso di solventi anche ecosostenibili ed ecocompatibili) e/o assistiti (es. microonde, ultrasuoni, etc.).
- Valutazione della cinetica di rilascio di molecole bioattive anche di origine naturale da sistemi micro/nanostrutturati mediante cromatografia liquida ad elevata pressione (HPLC).
- Determinazione qualitativa del finger-printing delle molecole di interesse mediante spettroscopia infrarossa in trasformata di Fourier (FT-IR).
- Determinazione quali-quantitativa delle molecole di interesse mediante cromatografia liquida associata alla spettrometria di massa (LC-MS/MS).
- Test di biocompatibilità delle molecole bioattive estratte.

ISTRUZIONE E FORMAZIONE

GIUGNO 2017 – APRILE 2018 — Borsa di studio

Centro Interuniversitario per le Ricerche in Neuroscienze (CIRN), Università degli Studi della Campania Luigi Vanvitelli, Via Pansini, Napoli edificio 10.

Progetto POR FSER 2001/2013" - obiettivo Operativo 2 - Capofila Farmaceutici DAMOR SRL. Titolo: Nanotecnologia per il rilascio controllato di molecole bio-attive.

Principali mansioni e responsabilità

- Determinazione delle dimensioni, della carica di superficie e dell'indice di polidispersione di nanoparticelle mediante "Dinamic Light Scattering - DLS", Nanoparticle tracking analysis (NTA), ed ottimo utilizzo di tecniche cromatografiche ad alte prestazioni (HPLC). Estrazione e caratterizzazione di molecole bioattive di origine naturale.
- Determinazione quali-quantitativa delle molecole di interesse mediante cromatografia liquida associata alla spettrometria di massa (LC-MS/MS).
- Determinazione qualitativa del finger-printing delle molecole di interesse mediante spettroscopia infrarossa in trasformata di Fourier (FT-IR) e Spettrometria di massa.

GENNAIO 2017 - MAGGIO 2017

Tirocinio volontario

Istituto di Bioscienze e Biorisorse, CNR-UOS di Napoli, Via Pietro Castellino, 111.

Progetto “Materiali Avanzati Per la Ricerca ed il Comparto Agroalimentare – MAReA”. Progettazione di nuovi polimeri funzionalizzati con molecole bioattive di origine naturali in grado di inibire la formazione di biofilm microbici e di aumentare la shelf–life di prodotti alimentari. Ente/Istituzione finanziatrice: MIUR; n° 0000732 data 04/03/2014

Principali mansioni e responsabilità

- Valutazione, mediante tecniche cromatografiche quali HPLC, della cinetica di rilascio di molecole bioattive in grado di inibire biofilm microbici
- Determinazione qualitativa del finger-printing delle molecole di interesse mediante spettroscopia infrarossa in trasformata di Fourier (FT-IR) e Spettrometria di massa.

OTTOBRE 2012 – DICEMBRE 2016

Dottorato di ricerca

Scienze Mediche Cliniche e Sperimentale. Conseguito in data 15-12-2016

XXIX ciclo presso l’Università degli Studi della Campania Luigi Vanvitelli.

Tesi di dottorato dal titolo: “Epigenetic deregulation of carnitine system by miRNAs induces metabolic reprogramming in cancer cells.”. Reg. Fol. 218 n. 2596.

Principali abilità professionali acquisite

- Analisi del profilo di espressione dei miRNA (sia da cellule che da tessuti) dopo Next Generation Sequencing (NGS).
- Utilizzo di algoritmi di predizione bioinformatica quali miRBase, DIANA Tool, TargetScan.
- Identificazione di potenziali target mediante tecniche di biologia molecolare avanzata

DICEMBRE 2009 – MARZO 2012

Laurea Magistrale

Biotecnologie Mediche (LM9). Conseguita in data 29-03-2012

Università degli Studi di Napoli Federico II .N. Reg. CE2012N7952700013

Tesi dal titolo: “Patogenesi della Sindrome di Down: ruolo di NFAT, NF-kB e del sistema ubiquitina proteasoma”

Votazione 110/110 e lode.

Principali abilità professionali acquisite

- Estrazione di proteine ed acidi nucleici
- EMSA, Real-Time PCR, Western blot
- Analisi di microarray,

SETTEMBRE 2006 – DICEMBRE 2009

Laurea Triennale

Biotecnologie per la salute curriculum medico Conseguita in data 19/12/2009

Università degli Studi di Napoli Federico II

Tesi dal titolo: “Analisi mediante Southern blot dell’inattivazione del gene rel A nel ceppo 93/4286 di Neisseria meningitidis”

Votazione 110/110.

Principali abilità professionali acquisite

- Culture e crescita batterica
- Tecniche di clonaggio

COMPETENZE PERSONALI

Lingua madre: Italiano

Altre lingue

	COMPRENSIONE		PARLATO		PRODUZIONE SCRITTA
	Ascolto	Lettura	Interazione	Produzione orale	
Inglese	B2	B2	B2	B2	B2

Livelli: A1/A2: Utente base - B1/B2: Utente intermedio - C1/C2: Utente avanzato
Quadro Comune Europeo di Riferimento delle Lingue

COMPETENZE COMUNICATIVE, ORGANIZZATIVE E GESTIONALI

▪ Ottima predisposizione al lavoro in team ma capace allo stesso tempo di organizzare personalmente ed indipendentemente il suo lavoro. Persona responsabile, dotata di capacità organizzative, di comunicazione e di problem-solving, pronta ad apprendere sempre più dalle esperienze.

Competenze tecnico-professionali

Tecniche per l'isolamento e l'identificazione di molecole biologicamente attive:

- Estrazione mediante metodi convenzionali (uso di solventi anche ecosostenibili ed ecocompatibili) e/o assistiti (es. microonde, ultrasuoni, etc.);
- Cromatografia su strato sottile (TLC);
- Analisi quali-quantitativa mediante tecniche cromatografiche strumentali (GC/MS, HPLC, HPCL/ESI/MS).

Tecniche di sintesi e caratterizzazione di sistemi micro- nano-strutturate per il rilascio controllato di molecole bioattive:

- Sintesi di micro-nano-particolati mediante tecniche di emulsione singola o doppia, nanoprecipitazione;
- Caratterizzazione chimico-fisica mediante dinamic light scattering (DLS) per l'identificazione delle dimensioni, della carica di superficie e dell'indice di polispersione.
- Caratterizzazione e conta (particle number) delle nonostrutture mediate Nanoparticle tracking analysis (NTA).

Tecniche di biologia cellulare:

- Coltura, mantenimento e manipolazione di linee cellulari primarie, fibroblastiche, tumorali, leucemiche e staminali.
- Tecniche biologiche per la determinazione della vitalità cellulare (Trypan Blue assay, MTT assay, LDH).

Tecniche di biochimica e biologia molecolare:

- Estrazione proteica / RNA e DNA da cellule e tessuti;
- Valutazione dei livelli di espressione proteica mediante Western blotting;
- Isolamento e caratterizzazione di esosomi e microRNA esosomiali da plasma, cellule e tessuti;
- Analisi bioinformatica di target molecolari con differenti tool: MiRBase, TargetScan, miRPath, DianaTool;
- Analisi dell'espressione genica mediante PCR e Real Time PCR, analisi microarray;

Tecniche di diagnostica microbiologica:

- Preparazione terreni di coltura, isolamento, mantenimento e crioconservazione di ceppi batterici in coltura pura;
- Tecniche di clonaggio

Competenze digitali

AUTOVALUTAZIONE				
Elaborazione delle informazioni	Comunicazione	Creazione di Contenuti	Sicurezza	Risoluzione di problemi
Avanzato	Avanzato	Avanzato	Intermedio	Avanzto

Livelli: Utente base - Utente intermedio - Utente avanzato
Competenze digitali - Scheda per l'autovalutazione

▪ Ottima conoscenza di Microsoft Office, Posta elettronica, Internet, Power point, Photoshop, Graphpad e programmi Bionformatici

Patente di guida B

CORSI DI ALTA FORMAZIONE CON ESAME FINALE, MASTER UNIVERSITARI

GENNAIO 2020– FEBBRAIO 2020

Corso di alta formazione per l'utilizzo degli strumenti di cromatografia in fase liquida e in fase gassosa con detector di massa LC-MS/MS e GC-MS.

Principali mansioni e responsabilità: utilizzo di metodi di troubleshooting per il miglioramento dei settaggi ed in caso di malfunzionamento degli strumenti.

Strumenti utilizzati: LCMS-8060 con sistema UHPLC Nexera XR, e NEXIS GC-2030 con detector GCMS QP 2020 NX.

DICEMBRE 2017 – GENNAIO 2018

Corso di alta formazione per l'utilizzo degli strumenti di cromatografia in fase liquida e in fase gassosa con detector di massa LC-MS/MS e GC-MS.

Principali mansioni e responsabilità: Sviluppo e la messa a punto di metodi analitici per la ricerca quali-quantitativa di polifenoli e altre molecole bioattive anche di origine gassosa.

Strumenti utilizzati: LCMS-8060 con sistema UHPLC Nexera XR, e NEXIS GC-2030 con detector GCMS QP 2020 NX.

OTTOBRE 2012 – OTTOBRE 2013

Master in "Esperto in processi innovativi di sintesi biomolecolare applicata a tecniche di epigenetica" (Programma Operativo Nazionale "Ricerca e Competitività" 2007-2013, PON01_02512).

Enti proponenti: Cosvitec Soc cons a r.l., via Galileo Ferraris 171, Napoli; Consiglio Nazionale delle Ricerche (CNR), Via Pietro Castellino, 111, Napoli. Tirocinio svolto il CNR di Napoli Istituto di Biochimica delle Proteine. Attestato n.1217

ABILITAZIONI PROFESSIONALI E ISCRIZIONI AD ALBI

LUGLIO 2013

Tipologia: Abilitazione alla professione di Biologo.
Data di conseguimento: 2°sessione anno 2013
Università del Sannio, Benevento. N° 254 registro rilascio documenti

ESPERIENZE ALL'ESTERO

MAGGIO2016 - AGOSTO 2016

Visiting scientist presso Early Clinical Trials Units Oncology Department University Hospital Antwerp, Wilrijstraat 10, 2650 Edegem, Belgium.

Titolo Progetto: Isolation and Identification of miRNAs in exosomes derived from serum, plasma and tissue of lung cancer patients".

Principali mansioni e responsabilità: Estrazione, purificazione ed analisi di miRNA e proteine esosomiali da cellule, sangue (siero e plasma) e tessuti.

PARTECIPAZIONE A PROGETTI FINANZIATI

FEBBRAIO 2020 - AD OGGI

Progetto CARIPLO 2008-1001-Cup: C15J19000150007. Titolo: High added-value bioactive polyphenols recovered from waste of olive oil production.

Finalità del progetto: Il progetto mira a recuperare i polifenoli ad alto valore aggiunto come l'idrossitirosolo ed il suo precursore l'oleuropeina da due scarti della produzione di olio d'oliva: le acque reflue del frantoio e il panello di filtrazione dell'olio d'oliva per la realizzazione di scaffold bioattivi finalizzati alla rigenerazione ossea e cartilaginea.

GENNAIO 2015 - SETTEMBRE 2021

Progetto SORRISO PON 03 PE_00110_1/ptd1_000410.Titolo: Sviluppo di nanotecnologie Orientate alla Rigenerazione e Ricostruzione tissutale, Implantologia e Sensoristica in Odontoiatria/oculistica (SORRISO)

Finalità del progetto: Il progetto "SORRISO" propone l'utilizzo di nanotecnologie ecosostenibili per la progettazione e la sintesi di dispositivi innovativi volti alla valorizzazione di molecole naturali derivanti da scarti della filiera agroalimentare (economia circolare)

OTTOBRE 2013 - MARZO 2018

Progetto MAReA PON_03_PE_00106_1. Titolo: MAReA-Materiali Avanzati Per la Ricerca ed il Comparto Agroalimentare

Finalità del progetto: progettazione di nuovi polimeri funzionalizzati con molecole bioattive di origine naturali in grado di inibire la formazione di biofilm microbici e di aumentare la shelf–life di prodotti alimentari

GIUGNO 2017 – APRILE 2018

Progetto PO FESR 2007-2013. Titolo: “Nanotecnologie per il rilascio controllato di molecole bioattive”.

Finalità del progetto: Sintesi di nuovi nanodispositivi ecocompatibili per il rilascio di molecole bioattive mediante l’impiego di tecnologie abilitanti.

PARTECIPAZIONE SU INVITO A CONFERENZE INTERNAZIONALI/NAZIONALI

SETTEMBRE 2021

Invited Speaker al Workshop " Strategie innovative per la rigenerativa dentale " Fiuggi, 24 Settembre 2021. *Rigenerativa dentale: un approccio biologico*

RICONOSCIMENTI E PREMI

APRILE 2016

Menzione D’onore per il poster: “Membrane bioattive per la rigenerazione osseo guidata post-impianto”, 23° Congresso Nazionale dei Docenti Universitari in discipline Odontostomatologiche. Roma, 14-16 Aprile 2016

PUBBLICAZIONI SCIENTIFICHE

L’attività scientifica della dott.ssa Valentino è documentata da pubblicazioni su riviste internazionali con collegio dei referees e citate su ISI Web of Knowledge – Journal Citation Reports (JCR) e/o su Scopus.

Indice di Hirsch/H- index (fonte Scopus/WOS): 9

1. **Valentino A**, Di Cristo F, Bosetti M, Amaghnouje A, Bousta D, Conte R, and Calarco A. Bioactivity and Delivery Strategies of Phytochemical Compounds in Bone Tissue Regeneration. APPLIED. SCIENCES. 2021, 11, 5122. **IF: 2.68** Review in Rivista. Ruolo svolto: First author
2. Di Salle A, Viscusi G, Di Cristo F, **Valentino A**, Gorrasi G, Lamberti E, Vittoria V, Calarco A, and Peluso G. Antimicrobial and Antibiofilm Activity of Curcumin-Loaded Electrospun Nanofibers for the Prevention of the Biofilm-Associated Infections. MOLECULES 2021, 26, 4866. **IF 4.40** Citations: 1 Articolo in Rivista. Ruolo svolto: Co-author.
3. Bonadies I, Di Cristo F, **Valentino A**, Peluso G, Calarco A, Di Salle A. pH-Responsive Resveratrol-Loaded Electrospun Membranes for the Prevention of Implant-Associated Infections. NANOMATERIALS. 2020, 10(6): 1175. IF: 5.07 Citations: 7 Articolo in Rivista. Ruolo svolto: Co-author.
4. **Valentino A,** Conte R, Di Cristo F, Peluso G, Cerruti P, Di Salle A, Calarco A. Cationic Polymer Nanoparticles-Mediated Delivery of miR-124 Impairs umorigenicity of Prostate Cancer Cells. INTERNATIONAL JOURNAL OF MOLECULAR SCIENCES. 2020, 21(3): 869. **IF: 5.92** Citations: 10 Articolo in Rivista. Ruolo svolto: First author.
5. **Valentino A,** Di Meo F, Petillo O, Peluso G, Filosa S, Crispi S. Bioactive Polyphenols and Neuromodulation: Molecular Mechanisms in Neurodegeneration. INTERNATIONAL JOURNAL OF MOLECULAR SCIENCES. 2020, 21(7): 2564. **IF: 4.50** Citations: 15 Review in Rivista. Ruolo svolto: First author.
6. Di Cristo F, Finicelli M, Digilio FA, Paladino S, **Valentino A**, Scialo F, D'Apolito M, Saturnino C, Galderisi U, Giordano A, Melone MAB, Peluso G. Meldonium improves Huntington's disease mitochondrial dysfunction by restoring peroxisome proliferator-activated receptor gamma coactivator 1 alpha expression. JOURNAL OF CELLULAR PHYSIOLOGY. 2019,

234(6): 9233-9246. **IF: 6.38** Citations: 6 Articolo in Rivista. Ruolo svolto: Co-author.

7. Conte R, De Luise A, **Valentino A**, Di Cristo F, Petillo O, Riccitiello F, Di Salle A, Calarco A, Peluso G. Hydrogel Nanocomposite Systems: Characterization and Application in Drug-Delivery Systems in nanocarriers for drug delivery: NANOSCIENCE AND NANOTECHNOLOGY IN DRUG DELIVERY. Book series: Micro & Nano Technologies. 2019, 319-349. Citations: 5 Review in Rivista. Ruolo svolto: Co-author.

8. Reclusa P, Laes JF, Malapelle U, **Valentino A**, Rocco D, Gil-Bazo I, Rolfo C. EML4-ALK translocation identification in RNA exosomal cargo (ExoALK) in SCLC patients: a novel role for liquid biopsy. TRANSLATIONAL CANCER RESEARCH. 2019, 8(1): S76-S78. **IF: 1.24** Citations: 11 Articolo in Rivista. Ruolo svolto: Co-author.

9. **Valentino A,** Melone MAB, Margarucci S, Galderisi U, Giordano A, Peluso G. The carnitine system and cancer metabolic plasticity. CELL DEATH & DISEASE. 2018, 9: 228. **IF: 8.47** Citations: 71 Review in Rivista. Ruolo svolto: First author

10. **Valentino A**, Calarco A, Di Salle A, Finicelli M, Crispi S, Calogero RA, Riccardo F, Sciarra A, Gentilucci A, Galderisi U, Margarucci S, Peluso G. Deregulation of MicroRNAs mediated control of carnitine cycle in prostate cancer: molecular basis and pathophysiological consequences. ONCOGENE. 2017 36(43): 6030-6040. **IF: 9.86** Citations: 29 Articolo in Rivista. Ruolo svolto: First author.

11. **Valentino A**, Reclusa P, Sirera R, Giallombardo M, Camps C, Pauwels P, Crispi S, Rolfo C. Exosomal microRNAs in liquid biopsies: future biomarkers for prostate cancer. CLINICAL & TRANSLATIONAL ONCOLOGY. 2017, 19(6): 651-657. **IF: 3.40** Citations: 51 Review in Rivista. Ruolo svolto: First author

12. Conte R, De Luca I, **Valentino A**, Di Salle A, Calarco A, Riccitiello F, Peluso G. Recent advances in bioartificial polymeric materials based nanovectors. PHYSICAL SCIENCES REVIEWS. 2017, 2(4): UNSP 20160131. Review in Rivista. Ruolo svolto: Co-author

13. **Valentino A,** Reclusa P, Sirera R, Dietrich MF, Luis Raez LE, Rolfo C. Circulating MicroRNAs and Long Noncoding RNAs: Liquid Biomarkers in Thoracic Cancer. *Cancer Transl Med 2017;3(2):53–57.* Review in Rivista. Ruolo svolto: First author

14. Reclusa P, Sirera R, Araujo A, Giallombardo M, **Valentino A,** Sorber L, Bazo IG, Pauwels P, Rolfo C. Exosomes genetic cargo in lung cancer: a truly Pandora's box. Transl Lung Cancer Res. 2016 Oct;5(5):483-491. doi: 10.21037/tlcr.2016.10.06. PMID: 27826529; PMCID: PMC5099517. **IF: 6.49** Citations: 26. Review in Rivista. Ruolo svolto: Co-author

15. Conte R, Calarco A, Napoletano A, **Valentino A**, Margarucci S, Di Cristo F, Di Salle A, Peluso G. Polyphenols Nanoencapsulation for Therapeutic Applications J. Biomol. Res. Ther 5 (2). Review in Rivista. Ruolo svolto: Co-author

16. Fico A, Alfano D, **Valentino A**, Vasta V, Cavalcanti E, Travali S, Patriarca EJ, Caputo E. c-Myc modulation: a key role in melanoma drug response. Cancer Biol Ther. 2015 Sep 2;16(9):1375-86. Epub 2015 Apr 2. **IF: 4.74** Citations: 5. Articolo in Rivista. Ruolo svolto: Co-author.

17. Caputo E, Wang E**, Valentino A**, Crispi S, De Giorgi V, Fico A, Ficili B, Capone M, Anniciello A, Cavalcanti E, Botti G, Mozzillo N, Ascierto PA, Marincola FM, Travali S. Ran signaling in melanoma: implications for the development of alternative therapeutic strategies. Cancer Lett. 2015 Feb 1;357(1):286-96. Epub 2014 Nov 20. **IF: 8.67** Citations: 9. Articolo in Rivista. Ruolo svolto: Co-author.

18. Granese B, Scala I, Spatuzza C, **Valentino A,** Coletta M, Vacca RA, De Luca P, Andria G. Validation of microarray data in human lymphoblasts shows a role of the ubiquitin proteasome system and NF-kB in the pathogenesis of Down syndrome**.** BMC Med Genomics. 2013 Jul 5;6:24. IF: 3.063 Citations: 16. Articolo in Rivista. Ruolo svolto: Co-author.

CONTRIBUTI A CONVEGNI

Valentino A, Crispi S, Filosa S, Margarucci S, Calogero R, Riccardo F, Galderisi U, Peluso G. MiRNAs: a connection between fatty acid metabolism and cancerogenesis in prostate cells.

Gianlombardo M, Reclusa P, **Valentino A**, Sirera R, Pauwel P, Rolfo C. Evaluation of Different Exosomal RNA Isolation Methods in NSCLC Liquid Biopsies. Meeting Abstract **IF: 15.60** Citations:1

Rolfo C, Laes JF, Reclusa P, **Valentino A**, Lienard M, Gil Bazo I, Malapelle U et al,. Exo-ALK Proof of

Concept: Exosomal Analysis of ALK Alterations in Advanced NSCLC Patients. Meeting Abstract **IF: 15.60** Citations:4

Valentino A, Di Salle A, Crispi S, Di Cristo F, Napoletano A, Galderisi U and Peluso G. Roles of microRNAs in the regulation of prostate cancer metabolism

I. De Luca, A. **Valentino, A**. Di Salle, A. De Luise, F. Di Cristo, G. Peluso and A. Calarco. Mitocondria toxicity of PEI-based nanoparticles is reduced by acetylation of amines

De Luise, A. Calarco, **Valentino A**, S. Margarucci, G. Peluso, S. Rengo, A. Di Salle. Electrospun membranes loading osteogenic-bioactive molecole for guided bone regeneration after dental implantation.

Di Cristo F., Napoletano A., Conte R., **Valentino A**, Caporale A., Di Mole T., Peluso G., Saturnino C. Effect of Etomoxir on Huntington's disease models.

Melone M, Di Cristo F, Digilio FA, Paladino S, **Valentino A**, Finicelli M, et al. Are mitochondria a possible therapeutic target in huntington's disease? Meeting Abstract. **IF: 10.28**

Dati personali

Autorizzo il trattamento dei miei dati personali ai sensi del Decreto Legislativo 30 giugno 2003, n. 196 "Codice in materia di protezione dei dati personali".

DATA

14/12/2021

FIRMA

Cognome VALENTINO
Nome ANNA
nato il 17-03-1988
(atto n. 00364 p. 2 s. A 1988)
a NAPOLI (NA)
Cittadinanza Italiana
Residenza AFRAGOLA (NA)
Via MESSINA 4
Stato civile STATO LIBERO
Professione Omessa la qualifica professionale (Art. 35 D.P.R. 30-5-1989 N. 223)

CONNOTATI E CONTRASSEGNI SALIENTI

Statura 158
Capelli Castani
Occhi Castani
Segni particolari

Firma del titolare Anna Valentino

AFRAGOLA li 12-04-2012

Impronta del dito indice sinistro

IL SINDACO

ISTRUTTORE AMMINISTRATIVO

Tucillo Elvira

Scadenza : 17-03-2023
Diritti : 5,16

AT 2912251

REPVBBLICA ITALIANA

COMVNE DI
AFRAGOLA

CARTA D'IDENTITA'

N°AT 2912251

DI
VALENTINO ANNA

Anna Valentino

Allegato C

INFORMATIVA SUL TRATTAMENTO DEI DATI PERSONALI RESA

AI SENSI DELL'ART. 13 DEL REGOLAMENTO UE 2016/679

Ai sensi dell'art. 13 del predetto Regolamento, La informiamo che:

1) I suoi dati personali verranno trattati per le seguenti finalità: svolgimento della procedura selettiva, compreso l'eventuale utilizzo di graduatorie e per il successivo eventuale conferimento dell'assegno, per l'esecuzione dei compiti di interesse pubblico o comunque connessi all'esercizio dei pubblici poteri affidati al Consiglio Nazionale delle Ricerche. I dati saranno trattati per il tempo necessario alla selezione e, in caso di conferimento dell'assegno, per tutto il periodo in cui intercorre il rapporto instaurato con il titolare dell'assegno e, successivamente alla cessazione, per l'eventuale adempimento di obblighi di legge in conformità alle norme vigenti sulla conservazione degli atti amministrativi.

2) I dati verranno trattati in forma digitale ed analogica, con modalità di organizzazione ed elaborazione correlate alle finalità sopra indicate e, comunque, in modo da garantirne la sicurezza e la riservatezza.

3) Il conferimento dei dati è obbligatorio per l'espletamento della procedura selettiva; l'eventuale rifiuto di fornire tali dati comporta la mancata possibilità di partecipazione alla procedura stessa.

4) Possono venire a conoscenza dei dati in questione, per il conseguimento delle finalità sopra indicate, il Direttore/Dirigente della Struttura che ha emanato l'avviso di selezione, il responsabile del procedimento, il personale incaricato della gestione delle diverse fasi del procedimento, i componenti della commissione esaminatrice e il segretario.

5) Il Titolare del trattamento è: il Consiglio Nazionale delle Ricerche – Piazzale Aldo Moro n. 7 – 00185 Roma PEC: protocollo-ammcen@pec.cnr.it, il cui punto di contatto è indicato nell'articolo 10 dell'avviso di selezione, rubricato "Trattamento dei dati personali".

6) I dati di contatto del Responsabile della protezione dei dati sono: E-mail: rpd@cnr.it; PEC: protocollo-ammcen@pec.cnr.it presso il Consiglio Nazionale delle Ricerche – Piazzale Aldo Moro n. 7 – 00185 Roma.

7) La graduatoria finale di merito verrà pubblicata con le modalità indicate nell'art. 7 del bando di selezione, rubricato "Modalità di selezione e graduatoria".

8) Saranno altresì diffusi sul sito web del CNR nella sezione "Amministrazione Trasparente" ai sensi e per gli effetti dell'art. 15 comma 1, del D. Lgs. n. 33/2013, le seguenti informazioni del candidato vincitore: a) gli estremi dell'atto di conferimento dell'assegno; b) il curriculum vitae presentato dal candidato; c) i compensi, comunque denominati, relativi all'assegno di ricerca.

9) Al termine della procedura selettiva, nei limiti pertinenti le finalità sopra indicate, i dati del candidato potranno essere comunicati a soggetti terzi, in conformità agli obblighi previsti da leggi, regolamenti, normativa nazionale e comunitaria, nonché da disposizioni impartite da autorità a ciò legittimate da organi di vigilanza e di controllo, ai sensi dell'art. 6 del Reg. UE 2016/679.

10) In qualità di interessato, il candidato ha il diritto di chiedere al Titolare l'accesso ai dati personali che lo riguardano nonché di esercitare i diritti di cui agli articoli 15 e seguenti del Regolamento (UE) 2016/679, tra cui richiedere la rettifica o la cancellazione degli stessi o la limitazione del trattamento o di opporsi al trattamento presentando apposita istanza al contatto di cui al precedente punto 5.

11) In qualità di interessato, ricorrendone i presupposti, il candidato può presentare reclamo al Garante per la protezione dei dati personali quale autorità di controllo secondo le procedure previste.

La sottoscritta Valentino Anna

nata a Napoli il 17/03/1988 residente ad Afragola in Via Messina n° 4 C.A.P. 80021

Per presa visione

Data
14/12/2021 (Firma leggibile)

ELENCO LAVORI TRASMESSI PER VIA TELEMATICA

1. **Valentino A**, Di Cristo F, Bosetti M, Amaghnouje A, Bousta D, Conte R, and Calarco A. Bioactivity and Delivery Strategies of Phytochemical Compounds in Bone Tissue Regeneration. APPLIED. SCIENCES. **2021**, *11*, 5122.

2. Di Salle A, Viscusi G, Di Cristo F, **Valentino A**, Gorrasi G, Lamberti E, Vittoria V, Calarco A, and Peluso G. Antimicrobial and Antibiofilm Activity of Curcumin-Loaded Electrospun Nanofibers for the Prevention of the Biofilm-Associated Infections. MOLECULES 2021, 26, 4866.

3. Bonadies I, Di Cristo F, **Valentino A**, Peluso G, Calarco A, Di Salle A. pH-Responsive Resveratrol-Loaded Electrospun Membranes for the Prevention of Implant-Associated Infections. NANOMATERIALS. 2020, 10(6): 1175.

4. **Valentino A,** Conte R, Di Cristo F, Peluso G, Cerruti P, Di Salle A, Calarco A. Cationic Polymer Nanoparticles-Mediated Delivery of miR-124 Impairs umorigenicity of Prostate Cancer Cells. INTERNATIONAL JOURNAL OF OLECULAR SCIENCES. 2020, 21(3): 869.

5. **Valentino A,** Di Meo F, Petillo O, Peluso G, Filosa S, Crispi S. Bioactive Polyphenols and Neuromodulation: Molecular Mechanisms in Neurodegeneration. INTERNATIONAL JOURNAL OF MOLECULAR SCIENCES. 2020, 21(7): 2564

6. Di Cristo F, Finicelli M, Digilio FA, Paladino S, **Valentino A**, Scialo F, D'Apolito M, Saturnino C, Galderisi U, Giordano A, Melone MAB, Peluso G. Meldonium improves Huntington's disease mitochondrial dysfunction by restoring peroxisome proliferator-activated receptor gamma coactivator 1 alpha expression. JOURNAL OF CELLULAR PHYSIOLOGY. 2019, 234(6): 9233-9246.

7. Conte R, De Luise A, **Valentino A**, Di Cristo F, Petillo O, Riccitiello F, Di Salle A, Calarco A, Peluso G. Hydrogel Nanocomposite Systems: Characterization and Application in Drug-Delivery Systems in NANOCARRIERS FOR DRUG DELIVERY: NANOSCIENCE AND NANOTECHNOLOGY IN DRUG DELIVERY. Book series: Micro & Nano Technologies. 2019, 319-349.

8. Reclusa P, Laes JF, Malapelle U, **Valentino A**, Rocco D, Gil-Bazo I, Rolfo C. EML4-ALK translocation identification in RNA exosomal cargo (ExoALK) in SCLC patients: a novel role for liquid biopsy. TRANSLATIONAL CANCER RESEARCH. 2019, 8(1): S76-S78.

9. **Valentino A,** Melone MAB, Margarucci S, Galderisi U, Giordano A, Peluso G. The carnitine system and cancer metabolic plasticity. CELL DEATH & DISEASE. 018, 9: 228.

10. **Valentino A**, Calarco A, Di Salle A, Finicelli M, Crispi S, Calogero RA, Riccardo F, Sciarra A, Gentilucci A, Galderisi U, Margarucci S, Peluso G. Deregulation of MicroRNAs mediated control of carnitine cycle in prostate cancer: molecular basis and pathophysiological consequences. ONCOGENE. 2017 36(43): 6030-6040.

11. **Valentino A**, Reclusa P, Sirera R, Giallombardo M, Camps C, Pauwels P, Crispi S, Rolfo C. Exosomal microRNAs in liquid biopsies: future biomarkers for prostate cancer. CLINICAL & TRANSLATIONAL ONCOLOGY. 2017, 19(6): 651-657.

12. Conte R, De Luca I, **Valentino A**, Di Salle A, Calarco A, Riccitiello F, Peluso G. Recent advances in bioartificial polymeric materials based nanovectors. PHYSICAL SCIENCES REVIEWS. 2017, 2(4): UNSP 20160131.

13. Reclusa P, Sirera R, Araujo A, Giallombardo M, **Valentino A**, Sorber L, Bazo IG, Pauwels P, Rolfo C. Exosomes genetic cargo in lung cancer: a truly Pandora's box. Transl Lung Cancer Res. 2016 Oct;5(5):483-491. doi: 10.21037/tlcr.2016.10.06. PMID: 27826529; PMCID: PMC5099517.

14. **Valentino A,** Pablo Reclusa, Rafael Sirera, Martin Frederik Dietrich, Luis Estuardo Raez, Christian Rolfo. Circulating MicroRNAs and Long Noncoding RNAs: Liquid Biomarkers in Thoracic Cancer. *Cancer Transl Med 2017;3(2):53–57*

15. R Conte, A Calarco, A Napoletano, **Valentino A**, S Margarucci, F Di Cristo, Di Salle A, Peluso G. Polyphenols Nanoencapsulation for Therapeutic Applications J. Biomol. Res. Ther 5 (2).

16. Fico A, Alfano D, **Valentino A**, Vasta V, Cavalcanti E, Travali S, Patriarca EJ, Caputo E. c-Myc modulation: a key role in melanoma drug response. Cancer Biol Ther. 2015 Sep 2;16(9):1375-86. Epub 2015 Apr 2.

17. Caputo E, Wang E**, Valentino A**, Crispi S, De Giorgi V, Fico A, Ficili B, Capone M, Anniciello A, Cavalcanti E, Botti G, Mozzillo N, Ascierto PA, Marincola FM, Travali S. Ran signaling in melanoma: implications for the development of alternative therapeutic strategies. Cancer Lett. 2015 Feb 1;357(1):286-96. Epub 2014 Nov 20.

18. Granese B, Scala I, Spatuzza C, **Valentino A**, Coletta M, Vacca RA, De Luca P, Andria G. Validation of microarray data in human lymphoblasts shows a role of the ubiquitin proteasome system and NF-kB in the pathogenesis of Down syndrome. BMC Med Genomics. 2013 Jul 5;6:24.

Data 14/12/2021 *Firma*

applied sciences

MDPI

Review

Bioactivity and Delivery Strategies of Phytochemical Compounds in Bone Tissue Regeneration

Anna Valentino [1,2,†], Francesca Di Cristo [3,†], Michela Bosetti [1], Amal Amaghnouje [4], Dalila Bousta [4], Raffaele Conte [5,*] and Anna Calarco [2,*]

[1] Dipartimento di Scienze del Farmaco, Università del Piemonte Orientale "A. Avogadro", Largo Donegani, 2, 28100 Novara, Italy; anna.valentino@uniupo.it (A.V.); michela.bosetti@uniupo.it (M.B.)
[2] Research Institute on Terrestrial Ecosystems (IRET)-CNR, Via Pietro Castellino 111, 80131 Naples, Italy
[3] Elleva Pharma S.R.L. via Pietro Castellino 111, 80131 Naples, Italy; francesca.dicristo@ellevapharma.com
[4] Laboratory of Biotechnology, Environment, Agrifood, and Health, University of Sidi Mohamed Ben Abdellah, 30000 Fez, Morocco; Amal.amaghnouje@usmba.ac.ma (A.A.); Boustadalila@usmba.ac.ma (D.B.)
[5] AMES Group Polydiagnostic Center, via Padre Carmine Fico, 24, 80013 Casalnuovo di Napoli, Italy; raffaele.conte86@tiscali.it
* Correspondence: raffaele.conte86@tiscali.it (R.C.); anna.calarco@cnr.it (A.C.)
† These authors contributed equally to this work.

Abstract: Plant-derived secondary metabolites represent a reservoir of phytochemicals for regenerative medicine application because of their varied assortment of biological properties including anti-oxidant, anti-inflammatory, antibacterial, and tissue remodeling properties. In addition, bioactive phytochemicals can be easily available, are often more cost-effective in large-scale industrialization, and can be better tolerated compared to conventional treatments mitigating the long-lasting side effects of synthetic compounds. Unfortunately, their poor bioavailability and lack of long-term stability limit their clinical impact. Nanotechnology-based delivery systems can overcome these limitations increasing bioactive molecules' local effectiveness with reduction of the possible side effects on healthy bone. This review explores new and promising strategies in the area of delivery systems with particular emphasis on solutions that enhance bioavailability and/or health effects of plant-derived phytochemicals such as resveratrol, quercetin, epigallocatechin-3-gallate, and curcumin in bone tissue regeneration.

Keywords: bone regeneration; phyto-bioactive compounds; molecular signaling pathways; bone-devices

Citation: Valentino, A.; Di Cristo, F.D.; Bosetti, M.; Amaghnouje, A.; Bousta, D.; Conte, R; Calarco A. Bioactivity and Delivery Strategies of Phytochemical Compounds in Bone Tissue Regeneration. *Appl. Sci.* **2021**, *11*, 5122. https://doi.org/10.3390/app11115122

Academic Editor: Won Ho Park

Received: 16 April 2021
Accepted: 27 May 2021
Published: 31 May 2021

1. Introduction

Bone defect, due to traumatic injury, congenital disease, or tumor resection, represents a severe ailment affecting millions of people. However, bone regeneration is a complex and dynamic process that involves several actors including osteoprogenitor cells that respond to intracellular and extracellular molecular signaling pathways to ensure bone functional recovery [1,2]. Although the bone tissue is capable of self-repair and renew, regenerative medicine approaches are essential to promote and speed up the healing of bone defects recovering the normal and healthy function of the skeletal system [3]. The conventionally therapeutic approaches have demonstrated a limited efficacy due, for example, to graft rejection, pathogen transmission, and invasive surgical procedures [4]. Owing to the drawbacks and limitations of many bone grafts, bioactive materials that integrate various delivery vehicles, bioactive molecules, stem cells, or demineralized bone matrix may help bone repair creating microenvironments that favor and guide bone regeneration [5,6]. An engineering bone substitute should operate as a proper template for new bone ingrowth showing osteogenic properties (osteoinductive and/or

osteoconductive) and being biocompatible with the host tissue. In the last decades, the nanotechnological approach has made great strides in the design of materials able to mimic the natural characteristics of the bone. To improve bone formation/regeneration, phytochemicals such as curcumin, resveratrol, oleuropein, quercetin, etc., have often been incorporated into biomaterials as a natural and non-toxic therapeutic alternative to traditional treatments [7,8]. Phyto-bioactive substances, defined as non-nutritive plant secondary metabolites, could interact with enzymes, proteins, and membrane receptors modulating cell-signal transduction cascade and specific molecular pathways leading to bone anabolic effects and decreasing bone resorption [9,10]. In addition, epidemiological studies have reported a correlation between a diet rich in biologically active factors such as fruits, vegetables, and olive oil and the reduced risk of bone loss and bone-related trauma [11,12]. However, these compounds present in vivo limited biological activity, lack long-term stability, and are subject to oxidation overtime under exposure to oxygen, light, moisture, and heat [13,14]. Therefore, a nanotechnological approach that involves controlled drug delivery systems for natural bioactive molecules could be a solution to avoid invasive procedures and minimize off-target cell behaviors. In addition, these alternative strategies could provide phytochemicals better performance, enhance their low water solubility or very short circulating half-life, improving the functionality and clinical utility [3,15]. This review attempts to summarize the recent works involving delivery systems (i.e., synthetic ceramic, scaffolds, nanoparticles) and phytochemicals to guarantee the protection of natural biomolecules from environmental degradation, to modulate compounds release, and to prolong delivery at localized injury sites. A short chapter on the structure of bone tissue, its functional activities, and the regulatory mechanisms of bone remodeling/regeneration will help in understanding the results discussed.

2. Bone Structure and Function

Bone is a metabolically active tissue with self-healing capability, in constant renewal, adapting its structure to mechanical stimuli, stress, hormonal changes, and repairing structural injuries through a process of remodeling [16]. Bone homeostasis is preserved by the coordinated action between osteoblasts (bone-generating cells derived from mesenchymal stem cells, MSCs) responsible for bone growth and osteoclasts (multinucleated bone-resorbing cells differentiated from the hematopoietic stem) involved in bone resorption [17]. During bone matrix synthesis, first osteoblasts secrete the organic matrix: collagen proteins, mainly collagen type I and non-collagen proteins, such as osteonectin (ON), osteocalcin (OCN), bone sialoprotein (BSPI/II), and osteopontin (OPN), and proteoglycan [18–20]. Secondly, deposition and mineralization of the bone matrix take place through the production of a protein mixing called osteoid that promotes calcium and phosphate adhesion, resulting in the organization and mineralization of new bone [21,22]. Mature osteocytes (derived from MSCs through osteoblastic differentiation) are completely trapped inside the mineralized bone matrix. Due to their strategic location, osteocytes maintain the connections to other osteocytes and osteoblasts and react to several biochemical signaling paths and mechanical stimuli contributing to the regulation of calcium and phosphate homeostasis [23]. When bone resorption should not take place, lining cells avoid direct interface among osteoclasts and bone matrix, playing a significant role in calcium homeostasis and osteoclast differentiation [24–27]. Osteoclasts resorb bone through the release of enzymes and acids capable of dissolving and digesting minerals in the bone, but they also secrete cytokines that affect the activity of surrounding cells inducing mesenchymal stem cells and osteoblasts to initiate osteogenesis in resorption lacuna (remodeling) or another non resorbed site (modeling) [28–30]. The RANKL/RANK/OPG system is a crucial mediator of osteoclastogenesis. In particular, the interaction of RANK with RANKL is required for osteoclast formation, differentiation, activation, and survival. On the contrary, OPG can block RANK/RANKL interaction, thus

preventing osteoclast differentiation and activation [31,32]. Irregularities in osteoclastic activity lead to disorders such as osteoporosis and osteopetrosis [33].

3. Bone Regeneration Process

The bone healing process is a complex mechanism of bone regeneration, which involves inflammation, bone production, and bone remodeling phases [34]. Inflammation is usually observed immediately following the fracture at the injury site since tissues swell, bone cells die, and blood vessels break, with consequent formation of hematoma, a source of hematopoietic cells capable of secreting growth factors. The injury to bone leads to the secretion of pro-inflammatory factors like tumor necrosis factor-alpha (TNF-α), bone morphogenetic proteins (BMPs), and interleukins (IL-1, IL-6, IL-11, IL-23). These molecules attract, at the fracture site, macrophages, monocytes, and lymphocytes able to take out damaged necrotic tissue and secrete factors (i.e., vascular endothelial growth factor, VEGF) to stimulate angiogenesis and healing [35]. MSCs migrate to the fracture site and, under BMPs control, start to differentiate into fibroblasts, osteoblasts, and chondroblasts. As a result, chondrogenesis begins to occur, and a fibrocartilaginous callus (also called "soft callus") forms within two weeks. The soft callus undergoes endochondral ossification, which converts fibrocartilaginous callus to bony callus (also identified as "hard callus"). The expression of RANKL promotes further differentiation of chondroblasts, osteoblasts, and osteoclasts [36–38]. Bone regeneration is thinly modulated by several signaling pathways and transcriptional factors. During the early stages of bone healing, the Wnt pathway suppresses the differentiation of mesenchymal stem cells into osteoblasts, while in the later stages it controls the commitment of the undifferentiated cells to the osteoblasts [39]. Notch signaling is another potential pathway with osteoinductive properties. Notch receptors, through their ligand (Jag-1), increase the expression of genes related to osteoblasts as ALP and BSP, inducing osteoclastogenesis [40]. An interesting study demonstrates that the functionalization of titanium implant surface with Jag-1 contributes to the enhancement of osteoblast differentiation, improving osteogenic properties [41]. Indeed, the activation of the Notch pathway leads to an increase of osteogenic differentiation, as highlighted by an upregulation of osteogenic markers, in particular BSP and OCN; bone differentiation proteins as BMP2 and BMP6; and growth/differentiation factor 15 (GDF15) [42]. Several other factors are implicated in bone regeneration processes, such as mitogen-activated protein kinase (MAPK) associated pathways, phosphatidylinositol-4,5-bisphosphate 3-kinase (PI3K)/Akt, growth factors as fibroblast growth factors (FGFs), insulin-like growth factors (IGFs), and VEGF [43]. MAPKs pathway takes part in bone formation and bone healing post-fracture through the transduction of signals induced by numerous growth factors or adhesion molecules. The (PI3K)/Akt signaling pathway promotes the expression of OPG, Runx2, *p*-Akt, and BMP-2 proteins, as well as the proliferation, differentiation, and osteogenesis of osteoblasts [44]. Devi and Dixit demonstrated that the release of rh-VEGF, rh-IGF-I from a polylactide-polyglycolide acid membrane and β-tricalcium phosphate bone graft led to better clinical results such as bone pocket reduction and bone filling simultaneously with respect to growth factors used alone [45]. Furthermore, FGF signaling plays a pivotal role in the intramembranous and endochondral signaling pathway regulating process in osteoprogenitor cells [46]. It has been reported that treatment with hydrogel-bFGF after a fracture has a higher rate of mineralization, as well as an upregulation of Runx2 and osteocalcin in mice [47,48]. Normal bone development requires the downregulation of Runx2 to form mature bone [49].

4. Bioactive Phytochemicals and Bone Signaling Pathways

Phyto-bioactive compounds (i.e., polyphenolic compounds, carotenoids, tocopherols, and phytosterols) are defined as natural secondary metabolites available in fruits, vegetables, grains, and other plant-based foods which provide health benefits and reduce the risk of major chronic diseases [50–53]. In addition to health benefits, bioactive

molecules of natural origin are being used as prominent alternatives to chemical preservatives and additives [54–56] as well as in the green synthesis of nanomaterials (i.e., graphene nanosheets, gold nanoparticles, etc.) [57–61]. In bone regenerative medicine, their antioxidant and anti-inflammatory beneficial properties can regulate bone regeneration signaling pathways, offering an innovative potential therapeutic strategy [62]. Notably, phytochemicals target several critical molecular pathways involved in bone metabolism, such as estrogen signaling pathway, MAPK cascade, Wnt/β-catenin, sirtuin 1 (Sirt1), TGF-β/BMP, PI3K/Akt, and adenosine monophosphate protein kinase (AMPK) [63]. These pathways can be split into three main classes based on their activity: anti-inflammatory, antioxidants, and bone cell differentiation activity (Figure 1).

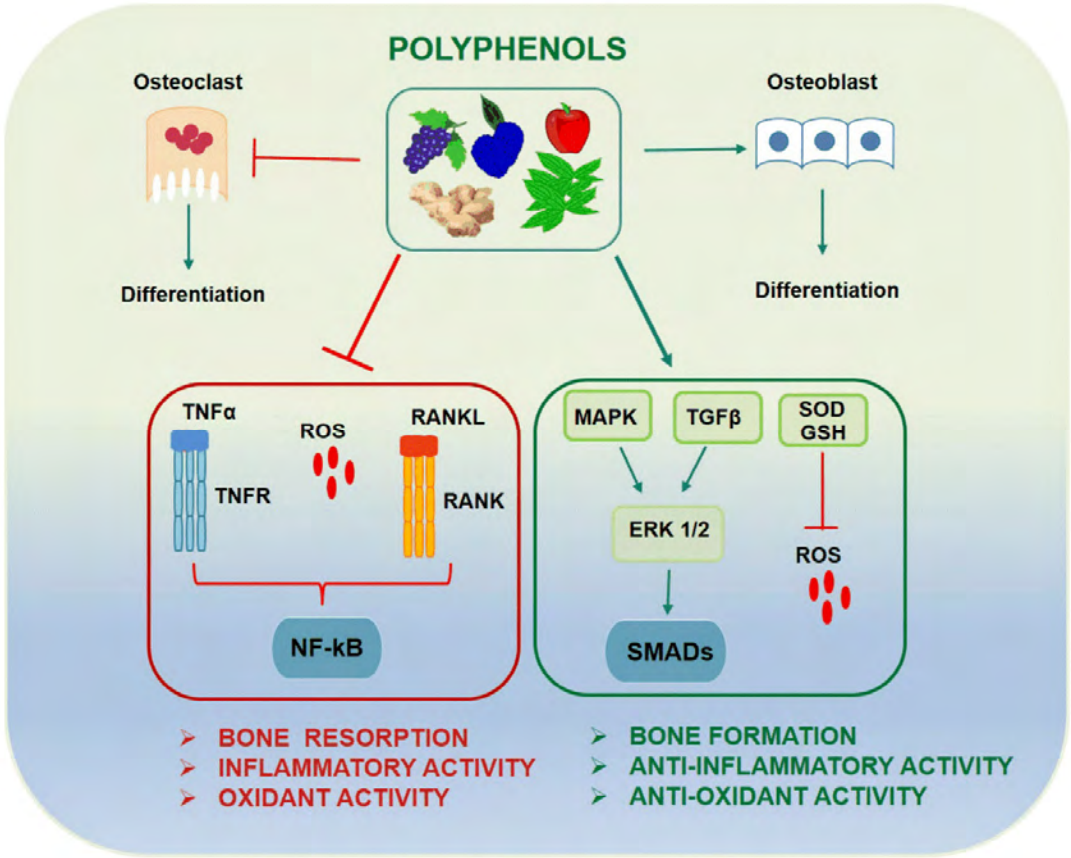

Figure 1. Signaling pathways involved in bone formation (green box) and bone resorption (red box). Polyphenols positively regulate MAPKs/TGFβ/ERK1-2 pathway that activates and translocate Smads complex into the nucleus. Activated Smads regulate the expression of transcriptional factors and coactivators important in osteoblasts differentiation and bone formation process including Dlx5, Runx2, and Osx. Polyphenols also up-regulate genes involved in antioxidant activity such as superoxide dismutase (SOD) and *g*lutathione *s*ynthetase (GSH). At the same time, polyphenols down-regulate RANKL and TNF*α*, two master gene regulators of osteoclasts differentiation and inflammatory pathways, respectively.

4.1. Anti-Inflammatory Activity

The anti-inflammatory activity of phyto-molecules is related to the inhibition of genes expression such as TNF-*α*, [64] monocyte chemotactic protein (MCP)-1, [65] and matrix metalloproteinases (MMPs) [66], and the decrease of pro-inflammatory molecules, such as IL-6, IL-10, and IL-1β [67–69]. For example, curcumin, an extract from *Curcuma longa*, has been extensively studied due to its ability to inhibit NF-kB and the activation of the activator protein 1 (AP-1) after an inflammatory stimulus [70]. This bioactive molecule

suppresses the transcription of pro-inflammatory genes, such as TNFα, IL-6, [64] cyclooxygenase 2 (COX2), and inducible nitric oxide synthase iNOS [71], and contributes to inhibition of MMPs synthesis [72]. Similarly, dried plum polyphenols and tannins indirectly suppress osteoclast differentiation and activity via lowering TNF-α and NO production [73,74] and down-regulating RANKL expression. Epigallocatechin gallate (EGCG), the most abundant catechin in green tea, exerts an anti-inflammatory effect through MAPKs pathway. Moreover, EGCG reduces the phosphorylation levels of MEK1/2and Raf-1 upstream of ERK1/2 MAPK cascade, [75] promoting bone anabolism, enhancing osteoblasts proliferation, differentiation, and mineralization, and decreasing inflammatory mediators [76,77]. Flavonoids, polyphenols present at relatively low concentrations in most fruit and vegetables, are known as food-based anti-inflammatory agents. Important flavonoids such as quercetin, quercitrin, icaritin, and phloridzin, through downregulation of COX-2 and hypoxia-inducible factor 1-alpha (HIF-1α) pathways, help to reduce the production of prostaglandin E2 (PGE2), [78] exerting anti-inflammatory and antioxidant actions simultaneously [79].

4.2. Antioxidants Activity

Phytochemicals that operate as direct antioxidant substances are able to activate and regulate antioxidant enzymes, with simultaneous action on the inhibition of oxidases, cyclooxygenases, and other enzymes such as iNOS, involved in radical generation [80]. In general, polyphenols, thanks to their B-ring hydroxyl configuration, display a significant antioxidant action that enhances with the increasing of the total number of OH groups and the attendance of the 3,4-catechol structure [81]. By decreasing the oxidative state, bioactive molecules provide for osteoblasts proliferation, activity, and differentiation through the involvement of crucial molecular signaling pathways.

The ROS-scavenging activity is particularly visible in icaritin (a flavonoid isolated from *Epimedium pubescens*), which can reduce superoxide generation in osteoclasts by indirect action on NFATc1 [82] and in naringin, a flavanone with effects on lipid peroxidation, glutathione (GSH) oxidation, and DNA cleavage [83]. Through the same mechanism of action, curcumin and resveratrol (a polyphenolic compound found in grapes and wine) upregulate in the osteoclast the antioxidant enzymes like glutathione peroxidase (Gpx)-1 and superoxide dismutase (SOD), thus modulating ROS levels [84,85]. Curcumin acts on osteoclastogenesis contributing to mitigate bone loss during osteoclast formation and function, preventing ROS and cytokine production. Myricitrin, a glycoside from myricetin, is able to inhibit bone-resorbing cytokines production under oxidative conditions, displaying protective effects against osteoblast cytotoxicity [86]. On the other hand, polyphenols can exert their antioxidant activity through a mechanism of chelation interacting with metals, in particular, Fe and Zn [87,88]. The EGCG shows cytotoxic properties on osteoclasts thanks to its reductive action on Fe (III) catalyzed by the Fenton reaction, leading to hydroxyl radical's generation [89,90].

4.3. Bone Cells Differentiation Activity

Phytomolecules are not only responsible for bone resorption inhibition, but also promote bone formation by aiming at osteoblasts differentiation. For example, EGCG positively acts on osteoblast differentiation and MSC proliferation by upregulating BMP2 and Runx2 expression [91]. Likewise, myricetin can promote osteoblast differentiation and activity, by targeting SMAD-1/5/8, downstream of BMP signaling [92]. It has been demonstrated that myricetin and Baicalin affect osteoblast and osteoclast differentiation and function also through Wnt/β-catenin pathway [93,94]. Additionally, due to structural similarity to mammalian estrogens, some polyphenols can bind estrogen receptors (Ers) that are called phytoestrogens [95]. Among them, vanillic acid upregulates the expression of osteoblastic differentiation markers, i.e., Runx2, OCN, and OPG, by activating ERs pathway [96]. Rutin, instead, downregulates the RUNX suppressor genes [97] and exerts its osteogenic effect through an ER-mediated mechanism [98]. In addition, phyto-derived

neurotransmitters such as dopamine, commonly found in fruit and vegetables (in particular bananas), promote VEGF and bFGF expression, leading to enhanced angiogenesis and osteogenesis [99]. Furthermore, several studies have highlighted the crucial role of polyphenols in regulating gene activation or silencing through epigenetic modifications such as DNA methylation and histone modification [100]. Resveratrol is one of the main activators of Sirt, a known NAD-dependent deacetylase, which induces a conformational change in proteins, translating into an increase in enzymatic activity [101]. Resveratrol induces the MSC differentiation into osteoblasts via a very complex mechanism, which could be direct or indirect. Indirectly, resveratrol, through the interaction of Sirt1 with nuclear receptor co-repressor (NcoR), inhibits peroxisome proliferator-activated receptor gamma (PPARγ) [102], while directly activating RUNX2 transcription factor by forming a Sirt1-Runx2 complex [103]. Resveratrol-mediated activation of Sirt1 enhances phosphorylation of downstream kinases involved in osteoblastic differentiation, such as PKB/Akt, SMAD1/5/8, AMPK, and MAPKs [104,105]. Furthermore, quercetin stimulates osteoblast differentiation through the stimulation of the expression of TGF-β1, BMP-2, and Runx2, via activation of ERK1/2, p38, and JNK MAPKs [106]. Finally, curcumin regulates the expression of genes implicated in RANKL-induced osteoclast differentiation through the suppression of NF-kB [107]. Table 1 recaps the phytochemical-related bone regeneration signaling pathways.

The cellular responses resulting from the activation of different biological pathways underline the importance of natural bioactive molecules and their ability to modulate inflammatory processes, oxidative stress, and cellular differentiation.

Table 1. Summary of phytochemical signaling pathways for bone regeneration.

Phytochemical	Signaling Pathway	Reference
Curcumin	NF-kB pathways, Redox-sensitive signaling pathways	[75,89,90]
EGCG	MAPKs signaling pathways	[82]
Quercetin	COX2/HIF1αsignaling ERK1-2/MAPKs signaling	[83,84,108]
Resveratrol	Redox-sensitive signaling pathways Sirt/RUNX2 signaling MAPKs pathways	[89,90,109]
Incaritin	NFATc signaling	[87]
Naringin	*Glutathione Pathway (GSH)*	[88]
Myricetin	SMAD/BMP signaling Wnt/β-catenin signaling	[97]
Vanillic acid	ERs pathways	[101]
Rutin	ERs pathways	[102,103]

5. Phytochemical-Delivery Vehicles in Bone Tissue Regeneration

To date, the most effective treatment for bone-defect restoration is represented by living tissue transplantation (autologous bone) and/or devitalized donor bone (allograft) because of their notable osteoconductive and osteoinductive properties [108,109]. However, the potential for disease transmission, the limited amount of donor tissue, and postoperative pain at the donor site represent some of drawbacks related to these approaches. To overcome these challenges, new and promising strategies involving delivery systems and phytochemicals have been developed in bone tissue regeneration [110–113]. A successful delivery system should be able to protect phytochemicals from degradation, enhancing their poor bioavailability and minimizing off-target tissue effects [114,115]. These constructs, determining a localized delivery of the natural bioactive

molecules, should promote the normal process of bone regeneration and minimize tissue toxicity caused by systemic drug administration (Figure 2) [116].

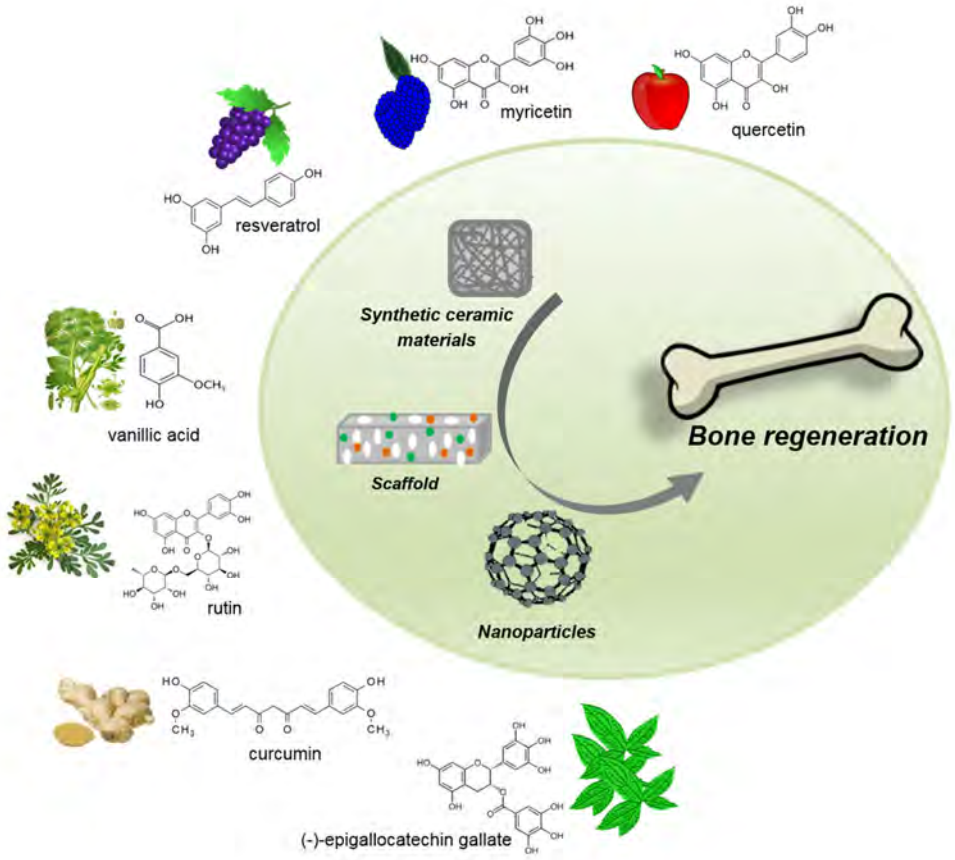

Figure 2. Schematic representation of the main phyto-bioactive nano delivery systems involved in bone regeneration.

5.1. Ceramics

Synthetic ceramic materials are inorganic material favorably used in dentistry that proved excellent mechanical properties and osteo-conduciveness owing to their good biocompatibility, reproducibility, non-immunogenicity [117,118]. Ceramic nanocomposites in the form of particles or nanofibers could mimic the hierarchical arrangement of native bone mineral phase, providing a functional scaffold for cell adhesion [119–122], but are not able to prevent the cause of bone resorption, to control specific anti-osteoclastogenic actions, or to counteract the damage related to oxidative stress. To overcome these disadvantages, polyphenols are widely used to enhance periodontal regeneration or to re-mineralize bone tissue, due to their antioxidant, free-radical scavenging, and antimicrobial properties [123–125]. The preparation of these composites is often optimized to form nanopores (pore diameter < 0.1 μm) to increase the specific surface area of the scaffolds, allowing for better drug loading and higher bioactivity [125]. For example, Iviglia G et al. patented a polyphenol-based collagen gel with granular ceramic fillers to fill the peri-implant bone defects. Such material, characterized by strong mechanical scaffolding properties, combines the pro-osteogenic action of collagen with the anti-inflammatory, antioxidant, and anti-osteoclastogenic activity of a polyphenolic mixture extracted from the pomace of the *Croatina* grape variety [126]. In vitro and in vivo results demonstrated that both the control of inflammation and oxidative stress and the enhancement of early bone matrix deposition are necessary in the

case of oral disease. Cazzola M et al. produced a silica-based bioactive glass coupled with gallic acid and polyphenols extracted from red grape skins and green tea leaves. These modified bioactive glasses showed enhanced free radical scavenging activity [127]. Zhou et al. proposed a simple protocol to functionalize porous calcium phosphate ceramics (PCPC) using dietetic tea polyphenols (TP). TP molecules modulated the nucleation and crystallization of calcium phosphate nanorods and promoted bone mesenchymal stem cell (BMSC) proliferation and differentiation, increasing BMP2, ErK/MAPK, and JNK/MAPK levels and cell mineralization capacity [128].

5.2. Scaffolds

Since the scaffold surface functionalization with polyphenols increases the bone regeneration capacity, the use of enriched scaffolds is considered a promising tool for bone bioengineering [129–131]. Ideally, a scaffold should mimic the extracellular matrix characteristics of the organ of interest to form cell/tissue-specific combination, pattern/topology, and mechanical properties able to support tissue formation [131]. The combination of scaffolds and phytochemicals is used to improve adhesion, growth, or differentiation of cells through the action of the bioactive compound for which the release can be controlled through three methods. When drugs are incorporated into the matrix of the scaffold, the release kinetics are regulated by the degradation of the polymer. Similarly, when scaffold surfaces are coated with a polymer/drug layer, the release is controlled by diffusion and degradation of the coating polymer. Conversely, the integration of micro-nano spheres into scaffolds offers a third mechanism of release based on the degradation of the scaffold and the consequent diffusion of the particle [132]. For example, Santin M et al. used biodegradable antioxidant scaffolds based on soybean (SB), as bone filler. This material showed an in vitro block of osteoclast activation succeeding incubation with SB, with a parallel inhibitory effect on monocyte/macrophage activity and an improved ability to induce mineralization in osteoblasts [133]. In another study, the SB granules implanted in rabbits led to bone repair with distinctive morphology from non-treated defects [134].

Wang W et al. produced scaffolds loaded with resveratrol by grafting the polyphenol to polyacrylic acid (PAA) and integrating this molecular drug into atelocollagen (Coll) hydrogels (Coll/PAA-RSV) [135]. These scaffolds supported the growth of chondrocytes and BMSCs protecting cells against reactive oxygen species. Moreover, the in vivo implantation on rabbits led to the disappearance of osteochondral defects and the integration of the newly formed tissue with surrounding tissue and subchondral bone. Li et al. functionalized a poly-ε-caprolactone (PCL) surface with resveratrol, obtaining an osteogenic porous material. The presence of polyphenol on a scaffold surface increases the mineralization in stromal cells with an improvement in bone regenerating capacity [136]. Kamath MS et al. formulated a porous composite scaffold integrating PLC with resveratrol-loaded albumin nanoparticles. This 3D material produced a significant increment in cell proliferation, ALP activity, and mineralization imparting osteogenic properties to PCL scaffold [137]. Riccitiello et al. synthesized a PLA electrospinning membrane able to release resveratrol in a tunable manner for the preservation of the alveolar socket after tooth extraction. The controlled release of resveratrol influenced in vitro osteoblast and osteoclast differentiation [138]. In another work, the resveratrol released form PLA membrane presents a significant antibacterial and antibiofilm activity versus *Pseudomonas aeruginosa* and *Streptococcus mutans*, becoming a promising solution for the prevention of implant-associated infections [51]. For cranio-facial tissue-engineering applications, Wang et al. combine a collagen scaffold loaded with resveratrol with human adipose stem cells (hASCs). This composite promotes epidermal wound healing and bone mineralization [139]. Wang et al. introduced dopamine (D) onto strontium-doped calcium polyphosphate (SCPP) scaffolds with silk fibroin (SF). SCPP/D/SF stimulated angiogenic factor secretion, osteogenesis, and had great biocompatibility (Figure 3). Then, SCPP/D/SF could fulfill a role as a potential scaffold for

bone tissue engineering with the ability to speed up bone regeneration and vascularization. (Figure 4) [140]. Dhand et al. reported the synthesis by electrospinning of bone-like composite structures containing catecholamines and Ca(2+). Human fetal osteoblasts seeded on these collagen scaffolds exhibited enhanced cell adhesion, penetration, proliferation, and differentiation as well as increased osteogenic expression of osteocalcin, osteopontin, and bone matrix elements [141]. Lee et al. reported an easy, multifunctional surface modification using catechin to enhance the polymeric scaffolds functionality for bone regeneration by stem cells. These catechin-functionalized polymer nanofiber scaffolds, in a critical-sized calvarial bone defect, markedly supported bone formation by hADSC transplantation [142].

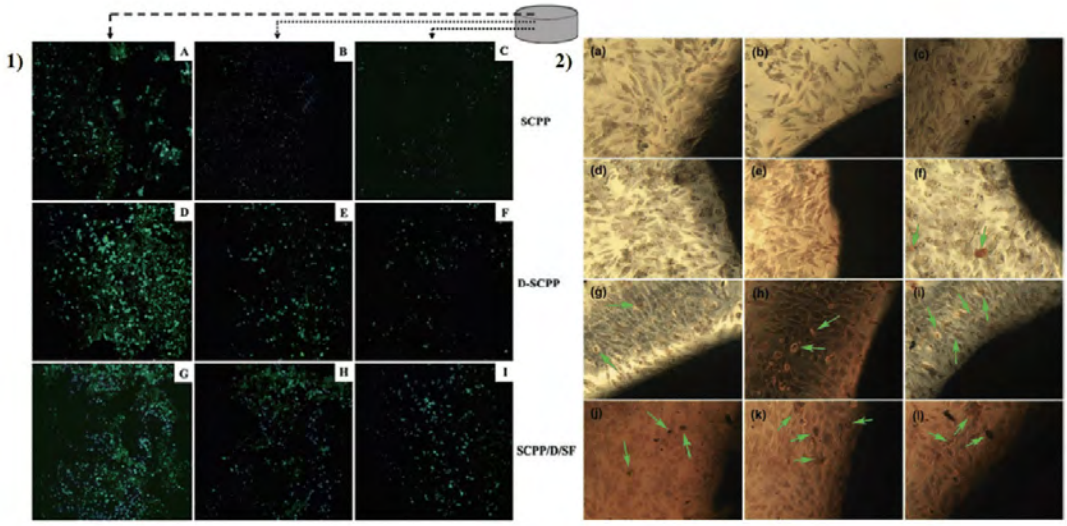

Figure 3. Image (**1**) represents cells cultured with different scaffolds. Image (**2**) shows scaffolds alizarin red staining on day 4 (a–c), day 7 (d–f), day 10 (g–i), day 14 (j–l); SCPP (a, d, g, j), D-SCPP (b, e, h, k), SCPP/D/SF (c, f, i, l), respectively. Green arrows: calcium nodules. Courtesy of: Wang X, Gu Z, Jiang B, Li L, Yu X. Surface modification of strontium-doped porous bioactive ceramic scaffolds via poly(DOPA) coating and immobilizing silk fibroin for excellent angiogenic and osteogenic properties. Biomater Sci. 2016 Apr;4(4):678–88. doi: 10.1039/c5bm00482a. Epub 2016 Feb 12. PMID: 26870855.

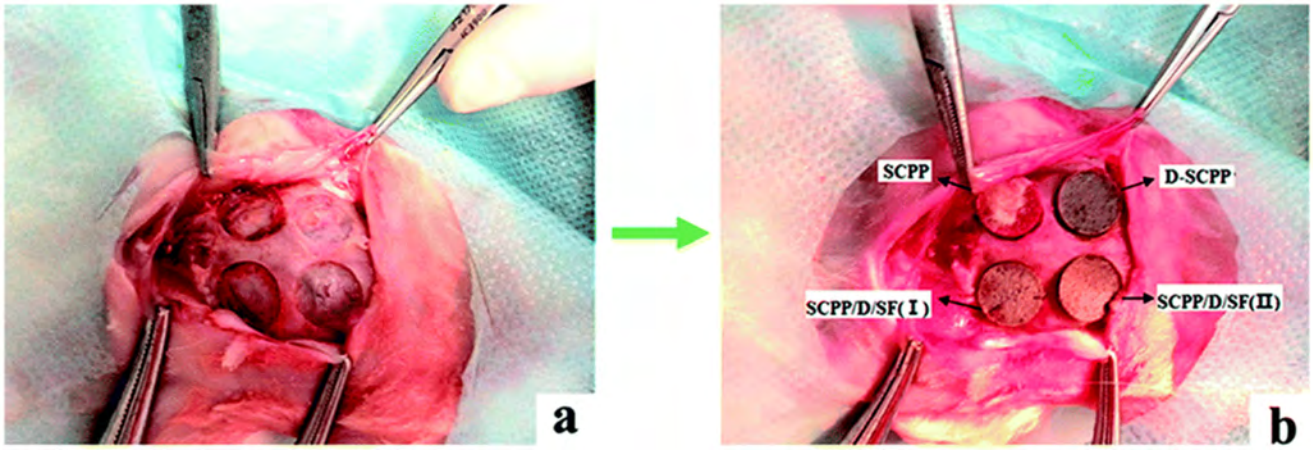

Figure 4. Photographs of animal modeling in vivo. Defects on the cranial bone (**a**) and (**b**) materials implanted. Courtesy of: Wang X, Gu Z, Jiang B, Li L, Yu X. Surface modification of strontium-doped porous bioactive ceramic scaffolds via poly(DOPA) coating and immobilizing silk fibroin for excellent angiogenic and osteogenic properties. Biomater Sci. 2016 Apr;4(4):678–88. doi: 10.1039/c5bm00482a. Epub 2016 Feb 12. PMID: 26870855.

5.3. Nanoparticles

The therapeutic efficacy of natural bioactive molecules can be improved by nanotechnological approaches. The design of drug delivery systems with pre-determined physico-chemical properties permits an increase of phytochemical bioavailability and reduces their toxic side effects [53]. For example, positive surface charges could facilitate the transport of nanoparticles through small intestinal epithelial cells improving the oral bioavailability, while the introduction of polyethylene glycol chains limits opsonization prolonging circulation times [143–145]. Moreover, the modulation of structure-property relationships (i.e., size, geometry or shape, material composition, etc.) of nanoparticles can influence the transport mechanism, facilitating their internalization into the target cells.

He L et al. produced tea polyphenol-modified calcium phosphate nanoparticles (TP-CaP) able to enhance remineralization of preformed enamel lesions on bovine incisors. Moreover, the released tea polyphenols inhibited bacterial growth and enzyme activities [146]. Wang produced gold nanoparticles (Au-NPs) formed using Anogeissus latifolia (A. latifolia) phytochemicals. Such nano-vehicles showed great osteoinductive potential and analgesic properties and were characterized by exceptional blood compatibility and cytocompatibility [147]. Felice et al. synthesized polyphenol-based mucoadhesive polymeric nanoparticles (GSE-NP) able to protect endothelial progenitor cells (EPCs) from oxidative stress. These vehicles demonstrated strong antioxidant capacity thanks to their high content in total polyphenols [148]. Del Prado Audelo et al. synthesized nanoparticles of PCL and Pluronic® F-68, loaded with curcumin. These nanoparticles were able to reduce cell proliferation without affecting cell migration and adhesion, and decrease the oxidative stress induced by hydrogen peroxide exhibiting a cytoprotective effect [149]. Finally, Malathy S and Priya R Iyer used chitosan to prepare Naringin-loaded chitosan nanoparticles (NCN). The NCN had strong anti-inflammatory, anti-coagulant, antioxidant, and anti-cancerous effects. Furthermore, these nanoparticles promoted osteoblast differentiation, so they could be considered an efficient model for bone tissue regeneration [150]. All described delivery systems are summarized in Table 2.

Table 2. Summary of bioactive compounds-based devices system and their effects on bone regeneration.

Bioactive Compound	Device	Effect	Ref
- Gallic acid - Tea polyphenols	Synthetic ceramic materials	- pro-osteogenic - anti-inflammatory - antioxidant	[128,134]
- Resveratrol - Phlorotannins - Catechins	Scaffolds -hydrogel - PLGA - PCL and PLA	- antioxidant - pro-differentiating - pro-osteogenic - wound healing - osteopromotive	[135–137,142]
- EGCG - Catechin - Pro-anthocyanidins - Curcumin - Naringin	Nanoparticles - TP-CaP - Au-NPs - GSE-NP - Cur–PCL	- osteoblast differentiation - osteoblast proliferation - cytoprotective -remineralization - antioxidant - anti-inflammatory	[147–150]

6. Conclusions

In this review paper, recent developments in delivery systems for phytochemicals release for bone tissue regeneration were discussed. Despite the updates reviewed in this paper, more work is required to develop materials that can present controlled release kinetics and degradation, and that directly influence the rate of new bone formation. Soon, researchers, in accordance with clinicians, might be able to design and develop new

delivery systems with improved characteristics that mimic bone microenvironment at the site of implantation, promoting the inflammation, angiogenesis, and osteogenesis phases of new bone formation. The interaction between a nanotechnological approach and natural-derived compounds with osteogenic, anti-oxidant, antimicrobial, and anti-inflammatory activities will open up a new era of advanced treatment and solutions to prevent and/or treat bone-related complications.

Author Contributions: Conceptualization, A.C. and R.C.; writing—original draft preparation, A.V., F.D.C., and R.C.; writing—review and editing, A.V., F.D.C., R.C., and A.C.; visualization, A.A. and D.B.; supervision, M.B. and A.C.; funding acquisition, A.C. and M.B. All authors have read and agreed to the published version of the manuscript.

Funding: This work was financially supported by the Italian Ministry of University and Research, PON 03PE_00110_1/ptd1_000410 Titolo: Sviluppo di nanotecnologie Orientate alla Rigenerazione e Ricostruzione tissutale, Implantologia e Sensoristica in Odontoiatria/oculistica (SORRISO) (approval date 02/01/2019); POR Campania FESR 2014_2020 "Tecnologie abilitanti per la sintesi eco-sostenibile di nuovi materiali per la Restaurativa dentale"—ABILTECH (approval date 29 October 2018).This work was supported also by grant from Fondazione Cariplo, "High added-value bioactive polyphenols recovered from waste of olive oil production" (agreement 2018-1001), "Economia Circolare-Ricerca per un Futuro Sostenibile" program.

Institutional Review Board Statement: Not applicable.

Informed Consent Statement: Not applicable.

Acknowledgments: We would like to extend our sincere thanks to the project H2020- MSCA-RISE-Marie Sklodowska-Curie Actions (MSCA) Research and Innovation Staff Exchange (RISE) for funding this work, Project Acronym: VAHVISTUS-Project Number: 734759.

Conflicts of Interest: The authors have not declared any conflict of interest.

References

1. Li, Y.; Liu, C. Nanomaterial-based bone regeneration. *Nanoscale* **2017**, *9*, 4862–4874, doi:10.1039/c7nr00835j.
2. Bosetti, M.; Leigheb, M.; Brooks, R.A.; Boccafoschi, F.; Cannas, M.F. Regulation of osteoblast and osteoclast functions by FGF-6. *J. Cell. Physiol.* **2010**, *225*, 466–471, doi:10.1002/jcp.22225.
3. Yi, H.; Ur Rehman, F.; Zhao, C.; Liu, B.; He, N. Recent advances in nano scaffolds for bone repair. *Bone Res.* **2016**, *4*, 16050, doi:10.1038/boneres.2016.50.
4. Webber, M.J.; Khan, O.F.; Sydlik, S.A.; Tang, B.C.; Langer, R. A perspective on the clinical translation of scaffolds for tissue engineering. *Ann. Biomed. Eng.* **2015**, *43*, 641–656, doi:10.1007/s10439-014-1104-7. .
5. Bosetti, M.; Lloyd, A.W.; Santin, M.; Denyer, S.P.; Cannas, M. Effects of phosphatidylserine coatings on titanium on inflammatory cells and cell-induced mineralisation in vitro. *Biomaterials* **2005**, *26*, 7572–7578, doi:10.1016/j.biomaterials.2005.05.033. .
6. Bosetti, M.; Boccafoschi, F.; Calarco, A.; Leigheb, M.; Gatti, S.; Piffanelli, V.; Peluso, G.; Cannas, M. Behaviour of human mesenchymal stem cells on a polyelectrolyte-modified HEMA hydrogel for silk-based ligament tissue engineering. *J. Biomater. Sci. Polym. Ed.* **2008**, *19*, 1111–1123, doi:10.1163/156856208785540145. .
7. Byberg, L.; Bellavia, A.; Larsson, S.C.; Orsini, N.; Wolk, A.; Michaëlsson, K. Mediterranean Diet and Hip Fracture in Swedish Men and Women. *J. Bone Miner. Res. Off. J. Am. Soc. Bone Miner. Res.* **2016**, *31*, 2098–2105, doi:10.1002/jbmr.2896.
8. Lambert, M.N.T.; Thybo, C.B.; Lykkeboe, S.; Rasmussen, L.M.; Frette, X.; Christensen, L.P.; Jeppesen, P.B. Combined bioavailable isoflavones and probiotics improve bone status and estrogen metabolism in postmenopausal osteopenic women: A randomized controlled trial. *Am. J. Clin. Nutr.* **2017**, *106*, 909–920, doi:10.3945/ajcn.117.153353.
9. Nijveldt, R.J.; van Nood, E.; van Hoorn, D.E.; Boelens, P.G.; van Norren, K.; van Leeuwen, P.A. Flavonoids: A review of probable mechanisms of action and potential applications. *Am. J. Clin. Nutr.* **2001**, *74*, 418–425, doi:10.1093/ajcn/74.4.418.
10. Fraga, C.G.; Galleano, M.; Verstraeten, S.V.; Oteiza, P.I. Basic biochemical mechanisms behind the health benefits of polyphenols. *Mol. Asp. Med.* **2010**, *31*, 435–445, doi:10.1016/j.mam.2010.09.006.
11. Di Meo, F.; Valentino, A.; Petillo, O.; Peluso, G.; Filosa, S.; Crispi, S. Bioactive Polyphenols and Neuromodulation: Molecular Mechanisms in Neurodegeneration. *Int. J. Mol. Sci.* **2020**, *21*, 2564.
12. Pandey, K.B.; Rizvi, S.I. Plant polyphenols as dietary antioxidants in human health and disease. *Oxid. Med. Cell. Longev.* **2009**, *2*, 270–278, doi:10.4161/oxim.2.5.9498.
13. Scalbert, A.; Williamson, G. Dietary intake and bioavailability of polyphenols. *J. Nutr.* **2000**, *130* (Suppl. 8S), 2073s–2085s, doi:10.1093/jn/130.8.2073S.

14. D'Archivio, M.; Filesi, C.; Varì, R.; Scazzocchio, B.; Masella, R. Bioavailability of the polyphenols: Status and controversies. *Int. J. Mol. Sci.* **2010**, *11*, 1321–1342, doi:10.3390/ijms11041321.
15. Zhu, L.; Luo, D.; Liu, Y. Effect of the nano/microscale structure of biomaterial scaffolds on bone regeneration. *Int. J. Oral Sci.* **2020**, *12*, 6, doi:10.1038/s41368-020-0073-y.
16. Ansari, M. Bone tissue regeneration: Biology, strategies and interface studies. *Prog. Biomater.* **2019**, *8*, 223–237, doi:10.1007/s40204-019-00125-z.
17. Rosenberg, N.; Rosenberg, O.; Soudry, M. Osteoblasts in bone physiology-mini review. *Rambam Maimonides Med. J.* **2012**, *3*, e0013, doi:10.5041/rmmj.10080.
18. Ducy, P.; Zhang, R.; Geoffroy, V.; Ridall, A.L.; Karsenty, G. Osf2/Cbfa1: A Transcriptional Activator of Osteoblast Differentiation. *Cell* **1997**, *89*, 747–754, doi:10.1016/S0092-8674(00)80257-3.
19. Fakhry, M.; Hamade, E.; Badran, B.; Buchet, R.; Magne, D. Molecular mechanisms of mesenchymal stem cell differentiation towards osteoblasts. *World J. Stem Cells* **2013**, *5*, 136–148, doi:10.4252/wjsc.v5.i4.136.
20. Nakashima, K.; Zhou, X.; Kunkel, G.; Zhang, Z.; Deng, J.M.; Behringer, R.R.; de Crombrugghe, B. The novel zinc finger-containing transcription factor osterix is required for osteoblast differentiation and bone formation. *Cell* **2002**, *108*, 17–29, doi:10.1016/s0092-8674(01)00622-5.
21. James, R.; Deng, M.; Laurencin, C.T.; Kumbar, S.G. Nanocomposites and bone regeneration. *Front. Mater. Sci.* **2011**, *5*, 342–357, doi:10.1007/s11706-011-0151-3.
22. Sikavitsas, V.I.; Temenoff, J.S.; Mikos, A.G. Biomaterials and bone mechanotransduction. *Biomaterials* **2001**, *22*, 2581–2593, doi:10.1016/S0142-9612(01)00002-3.
23. Brannigan, K.; Griffin, M. An Update into the Application of Nanotechnology in Bone Healing. *Open Orthop. J.* **2016**, *10*, 808–823, doi:10.2174/1874325001610010808.
24. Miller, S.C.; de Saint-Georges, L.; Bowman, B.M.; Jee, W.S. Bone lining cells: Structure and function. *Scanning Microsc.* **1989**, *3*, 953–960; discussion 60-1.
25. Aarden, E.M.; Nijweide, P.J.; Burger, E.H. Function of osteocytes in bone. *J. Cell. Biochem.* **1994**, *55*, 287–299, doi:10.1002/jcb.240550304.
26. Andersen, T.L.; Sondergaard, T.E.; Skorzynska, K.E.; Dagnaes-Hansen, F.; Plesner, T.L.; Hauge, E.M.; Plesner, T.; Delaisse, J.M. A physical mechanism for coupling bone resorption and formation in adult human bone. *Am. J. Pathol.* **2009**, *174*, 239–247, doi:10.2353/ajpath.2009.080627.
27. Everts, V.; Delaissé, J.M, Korper, W.; Jansen, D.C.; Tigchelaar-Gutter, W.; Saftig, P.; Beertsen, W. The Bone Lining Cell: Its Role in Cleaning Howship's Lacunae and Initiating Bone Formation. *J. Bone Miner. Res.* **2002**, *17*, 77–90, doi:10.1359/jbmr.2002.17.1.77.
28. Boyce, B.F.; Hughes, D.E.; Wright, K.R.; Xing, L.; Dai, A. Recent advances in bone biology provide insight into the pathogenesis of bone diseases. *Lab. Investig. J. Tech. Methods Pathol.* **1999**, *79*, 83–94.
29. Crockett, J.C.; Mellis, D.J.; Scott, D.I.; Helfrich, M.H. New knowledge on critical osteoclast formation and activation pathways from study of rare genetic diseases of osteoclasts: Focus on the RANK/RANKL axis. *Osteoporos. Int. J. Establ. Result Coop. Eur. Found. Osteoporos. Natl. Osteoporos. Found. USA* **2011**, *22*, 1–20, doi:10.1007/s00198-010-1272-8.
30. Boyce, B.F.; Xing, L. Functions of RANKL/RANK/OPG in bone modeling and remodeling. *Arch. Biochem. Biophys.* **2008**, *473*, 139–146, doi:10.1016/j.abb.2008.03.018.
31. Yavropoulou, M.P.; Yovos, J.G. Osteoclastogenesis—Current knowledge and future perspectives. *J. Musculoskelet. Neuronal Interact.* **2008**, *8*, 204–216.
32. Phan, T.C.; Xu, J.; Zheng, M.H. Interaction between osteoblast and osteoclast: Impact in bone disease. *Histol. Histopathol.* **2004**, *19*, 1325–1344, doi:10.14670/hh-19.1325.
33. Kular, J.; Tickner, J.; Chim, S.M.; Xu, J. An overview of the regulation of bone remodeling at the cellular level. *Clin. Biochem.* **2012**, *45*, 863–873, doi:10.1016/j.clinbiochem.2012.03.021.
34. Schindeler, A.; McDonald, M.M.; Bokko, P.; Little, D.G. Bone remodeling during fracture repair: The cellular picture. *Semin. Cell Dev. Biol.* **2008**, *19*, 459–466, doi:10.1016/j.semcdb.2008.07.004.
35. Sheen, J.R.; Garla, V.V. *Fracture Healing Overview*; StatPearls Publishing: Treasure Island, FL, USA, 2019.
36. Ghiasi, M.S.; Chen, J.; Vaziri, A.; Rodriguez, E.K.; Nazarian, A. Bone fracture healing in mechanobiological modeling: A review of principles and methods. *Bone Rep.* **2017**, *6*, 87–100, doi:10.1016/j.bonr.2017.03.002.
37. Marsell, R.; Einhorn, T.A. The biology of fracture healing. *Injury* **2011**, *42*, 551–555, doi:10.1016/j.injury.2011.03.031.
38. Kostenuik, P.; Mirza, F.M. Fracture healing physiology and the quest for therapies for delayed healing and nonunion. *J. Orthop. Res. Off. Publ. Orthop. Res. Soc.* **2017**, *35*, 213–223, doi:10.1002/jor.23460.
39. Krishnan, V.; Bryant, H.U.; Macdougald, O.A. Regulation of bone mass by Wnt signaling. *J. Clin. Investig.* **2006**, *116*, 1202–1209, doi:10.1172/jci28551.
40. Zhu, F.; Sweetwyne, M.T.; Hankenson, K.D. PKCδ is required for Jagged-1 induction of human mesenchymal stem cell osteogenic differentiation. *Stem Cells* **2013**, *31*, 1181–1192, doi:10.1002/stem.1353.
41. Dishowitz, M.I.; Zhu, F.; Sundararaghavan, H.G.; Ifkovits, J.L.; Burdick, J.A.; Hankenson, K.D. Jagged1 immobilization to an osteoconductive polymer activates the Notch signaling pathway and induces osteogenesis. *J. Biomed. Mater. Res. Part A* **2014**, *102*, 1558–1567, doi:10.1002/jbm.a.34825.

42. Chakravorty, N.; Hamlet, S.; Jaiprakash, A.; Crawford, R.; Oloyede, A.; Alfarsi, M.; Xiao, Y.; Ivanovski, S. Pro-osteogenic topographical cues promote early activation of osteoprogenitor differentiation via enhanced TGFβ, Wnt, and Notch signaling. *Clin. Oral Implants Res.* **2014**, *25*, 475–486, doi:10.1111/clr.12178.
43. Herford, A.S.; Stoffella, E.; Tandon, R. Reconstruction of mandibular defects using bone morphogenic protein: Can growth factors replace the need for autologous bone grafts? A systematic review of the literature. *Plast. Surg. Int.* **2011**, *2011*, 165824, doi:10.1155/2011/165824.
44. Zheng, A.Q.; Xiao, J.; Xie, J.; Lu, P.P.; Ding, X. bFGF enhances activation of osteoblast differentiation and osteogenesis on titanium surfaces via PI3K/Akt signaling pathway. *Int. J. Clin. Exp. Pathol.* **2016**, *9*, 4680–4692.
45. Devi, R.; Dixit, J. Clinical Evaluation of Insulin like Growth Factor-I and Vascular Endothelial Growth Factor with Alloplastic Bone Graft Material in the Management of Human Two Wall Intra-Osseous Defects. *J. Clin. Diagn. Res. JCDR* **2016**, *10*, ZC41–ZC46, doi:10.7860/jcdr/2016/21333.8476.
46. Ornitz, D.M.; Marie, P.J. FGF signaling pathways in endochondral and intramembranous bone development and human genetic disease. *Genes Dev.* **2002**, *16*, 1446–1465, doi:10.1101/gad.990702.
47. Furuya, H.; Tabata, Y.; Kaneko, K. Bone regeneration for murine femur fracture by gelatin hydrogels incorporating basic fibroblast growth factor with different release profiles. *Tissue Eng. Part A* **2014**, *20*, 1531–1541, doi:10.1089/ten.tea.2012.0763.
48. Liu, T.M.; Lee, E.H. Transcriptional regulatory cascades in Runx2-dependent bone development. *Tissue Eng. Part B Rev.* **2013**, *19*, 254–263, doi:10.1089/ten.TEB.2012.0527.
49. Zhang, X.; Yang, M.; Lin, L.; Chen, P.; Ma, K.T.; Zhou, C.Y.; Ao, Y.F. Runx2 overexpression enhances osteoblastic differentiation and mineralization in adipose--derived stem cells in vitro and in vivo. *Calcif. Tissue Int.* **2006**, *79*, 169–178, doi:10.1007/s00223-006-0083-6.
50. Conte, R.; Luca, I.D.; Luise, A.D.; Petillo, O.; Calarco, A.; Peluso, G. New Therapeutic Potentials of Nanosized Phytomedicine. *J. Nanosci. Nanotechnol.* **2016**, *16*, 8176–8187, doi:10.1166/jnn.2016.12809.
51. Bonadies, I.; Di Cristo, F.; Valentino, A.; Peluso, G.; Calarco, A.; Di Salle, A. pH-Responsive Resveratrol-Loaded Electrospun Membranes for the Prevention of Implant-Associated Infections. *Nanomaterials* **2020**, *10*, 1175, doi:10.3390/nano10061175.
52. Amrati, F.E.; Bourhia, M.; Slighoua, M.; Ibnemoussa, S.; Bari, A.; Ullah, R.; Amaghnouje, A.; Di Cristo, F.; El Mzibri, M.; Calarco, A.; et al. Phytochemical Study on Antioxidant and Antiproliferative Activities of Moroccan Caralluma europaea Extract and Its Bioactive Compound Classes. *Evid. Based Complement. Altern. Med.* **2020**, *2020*, 8409718, doi:10.1155/2020/8409718. .
53. Conte, R.; Marturano, V.; Peluso, G.; Calarco, A.; Cerruti, P. Recent Advances in Nanoparticle-Mediated Delivery of Anti-Inflammatory Phytocompounds. *Int. J. Mol. Sci.* **2017**, *18*, 709, doi:10.3390/ijms18040709.
54. Moccia, F.; Agustin-Salazar, S.; Berg, A.L.; Setaro, B.; Micillo, R.; Pizzo, E.; Weber, F.; Gamez-Meza, N.; Schieber, A.; Cerruti, P. Pecan (Carya illinoinensis (Wagenh.) K. Koch) Nut Shell as an Accessible Polyphenol Source for Active Packaging and Food Colorant Stabilization. *ACS Sustain. Chem. Eng.* **2020**, *8*, 6700–6712, doi:10.1021.
55. Marturano, V.; Bizzarro, V.; De Luise, A.; Calarco, A.; Ambrogi, V.; Giamberini, M.; Tylkowski, B.; Cerruti, P. Essential oils as solvents and core materials for the preparation of photo-responsive polymer nanocapsules. *Nano Res.* **2018**, *11*, 2783–2795, doi:10.1007/s12274-017-1908-5.
56. Agustin-Salazar, S.; Gamez-Meza, N.; Medina-Juárez, L.A.; Malinconico, M.; Cerruti, P. Stabilization of Polylactic Acid and Polyethylene with Nutshell Extract: Efficiency Assessment and Economic Evaluation. *ACS Sustain. Chem. Eng.* **2017**, *5*, doi:10.1021/acssuschemeng.6b03124.
57. Agustin-Salazar, S.; Gamez-Meza, N.; Medina-Juàrez, L.À.; Soto-Valdez, H.; Cerruti, P. From Nutraceutics to Materials: Effect of Resveratrol on the Stability of Polylactide. *ACS Sustain. Chem. Eng.* **2014**, *2*, 1534–1542, doi:10.1021/sc5002337.
58. Srivastava, S.K.; Ogino, C.; Kondo, A. Green synthesis of thiolated graphene nanosheets by alliin (garlic) and its effect on the deposition of gold nanoparticles. *RSC Adv.* **2013**, *4*, 5986, doi:10.1039/C3RA45353G.
59. Elif, Ö.; Belma, Ö.; İlkay, Ş. Production of biologically safe and mechanically improved reduced graphene oxide/hydroxyapatite composites. *Mater. Res. Express* **2017**, *4*, 015601, doi:10.1088/2053-1591/aa5464.
60. Alegria, E.C.B.A.; Ribeiro, A.P.C.; Mendes, M.; Ferraria, A.M.; do Rego, A.M.B.; Pombeiro, A.J.L. Effect of Phenolic Compounds on the Synthesis of Gold Nanoparticles and its Catalytic Activity in the Reduction of Nitro Compounds. *Nanomaterials* **2018**, *8*, 320, doi:10.3390/nano8050320.
61. Swilam, N.; Nematallah, K.A. Polyphenols profile of pomegranate leaves and their role in green synthesis of silver nanoparticles. *Sci. Rep.* **2020**, *10*, 14851, doi:10.1038/s41598-020-71847-5.
62. Conte, R.; Calarco, A.; Napoletano, A.; Valentino, A.; Margarucci, S.; Di Cristo, F.; Di Salle, A.; Peluso, G. Polyphenols Nanoencapsulation for Therapeutic Applications. *Biomol. Res. Ther.* **2016**, *5:2* doi: 10.4172/2167-7956.10001392016.
63. Torre, E. Molecular signaling mechanisms behind polyphenol-induced bone anabolism. *Phytochem. Rev.* **2017**, *16*, 1183–1226, doi:10.1007/s11101-017-9529-x.
64. Zhou, T.; Chen, D.; Li, Q.; Sun, X.; Song, Y.; Wang, C. Curcumin inhibits inflammatory response and bone loss during experimental periodontitis in rats. *Acta Odontol. Scand.* **2013**, *71*, 349–356, doi:10.3109/00016357.2012.682092.
65. Bandyopadhyay, S.; Lion, J.M.; Mentaverri, R.; Ricupero, D.A.; Kamel, S.; Romero, J.R.; Chattopadhyay, N. Attenuation of osteoclastogenesis and osteoclast function by apigenin. *Biochem. Pharmacol.* **2006**, *72*, 184–197, doi:10.1016/j.bcp.2006.04.018.
66. La, V.D.; Howell, A.B.; Grenier, D. Cranberry proanthocyanidins inhibit MMP production and activity. *J. Dent. Res.* **2009**, *88*, 627–632, doi:10.1177/0022034509339487.

67. Pang, J.L.; Ricupero, D.A.; Huang, S.; Fatma, N.; Singh, D.P.; Romero, J.R.; Chattopadhyay, N. Differential activity of kaempferol and quercetin in attenuating tumor necrosis factor receptor family signaling in bone cells. *Biochem. Pharmacol.* **2006**, *71*, 818–826, doi:10.1016/j.bcp.2005.12.023.
68. La, V.D.; Tanabe, S.; Grenier, D. Naringenin inhibits human osteoclastogenesis and osteoclastic bone resorption. *J. Periodontal Res.* **2009**, *44*, 193–198, doi:10.1111/j.1600-0765.2008.01107.x.
69. Comalada, M.; Ballester, I.; Bailón, E.; Sierra, S.; Xaus, J.; Gálvez, J.; Sánchez de Medina, F.; Zarzuelo, A. Inhibition of pro-inflammatory markers in primary bone marrow-derived mouse macrophages by naturally occurring flavonoids: Analysis of the structure–activity relationship. *Biochem. Pharmacol.* **2006**, *72*, 1010–1021, doi:10.1016/j.bcp.2006.07.016.
70. Bharti, A.C.; Takada, Y.; Aggarwal, B.B. Curcumin (diferuloylmethane) inhibits receptor activator of NF-kappa B ligand-induced NF-kappa B activation in osteoclast precursors and suppresses osteoclastogenesis. *J. Immunol.* **2004**, *172*, 5940–5947, doi:10.4049/jimmunol.172.10.5940.
71. Chowdhury, T.T.; Salter, D.M.; Bader, D.L.; Lee, D.A. Signal transduction pathways involving p38 MAPK, JNK, NFkappaB and AP-1 influences the response of chondrocytes cultured in agarose constructs to IL-1beta and dynamic compression. *Inflamm. Res. Off. J. Eur. Histamine Res. Soc.* **2008**, *57*, 306–313, doi:10.1007/s00011-007-7126-y.
72. Kumar, D.; Kumar, M.; Saravanan, C.; Singh, S.K. Curcumin: A potential candidate for matrix metalloproteinase inhibitors. *Expert Opin. Ther. Targets* **2012**, *16*, 959–972, doi:10.1517/14728222.2012.710603.
73. Bu, S.Y.; Hunt, T.S.; Smith, B.J. Dried plum polyphenols attenuate the detrimental effects of TNF-alpha on osteoblast function coincident with up-regulation of Runx2, Osterix and IGF-I. *J. Nutr. Biochem.* **2009**, *20*, 35–44, doi:10.1016/j.jnutbio.2007.11.012.
74. Bhatia, I.S.; Bajaj, K.L. Tannins in black-plum (*Syzygium cumini* L.) seeds. *Biochem. J.* **1972**, *128*, 56, doi:10.1042/bj1280056pa.
75. Tokuda, H.; Takai, S.; Matsushima-Nishiwaki, R.; Akamatsu, S.; Hanai, Y.; Hosoi, T.; Harada, A.; Ohta, T.; Kozawa, O. (−)-epigallocatechin gallate enhances prostaglandin F2α-induced VEGF synthesis via upregulating SAPK/JNK activation in osteoblasts. *J. Cell. Biochem.* **2007**, *100*, 1146–1153, doi:10.1002/jcb.21104.
76. Shen, C.L.; Yeh, J.K.; Cao, J.J.; Tatum, O.L.; Dagda, R.Y.; Wang, J.S. Green tea polyphenols mitigate bone loss of female rats in a chronic inflammation-induced bone loss model. *J. Nutr. Biochem.* **2010**, *21*, 968–974, doi:10.1016/j.jnutbio.2009.08.002.
77. Shen, C.L.; Cao, J.J.; Dagda, R.Y.; Chanjaplammootil, S.; Lu, C.; Chyu, M.C.; Gao, W.; Wang, J.S.; Yeh, J.K. Green tea polyphenols benefits body composition and improves bone quality in long-term high-fat diet-induced obese rats. *Nutr. Res.* **2012**, *32*, 448–457, doi:10.1016/j.nutres.2012.05.001.
78. Li, Y.; Yao, J.; Han, C.; Yang, J.; Chaudhry, M.T.; Wang, S.; Liu, H.; Yin, Y. Quercetin, Inflammation and Immunity. *Nutrients* **2016**, *8*, 167, doi:10.3390/nu8030167.
79. Hämäläinen, M.; Nieminen, R.; Asmawi, M.Z.; Vuorela, P.; Vapaatalo, H.; Moilanen, E. Effects of flavonoids on prostaglandin E2 production and on COX-2 and mPGES-1 expressions in activated macrophages. *Planta Med.* **2011**, *77*, 1504–1511, doi:10.1055/s-0030-1270762.
80. Procházková, D.; Boušová, I.; Wilhelmová, N. Antioxidant and prooxidant properties of flavonoids. *Fitoterapia* **2011**, *82*, 513–523, doi:10.1016/j.fitote.2011.01.018.
81. Sekher Pannala, A.; Chan, T.S.; O'Brien, P.J.; Rice-Evans, C.A. Flavonoid B-Ring Chemistry and Antioxidant Activity: Fast Reaction Kinetics. *Biochem. Biophys. Res. Commun.* **2001**, *282*, 1161–1168, doi:10.1006/bbrc.2001.4705.
82. Huang, J.; Yuan, L.; Wang, X.; Zhang, T.-L.; Wang, K. Icaritin and its glycosides enhance osteoblastic, but suppress osteoclastic, differentiation and activity in vitro. *Life Sci.* **2007**, *81*, 832–840, doi:10.1016/j.lfs.2007.07.015.
83. Cavia-Saiz, M.; Busto, M.D.; Pilar-Izquierdo, M.C.; Ortega, N.; Perez-Mateos, M.; Muñiz, P. Antioxidant properties, radical scavenging activity and biomolecule protection capacity of flavonoid naringenin and its glycoside naringin: A comparative study. *J. Sci. Food Agric.* **2010**, *90*, 1238–1244, doi:10.1002/jsfa.3959.
84. Kim, W.K.; Ke, K.; Sul, O.J.; Kim, H.J.; Kim, S.H.; Lee, M.H.; Kim, H.J.; Kim, S.Y.; Chung, H.T.; Choi, H.S. Curcumin protects against ovariectomy-induced bone loss and decreases osteoclastogenesis. *J. Cell. Biochem.* **2011**, *112*, 3159–3166, doi:10.1002/jcb.23242.
85. Zhao, L.; Wang, Y.; Wang, Z.; Xu, Z.; Zhang, Q.; Yin, M. Effects of dietary resveratrol on excess-iron-induced bone loss via antioxidative character. *J. Nutr. Biochem.* **2015**, *26*, 1174–1182, doi:10.1016/j.jnutbio.2015.05.009.
86. Huang, Q.; Gao, B.; Wang, L.; Hu, Y.Q.; Lu, W.G.; Yang, L.; Luo, Z.J.; Liu, J. Protective effects of myricitrin against osteoporosis via reducing reactive oxygen species and bone-resorbing cytokines. *Toxicol. Appl. Pharmacol.* **2014**, *280*, 550–560, doi:10.1016/j.taap.2014.08.004.
87. Cherrak, S.A.; Mokhtari-Soulimane, N.; Berroukeche, F.; Bensenane, B.; Cherbonnel, A.; Merzouk, H.; Elhabiri, M. In Vitro Antioxidant versus Metal Ion Chelating Properties of Flavonoids: A Structure-Activity Investigation. *PLoS ONE* **2016**, *11*, e0165575, doi:10.1371/journal.pone.0165575.
88. Hider, R.C.; Liu, Z.D.; Khodr, H.H. *Metal Chelation of Polyphenols. Methods in Enzymology*; Academic Press: Cambridge, MA, USA, 2001; pp. 190–203.
89. Islam, S.; Islam, N.; Kermode, T.; Johnstone, B.; Mukhtar, H.; Moskowitz, R.W.; Goldberg, V.M.; Malemud, C.J.; Haqqi, T.M. Involvement of Caspase-3 in Epigallocatechin-3-gallate-Mediated Apoptosis of Human Chondrosarcoma Cells. *Biochem. Biophys. Res. Commun.* **2000**, *270*, 793–797, doi:10.1006/bbrc.2000.2536.
90. Nakagawa, H.; Wachi, M.; Woo, J.-T.; Kato, M.; Kasai, S.; Takahashi, F.; Lee, I.S.; Nagai, K. Fenton Reaction Is Primarily Involved in a Mechanism of (−)-Epigallocatechin-3-gallate to Induce Osteoclastic Cell Death. *Biochem. Biophys. Res. Commun.* **2002**, *292*, 94–101, doi:10.1006/bbrc.2002.6622.

91. Lin, S.-Y.; Kang, L.; Wang, C.-Z.; Huang, H.H.; Cheng, T.-L.; Huang, H.-T.; Lee, M.J.; Lin, Y.S.; Ho, M.L.; Wang, G.J.; Chen, G.H. (-)-Epigallocatechin-3-Gallate (EGCG) Enhances Osteogenic Differentiation of Human Bone Marrow Mesenchymal Stem Cells. *Molecules* **2018**, *23*, 3221, doi:10.3390/molecules23123221.
92. Hsu, Y.-L.; Chang, J.-K.; Tsai, C.-H.; Chien, T.-T.C.; Kuo, P.-L. Myricetin induces human osteoblast differentiation through bone morphogenetic protein-2/p38 mitogen-activated protein kinase pathway. *Biochem. Pharmacol.* **2007**, *73*, 504–514, doi:10.1016/j.bcp.2006.10.020.
93. Chen, J.R.; Lazarenko, O.P.; Wu, X.; Kang, J.; Blackburn, M.L.; Shankar, K.; Badger, T.M.; Ronis, M.J.J. Dietary-induced serum phenolic acids promote bone growth via p38 MAPK/β-catenin canonical Wnt signaling. *J. Bone Miner. Res. Off. J. Am. Soc. Bone Miner. Res.* **2010**, *25*, 2399–2411, doi:10.1002/jbmr.137.
94. Guo, A.J.; Choi, R.C.; Cheung, A.W.; Chen, V.P.; Xu, S.L.; Dong, T.T.; Chen, J.J.; Tsim, K.W.K. Baicalin, a flavone, induces the differentiation of cultured osteoblasts: An action via the Wnt/beta-catenin signaling pathway. *J. Biol. Chem.* **2011**, *286*, 27882–27893, doi:10.1074/jbc.M111.236281.
95. Patisaul, H.B.; Jefferson, W. The pros and cons of phytoestrogens. *Front. Neuroendocrinol.* **2010**, *31*, 400–419, doi:10.1016/j.yfrne.2010.03.003.
96. Xiao, H.H.; Gao, Q.G.; Zhang, Y.; Wong, K.C.; Dai, Y.; Yao, X.S.; Wong, M.S. Vanillic acid exerts oestrogen-like activities in osteoblast-like UMR 106 cells through MAP kinase (MEK/ERK)-mediated ER signaling pathway. *J. Steroid Biochem. Mol. Biol.* **2014**, *144 Pt, B.;* 382–391, doi:10.1016/j.jsbmb.2014.08.002.
97. Abdel-Naim, A.B.; Alghamdi, A.A.; Algandaby, M.M.; Al-Abbasi, F.A.; Al-Abd, A.M.; Eid, B.G.; Abdallah, H.M.; El-Halawany, A.M. Rutin Isolated from *Chrozophora tinctoria* Enhances Bone Cell Proliferation and Ossification Markers. *Oxid. Med. Cell. Longev.* **2018**, *2018*, 5106469, doi:10.1155/2018/5106469.
98. Rassi, C.M.; Lieberherr, M.; Chaumaz, G.; Pointillart, A.; Cournot, G. Modulation of osteoclastogenesis in porcine bone marrow cultures by quercetin and rutin. *Cell Tissue Res.* **2005**, *319*, 383–393, doi:10.1007/s00441-004-1053-9.
99. Lee, D.J.; Tseng, H.C.; Wong, S.W.; Wang, Z.; Deng, M.; Ko, C.-C. Dopaminergic effects on in vitro osteogenesis. *Bone Res.* **2015**, *3*, 15020, doi:10.1038/boneres.2015.20.
100. Schneider-Stock, R.; Ghantous, A.; Bajbouj, K.; Saikali, M.; Darwiche, N. Epigenetic mechanisms of plant-derived anticancer drugs. *Front. Biosci.* **2012**, *17*, 129–173, doi:10.2741/3919.
101. Howitz, K.T.; Bitterman, K.J.; Cohen, H.Y.; Lamming, D.W.; Lavu, S.; Wood, J.G.; Zipkin, R.E.; Chung, P.; Kisielewski, A.; Zhang, L.L.; et al. Small molecule activators of sirtuins extend Saccharomyces cerevisiae lifespan. *Nature* **2003**, *425*, 191–196, doi:10.1038/nature01960.
102. Shakibaei, M.; Shayan, P.; Busch, F.; Aldinger, C.; Buhrmann, C.; Lueders, C.; Mobasheri, A. Resveratrol mediated modulation of Sirt-1/Runx2 promotes osteogenic differentiation of mesenchymal stem cells: Potential role of Runx2 deacetylation. *PLoS ONE* **2012**, *7*, e35712, doi:10.1371/journal.pone.0035712.
103. Tseng, P.C.; Hou, S.M.; Chen, R.J.; Peng, H.W.; Hsieh, C.F.; Kuo, M.L.; Yen, M.L. Resveratrol promotes osteogenesis of human mesenchymal stem cells by upregulating RUNX2 gene expression via the SIRT1/FOXO3A axis. *J. Bone Miner. Res. Off. J. Am. Soc. Bone Miner. Res.* **2011**, *26*, 2552–2563, doi:10.1002/jbmr.460.
104. Lee, Y.M.; Shin, S.I.; Shin, K.S.; Lee, Y.R.; Park, B.H.; Kim, E.C. The role of sirtuin 1 in osteoblastic differentiation in human periodontal ligament cells. *J. Periodontal Res.* **2011**, *46*, 712–721, doi:10.1111/j.1600-0765.2011.01394.x.
105. Shakibaei, M.; Buhrmann, C.; Mobasheri, A. Resveratrol-mediated SIRT-1 interactions with p300 modulate receptor activator of NF-kappaB ligand (RANKL) activation of NF-kappaB signaling and inhibit osteoclastogenesis in bone-derived cells. *J. Biol. Chem.* **2011**, *286*, 11492–11505, doi:10.1074/jbc.M110.198713.
106. Li, Y.; Wang, J.; Chen, G.; Feng, S.; Wang, P.; Zhu, X.; Zhang, R. Quercetin promotes the osteogenic differentiation of rat mesenchymal stem cells via mitogen-activated protein kinase signaling. *Exp. Ther. Med.* **2015**, *9*, 2072–2080, doi:10.3892/etm.2015.2388.
107. Moon, H.J.; Ko, W.K.; Han, S.W.; Kim, D.S.; Hwang, Y.S.; Park, H.K.; Kwon, I.K. Antioxidants, like coenzyme Q10, selenite, and curcumin, inhibited osteoclast differentiation by suppressing reactive oxygen species generation. *Biochem. Biophys. Res. Commun.* **2012**, *418*, 247–253, doi:10.1016/j.bbrc.2012.01.005.
108. Oryan, A.; Alidadi, S.; Moshiri, A.; Maffulli, N. Bone regenerative medicine: Classic options, novel strategies, and future directions. *J. Orthop. Surg. Res.* **2014**, *9*, 18, doi:10.1186/1749-799X-9-18.
109. Liu, Y.; Lim, J.; Teoh, S.-H. Development of clinically relevant scaffolds for vascularised bone tissue engineering. *Biotechnol. Adv.* **2013**, *31*, 688–705. 10.1016/j.biotechadv.2012.10.003.
110. Zhu, G.; Zhang, T.; Chen, M.; Yao, K.; Huang, X.; Zhang, B.; Li, Y.; Liu, J.; Wang, Y.; Zhao, Z. Bone physiological microenvironment and healing mechanism: Basis for future bone-tissue engineering scaffolds. *Bioact. Mater.* **2021**, *6*, 4110–4140, doi:10.1016/j.bioactmat.2021.03.043.
111. Ogay, V.; Mun, E.A.; Kudaibergen, G.; Baidarbekov, M.; Kassymbek, K.; Zharkinbekov, Z.; Saparov, A. Progress and Prospects of Polymer-Based Drug Delivery Systems for Bone Tissue Regeneration. *Polymers* **2020**, *12*, 2881, doi:10.3390/polym12122881.
112. Cojocaru, F.-D.; Botezat, D.; Gardikiotis, I.; Uritu, C.-M.; Dodi, G.; Trandafir, L.; Rezus, C.; Rezus, E.; Tamba, B.-I.; Mihai, C.-T. Nanomaterials Designed for Antiviral Drug Delivery Transport across Biological Barriers. *Pharmaceutics* **2020**, *12*, 171, doi:10.3390/pharmaceutics12020171.
113. Newman, M.R.; Benoit, D.S. Local and targeted drug delivery for bone regeneration. *Curr. Opin. Biotechnol.* **2016**, *40*, 125–132, doi:10.1016/j.copbio.2016.02.029. Epub 2016 Apr 8.

114. Bosetti, M.; Bianchi, A.E.; Zaffe, D.; Cannas, M. Comparative in vitro study of four commercial biomaterials used for bone grafting. *J. Appl. Biomater. Funct. Mater.* **2013**, *11*, e80–e88, doi:10.5301/jabfm.5000149.
115. Ceresa, C.; Fracchia, L.; Marchetti, A.; Rinaldi, M.; Bosetti, M. Injectable Scaffolds Enriched with Silver to Inhibit Bacterial Invasion in Tissue Regeneration. *Materials* **2019**, *12*, 1931, doi:10.3390/ma12121931.
116. Susmita, B.; Naboneeta Sa Dishary, B. Natural medicine delivery from biomedical devices to treat bone disorders: A review. *Acta Biomater.* **2021**, *126*, 63–91, doi:10.1016/j.actbio.2021.02.034.
117. Tadic, D.; Epple, M. A thorough physicochemical characterisation of 14 calcium phosphate-based bone substitution materials in comparison to natural bone. *Biomaterials* **2004**, *25*, 987–994, doi:10.1016/s0142-9612(03)00621-5.
118. Yuan, H.; Yang, Z.; Li, Y.; Zhang, X.; De Bruijn, J.D.; De Groot, K. Osteoinduction by calcium phosphate biomaterials. *J. Mater. Sci. Mater. Med.* **1998**, *9*, 723–726, doi:10.1023/a:1008950902047.
119. Ramseier, C.A.; Rasperini, G.; Batia, S.; Giannobile, W.V. Advanced reconstructive technologies for periodontal tissue repair. *Periodontology 2000* **2012**, *59*, 185–202, doi:10.1111/j.1600-0757.2011.00432.x.
120. Reynolds, M.A.; Aichelmann-Reidy, M.E.; Branch-Mays, G.L. Regeneration of periodontal tissue: Bone replacement grafts. *Dent. Clin. N. Am.* **2010**, *54*, 55–71, doi:10.1016/j.cden.2009.09.003.
121. Kao, R.T.; Nares, S.; Reynolds, M.A. Periodontal regeneration—Intrabony defects: A systematic review from the AAP Regeneration Workshop. *J. Periodontol.* **2015**, *86* (Suppl. 2), S77–S104, doi:10.1902/jop.2015.130685.
122. Houde, V.; Grenier, D.; Chandad, F. Protective effects of grape seed proanthocyanidins against oxidative stress induced by lipopolysaccharides of periodontopathogens. *J. Periodontol.* **2006**, *77*, 1371–1379, doi:10.1902/jop.2006.050419.
123. Hirasawa, M.; Takada, K.; Makimura, M.; Otake, S. Improvement of periodontal status by green tea catechin using a local delivery system: A clinical pilot study. *J. Periodontal Res.* **2002**, *37*, 433–438, doi:10.1034/j.1600-0765.2002.01640.x.
124. Kushiyama, M.; Shimazaki, Y.; Murakami, M.; Yamashita, Y. Relationship between intake of green tea and periodontal disease. *J. Periodontol.* **2009**, *80*, 372–377, doi:10.1902/jop.2009.080510.
125. Diaz-Rodriguez, P.; Sánchez, M.; Landin, M. Drug-Loaded Biomimetic Ceramics for Tissue Engineering. *Pharmaceutics* **2018**, *10*, 272, doi:10.3390/pharmaceutics10040272.
126. Morra, M.C.C.; Bollati, D.; Iviglia, G. Inventor Compositions for Filling Bone and Periodontal Defects; WO 2015/014872 A. 2016.
127. Cazzola, M.; Corazzari, I.; Prenesti, E.; Bertone, E.; Vernè, E.; Ferraris, S. Bioactive glass coupling with natural polyphenols: Surface modification, bioactivity and anti-oxidant ability. *Appl. Surf. Sci.* **2016**, *367*, 237–248, doi:10.1016/j.apsusc.2016.01.138.
128. Zhou, K.; Ren, X.; Zhao, M.; Mei, X.; Zhang, P.; Chen, Z.; Zhu, X. Promoting proliferation and differentiation of BMSCs by green tea polyphenols functionalized porous calcium phosphate. *Regener. Biomater.* **2018**, *5*, 35–41, doi:10.1093/rb/rbx031.
129. Preethi Soundarya, S.; Sanjay, V.; Haritha Menon, A.; Dhivya, S.; Selvamurugan, N. Effects of flavonoids incorporated biological macromolecules based scaffolds in bone tissue engineering. *Int. J. Biol. Macromol.* **2018**, *110*, 74–87, doi:10.1016/j.ijbiomac.2017.09.014. Epub 2017 Sep 8.
130. Joseph, J.; Sundar, R.; John, A.; Abraham, A. Phytochemical Incorporated Drug Delivery Scaffolds for Tissue Regeneration. *Regen. Eng. Transl. Med.* **2018**, *4*, 167–176, doi:10.1007/s40883-018-0059-x.
131. Rekulapally, R.; Udayachandrika, K.; Hamlipur, S.; Nair, A.S.; Pal, B.; Singh, S. Tissue engineering of collagen scaffolds crosslinked with plant based polysaccharides. *Prog. Biomater.* **2021**, *10*, 29–41, doi:10.1007/s40204-021-00149-4.
132. Rambhia, K.J.; Ma, P.X. Controlled drug release for tissue engineering. *J. Control. Release* **2015**, *219*, 119–128, doi:10.1016/j.jconrel.2015.08.049. Epub 2015 Aug 29.
133. Santin, M.; Morris, C.; Standen, G.; Nicolais, L.; Ambrosio, L. A new class of bioactive and biodegradable soybean-based bone fillers. *Biomacromolecules* **2007**, *8*, 2706–2711, doi:10.1021/bm0703362.
134. Merolli, A.; Nicolais, L.; Ambrosio, L.; Santin, M. A degradable soybean-based biomaterial used effectively as a bone filler in vivo in a rabbit. *Biomed. Mater.* **2010**, *5*, 015008, doi:10.1088/1748-6041/5/1/015008.
135. Wang, W.; Sun, L.; Zhang, P.; Song, J.; Liu, W. An anti-inflammatory cell-free collagen/resveratrol scaffold for repairing osteochondral defects in rabbits. *Acta Biomater.* **2014**, *10*, 4983–4995, doi:10.1016/j.actbio.2014.08.022.
136. Li, Y.; Dånmark, S.; Edlund, U.; Finne-Wistrand, A.; He, X.; Norgård, M.; Blomén, E.; Hultenby, K.; Andersson, G.; Lindgren, U. Resveratrol-conjugated poly-ε-caprolactone facilitates in vitro mineralization and in vivo bone regeneration. *Acta Biomater.* **2011**, *7*, 751–758, doi:10.1016/j.actbio.2010.09.008.
137. Kamath, M.S.; Ahmed, S.S.; Dhanasekaran, M.; Santosh, S.W. Polycaprolactone scaffold engineered for sustained release of resveratrol: Therapeutic enhancement in bone tissue engineering. *Int. J. Nanomed.* **2014**, *9*, 183–195, doi:10.2147/ijn.s49460.
138. Riccitiello, F.; De Luise, A.; Conte, R.; D'Aniello, S.; Vittoria, V.; Di Salle, A.; Calarco, A.; Peluso, G. Effect of resveratrol release kinetic from electrospun nanofibers on osteoblast and osteoclast differentiation. *Eur. Polym. J.* **2018**, *99*, 289–297, doi:10.1016/j.eurpolymj.2017.12.035.
139. Wang, C.C.; Wang, C.H.; Chen, H.C.; Cherng, J.H.; Chang, S.J. Combination of resveratrol-containing collagen with adipose stem cells for craniofacial tissue-engineering applications. *Int. Wound, J.* **2018**, *15*, 660–672, doi:10.1111/iwj.12910.
140. Wang, Z.; Li, C.; Xu, J.; Wang, K.; Lu, X.; Zhang, H.; Qu, S.; Zhen, G.; Ren, F. Bioadhesive Microporous Architectures by Self-Assembling Polydopamine Microcapsules for Biomedical Applications. *Chem.Mater.* **2015**, *27*, 848–856. doi:10.1021/cm5038765.
141. Ko, E.; Yang, K.; Shin, J.; Cho, S.-W. Polydopamine-Assisted Osteoinductive Peptide Immobilization of Polymer Scaffolds for Enhanced Bone Regeneration by Human Adipose-Derived Stem Cells. *Biomacromolecules* **2013**, *14*, 3202–3213. doi:10.1021/bm4008343.

142. Lee, J.S.; Lee, J.S.; Lee, M.S.; An, S.; Yang, K.; Lee, K.; Yang, H.S.; Lee, H.; Cho, S.W. Plant Flavonoid-Mediated Multifunctional Surface Modification Chemistry: Catechin Coating for Enhanced Osteogenesis of Human Stem Cells. *Chem. Mater.* **2017**, *29*, 4375–4384, doi:10.1021/acs.chemmater.7b00802.
143. Pasche, S.; Vörös, J.; Griesser, H.J.; Spencer, N.D.; Textor, M. Effects of ionic strength and surface charge on protein adsorption at PEGylated surfaces. *J. Phys. Chem. B* **2005**, *109*, 17545–17552, doi:10.1021/jp050431+.
144. Verma, A.; Stellacci, F. Effect of surface properties on nanoparticle-cell interactions. *Small* **2010**, *6*, 12–21, doi:10.1002/smll.200901158.
145. Bertrand, N.; Wu, J.; Xu, X.; Kamaly, N.; Farokhzad, O.C. Cancer nanotechnology: The impact of passive and active targeting in the era of modern cancer biology. *Adv. Drug Deliv. Rev.* **2014**, *66*, 2–25, doi:10.1016/j.addr.2013.11.009. Epub 2013 Nov 22.
146. He, L.; Deng, D.; Zhou, X.; Cheng, L.; ten Cate, J.M.; Li, J.; Li, X.; Crielaard, W. Novel tea polyphenol-modified calcium phosphate nanoparticle and its remineralization potential. *Biomed. Mater. Res. Part B Appl. Biomater.* **2015**, *103*, 1525–1531. doi:10.1002/jbm.b.33333.
147. Wang, M.; Wang, L. Plant polyphenols mediated synthesis of gold nanoparticles for pain management in nursing care for dental tissue implantation applications. *J. Drug Deliv. Sci. Technol.* **2020**, *58*, 101753, doi:10.1016/j.jddst.2020.101753.
148. Felice, F.; Zambito, Y.; Belardinelli, E.; D'Onofrio, C.; Fabiano, A.; Balbarini, A.; Di Stefano, R. Delivery of natural polyphenols by polymeric nanoparticles improves the resistance of endothelial progenitor cells to oxidative stress. *Eur. J. Pharm. Sci.* **2013**, *50*, 393–399, doi:10.1016/j.ejps.2013.08.008.
149. M Luisa, D.P.-A., Griselda, R.-M.; Valentín, M.-L.; Carmina, O.-S.; Cristina, V.-M.; Jj, M.; Maykel, G.T.; David, Q.G.; Sánchez-Sánchez, R.; Leyva-Gómez, G. Curcumin-loaded poly-ε-caprolactone nanoparticles show antioxidant and cytoprotective effects in the presence of reactive oxygen species. *J. Bioact. Compat. Polym.* **2020**, *35*, 270–285, doi:10.1177/0883911520921499.
150. Malathy, S.; Iyer, P.R. Naringin Loaded Chitosan Nanoparticle for Bone Regeneration: A Preliminary in vitro Study. *J. Nanomed. Nanotechnol.* **2018**, *9*, 1–7.

molecules

MDPI

Article

Antimicrobial and Antibiofilm Activity of Curcumin-Loaded Electrospun Nanofibers for the Prevention of the Biofilm-Associated Infections

Anna Di Salle [1,†], Gianluca Viscusi [2,†], Francesca Di Cristo [3], Anna Valentino [1,4], Giuliana Gorrasi [2,*], Elena Lamberti [5], Vittoria Vittoria [5], Anna Calarco [1,*] and Gianfranco Peluso [1]

1 Research Institute of Terrestrial Ecosystems (IRET)—CNR, Via Castellino, 111, 80131 Naples, Italy; anna.disalle@cnr.it (A.D.S.); anna.valentino@uniupo.it (A.V.); gianfranco.peluso@cnr.it (G.P.)
2 Department of Industrial Engineering, University of Salerno, Via Giovanni Paolo II 132, 84084 Fisciano, Italy; gviscusi@unisa.it
3 Elleva Pharma s.r.l., Via Pietro Castellino 111, 80131 Naples, Italy; francesca.dicristo@ellevapharma.com
4 Department of Pharmaceutical Sciences, Università del Piemonte Orientale "A. Avogadro", Largo Donegani, 2, 28100 Novara, Italy
5 Nice Filler s.r.l., Via Loggia dei Pisani, 25, 80133 Naples, Italy; elena.lamberti@nicefiller.it (E.L.); vvittoria@unisa.it (V.V.)
* Correspondence: ggorrasi@unisa.it (G.G.); anna.calarco@cnr.it (A.C.)
† These authors equally contributed.

Abstract: Curcumin extracted from the rhizome of *Curcuma Longa* has been used in therapeutic preparations for centuries in different parts of the world. However, its bioactivity is limited by chemical instability, water insolubility, low bioavailability, and extensive metabolism. In this study, the coaxial electrospinning technique was used to produce both poly (ε-caprolactone) (PCL)–curcumin and core–shell nanofibers composed of PCL and curcumin in the core and poly (lactic acid) (PLA) in the shell. Morphology and physical properties, as well as the release of curcumin were studied and compared with neat PCL, showing the formation of randomly oriented, defect-free cylindrical fibers with a narrow distribution of the dimensions. The antibacterial and antibiofilm potential, including the capacity to interfere with the quorum-sensing mechanism, was evaluated on *Pseudomonas aeruginosa* PAO1, and *Streptococcus mutans*, two opportunistic pathogenic bacteria frequently associated with infections. The reported results demonstrated the ability of the Curcumin-loading membranes to inhibit both PAO1 and *S. mutans* biofilm growth and activity, thus representing a promising solution for the prevention of biofilm-associated infections. Moreover, the high biocompatibility and the ability to control the oxidative stress of damaged tissue, make the synthesized membranes useful as scaffolds in tissue engineering regeneration, helping to accelerate the healing process.

Keywords: electrospinning; drug delivery; biomedical applications; controlled release kinetics; curcumin

Citation: Di Salle, A.; Viscusi, G.; Di Cristo, F.; Valentino, A.; Gorrasi, G.; Lamberti, E.; Vittoria, V.; Calarco, A.; Peluso, G. Antimicrobial and Antibiofilm Activity of Curcumin-Loaded Electrospun Nanofibers for the Prevention of the Biofilm-Associated Infections. *Molecules* **2021**, *26*, 4866. https://doi.org/10.3390/molecules26164866

Academic Editors: Chiara Porro and Vassilios Roussis

Received: 25 June 2021
Accepted: 8 August 2021
Published: 11 August 2021

1. Introduction

Among natural compounds, curcumin (1,7-bis(4-hydroxy-3-methoxyphenyl)-1,6-heptadiene-3,5-dione), the main active components isolated from the rhizome of *Curcuma Longa* L., is well known for its beneficial effect on human health because of its outstanding anti-inflammatory [1], antioxidant [2], anticancer [3], wound healing [4,5], and antibacterial [6] properties. Despite these health-beneficial effects, curcumin exhibits poor bioavailability, photodegradation, and in vivo instability (i.e., low serum levels, limited tissue distribution, excessive metabolism, etc.) that limits its therapeutic efficacy. To date, there is a large body of published studies supporting the use of several nanoformulations to overcome these limitations [7–9].

In particular, electrospinning (ES) has emerged as a versatile technique for preparing nano and microfibers of natural and synthetic polymers. The electrospun fibers show fitness

in diversified technological fields such as filtration, protective clothing, wound healing, and other biomedical applications [10–13]. In particular, the use of electrospun fibers is highly promising for scaffolds in tissue engineering and drug delivery [13–17]. High surface area, high drug loading capacity, porosity, simultaneous delivery of different therapeutic agents, adequate mechanical strength, and cost-effectiveness are appealing characteristics for use in drug delivery systems [18–27]. In this context, the coaxial electrospinning technique, combining the properties from two different materials into a single core-sheath fiber, provides important and unique features relevant for biomedical applications [28–34].

The core–shell methodology might contribute to overcoming some challenges associated with electrospinning techniques (i.e., blending electrospinning, production of monolithic fibers, bilayer electrospinning) such as the incorporation of high compound loading, preservation of the activity and presence of burst effect. The use of core–shell structures allows for better tuning of the release kinetics by tailoring the thickness of shell polymer, which acts as a diffusion barrier for the compound loaded in the core as well as a protection of the active molecule from the sunlight or from microbiological attack for example. Then, coaxial fibers allow for the bioactive molecule to be located either in the core or shell layer in a simple one-step process and to modulate the thickness of fibrous material triggering the drug release kinetic [10]. Moreover, the drug release mechanism is mostly explained by the relative rates of erosion and diffusion of the entire fiber scaffold, hence the composition and the porosity of the single fibers can both modify this effect [35–38].

For these reasons, recently electrospinning technique was used in the treatment and prevention of biofilm-related infections, where the possibility to finely trigger the drug release may have a different impact on the bacterial/biofilm growth [39–41]. Biofilm is a complex multidimensional, self-sustained community of bacteria producing a matrix consisting of proteins, extracellular DNA, and polysaccharides, which are frequently associated with antibiotic resistance. Recently, several studies reported the use of electrospun fibers loaded with curcumin which ensure a controlled and sustained drug release in biomedical applications [5,42,43]. However, only a few papers described the fabrication and the application of coaxial electrospun mats loading curcumin [44,45]. Here we report the synthesis of coaxial membranes with two biodegradable polymers, poly (ε-caprolactone) (PCL) and poly (lactic acid) (PLA), used for the core and shell and loaded with curcumin in the core. The antibacterial and antibiofilm potential was evaluated on *Pseudomonas aeruginosa* PAO1, and *Streptococcus mutans*, two opportunistic pathogenic bacteria frequently associated with the infection of biomedical devices both in oral and in orthopedic implantology [46–48]. The Gram-negative bacterium PAO1 is responsible for several medical device-related infections (i.e., endocardial valve infection, ventilator-associated pneumonia, catheter-associated urinary tract infections, etc.), causing approximately 80% of severe infections in immunocompromised patients, of which 25–60% fatal [46,49,50]. *Streptococcus mutans*, moreover, is a Gram-positive bacterium present in the oral cavity and is one of the major contributors to dental biofilms [51,52].

The results reported herein demonstrate the ability of the single-needle-spinned PCL-Cur and the coaxial membrane PCL-Cur/PLA (PCL in the core and PLA in the shell) to inhibit both PAO1 and *S. mutans* biofilm growth and activity. The high biocompatibility and the ability to control the oxidative stress of damaged tissue, make the synthesized membranes useful as scaffolds in tissue engineering regeneration, helping to accelerate the healing process and to prevent biofilm-associated infections.

2. Results and Discussion

2.1. Morphological Analysis

Electrospinning conditions were optimized to produce fibrous mats with bead-less fibers [53,54]. By adopting the chosen final parameters (as reported in the experimental part), fibers loaded with curcumin were successfully fabricated. Representative SEM photographs and the fiber diameter distribution of the electrospun membranes are shown in Figure 1.

2.1. Morphological Analysis

Electrospinning conditions were optimized to produce fibrous mats with bead-less fibers [53,54]. By adopting the chosen final parameters (as reported in the experimental part), fibers loaded with curcumin were successfully fabricated. Representative SEM photographs and the fiber diameter distribution of the electrospun membranes are shown in Figure 1.

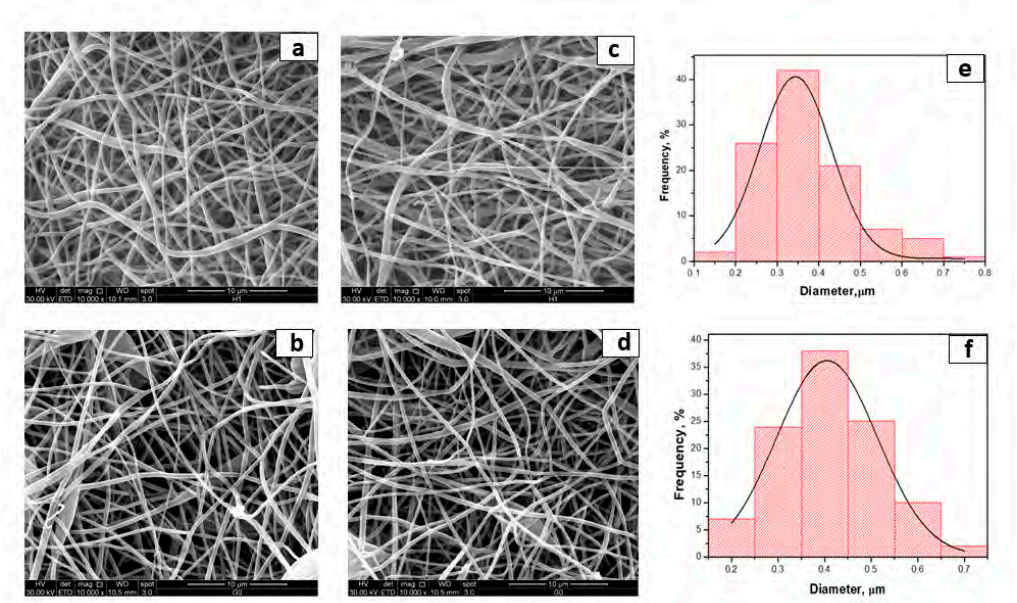

Figure 1. SEM photographs of (**a**) PCL; (**b**) PCL-PLA; (**c**) PCL-Cur; (**d**) PCL-Cur/PLA; (**e**) fiber distribution of PCL-Cur and (**f**) fiber distribution of PCL-Cur/PLA.

As shown in Figure 1, curcumin loading did not noticeably affect the fiber morphology. The electrospinning of PCL led to the defection of free fibers, with a narrow fiber diameter distribution of 344 nm. Even in the case of coaxial fibers, the fibers are well-formed and almost free of defects. Their dimensions are slightly smaller than the neat PCL membrane and are very similar. In Figure 2, the TEM analysis shows the morphology of coaxial nanofibers where the inner and outer diameters made of PCL-Cur and PLA, respectively, are clearly evident.

Figure 2. TEM images of PCL-Cur/PLA fiber.

It is evident that the core containing the drug is thicker than the shell of PLA; the PCL core is 286 nm, whereas the PLA shell is 60.5 nm.

2.2. Thermogravimetric Analysis

Thermogravimetric analysis was performed for investigating the degradation temperature of the coaxial fibers compared to the pure polymers. The thermal decomposition up to 700 °C in the air of the electrospun fibers, either PCL-Cur or coaxial PCL-Cur/PLA, are shown in Figure 3.

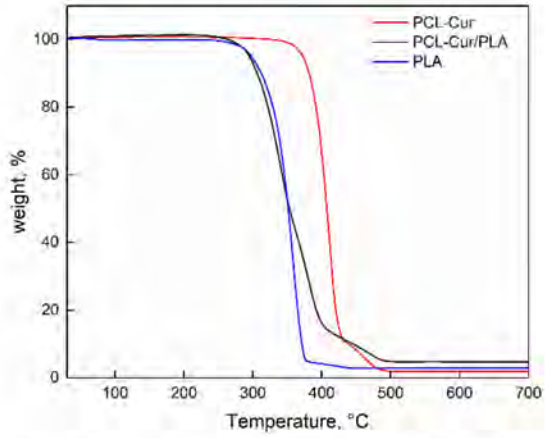

Figure 3. Thermogravimetric analysis of PCL-Cur, PCL-Cur/PLA and PLA.

The degradation behavior of the coaxial membrane is higher than the PCL-Cur. This is due to the presence of PLA that shows lower thermal stability. Table 1 reports the degradation temperatures as the onset and endset of the coaxial fibers compared to the pure polymers.

Table 1. Onset temperatures, endset temperatures and residue contents of electrospun membranes.

	PCL-Cur	PCL-Cur/PLA	PLA
Residue (%)	1.89	4.70	2.98
Onset (°C)	372	260	315
Endset (°C)	425	395	374

2.3. Mechanical Characterization

The mechanical properties of PCL-Cur membranes were evaluated from stress–strain curves and compared to the coaxial system. The mechanical parameters are reported in Table 2.

Table 2. Mechanical properties of electrospun membranes.

	PCL-Cur	PCL-Cur/PLA
E (MPa)	6.1 ± 0.5	48 ± 25
σ_{break} (MPa)	2.19 ± 1.1	1.31 ± 0.3
ε_{break} (mm/mm%)	139 ± 3.5	46 ± 11

Interestingly, the coaxial fibers show a higher mechanical modulus due to the strengthening of one material inside the other. At variance, the coaxial systems displayed a lower extensibility than PCL system as well as reduced stress at the breakpoint. This can be due to the dishomogeneity of the systems. However, the decrease of these parameters is not dramatic, and does not compromise the mechanical properties, also considering the increase of the elastic modulus.

2.4. Drug Release Analysis

As curcumin is poorly soluble in aqueous solutions, the release kinetic was determined in PBS/EtOH (90:10 *v/v*), a medium that facilitates the solubilization of the curcumin. As shown in Figure 4, PCL-Cur/PLA exhibited a significantly ($p < 0.001$) more sustained curcumin release, compared to PCL-Cur, after 2 h of incubation and throughout the experimental period.

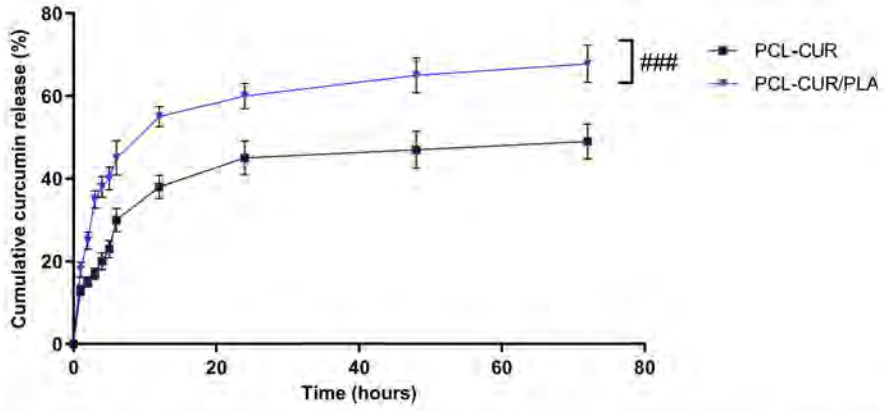

Figure 4. Cumulative curcumin release kinetic release profiles at 37 °C of PCL, and PCL-Cur/PLA incubated for 72 h in release medium (PBS/EtOH 90:10 *v/v*). For each sample, six different experiments were conducted, and the results expressed as the mean of the values obtained (mean ± SD). Statistically significant variations: ### $p < 0.001$ versus PCL-CUR.

Approximately 30 and 45% of the curcumin was released within the first 6 h from PCL-Cur and PCL-Cur/PLA, respectively, indicating that curcumin molecules weakly attached on the fiber surfaces have a high diffusion tendency. This initial burst release is followed by a slower and constant release, reaching 49 and 67.8% of a curcumin release after 72 h of incubation for PCL-Cur and PCL-Cur/PLA, respectively. From 72 h onwards, the release of curcumin reached a plateau, leveling off at around 52 and 69% for PCL-Cur and PCL-Cur/PLA, respectively (data not shown).

Moreover, the coaxial membrane PCL-Cur/PLA showed a higher curcumin loading efficiency in comparison to the PCL-Cur membrane, incorporating 70 ± 3% and 56 ± 2% of curcumin, respectively. The obtained data are in accordance with the literature, confirming the capacity of the coaxial spinning to load the drug and control the initial burst release more efficiently with respect to single-needle spinning [55,56]. Furthermore, the incorporation into the core–shell of the fiber is helpful to protect unstable active molecules from degradation, serving as a physical barrier [32,56].

2.5. Antibacterial and Antibiofilm Analyses

Biofilm inhibition was analyzed at different times, as reported in Figure 5.

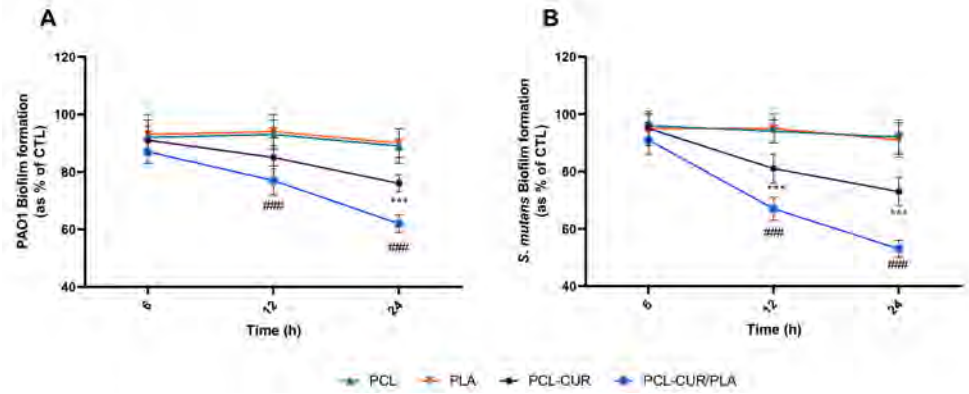

Figure 5. Antibiofilm activity of curcumin-loading membranes. Biofilm formation was evaluated by CV assay, after 6, 12, and 24 h of incubation at 37 °C in the presence of PAO1 (**A**), and *Streptococcus mutans* (**B**) as described in the material and methods section. Biofilm formation was reported as a percentage in comparison to the maximum amount of biofilm produced by PAO1 and *Streptococcus mutans* grown (bacterial positive controls). For each sample, six different experiments were conducted, and the results expressed as the mean of the values obtained (mean ± SD). Statistically significant variations: *** $p < 0.001$ versus PCL and PLA; ### $p < 0.001$ versus PCL-Cur.

The results indicated a significant decrease ($p < 0.001$) in both PAO1 and *S. mutans* biofilm formation only for the PCL-Cur and PCL-Cur/PLA, according to the release study.

In particular, the major effect was observed for PCL-Cur/PLA membrane whit a reduction of 38 ± 3%, 47 ± 3% in PAO1 and *S. mutans* biofilm formation, respectively. During the first stage of biofilm formation, only PCL-Cur/PLA significantly inhibited biofilm formation, resulting in a reduction of 23 ± 5%, 33 ± 4% in PAO1 and *S. mutans* biofilm formation, respectively after 12 h of incubation.

Moreover, to better understand the mechanism of action of curcumin released from membranes in the inhibition of biofilm formation/maturation, the mRNA level of several genes involved in the quorum-sensing process was evaluated by q-PCR.

In general, QS is regulated by different autoinducer molecules in Gram-negative and Gram-positive bacteria [57]. Indeed, Gram-negative bacteria such as PAO1 during the QS process produce extracellular autoinducers such as N-(3-oxododecanoyl)-L-homoserine lactone (3-*O*-C12-HSL) and *N*-butyryl-L-homoserine lactone (C4-HSL) that promote the transcription of virulence genes (i.e., exotoxin A, proteases, and rhamnolipids) [58,59]. Among them, rhamnolipids, which are of great importance acting as heat-stable extracellular hemolysins [60], are synthesized via *rhlAB* operon [61]. Conversely, Gram-positive bacteria such as *S. mutans* regulated the production of virulence factors via a two-component signal transduction system (TCSTS), consisting of a membrane-bound histidine kinase (HK) sensor protein, and a cognate cytoplasmic response regulator (RR) protein [62]. In *S. mutans*, the TCSTS consist principally in the operon ComAB/ComCDE where comC gene encodes competence-stimulating peptide (CSP), comD encodes HK sensor protein (ComD), and comE encodes an RR protein (ComE) [63].

As shown in Figure 6, both PCL-Cur and PCL-Cur/PLA significantly ($p < 0.001$) decreased the mRNA levels of all genes tested, compared to control (gene expression level in biofilm formed in the presence of PCL and PLA membranes). In particular, for PAO1, the relative expression levels of the virulence genes *rhlA*, and *rhlB* were significantly decreased by 0.85-, and 0.83-fold, respectively, after 6 h of incubation in the presence of PCL-Cur, while by 0.72- and 0.73-fold after 6 h of incubation in the presence of PCL-Cur/PLA. This reduction was more evident after 24 h of incubation, reaching a downregulation of 0.67- and 0.53-fold for PCL-Cur and 0.53- and 49-fold for PCL-Cur/PLA. The same behavior was observed for *S. mutans* biofilm, where the treatment with PCL-Cur and PCL-Cur/PLA for 6 h repressed the relative expression levels of *comC* and *comD* to 77% and 72% (PCL-Cur), and 37% and 49% (PCL-Cur/PLA), respectively, as compared to control values. After 24 h of incubation, only the relative expression level of com D significantly ($p < 0.001$) was downregulated, reaching a 29% decrease compared to control for PCL-CUR/PLA.

Antimicrobial activity was then analyzed at 6 and 24 h in the presence of prepared membranes. As reported in Figure 7, the antibacterial evaluation demonstrated that the electrospun membranes did not have a noticeable effect on both the *Pseudomonas aeruginosa* PAO1 and the *Streptococcus mutans* growth curves.

The reported results demonstrated that the curcumin released from electrospun membranes is able to affect biofilm formation without interfering with bacterial growth.

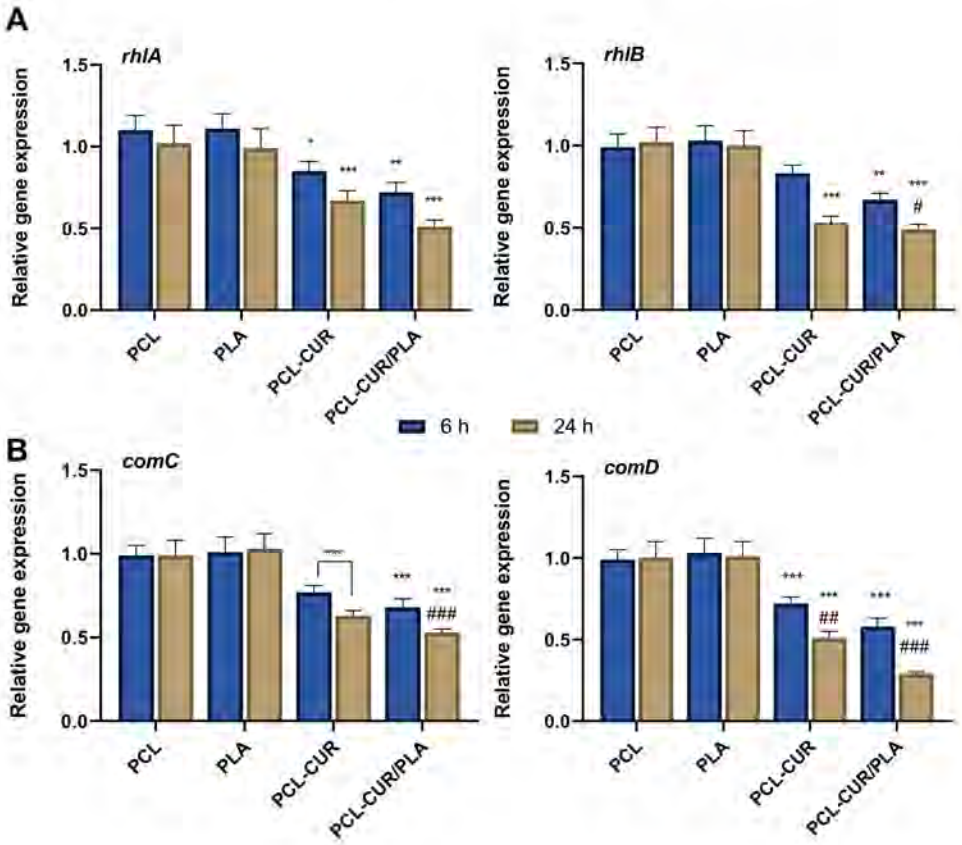

Figure 6. Evaluation of the effect of the CUR-loaded membranes on the expression of QS-related genes. (**A**) Relative RNA expression of *rhlA* and *rhlB* in PAO1; (**B**) relative RNA expression of *comC* and *comD* in *S. mutans*. Different gene expression levels were normalized to the level of 16sRNA gene transcripts. Gene expression levels of biofilm formed in the presence of PCL were used as control. Statistically significant variations: * $p < 0.05$ versus PCL and PLA; ** $p < 0.01$ versus PCL and PLA; *** $p < 0.001$ versus PCL and PLA; $^{\#}$ $p < 0.05$ versus PCL-CUR; $^{\#\#}$ $p < 0.01$ versus PCL-CUR; $^{\#\#\#}$ $p < 0.001$ versus PCL-CUR.

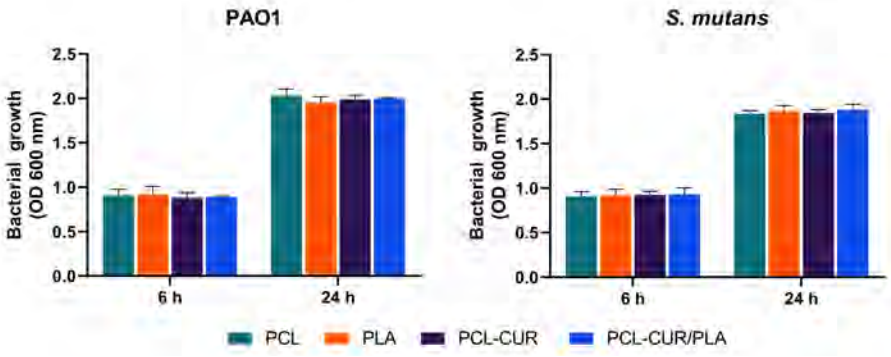

Figure 7. Antibacterial activity evaluated at 600 nm against *Pseudomonas aeruginosa* PAO1, and *Streptococcus mutans*. Bacterial growth in the presence of PCL and PLA were used as controls. For each sample, six different experiments were conducted, and the results expressed as the mean of the values obtained (mean ± SD).

2.6. Determination of DPPH Radical Scavenging Activity

Inflammation represents an adaptive physiological response to external and/or internal deleterious circumstances, including infection and tissue injuries. Extensive studies have suggested that continuous oxidative stress activates the inflammatory signaling cascade producing new free radicals that, in turn, lead to further oxidative stress, thus creating

a cycle. This altered status can cause various chronic diseases such as cancer, atherosclerosis, Alzheimer's disease, metabolic disorders, and so on [64,65]. Among the numerous phytochemicals, curcumin exhibited anti-inflammatory, antioxidative, and antitumor effects both on in vitro and in vivo models of human diseases [66]. The anti-inflammatory and antioxidative activity of curcumin is mostly related to the regulation of the NF-κB (nuclear factor k-light-chain-enhancer of activated B cells) pathway and the inhibition of the cyclooxygenase-2 (COX-2) [67]. Other studies reported the involvement of curcumin in the increase of reactive oxidative species (ROS) and glutathione production and inhibition of lipid peroxidation activity [68]. It has been suggested that the antioxidant activity of curcumin can be attributed either to the phenolic OH group or the CH_2 group of the β-diketone moiety [69,70]. Indeed, the radical scavenging activity of curcumin is 100-fold stronger than that of vitamin E or C both in vitro and in vivo [71].

The ability of curcumin released from membranes to produces an antioxidant effect was evaluated by the DPPH radical scavenging assay, a simple and highly sensitive method to evaluate the free radical scavenging activity of antioxidants [72].

As reported in Figure 8, a decrease in the concentration of DPPH radical was shown due to the scavenging ability of curcumin released from both PCL-Cur and PCL-Cur/PLA. However, the PCL-Cur/PLA coaxial membrane showed a significantly higher antioxidant activity with respect to PCL-Cur after 8, 24 and 48 h of immersion. No effect was observed in the presence of PLA-Cur and PLA-Cur/PCL membranes. Moreover, the results indicated that a longer immersion period (48 h) led to a reduction of antioxidant activity, likely due to decreasing stability of curcumin in alcohol solution.

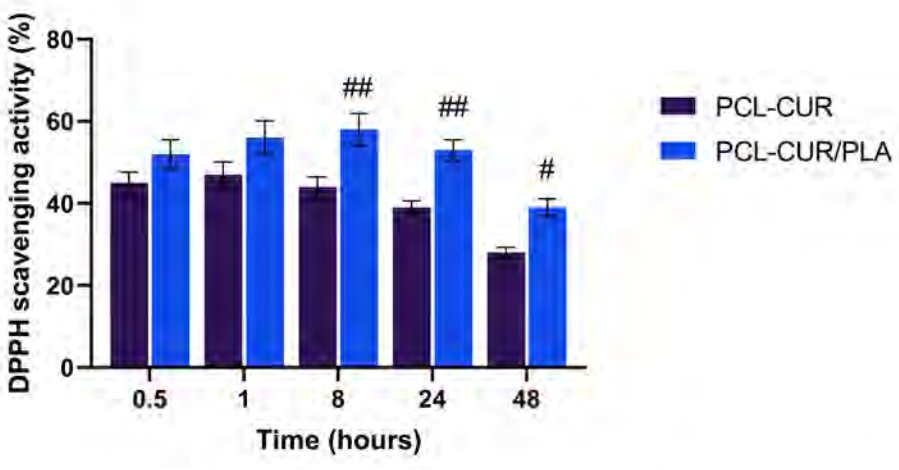

Figure 8. DPPH scavenging activity of Cur loading membranes. For each sample, six different experiments were conducted, and the results expressed as the mean of the values obtained (mean ± SD). Statistically significant variations: $^{\#\#}$ $p < 0.005$ versus PCL-Cur; $^{\#}$ $p < 0.05$ versus PCL-Cur.

2.7. Membranes Biocompatibility

To investigate the effect of curcumin extract on viability, human dermal fibroblasts (HDFs) were chosen as in vitro cell models. The results depicted in Figure 9 demonstrated that the extracts obtained in culture medium from all synthesized membranes did not elicit any cytotoxic effect. In particular, no influence on HDF metabolic activity was reported even after 72 h of incubation (Figure 9A). In addition, the low LDH level in the cell supernatant confirms the absence of cell membrane damage (Figure 9B).

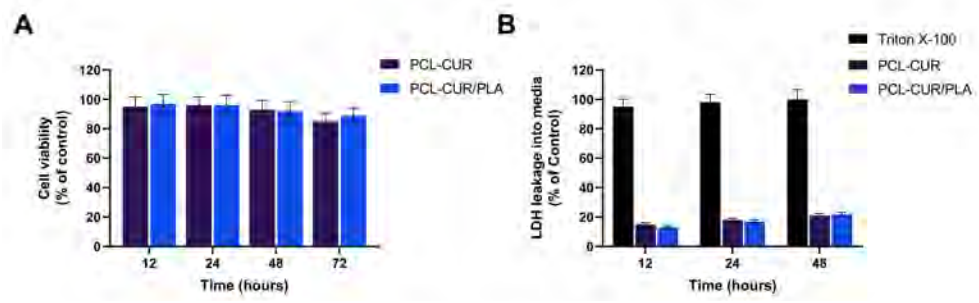

Figure 9. Cytotoxicity of curcumin released from Cur loading membranes tested via CCK-8 (**A**) and LDH (**B**) assays after 12, 24, 48, and 72 h of incubation. For each sample, six different experiments were conducted, and the results were expressed as the mean of the values obtained (mean ± SD).

Taken together, these results demonstrate that the fabricated membranes could be employed as scaffolds in tissue engineering regeneration to control the oxidative stress of damaged tissue, helping to accelerates the healing process.

3. Materials and Methods

3.1. Materials

Poly(ε-caprolactone) (PCL molecular weight of 80,000 Da) was purchased from Sigma Aldrich while poly (L-lactide-co-D,L-lactide) (PLA 4032 D-Mw = 160,000 g/mol) was purchased from NatureWorks (Minnetonka, MN, USA). Tetrahydrofuran (THF pure-CAS: 109-99-9), Ethanol (EtOH purity > 96%-CAS 64-17-5) and Phosphate Buffer Solution (PBS-pH = 7 ± 0.02-CAS: 7558-79-4) were purchased from Carlo Erba Reagents (Cornaredo-Milano). N,N-Dimethylformamide (DMF-CAS 68-12-2) and Curcumin (Cur) were purchased from Sigma Aldrich (Milan, Italy). Cell Counting Kit-8 (CCK-8) assay and Lactate dehydrogenase assay were from Roche Applied Science (Milan, Italy). Human dermal fibroblasts were purchased from the American Type Culture Collection ATCC (LGC Standards S.R.L., Sesto San Giovanni, Milan, Italy) and cultured in accordance with the manufacturer's instructions. Fetal bovine serum (FBS), Dulbecco's Modified Eagle's Medium (DMEM), sodium pyruvate, L-glutamine, penicillin, and streptomycin were purchased from Hyclone (Milan, Italy).

3.2. Preparation of Curcumin-Loaded Membranes Using Electrospinning

The electrospinning membranes were prepared by dissolving PCL and PLA in a solvent mixture THF/DMF (50:50 *v/v*) at 12% *w*/*w*. Curcumin was added to PCL solution at the drug to polymer ratio of 0.1:9.9 (*w*/*w*) and mixed for 4 h at 40 °C using a temperature-controlled stirring plate (300 rpm) to obtain a homogenous solution. Coaxial electrospun membranes were obtained by using a coaxial nozzle (EM-CAX-Ime electrospinning). Two separate volumetric pumps were used to process the polymeric solutions, prepared as previously described. The curcumin-loaded coaxial nanofibrous mats were processed by coaxial electrospinning; the drug-loaded solution constitutes the inner core, while the no-loaded solution is the outer shell. Before performing the experiment, each solution was fed in a 5 mL syringe pump. The sets of electrospinning conditions were reported in Table 3 and optimized to produce nanofibrous mats without bead formation [44]. Temperature and relative humidity were fixed for all the experiments and equal to 25 °C and 35%, respectively. The produced composite nanofibrous mats were marked as PCL-Cur and PCL-Cur (core)/PLA (shell).

Table 3. Processing parameters of fibrous membranes fabricated by electrospinning.

Sample	Polymer Concentration (% *w*/*w*)	Voltage (kV)	Distance (cm)	Flow Rate (mL/h)
PCL-Cur	12	17.5	18	0.5
Core: PCL-Cur Shell: PLA	Core: 12 Shell: 12	24	25	Core: 0.5 Shell: 0.7

A climate-controlled electrospinning apparatus EC-CLI (IME Technologies, WG Waalre, The Netherlands) was used to produce fibrous membranes. The vertical setup was chosen to carry out the experiments. Core–shell nanofibers were obtained through a coaxial apparatus containing two concentric needles. The diameters of the inner and outer needles were 0.8 mm and 1.2 mm, respectively. The inner needle was 0.20 mm longer than the outer needle. For all the experiments, an aluminum collector was used to recover the electrospun nanofibers.

3.3. Morphological Analises

3.3.1. Scanning Electron Microscopy (SEM)

SEM was carried out using a Quanta 200 F microscope (Thermo Fischer, Hillsboro, OR, USA) in high-vacuum mode. Before the analysis, electrospun membranes were covered with a thin film of gold using an Agar Automatic Sputter Coater (Mod. B7341, Stansted, UK) at 40 mA for 120 s prior to the analysis.

3.3.2. Transmission Electron Microscopy (TEM)

TEM was performed on a FEI Tecnai 200 kV electron microscope (Thermo Fischer, Hillsboro, OR, USA) operating at 100 keV. The samples for the TEM observation were prepared by directly depositing the as-spun fibers onto the copper grids.

3.4. Structural Characterization of Electrospinning Nanofibers

3.4.1. Thermogravimetric Analyses (TGA)

TGA were carried out in an air atmosphere with a Mettler TC-10 thermobalance (Mettler Toledo GmbH, Greifensee, Switzerland) from 25 °C to 800 °C at a heating rate of 10 °C/min.

3.4.2. Mechanical Properties

Mechanical properties were evaluated, in tensile mode, at room temperature using a dynamometric apparatus INSTRON 4301 (ITW Test and Measurement Italia S.r.l., Pianezza, Italy). Experiments were conducted at room temperature with a deformation rate of 5 mm/min. Elastic modulus was evaluated in the deformation range of 0.1%. Data were averaged on five samples.

3.5. Curcumin Entrapment Efficiency

Square pieces of membranes (ca. 2 cm^2) were weighted and dissolved in methanol (1:5 *w*/*v*) for 60 min and curcumin concentration was measured as reported above by HPLC. The curcumin loading efficiency (LE) was calculated as percentage respect to the loaded drug as follows:

$$\text{LE } (\%) = \frac{\text{curcumin concentration}}{\text{curcumin concentration initially added in the polymer solution}} \times 100$$

3.6. In Vitro Release Kinetic Measurement

The release of the curcumin from the membranes was determined as early described with some modifications [73]. Briefly, square pieces of membranes (ca. 2 cm^2) were weighed and placed into individual amber vials. Considering the very low solubility of the curcumin in aqueous solutions, the release kinetic was performed at 37 °C in PBS/EtOH

(90:10 *v/v*). At predetermined time intervals (every hour for 6 h, then at 12, 24, 48 and 72 h), supernatants were withdrawn, and the same amount of fresh solution was added back to the release medium. The curcumin concentration was measured using HPLC-UV with a linear elution gradient consisting of mobile phase A (0.1% acetic acid), B (Acetonitrile), and C (Methanol). The detection wavelength was set at 420 nm and Curcumin quantitation was based on a standard curve in PBS/EtOH (90:10 *v/v*). System control and data acquisition were performed using ChemStation software (Agilent Technologies). The results were presented in terms of cumulative release (percentage with respect to the loaded drug) as a function of time.

3.7. Antioxidant Activity

Antioxidant activity, as the free radical-scavenging ability of curcumin-loaded nanofibers, was examined using 1,1-dipheny-l-2-picryl hydrazyl (DPPH) assay as reported by Amrati et al. with slight modifications [74]. Samples of square pieces of membranes (ca. 1.5 × 2 cm) were dissolved in PBS/EtOH (90:10 *v/v*) for 0.5, 1, 8, 24 and 48 h and then ultrasonicated for 15 min. The dilution of the solutions was done in PBS/EtOH (90:10 *v/v*). Aliquots (500 µL) of those solutions were added to 2 mL of DPPH methanolic solution (60 µM) and kept in the dark at 37 °C for 1 h. The absorbance of the samples was determined at 517 nm using a microplate reader (Cytation 3, ASHI). A methanolic solution of free curcumin and polymers was used as a control. The percentage of inhibition of DPPH was calculated as follows:

$$\text{DPPH scavenging effect (\%)} = [(A_1 - A_0)/A_1] \times 100$$

where A_1 was the absorbance of the control (DPPH solution without sample) at 517; A_0 was the absorbance at 517 of the sample at different concentrations with DPPH. The antioxidant activity was expressed as % with respect to free curcumin.

3.8. Citotoxicity

3.8.1. Cell Proliferation Assay

Indirect cytotoxicity evaluation of curcumin-loaded membranes was conducted according to ISO 10993-5 standard test method as reported by Conte et al. with slight modifications [75]. Samples in a circular shape (1.5 cm in diameter) were exposed to UV radiation for 30 min for sterilization. Then, the samples were immersed in 10 *v/v* % serum containing DMEM medium for 24 h at 37 °C to produce the sample extraction. Human dermal fibroblasts (HDFs) were cultured in 96-well tissue-culture polystyrene plate (TCPS) at 2×10^3 cells/well in serum-containing DMEM for 16 h to allow cell attachment. After that, the medium was replaced with an extraction medium and HDFs were incubated for a further 12, 24 and 48 h. At the end of the incubation period, all CCK-8 solutions were added to each well, and the plate was then incubated under cell culture conditions for 1–4 h. The optical density of formazan salt at 450 nm was measured using a Citation 3 Cell Imaging Multi-Mode microplate reader (ASHI, Milan, Italy). The cytocompatibility of the membranes was expressed as a percentage relative to the control and calculated as:

$$\text{Cytocompatibility (\%)} = (\text{OD sample}/\text{OD control}) \times 100$$

where OD sample is the optical density of cells treated with curcumin extract and OD control is the optical density of untreated cells.

3.8.2. LDH Release Assay

Lactate dehydrogenase (LDH) release measurements were based on the measurement of lactate LDH released into the growth media when the integrity of the cell membrane is lost. For this assay, HDF cells were treated with extracts in the same way as described above. At the end of the incubation time, 100 µL of the culture supernatants were collected to a well, and LDH activity was detected at 450 nm as reported by manufacturing protocol.

As a positive control, cells were completely lysed with Triton X-100, according to Calarco et al. [76].

3.9. Antimicrobial Activity

3.9.1. Bacterial Strains and Culture Conditions

Pseudomonas aeruginosa PAO1 (ATCC® BAA-47™) and *Streptococcus mutans* (ATCC® 25175) were purchased from ATCC, and cultured following the ATCC's guidelines.

3.9.2. Antibacterial Activity

The capability of the curcumin-loaded membranes to inhibit bacterial growth was determined by monitoring the optical density (OD) at 600 nm of bacterial suspensions cultured in the presence of both PCL-Cur and coaxial PCL-Cur/PLA. All mats were cut of similar dimension, sterilized by UV radiation for 15 min at each side, and finally placed in a 12-well plate in the presence of 500 µL liquid broth as previously described [77]. Briefly, bacteria were inoculated approximately at 1×10^7 CFU/mL and incubated at 37 °C and 200 rpm in a microplate reader (Cytation 3). As a control, the growth curve was obtained in the presence of PCL mat. At scheduled times (6 h or 24 h), the optical density (OD) at 600 nm was recorded.

3.9.3. Biofilm Analysis

To investigate the ability of the curcumin-loaded membranes to inhibit the biofilm formation, a similar amount of PCL-Cur, and PCL-Cur/PLA were sterilized by UV radiation for 15 min at each side, placed in a 48-well polystyrene plate, and biofilm developed as described by Di Salle et al. with some modifications [78]. Briefly, 750 µL of liquid medium broth containing 1×10^7 CFU/mL of *S. mutans* or PAO1 were added and the cultures were incubated statically at 37 °C in a humid atmosphere. PLA or PCL mats incubated in liquid medium broth were used as a negative control, while 750 µL of PAO1 (1×10^7 CFU/mL) or *S. mutans* (1×10^7 CFU/mL) were used as positive controls.

The surface-adhered biofilm was quantified after 6, 12, and 24 h by the Crystal Violet (CV) assay. Each well was washed gently with sterile phosphate-buffered saline (PBS), and air-dried for 30 min. Then, a solution of 0.1% *w/v* Crystal Violet was added to each well. After 30 min, excess solution was removed, and any extra stain was removed by washing with PBS. The stained biofilms were solubilized in 96% ethanol and quantified by measuring the optical density (OD) at 570 nm using a microplate reader (Cytation 3, AHSI, Milan, Italy). Measurements were carried out in triplicate for each membrane.

3.9.4. Quorum Sensing (QS) Interfering

To determine the ability of the membranes to interfere with the quorum-sensing mechanism underlying the biofilm maturation process, the mRNA level of *rhlAB* genes for PAO1 and of *comCD* genes for *S. mutans* was quantified by real-time PCR (qRT-PCR). PAO1 and *S. mutans* biofilms were developed in the presence of synthesized membranes for 6 or 24 h, as previously described in a 48-well polystyrene plate. The bacterial pellet was then collected by centrifugation at 13,000× *g* for 10 min, and total RNA was extracted using TRIzol reagent (Invitrogen, Italy) as previously described [79]. Briefly, 0.2 µg of total RNA was retrotranscripted using AMV Reverse Transcriptase and random hexamers according to the provider's instruction (Promega, Milan, Italy). The resulting mixture was amplified by qRT-PCR using specific primers based on the previous literature as listed in Table 4.

Table 4. QPCR primers.

Gene	Forward Primer (5′—3′)	Reverse Primer (5′—3′)	Ref.
rhlA	AGCTGGGACGAATACACCA	GACTCCAGGTCGAGGAAATG	[80]
rhlB	GAGCGACGAACTGACCTACC	GTTGAACTTGGGGTGTACCG	[80]
comC	GACTTTAAAGAAATTAAGACTG	AAGCTTGTGTAAAACTTCTGT	[81]
comD	CTCTGATTGACCATTCTTCTGG	CATTCTGAGTTTATGCCCCTC	[81]
16SrRNA	CCTACGGGAGGCAGCAGTAG	CAACAGAGCTTTACGATCCGAAA	[82]
16SrRNA	CAAAACTACTGAGCTAGAGTACG	TAAGATCTCAAGGATCCCAACGGCT	[83]

qPCR and data collection were performed on 7900HT Fast Real-time PCR System (Applied Biosystems, Milan, Italy). The reactions were performed according to the manufacturer's instructions using SYBR Green PCR Master Mix (Invitrogen, Italy). All reactions were run in triplicate, normalized to the housekeeping gene (*16SrRNA*), and the results expressed as mean ±SD. The comparative cycle threshold ($2-\Delta\Delta Ct$) method was used to determine the relative quantification.

3.10. Statistical Analysis

Results were expressed as mean ± standard deviation (SD). Student's *t*-test was used for the curcumin release. For biochemical, antimicrobial investigations assay, and quantitative real-time PCR one-way analysis of variance (ANOVA) with Tukey's post-hoc test were used for statistical comparison. The difference was regarded as statistically significant when $p < 0.05$. All the data were analyzed with the GraphPad Prism version 6.01 statistical software package (GraphPad, San Diego, CA, USA).

4. Conclusions

In this study, electrospinning was used to produce nanofibrous membranes with the ability to release curcumin in a continuous and sustainable mode, eliciting both antibacterial and antibiofilm activity on *Pseudomonas aeruginosa* PAO1 and *Streptococcus mutans*—two opportunistic bacteria frequently associated with human infections. In particular, we observed a more important effect, especially after 12 h of incubation, with the coaxial respect to the single-needle electrospun membrane, showing a reduction of 23 ± 5%, 33 ± 4% in PAO1 and *S. mutans* biofilm formation, respectively. Our data also demonstrated the ability of CUR-loading membranes to inhibit signal-based biofilm formation, lowering the expression of several genes involved in the quorum-sensing mechanism that led to biofilm maturation.

Moreover, the presented results demonstrated good biocompatibility of both PCL-Cur, and PCL-Cur/PLA and a good antioxidant capacity already after 30 min of incubation.

Taken together, these results demonstrate that the fabricated membranes could be employed as scaffolds in tissue engineering regeneration to control the oxidative stress of damaged tissue, thus helping to accelerates the healing process.

Author Contributions: Conceptualization, A.C., A.D.S. and G.G.; investigation, G.V., A.V., F.D.C. and E.L.; writing—original draft preparation, G.G., A.D.S., G.P., V.V. and A.C.; writing—review and editing, G.G., A.D.S., G.P., V.V. and A.C.; supervision, A.D.S., G.G. and A.C.; funding acquisition, G.P. All authors have read and agreed to the published version of the manuscript.

Funding: This research was financially supported by the PON 03 PE_00110_1/ptd1_000410 Titolo: Sviluppo di nanotecnologie Orientate alla Rigenerazione e Ricostruzione tissutale, Implantologia e Sensoristica in Odontoiatria/oculistica (SORRISO).

Data Availability Statement: Not applicable.

Acknowledgments: The authors thank Orsolina Petillo for her technical support and editorial assistance.

Conflicts of Interest: The authors declare no conflict of interest.

Sample Availability: Not available.

References

1. Hasanzadeh, S.; Read, M.I.; Bland, A.R.; Majeed, M.; Jamialahmadi, T.; Sahebkar, A. Curcumin: An inflammasome silencer. *Pharmacol. Res.* **2020**, *159*, 104921. [CrossRef]
2. Banez, M.J.; Geluz, M.I.; Chandra, A.; Hamdan, T.; Biswas, O.S.; Bryan, N.S.; Von Schwarz, E.R. A systemic review on the antioxidant and anti-inflammatory effects of resveratrol, curcumin, and dietary nitric oxide supplementation on human cardiovascular health. *Nutr. Res.* **2020**, *78*, 11–26. [CrossRef]
3. D'Arcy, M.S. A review of the chemopreventative and chemotherapeutic properties of the phytochemicals berberine, resveratrol and curcumin, and their influence on cell death via the pathways of apoptosis and autophagy. *Cell Biol. Int.* **2020**, *44*, 1781–1791. [CrossRef]
4. Barbalho, S.M.; de Sousa Gonzaga, H.F.; de Souza, G.A.; de Alvares Goulart, R.; de Sousa Gonzaga, M.L.; de Alvarez Rezende, B. Dermatological effects of Curcuma species: A systematic review. *Clin. Exp. Dermatol.* **2021**, *46*, 825–833. [CrossRef]
5. Alven, S.; Nqoro, X.; Aderibigbe, B.A. Polymer-Based Materials Loaded with Curcumin for Wound Healing Applications. *Polymers* **2020**, *12*, 2286. [CrossRef] [PubMed]
6. Zheng, D.; Huang, C.; Huang, H.; Zhao, Y.; Khan, M.R.U.; Zhao, H.; Huang, L. Antibacterial Mechanism of Curcumin: A Review. *Chem. Biodivers.* **2020**, *17*, e2000171. [CrossRef] [PubMed]
7. Basu, P.; Maier, C.; Basu, A. Effects of Curcumin and Its Different Formulations in Preclinical and Clinical Studies of Peripheral Neuropathic and Postoperative Pain: A Comprehensive Review. *Int. J. Mol. Sci.* **2021**, *22*, 4666. [CrossRef]
8. Hesari, M.; Mohammadi, P.; Khademi, F.; Shackebaei, D.; Momtaz, S.; Moasefi, N.; Farzaei, M.H.; Abdollahi, M. Current Advances in the Use of Nanophytomedicine Therapies for Human Cardiovascular Diseases. *Int. J. Nanomed.* **2021**, *16*, 3293–3315. [CrossRef] [PubMed]
9. Mahjoob, M.; Stochaj, U. Curcumin nanoformulations to combat aging-related diseases. *Ageing Res. Rev.* **2021**, *69*, 101364. [CrossRef]
10. Liu, H.; Gough, C.R.; Deng, Q.; Gu, Z.; Wang, F.; Hu, X. Recent Advances in Electrospun Sustainable Composites for Biomedical, Environmental, Energy, and Packaging Applications. *Int. J. Mol. Sci.* **2020**, *21*, 4019. [CrossRef] [PubMed]
11. Croitoru, A.M.; Ficai, D.; Ficai, A.; Mihailescu, N.; Andronescu, E.; Turculet, C.F. Nanostructured Fibers Containing Natural or Synthetic Bioactive Compounds in Wound Dressing Applications. *Materials* **2020**, *13*, 2407. [CrossRef] [PubMed]
12. Luo, H.; Jie, T.; Zheng, L.; Huang, C.; Chen, G.; Cui, W. Electrospun Nanofibers for Cancer Therapy. *Adv. Exp. Med. Biol.* **2021**, *1295*, 163–190. [CrossRef] [PubMed]
13. Dziemidowicz, K.; Sang, Q.; Wu, J.; Zhang, Z.; Zhou, F.; Lagaron, J.M.; Mo, X.; Parker, G.J.M.; Yu, D.G.; Zhu, L.M.; et al. Electrospinning for healthcare: Recent advancements. *J. Mater. Chem. B* **2021**, *9*, 939–951. [CrossRef] [PubMed]
14. Tottoli, E.M.; Dorati, R.; Genta, I.; Chiesa, E.; Pisani, S.; Conti, B. Skin Wound Healing Process and New Emerging Technologies for Skin Wound Care and Regeneration. *Pharmaceutics* **2020**, *12*, 735. [CrossRef] [PubMed]
15. Deng, X.; Qasim, M.; Ali, A. Engineering and polymeric composition of drug-eluting suture: A review. *J. Biomed. Mater. Res. Part A* **2021**. [CrossRef]
16. Jeckson, T.A.; Neo, Y.P.; Sisinthy, S.P.; Gorain, B. Delivery of Therapeutics from Layer-by-Layer Electrospun Nanofiber Matrix for Wound Healing: An Update. *J. Pharm. Sci.* **2021**, *110*, 635–653. [CrossRef]
17. Luraghi, A.; Peri, F.; Moroni, L. Electrospinning for drug delivery applications: A review. *J. Control. Release Off. J. Control. Release Soc.* **2021**, *334*, 463–484. [CrossRef]
18. Elsner, J.J.; Egozi, D.; Ullmann, Y.; Berdicevsky, I.; Shefy-Peleg, A.; Zilberman, M. Novel biodegradable composite wound dressings with controlled release of antibiotics: Results in a guinea pig burn model. *Burns* **2011**, *37*, 896–904. [CrossRef]
19. Elsner, J.J.; Zilberman, M. Antibiotic-eluting bioresorbable composite fibers for wound healing applications: Microstructure, drug delivery and mechanical properties. *Acta Biomater.* **2009**, *5*, 2872–2883. [CrossRef]
20. Liu, S.-J.; Kau, Y.-C.; Chou, C.-Y.; Chen, J.-K.; Wu, R.-C.; Yeh, W.-L. Electrospun PLGA/collagen nanofibrous membrane as early-stage wound dressing. *J. Membr. Sci.* **2010**, *355*, 53–59. [CrossRef]
21. Meng, Z.X.; Xu, X.X.; Zheng, W.; Zhou, H.M.; Li, L.; Zheng, Y.F.; Lou, X. Preparation and characterization of electrospun PLGA/gelatin nanofibers as a potential drug delivery system. *Colloids Surf. B Biointerfaces* **2011**, *84*, 97–102. [CrossRef]
22. Noh, H.K.; Lee, S.W.; Kim, J.-M.; Oh, J.-E.; Kim, K.-H.; Chung, C.-P.; Choi, S.-C.; Park, W.H.; Min, B.-M. Electrospinning of chitin nanofibers: Degradation behavior and cellular response to normal human keratinocytes and fibroblasts. *Biomaterials* **2006**, *27*, 3934–3944. [CrossRef]
23. Powell, H.M.; Supp, D.M.; Boyce, S.T. Influence of electrospun collagen on wound contraction of engineered skin substitutes. *Biomaterials* **2008**, *29*, 834–843. [CrossRef]
24. Rho, K.S.; Jeong, L.; Lee, G.; Seo, B.-M.; Park, Y.J.; Hong, S.-D.; Roh, S.; Cho, J.J.; Park, W.H.; Min, B.-M. Electrospinning of collagen nanofibers: Effects on the behavior of normal human keratinocytes and early-stage wound healing. *Biomaterials* **2006**, *27*, 1452–1461. [CrossRef] [PubMed]
25. Teo, E.Y.; Ong, S.-Y.; Khoon Chong, M.S.; Zhang, Z.; Lu, J.; Moochhala, S.; Ho, B.; Teoh, S.-H. Polycaprolactone-based fused deposition modeled mesh for delivery of antibacterial agents to infected wounds. *Biomaterials* **2011**, *32*, 279–287. [CrossRef]

26. Thangaraju, E.; Rajiv, S.; Natarajan, T.S. Comparison of preparation and characterization of water-bath collected porous poly L–lactide microfibers and cellulose/silk fibroin based poly L-lactide nanofibers for biomedical applications. *J. Polym. Res.* **2015**, *22*, 24. [CrossRef]
27. Uttayarat, P.; Jetawattana, S.; Suwanmala, P.; Eamsiri, J.; Tangthong, T.; Pongpat, S. Antimicrobial electrospun silk fibroin mats with silver nanoparticles for wound dressing application. *Fibers Polym.* **2012**, *13*, 999–1006. [CrossRef]
28. Alharbi, H.F.; Luqman, M.; Khalil, K.A.; Elnakady, Y.A.; Abd-Elkader, O.H.; Rady, A.M.; Alharthi, N.H.; Karim, M.R. Fabrication of core-shell structured nanofibers of poly (lactic acid) and poly (vinyl alcohol) by coaxial electrospinning for tissue engineering. *Eur. Polym. J.* **2018**, *98*, 483–491. [CrossRef]
29. Khalf, A.; Madihally, S.V. Recent advances in multiaxial electrospinning for drug delivery. *Eur. J. Pharm. Biopharm.* **2017**, *112*, 1–17. [CrossRef] [PubMed]
30. McCann, J.T.; Li, D.; Xia, Y. Electrospinning of nanofibers with core-sheath, hollow, or porous structures. *J. Mater. Chem.* **2005**, *15*, 735–738. [CrossRef]
31. Naeimirad, M.; Zadhoush, A.; Kotek, R.; Esmaeely Neisiany, R.; Nouri Khorasani, S.; Ramakrishna, S. Recent advances in core/shell bicomponent fibers and nanofibers: A review. *J. Appl. Polym. Sci.* **2018**, *135*, 46265. [CrossRef]
32. Sultanova, Z.; Kaleli, G.; Kabay, G.; Mutlu, M. Controlled release of a hydrophilic drug from coaxially electrospun polycaprolactone nanofibers. *Int. J. Pharm.* **2016**, *505*, 133–138. [CrossRef]
33. Wang, J.; Windbergs, M. Controlled dual drug release by coaxial electrospun fibers—Impact of the core fluid on drug encapsulation and release. *Int. J. Pharm.* **2019**, *556*, 363–371. [CrossRef] [PubMed]
34. Xu, X.; Yang, Q.; Wang, Y.; Yu, H.; Chen, X.; Jing, X. Biodegradable electrospun poly(l-lactide) fibers containing antibacterial silver nanoparticles. *Eur. Polym. J.* **2006**, *42*, 2081–2087. [CrossRef]
35. Yakoub, L.K.; Mohammad, F.K. Medetomidine protection against diazinon-induced toxicosis in mice. *Toxicol. Lett.* **1997**, *93*, 1–8. [CrossRef]
36. Gopferich, A.; Langer, R. Modeling of polymer erosion. *Macromolecules* **1993**, *26*, 4105–4112. [CrossRef]
37. Reynolds, T.D.; Gehrke, S.H.; Ajaz, S.H.; Shenouda, L.S. Polymer Erosion and Drug Release Characterization of Hydroxypropyl Methylcellulose Matrices. *J. Pharm. Sci.* **1998**, *87*, 1115–1123. [CrossRef] [PubMed]
38. Tamada, J.A.; Langer, R. Erosion kinetics of hydrolytically degradable polymers. *Proc. Natl. Acad. Sci. USA* **1993**, *90*, 552. [CrossRef]
39. Preem, L.; Mahmoudzadeh, M.; Putrinš, M.; Meos, A.; Laidmäe, I.; Romann, T.; Aruväli, J.; Härmas, R.; Koivuniemi, A.; Bunker, A.; et al. Interactions between Chloramphenicol, Carrier Polymers, and Bacteria–Implications for Designing Electrospun Drug Delivery Systems Countering Wound Infection. *Mol. Pharm.* **2017**, *14*, 4417–4430. [CrossRef]
40. Preem, L.; Bock, F.; Hinnu, M.; Putrinš, M.; Sagor, K.; Tenson, T.; Meos, A.; Østergaard, J.; Kogermann, K. Monitoring of Antimicrobial Drug Chloramphenicol Release from Electrospun Nano- and Microfiber Mats Using UV Imaging and Bacterial Bioreporters. *Pharmaceutics* **2019**, *11*, 487. [CrossRef] [PubMed]
41. Zupančič, Š.; Preem, L.; Kristl, J.; Putrinš, M.; Tenson, T.; Kocbek, P.; Kogermann, K. Impact of PCL nanofiber mat structural properties on hydrophilic drug release and antibacterial activity on periodontal pathogens. *Eur. J. Pharm. Sci. Off. J. Eur. Fed. Pharm. Sci.* **2018**, *122*, 347–358. [CrossRef]
42. Agarwal, Y.; Rajinikanth, P.S.; Ranjan, S.; Tiwari, U.; Balasubramnaiam, J.; Pandey, P.; Arya, D.K.; Anand, S.; Deepak, P. Curcumin loaded polycaprolactone-/polyvinyl alcohol-silk fibroin based electrospun nanofibrous mat for rapid healing of diabetic wound: An in-vitro and in-vivo studies. *Int. J. Biol. Macromol.* **2021**, *176*, 376–386. [CrossRef] [PubMed]
43. Shababdoust, A.; Ehsani, M.; Shokrollahi, P.; Zandi, M. Fabrication of curcumin-loaded electrospun nanofiberous polyurethanes with anti-bacterial activity. *Prog. Biomater.* **2018**, *7*, 23–33. [CrossRef] [PubMed]
44. Llorens, E.; Ibañez, H.; Del Valle, L.J.; Puiggalí, J. Biocompatibility and drug release behavior of scaffolds prepared by coaxial electrospinning of poly(butylene succinate) and polyethylene glycol. *Mater. Sci. Eng. C Mater. Biol. Appl.* **2015**, *49*, 472–484. [CrossRef]
45. Sharifisamani, E.; Mousazadegan, F.; Bagherzadeh, R.; Latifi, M. PEG-PLA-PCL based electrospun yarns with curcumin control release property as suture. *Polym. Eng. Sci.* **2020**, *60*, 1520–1529. [CrossRef]
46. Canullo, L.; Rossetti, P.H.; Penarrocha, D. Identification of Enterococcus Faecalis and *Pseudomonas Aeruginosa* on and in Implants in Individuals with Peri-implant Disease: A Cross-Sectional Study. *Int. J. Oral Maxillofac. Implant.* **2015**, *30*, 583–587. [CrossRef] [PubMed]
47. Kaur, G.; Rajesh, S.; Princy, S.A. Plausible Drug Targets in the Streptococcus mutans Quorum Sensing Pathways to Combat Dental Biofilms and Associated Risks. *Indian J. Microbiol.* **2015**, *55*, 349–356. [CrossRef]
48. Persson, G.R.; Renvert, S. Cluster of Bacteria Associated with Peri-Implantitis. *Clin. Implant Dent. Relat. Res.* **2014**, *16*, 783–793. [CrossRef]
49. Maurice, N.M.; Bedi, B.; Sadikot, R.T. *Pseudomonas aeruginosa* Biofilms: Host Response and Clinical Implications in Lung Infections. *Am. J. Respir. Cell Mol. Biol.* **2018**, *58*, 428–439. [CrossRef]
50. Pericolini, E.; Colombari, B.; Ferretti, G.; Iseppi, R.; Ardizzoni, A.; Girardis, M.; Sala, A.; Peppoloni, S.; Blasi, E. Real-time monitoring of *Pseudomonas aeruginosa* biofilm formation on endotracheal tubes in vitro. *BMC Microbiol.* **2018**, *18*, 84. [CrossRef]
51. Astasov-Frauenhoffer, M.; Kulik, E.M. Cariogenic Biofilms and Caries from Birth to Old Age. *Monogr. Oral Sci.* **2021**, *29*, 53–64. [CrossRef]

52. Koo, H.; Xiao, J.; Klein, M.I.; Jeon, J.G. Exopolysaccharides produced by Streptococcus mutans glucosyltransferases modulate the establishment of microcolonies within multispecies biofilms. *J. Bacteriol.* **2010**, *192*, 3024–3032. [CrossRef] [PubMed]
53. Qin, X.-H.; Wang, S.-Y. Filtration properties of electrospinning nanofibers. *J. Appl. Polym. Sci.* **2006**, *102*, 1285–1290. [CrossRef]
54. Viscusi, G.; Lamberti, E.; Vittoria, V.; Gorrasi, G. Coaxial electrospun membranes of poly(ε-caprolactone)/poly(lactic acid) with reverse core-shell structures loaded with curcumin as tunable drug delivery systems. *Polym. Adv. Technol.* **2021**. [CrossRef]
55. Kabay, G.; Demirci, C.; Kaleli Can, G.; Meydan, A.E.; Daşan, B.G.; Mutlu, M. A comparative study of single-needle and coaxial electrospun amyloid-like protein nanofibers to investigate hydrophilic drug release behavior. *Int. J. Biol. Macromol.* **2018**, *114*, 989–997. [CrossRef]
56. Pant, B.; Park, M.; Park, S.J. Drug Delivery Applications of Core-Sheath Nanofibers Prepared by Coaxial Electrospinning: A Review. *Pharmaceutics* **2019**, *11*, 305. [CrossRef] [PubMed]
57. Rocha, F.R.; Regis, W.F.M.; Duarte, S.; Muniz, F.W.M.G.; Rodrigues, L.K.A. Effect of bioactive compounds on the regulation of quorum sensing network-associated genes and virulence in Streptococcus mutans—A systematic review. *Arch. Oral Biol.* **2020**, *119*, 104893. [CrossRef] [PubMed]
58. O'Loughlin, C.T.; Miller, L.C.; Siryaporn, A.; Drescher, K.; Semmelhack, M.F.; Bassler, B.L. A quorum-sensing inhibitor blocks *Pseudomonas aeruginosa* virulence and biofilm formation. *Proc. Natl. Acad. Sci. USA* **2013**, *110*, 17981. [CrossRef] [PubMed]
59. Pesci, E.C.; Pearson, J.P.; Seed, P.C.; Iglewski, B.H. Regulation of las and rhl quorum sensing in Pseudomonas aeruginosa. *J. Bacteriol.* **1997**, *179*, 3127–3132. [CrossRef]
60. Soberón-Chávez, G.; Lépine, F.; Déziel, E. Production of rhamnolipids by Pseudomonas aeruginosa. *Appl. Microbiol. Biotechnol.* **2005**, *68*, 718–725. [CrossRef] [PubMed]
61. Zhu, K.; Rock, C.O. RhlA converts beta-hydroxyacyl-acyl carrier protein intermediates in fatty acid synthesis to the beta-hydroxydecanoyl-beta-hydroxydecanoate component of rhamnolipids in Pseudomonas aeruginosa. *J. Bacteriol.* **2008**, *190*, 3147–3154. [CrossRef] [PubMed]
62. Li, Y.-H.; Tian, X.-L.; Layton, G.; Norgaard, C.; Sisson, G. Additive attenuation of virulence and cariogenic potential of Streptococcus mutans by simultaneous inactivation of the ComCDE quorum-sensing system and HK/RR11 two-component regulatory system. *Microbiology* **2008**, *154*, 3256–3265. [CrossRef] [PubMed]
63. Li, Y.-H.; Lau Peter, C.Y.; Lee Janet, H.; Ellen Richard, P.; Cvitkovitch Dennis, G. Natural Genetic Transformation ofStreptococcus mutans Growing in Biofilms. *J. Bacteriol.* **2001**, *183*, 897–908. [CrossRef] [PubMed]
64. Aggarwal, B.B.; Harikumar, K.B. Potential therapeutic effects of curcumin, the anti-inflammatory agent, against neurodegenerative, cardiovascular, pulmonary, metabolic, autoimmune and neoplastic diseases. *Int. J. Biochem. Cell Biol.* **2009**, *41*, 40–59. [CrossRef]
65. Xu, X.-Y.; Meng, X.; Li, S.; Gan, R.-Y.; Li, Y.; Li, H.-B. Bioactivity, Health Benefits, and Related Molecular Mechanisms of Curcumin: Current Progress, Challenges, and Perspectives. *Nutrients* **2018**, *10*, 1553. [CrossRef]
66. Sreedhar, R.; Arumugam, S.; Thandavarayan, R.A.; Karuppagounder, V.; Watanabe, K. Curcumin as a therapeutic agent in the chemoprevention of inflammatory bowel disease. *Drug Discov. Today* **2016**, *21*, 843–849. [CrossRef]
67. Willenbacher, E.; Khan, S.Z.; Mujica, S.C.; Trapani, D.; Hussain, S.; Wolf, D.; Willenbacher, W.; Spizzo, G.; Seeber, A. Erratum: Willenbacher, E.; et al. Curcumin: New Insights into an Ancient Ingredient against Cancer. *Int. J. Mol. Sci.* **2020**, *21*, 5725. [CrossRef]
68. Biswas, S.K.; McClure, D.; Jimenez, L.A.; Megson, I.L.; Rahman, I. Curcumin Induces Glutathione Biosynthesis and Inhibits NF-κB Activation and Interleukin-8 Release in Alveolar Epithelial Cells: Mechanism of Free Radical Scavenging Activity. *Antioxid. Redox Signal.* **2004**, *7*, 32–41. [CrossRef]
69. Portes, E.; Gardrat, C.; Castellan, A. A comparative study on the antioxidant properties of tetrahydrocurcuminoids and curcuminoids. *Tetrahedron* **2007**, *63*, 9092–9099. [CrossRef]
70. Priyadarsini, K.I.; Maity, D.K.; Naik, G.H.; Kumar, M.S.; Unnikrishnan, M.K.; Satav, J.G.; Mohan, H. Role of phenolic O-H and methylene hydrogen on the free radical reactions and antioxidant activity of curcumin. *Free Radic. Biol. Med.* **2003**, *35*, 475–484. [CrossRef]
71. Ruby, A.J.; Kuttan, G.; Dinesh Babu, K.; Rajasekharan, K.N.; Kuttan, R. Anti-tumour and antioxidant activity of natural curcuminoids. *Cancer Lett.* **1995**, *94*, 79–83. [CrossRef]
72. Saeed, N.; Khan, M.R.; Shabbir, M. Antioxidant activity, total phenolic and total flavonoid contents of whole plant extracts Torilis leptophylla L. *BMC Complementary Altern. Med.* **2012**, *12*, 221. [CrossRef]
73. Riccitiello, F.; De Luise, A.; Conte, R.; D'Aniello, S.; Vittoria, V.; Di Salle, A.; Calarco, A.; Peluso, G. Effect of resveratrol release kinetic from electrospun nanofibers on osteoblast and osteoclast differentiation. *Eur. Polym. J.* **2018**, *99*, 289–297. [CrossRef]
74. Amrati, F.e.-z.; Bourhia, M.; Slighoua, M.; Ibnemoussa, S.; Bari, A.; Ullah, R.; Amaghnouje, A.; Di Cristo, F.; El Mzibri, M.; Calarco, A.; et al. Phytochemical Study on Antioxidant and Antiproliferative Activities of Moroccan Caralluma europaea Extract and Its Bioactive Compound Classes. *Evid. Based Complementary Altern. Med.* **2020**, *2020*, 8409718. [CrossRef]
75. Conte, R.; Valentino, A.; Di Cristo, F.; Peluso, G.; Cerruti, P.; Di Salle, A.; Calarco, A. Cationic Polymer Nanoparticles-Mediated Delivery of miR-124 Impairs Tumorigenicity of Prostate Cancer Cells. *Int. J. Mol. Sci.* **2020**, *21*, 869. [CrossRef] [PubMed]
76. Calarco, A.; Bosetti, M.; Margarucci, S.; Fusaro, L.; Nicolì, E.; Petillo, O.; Cannas, M.; Galderisi, U.; Peluso, G. The genotoxicity of PEI-based nanoparticles is reduced by acetylation of polyethylenimine amines in human primary cells. *Toxicol. Lett.* **2013**, *218*, 10–17. [CrossRef]

77. Bonadies, I.; Di Cristo, F.; Valentino, A.; Peluso, G.; Calarco, A.; Di Salle, A. pH-Responsive Resveratrol-Loaded Electrospun Membranes for the Prevention of Implant-Associated Infections. *Nanomaterials* **2020**, *10*, 1175. [CrossRef]
78. Di Salle, A.; Spagnuolo, G.; Conte, R.; Procino, A.; Peluso, G.; Rengo, C. Effects of various prophylactic procedures on titanium surfaces and biofilm formation. *J. Periodontal Implant. Sci.* **2018**, *48*, 373–382. [CrossRef]
79. Calarco, A.; Di Salle, A.; Tammaro, L.; De Luca, I.; Mucerino, S.; Petillo, O.; Riccitiello, F.; Vittoria, V.; Peluso, G. Long-Term Fluoride Release from Dental Resins Affects STRO-1+ Cell Behavior. *J. Dent. Res.* **2015**, *94*, 1099–1105. [CrossRef] [PubMed]
80. Prateeksha; Rao, C.V.; Das, A.K.; Barik, S.K.; Singh, B.N. ZnO/Curcumin Nanocomposites for Enhanced Inhibition of *Pseudomonas aeruginosa* Virulence via LasR-RhlR Quorum Sensing Systems. *Mol. Pharm.* **2019**, *16*, 3399–3413. [CrossRef]
81. Li, B.; Li, X.; Lin, H.; Zhou, Y. Curcumin as a Promising Antibacterial Agent: Effects on Metabolism and Biofilm Formation in S. mutans. *BioMed Res. Int.* **2018**, *2018*, 4508709. [CrossRef] [PubMed]
82. Wang, C.; Hou, J.; van der Mei, H.C.; Busscher, H.J.; Ren, Y. Emergent Properties in Streptococcus mutans Biofilms Are Controlled through Adhesion Force Sensing by Initial Colonizers. *mBio* **2019**, *10*, e01908-19. [CrossRef] [PubMed]
83. Lenz Ailyn, P.; Williamson Kerry, S.; Pitts, B.; Stewart Philip, S.; Franklin Michael, J. Localized Gene Expression in *Pseudomonas aeruginosa* Biofilms. *Appl. Environ. Microbiol.* **2008**, *74*, 4463–4471. [CrossRef] [PubMed]

nanomaterials

MDPI

Article

pH-Responsive Resveratrol-Loaded Electrospun Membranes for the Prevention of Implant-Associated Infections

Irene Bonadies [1,†], Francesca Di Cristo [2,†], Anna Valentino [2], Gianfranco Peluso [3], Anna Calarco [3,*] and Anna Di Salle [3]

1 Institute for Polymers, Composites and Biomaterials (IPCB-CNR) Via Campi Flegrei, 34, 80078 Pozzuoli (NA), Italy; irene.bonadies@cnr.it
2 Elleva Pharma S.R.L. Via Pietro Castellino, 111, 80131 Naples, Italy; francesca.dicristo@ellevapharma.com (F.D.C.); anna.valentino@ellevapharma.com (A.V.)
3 Research Institute on Terrestrial Ecosystems (IRET)—CNR, Via Pietro Castellino 111, 80131 Naples, Italy; gianfranco.peluso@cnr.it (G.P.); anna.disalle@cnr.it (A.D.S.)
* Correspondence: anna.calarco@cnr.it
† These authors contributed equally to this work.

Received: 7 May 2020; Accepted: 12 June 2020; Published: 16 June 2020

Abstract: To date, the implant-associated infections represent a worldwide challenge for the recently reported bacterial drug resistance that can lead to the inefficacy or low efficacy of conventional antibiotic therapies. Plant polyphenolic compounds, including resveratrol (RSV), are increasingly gaining consensus as valid and effective alternatives to antibiotics limiting antibiotic resistance. In this study, electrospun polylactic acid (PLA) membranes loaded with different concentrations of RSV are synthesized and characterized in their chemical, morphological, and release features. The obtained data show that the RSV release rate from the PLA-membranes is remarkably higher in acidic conditions than at neutral pH. In addition, a change in pH from neutral to slightly acidic triggers a significant increase in the RSV release. This behavior indicates that the PLA-RSV membranes can act as drug reservoir when the environmental pH is neutral, starting to release the bioactive molecules when the pH decreases, as in presence of oral bacterial infection. Indeed, our results demonstrate that PLA-RSV2 displays a significant antibacterial and antibiofilm activity against two bacterial strains, *Pseudomonas aeruginosa* PAO1, and *Streptococcus mutans*, responsible for both acute and chronic infections in humans, thus representing a promising solution for the prevention of the implant-associated infections.

Keywords: bioresorbable membrane; phytochemicals; resveratrol; polylactic acid; electrospinning; antibiofilm

1. Introduction

Over the past decades, osseointegrated implants have emerged as a major clinical therapeutic approach to replace missing teeth or restore the structure or function of the musculoskeletal system [1]. With the increasing number of implants applied in clinical environments, evidence revealed that the device-associated infections (defined as peri-implantitis) damage the epithelial and mucosal barriers, either impeding host defense mechanisms or serving as microorganism reservoirs, leading to the failure of the implant [2]. Peri-implantitis represents a pathological condition involving both the soft and the hard tissue around implants, characterized by local tissue inflammation that may result in severe bone loss around the implant [3,4]. The inflammatory process involves proliferation of pathogenic bacteria and may occur either shortly after implantation or after several years [3]. The progressive

loss of contact between the connective tissue and the implant surface enables the bacterial biofilm to move down into the peri-implant pocket, thereby decreasing implant osseointegration. This process may be exacerbated by the oral pH drop that is a consequence of sugar consumption or sustained microorganism metabolism, as in the biofilm presence [5,6]. Indeed, when the environmental pH reaches values of <5.5, a mineral imbalance between the tooth and the salivary/plaque fluid is generated, resulting in a net tooth loss of hydroxyapatite that blocks the mineralization process [7].

The current non-surgical therapy of peri-implantitis consists of the use of strict aseptic procedures and the administration of systemic antibiotics. However, currently, there is no treatment that acts against the bacteria simultaneously promoting regeneration of the damaged tissue. Additionally, local or systemic administered antibiotics are largely ineffective for peri-implant infections due to bacterial drug resistance, poor drug penetration, and suboptimal bioavailability at the site of infection [2]. Recent studies have demonstrated the effectiveness of plant secondary metabolites (phytochemicals) where bacterial resistance mechanisms, including multidrug resistance, make traditional therapy unsuccessful, even in the control of biofilms [8,9]. In this respect, phytochemicals exert their antibacterial activity through different mechanisms of action including bacterial membrane damage, inhibition of enzymes and toxins, and bacterial biofilm formation. Therefore, plant-derived biomolecules could be used alone or as synergists/potentiators of less effective antibacterial products [8].

Resveratrol (RSV), a stilbenoid polyphenolic compound present in red wine and numerous plants, has demonstrated several health-beneficial effects such as antioxidant, anticancer, anti-inflammatory, and bone regeneration [10]. Numerous studies reported the antimicrobial activity of RSV against a wide range of bacterial [11–14], viral [15], and fungal species [14] due to the reduction of microorganism motility [16], inhibition of biofilm formation [11], and interference with quorum sensing [17]. Nevertheless, the exact mechanism of the antibacterial and antibiofilm activity of RSV remains uncertain. However, the clinical applications of these results remain controversial, due to RSV poor pharmacokinetics, low water solubility, and in vivo rapid metabolism [18,19]. The local administration into the peri-implant region could address this issue as it helps avoiding systemic degradation of RSV, increasing its therapeutic concentration.

Several studies have been conducted in the area of biomaterials to develop local drug delivery systems that are able to improve the tissue/bone regeneration and treat peri-implant bone infection which limits the osseointegration of the implant [20,21]. In this context, electrospinning represents a simple and cost-effective process to obtain, from a wide range of polymers, drug release devices with high porosity, high surface area, and nanoscale-sized fibers [22]. Electrospun loaded membranes for the treatment of peri-implantitis have been previously reported [23,24]. Li et al. and Zhang et al. fabricated poly(lactic-co-glycolic) acid (PLGA) nanofibers able to release gentamicin and vancomycin, respectively, that can prevent implanted-related infections [21,25]. In particular, PLGA-coated titanium implant with gentamicin, achieving a significant reduction in adhesion of *Staphylococcus aureus* and no cytotoxicity on osteoblasts [21]. In addition, Zhang et al. determine nanofibers with antibacterial properties both in vitro and in vivo against *S. aureus* [25]. Shahi et al. produced tetracycline-containing fibers able to inhibit the growth and the biofilm formation of peri-implantitis-associated pathogens [26]. In particular, membranes manufactured from a polymer blend solution of poly(D,L-lactic acid) (PLA), poly(ε-caprolactone) (PCL), and gelatin (GEL) with different concentrations of tetracycline were obtained. The biofilm reduction was proportional to the tetracycline content. In another research, Baranowska-Korczyc et al. synthesized electrospun PCL membranes loaded with ampicillin that exhibited a good antibacterial activity against an oral strain of *Streptococcus sanguinis* and low cytotoxic effect on gingival fibroblasts [27]. However, to date, no instances of electrospun devices incorporating phytochemicals have been reported for the treatment of peri-implant infections.

In this paper, electrospun PLA nanofiber membranes loaded with different amounts of RSV were produced, characterized, and their antibacterial and antibiofilm potential evaluated on *Pseudomonas aeruginosa* PAO1, *Streptococcus mutans*, and on a mixed culture of both bacteria to simulate the naturally occurring multispecies biofilm system (dual system).

PAO1, one of the most important Gram-negative bacteria, is responsible for both acute and chronic infections in humans. *P. aeruginosa* biofilms were reported to cause several medical device-related infections such as endocardial valve infection through endocardial tubes, ventilator-associated pneumonia, and catheter-associated urinary tract infections [28,29]. Additionally, PAO1 was recovered in patients affected by peri-implant disease in several oral sites [30].

Streptococcus mutans, a gram-positive bacterium present in the supragingival region of both healthy people and subjects with periodontal disease, is considered as one of the major contributors in the formation and development of the extracellular polysaccharide matrix in dental biofilms [31]. Indeed, after sucrose consumption, when the oral environment shows a low pH (<5.5) and a strong presence of glycan, bacterial species such as *S. mutans* start to produce water-insoluble glucan, one of the first molecules that significantly contribute to biofilm formation [32]. Then, the glucans synthesized by *S. mutans* provide the substrate for the adhesion of the latecomer bacterial strains [31,33].

The results reported herein demonstrate the ability of the PLA-RSV membranes to release RSV in a tunable and sustained manner, with a release kinetics strongly affected by the pH of the medium. Indeed, the change in pH (from neutral to slightly acidic) triggers a significant increase in the RSV release, demonstrating that the proposed membranes act as pH-responsive RSV reservoirs able to quickly release RSV only in the case of bacterial infection when the pH decreases. Our results, moreover, demonstrate the ability of PLA-RSV membranes to induce a significant antibacterial and antibiofilm activity against PAO1, *S. mutans*, and a mixed culture of both bacteria at pH < 5.5.

Taken together, the reported data suggest that PLA-RSV membranes can represent a promising solution for the prevention of the implant-associated infections, both as barrier membranes during a socket preservation period and as implant coating for prolonged time use.

2. Materials and Methods

2.1. Materials

Polylactic acid (PLA, Ingeo 4032D) with 0.7 mol% L-isomer, Mw = 2.1×10^5 g mol^{-1}, and the polydispersity (PDI) = 1.7 were supplied by NatureWorks LLC (Minnetonka, Minnesota, USA). *N*,*N*-Dimethylformamide (DMF), acetone with a purity of ≥99.8%, and resveratrol (RSV) were purchased from Sigma-Aldrich (Milan, Italy) and used without further purification.

2.2. Preparation of Electrospinning Solutions and Membrane Manufacturing

Electrospun membranes containing resveratrol were realized starting from PLA solutions containing different amounts of resveratrol. Neat PLA solutions (coded as PLA) were prepared by dissolving 12.5% wt. PLA in acetone/DMF (80/20 v/v) at 60 °C; after that, 0.8% and 3.2% wt of RSV with respect to PLA (w/w) were directly added to the polymer solution (coded as PLA-RSV1 and PLA-RSV2, respectively). The solutions were stirred before use for at least 6 h at 60 °C. All the solutions were electrospun with a NANON01 equipment (MECC Co., Ltd., Fukuoka, Japan) by using a single nozzle and a plate collector at room temperature and 10% relative humidity. After optimization of the process parameters, the flow rate was fixed at 0.5 mL h^{-1}. The applied voltage and the distance between the nozzle and the collector, which was covered with aluminum foil, were adjusted to 20 kV and 30 cm, respectively, to obtain defect-free fibers for further characterizations.

2.3. Membranes Characterization

The morphology of the membranes was evaluated using a FEI Phenom Desktop Scanning Electron Microscope (Eindhoven, The Netherlands). Before analysis, the samples were sputtered/coated with an Au-Pd alloy using a Baltec Med 020 Sputter Coater System (Leica, Milan, Italy) and then mounted on aluminum stubs. The average fiber-diameter distribution was analyzed using the ImageJ software 1.51 April 2018 (NIH, Bethesda, MD, USA).

The chemical composition of membranes was investigated by means of Fourier Transformed Infrared Spectroscopy coupled with attenuated total reflectance technique (ATR-FTIR). The spectra were acquired in the spectral region between 4000 and 400 cm^{-1}. The analysis was performed using the Origin software (OriginPro 8.1 SR0, 2009 October, OriginLab Corporation, Northampton MA, USA). Resveratrol spectrum was considered as positive control.

2.4. In Vitro Drug Release from RSV-Loaded Membranes

The RSV release was investigated as reported by Riccitiello et al. with some modifications [34]. Briefly, circular pieces of membranes (30 mm diameter) were weighed and placed into individual vials covered with aluminum foil to prevent drug degradation caused by light. The release kinetics was performed at 37 °C in artificial saliva medium containing 4 g of sucrose (SAGF-suc), as reported by Cavazana et al. [5]. The pH was adjusted to 4.8 and 6.8 with HCl and NaOH, respectively. At predetermined time intervals (every hour for 24 h, then every 3 days over 90 days), supernatants were withdrawn, and the same amount of fresh solution was added back to the release medium to maintain the sink condition. The RSV concentration was measured using HPLC-UV with a linear elution gradient consisting of mobile phase A (0.1% acetic acid), B (Acetonitrile), and C (Methanol). The detection wavelength was set at 290 nm and RSV quantitation was based on a standard curve in SAGF-suc. The resveratrol stock standard of 1 mg/mL was prepared in methanol. Before injection, the standards and samples were filtered through a 0.22 µm pore-size filter (Millipore, Milan, Italy). System control and data acquisition were performed using the ChemStation software 4.03 Jan 27, 2020 (Agilent Technologies). The results were presented in terms of cumulative release as a function of time.

2.5. Bacterial Strains and Culture Conditions

Pseudomonas aeruginosa PAO1 (ATCC® BAA-47™) and *Streptococcus mutans* (ATCC® 25175) were obtained from the American Type Culture Collection (ATCC, LGC Standards S.R.L., Sesto San Giovanni, Milan, Italy), and cultivated following the ATCC guidelines. Briefly, PAO 1 and *S. mutans* were cultured for 18 h on trypticase soy broth agar and trypticase soy yeast extract agar (Thermo Fisher Scientific, Waltham, MA, USA), respectively. Subsequently, one colony was resuspended in 5 mL of liquid broth medium and incubated overnight at 37 °C and 200 rpm.

2.6. Antibacterial Activity

The capability of the RSV-loaded membranes to inhibit bacterial growth was assessed by monitoring the bacterial growth rate. Each electrospun membrane of similar dimension, previously sterilized by UV radiation for 15 min at each side, was placed in a 12-well plate, covered with 500 µL of liquid broth supplemented with 20% of sucrose [5], and inoculated with a bacterial suspension containing a microbial concentration of approximately 1×10^7 CFU/mL. The plate was incubated at 37 °C and 200 rpm in a microplate reader (Cytation 3; AHSI, Milan, Italy). At scheduled times (6 h, 24 h, or 48 h), the optical density (OD) at 600 nm was recorded. Moreover, culture pH was monitored using a pH electrode (Mettler-Toledo, Milan, Italy).

2.7. Biofilm Analysis

Biofilm was developed as described by Di Salle et al. with some modifications [35]. Briefly, each electrospun membrane of similar dimension was sterilized by UV radiation for 15 min at each side. Then, the membranes were placed in a 48-well polystyrene plate, covered with 750 µL of liquid medium broth supplemented with 20% of sucrose and containing *S. mutans*, PAO1 or a mixed culture of both bacteria (PAO1-*S. mutans*), with a concentration of 1×10^7 CFU/mL. The cultures were incubated statically at 37 °C in a humid atmosphere for 16 h, until a mature biofilm was obtained. Liquid medium broth without bacteria was used as negative control, while 750 µL of PAO1 (1×10^7 CFU/mL), *S. mutans* (1×10^7 CFU/mL), PAO1-*S. mutans* (1×10^7 CFU/mL each), and 200 µM resveratrol were used as positive controls.

Crystal violet (CV) assay was used to determine biofilm formation, as previously described [35]. Briefly, each well was washed twice with sterile PBS for removal of non-attached bacteria, air-dried for 15 min, stained with 0.1% w/v crystal violet for 30 min, and then re-washed with 5 × PBS to remove any extra stain. Then, the stained biofilms were solubilized in 96% ethanol and absorbance measured at 570 nm using a microplate reader (Cytation 3, AHSI, Milan, Italy).

The number of biofilm viable bacterial cells was determined with the BacTiter-Glo™ Microbial Cell Viability Assay (Promega, Milan, Italy) and with the Live/Dead Cell Double Staining Kit (Sigma Aldrich, Milan, Italy). The tests were performed following the manufacturer's protocol. The BacTiterGlo™ assay is based on the luciferase reaction driven by ATP released from lysed bacterial cells. Therefore, to quantify the ATP present in the culture, 250 µL of PBS and 250 µL of BacTiter-Glo™ Reagent were added to each well, mixed, and incubated at room temperature for 5 min. The luminescence as relative light units (RLU) was measured in a microplate reader (Cytation 3, ASHI, Bernareggio, Italy) and correlated with the number of metabolically active bacteria, using an ATP calibration curve.

Staining with the LIVE/DEAD® Biofilm viability kit (Molecular Probes, Life Technologies Ltd., Milan, Italy) was performed according to the manufacturer's instructions. Briefly, a working solution of fluorescent stains was prepared by adding 3 µL of SYTO® 9 stain and 3 µL of propidium iodide (PI) stain to 1 mL of filter-sterilized water. Two hundred microliters of staining solution were deposited on the disc surface and, after 15 min incubation at room temperature in the dark, samples were washed with sterile saline in order to remove the excess dyes and rinsed with water from the base of the support material. Fluorescence was detected using Cytation 3 with 490 nm excitation for simultaneous monitoring of viable and dead cells. Measurements were carried out in triplicate for each membrane.

2.8. Statistical Analysis

All quantitative data are presented as the mean ± SD. Each experiment was performed at least three times. Student's *t* test was used for the resveratrol release. Statistical analyses for the antibacterial and antibiofilm assays were performed by 1-way analysis of variance (ANOVA) with Bonferroni's post hoc test. All the data were analyzed with the GraphPad Prism version 8.01 statistical software package (GraphPad, CA, USA).

3. Results

3.1. Membrane Characterization

Nowadays, biodegradable polymers such as aliphatic polyesters have replaced traditional non-degradable materials for biomedical application due to their ability to degrade and be absorbed by the body without elicit adverse effects [36,37]. Among them, electrospun PLA-based nanofibers represent one of the most promising drug release systems because of their superior chemical and mechanical properties, their versatility in fabrication, biodegradability, and compatibility with biomolecules and cells [38]. Riccitiello et al. fabricated uniform defect-free fibers of PCL and PLA that were able to release RSV in a tunable and sustained manner. Both membranes showed similar in vitro osteoinductive capacity on dental pulp stem cells, while the lower resveratrol-releasing membrane (PLA-RSV) was able to inhibit osteoclast differentiation [34]. The bactericidal properties of PLA membranes with high loadings of titanium dioxide nanoparticles (TiO_2) were reported by Toniatto and co-workers [39]. In addition, the nanostructured PLA/TiO_2 nanofibers demonstrated no mammalian cell toxicity, suggesting a wide range of biomedical applications.

To evaluate the effect of release media on membrane fiber morphology, stability, and release kinetic, PLA membranes with two RSV concentrations (PLA-RSV1 and PLA-RSV2) were characterized before and after the in vitro RSV release test.

SEM micrographs and diameters distribution of the PLA-RSV fibers containing different amounts of RSV are shown in Figure 1. All membranes exhibited a three-dimensional interconnected pore structure. For all analyzed compositions, fibers have a smooth and regular surface, with a uniform

uniform bead-free diameter, and no appearance of drug aggregates. A monomodal distribution was observed for all samples; the addition and the amount of RSV did not affect the average diameter of fibers that was 0.540 ± 0.103, 0.531 ± 0.075, and 0.545 ± 0.054 µm for PLA, PLA-RSV1, and PLA-RSV2, respectively.

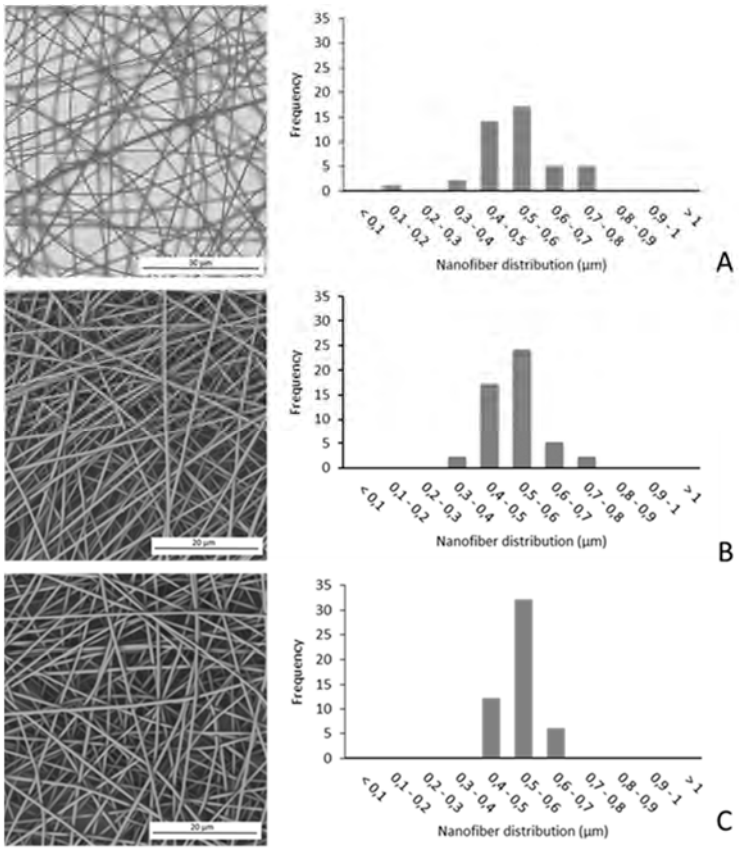

Figure 1. SEM micrographs (left) and size-distribution of fibers (right), expressed as % number (frequency), prepared from polylactic acid (PLA) solutions containing various amounts of resveratrol (RSV): (**A**) PLA; (**B**) PLA-RSV1; (**C**) PLA-RSV2.

FTIR analysis of PLA and PLA-RSV membranes revealed the characteristic peaks of both RSV and PLA (Figure 2). Despite several vibration bands of PLA and RSV overlapping, it was possible to highlight the vibration of phenol OH at 3505 cm^{-1}, the C=C aromatic double bond stretching related to the aromatic rings of RSV at 1608 cm^{-1}, the C–C olefinic stretching at 1599 cm^{-1}, and the in-plane C–H bending of phenyl rings at 1516 cm^{-1}. The intensity of RSV peaks increased with the amount of RSV in the fibers. Furthermore, peaks at 1749 cm^{-1} (C=O stretching) and 1453 cm^{-1} ($-CH_3$ bending) related to PLA were evident [40,41]. Interestingly, these peaks shifted to lower wavenumbers in comparison with the same bands in the pure RSV (3201, 1605, 1583, and 1510 cm^{-1}) and PLA (1752 cm^{-1}) spectra, indicating the presence of hydrogen-bonding interactions between the phenol OH of RSV and the carbonyl oxygen of the PLA matrix [42].

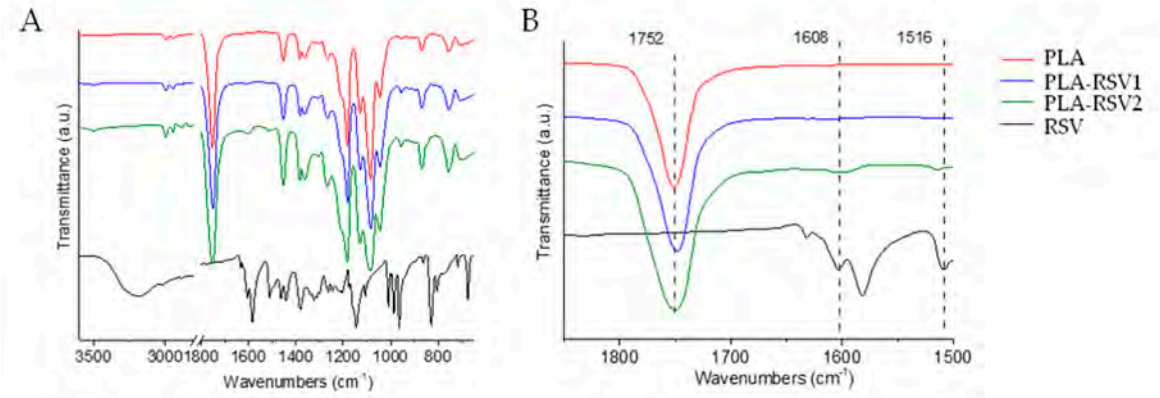

Figure 2. (**A**) FTIR-ATR spectra of RSV, neat PLA fibers, PLA fibers containing RSV1 and RSV2; **(B)** Zoom in the range of 2000–1400 cm^{-1}.

3.2. pH-Dependent RSV Release

The local delivery of a bioactive molecule from the electrospun membrane is significantly influenced by the polymer–drug interaction and the physicochemical properties of the membrane, such as drug encapsulation efficiency, drug distribution inside the micro/nanofibers, and drug release kinetics [43,44].

In particular, the mechanism of drug release from polyester nanofibers is characterized by a two-phase release behavior: first, the embedded compound desorbs through fiber nanopores or from the outer surface of the fibers in contact with the medium, then the drug captured between polymer chains is released [45,46]. To mimic the peri-implant microenvironment, characterized by subtle variations of pH level or degree of inflammation, in vitro cumulative release of RSV from PLA membranes was performed at different pH conditions, namely, pH 4.8 and pH 6.8, in artificial saliva supplemented with sucrose (SAGF-suc). As shown in Figure 3A,B, a burst release was noticed on the first day, suggesting that RSV located in the outer surface of the fibers quickly diffuses in the medium [47]. It is worth noting that in acidic conditions the RSV release rate from the PLA-RSV membranes was remarkably higher than that at neutral pH. In particular, after one day of incubation at pH 4.8, the RSV release for PLA-RSV1 and PLA-RSV2 was two- and five-fold higher, respectively, than that at pH 6.8. Subsequently, a slow but sustained release continued at pH 4.8 for 46 days, reaching a concentration of 5.57 ± 0.56 and 16.52 ± 1.62 µM at that time for PLA-RSV1 and PLA-RSV2, respectively. Instead, at neutral pH, the RSV amount released from PLA-RSV1 and PLA-RSV2 was approximately 50% and 75% lower than that released at pH 4.8 in 46 days highlighting that the effect of pH was more significant in the case of higher RSV loading. Furthermore, while 50% of RSV was released from PLA-RSV2 at the end of 46 days at pH 4.8, only 14.9% was released in the same time at pH 6.8. To better understand the impact of the pH on the RSV release, the PLA-RSV2 sample was first immersed in SAGF-suc pH 6.8 for 7 days and then transferred to pH 4.8. As shown in Figure 3B, the change in pH led to a sudden increase (~3.4-fold, $p < 0.001$) in the RSV concentration, due to the faster release of RSV entrapped in the fiber surface. It should be also noted that the slope of the release curve at pH 4.8 was about three times higher than that at pH 6.8, as the acidic pH also induced faster release of the drug captured in the bulk polymer fiber. The results demonstrate that the membranes can be stored for several days at physiological pH before RSV is quickly released when the pH decreases, as in the case of bacterial infection.

The local delivery of a bioactive molecule from the electrospun membrane is significantly influenced by the polymer–drug interaction and the physicochemical properties of the membrane, such as drug encapsulation efficiency, drug distribution inside the micro/nanofibers, and drug release kinetics [43,44].

In particular, the mechanism of drug release from polyester nanofibers is characterized by a two-phase release behavior: first, the embedded compound desorbs through fiber nanopores or from the outer surface of the fibers in contact with the medium, then the drug captured between polymer chains is released [45,46]. To mimic the peri-implant microenvironment, characterized by subtle variations of pH level or degree of inflammation, in vitro cumulative release of RSV from PLA membranes was performed at different pH conditions, namely, pH 4.8 and pH 6.8, in artificial saliva supplemented with sucrose (SAGF-suc). As shown in Figure 3A,B, a burst release was noticed on the first day, suggesting that RSV located in the outer surface of the fibers quickly diffuses in the medium [47]. It is worth noting that in acidic conditions the RSV release rate from the PLA-RSV membranes was remarkably higher than that at neutral pH. In particular, after one day of incubation at pH 4.8, the RSV release for PLA-RSV1 and PLA-RSV2 was two- and five-fold higher, respectively, than that at pH 6.8. Subsequently, a slow but sustained release continued at pH 4.8 for 46 days, reaching a concentration of 5.57 ± 0.56 and 16.52 ± 1.62 µM at that time for PLA-RSV1 and PLA-RSV2, respectively. Instead, at neutral pH, the RSV amount released from PLA-RSV1 and PLA-RSV2 was approximately 50% and 75% lower than that released at pH 4.8 in 46 days highlighting that the effect of pH was more significant in the case of higher RSV loading. Furthermore, while 50% of RSV was released from PLA-RSV2 at the end of 46 days at pH 4.8, only 14.9% was released in the same time at pH 6.8. To better understand the impact of the pH on the RSV release, the PLA-RSV2 sample was first immersed in SAGF-suc pH 6.8 for 7 days and then transferred to pH 4.8. As shown in Figure 3B, the change in pH led to a sudden increase (~3.4-fold, $p < 0.001$) in the RSV concentration, due to the faster release of RSV entrapped in the fiber surface. It should be also noted that the slope of the release curve at pH 4.8 was about three times higher than that at pH 6.8, as the acidic pH also induced faster release of the drug captured in the bulk polymer fiber. The results demonstrate that the membranes can be stored for several days at physiological pH before RSV is quickly released when the pH decreases, as in the case of bacterial infection.

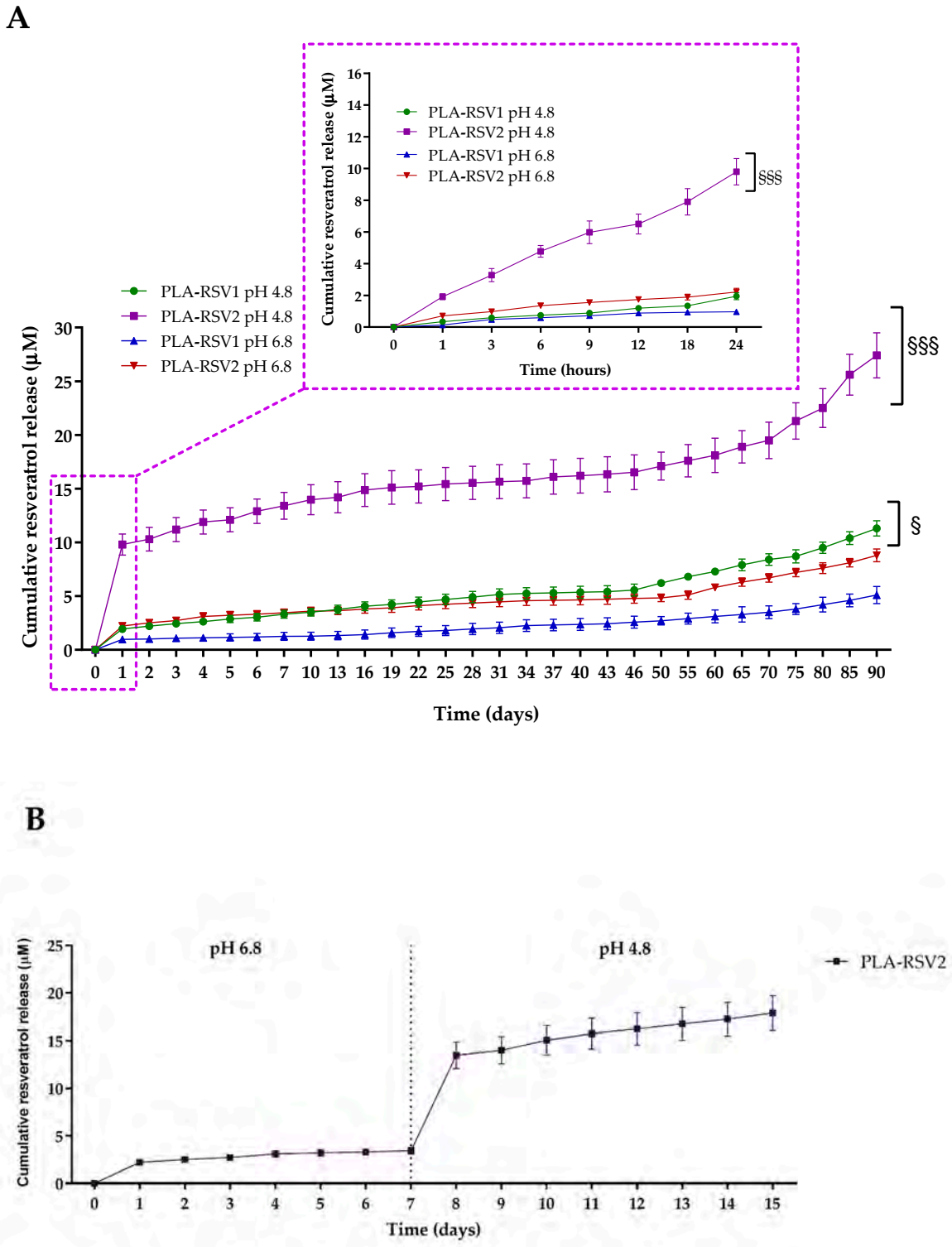

Figure 3. (**A**) In vitro drug release profiles at 37 °C of PLA-RSV membranes incubated for 46 days in artificial saliva (pH 6.8) and in SAGF simulated gastric fluid (pH 4.8) from 0 to 15 days. Profiles of PLA-RSV2 membranes in SAGF at pH 6.8 and pH 4.8 from 0 to 15 days. For each sample, six different specimens were tested, and the results expressed as the mean of the values obtained (mean ± SD). Statistically significant variations: §§§ $p < 0.001$ and § $p < 0.05$ versus pH 6.8.

The morphological analysis carried out on the samples after the release test reveals no massive deterioration of fibers even after 46 days incubation for both pH values (Figure 4). A close inspection

Nanomaterials **2020**, *10*, x FOR PEER REVIEW 9 of 18

of the polymer surface after 46 days incubation (inset in Figure 4) revealed massive fiber swelling, which led to an increase in fiber diameter proportional to the amount of RSV, and remarkably affected by the pH of the release medium.

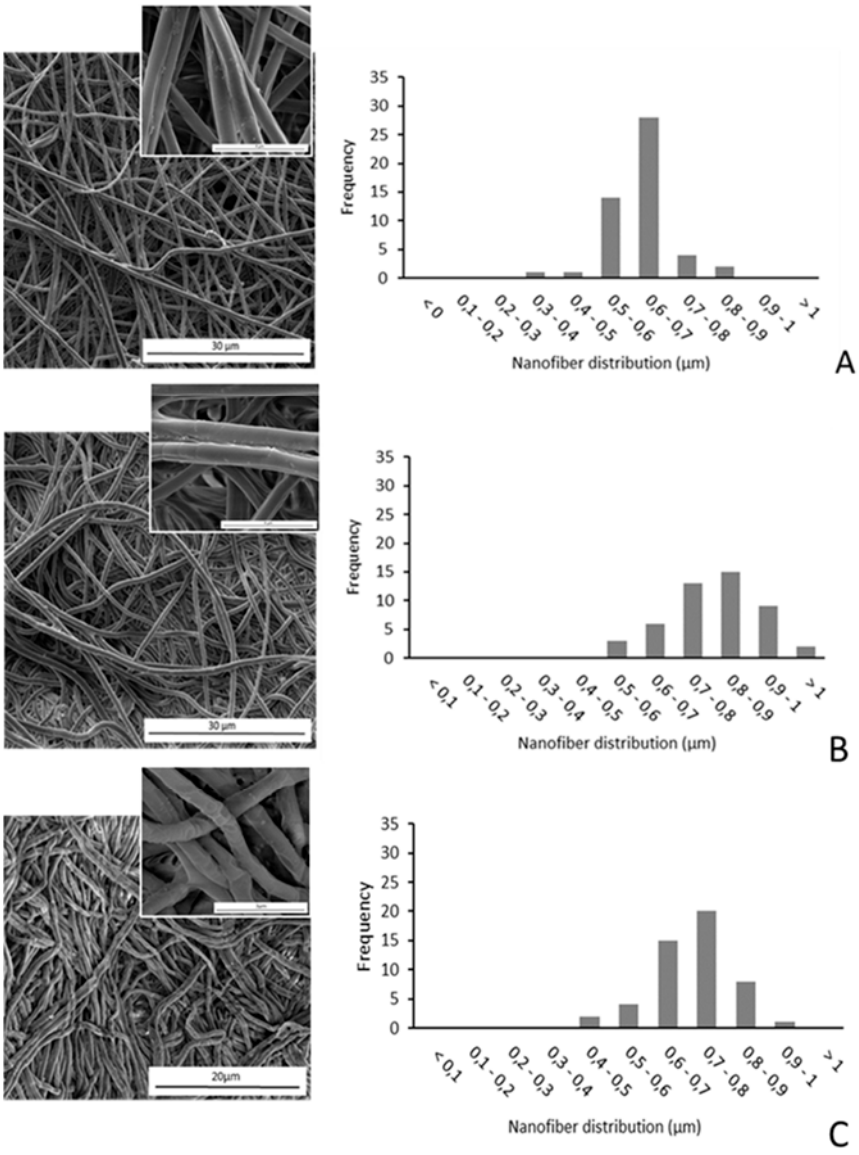

Figure 4. SEM micrographs (left) and size-distribution of fibers (right), expressed as % number (frequency), prepared from PLA solutions containing various amounts of RSV after a 46-day release test: (**A**) PLA-RSV1, pH 4.8, (**B**) PLA-RSV2, pH 4.8, (**C**) PLA-RSV2, pH 6.8.

Figure 4. SEM micrographs (left) and size-distribution of fibers (right), expressed as % number (frequency), prepared from PLA solutions containing various amounts of RSV after a 46-day release test: (**A**) PLA-RSV1, pH 4.8, (**B**) PLA-RSV2, pH 4.8, (**C**) PLA-RSV2, pH 6.8.

As shown in Figure 5, in the case of PLA-RSV2, the immersion for 46 days at pH 6.8 and 4.8 resulted in a diameter increase by about 31% and 51%, respectively. This increase in nanofiber diameters is due to the swelling process occurring during incubation in SAGF-suc for the release test. For PLA-RSV1 the diameter variation resulted negligible at both pH examined. As reported in literature, soaking of the nanofibers allows the water molecules to penetrate into the fiber interior, resulting in the swelling process. Remarkably, acidic conditions significantly enhance the ability of water to penetrate the polymer, giving rise to a higher swelling ratio [48,49].

As shown in Figure 5, in the case of PLA-RSV2, the immersion for 46 days at pH 6.8 and 4.8 resulted in a diameter increase by about 31% and 51%, respectively. This increase in nanofiber diameters is due to the swelling process occurring during incubation in SAGF-suc for the release test. For PLA-RSV1 the diameter variation resulted negligible at both pH examined. As reported in literature, soaking of the nanofibers allows the water molecules to penetrate into the fiber interior, resulting in the swelling process. Remarkably, acidic conditions significantly enhance the ability of water to penetrate the polymer, giving rise to a higher swelling ratio [48,49].

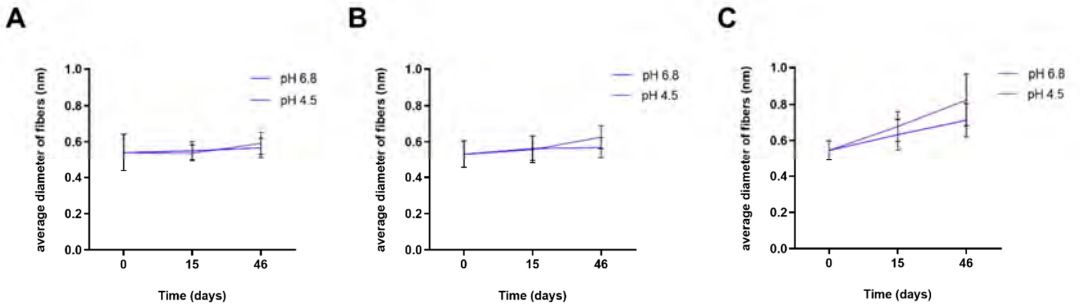

Figure 5. Average diameters of fibers prepared from PLA solutions containing various amounts of RSV after incubation in SAGF-suc (pH 4.5 and pH 6.8) for 15 and 46 days: (**A**) PLA, (**B**) PLA-RSV1, and (**C**) PLA-RSV2.

FTIR analysis of PLA and PLA-RSV membranes after incubation in the release medium at different pH values provides further insights about the release mechanism of the membranes (Figure 6). First, the decrease of the RSV peak at 1608 cm^{-1} confirms that RSV is released from the fibers. Further, a slight shift of the C=O absorption band to higher wavenumbers, from 1749 to 1751 cm^{-1}, for PLA-RSV2 at pH 4.5, was noticed after the 46-day immersion tests in the release medium, confirming the disruption of the hydrogen bonding between RSV hydroxyl and PLA carbonyl groups.

Taking into account the results gathered from SEM observations and FTIR spectroscopy, and considering that in the experimentally used pH conditions the influence of pH on the PLA degradation rate is negligible [50–52], the high RSV release is ascribed to the activity of the water molecules that provide the driving force for the RSV diffusion as the membrane swells in acidic conditions [53]. Additionally, a slightly higher RSV solubility in acidic media can further contribute to the enhancement of the RSV release at pH 4.5 [54]. It is also worth noting that for longer incubation times (Figure 5A) the shape of the release curve exhibited a significant upward deviation at times exceeding 30 days. This outcome suggests the occurrence of polymer degradation, thereby resulting in a further acceleration of the RSV release. To sum up, the overall kinetics of the RSV release was characterized by a three-phase profile. At the very beginning, the compound embedded in the outer surface quickly desorbs from the fibers. Subsequently, the drug captured in the core diffuses out of the fibers [55]. In this regard, the acidic pH enhances the water-induced swelling, which is the main reason responsible for the RSV release. Afterwards, the effect of polymer degradation on RSV release becomes more significant, giving rise to a further acceleration of RSV diffusion. It should be also noted that the effect of pH was more significant in the case of higher RSV loading.

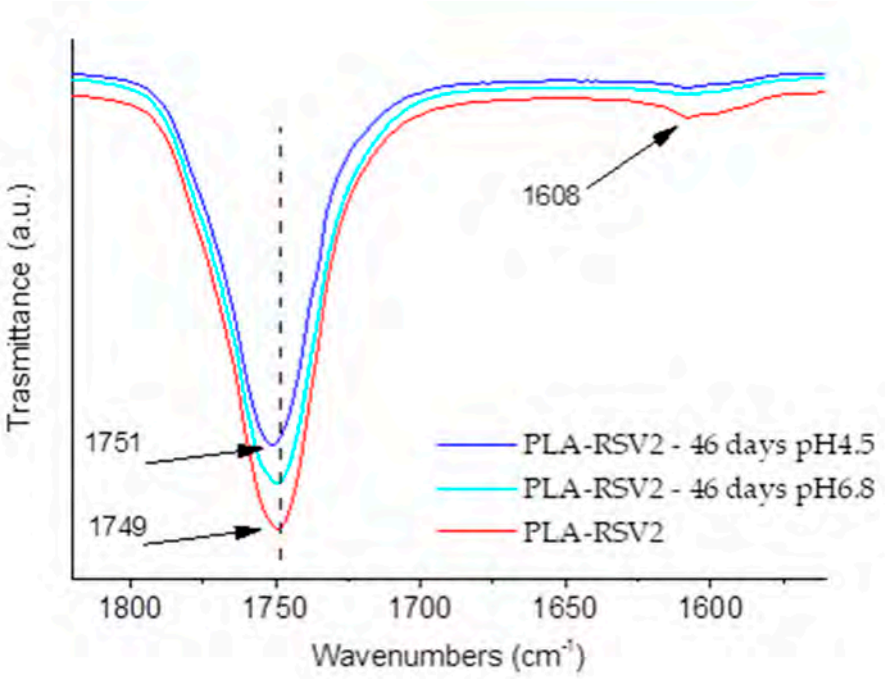

Figure 6. ATR spectra of RSV, neat PLA fibers, and PLA fibers containing RSV2 after the release test (pH 4.5 and pH 6.8—46 days) in the range of 1820–1560 cm^{-1}.

3.3. Antibacterial and Antibiofilm Activity

Phytochemicals may represent a valid alternative or adjunctive to antibiotics for mitigating implant-related infections, thanks to their reduced risk of developing resistant bacterial strains [56,57]. In addition, plant-derived compounds may exert in vitro synergistic effects when combined with conventional antibiotics [58]. Phenolic compounds, such as resveratrol, play an important role in enhancing antibiotic activity against resistant pathogens reducing, for example, the efflux pumps activity or acting as an employing EP inhibitors (EPIs) strand [14,59]. Phenolic terpenes such as carvacrol, thymol, and geraniol have been found to exhibit marked antibiofilm activity against both fungal and bacterial biofilms encountered in food processing environments and biomedicine [60,61]. Furthermore, several studies also reported the efficacy of resveratrol in the inhibition of formation and elimination of both Gram-positive and Gram-negative bacterial biofilm [13,62,63].

The capability of RSV-loaded PLA fibers to inhibit bacterial growth was determined by monitoring the growth rate of *S. mutans*, PAO1, and a mixed culture of both bacteria (PAO1-*S. mutans*) at 600 nm. The growth medium was supplemented with 20% of sucrose to mimic clinical conditions related to dental diseases such as periodontal diseases. Several studies, indeed, indicated how the presence of sugars in the diet increases the bacterial acid lactic production that lead to an environmental pH decrease [5,7].

The pH of the culture medium was measured at the beginning of the test, and after specific time-points throughout the experiment. It was found that pH reached acidic values already after the first 6 h of growth (Table 1).

Table 1. pH of the bacterial cultures.

Time	PAO1	*S. mutans*	PAO1-*S. mutans*
6 h	4.82 ± 0.26	4.86 ± 0.51	4.83 ± 0.55
12 h	4.87 ± 0.51	4.80 ± 0.46	4.85 ± 0.53
24 h	4.88 ± 0.43	4.81 ± 0.35	4.84 ± 0.39

As shown in Figure 7, the PLA-RSV2 membrane was able to significantly inhibit bacterial growth already after 12 h of incubation ($p < 0.01$). In particular, the greatest effect was observed on

Nanomaterials **2020**, *10*, x FOR PEER REVIEW 12 of 18

Pseudomonas aeruginosa at 24 h, showing a 57% of growth inhibition with respect to the control ($p < 0.001$). No effect was observed in the presence of PLA-RSV1.

Pseudomonas aeruginosa at 24 h, showing a 57% of growth inhibition with respect to the control ($p <$ 0.001). No effect was observed in the presence of PLA-RSV1.

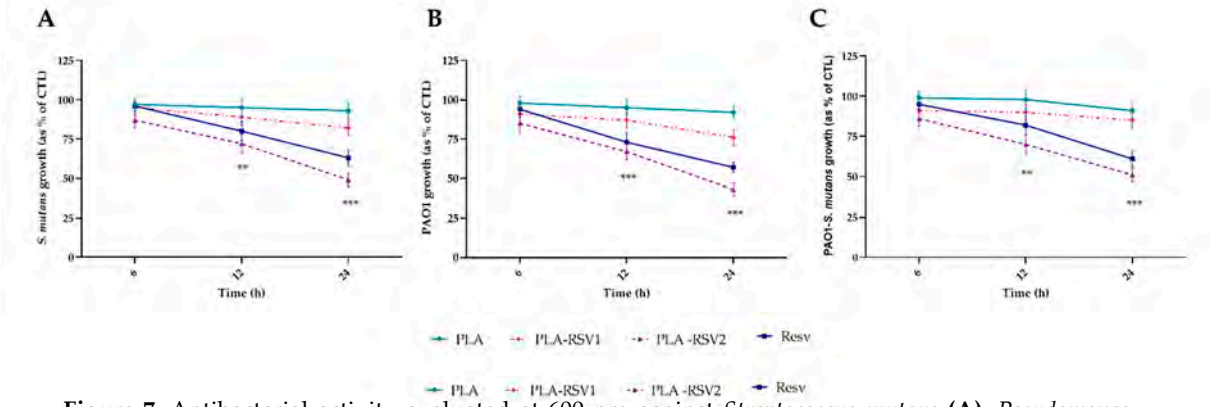

Figure 7. Antibacterial activity evaluated at 600 nm against *Streptococcus mutans* **(A)**, *Pseudomonas aeruginosa* PAO1 **(B)**, and PAO1-*S. mutans* **(C)** of PLA, PLA-RSV1, and PLA-RSV2. Bacterial growth in absence of membranes was used as bacterial positive control (CTL) while 200 uM resveratrol was used as positive standard control (RSV). Data were reported as a percentage in comparison with a bacterial positive control. For each sample, six different experiments were conducted and the results expressed as the mean of the values obtained (mean ± SD). Statistically significant variations: ** $p <$ 0.01, and *** $p < 0.001$ versus PLA and PLA-RSV1.

Figure 7. Antibacterial activity evaluated at 600 nm against *Streptococcus mutans* **(A)**, *Pseudomonas aeruginosa* PAO1 **(B)**, and PAO1-*S. mutans* **(C)** of PLA, PLA-RSV1, and PLA-RSV2. Bacterial growth in absence of membranes was used as bacterial positive control (CTL) while 200 uM resveratrol was used as positive standard control (RSV). Data were reported as a percentage in comparison with a bacterial positive control. For each sample, six different experiments were conducted and the results expressed as the mean of the values obtained (mean ± SD). Statistically significant variations: ** $p <$ 0.01, and *** $p < 0.001$ versus PLA and PLA-RSV1.

Biofilm inhibition was analyzed at different times in order to evaluate the resveratrol effect on biofilm development. As shown in Figure 8, a significant reduction ($p < 0.001$) in biofilm formation analyzed with CV assay, regardless of the bacterial strain used, was observed only in PLA-RSV2 membrane. Already after 6 h of incubation in presence of the membrane, a reduction of about 77 ± 8%, 60 ± 6%, and 65 ± 6% was detected in *S. mutans*, PAO1, and PAO1-*S. mutans* biofilm, respectively, and it was attributed to the release of resveratrol from the membrane. After 24 h of incubation, the reduction ranged from 27 ± 3% for *S. mutans* biofilm to 52 ± 5% for PAO1 biofilm.

Biofilm inhibition was analyzed at different times in order to evaluate the resveratrol effect on biofilm development. As shown in Figure 8, a significant reduction ($p < 0.001$) in biofilm formation analyzed with CV assay, regardless of the bacterial strain used, was observed only in PLA-RSV2 membrane. Already after 6 h of incubation in presence of the membrane, a reduction of about 77 ± 8%, 60 ± 6%, and 65 ± 6% was detected in *S. mutans*, PAO1, and PAO1-*S. mutans* biofilm, respectively, and it was attributed to the release of resveratrol from the membrane. After 24 h of incubation, the reduction ranged from 27 ± 3% for *S. mutans* biofilm to 52 ± 5% for PAO1 biofilm.

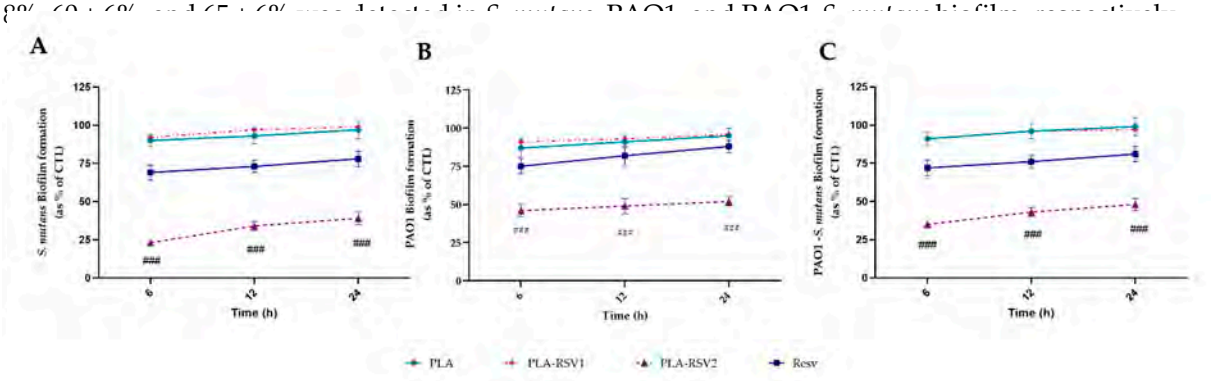

Figure 8. Antibiofilm activity of RSV-loading membranes. Biofilm formation was evaluated by crystal violet (CV) assay, after 6, 12, and 24 h of incubation at 37 °C in presence of **(A)** *Streptococcus mutans*, **(B)** PAO1, and **(C)** PAO1-*S. mutans* as described in the material and methods section. Biofilm formation was reported as a percentage in comparison with to the maximum amount of biofilm produced by *Streptococcus mutans*, PAO1, and PAO1-*S. mutans* grown (bacterial positive controls). A total of 200 uM resveratrol was used as positive standard control (RSV). For each sample, six different experiments were conducted, and the results expressed as the mean of the values obtained (mean ± SD). Statistically significant variations: ### $p < 0.001$ versus RSV, PLA, and PLA-RSV1.

Figure 8. Antibiofilm activity of RSV-loading membranes. Biofilm formation was evaluated by crystal violet (CV) assay, after 6, 12, and 24 h of incubation at 37 °C in presence of **(A)** *Streptococcus mutans*, **(B)** PAO1, and **(C)** PAO1-*S. mutans* as described in the material and methods section. Biofilm formation was reported as a percentage in comparison with to the maximum amount of biofilm produced by *Streptococcus mutans*, PAO1, and PAO1-*S. mutans* grown (bacterial positive controls). A total of 200 uM resveratrol was used as positive standard control (RSV). For each sample, six different experiments were conducted, and the results expressed as the mean of the values obtained (mean ± SD). Statistically significant variations: ### $p < 0.001$ versus RSV, PLA, and PLA-RSV1.

Metabolic analysis of biofilm, performed quantifying the amount of cellular adenosine triphosphate (ATP) that is directly related to bacterial metabolic activity [64], confirmed the CV results.

Metabolic analysis of biofilm, performed quantifying the amount of cellular adenosine triphosphate (ATP) that is directly related to bacterial metabolic activity [64], confirmed the CV results.

Figure 9 shown that PLA-RSV2 membrane was able to reduce biofilm activity already at 6 h and maintaining its activity until 24 h. The observed reduction after 6 h of incubation ranged from 27 ± 3% for *S. mutans* biofilm to 52 ± 5% for PAO1 biofilm.

Nanomaterials **2020**, *10*, 1175 13 of 18

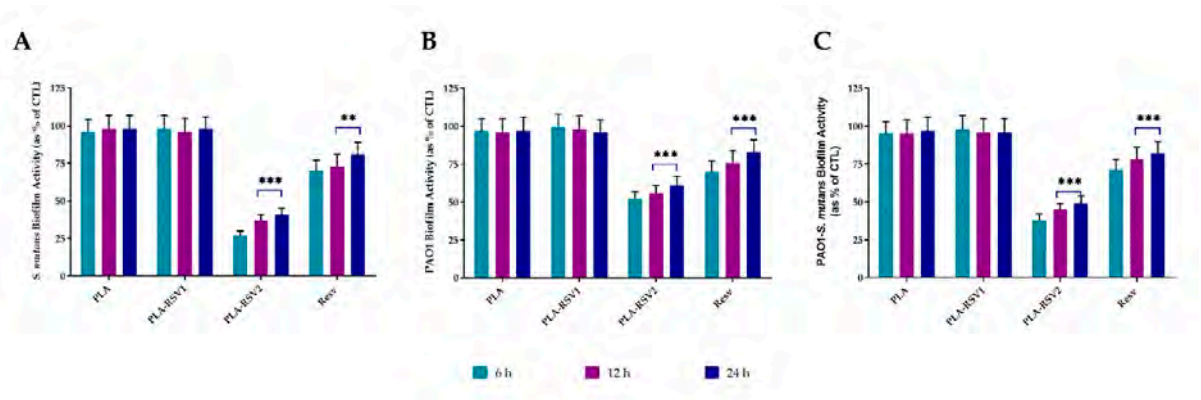

Figure 9. Biofilm metabolic activity of RSV-loading membranes. Biofilm metabolic reduction was quantified using BacTiterGlo™ assay and correlating the recorded luminescence with ATP nmoles, after 6, 12, and 24 h of incubation at 37 °C in presence of (**A**) *Streptococcus mutans*, (**B**) PAO1, and (**C**) PAO1-*S. mutans* as described in the material and methods section. Biofilm activity was reported as a percentage in comparison with positive bacterial controls. A total of 200 µM resveratrol was used as positive standard control (RSV). For each sample, six different experiments were conducted, and the results expressed as the mean of the values obtained (mean ± SD). Statistically significant variations: ** $p < 0.01$ and *** $p < 0.001$ versus PLA and PLA-RSV1.

Figure 9. Biofilm metabolic activity of RSV-loading membranes. Biofilm metabolic reduction was quantified using BacTiterGlo™ assay and correlating the recorded luminescence with APT nmoles, after 6, 12, and 24 h of incubation at 37 °C in presence of (**A**) *Streptococcus mutans*, (**B**) PAO1, and (**C**) PAO1-*S. mutans* as described in the material and methods section. Biofilm activity was reported as a percentage in comparison with positive bacterial controls. A total of 200 µM resveratrol was used as positive standard control (RSV). For each sample, six different experiments were conducted, and the results expressed as the mean of the values obtained (mean ± SD). Statistically significant variations: ** $p < 0.01$ and *** $p < 0.001$ versus PLA and PLA-RSV1.

The susceptibility of *S. mutans* and *P. aeruginosa* to RSV was further evaluated via the Live/Dead BacLight Bacterial Viability Kit. The fluorescent dye Syto 9 (green) penetrates bacterial membrane of both live and dead bacteria, while propidium iodide (red) selectively enters damaged bacteria membrane allowing differentiation between live and dead cells [65].

The susceptibility of *S. mutans* and *P. aeruginosa* to RSV was further evaluated via the Live/Dead BacLight Bacterial Viability Kit. The fluorescent dye Syto 9 (green) penetrates bacterial membrane of both live and dead bacteria, while propidium iodide (red) selectively enters damaged bacteria membrane allowing differentiation between live and dead cells [65].

As shown in Figure 10A,E,I, PLA membrane exhibited a well-organized, undisturbed biofilm with a lower live/dead cell ratio indicative of a general bacterial population in stationary phase growth. According to the BacTiterGlo™ results, there were no significant changes in viability of biofilm formed by *Streptococcus mutans* (Figure 10C), PAO1 (Figure 10G), and PAO1-*S. mutans* (Figure 10K) on PLA-RSV1 membranes in regards to PLA. In contrast, the biofilm formed by *S. mutans* or PAO1-*S. mutans* on PLA-RSV2 membrane (Figure 10D,H) represents a lessened biofilm mass/architecture with a significant proportion of dead cells confirming the antibacterial activity of the manufactured membrane. In the case of PAO1 (Figure 10L), an overlap between red and green was observed (labeled as yellow), which indicates the initial stages of apoptotic processes. Biofilm treated with 200 µM RSV exhibited a higher live/dead cell ratio in regards to PLA membrane for all the microorganisms analyzed (Figure 10B,F,J). Thus, these qualitative findings further confirmed that the newly fabricated PLA-RSV2 membrane possessed good antibiofilm activity inducing a cell membrane damage.

As shown in Figure 10A,E,I, PLA membrane exhibited a well-organized, undisturbed biofilm with a lower live/dead cell ratio indicative of a general bacterial population in stationary phase growth. According to the BacTiterGlo™ results, there were no significant changes in viability of biofilm formed by *Streptococcus mutans* (Figure 10C), PAO1 (Figure 10G), and PAO1-*S. mutans* (Figure 10K) on PLA-RSV1 membranes in regards to PLA. In contrast, the biofilm formed by *S. mutans* or PAO1-*S. mutans* on PLA-RSV2 membrane (Figure 10D,H) represents a lessened biofilm mass/architecture with a significant proportion of dead cells confirming the antibacterial activity of the manufactured membrane. In the case of PAO1 (Figure 10L), an overlap between red and green was observed (labeled as yellow), which indicates the initial stages of apoptotic processes. Biofilm treated with 200 µM RSV exhibited a higher live/dead cell ratio in regards to PLA membrane for all the microorganisms analyzed (Figure 10B,F,J). Thus, these qualitative findings further confirmed that the newly fabricated PLA-RSV2 membrane possessed good antibiofilm activity inducing a cell membrane damage.

Thus, these qualitative findings further confirmed that the newly fabricated PLA-RSV2 membrane possessed good antibiofilm activity inducing a cell membrane damage.

Nanomaterials **2020**, *10*, x FOR PEER REVIEW 14 of 18

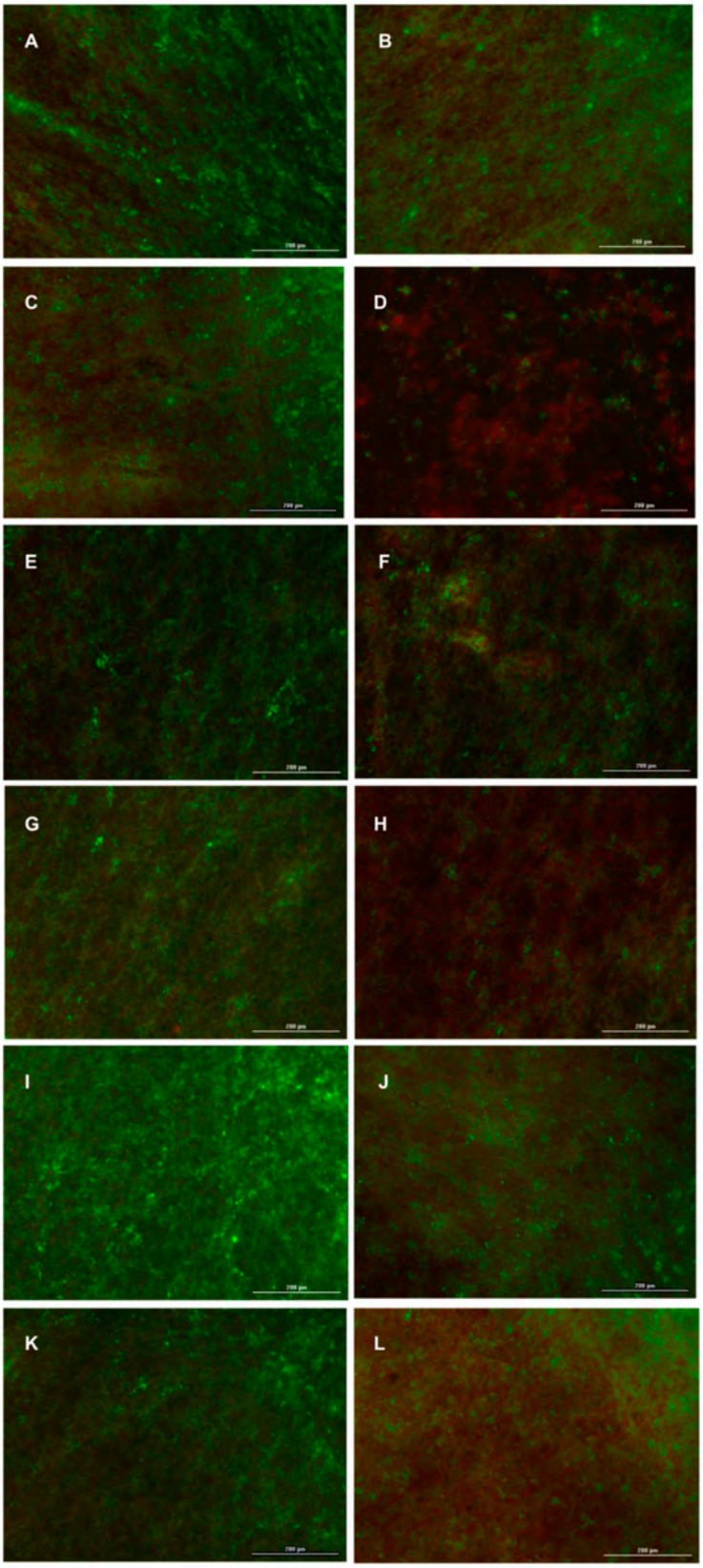

Figure 10. Fluorescent microscopy images of live/dead staining of (**A**–**D**) *S. mutans*, (**E**–**H**) PAO1, and (**I**–**L**) *S. mutans*/PAO1 on (**A**,**B**,**E**,**F**,**I**,**J**) PLA, (**C**,**G**,**K**) PLA-RSV1, and (**D**,**H**,**L**) PLA-RSV2. RSV was used as positive control (**B**,**F**,**J**). Live bacteria were stained green, and dead bacteria were stained red. Live and dead bacteria in proximity resulted in yellow/orange color.

Taken together, these results indicated that the PLA-RSV2 membrane was able to control the biofilm formation process inhibiting the bacterial ability to reproduce and form a mature biofilm during the 24 h. Indeed, PLA-RSV2 released a resveratrol concentration capable of producing a significant antimicrobial and antibiofilm effect already after 6 h of incubation.

4. Conclusions

In this paper, electrospun PLA nanofiber membranes loaded with different amounts of RSV were produced, characterized, and their antibacterial and antibiofilm potential evaluated on *Pseudomonas aeruginosa* PAO1 and *Streptococcus mutans* responsible for both acute and chronic infections in humans. The reported results demonstrated that resveratrol released from PLA-RSV2 membrane was able to induce, already after 6 h, a significant decrease of both bacterial growth and biofilm formation. Moreover, the PLA-RSV membranes capability to release RSV only at pH < 5.5 (as in presence of oral bacterial infection) acting as drug reservoir when the environmental pH is neutral, represents an interesting solution in the prevention of implant-associated infections. For this purpose, the PLA-RSV membranes could be used both as barrier membranes during socket preservation period and as implant coating for prolonged time use, taking advance of their pH-responsive release ability.

Author Contributions: Conceptualization, A.C. and A.D.S.; investigation, I.B., A.V., and F.D.C.; writing—original draft preparation, I.B., A.D.S., G.P. and A.C.; writing—review and editing, I.B., A.D.S., and A.C.; supervision, A.D.S. and A.C.; funding acquisition, A.C. and G.P. All authors have read and agreed to the published version of the manuscript.

Funding: This research was financially supported by the PON 03 PE_00110_1/ptd1_000410 Titolo: Sviluppo di nanotecnologie Orientate alla Rigenerazione e Ricostruzione tissutale, Implantologia e Sensoristica in Odontoiatria/oculistica (SORRISO); POR Campania FESR 2014_2020 "Tecnologie abilitanti per la sintesi eco-sostenibile di nuovi materiali per la restaurativa dentale"—ABILTECH, and EU funding within the Horizon 2020 Program, under the MSCA-RISE 2016 Project "VAHVISTUS" (Grant 734759).

Acknowledgments: The authors thank Orsolina Petillo for her technical support and editorial assistance. The authors gratefully acknowledge Cristina Del Barone (IPCB-CNR) for her support with electron microscopy analysis.

Conflicts of Interest: The authors declare no conflict of interest.

References

1. Zderic, I.; Steinmetz, P.; Benneker, L.M.; Sprecher, C.; Röhrle, O.; Windolf, M.; Boger, A.; Gueorguiev, B. Bone cement allocation analysis in artificial cancellous bone structures. *J. Orthop. Translat.* **2017**, *8*, 40–48. [CrossRef] [PubMed]
2. Arciola, C.R.; Campoccia, D.; Montanaro, L. Implant infections: Adhesion, biofilm formation and immune evasion. *Nat. Rev. Microbiol.* **2018**, *16*, 397–409. [CrossRef] [PubMed]
3. Peixoto, C.D.; Almas, K. The implant surface characteristics and peri-implantitis. An evidence-based update. *Odontostomatol. Trop.* **2016**, *39*, 23–35. [PubMed]
4. Schwarz, F.; Derks, J.; Monje, A.; Wang, H.L. Peri-implantitis. *J. Periodontol.* **2018**, *89* (Suppl. 1), S267–S290. [CrossRef] [PubMed]
5. Cavazana, T.P.; Pessan, J.P.; Hosida, T.Y.; Monteiro, D.R.; Botazzo Delbem, A.C. pH changes of mixed biofilms of Streptococcus mutans and Candida albicans after exposure to sucrose solutions in vitro. *Arch. Oral Biol.* **2018**, *90*, 9–12. [CrossRef] [PubMed]
6. Bowen, W.H. The Stephan Curve revisited. *Odontology* **2013**, *101*, 2–8. [CrossRef]
7. Fejerskov, O. Changing Paradigms in Concepts on Dental Caries: Consequences for Oral Health Care. *Caries Res.* **2004**, *38*, 182–191. [CrossRef]
8. Barbieri, R.; Coppo, E.; Marchese, A.; Daglia, M.; Sobarzo-Sánchez, E.; Nabavi, S.F.; Nabavi, S.M. Phytochemicals for human disease: An update on plant-derived compounds antibacterial activity. *Microbiol. Res.* **2017**, *196*, 44–68. [CrossRef]
9. Lahiri, D.; Dash, S.; Dutta, R.; Nag, M. Elucidating the effect of anti-biofilm activity of bioactive compounds extracted from plants. *J. Biosci.* **2019**, *44*, 52. [CrossRef]

10. Salehi, B.; Mishra, A.P.; Nigam, M.; Sener, B.; Kilic, M.; Sharifi-Rad, M.; Fokou, P.V.T.; Martins, N.; Sharifi-Rad, J. Resveratrol: A Double-Edged Sword in Health Benefits. *Biomedicines* **2018**, *6*, 91. [CrossRef]
11. He, Z.; Huang, Z.; Zhou, W.; Tang, Z.; Ma, R.; Liang, J. Anti-biofilm Activities from Resveratrol against Fusobacterium nucleatum. *Front. Microbiol.* **2016**, *7*, 1065. [CrossRef] [PubMed]
12. Lee, J.H.; Cho, H.S.; Joo, S.W.; Chandra Regmi, S.; Kim, J.A.; Ryu, C.M.; Ryu, S.Y.; Cho, M.H.; Lee, J. Diverse plant extracts and trans-resveratrol inhibit biofilm formation and swarming of Escherichia coli O157:H7. *Biofouling* **2013**, *29*, 1189–1203. [CrossRef] [PubMed]
13. Lee, J.H.; Kim, Y.G.; Raorane, C.J.; Ryu, S.Y.; Shim, J.J.; Lee, J. The anti-biofilm and anti-virulence activities of trans-resveratrol and oxyresveratrol against uropathogenic Escherichia coli. *Biofouling* **2019**, *35*, 758–767. [CrossRef] [PubMed]
14. Vestergaard, M.; Ingmer, H. Antibacterial and antifungal properties of resveratrol. *Int. J. Antimicrob. Agents* **2019**, *53*, 716–723. [CrossRef] [PubMed]
15. Abba, Y.; Hassim, H.; Hamzah, H.; Noordin, M.M. Antiviral Activity of Resveratrol against Human and Animal Viruses. *Adv. Virol.* **2015**, *2015*, 184241. [CrossRef]
16. Haranahalli, K.; Tong, S.; Ojima, I. Recent advances in the discovery and development of antibacterial agents targeting the cell-division protein FtsZ. *Bioorg. Med. Chem.* **2016**, *24*, 6354–6369. [CrossRef] [PubMed]
17. Truchado, P.; Tomás-Barberán, F.A.; Larrosa, M.; Allende, A. Food phytochemicals act as Quorum Sensing inhibitors reducing production and/or degrading autoinducers of Yersinia enterocolitica and Erwinia carotovora. *Food Control* **2012**, *24*, 78–85. [CrossRef]
18. Chimento, A.; De Amicis, F.; Sirianni, R.; Sinicropi, M.S.; Puoci, F.; Casaburi, I.; Saturnino, C.; Pezzi, V. Progress to Improve Oral Bioavailability and Beneficial Effects of Resveratrol. *Int. J. Mol. Sci.* **2019**, *20*, 1381. [CrossRef]
19. Machado, N.D.; Fernández, M.A.; Díaz, D.D. Recent Strategies in Resveratrol Delivery Systems. *ChemPlusChem* **2019**, *84*, 951–973. [CrossRef]
20. Dorati, R.; DeTrizio, A.; Modena, T.; Conti, B.; Benazzo, F.; Gastaldi, G.; Genta, I. Biodegradable Scaffolds for Bone Regeneration Combined with Drug-Delivery Systems in Osteomyelitis Therapy. *Pharmaceuticals* **2017**, *10*, 96. [CrossRef] [PubMed]
21. Li, L.; Zhou, G.; Wang, Y.; Yang, G.; Ding, S.; Zhou, S. Controlled dual delivery of BMP-2 and dexamethasone by nanoparticle-embedded electrospun nanofibers for the efficient repair of critical-sized rat calvarial defect. *Biomaterials* **2015**, *37*, 218–229. [CrossRef] [PubMed]
22. Pillay, V.; Dott, C.; Choonara, Y.E.; Tyagi, C.; Tomar, L.; Kumar, P.; du Toit, L.C.; Ndesendo, V.M.K. A Review of the Effect of Processing Variables on the Fabrication of Electrospun Nanofibers for Drug Delivery Applications. *J. Nanomater.* **2013**, *2013*, 789289. [CrossRef]
23. Lian, M.; Sun, B.; Qiao, Z.; Zhao, K.; Zhou, X.; Zhang, Q.; Zou, D.; He, C.; Zhang, X. Bi-layered electrospun nanofibrous membrane with osteogenic and antibacterial properties for guided bone regeneration. *Colloids Surf. B* **2019**, *176*, 219–229. [CrossRef] [PubMed]
24. Wang, J.; Zhan, L.; Zhang, X.; Wu, R.; Liao, L.; Wei, J. Silver Nanoparticles Coated Poly (L-Lactide) Electrospun Membrane for Implant Associated Infections Prevention. *Front. Pharmacol.* **2020**, *11*, 431. [CrossRef] [PubMed]
25. Zhang, L.; Yan, J.; Yin, Z.; Tang, C.; Guo, Y.; Li, D.; Wei, B.; Xu, Y.; Gu, Q.; Wang, L. Electrospun vancomycin-loaded coating on titanium implants for the prevention of implant-associated infections. *Int. J. Nanomed.* **2014**, *9*, 3027–3036. [CrossRef]
26. Shahi, R.G.; Albuquerque, M.T.P.; Münchow, E.A.; Blanchard, S.B.; Gregory, R.L.; Bottino, M.C. Novel bioactive tetracycline-containing electrospun polymer fibers as a potential antibacterial dental implant coating. *Odontology* **2017**, *105*, 354–363. [CrossRef]
27. Baranowska-Korczyc, A.; Warowicka, A.; Jasiurkowska-Delaporte, M.; Grześkowiak, B.; Jarek, M.; Maciejewska, B.M.; Jurga-Stopa, J.; Jurga, S. Antimicrobial electrospun poly(ε-caprolactone) scaffolds for gingival fibroblast growth. *RSC Adv.* **2016**, *6*, 19647–19656. [CrossRef]
28. Maurice, N.M.; Bedi, B.; Sadikot, R.T. Pseudomonas aeruginosa Biofilms: Host Response and Clinical Implications in Lung Infections. *Am. J. Respir. Cell Mol. Biol.* **2018**, *58*, 428–439. [CrossRef]
29. Pericolini, E.; Colombari, B.; Ferretti, G.; Iseppi, R.; Ardizzoni, A.; Girardis, M.; Sala, A.; Peppoloni, S.; Blasi, E. Real-time monitoring of Pseudomonas aeruginosa biofilm formation on endotracheal tubes in vitro. *BMC Microbiol.* **2018**, *18*, 84. [CrossRef]

30. Canullo, L.; Rossetti, P.H.; Penarrocha, D. Identification of Enterococcus Faecalis and Pseudomonas Aeruginosa on and in Implants in Individuals with Peri-implant Disease: A Cross-Sectional Study. *Int. J. Oral Maxillofac. Implants* **2015**, *30*, 583–587. [CrossRef]
31. Koo, H.; Xiao, J.; Klein, M.I.; Jeon, J.G. Exopolysaccharides produced by Streptococcus mutans glucosyltransferases modulate the establishment of microcolonies within multispecies biofilms. *J. Bacteriol.* **2010**, *192*, 3024–3032. [CrossRef] [PubMed]
32. Dani, S.; Prabhu, A.; Chaitra, K.R.; Desai, N.C.; Patil, S.R.; Rajeev, R. Assessment of Streptococcus mutans in healthy versus gingivitis and chronic periodontitis: A clinico-microbiological study. *Contemp. Clin. Dent.* **2016**, *7*, 529–534. [CrossRef] [PubMed]
33. Yang, Y.; Mao, M.; Lei, L.; Li, M.; Yin, J.; Ma, X.; Tao, X.; Yang, Y.; Hu, T. Regulation of water-soluble glucan synthesis by the Streptococcus mutans dexA gene effects biofilm aggregation and cariogenic pathogenicity. *Mol. Oral Microbiol.* **2019**, *34*, 51–63. [CrossRef] [PubMed]
34. Riccitiello, F.; De Luise, A.; Conte, R.; D'Aniello, S.; Vittoria, V.; Di Salle, A.; Calarco, A.; Peluso, G. Effect of resveratrol release kinetic from electrospun nanofibers on osteoblast and osteoclast differentiation. *Eur. Polym. J.* **2018**, *99*, 289–297. [CrossRef]
35. Di Salle, A.; Spagnuolo, G.; Conte, R.; Procino, A.; Peluso, G.; Rengo, C. Effects of various prophylactic procedures on titanium surfaces and biofilm formation. *J. Periodontal. Implant. Sci.* **2018**, *48*, 373–382. [CrossRef] [PubMed]
36. Conte, R.; Di Salle, A.; Riccitiello, F.; Petillo, O.; Peluso, G.; Calarco, A. Biodegradable polymers in dental tissue engineering and regeneration. *AIMS Mater. Sci.* **2018**, *5*, 1073–1101. [CrossRef]
37. Manavitehrani, I.; Fathi, A.; Badr, H.; Daly, S.; Negahi Shirazi, A.; Dehghani, F. Biomedical Applications of Biodegradable Polyesters. *Polymers* **2016**, *8*, 20. [CrossRef]
38. Narayanan, G.; Vernekar, V.N.; Kuyinu, E.L.; Laurencin, C.T. Poly (lactic acid)-based biomaterials for orthopaedic regenerative engineering. *Adv. Drug Deliv. Rev.* **2016**, *107*, 247–276. [CrossRef] [PubMed]
39. Toniatto, T.V.; Rodrigues, B.V.M.; Marsi, T.C.O.; Ricci, R.; Marciano, F.R.; Webster, T.J.; Lobo, A.O. Nanostructured poly (lactic acid) electrospun fiber with high loadings of TiO(2) nanoparticles: Insights into bactericidal activity and cell viability. *Mater. Sci. Eng. C* **2017**, *71*, 381–385. [CrossRef] [PubMed]
40. Agarwal, A.; Kharb, V.; Saharan, V. Process optimisation, characterisation and evaluation of resveratrol-phospholipid complexes using Box-Behnken statistical design. *Int. Curr. Pharm. J.* **2014**, *3*, 301–308. [CrossRef]
41. Bonadies, I.; Longo, A.; Androsch, R.; Jehnichen, D.; Göbel, M.; Di Lorenzo, M.L. Biodegradable electrospun PLLA fibers containing the mosquito-repellent DEET. *Eur. Polym. J.* **2019**, *113*, 377–384. [CrossRef]
42. Mamidi, N.; Romo, I.L.; Barrera, E.V.; Elías-Zúñiga, A. High throughput fabrication of curcumin embedded gelatin-polylactic acid forcespun fiber-aligned scaffolds for the controlled release of curcumin. *MRS Commun.* **2018**, *8*, 1395–1403. [CrossRef]
43. Chen, S.; Li, R.; Li, X.; Xie, J. Electrospinning: An enabling nanotechnology platform for drug delivery and regenerative medicine. *Adv. Drug Deliv. Rev.* **2018**, *132*, 188–213. [CrossRef]
44. Thakkar, S.; Misra, M. Electrospun polymeric nanofibers: New horizons in drug delivery. *Eur. J. Pharm. Sci.* **2017**, *107*, 148–167. [CrossRef] [PubMed]
45. Ding, J.; Zhang, J.; Li, J.; Li, D.; Xiao, C.; Xiao, H.; Yang, H.; Zhuang, X.; Chen, X. Electrospun polymer biomaterials. *Prog. Polym. Sci.* **2019**, *90*, 1–34. [CrossRef]
46. Srikar, R.; Yarin, A.L.; Megaridis, C.M.; Bazilevsky, A.V.; Kelley, E. Desorption-limited mechanism of release from polymer nanofibers. *Langmuir* **2008**, *24*, 965–974. [CrossRef]
47. Toncheva, A.; Paneva, D.; Manolova, N.; Rashkov, I. Electrospun poly (L-lactide) membranes containing a single drug or multiple drug system for antimicrobial wound dressings. *Macromol. Res.* **2011**, *19*, 1310–1319. [CrossRef]
48. Magiera, A.; Markowski, J.; Pilch, J.; Blazewicz, S. Degradation Behavior of Electrospun PLA and PLA/CNT Nanofibres in Aqueous Environment. *J. Nanomater.* **2018**, *2018*, 8796583. [CrossRef]
49. Mucha, M.; Michalak, I.; Draczyński, Z. Modified Dibutyrylchitin Films as Matrices for Controlled Ibuprofen Release. *Prog. Chem. Appl. Chitin Deriv.* **2013**, *18*, 139–147.
50. Codari, F.; Lazzari, S.; Soos, M.; Storti, G.; Morbidelli, M.; Moscatelli, D. Kinetics of the hydrolytic degradation of poly(lactic acid). *Polym. Degrad. Stab.* **2012**, *97*, 2460–2466. [CrossRef]

51. Nobile, M.R.; Cerruti, P.; Malinconico, M.; Pantani, R. Processing and properties of biodegradable compounds based on aliphatic polyesters. *J. Appl. Polym. Sci.* **2015**, *132*, 42481. [CrossRef]
52. Pistner, H.; Gutwald, R.; Ordung, R.; Reuther, J.; Mühling, J. Poly(l-lactide): A long-term degradation study in vivo: I. Biological results. *Biomaterials* **1993**, *14*, 671–677. [CrossRef]
53. Bode, C.; Kranz, H.; Fivez, A.; Siepmann, F.; Siepmann, J. Often neglected: PLGA/PLA swelling orchestrates drug release: HME implants. *J. Control. Release* **2019**, *306*, 97–107. [CrossRef] [PubMed]
54. Zupančič, Š.; Lavrič, Z.; Kristl, J. Stability and solubility of trans-resveratrol are strongly influenced by pH and temperature. *Eur. J. Pharm. Biopharm.* **2015**, *93*, 196–204. [CrossRef]
55. Xu, X.; Zhong, W.; Zhou, S.; Trajtman, A.; Alfa, M. Electrospun PEG–PLA nanofibrous membrane for sustained release of hydrophilic antibiotics. *J. Appl. Polym. Sci.* **2010**, *118*, 588–595. [CrossRef]
56. Khameneh, B.; Iranshahy, M.; Soheili, V.; Fazly Bazzaz, B.S. Review on plant antimicrobials: A mechanistic viewpoint. *Antimicrob. Resist. Infect. Control* **2019**, *8*, 118. [CrossRef]
57. Rossiter, S.E.; Fletcher, M.H.; Wuest, W.M. Natural Products as Platforms To Overcome Antibiotic Resistance. *Chem. Rev.* **2017**, *117*, 12415–12474. [CrossRef]
58. Betts, J.W.; Wareham, D.W. In vitro activity of curcumin in combination with epigallocatechin gallate (EGCG) versus multidrug-resistant Acinetobacter baumannii. *BMC Microbiol.* **2014**, *14*, 172. [CrossRef]
59. Klančnik, A.; Šikić Pogačar, M.; Trošt, K.; Tušek Žnidarič, M.; Mozetič Vodopivec, B.; Smole Možina, S. Anti-Campylobacter activity of resveratrol and an extract from waste Pinot noir grape skins and seeds, and resistance of Camp. jejuni planktonic and biofilm cells, mediated via the CmeABC efflux pump. *J. Appl. Microbiol.* **2017**, *122*, 65–77. [CrossRef]
60. Marturano, V.; Bizzarro, V.; Ambrogi, V.; Cutignano, A.; Tommonaro, G.; Abbamondi, G.R.; Giamberini, M.; Tylkowski, B.; Carfagna, C.; Cerruti, P. Light-Responsive Nanocapsule-Coated Polymer Films for Antimicrobial Active Packaging. *Polymers* **2019**, *11*, 68. [CrossRef]
61. Persico, P.; Ambrogi, V.; Carfagna, C.; Cerruti, P.; Ferrocino, I.; Mauriello, G. Nanocomposite polymer films containing carvacrol for antimicrobial active packaging. *Polym. Eng. Sci.* **2009**, *49*, 1447–1455. [CrossRef]
62. Lee, J.H.; Kim, Y.G.; Ryu, S.Y.; Cho, M.H.; Lee, J. Resveratrol oligomers inhibit biofilm formation of Escherichia coli O157:H7 and Pseudomonas aeruginosa. *J. Nat. Prod.* **2014**, *77*, 168–172. [CrossRef] [PubMed]
63. Morán, A.; Gutiérrez, S.; Martínez-Blanco, H.; Ferrero, M.A.; Monteagudo-Mera, A.; Rodríguez-Aparicio, L.B. Non-toxic plant metabolites regulate Staphylococcus viability and biofilm formation: A natural therapeutic strategy useful in the treatment and prevention of skin infections. *Biofouling* **2014**, *30*, 1175–1182. [CrossRef] [PubMed]
64. Abelho, M. Extraction and Quantification of ATP as a Measure of Microbial Biomass. In *Methods to Study Litter Decomposition: A Practical Guide*; Graça, M.A.S., Bärlocher, F., Gessner, M.O., Eds.; Springer: Dordrecht, The Netherlands, 2005; pp. 223–229. [CrossRef]
65. Robertson, J.; McGoverin, C.; Vanholsbeeck, F.; Swift, S. Optimisation of the Protocol for the LIVE/DEAD(®) BacLight(TM) Bacterial Viability Kit for Rapid Determination of Bacterial Load. *Front. Microbiol.* **2019**, *10*, 801. [CrossRef] [PubMed]

International Journal of Molecular Sciences

MDPI

Article

Cationic Polymer Nanoparticles-Mediated Delivery of miR-124 Impairs Tumorigenicity of Prostate Cancer Cells

Raffaele Conte [1,†], Anna Valentino [2,†], Francesca Di Cristo [2], Gianfranco Peluso [1], Pierfrancesco Cerruti [3,*], Anna Di Salle [1] and Anna Calarco [1,*]

[1] Research Institute on Terrestrial Ecosystems (IRET) – CNR, Via Pietro Castellino 111, 80131 Napoli, Italy; raffaele.conte86@tiscali.it (R.C.); gianfranco.peluso@cnr.it (G.P.); anna.disalle@cnr.it (A.D.S.)

[2] Elleva Pharma s.r.l. via P. Castellino, 111 – 80131 Napoli, Italy; anna.valentino@ellevapharma.com (A.V.); francesca.dicristo@ellevapharma.com (F.D.C.)

[3] Institute for Polymers, Composites and Biomaterials (IPCB-CNR) Via Campi Flegrei, 34, 80078 Pozzuoli (NA), Italy

* Correspondence: cerruti@ipcb.cnr.it (P.C.); anna.calarco@cnr.it (A.C.)

† These authors contributed equally to this work.

Received: 16 January 2020; Accepted: 28 January 2020; Published: 29 January 2020

Abstract: MicroRNAs (miRNAs) play a pivotal role in regulating the expression of genes involved in tumor development, invasion, and metastasis. In particular, microRNA-124 (miR-124) modulates the expression of carnitine palmitoyltransferase 1A (CPT1A) at the post-transcriptional level, impairing the ability of androgen-independent prostate cancer (PC3) cells to completely metabolize lipid substrates. However, the clinical translation of miRNAs requires the development of effective and safe delivery systems able to protect nucleic acids from degradation. Herein, biodegradable polyethyleneimine-functionalized polyhydroxybutyrate nanoparticles (PHB-PEI NPs) were prepared by aminolysis and used as cationic non-viral vectors to complex and deliver miR-124 in PC3 cells. Notably, the PHB-PEI NPs/miRNA complex effectively protected miR-124 from RNAse degradation, resulting in a 30% increase in delivery efficiency in PC3 cells compared to a commercial transfection agent (Lipofectamine RNAiMAX). Furthermore, the NPs-delivered miR-124 successfully impaired hallmarks of tumorigenicity, such as cell proliferation, motility, and colony formation, through CPT1A modulation. These results demonstrate that the use of PHB-PEI NPs represents a suitable and convenient strategy to develop novel nanomaterials with excellent biocompatibility and high transfection efficiency for cancer therapy.

Keywords: polymer nanoparticles; aminolysis; miR-124; gene delivery; polyhydroxybutyrate (PHB); polyethyleneimine (PEI); prostate cancer

1. Introduction

Prostate cancer (PC) remains a significant leading cause of male death in developed occidental countries [1,2]. Current PC therapies (e.g., surgery, hormonal therapy, radiation, or chemotherapy, etc.) aim to prolong patient survival, improving and maintaining quality of life. However, more than 80% of PC patients develop resistance to androgen deprivation therapy (ADT), a status named castration-resistant PC, leading to disease progression and metastases with poor survival [3].

Recently, the pivotal role of microRNAs (miRNAs) in PC initiation and progression as well as in modulating the response of PC to treatments has been underlined [4–6], suggesting their use as diagnostic biomarkers and alternative treatments [5,7–10]. In particular, microRNA-124 (miR-124) is a class of small non-coding RNAs significantly implicated in several types of human cancers, including hepatocellular carcinoma, glioblastoma, osteosarcoma, and breast cancer [11–13].

Several studies reported the suppressive role of miR-124 on prostate cancer cell proliferation, apoptosis, and metastasis [14–16]. Shi et al. showed that low expression of miR-124 contributes to the pathogenesis of PC via increased expression of the androgen receptor [17], while Kang et al. demonstrated miR-124 anti-proliferative and anti-aggressive effects related to the inhibition of PACE4 transcription [18]. Our previous study provided evidence that miR-124 is involved in PC deregulation of mitochondrial fatty acid (FA) oxidation via carnitine system modulation, targeting carnitine-palmitoyltransferase-1 A (CPT1A) [18]. Forced expression of the synthetic miR-124 mimic in androgen-dependent and androgen-independent PC cells (LNCaP and PC3, respectively) affects tumorigenic properties, regardless of their hormone sensitivity. Together, these studies suggest that administration of an miR-124 mimic may represent a promising therapeutic tool for PC management. However, the successful translation of miRNA therapy from bench to bedside is still a severe challenge due to the short half-life and poor stability of miRNA mimics. Indeed, their clinical translation requires effective delivery systems able to enhance cellular uptake in the tumor site as well as able to protect nucleic acids from degradation.

Nanoparticle (NP)-based targeted delivery, such as the use of cationic polymeric nanoparticles, represents the most promising solution to protect miRNAs from endosomal and/or lysosomal degradation, thus achieving their therapeutic effects [19–22]. Recently, few studies reported the therapeutic potential of miR-124 polymeric nanoparticles (NPs) in neurodegenerative disorders. Saraiva et al. fabricated polylactic-co-glycolic acid (PLGA) NPs containing perfluoro-1,5-crown ether and coated with protamine sulfate to complex microRNA-124. This formulation was able to enhance brain repair in in vitro and in vivo model of Parkinson's disease, leading to the amelioration of motor symptoms in mice treated with 6-hydroxydopamine [23]. In addition, Louw et al. synthetized chitosan miRNA-124 polyplexes that reduced neuronal inflammation in rat models of spinal cord injury [24]. To our knowledge, only Shi et al. reported the delivery of miR-124 in prostate cancer, as JetPEI (linear PEI derivative) complexes. The authors demonstrated that the intravenous administration of miR-124 polyplex inhibited the growth of androgen-dependent and -independent prostate cancer cells and increased tumor cell apoptosis in an enzalutamide-resistant xenograft model [16]. However, the clinical translation of JetPEI as a delivery vehicle presents a major hurdle, requiring appropriate drug formulation and optimization.

Several natural and synthetic biodegradable polymers have been employed in the synthesis of micro- and nano-vectors for nucleic acids delivery. For this purpose, mainly polysaccharides (such as dextran, cyclodextrins, chitosan), polyhydric polymers (polyvinyl alcohol, polyethylene glycol), and polyesters (PLGA, polycaprolactone, polylactic acid) have been utilized [25–27].

Poly(3-hydroxybutyrate) (PHB) has emerged as an alternative to the above mentioned biodegradable polymers because of its unique physiochemical and mechanical properties [28,29]. PHB exhibits excellent biocompatibility and hemocompatibility, generating a mild foreign-body response with no activation of the complement system. However, although the hydrolytic and enzymatic (via nonspecific lipases and esterases) in vivo degradation processes of PHB make this polymer a good candidate as an efficient delivery system [30,31], its application in gene delivery is limited due to its negative surface charge. Polyethyleneimine (PEI), a water-soluble polymer with protonable amino groups, has been widely used for nucleic acids complexation through electrostatic interactions [32–34]. However, its high transfection efficiency is frequently related to cellular toxicity due to polymer interference with cellular nuclear processes [35].

The present study reported, for the first time, the synthesis of PHB nanoparticles (PHB NPs), functionalized with low molecular weight PEI via aminolysis, and their use as effective cationic non-viral vectors to complex and deliver miR-124 in prostate cancer cells. The wet-chemical modification of polymeric surface prevented free PEI from being released in the living cell after delivery of the nucleic acid. Furthermore, the functionalization of the polymer via aminolysis represents a simple, rapid, and environmentally-safe procedure, which is easily scalable to an industrial environment. The physicochemical properties of cationic nanoparticles, such as the particle size, zeta potential, morphology, and stability, were evaluated. Additionally, the biocompatibility, cellular uptake, and

delivery efficiency of PHB-PEI NPs/miR-124 complexes were assessed in human prostate cancer cells, PC3, used as an in vitro cell model.

Our results showed that PHB-PEI NPs enhance cellular uptake of miR-124, in comparison to a commercially available Lipofectamine gene delivery system, decrease CPT1A expression and inhibit PC3 proliferation, migration, and invasion. Therefore, the high transfection efficiency and low cell toxicity make PHB-PEI NPs a promising delivery system for the treatment of prostate cancer in clinical trials.

2. Results and Discussion

2.1. Nanoparticles Synthesis and Characterization

Recently, scientific evidence established the master regulator role of miRNAs in tumor initiation, progression, and metastasis, shedding light on miRNAs as a promising strategy for cancer therapy. In comparison to 'one-drug-one-target' treatments (i.e., chemotherapeutic and/or radiotherapeutic agents), miRNA-based therapies offer the advantage of concurrently regulating multiple cellular targets, restoring or repressing miRNA expression and activity [10]. However, miRNAs clinical translation results in several off-target effects due to poor miRNA pharmacokinetic profile, rapid in vivo clearance, and limited delivery at the tumor site. Cationic polymeric vectors could potentially overcome these limitations, protecting nucleic acid from enzymatic degradation and increasing their bioavailability and loading efficiency. Therefore, they are regarded as efficient tools in in vitro and in vivo miRNA systemic delivery for cancer therapy [36].

Due to its high cationic charge density at physiological pH, polyethyleneimine (PEI) is a potential candidate for gene delivery. Indeed, it is well known that PEI induces a rapid intracellular uptake and miRNA release via an endocytic mechanism ('proton sponge effect') [37]. However, this strong positive surface charge causes severe cytotoxicity and nonspecific binding with serum [38]. To exploit the high transfection efficiency of PEI while limiting cellular toxicity, herein a two-step procedure, including preparation of PHB NPs followed by surface modification with PEI, was developed for the preparation of PHB-PEI NPs (Scheme 1).

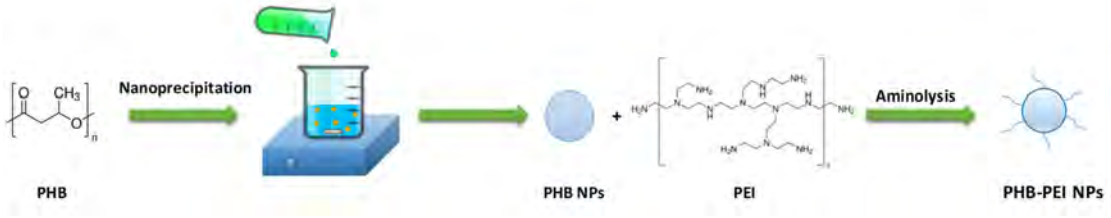

Scheme 1. Preparation route of polyethyleneimine-functionalized PHB nanoparticles (PHB-PEI NPs) by nanoprecipitation and aminolysis.

PHB NPs were prepared in Pluronic F-127 aqueous solution by nanoprecipitation. First, the optimal process parameters were determined to achieve NPs with the desired size and narrow polydispersity index (PDI). As reported in Table S1, the mean particle size ranged from 138 to 705 nm and was strongly affected by polymer and surfactant concentration. In particular, the NPs size was directly and inversely proportional to PHB and Pluronic F-127 concentrations, respectively. Indeed, larger nanoparticles formed at higher polymer concentrations due to lower diffusion coefficient of solvent in water [39] and, when an insufficient amount of surfactant resulted in a reduced interfacial stability, leading to particle coalescence. According to the Dynamic Light Scattering (DLS) results, PHB NPs obtained using 8.33 mg/mL PHB and 2 wt % Pluronic F-127 solutions, which showed a hydrodynamic diameter of 138 nm and moderate dispersity (Figure 1a and supplementary Table S1), were selected for the subsequent surface modification reaction. Aminolysis is an easy-to-perform chemical modification which allows the engraft of free $-NH_2$ groups along the polyester chains [31,40].

Upon aminolysis, one of the amino groups of branched PEI reacts with the ester group of PHB to form an amide bond, leaving the others amine groups of PEI available for nucleic acids complexation. Aminolysis was performed by immersing pristine PHB NPs in PEI–isopropanol solution at varying concentrations (12%, 24%, 48% w/v) for regular intervals, up to a maximum of 60 min (supplementary Table S2). The treatment with 24% PEI for 15 min at 50 °C resulted in the highest amount of $–NH_2$ groups on the PHB NPs surface (38.2 mmol $-NH_2$/g) as determined by quantitative ninhydrin assay. DLS analysis demonstrated a slight increase in hydrodynamic diameter (151.6 ± 62.8 nm) (Figure 1a), while the zeta potential dramatically increased following aminolysis, from −26.8 ± 6.9 to 37.1 ± 2.5 mV (Figure 1b), confirming the successful surface modification.

Size and morphology of the NPs were further characterized by TEM and SEM, which showed that they were spherical and regular in size (around 150 nm) with a smooth surface (Figure 1c,d). Electron microscopy did not show any significant size differences between PHB NPs and PHB-PEI NPs and the PEI coating was not clearly distinguishable (Figure 1e). SEM also confirmed that PHB nanoparticles maintained their low propensity to agglomerate even after surface modification (Figure 1f). Indeed, both PHB NPs and PHB-PEI NPs were easily redispersed in water after isolation.

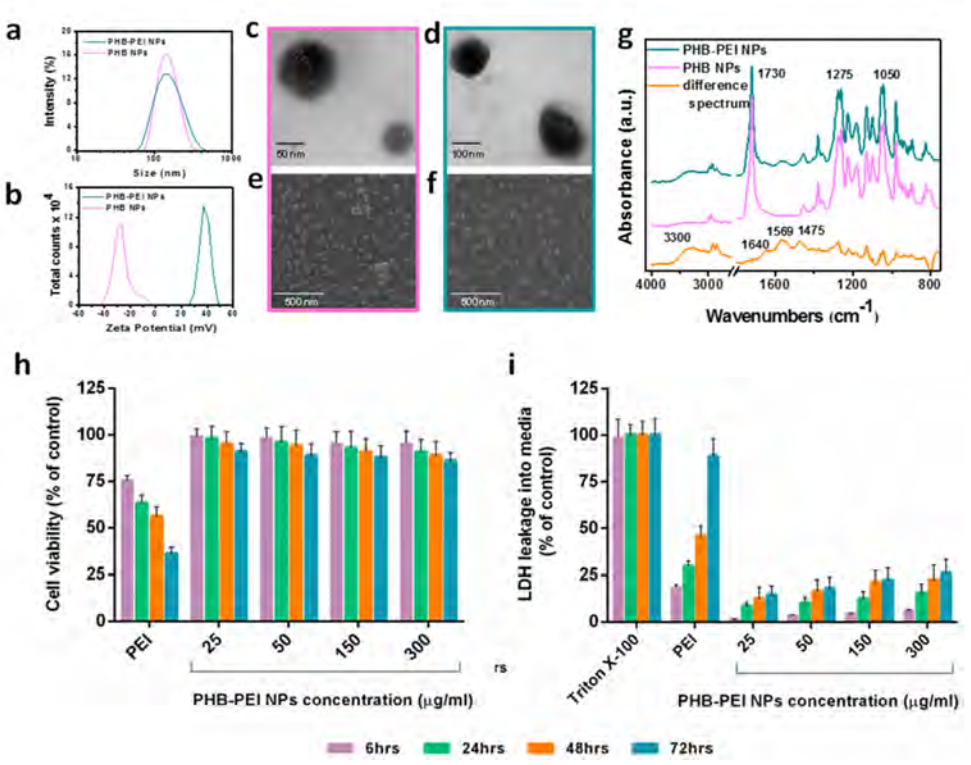

Figure 1. Size, morphological, chemical characterization, and cytotoxicity of PHB based NPs. (**a**) Size distribution and (**b**) zeta potential of PHB and PHB-PEI NPs. TEM and SEM images of: (**c**, **e**) PHB, and (**d**, **f**) PHB-PEI NPs. (**g**) FTIR-ATR spectra of PHB and PHB-PEI NPs along with difference spectra. (**h**, **i**) In vitro cytotoxicity of PHB-PEI NPs. Cytotoxicity was determined in PC3 cells after 6, 24, 48, and 72 h of incubation with varying concentrations of PHB-PEI NPs using: (**h**) the Cell Counting Kit-8 (CCK-8) assay, and (**i**) the Lactate Dehydrogenase (LDH) assay. Untreated cells were used as control. Data are presented as the mean ± SD for three independent measurements.

Chemical characterization of the NPs was performed by FTIR spectroscopy. FTIR-ATR spectra of pristine PHB NPs and PHB-PEI NPs are reported in Figure 1g, along with their difference spectra. The PHB NPs spectrum showed the presence of main absorption peaks of PHB at 2980 and 2940 cm^{-1} due to the aliphatic backbone at 1730 cm^{-1}, ascribed to the ester carbonyl stretching, and at 1275 cm^{-1}, corresponding to the bending of C-H bonds. Moreover, a pattern of bands between 1000 and 1250 cm^{-1} accounted for the stretching of the C-O bond of the carboxyl groups [41]. PHB-PEI NPs and the

difference spectrum clearly revealed absorption peaks that can be assigned to grafted PEI. Specifically, amide I and amide II stretching bands at 1640 and 1568 cm^{-1}, respectively, were noticed, along with the peak at 1475 cm^{-1}, indicative of the in-plane bending of CH_2 groups. Moreover, the broad absorption at 3300 cm^{-1} was assigned to the stretching vibration of primary amines [42].

PEI transfection is accompanied with certain degrees of cytotoxicity, depending on polymer molecular weight. PEI may induce cell cytotoxicity due the cell membrane destabilization and/or by interfering with host-gene expression in the nucleus [43]. However, it has been demonstrated that low molecular weight PEI shows lower cytotoxicity compared to high molecular weight PEI [34,44]. In order to determine if aminolysis can reduce the toxicity of PEI, the biocompatibility of PHB-PEI NPs was assessed after incubation of cells with varying concentrations of NPs. CCK-8 and LDH assays were performed on different cell lines (Caco-2, MCF-7, MCF10A, and PC3 cells), for up to 72 h. As reported in Figure 1h and Figure S1a–c, no changes in cell viability were observed in all cell lines after 72 h of incubation (>85% cell viability) with respect to the control. On the contrary, cells treated with PEI (25 μg/mL) showed a significant reduction in cell viability ($p < 0.01$). Moreover, the addition of PHB-PEI NPs to cell cultures induced only minimal or negligible damage to cell membrane integrity, as evidenced by the low LDH release even after 72 h at all tested concentrations (Figure 1i and supplementary Figure S1d–f). The reported results confirmed that aminolysis considerably reduced the PEI-induced toxicity by preventing the release of free toxic primary amino groups in the cell.

2.2. Characterization of PHB-PEI NPs/miR-124 Complexes (miR-124 NPs)

The ability of PHB-PEI NPs to electrostatically interact, at different N/P ratios (1:1, 5:1, 10:1), with phosphate groups on the miRNA backbone was determined by gel retardation assay. As depicted in Figure 2a, the intensity of migrating free miRNA decreased gradually with an increase in the N/P ratio. In particular, PHB-PEI NPs were able to condense miRNA already at an N/P ratio of 5, forming a stable miRNA/NPs complex at an N/P of 10.

As a prerequisite to obtaining an efficient miRNA delivery system for therapeutic applications, the cationic NPs should protect nucleic acids from nuclease degradation both in serum and extracellular matrix [21]. q-PCR data (Figure 2b) revealed that ~90% of intact miR-124 was also detected after 24 h of incubation in the growth medium when complexed with PHB-PEI NPs at an N/P ratio of 10, while free miR-124, used as control, was already completely degraded after 1 h of incubation (supplementary Figure S2). These results demonstrated that PHB-PEI NPs are able to protect nucleic acid from nuclease degradation for extended period of times.

The cellular internalization of the complex is modulated by its physico-chemical properties, such as particle size and zeta potential [45–47]. Therefore, the nanocomplexes' average hydrodynamic diameter and zeta potential were determined by dynamic and electrophoretic light scattering, respectively. As shown in Figure 2c, at a low N/P ratio, particles larger than pristine PHB-PEI NPs formed (hydrodynamic diameter = 181.4 ± 38.6 at N/P = 1), whose size tended to decrease when the N/P ratio increased, reaching the value of 157.6 ± 30.8 at N/P = 10. In addition, at N/P ratio = 1, the strongly positive zeta potential of the NPs complex declined (10.47 ± 1.27 mV) due to the presence of negatively charged miRNA on NPs surface (Figure 2d). However, at N/P = 10, the surface charge of the nanocomplex increased considerably, confirming the ability of PHB-PEI NPs to completely complex miRNA, in accordance with the gel retardation results.

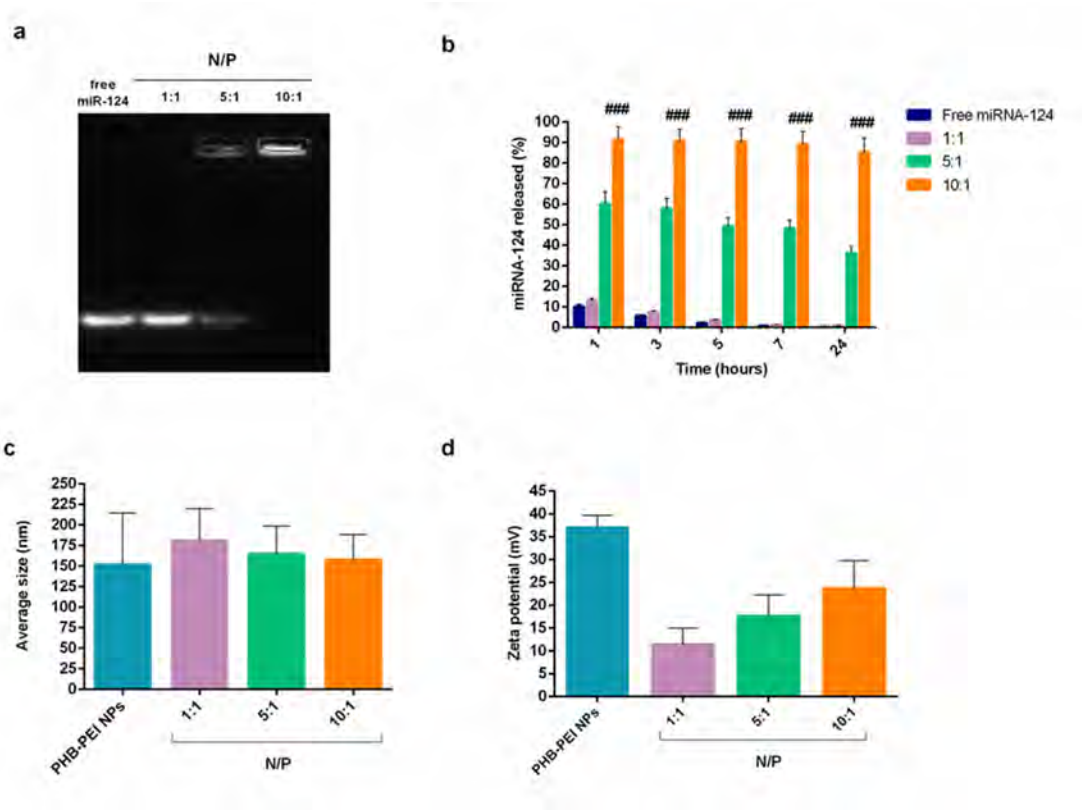

Figure 2. Characterization of PHB-PEI NPs/miR-124 complexes. (**a**) Electrophoretic mobility of miR-124 NPs at different N/P ratios. (**b**) miRNA-124 release profile evaluated by qRT-PCR analysis for 24 h in growth medium. Free miR-124 was used as control. (**c**) Average hydrodynamic diameter and (**d**) zeta potential of miR-124 NPs at different N/P ratios (mean ± SD, n = 6). Statistically significant variations: ### $p < 0.001$ N/P 10:1 versus N/P 5:1, N/P 1:1, and free miR-124.

2.3. Cellular Uptake of miR-124 NPs

Several reports have shown that miRNAs can be efficiently delivered into the cancer cell by nano-sized, non-viral vectors, minimizing the poor cellular uptake of free nucleic acids due to the charge repulsion between the cell membrane and miRNAs [48]. Inter alia, Shi et al. reported the delivery of miR-124 in prostate cancer as JetPEI complexes. The authors demonstrated that the intravenous administration of miR-124 polyplex inhibited the growth of androgen-dependent and -independent prostate cancer cells and increased tumor cell apoptosis in an enzalutamide-resistant xenograft model [16]. However, the clinical translation of JetPEI as a delivery vehicle requires appropriate drug formulation and optimization to avoid cytotoxic effects. To investigate the role of PHB-PEI NPs in miR-124 intracellular delivery, the transfection efficiency of miR-124 NPs was assessed by flow cytometry. Lipofectamine RNAiMAX (iMAX) was used as a control. Interestingly, in comparison with miRNA transfected using the commercial transfection agent (Cy5-miR-124-iMAX), Cy5-miR-124 NPs at an N/P ratio 10:1 induced a significant ($p < 0.01$) 30% increase in Cy5-positive PC3 (92.6 ± 6.20% and 70.5 ± 5.63%, respectively, Figure 3a). Furthermore, the transfection at N/P ratios below 10 resulted in a low signal inside cells, probably due to the weak interactions between NPs and miRNA. Fluorescence microscopy was also performed to evaluate subcellular distributions of Cy5-miR-124 in PC3 cells. As depicted in Figure 3b, a strong and diffuse fluorescence was observed in the cytoplasm of cells treated with the nanocomplex compared to PC3 incubated with lipofectamine. These results confirmed the advantages of using nontoxic PHB-PEI NPs to remarkably enhance miRNA delivery.

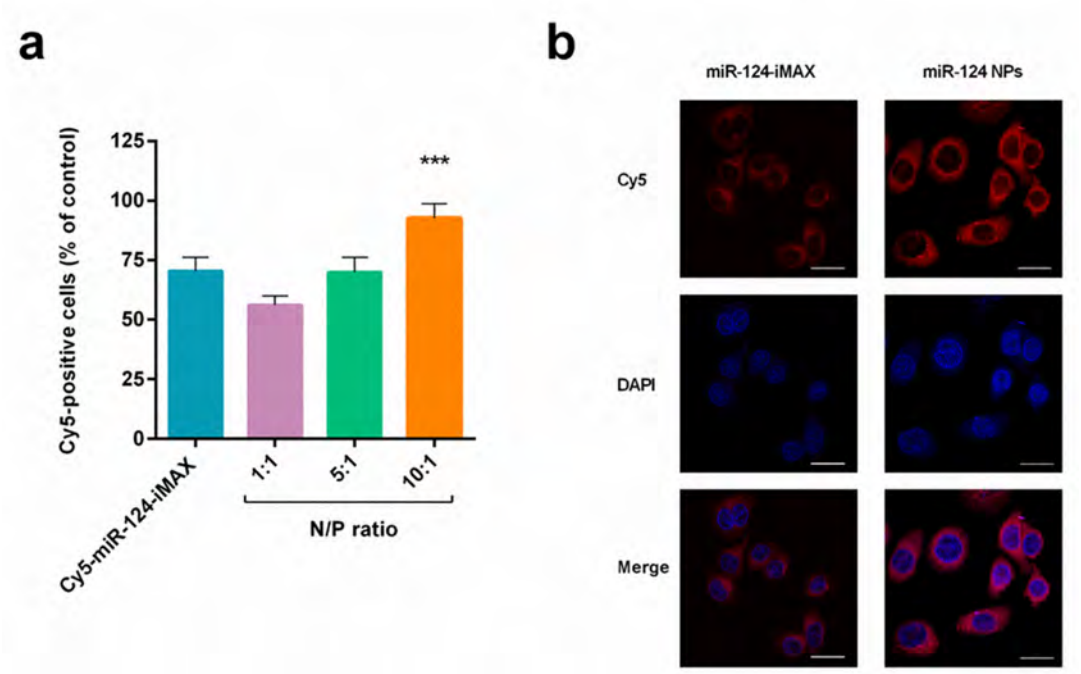

Figure 3. Intracellular delivery efficiency of PHB-PEI NPs/miR-124 complexes. (**a**) PC3 uptake of miR-124 NPs analyzed by Fluorescent Activated Cell Sorting (FACS). To facilitate observations, miR-124 was labeled with the Cy5 fluorescent probe (red) to form Cy5-miR-124-NPs at different N/P ratios (1:1 to 10:1). Lipofectamine RNAiMAX (iMAX) was used as a control. Cells were incubated with fluorescent nanocomplexes for 4 h, washed with PBS, and incubated for another 20 h prior to analysis by flow cytometer (mean ± SD, $n = 6$). Statistically significant variations: *** $p < 0.001$ N/P 10:1 versus N/P 5:1, N/P 1:1, and iMAX. (**b**) Fluorescence images of PC3 cells incubated with Cy5-miR-124-NPs (N/P ratio 10:1) or Cy5-miR-124-iMAX for 4 h. Magnification 40×, scale bar is 50 μm.

2.4. Anti-Cancer Effects of miR-124 NPs

Lipid metabolism dysregulation, due to abnormal expression of various genes, proteins, and signaling pathways, plays a pivotal role both in carcinogenesis and some metabolic syndromes [49–51]. Prostate cancer cells differ from many other cancer types in that they promote fatty acid oxidation (FAO) to fuel their energy and metabolic intermediate needs, even under nutrient-replete conditions. Indeed, mitochondrial FAO produces much more ATP/mole than oxidation of glucose or amino acids [49]. Several studies reported that carnitine palmitoyltransferase 1A (CPT1A), the key enzyme of mitochondrial FAO in both healthy and cancer cells, is strongly expressed in several cancers, including the hormone-dependent breast and prostate cancers [52]. CPT1A transfers the acyl group of a long-chain fatty acyl-CoA from coenzyme A to carnitine. Evidences have shown that the downregulation of CPT1A via inhibition/depletion impairs cancer cell proliferation in lung, gastric, prostate, lymphoma, and leukemia [53–55]. Schlaepfer et al. demonstrated that etomoxir, an irreversible inhibitor of CPT1A, is able to induce cytotoxicity in the androgen-dependent prostate cell lines as well as patient-derived prostate cancer cells [56,57]. Moreover, pharmacological blockage of CPT1A leads to a dose- and time-dependent cell growth reduction and apoptosis in leukemia cell lines and primary hematopoietic malignant cells [58].

Our previous research revealed that in prostate cancer cells, such as PC3, the downregulation of miR-124 induces an increase in both the expression and activity of CPT1A, allowing malignant cells to be more prone to fatty acid utilization with respect to normal cells [29]. Altogether, these observations suggest that lipid oxidation is an important player in the plasticity of cancer cells, allowing them to survive even in harsh environments such as androgen deprivation [59,60]. Based on the results reported above, miR-124 NPs at N/P = 10 was employed in the study. The functionality

of the miR-124 released by PHB-PEI NPs was determined by evaluating the expression level of CPT1A by both qPCR (Figure 4a) and Western blot (Figure 4b) analyses. As reported in Figure 4, a significant ($p < 0.001$) downregulation of the investigated target was observed 24 h after transfection at both transcriptional and translation level compared to non-transfected cells (CTL) or miR-NC-NPs-mediated transfection. In addition, the CPT1A immunofluorescence stain revealed a low expression in cells treated with miR-124 NPs with respect to control cells (Figure 4c).

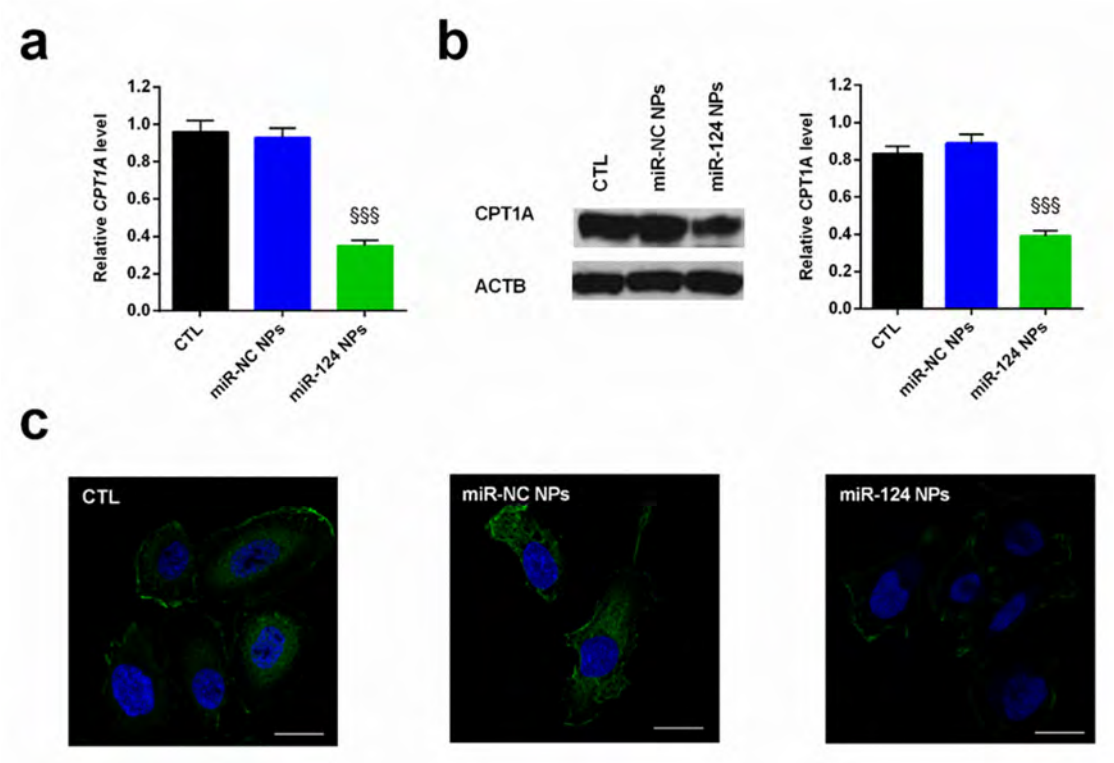

Figure 4. Expression of CPT1A in the PC3 cells in the presence of nanocomplexes. Cells were cultured for 24 h after transfection with miR-124-NPs or miR-NC-NPs at a 10:1 N/P ratio. The untreated cells were used as control (CTL). (**a**) miRNA target level (CPT1A) was quantified by quantitative real-time PCR (qPCR) and normalized to actin (ACTB) as a housekeeping gene. The comparative cycle threshold (CT) method ($2^{-\Delta\Delta Ct}$) was applied to calculate relative differences in qPCR results. (**b**) Western blot analysis of CPT1A protein was performed on total PC3 protein fraction. The protein expression was normalized to the housekeeping protein ACTB. The bars represent the mean ± SD, $n = 3$. Statistically significant variations: §§§ $p < 0.001$ miRNA versus miR-NC and CTL. (**c**) Representative fluorescent images of CPT1A expression. Immunofluorescence stain was performed with a FITC-labeled secondary antibody and counterstained with DAPI. Magnification 40×, scale bar is 50 μm.

The ability of miR-124 NPs to interfere with malignant cell functionality (cell proliferation, motility, and colony formation) was confirmed on PC3 cells transfected with miR-124 NPs as well as miR-NC (Figure 5). As reported in Figure 5a, the cell growth rate significantly ($p < 0.001$) decreased after forced overexpression of miR-124 compared with the miRNA-negative control. Similarly, colony-formation assay demonstrated that the gain in function of miR-124 reduced the ability of transfected cells to self-renew (Figure 5b). In addition, the wound healing assay confirmed the influence of miR-124 released by PHB-PEI NPs on PC3's migratory capability (78%, $p < 0.01$) compared to non-transfected cells (Figure 5c). Moreover, the number of PC3 cells crossing the Matrigel decreased of about 75% compared with the control cells (Figure 5d).

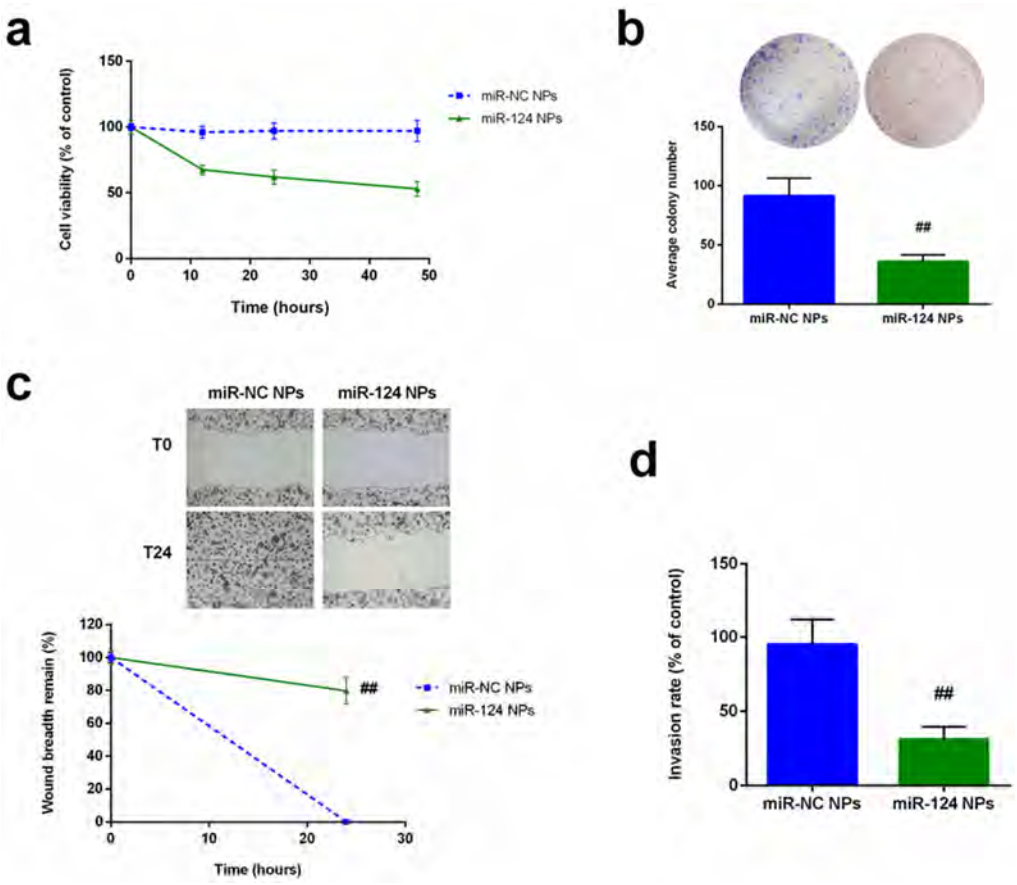

Figure 5. Influence of forced expression of miR-124 on PC3 proliferation, migration, and invasion. (**a**) Cell proliferation of PC3 cells was determined by CCK8 assay after 12, 24, and 48 h. (**b**) Colony formation assay was performed after 14 days of culture. For quantification, colonies with at least 50 cells were considered. Representative micrographs were obtained using phase contrast microscope after staining with crystal violet. (**c**) Wound-healing assay performed on transfected PC3 cell, and wound closure rate measured by detecting the closure distance after 24 h. Representative micrographs of the cell migration (top) and quantification (bottom) from three independent experiments are presented. (**d**) Transwell invasion assay with Matrigel performed in miR-124-NPs or miR-NC-NPs-transfected PC3 cells after 24 h. Five random fields in each well were counted under a microscope. The bars represent the mean ± SD, $n = 3$. Statistically significant variations: ## $p < 0.01$, miRNA versus miR-NC.

Together, the evidence demonstrates that miR-124 NPs represent a promising delivery system to target lipid oxidation in prostate and other cancers intervening in tumor progression and inhibition of metastasis and relapse.

3. Materials and Methods

3.1. Materials

Bacterial poly(3-hydroxybutyrate) (PHB), coded T19, was supplied by Biomer (Schwalbach, Germany). The number and weight average molecular weight, Mn and Mw, as determined by gel permeation chromatography (GPC), were 193 and 223 kg mol^{-1}, respectively. Branched polyethylenimine (PEI) with an Mw of 800 kg mol^{-1} (800 D-PEI, ratio of primary:secondary:tertiary amine groups 1:0.82:0.7), Coumarin-6 (C6), and Pluronic F-127 were obtained from Sigma-Aldrich (Milan, Italy). Microfiltered (0.22 μm) double distilled water (milliQ) was used throughout the studies. Fetal bovine serum (FBS), Roswell Park Memorial Institute (RPMI) 1640 medium, Dulbecco's

modified Eagle's medium (DMEM), sodium pyruvate, L-glutamine, penicillin, and streptomycin were purchased from Hyclone (Milan, Italy). All other chemicals and solvents used were of the highest grade commercially available (Sigma-Aldrich).

3.2. Synthesis and Functionalization of PHB NPs

PHB NPs were synthesized by nanoprecipitation, as previously reported [61], with minor modifications. Varying amounts of PHB were dissolved in N,N-Dimethylformamide (DMF) and the resulting solution was dropped in an aqueous solution of Pluronic F-127 under moderate magnetic stirring (solvent/non solvent ratio 1:5) (Table S1). The resulting suspension was kept under 300 rpm stirring overnight at room temperature, then centrifuged (18,000 rpm, 4 °C, 45 min). The obtained pellet was washed with milliQ water and, finally, freeze-dried. C6-loaded PHB NPs were prepared by adding C6 to the organic phase in a 10:1 polymer/drug ratio. Cationic PHB NPs were prepared through aminolysis to obtain PEI surface functionalized PHB nanoparticles (PHB-PEI NPs). Aminolysis was carried out by suspending PHB NPs in 800 D-PEI isopropanol solutions for a determined period of time at 50 °C. The effect of PEI concentration (from 12 to 48 wt %) and reaction time (0 to 60 min) on the amount of grafted PEI was systematically investigated. PHB-PEI NPs were recovered by centrifugation (13,300 rpm, 25 °C, 45 min), rinsed twice with distilled water, and freeze-dried.

3.3. Nanoparticles Characterization

Particle size and zeta potential were measured using a Zetasizer Nano ZS instrument (Malvern Instruments Ltd, Malvern, UK) on NPs dispersions in milliQ water. Size estimation with DLS was performed as follows: sampling time 60 s, temperature 25 °C, analysis with backscatter angle at 173°, viscosity of the dispersant 10,141 cp, and refraction index 1.5290. Zeta potential quantification with laser doppler micro-electrophoresis had the same settings. Smoluchowski approximation was used for the algorithm. Results are shown as mean ± SD (n = 3). Scanning electron microscopy (SEM) characterization of neat and PEI-functionalized PHB NPs were made with an FEI Quanta 200 FEG scanning electron microscope (Eindhoven, Netherlands). Prior to observation, the samples were transferred on an aluminum stub and coated with Au–Pd alloy by means of a sputtering device (MED 020, Bal-Tec AG) in order to provide a homogeneous layer of metal of 18 ± 0.2 nm. Transmission electron microscopy (TEM) analysis was carried out by an FEI Tecnai G2 Spirit TWIN 120 kV with emission source LaB6 and mounting FEI Eagle 4k CCD camera (on the bottom) and Olympus SIS MegaView G2 CCD Camera (on the side). NPs samples were prepared by casting a drop of nanoparticle water dispersion on a copper grid coated with a thin layer of carbon. Fourier transform infrared-attenuated total reflectance (FTIR-ATR) spectra were recorded on a Perkin Elmer Spectrum 100 spectrometer (Milan, Italy), equipped with a universal ATR diamond crystal sampling accessory. The spectra of PEI, as well as of PHB and PHB-PEI NPs, were acquired as an average of 64 scans in the range 4000–480 cm^{-1}, with a resolution of 4 cm^{-1}. Prior to measurements, the samples were kept at 60 °C under vacuum for 24 h. The amount of primary amino groups formed on the PHB-PEI NPs was determined by ninhydrin assay as described by Zhu et al. [38]. The NPs were solubilized in a 0.5 mL of CHCl3/DMF 3:1 *v*/*v* solution and mixed with 0.5 mL of 0.01 M ninhydrin solution ($CHCl_3$/DMF 3:1 *v*/*v*). To promote the reaction between ninhydrin and the amino groups of the NPs, the solution was heated at 80 °C for 15 min. Once reacted, the sample turned blue. The absorbance of the solution was recorded at 558 nm using a Varian DMS 200 UV/Vis spectrophotometer (Milan, Italy). Standard solutions of 800 D-PEI (0.0001, 0.0005, 0.001, 0.005, 0.01, and 0.05 mM) were prepared and reacted with ninhydrin in $CHCl_3$/DMF 3:1 *v*/*v* to obtain the calibration curve of standard solution. The absorbance of the PHB-PEI NPs dispersions was then compared with that of standard solution to determine the amine content of the PHB-PEI NPs.

3.4. PHB-PEI NPs Cytocompatibility

To assess PHB-PEI NPs cytocompatibility, a Cell Counting Kit-8 (CCK-8) assay was carried out. Briefly, PC3, Caco-2, MCF-7, and MCF10A cells were seeded in a 96-well plate in 100 μL at a density of 4×10^3 cells/well 24 h before treatment. After 24 h, the cells were treated with 10 μL of PHB-PEI NPs at different concentrations (25–250 μg/mL) and incubated at 37 °C for 24–72 h. Then, 10 μL of CCK-8 solution were added to each well, and the plate was then incubated under cell culture conditions for 1–4 h. The optical density of formazan salt at 450 nm was measured using a Cytation 3 Cell Imaging Multi-Mode microplate reader (Biotek, Milan, Italy)). PHB-PEI NPs cytocompatibility was expressed as a percentage relative to the control and calculated by the equation:

$$\text{Cytocompatibility (\%)} = (\text{OD sample}/\text{OD control}) \times 100 \quad (1)$$

where OD sample is the optical density of cells treated with PHB-PEI NPs and OD control is the optical density of untreated cells.

3.5. PHB-PEI NPs/miRNA Complex (miR-124 NPs) Formation and Characterization

miR-124 NPs were investigated at various N/P ratios (ratio of amine groups of NPs to phosphate groups of miRNAs) from 0.5 to 20. Complexation between miRNAs (diluted in RNase-free DEPC-treated water) and NPs suspensions was achieved by gentle pipetting and incubation at room temperature for 30 min. To confirm complexation, RNase protection, and release ability, miR-124 NPs were loaded onto 2% agarose gels containing GelStar nucleic acid gel stain (Lonza, Milan, Italy) and gel electrophoresis assays were performed at 80 V for 40 min in Tris-acetate EDTA (TAE) buffer. Images were acquired using a Bio-Rad VersaDoc MP 4000 Molecular Imager (Milan, Italy). Quantity One 1.1 software (Bio-Rad) was used for band integration and background correction. The zeta potential and size of miR-124 NPs were measured by the Malvern Zetasizer Nano ZS equipment as described above. In vitro miRNA stability in culture medium and serum was performed as reported by Devulapally et al. [47] with some modifications. Briefly, 50 pmols of miRNA equivalent of miR-124-loaded NPs were dispersed in Dulbecco's Modified Eagle's Medium (DMEM) supplemented with 2% fetal bovine serum (FBS) and 1% penicillin and streptomycin and incubated at 37 °C and 5% CO_2 for 0 to 1 days in a humidified atmosphere. At each time point, the reactions were terminated by adding 0.5 M of ethylenediaminetetraacetic acid and the samples were incubated at 37 °C for 1h in presence of 1% heparin sodium solution. Released free miRNAs from NPs were carefully separated by an ultracentrifuge filter device with 100 kDa MWCO Membrane (Millipore, Milan Italy) by centrifuging at 3000 rpm. The concentrated samples were washed and centrifuged several times with DNAse/RNAase free water (Invitrogen, Milan, Italy) and finally used for q-PCR, as reported in sections 3.7 and 3.8. For the RNase A protection assay, miR-124 NPs were incubated with 1 ng RNase A at 37 °C for 1 h. The nuclease activity of RNase A was terminated by treatment with 25 mM sodium dodecyl sulfate (SDS, Sigma-Aldrich) at 60 °C for 5 min. The absorbance of RNA at 260 nm was measured continuously for 1 h and the values were plotted vs. time.

3.6. Cell Culture

The human prostate adenocarcinoma cell line, PC3, as well as human adenocarcinoma cells (Caco-2), human breast carcinoma cells (MCF-7), and normal breast cells (MCF10A) were obtained from American Type Culture Collection (ATCC). PC3 and MCF10A were maintained in DMEM-F12, while the other cell lines were maintained in DMEM, all supplemented with 10% FBS, 1% L-glutamine, 50 U/mL penicillin, and 50 mg/mL streptomycin at 37 °C in a humidified atmosphere containing 5% CO_2. MCF-10A were also supplemented with epidermal growth factor 20 ng/mL, cholera toxin 100 ng/mL, and insulin 10 μg/mL. Cells were tested for contamination, including mycoplasma, and used within 2 to 4 months.

3.7. miRNAs Transient Transfection

The day before transfection, 1×10^5 cells were seeded under standard conditions into a 6-well plate in growth medium without antibiotics and transfected for 24 h using PHB-PEI NPs. Hsa-miR-124-3p, mirVana miRNA mimic (Ambion), and mirVana miRNA mimic negative control #1 (miR mimic NC, Ambion) were purchased from Applied Biosystems (Milan, Italy). For convenience, hsa-miR-124-3p mimic and the negative control are hereafter referred to as miR-124 and miR-NC, respectively. Forced expression of mimics were confirmed by qRT-PCR using TaqMan Universal PCR Master Mix (Applied Biosystem) and normalized to RNU6B. Transfected cells were used in further analyses.

3.8. RNA Isolation, Reverse Transcription, and Quantitative Real-Time PCR

Total RNA (mRNA and miRNAs) was extracted from cells after miR-124 NPs and miR-NC NPs transfection using QIAzol reagent (Qiagen, Milan, Italy) according to the manufacturer's instructions. For retro-transcription, total RNA (0.2 μg) was treated as described in Promega standard protocol and amplified by qPCR using specific primers for carnitine palmitoyltransferase 1A (CPT1A) and β-actin (ACTB), as listed in Table 1. Quantitative PCR (qPCR) was run on a 7900HT fast real-time PCR System (Applied Biosystem). The reactions were performed according to the manufacturer's instructions using SYBR Green PCR Master mix (Invitrogen). All reactions were run in triplicate, normalized to the housekeeping gene (ACTB), and the results expressed as mean ±SD. The $2^{-\Delta\Delta Ct}$ method was used to determine the relative quantification.

Table 1. Sequence of primers used in real-time polymerase chain reaction.

Genes	Forward primers (5′–3′)	Reverse primers (5′–3′)
ACTB	TTAGTTGCGTTACACCCTTTC	ACCTTCACCGTTCCAGTT
CPT1A	CTGGACAATACCTCGGAGCC	TCTAACGTCACGAAGAACGCT

3.9. Western Blotting

PC3 cells were grown to 70%–80% confluence and, after miR-124 NPs and miR-NC NPs transfection, pellets were lysed in ice-cold buffer containing 50 mM Tris-HCl (pH 7.5), 125 mM NaCl, 1% NP-40, 5.3 mM NaF, 1.5 mM NaP, 1 mM orthovanadate, 175 mg/mL octylglucopyranoside, 1 $mg{\cdot}mL^{-1}$ protease inhibitor cocktail, and 0.25 $mg{\cdot}mL^{-1}$ 4-(2-aminoethyl) benzenesulfonyl fluoride hydrochloride (AEBSF). Cell pellets were centrifuged and the supernatants were resuspended in SDS sample buffer, then were normalized for equal protein concentration before separation by sodium dodecyl sulfate (SDS) polyacrylamide gel electrophoresis. SDS polyacrylamide gel electrophoresis and immunoblotting were carried out according to standard procedures in triplicate, using 30 μg of total protein lysate. Antibodies were mouse monoclonal anti–carnitine palmitoyltransferase 1A (1:1000, Abcam, Milan Italy) and mouse monoclonal Anti-β-Actin (ACTB, 1:1000, Sigma-Aldrich). Anti-mouse was used as a secondary antibody (1:5.000, Santa Cruz, Milan Italy). The relative expression, normalized with respect to the housekeeping protein (ACTB), was quantified densitometrically using Quantity One 1-D analysis software (Bio-Rad).

3.10. miR-124 NPs Cell Viability and Colony Forming Assay

To assess miR-124 NPs-transfected cell proliferation, a CCK-8 assay was performed. PC3 cells were grown in 96-well plates at a density of 2.0 × 104 cells/well. Cells were treated with miR-124 NPs suspended in complete culture medium and diluted to the appropriate concentration (25–250 μg/mL). Cell proliferation at 0, 24, 48, and 72 h was determined by CCK8 assay following the manufacturer's protocol. The absorbance of each well was measured with a microplate reader (Cytation3, ASHI) at 450 nm. For colony formation assay, cells were counted and seeded in 6-well plates (in triplicate) at a density of 500 cells/well. Cells were treated with PHB-PEI NPs and miR-124 NPs at 50 μg/mL. The plates were incubated at 37 °C in a 5% CO_2 humidified incubator. The culture medium was replaced every 3 days. After 14 days in culture, cells were stained with crystal violet

and counted. Colonies with at least 50 cells were considered for quantification. Representative plates were photographed using a phase contrast microscope (Leica, Milan, Italy).

3.11. Cellular Uptake of miRNA

To assess the cellular uptake and binding of miR-124, PC3 cells were seeded on a microscope slide at a density of 4.5 × 104 cells in 24-well plates. Then, they were incubated with 100 nM of free Cy5-miRNA or PHB-PEI/Cy5-miRNA nanocomplexes at 37 °C for 0, 15, and 60 min. Cells were then washed 2 times with phosphate-buffered saline (PBS) and incubated in fixing solution (3.7% formaldehyde in PBS) for 15 min at room temperature. The microscope slides were mounted onto coverslips using ProLong Gold Antifade reagent with DAPI (Thermo Fisher Scientific, Milan, Italy). The percentage of miRNA uptake and binding was determined by measuring FAM-miRNA positive cells. NPs uptake was visualized by a Cytation 3 Cell Imaging Multi-Mode Reader fluorescent microscope (Biotek) at 520 nm.

3.12. miR-124 NPs Tumor Cell Migration and Invasion Assays

A scratch wound healing model was conducted to check the migratory ability of PC3 cells following the transfection treatment. PC3 cells were plated at a density of 1 × 105 cells in 2-well Lab-Tek Chamber Slide (Sigma-Aldrich). After overnight incubation, cells were transfected with mimics or miR-NC. Wounds were created in confluent cells using a 200 μL pipette tip. The cells were rinsed several times with media to remove any free-floating cells or debris and the speed of wound closure was monitored after 24 h by measuring the change in distance of the wound edges. Each experiment was conducted in triplicate and representative scrape lines were photographed using a phase contrast microscope (Leica). For the invasion assays, after 24 h transfection, 1 × 105 cells in serum-free media were seeded onto the transwell migration chambers (8 μm pore size, Millipore). The insert in the upper chamber was coated overnight with 1 mg·mL^{-1} BD Matrigel Matrix (BD Biosciences, Milan, Italy). A medium containing 10% FBS was added to the lower chamber. After 24 h, the non-invading cells were removed with a cotton-tipped swab and cells at the bottom of the Matrigel were stained with May–Grunewald–Giemsa stain (Sigma-Aldrich). Stained cells were counted under a microscope (Leica) at 200X magnification in 5 random fields in each well. Experiments were independently repeated three times.

3.13. Statistical Analyses

All values are expressed as mean ± standard deviation (SD). Each experiment was performed at least three times. A one-way analysis of variance (ANOVA) was used for statistical analysis, followed by Bonferroni's test for multiple comparisons to determine significance differences between groups. All the data were analyzed with the GraphPad Prism version 6.01 statistical software package (San Diego, CA, USA)

4. Conclusions

Aminolysis is a straightforward and easy-to-perform route to prepare PHB-based cationic NPs. The latter are successfully used as non-viral vectors to deliver miR-124 in androgen-independent prostate cancer (PC3) cells. The functionalization of PHB NPs with low-molecular-weight PEI results in NPs with high miR-124 loading capacity, which exhibit no significant cytotoxicity effect, even after 72 h. Furthermore, optimization of the N/P ratio contributes to a stable and uniform miR-124 NPs dispersion in aqueous solution and effectively protects miR-124 from RNAse degradation. PHB-PEI NPs showed 30% higher transfection efficiency compared to Lipofectamine RNAiMAX. A dramatic impairment of miR-124 NPs-transfected PC3 cell proliferation, motility, and colony formation was found due to the downregulation of CPT1A at both the transcriptional and translation level compared to non-transfected cells. Furthermore, the tumor-targeting efficacy of the reported delivery system should be assessed in in vivo models to validate the use of PHB-PEI NPs in non-invasive treatment of prostate cancer.

Supplementary Materials: Supplementary Materials can be found at www.mdpi.com/xxx/s1.

Author Contributions: Conceptualization, P.C. and A.C.; methodology, R.C., A.V., and F.D.C.; investigation, R.C., A.V., and F.D.C.; writing—original draft preparation, R.C. and A.V.; data curation A.D.S.; writing—review and editing, P.C., G.P., and A.C.; supervision, P.C. and A.C.; funding acquisition, P.C., G.P., and A.C. All authors have read and agreed to the published version of the manuscript.

Funding: This work was financially supported by the Italian Ministry of University and Research, grant PRIN 2012: "Nanotecnologie per variare i programmi di sviluppo osseo nella parete vasale per la prevenzione e trattamento delle patologie associate alla calcificazione ectopica arteriosa" (201288JKYY_003); PON 03 PE_00110_1/ptd1_000410 Titolo: Sviluppo di nanotecnologie Orientate alla Rigenerazione e Ricostruzione tissutale, Implantologia e Sensoristica in Odontoiatria/oculistica (SORRISO); POR Campania FESR 2014_2020 "Tecnologie abilitanti per la sintesi eco-sostenibile di nuovi materiali per la restaurativa dentale" – ABILTECH, and EU funding within the Horizon 2020 Program, under the MSCA-RISE 2016 Project "VAHVISTUS" (Grant 734759)

Acknowledgments: The authors gratefully acknowledge Cristina Del Barone (IPCB-CNR) for her support with electron microscopy analysis.

Conflicts of Interest: The authors declare no conflict of interest.

References

1. Siegel, R.L.; Miller, K.D.; Jemal, A. Cancer statistics, 2019. *Ca: A Cancer J. Clin.* **2019**, *69*, 7–34, doi:10.3322/caac.21551.
2. Saad, F.; Fizazi, K. Androgen Deprivation Therapy and Secondary Hormone Therapy in the Management of Hormone-sensitive and Castration-resistant Prostate Cancer. *Urology* **2015**, *86*, 852–861, doi:10.1016/j.urology.2015.07.034.
3. Nuhn, P.; De Bono, J.S.; Fizazi, K.; Freedland, S.J.; Grilli, M.; Kantoff, P.W.; Sonpavde, G.; Sternberg, C.N.; Yegnasubramanian, S.; Antonarakis, E.S. Update on Systemic Prostate Cancer Therapies: Management of Metastatic Castration-resistant Prostate Cancer in the Era of Precision Oncology. *Eur Urol* **2019**, *75*, 88–99, doi:10.1016/j.eururo.2018.03.028.
4. Vanacore, D.; Boccellino, M.; Rossetti, S.; Cavaliere, C.; D'Aniello, C.; Di Franco, R.; Romano, F.J.; Montanari, M.; La Mantia, E.; Piscitelli, R.; et al. Micrornas in prostate cancer: An overview. *Oncotarget* **2017**, *8*, 50240–50251, doi:10.18632/oncotarget.16933.
5. Bryzgunova, O.E.; Konoshenko, M.Y.; Laktionov, P.P. MicroRNA-guided gene expression in prostate cancer: Literature and database overview. *J. Gene Med.* **2018**, *20*, e3016-e3016, doi:10.1002/jgm.3016.
6. Ni, J.; Bucci, J.; Chang, L.; Malouf, D.; Graham, P.; Li, Y. Targeting MicroRNAs in Prostate Cancer Radiotherapy. *Theranostics* **2017**, *7*, 3243–3259, doi:10.7150/thno.19934.
7. Kanwal, R.; Plaga, A.R.; Liu, X.; Shukla, G.C.; Gupta, S. MicroRNAs in prostate cancer: Functional role as biomarkers. *Cancer Lett* **2017**, *407*, 9–20, doi:10.1016/j.canlet.2017.08.011.
8. Shukla, K.K.; Misra, S.; Pareek, P.; Mishra, V.; Singhal, B.; Sharma, P. Recent scenario of microRNA as diagnostic and prognostic biomarkers of prostate cancer. *Urol. Oncol.* **2017**, *35*, 92–101, doi:10.1016/j.urolonc.2016.10.019.
9. Bertoli, G.; Cava, C.; Castiglioni, I. MicroRNAs: New Biomarkers for Diagnosis, Prognosis, Therapy Prediction and Therapeutic Tools for Breast Cancer. *Theranostics* **2015**, *5*, 1122–1143, doi:10.7150/thno.11543.
10. Ganju, A.; Khan, S.; Hafeez, B.B.; Behrman, S.W.; Yallapu, M.M.; Chauhan, S.C.; Jaggi, M. miRNA nanotherapeutics for cancer. *Drug Discov. Today* **2017**, *22*, 424–432, doi:10.1016/j.drudis.2016.10.014.
11. Mucaj, V.; Lee, S.S.; Skuli, N.; Giannoukos, D.N.; Qiu, B.; Eisinger-Mathason, T.S.K.; Nakazawa, M.S.; Shay, J.E.S.; Gopal, P.P.; Venneti, S.; et al. MicroRNA-124 expression counteracts pro-survival stress responses in glioblastoma. *Oncogene* **2015**, *34*, 2204–2214, doi:10.1038/onc.2014.168.
12. Lee, Y.; Kim, H.J.; Park, C.K.; Kim, Y.-G.; Lee, H.-J.; Kim, J.-Y.; Kim, H.-H. MicroRNA-124 regulates osteoclast differentiation. *Bone* **2013**, *56*, 383–389, doi:10.1016/j.bone.2013.07.007.
13. Li, L.; Luo, J.; Wang, B.; Wang, D.; Xie, X.; Yuan, L.; Guo, J.; Xi, S.; Gao, J.; Lin, X.; et al. Microrna-124 targets flotillin-1 to regulate proliferation and migration in breast cancer. *Mol. Cancer* **2013**, *12*, 163–163, doi:10.1186/1476-4598-12-163.

14. Zhu, J.; Wang, S.; Zhang, W.; Qiu, J.; Shan, Y.; Yang, D.; Shen, B. Screening key microRNAs for castration-resistant prostate cancer based on miRNA/mRNA functional synergistic network. *Oncotarget* **2015**, *6*, 43819–43830, doi:10.18632/oncotarget.6102.
15. Chu, M.; Chang, Y.; Guo, Y.; Wang, N.; Cui, J.; Gao, W.-Q. Regulation and methylation of tumor suppressor miR-124 by androgen receptor in prostate cancer cells. *Plos ONE* **2015**, *10*, e0116197, doi:10.1371/journal.pone.0116197.
16. Shi, X.-B.; Ma, A.-H.; Xue, L.; Li, M.; Nguyen, H.G.; Yang, J.C.; Tepper, C.G.; Gandour-Edwards, R.; Evans, C.P.; Kung, H.-J.; et al. miR-124 and Androgen Receptor Signaling Inhibitors Repress Prostate Cancer Growth by Downregulating Androgen Receptor Splice Variants, EZH2, and Src. *Cancer Res.* **2015**, *75*, 5309–5317, doi:10.1158/0008-5472.CAN-14-0795.
17. Shi, X.B.; Xue, L.; Ma, A.H.; Tepper, C.G.; Gandour-Edwards, R.; Kung, H.J.; deVere White, R.W. Tumor suppressive miR-124 targets androgen receptor and inhibits proliferation of prostate cancer cells. *Oncogene* **2013**, *32*, 4130–4138, doi:10.1038/onc.2012.425.
18. Valentino, A.; Calarco, A.; Di Salle, A.; Finicelli, M.; Crispi, S.; Calogero, R.A.; Riccardo, F.; Sciarra, A.; Gentilucci, A.; Galderisi, U.; et al. Deregulation of MicroRNAs mediated control of carnitine cycle in prostate cancer: Molecular basis and pathophysiological consequences. *Oncogene* **2017**, *36*, 6030–6040, doi:10.1038/onc.2017.216.
19. Hu, J.; Sheng, Y.; Shi, J.; Yu, B.; Yu, Z.; Liao, G. Long Circulating Polymeric Nanoparticles for Gene/Drug Delivery. *Curr. Drug Metab.* **2018**, *19*, 723–738, doi:10.2174/1389200219666171207120643.
20. Fujita, Y.; Kuwano, K.; Ochiya, T. Development of small RNA delivery systems for lung cancer therapy. *Int. J. Mol. Sci.* **2015**, *16*, 5254–5270, doi:10.3390/ijms16035254.
21. Muthiah, M.; Park, I.-K.; Cho, C.-S. Nanoparticle-mediated delivery of therapeutic genes: Focus on miRNA therapeutics. *Expert Opin. Drug Deliv.* **2013**, *10*, 1259–1273, doi:10.1517/17425247.2013.798640.
22. Mauri, E.; Perale, G.; Rossi, F. Nanogel Functionalization: A Versatile Approach To Meet the Challenges of Drug and Gene Delivery. *ACS Appl. Nano Mater.* **2018**, *1*, 6525–6541, doi:10.1021/acsanm.8b01686.
23. Saraiva, C.; Paiva, J.; Santos, T.; Ferreira, L.; Bernardino, L. MicroRNA-124 loaded nanoparticles enhance brain repair in Parkinson's disease. *J. Control. Release* **2016**, *235*, 291–305, doi:10.1016/j.jconrel.2016.06.005.
24. Louw, A.M.; Kolar, M.K.; Novikova, L.N.; Kingham, P.J.; Wiberg, M.; Kjems, J.; Novikov, L.N. Chitosan polyplex mediated delivery of miRNA-124 reduces activation of microglial cells in vitro and in rat models of spinal cord injury. *Nanomedicine* **2016**, *12*, 643–653, doi:10.1016/j.nano.2015.10.011.
25. Schulze, J.; Kuhn, S.; Hendrikx, S.; Schulz-Siegmund, M.; Polte, T.; Aigner, A. Spray-Dried Nanoparticle-in-Microparticle Delivery Systems (NiMDS) for Gene Delivery, Comprising Polyethylenimine (PEI)-Based Nanoparticles in a Poly(Vinyl Alcohol) Matrix. *Small* **2018**, *14*, doi:10.1002/smll.201701810.
26. Pandey, A.P.; Sawant, K.K. Polyethylenimine: A versatile, multifunctional non-viral vector for nucleic acid delivery. *Mater. Sci. Eng. C* **2016**, *68*, 904–918, doi:10.1016/j.msec.2016.07.066.
27. Peng, L.; Wagner, E. Polymeric Carriers for Nucleic Acid Delivery: Current Designs and Future Directions. *Biomacromolecules* **2019**, *20*, 3613–3626, doi:10.1021/acs.biomac.9b00999.
28. Shrivastav, A.; Kim, H.-Y.; Kim, Y.-R. Advances in the applications of polyhydroxyalkanoate nanoparticles for novel drug delivery system. *Biomed. Res. Int* **2013**, *2013*, 581684–581684, doi:10.1155/2013/581684.
29. Nigmatullin, R.; Thomas, P.; Lukasiewicz, B.; Puthussery, H.; Roy, I. Polyhydroxyalkanoates, a family of natural polymers, and their applications in drug delivery. *J. Chem. Technol. Biotechnol.* **2015**, *90*, 1209–1221, doi:10.1002/jctb.4685.
30. Meng, D.-C.; Chen, G.-Q. Synthetic Biology of Polyhydroxyalkanoates (PHA). *Adv. Biochem. Eng. Biotechnol.* **2018**, *162*, 147–174, doi:10.1007/10_2017_3.
31. Pişkin, E. Biodegradable polymers as biomaterials. *J. Biomater. Sci. Polym. Ed.* **1995**, *6*, 775–795, doi:10.1163/156856295x00175.
32. Calarco, A.; Bosetti, M.; Margarucci, S.; Fusaro, L.; Nicolì, E.; Petillo, O.; Cannas, M.; Galderisi, U.; Peluso, G. The genotoxicity of PEI-based nanoparticles is reduced by acetylation of polyethylenimine amines in human primary cells. *Toxicol. Lett.* **2013**, *218*, 10–17, doi:10.1016/j.toxlet.2012.12.019.
33. Höbel, S.; Aigner, A. Polyethylenimines for siRNA and miRNA delivery in vivo. *Wiley Interdiscip. Rev. Nanomed. Nanobiotechnol.* **2013**, *5*, 484–501, doi:10.1002/wnan.1228.
34. d'Ayala, G.G.; Calarco, A.; Malinconico, M.; Laurienzo, P.; Petillo, O.; Torpedine, A.; Peluso, G. Cationic copolymers nanoparticles for nonviral gene vectors: Synthesis, characterization, and application in gene delivery. *J. Biomed. Mater. Res. A* **2010**, *94*, 619–630, doi:10.1002/jbm.a.32752.

35. Moret, I.; Esteban Peris, J.; Guillem, V.M.; Benet, M.; Revert, F.; Dasí, F.; Crespo, A.; Aliño, S.F. Stability of PEI-DNA and DOTAP-DNA complexes: Effect of alkaline pH, heparin and serum. *J. Control. Release* **2001**, *76*, 169–181, doi:10.1016/s0168-3659(01)00415-1.
36. Sun, X.; Zhang, N. Cationic polymer optimization for efficient gene delivery. *Mini Rev. Med. Chem.* **2010**, *10*, 108–125, doi:10.2174/138955710791185109.
37. Zhupanyn, P.; Ewe, A.; Büch, T.; Malek, A.; Rademacher, P.; Müller, C.; Reinert, A.; Jaimes, Y.; Aigner, A. Extracellular vesicle (ECV)-modified polyethylenimine (PEI) complexes for enhanced siRNA delivery in vitro and in vivo. *J. Control. Release* **2019**, *319*, 63–76, doi:10.1016/j.jconrel.2019.12.032.
38. Zhou, Y.; Yu, F.; Zhang, F.; Chen, G.; Wang, K.; Sun, M.; Li, J.; Oupický, D. Cyclam-Modified PEI for Combined VEGF siRNA Silencing and CXCR4 Inhibition To Treat Metastatic Breast Cancer. *Biomacromolecules* **2018**, *19*, 392–401, doi:10.1021/acs.biomac.7b01487.
39. Huang, W.; Zhang, C. Tuning the Size of Poly(lactic-co-glycolic Acid) (PLGA) Nanoparticles Fabricated by Nanoprecipitation. *Biotechnol. J.* **2018**, *13*, doi:10.1002/biot.201700203.
40. Croll, T.I.; O'Connor, A.J.; Stevens, G.W.; Cooper-White, J.J. Controllable surface modification of poly(lactic-co-glycolic acid) (PLGA) by hydrolysis or aminolysis I: Physical, chemical, and theoretical aspects. *Biomacromolecules* **2004**, *5*, 463–473, doi:10.1021/bm0343040.
41. Auriemma, M.; Piscitelli, A.; Pasquino, R.; Cerruti, P.; Malinconico, M.; Grizzuti, N. Blending poly(3-hydroxybutyrate) with tannic acid: Influence of a polyphenolic natural additive on the rheological and thermal behavior. *Eur. Polym. J.* **2015**, *63*, 123–131, doi:https://doi.org/10.1016/j.eurpolymj.2014.12.021.
42. Lakard, B.; Herlem, G.; Lakard, S.; Antoniou, A.; Fahys, B. Urea potentiometric biosensor based on modified electrodes with urease immobilized on polyethylenimine films. *Biosens. Bioelectron.* **2004**, *19*, 1641–1647, doi:https://doi.org/10.1016/j.bios.2003.12.035.
43. Godbey, W.T.; Wu, K.K.; Mikos, A.G. Poly(ethylenimine)-mediated gene delivery affects endothelial cell function and viability. *Biomaterials* **2001**, *22*, 471–480, doi:10.1016/s0142-9612(00)00203-9.
44. Kunath, K.; von Harpe, A.; Fischer, D.; Petersen, H.; Bickel, U.; Voigt, K.; Kissel, T. Low-molecular-weight polyethylenimine as a non-viral vector for DNA delivery: Comparison of physicochemical properties, transfection efficiency and in vivo distribution with high-molecular-weight polyethylenimine. *J. Control. Release* **2003**, *89*, 113–125, doi:10.1016/s0168-3659(03)00076-2.
45. Morachis, J.M.; Mahmoud, E.A.; Almutairi, A. Physical and chemical strategies for therapeutic delivery by using polymeric nanoparticles. *Pharm. Rev.* **2012**, *64*, 505–519, doi:10.1124/pr.111.005363.
46. Murugan, K.; Choonara, Y.E.; Kumar, P.; Bijukumar, D.; du Toit, L.C.; Pillay, V. Parameters and characteristics governing cellular internalization and trans-barrier trafficking of nanostructures. *Int. J. Nanomed.* **2015**, *10*, 2191–2206, doi:10.2147/IJN.S75615.
47. Devulapally, R.; Sekar, N.M.; Sekar, T.V.; Foygel, K.; Massoud, T.F.; Willmann, J.K.; Paulmurugan, R. Polymer nanoparticles mediated codelivery of antimiR-10b and antimiR-21 for achieving triple negative breast cancer therapy. *ACS Nano* **2015**, *9*, 2290–2302, doi:10.1021/nn507465d.
48. Wong, L.-Y.; Xia, B.; Wolvetang, E.; Cooper-White, J. Targeted, Stimuli-Responsive Delivery of Plasmid DNA and miRNAs Using a Facile Self-Assembled Supramolecular Nanoparticle System. *Biomacromolecules* **2018**, *19*, 353–363, doi:10.1021/acs.biomac.7b01462.
49. Zadra, G.; Photopoulos, C.; Loda, M. The fat side of prostate cancer. *Biochim. Biophys. Acta* **2013**, *1831*, 1518–1532, doi:10.1016/j.bbalip.2013.03.010.
50. Long, J.; Zhang, C.-J.; Zhu, N.; Du, K.; Yin, Y.-F.; Tan, X.; Liao, D.-F.; Qin, L. Lipid metabolism and carcinogenesis, cancer development. *Am. J. Cancer Res.* **2018**, *8*, 778–791.
51. Galbraith, L.; Leung, H.Y.; Ahmad, I. Lipid pathway deregulation in advanced prostate cancer. *Pharm. Res.* **2018**, *131*, 177–184, doi:10.1016/j.phrs.2018.02.022.
52. Qu, Q.; Zeng, F.; Liu, X.; Wang, Q.J.; Deng, F. Fatty acid oxidation and carnitine palmitoyltransferase I: Emerging therapeutic targets in cancer. *Cell Death Dis.* **2016**, *7*, e2226, doi:10.1038/cddis.2016.132.
53. Melone, M.A.B.; Valentino, A.; Margarucci, S.; Galderisi, U.; Giordano, A.; Peluso, G. The carnitine system and cancer metabolic plasticity. *Cell Death Dis.* **2018**, *9*, 228–228, doi:10.1038/s41419-018-0313-7.
54. Aiderus, A.; Black, M.A.; Dunbier, A.K. Fatty acid oxidation is associated with proliferation and prognosis in breast and other cancers. *BMC Cancer* **2018**, *18*, 805–805, doi:10.1186/s12885-018-4626-9.
55. Koundouros, N.; Poulogiannis, G. Reprogramming of fatty acid metabolism in cancer. *Br. J. Cancer* **2020**, *122*, 4–22, doi:10.1038/s41416-019-0650-z.

56. Stoykova, G.E.; Schlaepfer, I.R. Lipid Metabolism and Endocrine Resistance in Prostate Cancer, and New Opportunities for Therapy. *Int J. Mol. Sci.* **2019**, *20*, 2626, doi:10.3390/ijms20112626.
57. Schlaepfer, I.R.; Rider, L.; Rodrigues, L.U.; Gijón, M.A.; Pac, C.T.; Romero, L.; Cimic, A.; Sirintrapun, S.J.; Glodé, L.M.; Eckel, R.H.; et al. Lipid catabolism via CPT1 as a therapeutic target for prostate cancer. *Mol. Cancer* **2014**, *13*, 2361–2371, doi:10.1158/1535-7163.MCT-14-0183.
58. Ricciardi, M.R.; Mirabilii, S.; Allegretti, M.; Licchetta, R.; Calarco, A.; Torrisi, M.R.; Foà, R.; Nicolai, R.; Peluso, G.; Tafuri, A. Targeting the leukemia cell metabolism by the CPT1a inhibition: Functional preclinical effects in leukemias. *Blood* **2015**, *126*, 1925–1929, doi:10.1182/blood-2014-12-617498.
59. Flaig, T.W.; Salzmann-Sullivan, M.; Su, L.-J.; Zhang, Z.; Joshi, M.; Gijón, M.A.; Kim, J.; Arcaroli, J.J.; Van Bokhoven, A.; Lucia, M.S.; et al. Lipid catabolism inhibition sensitizes prostate cancer cells to antiandrogen blockade. *Oncotarget* **2017**, *8*, 56051–56065, doi:10.18632/oncotarget.17359.
60. Wang, Y.-N.; Zeng, Z.-L.; Lu, J.; Wang, Y.; Liu, Z.-X.; He, M.-M.; Zhao, Q.; Wang, Z.-X.; Li, T.; Lu, Y.-X.; et al. CPT1A-mediated fatty acid oxidation promotes colorectal cancer cell metastasis by inhibiting anoikis. *Oncogene* **2018**, *37*, 6025–6040, doi:10.1038/s41388-018-0384-z.
61. Fessi, H.; Puisieux, F.; Devissaguet, J.P.; Ammoury, N.; Benita, S. Nanocapsule formation by interfacial polymer deposition following solvent displacement. *Int. J. Pharm.* **1989**, *55*, R1–R4,doi:https://doi.org/10.1016/0378-5173(89)90281-0.

International Journal of Molecular Sciences

MDPI

Review

Bioactive Polyphenols and Neuromodulation: Molecular Mechanisms in Neurodegeneration

Francesco Di Meo [1,2,†], Anna Valentino [3,†], Orsolina Petillo [4], Gianfranco Peluso [4], Stefania Filosa [1,5,*,‡] and Stefania Crispi [1,6,*,‡]

[1] Institute of Biosciences and BioResources-UOS Naples CNR, Via P. Castellino, 111-80131 Naples, Italy; francesco.dimeo.90@gmail.com
[2] Department of Biology, University of Naples Federico II, Complesso Universitario Monte Sant'Angelo Via Cinthia, 80126 Naples, Italy
[3] Elleva Pharma s.r.l., Via P. Castellino 111, 80131 Naples, Italy; anna.valentino@ellevapharma.com
[4] Institute on Terrestrial Ecosystems (IRET) CNR, Via P. Castellino 111, 80131 Naples, Italy; orsolina.petillo@cnr.it (O.P.); gianfranco.peluso@cnr.it (G.P.)
[5] IRCCS Neuromed, Localitá Camerelle, 86077 Pozzilli (IS), Italy
[6] Stazione Zoologica Anton Dohrn, Villa Comunale, 80121 Napoli, Italy
* Correspondence: stefania.filosa@ibbr.cnr.it (S.F.); stefania.crispi@ibbr.cnr.it (S.C.)
† These authors contributed equally to this work.
‡ These authors contributed equally to this work.

Received: 3 March 2020; Accepted: 3 April 2020; Published: 7 April 2020

Abstract: The interest in dietary polyphenols in recent years has greatly increased due to their antioxidant bioactivity with preventive properties against chronic diseases. Polyphenols, by modulating different cellular functions, play an important role in neuroprotection and are able to neutralize the effects of oxidative stress, inflammation, and apoptosis. Interestingly, all these mechanisms are involved in neurodegeneration. Although polyphenols display differences in their effectiveness due to interindividual variability, recent studies indicated that bioactive polyphenols in food and beverages promote health and prevent age-related cognitive decline. Polyphenols have a poor bioavailability and their digestion by gut microbiota produces active metabolites. In fact, dietary bioactive polyphenols need to be modified by microbiota present in the intestine before being absorbed, and to exert health preventive effects by interacting with cellular signalling pathways. This literature review includes an evaluation of the literature in English up to December 2019 in PubMed and Web of Science databases. A total of 307 studies, consisting of research reports, review articles and articles were examined and 146 were included. The review highlights the role of bioactive polyphenols in neurodegeneration, with a particular emphasis on the cellular and molecular mechanisms that are modulated by polyphenols involved in protection from oxidative stress and apoptosis prevention.

Keywords: polyphenols; neuroprotection; apoptosis prevention; oxidative stress; gut microbiota

1. Introduction

An improvement in socio-economic conditions, especially in developed countries, results in an increase in elderly people. This determines a corresponding enlargement of the pathologies linked to brain aging, such as cognitive and neurodegenerative diseases. The potential mechanisms underpinning brain neurodegeneration have not yet been completely elucidated; nevertheless, oxidative stress and inflammation are considered the main effectors of brain decline.

Nowadays, there is a growing interest in dietary polyphenol nutrients since different epidemiological studies have suggested that diets rich in plant-derived phytochemicals and, in particular, polyphenols, are beneficial to human health [1]

Among phytochemicals, polyphenols are the major group of compounds produced by plants as secondary metabolites that protect plants against reactive oxygen species (ROS), ultraviolet radiation (UV), pathogens, parasites and plant predators. They act as natural antioxidants thanks to their metal-chelating and free radical scavenger properties. Bioactive polyphenols have been reported to prevent the age-related cognitive decline typical of neurodegenerative diseases. Dietary bioactive polyphenols can also modulate cognitive deficits and synaptic plasticity and promote neurogenesis [2,3].

Neurodegenerative diseases are characterized by the progressive loss of function of a specific population of neurons and neural stem cells that results in sensory and motor deficits and cognitive impairment. Different signaling pathways are involved in neurodegeneration, including oxidative stress, inflammation and apoptosis. Bioactive polyphenols are able to counteract these processes by directly scavenging free radical species inhibiting 'pro-oxidant' enzymes, activating anti-oxidant enzymes [4] or intervening in apoptotic pathways [5].

Polyphenols act by preventing the DNA damage triggered by hydrogen peroxide (H_2O_2) and by transition metals such as copper and iron. Iron-mediated oxidative DNA damage by hydroxyl radical (•OH) is the primary cause of cell death under oxidative stress conditions for both prokaryotes and eukaryotes [6]. Polyphenols can also directly scavenge ROS or inhibit the expression of molecules sensitive to oxidative stress such as nuclear factor-kB (Nf-κB) and activator protein-1 (AP-1) [7].

The molecular mechanism of neuroprotection involves the regulation of the mitochondrial apoptosis cascade, which is finely tuned by the imbalance by between B-cell lymphoma-2 (Bcl-2) and Bcl-2-associated X protein (Bax). Phytochemical neuroprotection can be achieved by introducing anti-apoptotic Bcl-2, thus preventing apoptosis [8].

Bioactive polyphenols can exert neuromodulatory effects, activating different intracellular signaling pathways that are crucial for neuroprotection. The PI3K/Akt (Phosphoinositide 3-kinases/Akt) pathway prevents apoptosis by upregulating the expression of Bcl-2; the PKC-ERK1/2 (Protein kinase C/ Extracellular signal-regulated protein kinases 1 and 2) pathway decreases Bcl-2 (B-cell lymphoma 2), Bcl-w (Bcl-2-Like Protein 2) and Bcl-xL (B-cell lymphoma-extra large), which are other anti-apoptotic proteins; Akt-ERK1/2 inhibits the pro-apoptotic activity of Bad (BCL2 associated agonist of cell death) and Bim (Bcl-2-interacting mediator) and activates caspases 9 and 3 [9,10].

The neuroprotective effects of polyphenols can be carried out through synthesis of neurotrophic factors, such as brain-derived neurotrophic factor (BDNF), nerve growth factor (NGF) or glial cell line-derived neurotrophic factor (GDNF). They can exert neurotrophic activity by binding the cognate receptors and activating the downstream neuroprotective pathways [11].

The beneficial health effects of bioactive phenolic compounds mainly depend on their bioavailability and absorption rate. These characteristics can be modulated through interaction with other dietary nutrients and through the action of enzymes present in the small intestine and in the liver. Polyphenols are usually recognized as xenobiotics by the human body. After ingestion, their absorption through the gut barrier can be increased following specific biotransformation and conjugation such as methylation, sulfation and glucuronidation [12].

Polyphenols are effective in neuroprotection in a different way—directly, by affecting brain functions and indirectly, by modulating gut microbiota composition and the metabolites produced. Both actions determine the production of neurotransmitters and neuropeptides that are able to influence the brain functions.

In this review, we discuss the different cellular and molecular mechanisms by which dietary bioactive polyphenols exert neuroprotective functions. The review evaluates the main publications in the field, providing a comprehensive analysis of the efficacy of bioactive polyphenols.

2. Methodology

We performed a literature review, searching within the PubMed and Web of Science database. As keywords, we used the terms: oxidative stress, antioxidant, polyphenols, neurodegeneration, neuroprotection, Alzheimer's disease, Parkinson's disease, and Huntington's disease. Research reports, review articles and articles in English published up to December 2019 were selected and evaluated. In addition, we examined the citations therein and included them when appropriate. In total, we examined 307 references and included 146 of them in the present review.

3. Oxidative Stress and Polyphenols

Oxidative stress occurs when ROS accumulate in the cells for excessive production or insufficient neutralization. ROS are a contradiction for the cells. They are produced in normal metabolism as part of several physiologic processes and, when present in physiologic concentrations, they control redox homeostasis in the cell. However, an imbalance between their production and the ability of the cell to enforce antioxidant defense mechanisms may affect cellular structure and functional integrity, resulting in cell damage and leading to necrotic or apoptotic cell death [13–15].

ROS cause severe molecular damage in the major cell components such as protein oxidation, lipid oxidation, DNA oxidation, and glycoxidation. They can be divided into free radicals and nonradicals. Free radicals are the molecular species containing at least one unpaired electron in the shell around the atomic nucleus.

Among free radicals, H_2O_2 is one of the most important ROS with a physiological significance. H_2O_2 is formed in the cells in a reaction catalyzed by the superoxide dismutase enzyme (SOD) and also, at relatively low concentrations, it can penetrate the biological membranes and cause severe damage to cellular macromolecules. ROS increase with exposure to the environment. To counterbalance the effect of oxidants, cells have evolved an intricate network of defense mechanisms. Indeed, depending on the intensity and duration of oxidative stress, the cell response can be different, ranging from cell proliferation to cell cycle arrest or cell death by apoptosis or necrosis [16].

The adverse effects of ROS can be inactivated by the action of antioxidants [17]. They are defined as compounds able to inhibit the oxidation of any molecule, even when present at very low concentration [18]. By inhibiting or quenching free radical reactions, antioxidants delay or block cellular damage.

It is widely accepted that neurodegenerative development is associated with oxidative stress that determines severe injury in the cell. In fact, oxidative stress can result in deep biological damage. An imbalance in redox regulation determines the overproduction of ROS with the induction of progressive cellular damage, which is fundamental in neurodegenerative diseases. The production of excessive ROS in neuronal tissue is mainly due to the activity of excitatory amino acids and neurotransmitters [19]. Thus, neuronal cells need antioxidants to scavenge and prevent the formation of ROS.

The body protects itself from ROS by using enzymatic antioxidant mechanisms [20]. The antioxidant enzymes reduce the levels of lipid hydroperoxide and H_2O_2; thus, they are important in preventing lipid peroxidation and maintaining the structure and function of cell membranes.

The nonenzymatic antioxidants are the natural antioxidants present in plants. Among them, polyphenols are the most powerful antioxidants able to balance the cellular ROS by activating antioxidant signaling pathways [21,22]. Different studies indicate that dietary antioxidants consumed daily exert a protective role [23].

Plants produce nonenzymatic antioxidants such as vitamins that act to interrupt free radical chain reactions. Vitamin C is present in all plant cells and it has intracellular and extracellular antioxidant capacity. Vitamin E is present exclusively in plastids. It represents the principal defense against oxidative membrane damage, being concentrated in the hydrophobic bilayer of the cell membrane. Vitamin E avoids lipid peroxidation, thus protecting polyunsaturated fatty acids (PUFA) from reactive oxygen damage [24].

Antioxidant plant polyphenols belong to different groups: phenolic acids, phenolic diterpenes, volatile oils, flavonoids and stilbene (Figure 1) [25]. All act as ROS scavengers, or induce antioxidant enzymes [26].

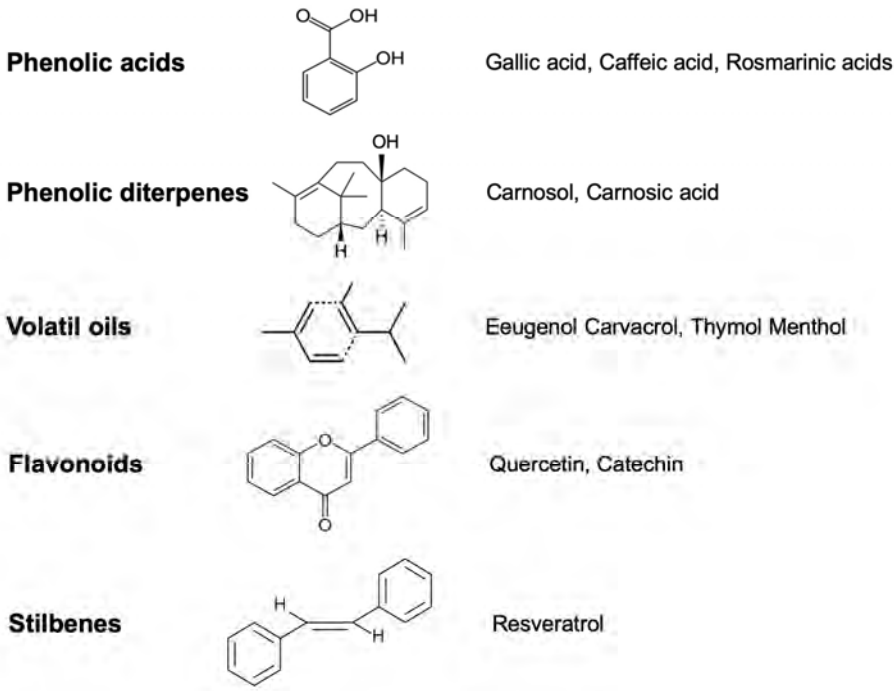

Figure 1. Typical representatives of antioxidant polyphenol classes with their basic chemical structure.

Phenolic acids exert their antioxidant action, trapping free radicals [27]. The antioxidant mechanism of phenolic diterpenes is related to the scavenging activities of lipid free radicals and to the inhibition of low-density lipoprotein oxidation [28]. Volatile oils, as well as phenolic compounds, act as antioxidants by reacting with peroxyl radicals [29]. Flavonoids are the most abundant class of plant polyphenols, due to their metal-chelating and free radical scavenger properties [30]. On the contrary, stilbenes scavenge hydroxyl radicals.

Other non-flavonoid polyphenols present in foods have antioxidant properties. Among them, curcumin, from turmeric Curcuma longa, prevents lipid peroxidation by scavenging H_2O_2 and hydroxyl radicals. Curcumin can also act as an antioxidant, reducing ferric ion (Fe^{3+}) and chelating ferrous ion (Fe^{2+}) [31].

4. Molecular Pathways Involved in Neuroprotection of Polyphenols

Although cells are equipped with a high variety of antioxidants, some tissues and organs are much more vulnerable than others to oxidative stress, probably because of their elevated consumption of oxygen and the consequent generation of large amounts of ROS. Several observations suggest that the brain is particularly vulnerable to oxidative stress [32] and oxidative stress has been implicated in the pathogenesis of many clinical conditions and in the process of aging.

Oxidative stress has been found to be increased in several human age-related degenerative diseases, including genetically-linked neurodegenerative diseases, like Alzheimer's disease (AD), Parkinson's disease (PD), and Huntington's disease (HD) [33]. However, whether oxidative stress is a primary cause or a downstream consequence of these neuropathological conditions or, more in general, of the aging process is still an open question [34].

Neurons are particularly sensitive to oxidative stress because, being postmitotic cells, they will not be replaced. Moreover, the ability of cells to respond to oxidative protein damage also seems to decline with age [35]. Since the antioxidant systems are overwhelmed in pathological conditions, the use of natural molecules like polyphenols can be viewed as a novel antioxidant therapeutic strategy to reduce neuronal ROS and ameliorate the neurodegenerative process.

Polyphenols, due to their ability to modulate multiple cellular processes including redox balance, have invaluable potential as antioxidant agents.

Polyphenols such as resveratrol from grapes and wine, curcumin from tumeric, and epigallocatechin-3-gallate from green tea (EGCG), are able to protect against neurodegenerative diseases by activating the protein kinases signaling molecular pathways such as Keap1/Nrf-2/ARE, the major protective pathway against endogenous and exogenous ROS [36,37]. The interaction between Keap1 and bioactive molecules leads to the disruption of the Keap1/Nrf2 complex, allowing Nrf2 to translocate to the nucleus where it binds adenylate and uridylate (AU)-rich elements (AREs) and triggers the expression of antioxidant proteins such as heme oxygenase-1 [38].

Polyphenols also stimulate neurotrophic receptor factors with a pivotal role in the maintenance of neuronal health. Examples are BDNF, which is involved in learning and memory [39], NGF, which is crucial for the survival of brain neurons [40], and GDNF, which regulates cell survival and synaptic plasticity [41]. Several studies reported that different flavonoids, including resveratrol, are able to enhance the expression of these factors. Quercetin and genistein were shown to stimulate NGF-induced neurite outgrowth [42,43]. Resveratrol is able to induce the release of BDNF and GDNF, thus protecting cells from neurotoxicity [44,45].

The neuroprotective role of polyphenols is carried out by activating the pathways that, in cells, regulate transcription, translation, proliferation, growth and survival, such as PI3K/Akt, PKC-ERK1/2, Akt-ERK1/2 and MAPK (Mitogen-activated protein kinase). Their binding to Trk receptors (tyrosine receptor kinases) activates the protein kinase cascades and, finally, cAMP (3',5'-cyclic adenosine monophosphate)response element-binding protein (CREB), increasing the expression of Bcl-2, Bcl-xL and of neurotrophic factors [46]. In addition, this binding promotes receptor dimerization and autophosphorylation by activating the downstream signaling cascades and promoting the survival of motor neurons, hippocampal neuronal cells, and spinal ganglion neurons [47].

A flavone derivative has been reported to act as a TrkB agonist and to activate the downstream signaling pathway [48]. More recently, resveratrol was shown to exert neuroprotection through its interaction with Trk receptors [49].

In the brain, the anti-inflammatory action of polyphenols leads to neuroprotective effects. In fact, polyphenols inhibit the release of cytokines from activated glia and they also downregulate pro-inflammatory transcription factors such as NF-κB [50]. For example, quercetin determines a strong neuroprotective effect, repressing NF-κB [51]; catechin, after stress injury, increases cell survival by downregulating the NF-κB and MAP kinase pathways [52].

The molecular mechanisms modulated by polyphenols are summarized in Figure 2.

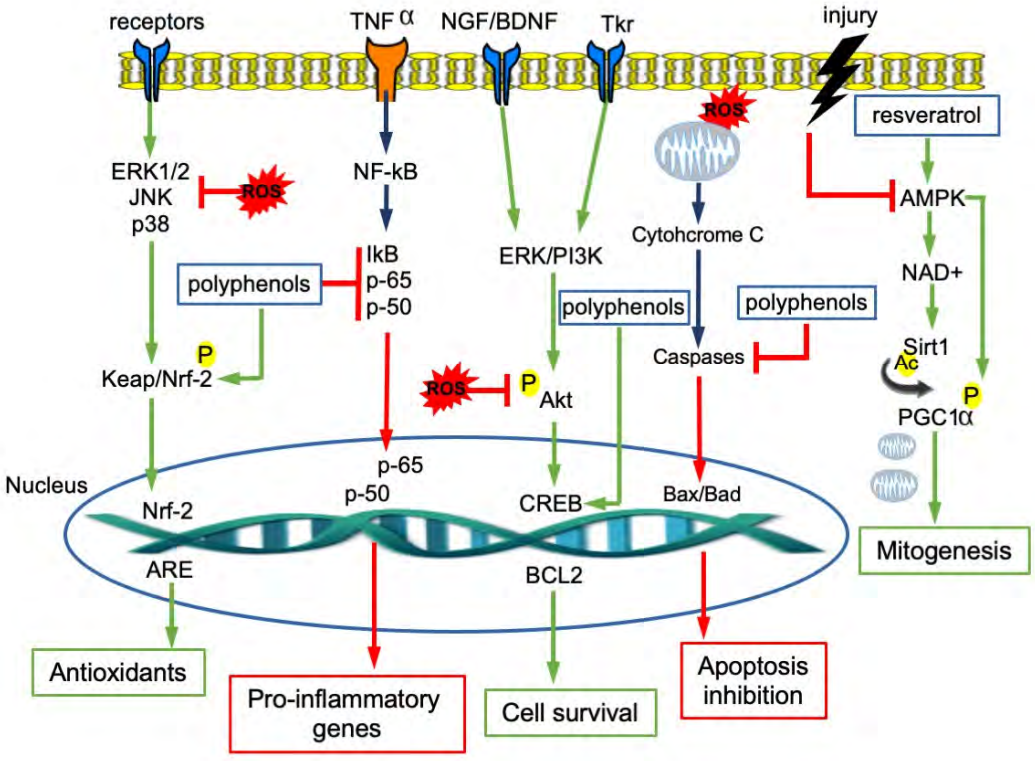

Figure 2. Intracellular signaling pathways involved in neuroprotection and modulated by polyphenols.

5. Effect of Polyphenols on Neurodegenerative Disorders

Despite the variability in the clinical picture of neurodegenerative disorders, these diseases share common molecular traits. Inflammation and oxidative stress are responsible for the disruption of the functions of the neurovascular units in AD, PD, HD and dementia. ROS are able to interact with different neuronal signaling pathways, such as protein kinase and lipid kinase signaling cascades [53,54] (Table 1).

Table 1. Signaling pathways activated by polyphenols in neurodegenerative diseases.

Polyphenol	Signaling Pathway	References
Resveratrol	SIRT1/PGC-1 PI3K/Akt	[52,55]
Curcumin	AMPK/NF-kB PI3K/Akt/GSK-3β	[56–58]
Quercetin	MAPK/AKT/ PI3K ERK/CREB	[59]
Catechins (EGCG)	PKC/MAPK/PI3K/Akt MEK/ERK1/2	[60–62]

5.1. Alzheimer's Disease

AD is the most frequent form of dementia in the elderly population [63], with progressive neurodegeneration. It is characterized by the deposition of Amyloid β (Aβ) peptides as Aβ plaques and intracellular neurofibrillary tangles [64,65] that ultimately lead to a gradual deterioration in brain structure and to the loss of intellectual function [66].

The presence of amyloid beta (Aβ) peptides in Alzheimer's disease confers oxidative insult on neurons and glial cells, leading to a change in synaptic plasticity [67]. The neuronal cytotoxicity in AD seems to be imputable to N-methyl- D-aspartic acid (NMDA) receptor activation coupled with ROS production [68]. This mechanism, through the PKC/MAPK pathways, leads to the release of arachidonic acid, involved in AD neuron apoptosis. Aβ peptides and ROS promote neurotoxicity in AD, inactivating PI3k/Akt pathways. The Akt inactivation regulates various pro-apoptotic mediators [56]. Several studies indicated that a diet rich in polyphenols inhibits the above-mentioned pathways [69]. Curcumin displays anti-amyloidogenic properties, preventing the neurodegenerative process in AD through the inhibition of MAPK and PI-3K pathways [70]. In addition, curcumin is able to block the BDNF decrease in rats inoculated with Aβ peptide, modulating the Akt/GSK-3β signaling pathway, thus determining a cognitive improvement [71]. Recently, it has been reported in an AD mouse model that curcumin reduced Aβ production through the inhibition of β-secretase (BACE-1), the enzyme that is responsible for the proteolytic processing of the amyloid precursor protein [72].

The antioxidant activity of resveratrol protects the memory decline in AD. In cells, it has been reported that resveratrol suppresses Aβ-induced ROS generation and apoptosis [73]. Another study reported that resveratrol exerts a neuroprotective role through its modulation of the PI3K/Akt signaling pathway [74]. SIRT1 (Sirtuin 1) in brain has been shown to be protective against neurodegeneration by deacetylating several transcription factors involved in neuronal protection and stress resistance [75]. Dietary resveratrol protects against Aβ formation and oxidative stress by modulating SIRT1 expression [76,77]. In particular, this ability is linked to the deacetylation of PGC-1α, to the presence of active proliferator-activated receptor-γ (PPAR-γ), and to the protection against mitochondrial damage by Bcl-2 upregulation [55]. EGCG was described as active towards AD in animal studies, being able to significantly reduce the cognitive decline and Aβ peptides, and to upregulate proteins related to synaptic plasticity [78]. EGCG prevents neuronal apoptosis from neurotoxic processes inhibiting BACE-1 [79]. In addition, EGCG significantly improves neuronal survival and hippocampal neurogenesis by activating the PI3K/Akt signaling pathway and inhibiting the MAPK pathway [80]. In vitro and in vivo studies reported the neuroprotective role of quercetin against Aβ toxicity, showing that this polyphenol determined cell viability increase with a reduction in neuronal oxidative stress [81]. Quercetin seems to inhibit the Aβ plaque aggregation and the formation of neurofibrillary tangles probably increasing the levels of apolipoprotein E, that has a key role in the clearance of Aβ [82]. A study performed in a triple transgenic mouse model of AD showed that quercetin, after three months treatment, was able to reduce the amount of the β-amyloid fibers with improvement of cognitive performances [83]. More recently, it was shown that a quercetin-enriched diet affected the latency in APP/PS1 mice only when administered at early stage. The effect was due to the inhibition of amyloidogenic processing through the reduction in the BACE-1 enzyme [84]. Finally, quercetin treatments in Drosophila models of AD indicated that this flavonoid could restore Aβ-induced perturbation by acting on cell cycle signaling pathways and DNA replication [85].

5.2. Parkinson's Disease

PD is a chronic and long-term degenerative disorder, characterized by the loss of dopaminergic neurons in the substantia nigra, which determines clinical motor deficits such as rigidity, bradykinesia and tremors [57].

Oxidative stress remains the strongest leading theory to explain the progressive loss of dopaminergic neurons in substantia nigra in PD patients [58]. Microglia produce high levels of ROS through NADPH oxidase, which induces the PKC delta and ERK1/2 pathways' activation of genes involved in apoptosis [59]. The neuroprotective effect of polyphenols, has been linked to their free

radical scavenging and anti-inflammatory properties, both in cellular and animal models [60,61]. They are able to reduce neurotoxicity by interacting with protein aggregates such as α-synuclein [62].

Different studies using in vitro and in vivo models of toxin- induced PD indicated that curcumin reduces oxidative stress with a reduction in apoptosis through the Akt/Nrf2 signaling pathway, since an increase in antioxidant enzyme activity via Nrf2 transcription was detected [86–88]. Several experiments also reported that curcumin in PD is able to counteract the decrease in the enzyme tyrosine hydroxylase—the rate-limiting enzyme involved in dopamine synthesis—which has been suggested to be causative in the onset of PD [89]. Curcumin exerts neuroprotective effects in PD by inhibiting oxidative stress through the decrease in ROS, TNF-α and IL-6 and the concomitant increase in Glutathione (GSH) levels [90]. On the other hand, in PD, curcumin not only acts as an antioxidant, but also as anti-inflammatory, reducing the production of TNF-α and Interleukin-6 (IL-6). The beneficial effect of curcumin in the pathophysiology of PD can be also linked to the ability to decrease toll-like receptor 4 (TLR4) and its downstream effectors (NF-κB, IRF3 (Interferon Regulatory Factor 3) and MyD88 (Myeloid differentiation primary response 88) [91].

Resveratrol seems to be a direct modulator in PD-affected pathways. Numerous in vitro studies have demonstrated that this molecule is able to prevent the rotenone-induced autophagic dysfunction by promoting the degradation of α-synuclein [92]. Other studies showed that resveratrol has a protective effect acting on the AKT/GSK-3β signaling pathway [93] or by inhibiting apoptosis through the upregulation of antioxidant enzymes [94]. In addition, resveratrol neurotrophic effects are accomplished through CREB activation in the hippocampus and amygdala neurons, thus reducing oxidative damage induced by neurotoxins [11]. The antioxidant effects of quercetin in PD have not been fully elucidated. Some studies reported that quercetin protected neurons in a rotenone-induced rat model of PD in a dose-dependent manner, upregulating mitochondrial complex-I activity. This molecular mechanism strongly suggests that quercetin has the ability to repair defective mitochondrial electron transport, a hallmark of PD. In addition, quercetin decreases glutathione levels and increases catalase and superoxide dismutase [95]. EGCG in PD exerts neuroprotective effects through AMPK activation, which positively regulates the mitochondrial biogenesis needed for dopaminergic neuronal survival. EGCG in vivo has been reported to preserve the loss of dopaminergic neurons by inhibiting neuronal nitric oxide synthase [96]. EGCG was also shown to prevent striatal dopamine depletion and dopaminergic neuron loss in substantia nigra [97].

5.3. Huntington's Disease and Vascular Dementia

In addition to AD and PD, two other neurodegenerative disorders, Huntington's disease and dementia, are characterized by a total compromise in cognition. The role of polyphenols in prevention/treatment is not so extensively studied in these two neurodegenerative diseases.

HD is a dominantly inherited neurodegenerative disorder characterized by progressive striatal and cortical neurodegeneration with associated motor and cognitive defects. The disease-causing mutation is an expansion of a CAG trinucleotide repeat (>36 repeats) encoding a polyglutamine stretch in the N-terminal region of the huntingtin protein, a ubiquitous protein whose function is still unclear [98]. Mutated Huntington is expressed not only in the brain neurons, but also in the enteric neurons [99,100]. HD has also been associated with mitochondrial dysfunction and oxidative stress, as possible disease mechanisms [101,102]. HD cellular models displayed a deregulation in mitochondrial membrane potential and respiration, implicating a decline in mitochondrial function. It has been reported that resveratrol in HD increases the transcription of genes associated to mitochondrial function [103].

To date, only a few studies have analyzed the effects of curcumin in HD. It has been described that curcumin treatment in a rat model of HD reduced mitochondrial damage and exerted antioxidant effects by activating the Nrf2 pathway [104]. A different study using *Drosophila melanogaster* as an HD model showed that curcumin protects against neurodegeneration, suppressing polyglutamine cytotoxicity and cell death [105]. The neuroprotective role of curcumin has been recently reported in an HD transgenic animal model. This study evidenced that curcumin protected the brain from neuropathological and phenotypic complications associated to the disease [106]. It has

been reported that resveratrol in HD increases the transcription of genes associated to mitochondrial function [103]. Resveratrol in HD seems to modulate SIRT. Resveratrol in mouse models of HD has been shown to strongly increase transcription of mitochondrial genes and to enhance mitochondrial function. This activity determines an improvement of motor function in HD transgenic mice [103]. Quercetin was able to reduce mitochondrial oxidative stress in HD. This effect leads to an increase in motor skills and coordination, as reported in a drug-induced HD model. Indeed, a reduction in the neuro-inflammatory response and an increased number of astrocytes and decreased microglial proliferation were observed in core lesions [107,108].

Vascular dementia arises from chronic vascular damages in the brain. Cerebral ischemia, increasing ROS production, induces neuronal injury accompanied by a progressive decline in memory and cognitive function [109]. In dementia, curcumin, resveratrol and catechins act as free radical scavengers, as well as natural anti-inflammatory agents, by suppressing the TNF-mediated NF-κB activation. In addition, they act to upregulate endogenous antioxidant enzymes and downregulate enzymes involved in the production of ROS [110]. Curcumin was shown to restore memory deficit in an induced mouse model of memory impairment, thanks to its antioxidant action and to the improvement of cerebral circulation [111]. Resveratrol was neuroprotective against vascular dementia by reducing cell death in the hippocampus and preventing the loss of reference memory [112]. In a rat model of vascular dementia, resveratrol was able to restore the cognitive deficits, to reverse oxidative stress levels and BDNF depletion [113]. In a mouse model of dementia, treatment with quercetin restored cognitive deficit and energy metabolism by directly scavenging superoxide, hydroxyl radicals and by inhibiting various oxidases [114]. A summary of the effects of polyphenols in neurodegenerative diseases is reported in Table 2.

Table 2. Summary of the effects of polyphenol treatment from in vitro and in vivo studies.

Pathology	Type of Study	Polyphenols (dose)	Time	Effect	References
Alzheimer's disease	mice	grape extract (5–20 μM)	5 months	Inhibition of Aβ oligomerization	[3]
Parkinson's disease	neuroblastoma cell line	caffeic acid (10–100 μM)	1 hour	Prevention of apoptotic cell death	[9]
Neurodegenerative disorders	neonatal mouse cerebellum cells	curcumin (1–50 μM)	24 hours	Enhancement and repair of neural plasticity	[37]
Alzheimer's disease	rats	curcumin (50–200 mg/kg)	7 days	Improvement of cognitive deficits	[71,72]
CNS disorders	mice	Resveratrol (20 mg/kg)	7 days	Regulation of pathway involved in CNS disorder and aging	[73]
Alzheimer's disease	mice	Resveratrol (24 mg/kg)	45 days	Anti-oxidant effect against beta-amyloid plaque formation	[76,77]
Alzheimer's disease	mice	ECGC (50 mg/kg)	6 months	Reduction in A-β deposition	[78]
Alzheimer's disease	human brain microvascular endothelial cells	Quercetin (0.3–30 μmol/L)	24 hours	Increase in cell viability and of antioxidant activity	[81]
Parkinson's disease	primary rat mesencephalic cells	Catechin, quercetin (40 μM)	48 hours	Protective effect on DA neurons under oxidative stress	[61]70
Parkinson's disease	rodent model	Curcumin 30 mg/kg)	4 days	Neuroprotective actions (anti-inflammatory and anti-oxidative)	[88,91,115]
Parkinson- like disease	dopaminergic-like cells	Resveratrol (50–200 μM)	12 hours	Neuroprotective effects by inhibiting apoptosis caused by oxidative stress	[92]
Parkinson's disease	rats	Resveratrol (20 mg/kg)	21 days	Prevention of neuronal death	[94,95]
Parkinson's disease	rats	Quercetin (25–75 mg/kg)	4 days	Neuroprotective effect observed in neurotoxin-induced Parkinsonism	[95]

Parkinson's disease	mice	ECGC (20 mg/kg)	5 days	Preventive effects on NOS	[96,97]
Huntington's disease	mice	ECGC (1 mg/kg)	28 days	Improvement of gene transcription associated to mitochondrial function	[103]
Huntington's disease	rats	Curcumin (40 mg/kg)	7 days	Amelioration of mitochondrial dysfunctions	[104,105]
Huntington's disease	mice	Curcumin (20–40 mg/kg)	7 days	Alleviation of debilitating symptoms associated with the disease	[106]
Huntington's disease	rats	Quercetin (25–50 mg/kg)	4 days	Potential use for inflammatory damages	[107,108]
Memory and cerebral blood flow	mice	Curcumin (10–50 mg/kg)	21 days	Beneficial effects of oxidative stress associated with neurodegenerative disorders	[111]
Dementia	rats	Resveratrol (10–20 mg/kg)	4 days	Neurorestorative effects	[113]
Memory dysfunction	mice	Quercetin (2.5–10 mg/kg)	21 days	Protective toward off dementia and neurodegenerative disorders	[114]

6. Bioactivity of Polyphenols and Gut Microbiota Interplay

Most of the polyphenols from plants ingested in the diet undergo intestinal transformation before being absorbed by enterocytes and colonocytes. The modifications can be either by enzymes produced by the enterocytes themselves or by the microbiota present in the intestine (Figure 3).

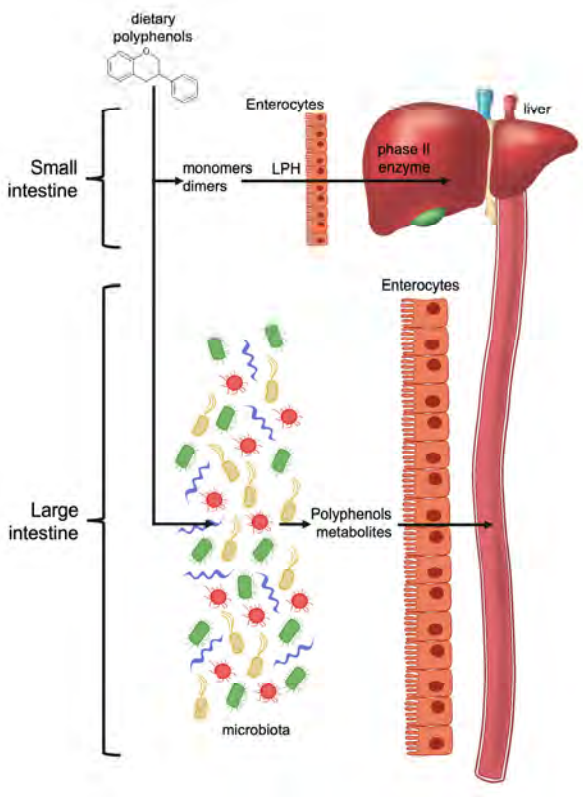

Figure 3. Dietary polyphenol metabolism in small and large intestine. In the small intestine, low molecular weight polyphenols, monomers or dimers, can be absorbed directly or after phase II reaction metabolic conversion. In the large intestine, high molecular weight and conjugated polyphenols are absorbed after transformation processes by enzymes produced by bacteria.

The bioavailability of native polyphenols is very low after recruitment at circulating levels. Polyphenols, to be effective, must be transformed into potentially more bioactive compounds, such as low-molecular weight metabolites [116].

Gut microbiota is essential in transforming numerous compounds that reach the colon, thanks to the capacity of microorganisms to produce a huge and varied range of enzymes.

Enzymatic conjugation processes are needed to reduce the potential toxic effects of polyphenols. These modifications result in the formation of polyphenol metabolites that show new biological activities [117].

The two main factors determining the modification of dietary polyphenols in the gastrointestinal tract are the chemical polyphenols' structure and the individual variety of gut microbiota composition. In fact, the structural subfamily and its scaffold enable only some transformations, thus reducing the kind (class, species) of final bioactive compounds that are produced. Some modifications of polyphenols can occur through enzymes produced by the majority of bacteria, while others require enzymes produced by specific bacterial species. The presence or absence of these bacteria in the individual's microbiota will cause different biotransformation of dietary polyphenols. This means that beneficial effects for consumers depend on the dietary polyphenols and on the individual's microbiota composition.

Polyphenols are molecules with high complexity and for this reason they generally reach the large intestine without modifications. The most complex oligomers are not absorbed in the small intestine, but are processed in the colon by microbiota [118].

EGCG, for example, is transformed in aglycones and gallate, which is further decarboxylated into pyrogallol. In vitro pyrogallol drastically inhibits monocyte migration by reducing levels of inflammatory macrophage differentiation. In addition, pyrogallol increases the phosphorylation of PI3K-AKT and AMPK and reduces caspase levels. In this way, it inhibits monocyte-associated cell death [119]. Pyrogallol is also a GPR35 agonist. GPR35 is an orphan G protein-coupled receptor and is associated to inflammation, cardiovascular diseases, metabolic disorders, Parkinson's disease and other neuronal disorders. GPR35 agonists, as catechol-O-methyl transferase inhibitors, are commonly used for the treatment of Parkinson's disease [120]. Pyrogallol can also block aggregate formation in α-synuclein [121]. The presence of aberrant soluble oligomeric conformations of α-synuclein may contribute to PD pathogenesis. Another example is curcumin that is modified in the colon tract by a specific enzyme produced by *E. coli*. This bacterium converts curcumin in its active metabolite, tetrahydrocurcumin, in a two-step reduction reaction. This metabolite shows both greater in vitro and in vivo antioxidant activity than curcumin [122]. Resveratrol bioavailability is greatly increased by gut microbiota metabolism. Resveratrol in plants is present as a glycosidic form of piceid, that is a stilbenoid glucoside. Two different bacteria—*Bifidobacteria infantis* and *Lactobacillus acidophilus*—convert piceid into resveratrol [123]. Then, resveratrol is further metabolized to obtain the active aglycone form by *Slackia equolifaciens* and *Adlercreutzia equolifaciens* [124].

Bacteria in the gut can cleave the ring structure of several flavonoids into short-chain fatty acids (SCFAs) like hydroxyphenylacetic and hydroxyphenylpropionic acids, as well as into acetate and butyrate [125]. Some polyphenols, like quercetin, are not modified in SCFAs; nonetheless, they can enhance the production of SCFAs, especially butyric acid [126].

Dietary polyphenols show neuroprotective potential, but their selective permeability across the blood–brain barrier (BBB) limits their bioavailability, thus limiting their protective efficacy. The BBB is a dynamic interface that regulates molecular interactions between the blood and the neuronal tissue, having an essential role in providing nutrients and other molecules and regulating the access of compounds to the brain. After intestinal absorption, some polyphenol metabolites can reach concentrations in the bloodstream that can exert effects in vivo. However, the effective brain uptake of these polyphenols' metabolites, and their possible direct neuroprotective potential, is still controversial, given that the exact mechanisms by which they may permeate the BBB are not completely understood. Nerveless, polyphenol microbial metabolites largely showed greater permeability through gut and blood–brain barriers compared to their parent compounds. For

example, 5-(hydroxyphenyl)-γ-valerolactone-*O*-sulfate, a secondary microbial metabolite of the flavan-3-ols, is able to reach the brain and cross the BBB in in silico, in vitro and in vivo models [127]. Microbial metabolites derived from dietary lignans, a class of polyphenols, like equol and enterolactone, passively cross both the gut and BBB barriers and show protective ability against inflammation in microglia [128]. A recent study demonstrates that microbial polyphenol metabolites could be transported across the BBB endothelium [129]. In vitro experiments showed that some polyphenols' metabolites cross BBB by transmembrane diffusion and their lipophilicity can determine greater or minor uptake [130]. Nevertheless, it is not clear whether the primary route by which polyphenols' metabolites cross the BBB happens by simple diffusion or by carrier-mediated transport.

Gut microbiota and polyphenols influence each other. Gut microbiota transforms polyphenols, improving bioavailability and health effects. At the same time, dietary polyphenols regulate microbiota composition, favoring the growth of some bacteria and avoiding the growth of pathogens. Specifically, dietary polyphenols have shown the ability to modulate gut microbiota composition and function, interfering with bacterial quorum sensing, membrane permeability, as well as sensitizing bacteria to xenobiotics.

Specific polyphenols modulate microbiota community composition, modifying the ratio of bacteroides/firmicutes, the most frequent bacteria genera present in the distal gut [131]. For example, resveratrol presented a significant antibacterial activity towards clinically important bacteria, such as *Salmonella enterica*, *Enterococcus faecalis*, and *Escherichia coli* [132]. The effects of polyphenols on gut microbiota have been shown in human studies. Dietary polyphenols' mechanism of action is different in Gram-positive and Gram-negative bacteria due to changes in cell membrane structure. Polyphenols bind bacterial cell membranes in a concentration-dependent manner; thus, they modify their membrane and alter their growth. Catechins reacted with the dissolved oxygen in aqueous solution, resulting in the generation of hydrogen peroxide. H_2O_2 modifies the permeability of the microbial cell membrane, thus sensitizing the bacteria to the effects of antibiotics [133].

Thus, different polyphenols can change the composition of the microbiota (Table 3), and different bacterial populations possess different enzymes that can change the metabolism of dietary polyphenols in different ways. For example, the intake of catechins, which occur in green tea and black tea, considerably boosted the growth and development of members of *E. coli*. As mentioned above, *E. coli* is able to modify curcumin in its active metabolite, tetrahydrocurcumin, which has to be anti-inflammatory and neuroprotective. So, polyphenols can modify the composition of gut microbiota which, in turn, produce secondary metabolites that have neuroprotective effects.

Table 3. Summary of the main findings of clinical trial studies related to the effects of polyphenols on gut microbiota by increase (+) or decrease (-) of specific strains.

Polyphenols		Bacteria	References
Catechin and epicatechin	+	*Clostridium coccoides–Eubacterium rectale*	[134]
	+	*E. coli*	
	−	*Clostridium histolyticum*	
Proanthocyanidin	+	*Bifidobacteria*	[135]
Pomegranate extract	+	*Odonbacter*	[136]
	+	*Faecalibacterium*	
	+	*Butyricicoccus*	
	+	*Butyricimonas*	
	+	*Bacteroides*	
	−	*Parvimonas*	
	−	*Metanobrevibacter*	
	−	*Metanosphaera*	
Cocoa flavonols	+	*Bifidobacterium*	[137]
	−	*Lactobacillus*	
	−	*Clostridia*	

Red wine	+	*Enterococcus*	[138]
	+	*Prevotella*	
	+	*Bacteroides*	
	+	*Bifidobacterium*	
	+	*Enterococcus*	
	+	*Bacteroides uniformis*	
	+	*Eggerthella lenta*	
	+	*Blautia coccoides*	
Orange juice	+	*Mogibacteriaceae*	[139]
	+	*Tissierellaceae*	
	+	*Veillonellaceae*	
	+	*Odoribacteraceae*	
	+	*Ruminococcaceae*	

However, gut microbiota can have a direct influence on brain function and alterations of the microbiota composition have been found in some neurodegenerative diseases, including PD and AD [140,141]. In addition, microbiota can exert neuroprotective effects by producing neurotransmitters and neuropeptides [142]. It has been shown that Streptococcus, Escherichia and Enterococcus spp. produce serotonin [143,144] and that Bifidobacterium infantis can modulate central serotonin transmission by increasing plasma tryptophan levels [145]. Meanwhile, different Lactobacillus and Bifidobacterium species are able to produce γ-aminobutyric acid (GABA), the principal inhibitory neurotransmitter in the central nervous system [146]. Therefore, gut microbiota can directly or indirectly contribute to neuroprotection.

7. Conclusions

The continuous increase in life expectancy is inversely correlated with quality of life during aging. During life there is, particularly in the brain, an accumulation of damage and a decrease in all of the mechanisms needed for cell repair. These processes can induce cell death.

Aging is one of the leading "risk factors" in the development of neurodegenerative processes. Indeed, neurodegenerative diseases are caused by nervous system dysfunction resulting from neuronal cell failure or cell death.

Neurodegenerative diseases increase with age and are becoming a big challenge for modern societies. Actually, neurodegenerative disorders in developed regions will have a strong increasing impact on medical and socio-economic conditions, since the population is becoming older. Therefore, it is essential to find strategies that help to prevent cognitive decline and improve the life quality of people living with dementia.

For thousands of years, it has been well known that food and health are related to each other. Indeed, even Hippocrates (400 BC), emphasized the importance of nutrition to prevent or cure diseases. In more recent years, different epidemiological studies have confirmed this thought, evidencing a strong link between the consumption of polyphenols and neurocognitive protection and suggesting that a polyphenol-rich diet can be an effective strategy to improve cognitive function in elderly populations.

Polyphenols are bioactive compounds contained in in food and beverages that are able to modulate the metabolic process, thus promoting health and preventing the age-related decline of cognitive, motor and sensory activities. Being antioxidants, polyphenols are able to counteract the oxidative damage accumulated in the cells. Moreover, they modulate different cellular signaling pathways, protecting cells from stress injury. Therefore, understanding the mechanisms by which polyphenols act at a molecular level is crucial in order to use them as dietary supplements to prevent neurodegenerative disorders.

Although polyphenols are abundant in fruits and vegetables and their intake can be increased in the diet, their bioavailability is also influenced by their chemical structure. Unlike in vitro, polyphenols in vivo have limited availability and they need to be metabolized rapidly in order to

overcome biological barriers. Thus, gut microbiota has a key role in the production of specific bioactive polyphenols' metabolites that are responsible for these health effects. Moreover, it is emerging that polyphenols can also modulate the bacterial composition of the gut microbiota, thus influencing the production of specific metabolites that act in modulating brain functions.

There is a growing attention being paid to food diversity, to the consumption of food rich in antioxidants and to developing novel food rich in the different bioactive nutrient groups. To date, the analysis of the impact of these products on neurodegeneration is limited, thus there is a need for an increasing number of studies to better evaluate the dose–effect relationship.

In conclusion, polyphenols and their metabolites are essential compounds with multiple biological activities. Their efficacy as antioxidants and their capacity to modulate pro-survival or anti-apoptotic signaling pathways are essential in preventing and slowing down neurodegenerative disorders. Moreover, considering that they are safe and have a very low toxicity, it is easy to test their efficacy in pre-clinical and clinical studies for the treatment of neurodegenerative diseases. Finally, different polyphenols, or their synthetic derivatives, have been patented as drugs against various human diseases in recent years.

Author Contributions: All authors actively participated in the review design, preparation and organization of the manuscript. They also extensively discussed the topics presented, giving positive criticism about the work. All authors have read and agreed to the published version of the manuscript.

Funding: This work was supported by the project PO FESR 2014-2020–Regione Campania, Asse 1–obiettivo specifico 1.2, Progetto "Sviluppo di nanotecnologie Orientate alla Rigenerazione e Ricostruzione tissutale, Implantologia e Sensoristica in Odontoiatria/oculistica (SORRISO)" (Grant Number: pdt1-000410) amd by CNR-DISBA project NutrAge.

Acknowledgments: FDM's PhD fellowship in Biology is supported by MIUR project PON "Dottorati Innovativi con caratterizzazione industriale" 2017–2018. We thank Dr. Chiara Nobile and Dr. Valentina Brasiello for their editing assistance. We thank Dr. Maria Rosaria Aletta for her bibliographic assistance and Dr. Maria Rosaria Chiummo for her help in reviewing the manuscript.

Conflicts of Interest: The authors confirm that there are no conflicts of interest.

References

1. Pandey, K.B.; Rizvi, S.I. Plant polyphenols as dietary antioxidants in human health and disease. Oxid. Med. Cell. Longev. 2009, 2, 270–278.
2. Fernandez-Fernandez, L.; Comes, G.; Bolea, I.; Valente, T.; Ruiz, J.; Murtra, P.; Ramirez, B.; Angles, N.; Reguant, J.; Morello, J.; et al. LMN diet, rich in polyphenols and polyunsaturated fatty acids, improves mouse cognitive decline associated with aging and Alzheimer's disease. *Behav. Brain Res.* **2012**, *228*, 261–271.
3. Liu, P.; Kemper, L.; Wang, J.; Zahs, K.; Ashe, K.; Pasinetti, G. Grape seed polyphenolic extract specifically decreases Aβ* 56 in the brains of Tg2576 mice. *J. Alzheimers Dis.* **2011**, *26*, 657–666.
4. Sandoval-Acuña, C.; Ferreira, J.; Speisky, H. Polyphenols and mitochondria: An update on their increasingly emerging ROS-scavenging independent actions. *Arch. Biochem. Biophys.* **2014**, *559*, 75–90.
5. Smolensky, D.; Rhodes, D.; McVey, D.S.; Fawver, Z.; Perumal, R.; Herald, T.; Noronha, L. High-polyphenol sorghum bran extract inhibits cancer cell growth through ROS induction, cell cycle arrest, and apoptosis. *J. Med. Food* **2018**, *21*, 990–998.
6. Mello-Filho, A.C.; Meneghini, R. Iron is the intracellular metal involved in the production of DNA damage by oxygen radicals. *Mutat. Res.* **1991**, *251*, 109–113.
7. Gupta, S.; Hastak, K.; Afaq, F.; Ahmad, N.; Mukhtar, H. Essential role of caspases in epigallocatechin-3-gallate-mediated inhibition of nuclear factor kappa B and induction of apoptosis. *Oncogene* **2004**, *23*, 2507–2522.
8. Kinarivala, N.; Patel, R.; Boustany, R.M.; Al-Ahmad, A.; Trippier, P.C. Discovery of aromatic carbamates that confer neuroprotective activity by enhancing autophagy and inducing the anti-apoptotic protein B-cell lymphoma 2 (Bcl-2). *J. Med. Chem.* **2017**, *60*, 9739–9756.
9. Nakaso, K.; Ito, S.; Nakashima, K. Caffeine activates the PI3K/Akt pathway and prevents apoptotic cell death in a Parkinson's disease model of SH-SY5Y cells. *Neurosci. Lett.* **2008**, *432*, 146–150.

10. Vauzour, D.; Vafeiadou, K.; Rice-Evans, C.; Williams, R.J.; Spencer, J.P. Activation of pro-survival Akt and ERK1/2 signalling pathways underlie the anti-apoptotic effects of flavanones in cortical neurons. *J. Neurochem.* **2007**, *103*, 1355–1367.
11. Moosavi, F.; Hosseini, R.; Saso, L.; Firuzi, O. Modulation of neurotrophic signaling pathways by polyphenols. *Drug Des. Devel.* **2016**, *10*, 23–42.
12. Di Meo, F.; Donato, S.; Di Pardo, A.; Maglione, V.; Filosa, S.; Crispi, S. New therapeutic drugs from bioactive natural molecules: The role of gut microbiota metabolism in neurodegenerative diseases. *Curr. Drug Metab.* **2018**, *19*, 478–489.
13. Filosa, S.; Fico, A.; Paglialunga, F.; Balestrieri, M.; Crooke, A.; Verde, P.; Abrescia, P.; Bautista, J.M.; Martini, G. Failure to increase glucose consumption through the pentose-phosphate pathway results in the death of glucose-6-phosphate dehydrogenase gene-deleted mouse embryonic stem cells subjected to oxidative stress. *Biochem. J.* **2003**, *370*, 935–943.
14. Fico, A.; Paglialunga, F.; Cigliano, L.; Abrescia, P.; Verde, P.; Martini, G.; Iaccarino, I.; Filosa, S. Glucose-6-phosphate dehydrogenase plays a crucial role in protection from redox-stress-induced apoptosis. *Cell Death Differ.* **2004**, *11*, 823–831-
15. Redza-Dutordoir, M.; Averill-Bates, D.A. Activation of apoptosis signalling pathways by reactive oxygen species. *Biochim. Biophys. Acta* **2016**, *1863*, 2977–2992.
16. Martindale, J.L.; Holbrook, N.J. Cellular response to oxidative stress: Signaling for suicide and survival. *J. Cell Physiol.* **2002**, *192*, 1–15.
17. Young, I.S.; Woodside, J.V. Antioxidants in health and disease. *J. Clin. Pathol.* **2001**, *54*, 176–186.
18. Halliwell, B. Antioxidant characterization. Methodology and mechanism. *Biochem. Pharm.* **1995**, *49*, 1341–1348.
19. Ward, R.J.; Dexter, D.T.; Crichton, R.R. Ageing, neuroinflammation and neurodegeneration. *Front. Biosci.* **2015**, *7*, 189–204.
20. Matés, J.M. Effects of antioxidant enzymes in the molecular control of reactive oxygen species toxicology. *Toxicology* **2000**, *153*, 83–104.
21. Qin, S.; Hou, D.X. Multiple regulations of Keap1/Nrf2 system by dietary phytochemicals. *Mol. Nutr. Food Res.* **2016**, *60*, 1731–1755.
22. Zhang, Y.J.; Gan, R.Y.; Li, S.; Zhou, Y.; Li, A.N.; Xu, D.P.; Li, H.B. Antioxidant phytochemicals for the prevention and treatment of chronic diseases. *Molecules* **2015**, *20*, 21138–21156.
23. Pisoschi, A.M.; Pop, A. The role of antioxidants in the chemistry of oxidative stress: A review. *Eur. J. Med. Chem.* **2015**, *97*, 55–74.
24. Kurutas, E.B. The importance of antioxidants which play the role in cellular response against oxidative/nitrosative stress: Current state. *Nutr. J.* **2016**, *15*, 71.
25. Shan, B.; Cai, Y.Z.; Sun, M.; Corke, H. Antioxidant capacity of 26 spice extracts and characterization of their phenolic constituents. *J. Agric. Food Chem.* **2005**, *53*, 7749–7759.
26. Lü, J.M.; Lin, P.H.; Yao, Q.; Chen, C. Chemical and molecular mechanisms of antioxidants: Experimental approaches and model systems. *J. Cell Mol. Med.* **2010**, *14*, 840–860.
27. Gheldof, N.; Engeseth, N.J. Antioxidant capacity of honeys from various floral sources based on the determination of oxygen radical absorbance capacity and inhibition of in vitro lipoprotein oxidation in human serum samples. *J. Agric. Food Chem.* **2002**, *50*, 3050–3055.
28. del Bano, M.J.; Lorente, J.; Castillo, J.; Benavente-Garcia, O.; del Rio, J.A.; Ortuno, A.; Quirin, K.W.; Gerard, D. Phenolic diterpenes, flavones, and rosmarinic acid distribution during the development of leaves, flowers, stems, and roots of *Rosmarinus officinalis*. *Antioxid. Act. J. Agric. Food Chem.* **2003**, *51*, 4247–4253.
29. Amorati, R.; Foti, M.C.; Valgimigli, L. Antioxidant activity of essential oils. *J. Agric. Food Chem.* **2013**, *61*, 10835–10847.
30. Tungmunnithum, D.; Thongboonyou, A.; Pholboon, A.; Yangsabai, A. Flavonoids and other phenolic compounds from medicinal plants for pharmaceutical and medical aspects: An overview. *Medicines* **2018**, *5*, 93.
31. Ak, T.; Gülçin, I. Antioxidant and radical scavenging properties of curcumin. *Chem. Biol. Interact.* **2008**, *174*, 27–37.
32. Foley, T.D. Reductive reprogramming: A not-so-radical hypothesis of neurodegeneration linking redox perturbations to neuroinflammation and excitotoxicity. *Cell Mol. Neurobiol.* **2019**, *39*, 577–590.

33. Cui, K.; Luo, X.; Xu, K.; Ven Murthy, M.R. Role of oxidative stress in neurodegeneration: Recent developments in assay methods for oxidative stress and nutraceutical antioxidants. *Prog. Neuropsychopharmacol. Biol. Psychiatry.* **2004**, *28*, 771–799.
34. Andersen, J.K. Oxidative stress in neurodegeneration: Cause or consequence? *Nat. Med.* **2004**, *10*, S18–S25.
35. Mattson, M.P.; Magnus, T. Ageing and neuronal vulnerability. *Nat. Rev. Neurosci.* **2006**, *7*, 278–294.
36. Lim, H.J.; Lee, K.S.; Lee, S.; Park, J.H.; Choi, H.E.; Go, S.H.; Kwak, H.J.; Park, H.Y. 15d-PGJ2 stimulates HO-1 expression through p38 MAP kinase and Nrf-2 pathway in rat vascular smooth muscle cells. *Toxicol. Appl. Pharm.* **2007**, *223*, 20–27.
37. Kim, S.J.; Son, T.G.; Park, H.R.; Park, M.; Kim, M.S.; Kim, H.S.; Chung, H.Y.; Mattson, M.P.; Lee, J. Curcumin stimulates proliferation of embryonic neural progenitor cells and neurogenesis in the adult hippocampus. *J. Biol. Chem.* **2008**, *283*, 14497–14505.
38. Bhakkiyalakshmi, E.; Dineshkumar, K.; Karthik, S.; Sireesh, D.; Hopper, W.; Paulmurugan, R.; Ramkumar, K.M. Pterostilbene-mediated Nrf2 activation: Mechanistic insights on Keap1: Nrf2 interface. *Bioorg. Med. Chem.* **2016**, *24*, 3378–3386.
39. Lu, B.; Chow, A. Neurotrophins and hippocampal synaptic transmission and plasticity. *J. Neurosci. Res.* **1999**, *58*, 76–87.
40. Chao, M.V.; Rajagopal, R.; Lee, F.S. Neurotrophin signalling in health and disease. *Clin. Sci.* **2006**, *110*, 167–173.
41. Sariola, H.; Saarma, M. Novel functions and signalling pathways for GDNF. *J. Cell Sci.* **2003**, *116*, 3855–3862.
42. Nakajima, K.; Niisato, N.; Marunaka, Y. Quercetin stimulates NGF-induced neurite outgrowth in PC12 cells via activation of Na(+)/K(+)/2Cl(−) cotransporter. *Cell Physiol. Biochem.* **2011**, *28*, 147–156.
43. Nakajima, K.; Niisato, N.; Marunaka, Y. Genistein enhances the NGF-induced neurite outgrowth. *Biomed. Res.* **2011**, *32*, 351–356.
44. Zhang, F.; Wang, Y.Y.; Liu, H.; Lu, Y.F.; Wu, Q.; Liu, J.; Shi, J.S. Resveratrol produces neurotrophic effects on cultured dopaminergic neurons through prompting astroglial BDNF and GDNF release. *Evid. Based Complement. Altern. Med* **2012**, *2012*, 937605.
45. Yuan, H.; Zhang, J.; Liu, H.; Li, Z. The protective effects of resveratrol on Schwann cells with toxicity induced by ethanol in vitro. *Neurochem. Int.* **2013**, *63*, 146–153.
46. Huang, E.J.; Reichardt, L.F. TRK receptors: Roles in neuronal signal transduction. *Annu. Rev. Biochem.* **2003**, *72*, 609–642.
47. Liu, C.; Chan, C.B.; Ye, K. 7,8-dihydroxyflavone, a small molecular TrkB agonist, is useful for treating various BDNF-implicated human disorders. *Transl. Neurodegener.* **2016**, *5*, 2.
48. Jang, S.W.; Liu, X.; Yepes, M.; Shepherd, K.R.; Miller, G.W.; Liu, Y.; Wilson, W.D.; Xiao, G.; Blanchi, B.; Sun, Y.E.; et al. A selective TrkB agonist with potent neurotrophic activities by 7,8-dihydroxyflavone. *Proc. Natl. Acad. Sci. USA* **2010**, *107*, 2687–2692.
49. Guo, Z.; Liu, Y.; Cheng, M. Resveratrol protects bupivacaine-induced neuro-apoptosis in dorsal root ganglion neurons via activation on tropomyosin receptor kinase A. *Biomed. Pharm.* **2018**, *103*, 1545–1551.
50. Spencer, J.P.; Vafeiadou, K.; Williams, R.J.; Vauzour, D. Neuroinflammation: modulation by flavonoids and mechanisms of action. *Mol. Asp. Med.* **2012**, *33*, 83–97.
51. Si, T.L.; Liu, Q.; Ren, Y.F.; Li, H.; Xu, X.Y.; Li, E.H.; Pan, S.Y.; Zhang, J.L.; Wang, K.X. Enhanced anti-inflammatory effects of DHA and quercetin in lipopolysaccharide-induced RAW264.7 macrophages by inhibiting NF-κB and MAPK activation. *Mol. Med. Rep.* **2016**, *14*, 499–508.
52. Baur, J.A.; Pearson, K.J.; Price, N.L.; Jamieson, H.A.; Lerin, C.; Kalra, A.; Prabhu, V.V.; Allard, J.S.; Lopez-Lluch, G.; Lewis, K.; et al. Resveratrol improves health and survival of mice on a high-calorie diet. *Nature* **2006**, *444*, 337–342.
53. Zhu, X.; Raina, A.K.; Lee, H.G.; Casadesus, G.; Smith, M.A.; Perry, G. Oxidative stress signalling in Alzheimer's disease. *Brain Res.* **2004**, *1000*, 32–39.
54. Di Pardo, A.; Amico, E.; Scalabrì, F.; Pepe, G.; Castaldo, S.; Elifani, F.; Capocci, L.; De Sanctis, C.; Comerci, L.; Pompeo, F.; et al. Impairment of blood-brain barrier is an early event in R6/2 mouse model of Huntington's disease. *Sci. Rep.* **2017**, *7*, 41316.
55. Knutson, M.D.; Leeuwenburgh, C. Resveratrol and novel potent activators of SIRT1: Effects on aging and age-related diseases. *Nutr. Rev.* **2008**, *66*, 591–596.
56. Polivka, J.; Janku, F. Molecular targets for cancer therapy in the PI3K/AKT/mTOR pathway. *Pharmacol. Therap.* **2014**, *142*, 164–175.

57. Alexander, G.E. Biology of Parkinson's disease: Pathogenesis and pathophysiology of a multisystem neurodegenerative disorder. *Dialogues Clin. Neurosci.* **2004**, *6*, 259–280.
58. Miller, R.L.; James-Kracke, M.; Sun, G.Y.; Sun, A.Y. Oxidative and inflammatory pathways in Parkinson's disease. *Neurochem. Res.* **2009**, *34*, 55–65.
59. Miller, R.L.; Sun, G.Y.; Sun, A.Y. Cytotoxicity of paraquat in microglial cells: Involvement of PKCδ- and ERK1/2-dependent NADPH oxidase. *Brain Res.* **2007**, *1167*, 129–139.
60. Weinreb, O.; Mandel, S.; Amit, T.; Youdim, M.B. Neurological mechanisms of green tea polyphenols in Alzheimer's and Parkinson's diseases. *J. Nutr. Biochem.* **2004**, *15*, 506–516.
61. Mercer, L.D.; Kelly, B.L.; Horne, M.K.; Beart, P.M. Dietary polyphenols protect dopamine neurons from oxidative insults and apoptosis: Investigations in primary rat mesencephalic cultures. *Biochem Pharm.* **2005**, *69*, 339–345.
62. Masuda, M.; Suzuki, N.; Taniguchi, S.; Oikawa, T.; Nonaka, T.; Iwatsubo, T.; Hisanaga, S.; Goedert, M.; Hasegawa, M. Small molecule inhibitors of alpha-synuclein filament assembly. *Biochemistry* **2006**, *45*, 6085–6094.
63. Andrieu, S.; Coley, N.; Lovestone, S.; Aisen, P.S.; Vellas, B. Prevention of sporadic Alzheimer's disease: Lessons learned from clinical trials and future directions. *Lancet Neurol.* **2015**, *14*, 926–944.
64. Haass, C.; Selkoe, D.J. Soluble protein oligomers in neurodegeneration: Lessons from the Alzheimer's amyloid beta-peptide. *Nat. Rev. Mol. Cell Biol.* **2007**, *8*, 101–112.
65. Querfurth, H.W.; LaFerla, F.M. Alzheimer's disease. *N. Engl. J. Med.* **2010**, *362*, 329–344.
66. Selkoe, D.J. Alzheimer's disease: Genes, proteins, and therapy. *Physiol. Rev.* **2001**, *81*, 741–766.
67. Selkoe, D.J. Alzheimer's disease results from the cerebral accumulation and cytotoxicity of amyloid beta-protein. *J. Alzheimers Dis.* **2001**, *3*, 75–80.
68. Snyder, E.M.; Nong, Y.; Almeida, C.G.; Paul, S.; Moran, T.; Choi, E.Y.; Nairn, A.C.; Salter, M.W.; Lombroso, P.J.; Gouras, G.K.; et al. Regulation of NMDA receptor trafficking by amyloid-beta. *Nat. Neurosci.* **2005**, *8*, 1051–1058.
69. Flanagan, E.; Müller, M.; Hornberger, M.; Vauzour, D. Impact of flavonoids on cellular and molecular mechanisms underlying age-related cognitive decline and neurodegeneration. *Curr. Nutr. Rep.* **2018**, *7*, 49–57.
70. Wang, R.; Li, Y.H.; Xu, Y.; Li, Y.B.; Wu, H.L.; Guo, H.; Zhang, J.Z.; Zhang, J.J.; Pan, X.Y.; Li, X.J. Curcumin produces neuroprotective effects via activating brain-derived neurotrophic factor/TrkB-dependent MAPK and PI-3K cascades in rodent cortical neurons. *Prog. Neuropsychopharmacol. Biol. Psychiatry* **2010**, *34*, 147–153.
71. Zhang, L.; Fang, Y.; Xu, Y.; Lian, Y.; Xie, N.; Wu, T.; Zhang, H.; Sun, L.; Zhang, R.; Wang, Z. Curcumin improves amyloid β-peptide (1–42) induced spatial memory deficits through BDNF-ERK signaling pathway. *PLoS ONE* **2015**, *10*, e0131525.
72. Zheng, K.; Dai, X.; Xiao, N.; Wu, X.; Wei, Z.; Fang, W.; Zhu, Y.; Zhang, J.; Chen, X. Curcumin ameliorates memory decline via inhibiting BACE1 expression and β-amyloid pathology in 5 × FAD transgenic mice. *Mol. Neurobiol.* **2017**, *54*, 1967–1977.
73. Zhao, Y.N.; Li, W.F.; Li, F.; Zhang, Z.; Dai, Y.D.; Xu, A.L.; Qi, C.; Gao, J.M.; Gao, J. Resveratrol improves learning and memory in normally aged mice through microRNA-CREB pathway. *Biochem. Biophys. Res. Commun.* **2013**, *435*, 597–602.
74. Fu, Z.; Yang, J.; Wei, Y.; Li, J. Effects of piceatannol and pterostilbene against β-amyloid-induced apoptosis on the PI3K/Akt/Bad signaling pathway in PC12 cells. *Food Funct.* **2016**, *7*, 1014–1023.
75. Donmez, G.; Outeiro, T.F. SIRT1 and SIRT2: Emerging targets in neurodegeneration. *EMBO Mol. Med.* **2013**, *5*, 344–352.
76. Karuppagounder, S.S.; Pinto, J.T.; Xu, H.; Chen, H.L.; Beal, M.F.; Gibson, G.E. Dietary supplementation with resveratrol reduces plaque pathology in a transgenic model of Alzheimer's disease. *Neurochem. Int.* **2009**, *54*, 111–118.
77. Wang, R.; Zhang, Y.; Li, J.; Zhang, C. Resveratrol ameliorates spatial learning memory impairment induced by Aβ. *Neuroscience* **2017**, *344*, 39–47.
78. Rezai-Zadeh, K.; Arendash, G.W.; Hou, H.; Fernandez, F.; Jensen, M.; Runfeldt, M.; Shytle, R.D.; Tan, J. Green tea epigallocatechin-3-gallate (EGCG) reduces beta-amyloid mediated cognitive impairment and modulates tau pathology in Alzheimer's transgenic mice. *Brain Res.* **2008**, *1214*, 177–187.

79. Evin, G.; Barakat, A.; Masters, C.L. BACE: Therapeutic target and potential biomarker for Alzheimer's disease. *Int. J. Biochem. Cell Biol.* **2010**, *42*, 1923–1926.
80. Ortiz-López, L.; Márquez-Valadez, B.; Gómez-Sánchez, A.; Silva-Lucero, M.D.; Torres-Pérez, M.; Téllez-Ballesteros, R.I.; Ichwan, M.; Meraz-Ríos, M.A.; Kempermann, G.; Ramírez-Rodríguez, G.B. Green tea compound epigallo-catechin-3-gallate (EGCG) increases neuronal survival in adult hippocampal neurogenesis in vivo and in vitro. *Neuroscience* **2016**, *322*, 208–220.
81. Li, Y.; Zhou, S.; Li, J.; Sun, Y.; Hasimu, H.; Liu, R.; Zhang, T. Quercetin protects human brain microvascular endothelial cells from fibrillar β-amyloid1–40-induced toxicity. *Acta Pharm. Sin. B* **2015**, *5*, 47–54.
82. Zhang, X.; Hu, J.; Zhong, L.; Wang, N.; Yang, L.; Liu, C.C.; Li, H.; Wang, X.; Zhou, Y.; Zhang, Y.; et al. Quercetin stabilizes apolipoprotein E and reduces brain Aβ levels in amyloid model mice. *Neuropharmacology* **2016**, *108*, 179–192.
83. Sabogal-Guáqueta, A.M.; Muñoz-Manco, J.I.; Ramírez-Pineda, J.R.; Lamprea-Rodriguez, M.; Osorio, E.; Cardona-Gómez, G.P. The flavonoid quercetin ameliorates Alzheimer's disease pathology and protects cognitive and emotional function in aged triple transgenic Alzheimer's disease model mice. *Neuropharmacology* **2015**, *93*, 134–145.
84. Lu, Y.; Liu, Q.; Yu, Q. Quercetin enrich diet during the early-middle not middle-late stage of Alzheimer's disease ameliorates cognitive dysfunction. *Am. J. Transl. Res.* **2018**, *10*, 1237–1246.
85. Kong, Y.; Li, K.; Fu, T.; Wan, C.; Zhang, D.; Song, H.; Zhang, Y.; Liu, N.; Gan, Z.; Yuan, L. Quercetin ameliorates Aβ toxicity in *Drosophila* AD model by modulating cell cycle-related protein expression. *Oncotarget* **2016**, *7*, 67716–67731.
86. Cui, Q.; Li, X.; Zhu, H. Curcumin ameliorates dopaminergic neuronal oxidative damage via activation of the Akt/Nrf2 pathway. *Mol. Med. Rep.* **2016**, *13*, 1381–1388.
87. Wu, J.; Li, Q.; Wang, X.; Yu, S.; Li, L.; Wu, X.; Chen, Y.; Zhao, J.; Zhao, Y. Neuroprotection by curcumin in ischemic brain injury involves the Akt/Nrf2 pathway. *PLoS ONE* **2013**, *8*, e59843.
88. Ramkumar, M.; Rajasankar, S.; Swaminathan Johnson, W.M.; Prabu, K.; Venkatesh Gobi, V. Demethoxycurcumin ameliorates rotenone-induced toxicity in rats. *Front. Biosci.* **2019**, *11*, 1–11.
89. Dauer, W.; Przedborski, S. Parkinson's disease: Mechanisms and models. *Neuron* **2003**, *39*, 889–909.
90. Wang, Y.L.; Ju, B.; Zhang, Y.Z.; Yin, H.L.; Liu, Y.J.; Wang, S.S.; Zeng, Z.L.; Yang, X.P.; Wang, H.T.; Li, J.F. Protective Effect of Curcumin Against Oxidative Stress-Induced Injury in Rats with Parkinson's Disease Through the Wnt/ β-Catenin Signaling Pathway. *Cell Physiol Biochem* **2017**, *43*, 2226-2241, doi:10.1159/000484302.
91. Yu, S.; Wang, X.; He, X.; Wang, Y.; Gao, S.; Ren, L.; Shi, Y. Curcumin exerts anti-inflammatory and antioxidative properties in 1-methyl-4-phenylpyridinium ion (MPP(+))-stimulated mesencephalic astrocytes by interference with TLR4 and downstream signaling pathway. *Cell Stress. Chaperones.* **2016**, *21*, 697–705.
92. Potdar, S.; Parmar, M.S.; Ray, S.D.; Cavanaugh, J.E. Protective effects of the resveratrol analog piceid in dopaminergic SH-SY5Y cells. *Arch. Toxicol.* **2018**, *92*, 669–677.
93. Zeng, W.; Zhang, W.; Lu, F.; Gao, L.; Gao, G. Resveratrol attenuates MPP. *Neurosci. Lett.* **2017**, *637*, 50–56.
94. Gaballah, H.H.; Zakaria, S.S.; Elbatsh, M.M.; Tahoon, N.M. Modulatory effects of resveratrol on endoplasmic reticulum stress-associated apoptosis and oxido-inflammatory markers in a rat model of rotenone-induced Parkinson's disease. *Chem. Biol. Interact.* **2016**, *251*, 10–16.
95. Karuppagounder, S.S.; Madathil, S.K.; Pandey, M.; Haobam, R.; Rajamma, U.; Mohanakumar, K.P. Quercetin up-regulates mitochondrial complex-I activity to protect against programmed cell death in rotenone model of Parkinson's disease in rats. *Neuroscience* **2013**, *236*, 136–148.
96. Choi, J.Y.; Park, C.S.; Kim, D.J.; Cho, M.H.; Jin, B.K.; Pie, J.E.; Chung, W.G. Prevention of nitric oxide-mediated 1-methyl-4-phenyl-1,2,3,6-tetrahydropyridine-induced Parkinson's disease in mice by tea phenolic epigallocatechin 3-gallate. *Neurotoxicology* **2002**, *23*, 367–374.
97. Levites, Y.; Weinreb, O.; Maor, G.; Youdim, M.B.; Mandel, S. Green tea polyphenol(−)-epigallocatechin-3-gallate prevents *N*-methyl-4-phenyl-1,2,3,6-tetrahydropyridine-induced dopaminergic neurodegeneration. *J. Neurochem.* **2001**, *78*, 1073–1082.
98. Walker, F.O. Huntington's Disease. Semin Neurol 2007, 27, 143-150, doi:10.1055/s-2007-971176.
99. Strong, T.V.; Tagle, D.A.; Valdes, J.M.; Elmer, L.W.; Boehm, K.; Swaroop, M.; Kaatz, K.W.; Collins, F.S.; Albin, R.L. Widespread expression of the human and rat Huntington's disease gene in brain and nonneural tissues. *Nat. Genet.* **1993**, *5*, 259–265.

100. Sciacca, S.; Favellato, M.; Madonna, M.; Metro, D.; Marano, M.; Squitieri, F. Early enteric neuron dysfunction in mouse and human Huntington's disease. *Parkinsonism Relat. Disord.* **2017**, *34*, 73–74.
101. Siddiqui, A.; Rivera-Sánchez, S.; Castro, M.e.R.; Acevedo-Torres, K.; Rane, A.; Torres-Ramos, C.A.; Nicholls, D.G.; Andersen, J.K.; Ayala-Torres, S. Mitochondrial DNA damage is associated with reduced mitochondrial bioenergetics in Huntington's disease. *Free Radic Biol Med* **2012**, *53*, 1478–1488.
102. Xun, Z.; Rivera-Sánchez, S.; Ayala-Peña, S.; Lim, J.; Budworth, H.; Skoda, E.M.; Robbins, P.D.; Niedernhofer, L.J.; Wipf, P.; McMurray, C.T. Targeting of XJB-5–131 to mitochondria suppresses oxidative DNA damage and motor decline in a mouse model of Huntington's disease. *Cell Rep.* **2012**, *2*, 1137–1142.
103. Naia, L.; Rosenstock, T.R.; Oliveira, A.M.; Oliveira-Sousa, S.I.; Caldeira, G.L.; Carmo, C.; Laço, M.N.; Hayden, M.R.; Oliveira, C.R.; Rego, A.C. Comparative mitochondrial-based protective effects of resveratrol and nicotinamide in Huntington's disease models. *Mol Neurobiol.* **2017**, *54*, 5385–5399.
104. Sandhir, R.; Yadav, A.; Mehrotra, A.; Sunkaria, A.; Singh, A.; Sharma, S. Curcumin nanoparticles attenuate neurochemical and neurobehavioral deficits in experimental model of Huntington's disease. *Neuromolecular. Med.* **2014**, *16*, 106–118.
105. Chongtham, A.; Agrawal, N. Curcumin modulates cell death and is protective in Huntington's disease model. *Sci. Rep.* **2016**, *6*, 18736.
106. Elifani, F.; Amico, E.; Pepe, G.; Capocci, L.; Castaldo, S.; Rosa, P.; Montano, E.; Pollice, A.; Madonna, M.; Filosa, S.; et al. Curcumin dietary supplementation ameliorates disease phenotype in an animal model of Huntington's disease. *Hum Mol Genet* **2019**, *28*, 4012–4021.
107. Sandhir, R.; Mehrotra, A. Quercetin supplementation is effective in improving mitochondrial dysfunctions induced by 3-nitropropionic acid: Implications in Huntington's disease. *Biochim. Biophys. Acta* **2013**, *1832*, 421–430.
108. Chakraborty, J.; Singh, R.; Dutta, D.; Naskar, A.; Rajamma, U.; Mohanakumar, K.P. Quercetin improves behavioral deficiencies, restores astrocytes and microglia, and reduces serotonin metabolism in 3-nitropropionic acid-induced rat model of Huntington's disease. *CNS Neurosci.* **2014**, *20*, 10–19.
109. Jellinger, K.A. The enigma of vascular cognitive disorder and vascular dementia. *Acta Neuropathol.* **2007**, *113*, 349–388.
110. Molino, S.; Dossena, M.; Buonocore, D.; Ferrari, F.; Venturini, L.; Ricevuti, G.; Verri, M. Polyphenols in dementia: From molecular basis to clinical trials. *Life Sci.* **2016**, *161*, 69–77.
111. Awasthi, H.; Tota, S.; Hanif, K.; Nath, C.; Shukla, R. Protective effect of curcumin against intracerebral streptozotocin induced impairment in memory and cerebral blood flow. *Life Sci.* **2010**, *86*, 87–94.
112. Anastácio, J.R.; Netto, C.A.; Castro, C.C.; Sanches, E.F.; Ferreira, D.C.; Noschang, C.; Krolow, R.; Dalmaz, C.; Pagnussat, A. Resveratrol treatment has neuroprotective effects and prevents cognitive impairment after chronic cerebral hypoperfusion. *Neurol. Res.* **2014**, *36*, 627–633.
113. Shen, D.; Tian, X.; Sang, W.; Song, R. Effect of melatonin and resveratrol against memory impairment and hippocampal damage in a rat model of vascular dementia. *Neuroimmunomodulation* **2016**, *23*, 318–331.
114. Tota, S.; Awasthi, H.; Kamat, P.K.; Nath, C.; Hanif, K. Protective effect of quercetin against intracerebral streptozotocin induced reduction in cerebral blood flow and impairment of memory in mice. *Behav. Brain Res.* **2010**, *209*, 73–79.
115. Jayaraj, R.; Elangovan, N.; Manigandan, K.; Singh, S.; Shukla, S. CNB-001 a novel curcumin derivative, guards dopamine neurons in MPTP model of Parkinson's disease. *BioMed Res. Int.* **2014**, doi:10.1155/2014/236182.
116. Selma, M.V.; Espín, J.C.; Tomás-Barberán, F.A. Interaction between phenolics and gut microbiota: Role in human health. *J. Agric. Food Chem.* **2009**, *57*, 6485–6501.
117. Aura, A. Microbial metabolism of dietary phenolic compounds in the colon. Phytochem. Rev. **2008**, 7, 407–429.
118. Deprez, S.; Mila, I.; Huneau, J.F.; Tome, D.; Scalbert, A. Transport of proanthocyanidin dimer, trimer, and polymer across monolayers of human intestinal epithelial Caco-2 cells. *Antioxid. Redox. Signal.* **2001**, *3*, 957–967.
119. Kang, S.M.; Lee, S.H.; Heo, S.J.; Kim, K.N.; Jeon, Y.J. Evaluation of antioxidant properties of a new compound, pyrogallol-phloroglucinol-6,6′-bieckol isolated from brown algae, *Ecklonia cava*. *Nutr. Res. Pract.* **2011**, *5*, 495–502.
120. Deng, H.; Fang, Y. The three catecholics benserazide, catechol and pyrogallol are GPR35 agonists. *Pharmaceuticals* **2013**, *6*, 500–509.

121. Di Giovanni, S.; Eleuteri, S.; Paleologou, K.E.; Yin, G.; Zweckstetter, M.; Carrupt, P.A.; Lashuel, H.A. Entacapone and tolcapone, two catechol O-methyltransferase inhibitors, block fibril formation of alpha-synuclein and beta-amyloid and protect against amyloid-induced toxicity. *J. Biol. Chem.* **2010**, *285*, 14941–14954.
122. Di Meo, F.; Margarucci, S.; Galderisi, U.; Crispi, S.; Peluso, G. Curcumin, gut microbiota, and neuroprotection. *Nutrients* **2019**, *11*, 2426.
123. Basholli-Salihu, M.; Schuster, R.; Mulla, D.; Praznik, W.; Viernstein, H.; Mueller, M. Bioconversion of piceid to resveratrol by selected probiotic cell extracts. *Bioprocess. Biosyst. Eng.* **2016**, *39*, 1879–1885.
124. Bode, L.M.; Bunzel, D.; Huch, M.; Cho, G.S.; Ruhland, D.; Bunzel, M.; Bub, A.; Franz, C.M.; Kulling, S.E. In vivo and in vitro metabolism of trans-resveratrol by human gut microbiota. *Am. J. Clin. Nutr.* **2013**, *97*, 295–309.
125. Blaut, M.; Schoefer, L.; Braune, A. Transformation of flavonoids by intestinal microorganisms. *Int. J. Vitam. Nutr. Res.* **2003**, *73*, 79–87.
126. Zheng, C.J.; Liu, R.; Xue, B.; Luo, J.; Gao, L.; Wang, Y.; Ou, S.; Li, S.; Peng, X. Impact and consequences of polyphenols and fructooligosaccharide interplay on gut microbiota in rats. *Food Funct.* **2017**, *8*, 1925–1932.
127. Angelino, D.; Carregosa, D.; Domenech-Coca, C.; Savi, M.; Figueira, I.; Brindani, N.; Jang, S.; Lakshman, S.; Molokin, A.; Urban, J.F.; et al. 5-(hydroxyphenyl)-γ-valerolactone-sulfate, a key microbial metabolite of flavan-3-ols, is able to reach the brain: Evidence from different in. *Nutrients* **2019**, *11*, 2678.
128. Johnson, S.L.; Kirk, R.D.; DaSilva, N.A.; Ma, H.; Seeram, N.P.; Bertin, M.J. Polyphenol microbial metabolites exhibit gut and blood-brain barrier permeability and protect murine microglia against LPS-induced inflammation. *Metabolites* **2019**, *9*, 78.
129. Figueira, I.; Garcia, G.; Pimpão, R.C.; Terrasso, A.P.; Costa, I.; Almeida, A.F.; Tavares, L.; Pais, T.F.; Pinto, P.; Ventura, M.R.; et al. Polyphenols journey through blood-brain barrier towards neuronal protection. *Sci. Rep.* **2017**, *7*, 11456.
130. Youdim, K.A.; Qaiser, M.Z.; Begley, D.J.; Rice-Evans, C.A.; Abbott, N.J. Flavonoid permeability across an in situ model of the blood-brain barrier. *Free Radic. Biol. Med.* **2004**, *36*, 592–604.
131. Filosa, S.; Di Meo, F.; Crispi, S. Polyphenols-gut microbiota interplay and brain neuromodulation. *Neural. Regen. Res.* **2018**, *13*, 2055–2059.
132. Bird, J.K.; Raederstorff, D.; Weber, P.; Steinert, R.E. Cardiovascular and antiobesity effects of resveratrol mediated through the gut microbiota. *Adv. Nutr.* **2017**, *8*, 839–849.
133. Arakawa, H.; Maeda, M.; Okubo, S.; Shimamura, T. Role of hydrogen peroxide in bactericidal action of catechin. *Biol. Pharm. Bull.* **2004**, *27*, 277–281.
134. Tzounis, X.; Vulevic, J.; Kuhnle, G.G.; George, T.; Leonczak, J.; Gibson, G.R.; Kwik-Uribe, C.; Spencer, J.P. Flavanol monomer-induced changes to the human faecal microflora. *Br. J. Nutr.* **2008**, *99*, 782–792.
135. Yamakoshi, J.; Tokutake, S.; Kikuchi, M.; Kubota, Y.; Konishi, H.; Mitsuoka, T. Effect of Proanthocyanidin-Rich Extract from Grape Seeds on Human Fecal Flora and Fecal Odor. *Microbial Ecology in Health and Disease* **2001**, *13*, 25-31.
136. García-Mediavilla, M.V.; Sánchez-Campos, S.; Tuñón, M.J. Fruit polyphenols, immunity and inflammation. *Br. J. Nutr.* **2010**, *104*, S15–S27.
137. Tzounis, X.; Rodriguez-Mateos, A.; Vulevic, J.; Gibson, G.R.; Kwik-Uribe, C.; Spencer, J.P. Prebiotic evaluation of cocoa-derived flavanols in healthy humans by using a randomized, controlled, double-blind, crossover intervention study. *Am. J. Clin. Nutr.* **2011**, *93*, 62–72.
138. Queipo-Ortuño, M.I.; Boto-Ordóñez, M.; Murri, M.; Gomez-Zumaquero, J.M.; Clemente-Postigo, M.; Estruch, R.; Cardona Diaz, F.; Andrés-Lacueva, C.; Tinahones, F.J. Influence of red wine polyphenols and ethanol on the gut microbiota ecology and biochemical biomarkers. *Am. J. Clin. Nutr.* **2012**, *95*, 1323–1334.
139. Brasili, E.; Hassimotto, N.M.A.; Del Chierico, F.; Marini, F.; Quagliariello, A.; Sciubba, F.; Miccheli, A.; Putignani, L.; Lajolo, F. Daily consumption of orange juice from *Citrus sinensis* L. Osbeck cv. Cara Cara and cv. Bahia differently affects gut microbiota profiling as unveiled by an integrated meta-omics approach. *J. Agric. Food Chem.* **2019**, *67*, 1381–1391.
140. Gerhardt, S.; Mohajeri, M.H. Changes of colonic bacterial composition in Parkinson's disease and other neurodegenerative diseases. *Nutrients* **2018**, *10*, 708.
141. Sun, M.F.; Shen, Y.Q. Dysbiosis of gut microbiota and microbial metabolites in Parkinson's disease. *Ageing Res. Rev.* **2018**, *45*, 53–61.

142. Hsiao, E.Y.; McBride, S.W.; Hsien, S.; Sharon, G.; Hyde, E.R.; McCue, T.; Codelli, J.A.; Chow, J.; Reisman, S.E.; Petrosino, J.F.; et al. Microbiota modulate behavioral and physiological abnormalities associated with neurodevelopmental disorders. *Cell* **2013**, *155*, 1451–1463.
143. Lyte, M. Probiotics function mechanistically as delivery vehicles for neuroactive compounds: Microbial endocrinology in the design and use of probiotics. *Bioessays* **2011**, *33*, 574–581.
144. Nzakizwanayo, J.; Dedi, C.; Standen, G.; Macfarlane, W.M.; Patel, B.A.; Jones, B.V. *Escherichia coli* Nissle 1917 enhances bioavailability of serotonin in gut tissues through modulation of synthesis and clearance. *Sci. Rep.* **2015**, *5*, 17324.
145. O'Mahony, S.M.; Clarke, G.; Borre, Y.E.; Dinan, T.G.; Cryan, J.F. Serotonin, tryptophan metabolism and the brain-gut-microbiome axis. *Behav. Brain Res.* **2015**, *277*, 32–48.
146. Yunes, R.A.; Poluektova, E.U.; Dyachkova, M.S.; Klimina, K.M.; Kovtun, A.S.; Averina, O.V.; Orlova, V.S.; Danilenko, V.N. GABA production and structure of *gad*B/*gad*C genes in *Lactobacillus* and *Bifidobacterium* strains from human microbiota. *Anaerobe* **2016**, *42*, 197–204.

Received: 18 July 2018 | Accepted: 19 September 2018

DOI: 10.1002/jcp.27602

ORIGINAL RESEARCH ARTICLE

WILEY Journal of Cellular Physiology

Meldonium improves Huntington's disease mitochondrial dysfunction by restoring peroxisome proliferator-activated receptor γ coactivator 1α expression

Francesca Di Cristo[1*] | Mauro Finicelli[2*] | Filomena Anna Digilio[2] | Simona Paladino[3] | Anna Valentino[1] | Filippo Scialò[4] | Maria D'Apolito[2] | Carmela Saturnino[5] | Umberto Galderisi[6,7] | Antonio Giordano[7,8] | Mariarosa Anna Beatrice Melone[1,7] | Gianfranco Peluso[9]

[1]Department of Medical, Surgical, Neurological, Metabolic Sciences, and Aging, 2nd Division of Neurology, Center for Rare Diseases and InterUniversity Center for Research in Neurosciences, University of Campania "Luigi Vanvitelli", Naples, Italy

[2]Institute of Bioscience and BioResources (IBBR), National Research Council (CNR), Naples, Italy

[3]Department of Molecular Medicine and Medical Biotechnology, University of Naples Federico II, Naples, Italy

[4]Institute for Cell and Molecular Bioscience, Campus for Ageing and Vitality, University of Newcastle, Newcastle-upon-Tyne, United Kingdom

[5]Department of Science, University of Basilicata, Potenza, Italy

[6]Department of Experimental Medicine, Biotechnology and Molecular Biology Section, University of Campania "Luigi Vanvitelli, Naples, Italy

[7]Department of Biology, Center for Biotechnology, College of Science and Technology, Sbarro Institute for Cancer Research and Molecular Medicine, Temple University, Philadelphia, Pennsylvania

[8]Department of Medicine, Surgery and Neuroscience, University of Siena, Siena, Italy

[9]Institute of Agro-environmental and Forest Biology (IBAF), National Research Council (CNR), Naples, Italy

Correspondence
Gianfranco Peluso, Institute of Agro-environmental and Forest Biology (IBAF), National Research Council (CNR), via P. Castellino, 111-80131, Naples, Italy.
Email: gianfranco.peluso@ibaf.cnr.it
Mariarosa Anna Beatrice Melone, University of Campania "Luigi Vanvitelli" Via Pansini, 5-80131, Naples, Italy.
Email marina.melone@unicampania.it

Funding information
Ministero dell`Istruzione, dell`Università e della Ricerca (MIUR, Italy), Grant/Award Numbers: Project PON—'Ricerca e Competitività 2007-2013 - PON01_01802, Prin 2010-2011 - 20109MXHMR".

Abstract

Mitochondrial dysfunction seems to play a fundamental role in the pathogenesis of neurodegeneration in Huntington's disease (HD). We assessed possible neuroprotective actions of meldonium, a small molecule affecting mitochondrial fuel metabolism, in in vitro and in vivo HD models. We found that meldonium was able to prevent cytotoxicity induced by serum deprivation, to reduce the accumulation of mutated huntingtin (mHtt) aggregates, and to upregulate the expression of peroxisome proliferator-activated receptor γ coactivator 1α (PGC-1α) in mHTT-expressing cells. The PGC-1α increase was accompanied by the increment of mitochondrial mass and by the rebalancing of mitochondrial dynamics with a promotion of the mitochondrial fusion. Meldonium-induced PGC-1α significantly alleviated motor dysfunction and prolonged the survival of a transgenic HD Drosophila model in which mHtt expression in the nervous system led to progressive motor performance deficits. Our study strongly suggests that PGC-1α, as a master coregulator of mitochondrial biogenesis, energy homeostasis, and antioxidant defense, is a potential therapeutic target in HD.

*Francesca Di Cristo and Mauro Finicelli contributed equally to this work.

KEYWORDS
Huntington, meldonium, mitochondrial dysfunction, neurodegeneration

1 | INTRODUCTION

Huntington's disease (HD) is a dominant inherited disorder characterized by neurodegeneration of cortical and striatal tissue. The mutation is an expansion of unstable CAG triplet repeats in exon 1 of the huntingtin gene (HTT), which lies on the short arm of chromosome 4. On translation, this leads to a polyglutamine tract at the N terminal of the mutant huntingtin protein (mHtt).

Researchers have ascribed the HD pathogenesis to a toxic gain of mHtt functions, which includes mHTT aggregate formation, transcriptional dysregulation, defective energy metabolism, and oxidative stress. It also consists of the loss of wild-type Htt functions, such as brain-derived neurotrophic factor translation, vesicle transport, and autophagy modulation. In addition, several converging lines of research have demonstrated that in different HD models mitochondrial biogenesis, dynamics, trafficking, and mitophagy are altered, resulting in a shortage of energy-generating organelles (Guedes-Dias et al., 2016; Guo et al., 2016; Li, Orr, & Li, 2010). Although researchers have made significant advances in understanding the genetic basis of this disease, they have not yet determined a direct cause–effect relationship between HD gene mutation and mitochondrial dysfunction. Mitochondrial dysfunction may also originate from mHtt-dependent transcriptional dysregulation which results in abnormal mitochondrial biogenesis and dynamics. Such dysregulation can also accumulate oxidative damage, inactivating some mitochondrial metabolic enzymes (Browne et al., 1997; Kumar, Vaish, & Ratan, 2014).

Moreover, in HD, additional metabolic alterations, which arise as a compensatory homeostatic response to the restrictions on energy production, might exacerbate mitochondrial dysfunction. Shifts in fluxes through the different branches of the energy-generating pathways could explain the stimulation of fatty acid (FA) oxidation to compensate for reduced glucose oxidation due to mHtt-dependent pyruvate dehydrogenase dysregulation (Cheng, Chang, Wu, & Chen, 2016; Graham et al., 2016; Naia et al., 2017).

However, compensatory shifts to generate energy from FAs may be detrimental to mitochondria since FA overloading might worsen mitochondrial impairment with an increase of reactive oxygen species (ROS) production.

Meldonium (mildronate; 3-(2,2,2-trimethylhydrazinium) propionate; THP; MET-88), is known as a cardioprotective drug whose mechanism of action is based mainly on preserving adenosine triphosphate production by optimizing energy metabolism during heart hypoxia (Dambrova, Liepinsh, & Kalvinsh, 2002).

Meldonium modulates cellular energy metabolism pathways by lowering intracellular l-carnitine levels and by reducing the formation of long-chain acylcarnitines. These changes redirect the FA metabolism from mitochondria to peroxisomes, which in turn stimulates short- and medium-chain FA mitochondrial utilization decreases the production of cytotoxic intermediate and free radicals from FA β-oxidation, and increases glucose metabolism (Dambrova et al., 2016). Researchers found that meldonium decreases protein expression related to inflammation and apoptosis in a Parkinson's disease rat model and an azidothymidine neurotoxicity model in mice. They also found that meldonium has several positive effects in Alzheimer's disease-model mice, including improvement of social recognition and spatial learning and a reduction of amyloid β peptide load (Beitnere et al., 2014; Isajevs et al., 2011; Pupure et al., 2008). Despite the significance of meldonium in some neurodegenerative disorders, little information is available concerning its treatment impact on HD and on the mitochondrial dysfunction that accompanies the disease. In this context, the first aim of the current study was to test the hypothesis that, compared with the control, meldonium administration would have an impact on the viability of STHdh$^{Q111/111}$ cells expressing mHtt and on the survival rate and physical activity of the fly HD model. A further aim of this study was to highlight potential mechanisms by which meldonium treatment may have biological effects by specifically focusing on an analysis of PGC-1α, which is to control mitochondria function, along with aspects of mitochondria dynamics alterations.

For the first time, we demonstrate that meldonium can ameliorate some mitochondrial dysfunction in both in vitro and in vivo HD models and that these beneficial effects are correlated to a restore of the PGC1-α expression that mHTT-expressing neurons impair.

2 | MATERIALS AND METHODS

2.1 | Chemicals and antibodies

Dulbecco's modified Eagle medium (DMEM), fetal bovine serum (FBS), streptomycin-penicillin, L-glutamine, and sodium pyruvate were purchased from EuroClone (Milan, Italy). The Cell Proliferation Kit I (3-(4,5-dimethylthiazol-2-yl)-2,5-diphenyl tetrazolium bromide [MTT]) was obtained from Sigma-Aldrich (Milan, Italy). Dichlorofluorescein (H_2DCF) was purchased from Life Technologies/Thermo Fisher Scientific (Milan, Italy). The following western blot antibodies were used in this study: anti-polyglutamine-expansion (1:2,000, MAB1574; Merck Millipore, Burlington, MA), anti-vinculin (1:25,000, AB129002; Abcam, Cambridge, UK), anti-PGC1α (1:1,000, AB54481; Abcam) and anti-glyceraldehyde 3-phosphate dehydrogenase (GAPDH; 1:10,000, AB2302; Merck Millipore). Peroxidase-conjugated secondary antibodies were antimouse and antirabbit (Bio-Rad, Hercules, CA). TRIzol reagent and SYBR Green PCR Master Mix were purchased from Invitrogen (Milan, Italy), and the High Capacity cDNA Reverse Transcription Kit was obtained from Promega (Milan, Italy). MitoTracker® Green FM and Mitotracker Red CMXRos were purchased from Life Technologies/Thermo Fisher Scientific (Milan, Italy). All chemicals and reagents, unless otherwise stated, were purchased from Sigma-Aldrich.

2.2 | Cell cultures

Conditionally immortalized wild-type STHdh$^{Q7/7}$ and mutant STHdh$^{Q111/111}$ striatal neuronal cell lines were a kind gift of Elena Cattaneo (Milan, Italy). STHdh$^{Q7/7}$ and STHdh$^{Q111/111}$ cell lines express endogenous levels of normal and mutant full-length huntingtin protein with 7 and 111 glutamines, respectively, and they were generated from wild-type Hdh$^{Q7/7}$ and homozygous Hdh$^{Q111/111}$ littermate embryos (Gines et al., 2003). Striatal cells were grown in a humidified atmosphere of 95% air and 5% CO_2 at 33°C in DMEM supplemented with 10% FBS, 1% streptomycin-penicillin, 2 mM L-glutamine, and 1 mM sodium pyruvate.

Cell viability of STHdh$^{Q111/111}$ and STHdh$^{Q7/7}$ cell lines was assessed by MTT Cell Proliferation Assay. Cells, at early passage (six to nine) were seeded at a density of 5×10^3 cells/well in 96-well plates and treated with increasing concentrations of meldonium (10, 20, and 50 μM) in the presence of DMEM containing 10% FBS, or 0.5% FBS for serum-deprived conditions. Absorbance was read at 550 nm on a Cytation 3 Imaging Reader (BioTek Instruments, Winooski, VT), after 4, 8, and 12 hr. Neuronal survival in the presence of meldonium was referred to nontreated neurons.

2.3 | Western blot analysis

Protein lysates from STHdh$^{Q111/111}$ and STHdh$^{Q7/7}$ cell lines were used for sodium dodecyl sulfate–polyacrylamide gel electrophoresis (SDS-PAGE). SDS-PAGE and immunoblotting were carried out according to standard procedures in triplicate. The relative expressions, normalized concerning the housekeeping proteins, were quantified densitometrically using the ImageJ Software (ImageJ; NIH).

2.4 | Mitochondrial staining

MitoTracker Green FM staining quantified the cellular content of mitochondria. STHdh$^{Q7/Q7}$ and STHdh$^{Q111/Q111}$ cells were seeded in 96-well plates (3.5×10^3 cells/well) for 24 hr, after which they were stimulated in quadruplicate wells with 50 μM meldonium for 72 hr. The cells were stained with 100 nM MitoTracker Green FM for 30 min in serum-free media, and fluorescence was measured with a Cytation 3 Multi-Mode Reader (BioTek) with excitation wavelength 490 nm and emission 516 nm.

The fluorescence was normalized to the mitochondrial proteins extracted as described by Mucerino et al. (2017), and measured using the bicinchoninic acid assay.

For confocal microscopy, cells cultured on 12-mm diameter glass coverslips were incubated with 200 nM MitoTracker® Red CMXRos for 20 min in a culture medium. After incubation, cells were fixed with cold methanol for 5 min, washed with phosphate-buffered saline (PBS), and then mounted in 50% glycerol in PBS. Images were acquired using a laser scanning microscope (LSM 510 META; Carl Zeiss MicroImaging, Inc.) equipped with a Plan Apo ×63 oil-immersion (NA 1.4) objective lens. Z-slices from the top to the bottom of the cell were collected, and three-dimensional reconstructions were carried out using LSM 510 Software. The mitochondrial network was classified according to the size of objects (length) using the ImageJ Software as previously described by Helguera et al. (2013).

2.5 | Drosophila stocks

Flies were reared on standard cornmeal-agar with a 12-hr on–off light cycle at 25°C. Fly stocks used in the current study were obtained from the Bloomington Stock Center (Bloomington, IN): 33808 w*; P{UAS-HTT.128Q.FL}f27b-8765 w;P{GAL4-elav.L}2-1521 w[*]; P{w[+ mC] = UAS-GFP.S65T}Myo31DF[T2].

2.6 | Meldonium treatment and crosses

Meldonium (14.6 mg) was added into the surface of assay fly food (AF; 2% Agar, 10% powdered yeast, 10% sucrose, 0.1% Nipagin), and left under gentle agitation for 3 hr at room temperature until dried. This food was used for growing experimental flies while controls were reared in AF devoid of meldonium. Water was supplemented in equal amounts in all the food conditions. Expression of polyglutamine-containing hHTT was driven by the bipartite expression system upstream activator sequence (UAS)-GAL4 in transgenic flies, as described by Brand and Perrimon (1993). To obtain HD model flies, we crossed females carrying the pan-neural driver elav-Gal4 to males from the UAS HTT128QFL strain. The parental strains elav/+ as well as UAS HTT128QFL and P{w[+ mC] = UAS-GFP.S65T}T2/P{GAL4-elav.L}2) were used as controls. For all assays, only one sex was used in this study.

2.7 | Feeding behavior

To determine whether the presence of meldonium in the medium could affect the feeding of the flies, we visually confirmed food intake by feeding flies on media containing the red food dye no. 40 (Tanimura, Isono, Takamura, & Shimada, 1982). For this experiment, we mixed red dye no. 40 (1 mg/ml) in the medium containing meldonium. The flies were allowed to feed on the dye-supplemented medium for 1 day, and their abdominal coloring was examined under a stereomicroscope.

2.8 | Lifespan analysis

Newly emerged adult flies with the desired genotype (P{UAS-HTT.128Q.FL}f27b/P{GAL4-elav.L}2) were collected under cold-induced anesthesia, sorted by sex, grouped in five cohorts of 20 insects, placed in vials containing 3.5 ml of AF supplemented or not with meldonium, and reared at 28°C. Flies were transferred to new vials containing fresh food every 3 days and deaths were recorded at each transfer. The experiment ended when no living flies remained in the vials. Lifespan of fruit flies was measured in three independent experiments ($n = 300$) per treatment. Obtained values were used to

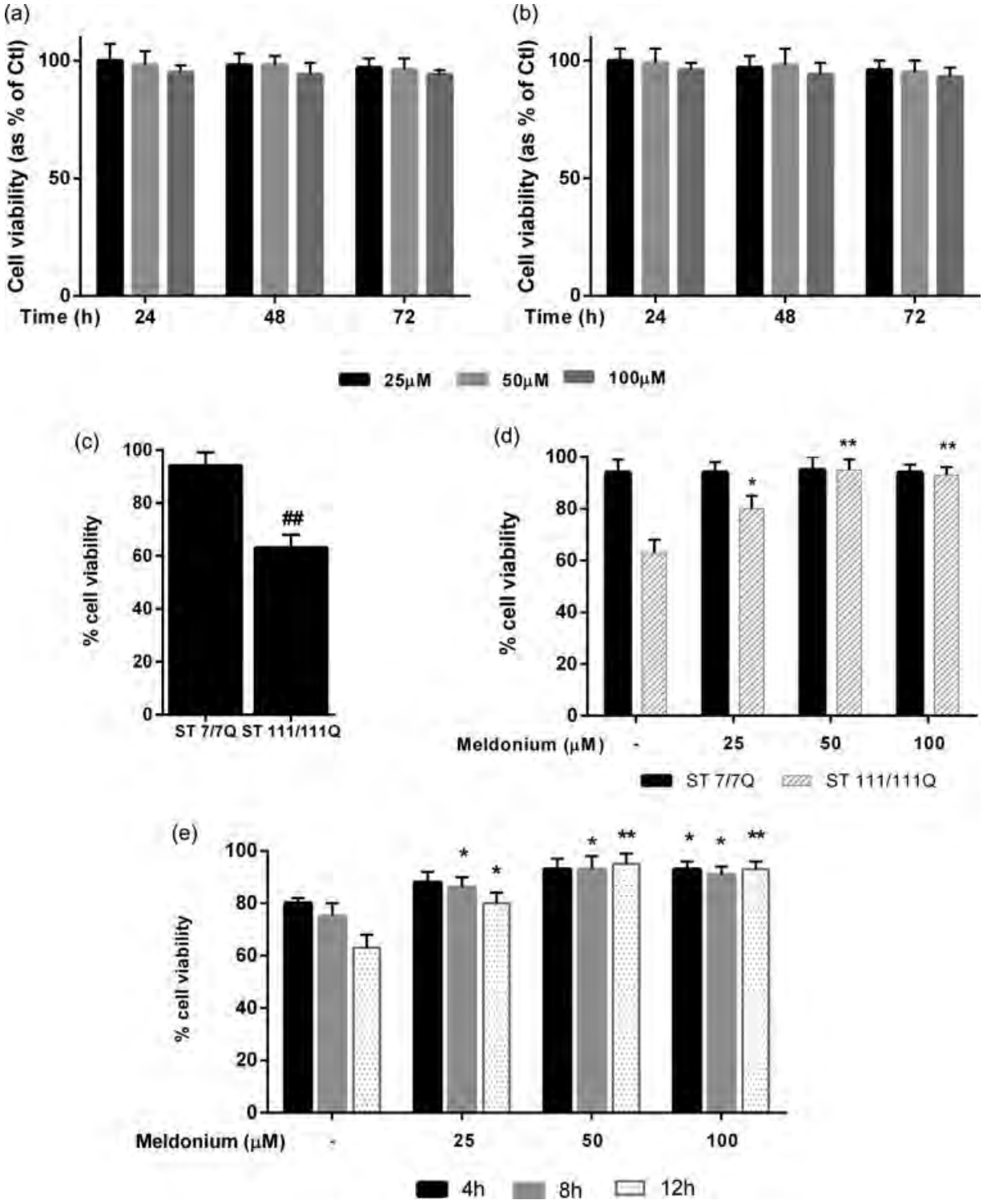

FIGURE 1 Meldonium protects STHdh$^{Q111/111}$ cells from mutated huntingtin (mHtt)-dependent cell death. Cell viability in (a) STHdh$^{Q7/7}$ and (b) STHdh$^{Q111/111}$ cells incubated 24, 48, and 72 hr with 25–50-100 μM meldonium. Cell viability percentage was normalized to untreated cells used as control (CTL). (c) Cell viability in STHdh$^{Q7/7}$ and STHdh$^{Q111/111}$ cells after serum deprivation. (d) Cell viability in STHdh$^{Q7/7}$ and STHdh$^{Q111/111}$ cells after serum deprivation and then incubated 12 hr with 25–50-100 μM meldonium. Data were normalized to STHdh$^{Q7/7}$ cells and untreated STHdh$^{Q111/111}$ cells, respectively. Statistical significance: $^{\#\#}p < 0.01$ versus STHdh$^{Q7/7}$ cell line; $^{*}p < 0.05$ and $^{**}p < 0.01$ versus untreated STHdh$^{Q111/111}$ cell line; one-way analysis of variance, with post-hoc Bonferroni's test. Bars represent the means ± *SD*; $n = 3$. (e) Cell viability in STHdh$^{Q111/111}$ cells after 4, 8, and 12 hr of serum deprivation in absence or in presence of 25–50-100 μM meldonium

calculate mean lifespan (mean survival days of all flies for each group), and maximum lifespan (maximum amount of days needed to reach 90% mortality).

2.9 | Negative geotaxis assay

Climbing assays were performed on newly emerged flies by the negative geotaxis assay. Briefly, 20 flies were placed in a graduated empty plastic vial (18 × 2.5 cm). After 60 min of acclimatization, the flies were gently tapped down to the bottom of the vial, and the number of flies that climbed above the 10-cm mark within 10 s after the tap was recorded. This assay was repeated for the same group two times, allowing for a 1-min rest period between each trial. The number of flies per group that passed the 10-cm mark was recorded as a percentage of total flies. Each trial was performed three times at each time point, and the data were expressed as an average of the replicates ($n = 300$).

2.10 | RNA isolation and quantitative real-time polymerase chain reaction (qRT-PCR)

Total RNA was extracted from STHdh$^{Q7/7}$ and STHdh$^{Q111/111}$ cell lines as well as meldonium-treated and nontreated hHTT flies using TRIzol reagent.

For in vivo studies, we analyzed the heads from five females and five males at different disease stages: presymptomatic (pre-HD; 0 days), early symptomatic (early-HD; 4 days), and late symptomatic (late-HD; 12 and 16 days). Retrotranscription (0.2 μg RNA) was performed according to the manufacturer's instructions (Promega). Two quantitative PCR (qPCR) amplification-specific primers for peroxisome proliferator-activated receptor γ coactivator 1α (*PGC-1α*, forward: GATGGCACGCAGCCCTAT, reverse: CTCGACACGGAGAGT TAAAGGAA) and β-actin (*Actb*, forward: TTAGTTGCGTTACACCC TTTC, reverse: ACCTTCACCGTTCCAGTT) were used, as reported by Cui et al. (2006). The following primers were used for the quantification of mitochondrial DNA (mtDNA) copy number in total DNA (extracted with phenol:chloroform) as described by Venegas, Wang, Dimmock, and Wong (2011): NADH-ubiquinone oxidoreductase chain 1 (*Nd1*), forward: CAGCCTGACCCATAGCCATA, reverse: ATTCTCCTTCTGTCAGGTCGAA); *Gapdh*, forward: GCAGTG GCAAAGTGGAGATT, reverse: GAATTTGCCGTGAGTGGAGT). The following specific oligonucleotide primers for *PGC-1/Spargel* and *rp49* genes were designed by Primer Express Software (Thermo Fisher Scientific). Primers used for *PGC-1/Spargel* were *srl* Fw (TCCGA GATCCGCAAAAAAGA) and *srl* Rv (CCCCAGTTGTTCCGGCTTAT); primers for *rp49* were Rp49RTFw (CAGTCGGATCGATATGCTAAGC) and Rp49RTRv (GGCATCAGATACTGTCCCTTGAA).

qPCR was run on a 7900HT Fast Real time-PCR System. The reactions were performed as reported by Mucerino et al. (2017). All reactions were run in triplicate, normalized to the housekeeping gene, and the results were expressed as mean ± *SD*. The $-2^{\Delta\Delta C_t}$ method was used to determine the relative abundance of mtDNA or genes of interest (Schmittgen & Livak, 2008).

2.11 | ROS detection

To measure ROS level, fly brains were incubated in 30 μM H_2DCF in PBS 1× buffer for 10 min, washed three times in PBS 1× buffer and imaged immediately. The intensity of the brains fluorescence was measured by using a Leica SP8 confocal and Digital Light Sheet (Leica, Wetzlar, Germany). The total (average) fluorescence intensity of each individual brain imaged was quantified using ImageJ.

2.12 | Statistical analyses

For both in vitro and in vivo experiments, all quantitative data were presented as the mean ± *SD*, and statistical significance was evaluated using the Student's *t* test or one-way analysis of variance, followed by post-hoc Bonferroni's test for multiple comparisons to determine any statistical differences between groups. Each experiment was performed at least three times. All the data were analyzed with the GraphPad Prism version 5.01 statistical software package (GraphPad, La Jolla, CA).

3 | RESULTS

3.1 | Meldonium protects STHdh$^{Q111/111}$ cells from death induced by serum deprivation

Before evaluating the effects of meldonium on in vivo HD models, we tested the molecule in several well-established in vitro assays.

First, we analyzed the effect of meldonium on immortalized striatal cell lines expressing wild-type (STHdh$^{Q7/7}$) or mutant full-length huntingtin protein (STHdh$^{Q111/111}$; Trettel et al., 2000).

As reported in Figure 1a,b a concentration of meldonium ranging from 25 to 100 μM did not affect cell viability in both striatal cell lines.

The mHtt bearing 111 glutamines in the N-terminal domain (Q111/Q111) can promote neuronal cell death depending on the culture conditions. In Figure 1c, we demonstrate that Q111/Q111 expression caused cytotoxicity under serum-deprived conditions, while STHdh$^{Q7/7}$ cells were resistant to serum deprivation. The effect of meldonium on striatal cells after serum deprivation was examined at different concentrations and time. The STHdh$^{Q111/Q111}$ cell viability following serum deprivation was improved by meldonium (Figure 1d,e).

Since researchers have demonstrated that both soluble forms of mHtt aggregates and insoluble mHtt deposits engender neurotoxicity, we carried out experiments to test the hypothesis that meldonium can affect STHdh$^{Q111/111}$ cell viability *via* a reduction of mHtt aggregates.

Interestingly, western blot analysis demonstrated that 50 μM meldonium significantly diminished ($p < 0.01$) the high molecular weight of mHtt aggregates in the STHdh$^{Q111/111}$ cell line (Figure 2). This supports the idea that meldonium's protective role could be related to an ability to modulate mHtt aggregation or degradation.

The meldonium concentration required to obtain a significant biological effect was 50 μM in all the assays performed: thus, the same concentration was used in conducting further experiments.

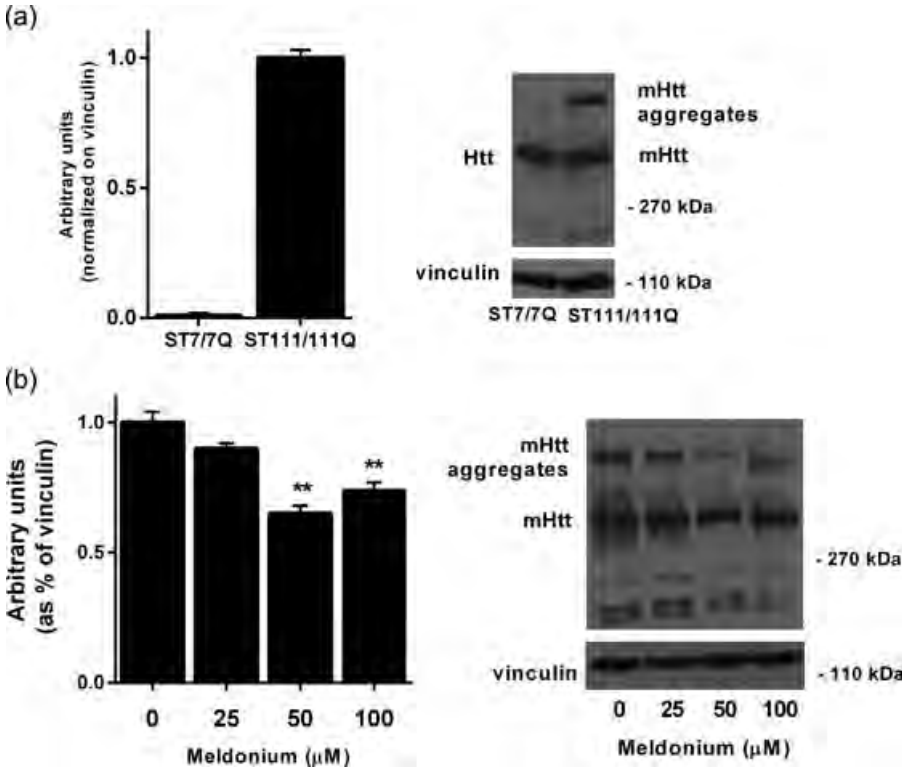

FIGURE 2 Meldonium decreases mutated huntingtin (mHtt) aggregates in the STHdh$^{Q111/111}$ cell line. (a) Representative western blot of mHtt aggregates in STHdh$^{Q111/111}$ cell line versus STHdh$^{Q7/7}$ cell line. (b) Representative western blot of mHtt aggregates in STHdh$^{Q111/111}$ cell line incubated for 72 hr in the presence of 25–50-100 μM meldonium. Densitometric quantification was performed on three different experiments and the results expressed as the mean of the values obtained (mean ± *SD*). Statistical significance: $^{**}p < 0.01$ versus untreated STHdh$^{Q111/111}$ cell line; one-way analysis of variance, with post-hoc Bonferroni's test. Bars represent the means ± *SD*; $n = 3$

3.2 | Meldonium induces PGC-1α expression

There is substantial evidence that the transcriptional coactivator PGC-1α pathway results impaired in HD and its upregulation could promote clearance of mHtt aggregates, thereby decreasing mHtt neurotoxicity (Tsunemi et al., 2012). Thus, we evaluated whether meldonium was able to increase PGC-1α expression in treated cells.

We confirmed that PGC-1α expression, at both the transcriptional level (Figure 3a) and translational level (Figure 3b), was significantly downregulated ($p < 0.01$) in the STHdh$^{Q111/111}$ cell line compared with the STHdh$^{Q7/7}$ cell line.

Again, meldonium treatment significantly increased the messenger RNA (mRNA) expression of PGC-1α in STHdh$^{Q111/111}$ cells (Figure 3a; $p < 0.01$), and the augmented amount of the PGC-1α protein also reflected this increment (Figure 3b; $p < 0.01$).

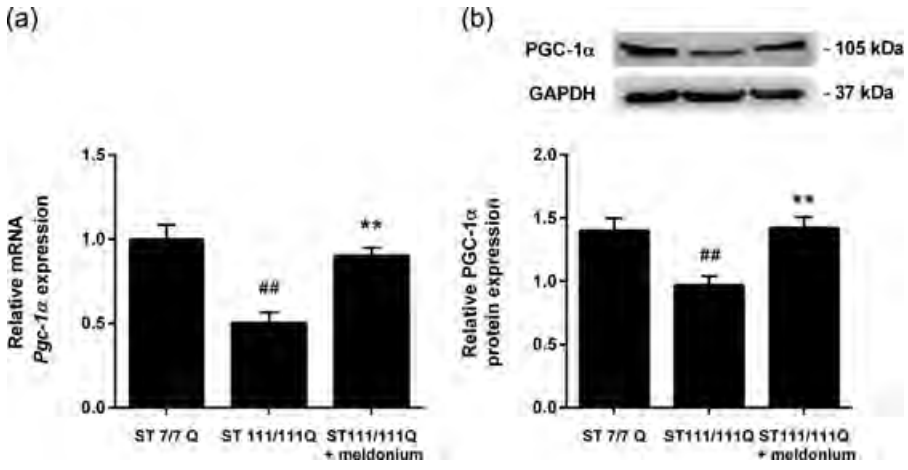

FIGURE 3 Meldonium restores the peroxisome proliferator-activated receptor γ coactivator 1α (PGC-1α) signaling pathway in STHdh$^{Q111/111}$ cell line. (a) PGC-1α messenger RNA expression in STHdh$^{Q7/7}$, STHdh$^{Q111/111}$, and 24 hr, 50 μM meldonium-treated STHdh$^{Q111/111}$ cells. (b) PGC-1α protein expression in STHdh$^{Q7/7}$, STHdh$^{Q111/111}$, and 24 hr, 50 μM meldonium-treated STHdh$^{Q111/111}$ cells. Representative cropped western blot of PGC-1α. Data were normalized to the housekeeping gene β-actin (*Actb*) and to the housekeeping protein glyceraldehyde 3-phosphate dehydrogenase (GAPDH), respectively. Statistical significance: $^{\#\#}p < 0.01$ versus STHdh$^{Q7/7}$ cells; $^{**}p < 0.01$ versus untreated STHdh$^{Q111/111}$ cells; one-way analysis of variance, with post-hoc Bonferroni's test. Bars represent the means ± *SD*; $n = 3$

3.3 | Meldonium affects mitochondrial mass and dynamics

Researchers have demonstrated that PGC-1α modulates mitochondrial biogenesis and mitochondrial dynamics in neuronal cells (Chiang et al., 2016; Dambrova et al., 2016). At first, we performed experiments to evaluate whether meldonium-treated cells exhibited an increase in mitochondrial mass. For these studies, STHdh$^{Q111/111}$ cells were treated with meldonium at the indicated concentrations for 72 hr, and then incubated with MitoTracker Green to determine mitochondrial mass. The fluorescent intensity changes, recorded and analyzed by Cytation 3 Multi-Mode Reader (BioTek), demonstrated that meldonium treatment induced a significant increase in mitochondrial mass levels (Figure 4a). As reported in Figure 4b, these results were corroborated by the analysis of mtDNA level in treated and untreated cell lines.

We also investigated mitochondrial dynamics in STHdh$^{Q7/7}$ and STHdh$^{Q111/111}$ cell lines by confocal microscopy after incubation with the MitoTracker Red dye. In agreement with previous reports (Dickey et al., 2017), we found that the STHdh$^{Q7/7}$ mitochondrial network exhibited a branched, tubular morphology, while it appeared fragmented with many small and short mitochondria in STHdh$^{Q111/111}$ cells (Figure 4c). In particular, we observed a significant decrease in the percentage of longer mitochondria (>3 μm) and a corresponding significant increase of shorter mitochondria in STHdh$^{Q111/111}$ cells (Figure 4d).

Confocal microscopy analysis showed that the tubular morphology of mitochondria was restored in STHdh$^{Q111/111}$ meldonium-treated cells (Figure 4c). Mitochondria appeared as long tubular structures extending in the whole cytosol, and only a small percentage of the mitochondrial network remained still fragmented (Figure 4d). As expected, we did not find any differences in STHdh$^{Q7/7}$ cells after meldonium treatment and we exclude any off-target effect (Figure 4c).

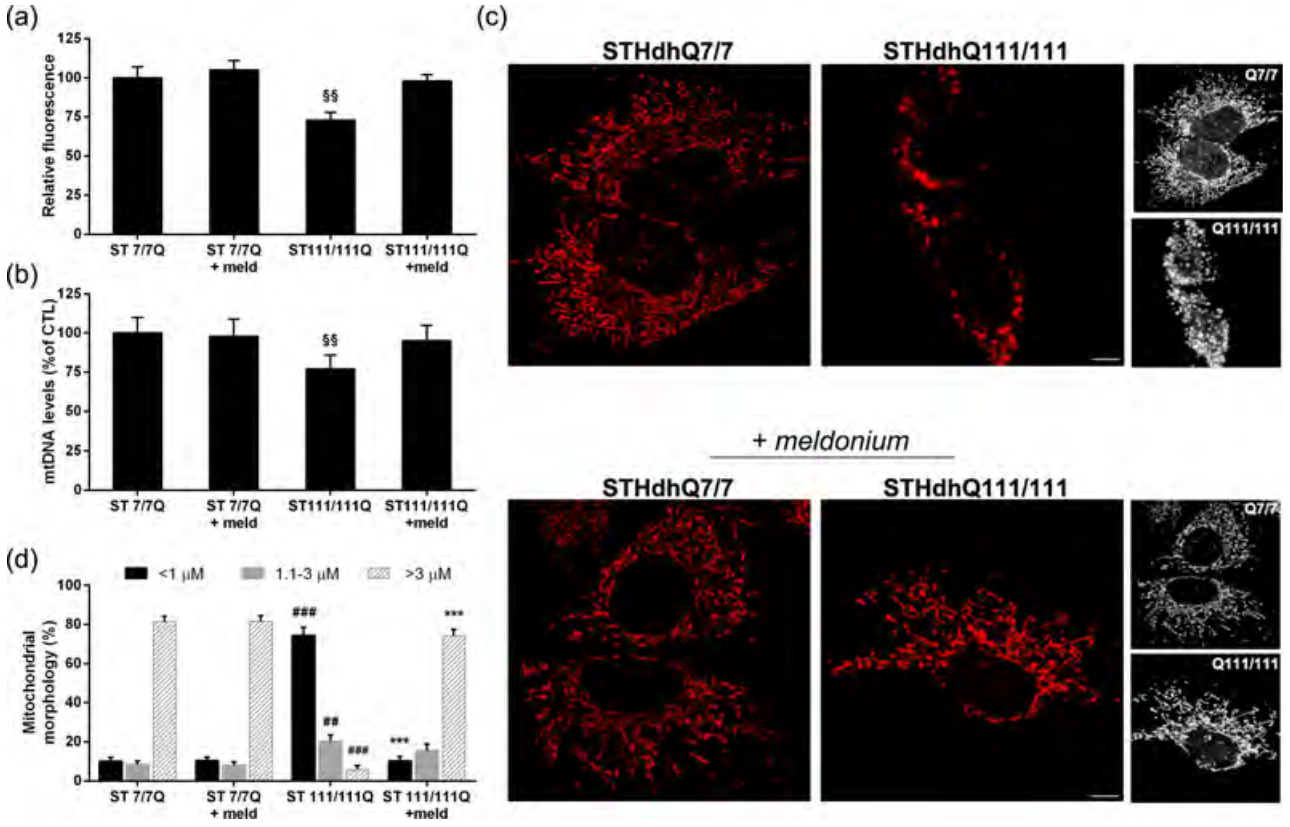

FIGURE 4 Meldonium improves mitochondrial mass and dynamics. (a) Cellular content of mitochondria in STHdh$^{Q7/7}$ and STHdh$^{Q111/111}$ cells with and without treatment with 50 μM meldonium for 72 hr. The mitochondria were stained with MitoTracker Green FM and the fluorescence was quantified with the Cytation 3 Multi-Mode Reader and expressed relative to the control condition (STHdh$^{Q7/7}$ cells without meldonium). Bars represent the mean ± *SD*; $n = 3$. Statistical significance: $^{§§}p < 0.01$ versus STHdh$^{Q7/7}$ cells and 72 hr, 50 μM meldonium-treated STHdh$^{Q7/7}$ and STHdh$^{Q111/111}$ cells; Student's *t* test. (b) Evaluation of mitochondrial DNA (mtDNA) copy number. Quantitative polymerase chain reaction was used to determine the mtDNA/nuclear DNA ratio in STHdh$^{Q7/7}$ and STHdh$^{Q111/111}$ cells with and without treatment with 50 μM meldonium for 72 hr. Bars represent the mean ± *SD*; $n = 3$. Statistical significance: $^{§§}p < 0.01$ versus STHdh$^{Q7/7}$ cells and 72 hr, 50 μM meldonium-treated STHdh$^{Q7/7}$ and STHdh$^{Q111/111}$ cells; one-way analysis of variance with post-hoc Bonferroni's test. (c) Representative images of STHdh$^{Q7/7}$ and STHdh$^{Q111/111}$ cells with and without treatment with 50 μM meldonium for 72 hr, stained with MitoTracker Red treatment. Images were acquired with a confocal microscope taking Z-slices from the top to the bottom of cells. The three-dimensional reconstruction is shown in small panels. Scale Bar=5 μm. (d) Quantification of mitochondrial shape according to length. Bars represent the mean ± *SD*; $n = 3$. Statistical significance: $^{###}p < 0.001$ versus untreated STHdh$^{Q7/7}$ cells; $^{***}p < 0.001$ versus untreated STHdh$^{Q111/111}$ cells; Student's *t* test [Color figure can be viewed at wileyonlinelibrary.com]

3.4 | Meldonium increased lifespan and survival rate in the fly HD model

To evaluate the potentiality of meldonium in vivo, we used a well-established *Drosophila melanogaster* model for HD (Q128HD-FL) in which the human HTT complementary DNA (cDNA), with 128 glutamine repeats, is expressed in all neuronal tissues (genotype: elav-Gal4/+; UAS-HttFL-Q128/+; Romero et al., 2008).

To investigate the effect of meldonium on Drosophila adults, we first confirmed whether feeding flies on food supplemented with this compound influences the food intake. With this aim, we used a red-dyed assay. We allowed the flies to feed for 1 day in the red-dyed assay food supplemented or not with meldonium. Importantly, the ingestion of the food with meldonium did not differ significantly from the food without meldonium (Figure 5a). We observed this result for flies expressing full-length human cDNA with 128 Q under the control of the elav-GAL4 driver as well as for the control strain expressing GFP under the elav-GAL4 driver.

Of interest, in the transgenic Q128HD-FL strain we used, HD had a very aggressive disease course and was usually fatal within 30 days. The flies developed age-dependent neurodegenerative phenotypes, with initial hyperactivity followed by a progressive loss of coordination and motor impairment.

To test whether meldonium could slow the course of the disease and the onset of pathological symptoms, we measured the survival rate as well as the ability of Q128HD-FL flies to climb a vial wall as a function of meldonium treatment.

Our results clearly indicate that meldonium-treated Q128HD-FL flies had significantly extended lifespans compared with untreated sibling flies (Figure 5b). Specifically, the mean lifespan of flies in the meldonium-treated group increased by 20%, and the maximum lifespan increased by about 19% ($p < 0.001$). Additionally, a comparison between the two lifespan curves revealed that meldonium significantly increased the survival rate of Q128HD-FL flies. As shown in Figure 5c, the two curves overlap in the first 13 days and diverge thereafter due to better survival of the meldonium group flies. The survival curve of untreated flies fell rapidly between 13 and 24 days, while the survival curve of treated flies slowly declined slowly declined between 18 and 24 days, dropping quickly thereafter ($p < 0.001$). Furthermore, the turning drop point of the treated fly group was later than the untreated group.

3.5 | Meldonium ameliorates htt-linked symptoms in HD flies

To study the effect of meldonium on neuronal dysfunction, we evaluated its impact on the motor function of Q128HD-FL transgenic flies grown on normal or meldonium-supplemented food. HD flies exhibited progressive abnormal movements with age because of impaired motor neuronal function, revealed by the climbing test, which exploits the strong negative geotaxis behavior of Drosophila. Our results show that meldonium treatment significantly improved the climbing ability of transgenic flies (Figure 5d). Motor dysfunction of nontreated flies was early and progressive and most prominent on Day 12 posteclosion when the flies tended to stay at the bottom of the vial or climb only a short distance. In contrast, the climbing ability of meldonium-treated flies was remarkably higher. Their motor disability arose later and was most prominent on Day 17 posteclosion. Moreover, the percentage of flies that achieved the target (10 s) was significantly higher at each age point examined ($p < 0.001$).

3.6 | Meldonium induces upregulation of the dPGC-1α gene in *D. melanogaster*

Results obtained on Htt-cells showed that meldonium treatment significantly enhances the levels of the PGC-1α transcript and protein (Figure 3). To investigate whether the observed upregulation of PGC-1α was evident also in the in vivo HD model, we analyzed the RNA levels of the *Spargel* (*srl*) gene, the only orthologue of the PGC-1 family in Drosophila (Gershman et al., 2007).

Consistent with the idea that the enhancement of PGC-1α activity may offer neuroprotection, we carried out a qRT-PCR assay to measure the level of the *Spargel* transcript in Drosophila. We first analyzed the *Spargel* mRNA expression in the progression of HD. Based on the motor dysfunction, we performed this assay at four different age steps: presymptomatic (pre-HD; 0 days old), early symptomatic (early-HD; 4 days old) and late symptomatic (late-HD; 12 and 16 days old) transgenic flies. Interestingly, we found that the level of the *Spargel* transcript decreased with the progression of HD with a significant decline in the late symptomatic Q128HD-FL (Figure 5e).

We next performed this assay in meldonium-treated siblings, and our results clearly indicate that in HD flies fed with meldonium, *Spargel* is significantly upregulated (about 1.6–1.8-fold) in all time points tested (Figure 5f).

In conclusion, the dPGC-1α/*Spargel* gene in *D. melanogaster* was significantly upregulated in the head tissues of the HD flies after meldonium treatment, starting from the early stage of HD.

3.7 | ROS level measurement

Given the critical role that oxidative stress can play in the development of HD, we compared the oxidative status of 10-day-old HD transgenic flies with the same flies following meldonium treatment. Our results clearly demonstrate that HD transgenic flies have an increased level of ROS when compared with wild-type flies (Figure 6), confirming the data obtained in other HD models (Scialò et al., 2016). In HD transgenic flies, meldonium supplementation reduced the level of oxidative stress in brain tissues (Figure 6).

4 | DISCUSSION

The results presented in this report indicate that meldonium corrects the HD phenotype in cellular and insect models, predominantly by

(a)

(b)

	Number of flies	Mean lifespan (days)	Change of mean lifespan (%)	Maximum lifespan (days)	Change of maximum lifespan (%)
No treatment	300	20 ± 1.85		24 ± 1	
Meldonium	300	24 ± 2.3	+20	27 ± 1,6	+19

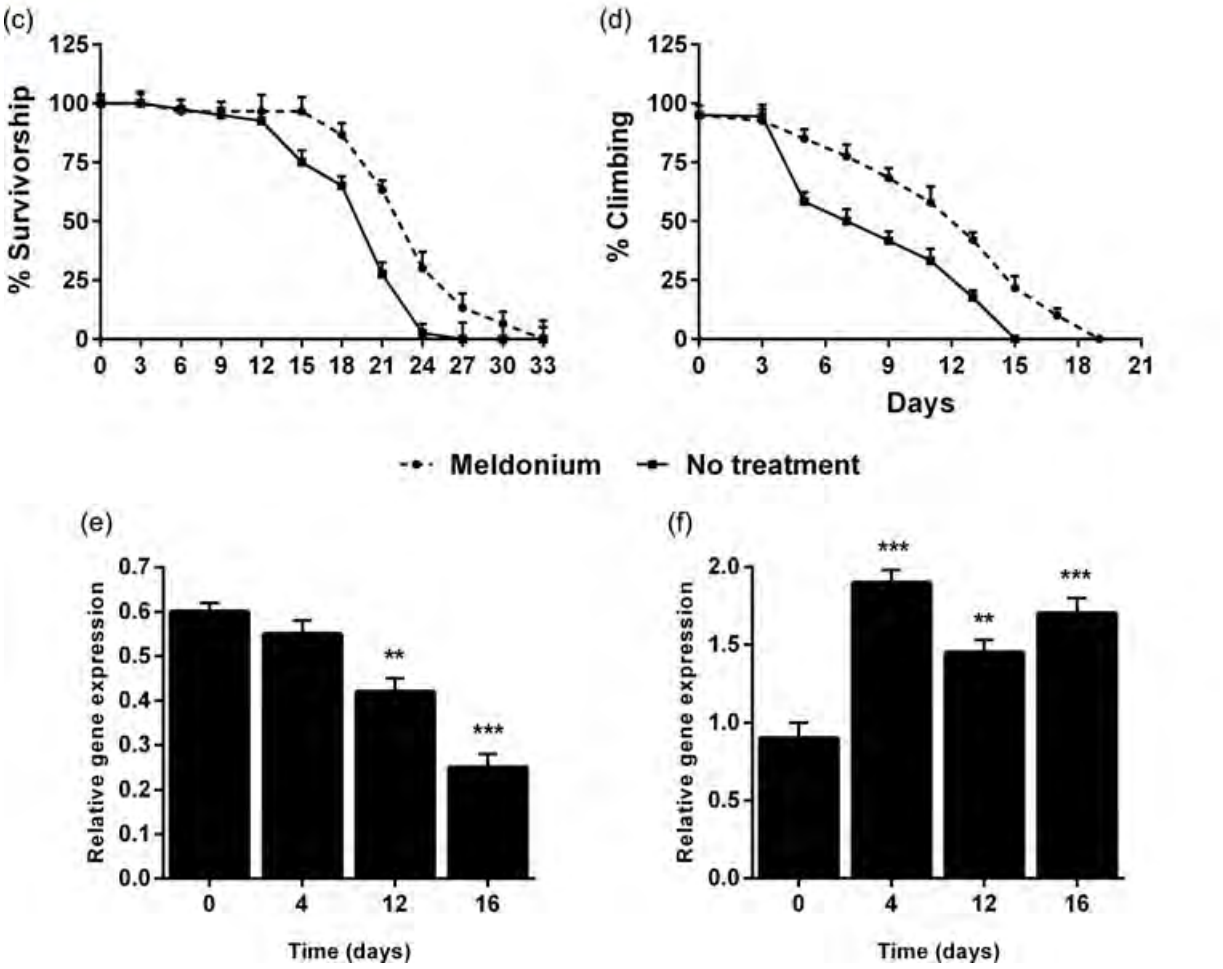

FIGURE 5 Meldonium effect on the fly Huntington's disease (HD) model. (a) Transgenic Q128HD-FL flies fed with red food and red food supplemented with meldonium. Both flies present the same coloration in the abdomen. (b) Lifespan of Q128HD-FL transgenic flies fed with meldonium and control diet. The data were given as mean ± *SD*; $n = 300$. Change lifespan % = control−treatment/control lifespan×100. Statistical significance: $^{***}p < 0.001$ versus flies fed with control diet; Student's *t* test. (c) Comparison of age-dependent survival curves of Q128HD-FL transgenic flies fed with diets either containing meldonium or not indicated highly significant differences ($p < 0.001$); $n = 300$; Student's *t* test. (d) Negative geotaxis assay in Q128HD-FL transgenic flies fed with meldonium and with control food. Treated flies showed defects in their climbing ability later than nontreated siblings. The data were given as mean ± *SD*; $n = 300$; $p < 0.001$ versus untreated group at each age point examined; one-way analysis of variance (ANOVA) with post-hoc Bonferroni's test. (e) *dPGC-1α/Spargel* messenger RNA (mRNA) expression in the progression of fly HD model. The levels of *Spargel* mRNA in each sample were normalized against the level of *rp49* based on standard curves. Statistical significance: $^{**}p < 0.01$ and $^{***}p < 0.001$ versus age-matched control parental strain; one-way ANOVA analysis with post-hoc Bonferroni's test. (f) *dPGC-1α/Spargel* mRNA expression in Q128HD-FL transgenic flies after meldonium treatment. The *dPGC-1α/Spargel* mRNA level in each sample was normalized against the level of *rp49* based on standard curves. The normalized levels of the *srl* transcript at four different age steps were then compared with those of age-matched untreated flies using the analysis of variance one-way ANOVA, followed by the post-hoc Bonferroni's test. Statistical significance: $^{**}p < 0.01$, $^{***}p < 0.001$ versus Q128HD-FL flies without meldonium supplementation. Bars represent the means ± *SD*; $n = 3$ [Color figure can be viewed at wileyonlinelibrary.com]

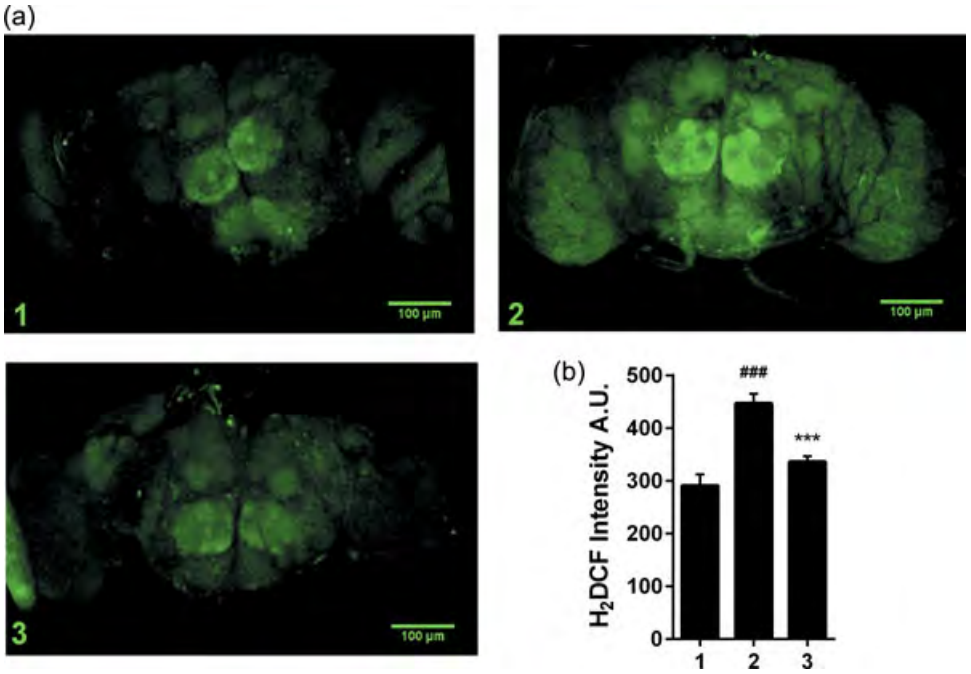

FIGURE 6 Meldonium reduces reactive oxygen species (ROS) production in Huntington's disease (HD) transgenic flies brains. (a) Representative images of Drosophila-dissected brains from control parental flies (1), Q128HD-FL flies without meldonium supplementation (2), and Q128HD-FL flies with meldonium supplementation (3). (b) Fluorescence intensity quantification of each individual brain imaged. Statistical significance: $^{###}p < 0.001$ versus control parental flies; $^{***}p < 0.001$ versus Q128HD-FL without meldonium supplementation; one-way analysis of variance with post-hoc Bonferroni's test. Bars represent the means ± *SD*; $n = 3$ [Color figure can be viewed at wileyonlinelibrary.com]

restoring a proper mitochondrial functionality as summarized in Scheme 1.

The ever-increasing understanding of how the mutant huntingtin protein causes neuronal dysfunction and death has produced a multitude of rational therapeutic targets. Many scientific reports have suggested the decisive involvement of mitochondrial dysfunction, including defects in bioenergetics, mitochondrial fusion/fission, mitochondrial movement, and transcription in the pathogenesis of HD (Kim et al., 2010). Whether correction of these mitochondria-associated dysfunctions is sufficient to inhibit the neurodegenerative process remains uncertain. Over the past years, without any definite success up to now, researchers have tested agents able to improve mitochondrial function and correct some mitochondrial defects for their therapeutic effects on in vitro and in vivo HD models (Rosenstock, Duarte, & Rego, 2010).

Meldonium inhibits endogenous carnitine synthesis and carnitine cell uptake, thus lowering carnitine availability inside the cell (Dambrova et al., 2016). Carnitine has a vital role in the metabolism of FAs as a substrate for the reversible acylation of coenzyme A and as a carrier for the transport of acyl units from cytosol across the inner mitochondrial membrane to the mitochondrial matrix, and vice versa (Adeva-Andany, Calvo-Castro, Fernandez-Fernandez, Donapetry-Garcia, & Pedre-Pineiro, 2017).

Therefore, the way through which meldonium hypothetically induces changes in glucose metabolism is by acting in the Randle cycle as a compensatory mechanism of decreased carnitine-dependent FA oxidation in mitochondria. Interestingly, the World Anti-Doping Agency (the regulatory body overseeing drug screening for international sporting events) has classified meldonium, for its metabolic activity, as a performance-enhancing drug, a category that also includes insulin and trimetazidine (Thevis, Kuuranne, & Geyer, 2018).

Administration of meldonium has already been shown to exert a neuroprotective action in different models of central nervous system diseases, including Parkinson's and Alzheimer's disease.

In the current study, we found that treatment with meldonium attenuated in vitro cytotoxicity induced by mHtt and decreased intracellular mHtt aggregate formation. To further test our results in vivo, we used a transgenic Drosophila model of HD in which the expression of Htt, with a 128Q expansion (Q128HD-FL) in the nervous system, leads to progressive motor performance deficits when compared with normal insects. Indeed, Q128HD-FL transgenic flies exhibit progressive abnormal movements with age because of impaired motor neuronal function, revealed by a climbing test, which exploits the strong negative geotaxis behavior of Drosophila. Our results demonstrate that meldonium-treated Q128HD-FL transgenic flies show a significant delay in disease onset with a concomitant lifespan increase, and they perform better than untreated Q128HD-FL flies. Again, the effects observed were related to an increased expression of *Spargel* (*srl*) gene, the only orthologue of the PGC-1 family in Drosophila (Gershman et al., 2007). A recent study based on an RNAi approach reported that knocking down the *Spargel* gene reduced the locomotion ability of adult flies (Merzetti & Staveley, 2015), inducing time-dependent impairment in their climbing ability

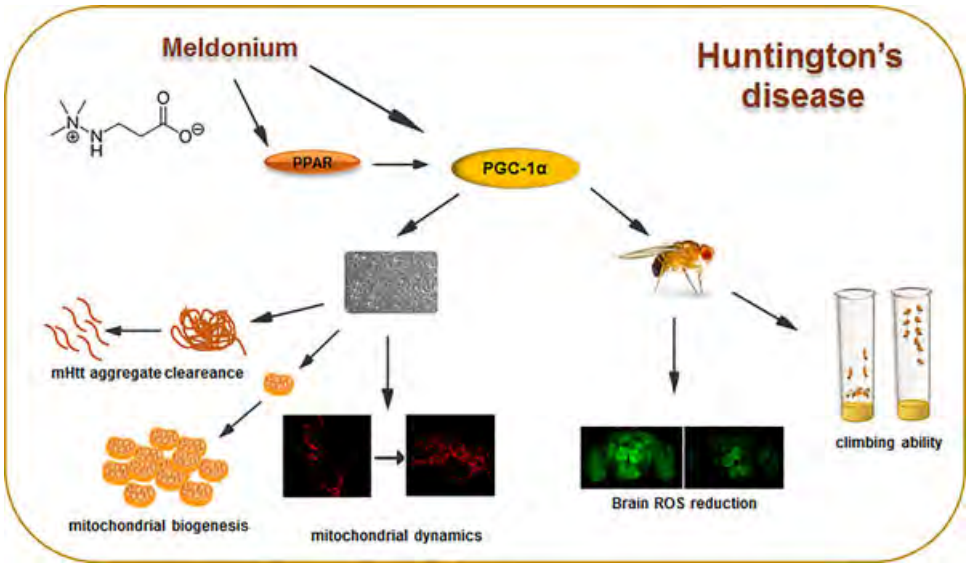

SCHEME 1 Regulatory mechanism of meldonium in Huntington's disease models. Schematic representation of two potential pathways involved in meldonium modulation mechanism of peroxisome proliferator-activated receptor γ coactivator 1α (PGC-1α). ROS: reactive oxygen species [Color figure can be viewed at wileyonlinelibrary.com]

(Ng et al., 2017). In contrast, *Spargel* overexpression significantly improved the climbing performance of parkin null flies, a strain of Drosophila characterized by disability in mobility.

Regarding the meldonium effects that we described, we cannot relate them in an oversimplified way to the reported mechanism of action of the drug on endogenous carnitine synthesis and tissue uptake leading to a reduction of cytotoxic intermediate products of FA β-oxidation. Alternatively, the long-term decline in mitochondrial FA oxidation induced by chronic treatment with meldonium might generate compensatory mechanisms that strongly reprogram cell metabolic phenotype. A recent study reported that meldonium modified the abundance of 189 mRNAs modulating fuel selection, highlighting the regulation of discrete cellular functions and metabolic pathways (Porter et al., 2017).

Interestingly, Liepinsh et al. (2008) revealed that long-term treatment with meldonium stimulated a compensatory activation of the PGC-1α signaling pathway. PGC-1α is the master coregulator of mitochondrial biogenesis, energy homeostasis, and antioxidant defense (Liu & Lin, 2011). Impaired PGC-1α expression and downstream signaling changes have been already demonstrated to underpin mitochondrial dysfunction in HD neurons (Johri, Chandra, & Flint beal, 2013). Therefore, an upregulation of this critical transcriptional coactivator, sitting at the crossroads of mitochondrial functions, would be beneficial in HD (McGill & Beal, 2006).

However, the transcriptional regulatory factors that link upstream signaling pathways to PGC1A gene expression in the brain are only partially defined. At the PGC-1α promoter, there are binding sites for transcription factors myocyte enhancer factor 2 (MEF2), forkhead box class O (FoxO1), activating transcription factor 2 (ATF2), and cAMP response element–binding protein (CREB), all of which enhance PGC-1α transcription. These factors, in turn, are modulated by different signaling pathways. Insulin activates Akt, which leads to cytoplasmic sequestration and inhibition of FoxO1. Cytokines and exercise activate p38 mitogen-activated protein kinase (p38MAPK), which phosphorylates and activates MEF2 and ATF2. Exercise also stimulates Ca^{2+} signaling, which, through calmodulin-dependent protein kinase IV and calcineurin A, induces CREB and MEF2-mediated PGC-1α transcription. Cold activates β3-adrenergic receptors in muscle and brown fat, leading to protein kinase A-mediated activation of CREB. Interestingly, in vivo studies have demonstrated that PPARγ activation by Rosiglitazone attenuates mutant HTT induced toxicity in HTT striatal cells (Quintanilla, Jin, Fuenzalida, Bronfman, & Johnson, 2008), and prevents PGC-1α reduction in HD mouse brain (Jin et al., 2013). In addition, it was demonstrated that bezafibrate, an agonist of Pan-PPAR, activated mitochondrial biogenesis and restored levels of PGC-1α, PPARs, and downstream genes in a transgenic mouse model of HD (Johri et al., 2012).

In our study, we showed that the results of meldonium treatment, including the in vivo effects, were coupled to PGC-1α or its orthologue *Spargel* (*srl*) gene overexpression. We might explain the same normalization of mitochondrial dynamics by the increase of PGC-1α expression, which in turn induces a balanced expression of fusion/fission genes by binding to their promoters and implying its direct role in the regulation of mitochondrial dynamics (Dabrowska et al., 2016). Future studies should clarify whether PPARγ activation mediates the PGC-1α elevation induced by meldonium or is related to other PPAR-independent mechanisms.

Finally, the studies reporting that supplementation of carnitine alone can exert only partial neuroprotective effects in HD experimental model are in agreement with our findings (Mehrotra, Sood, & Sandhir, 2015). Since an increase of free carnitine cannot modify the metabolic attitude of mHtt cells to utilize FA as mitochondrial fuel, carnitine can only alleviate the effects of the

mitochondrial overloading of long-chain FA, making it possible to export FA as acylcarnitines from cytosol to the bloodstream. Indeed, HD patients displayed a significantly distinctive metabolic pattern characterized by elevated levels of circulating acylcarnitines and low levels of free carnitine that turn out to be essential discriminators between patients with HD and normal controls (Cheng et al., 2016). This HD carnitine–acylcarnitines profile is the signature of an inefficient increase of FA utilization that produces toxic intermediates rather than generates energy. Hence, carnitine supplementation does not improve mitochondrial dysfunction in HD, which is why this treatment does not significantly modify the functional decline of HD patients (Mestre, Ferreira, Coelho, Rosa, & Sampaio, 2009).

Of interest, on January 1, 2016 the World Anti-Doping Agency (WADA) announced that "meldonium would be included on the Prohibited List because the WADA rates meldonium as a metabolic modulator whose performance-enhancing benefits can be applied to a wide range of athletic activities" (Dambrova & Liepinsh, 2016; Hughes, 2016). Although the decision to include meldonium on the WADA's Prohibited List did not mention any safety concerns, some authors have also questioned about the safety of meldonium in humans (Arduini & Zammit, 2016), Thus, more in vivo studies are needed not only to confirm the effects of meldonium on different animal models but in particular to investigate potential adverse effect(s) of the drug. Additionally or alternatively, meldonium analogues might be synthetized and selected on the basis of their ability to regulate PGC1 expression and activity with little or no interference on the carnitine system, to which doping effect is attributed (Schobersberger, Dünnwald, Gmeiner, & Blank, 2017). A study describing meldonium derivatives characterized by different ability to inhibit γ-Butyrobetaine hydroxylase, a key enzyme in the generation of carnitine in humans, was recently published (Tars et al., 2014).

ACKNOWLEDGEMENTS

The authors thank Daniela Cavaliere for the excellent technical assistance. The authors also thank the InterUniversity Center for Research in Neurosciences (CIRN), University of Campania "Luigi Vanvitelli", Naples.

This study was supported by Ministero dell'Istruzione, dell'Università e della Ricerca of Italy–MIUR: Project PON—"Ricerca e Competitività 2007–2013"—PON01_01802 title: "Sviluppo di molecole capaci di modulare vie metaboliche intracellulari redox-sensibili per la prevenzione e la cura di patologie infettive, tumorali, neurodegenerative e loro delivery mediante piattaforme nano tecnologiche," and Project Prin 2010–2011– 20109MXHMR" title "Neurodegenerazione e neuroprotezione: ruolo dell'espressione della neuroglobina indotta dagli ormoni estrogeni."

CONFLICTS OF INTEREST

The authors declare that there are no conflicts of interest.

ORCID

Umberto Galderisi http://orcid.org/0000-0003-0909-7403
Mariarosa Anna Beatrice Melone http://orcid.org/0000-0002-7213-9277
Gianfranco Peluso http://orcid.org/0000-0003-4352-9484

REFERENCES

Adeva-Andany, M. M., Calvo-Castro, I., Fernández-Fernández, C., Donapetry-García, C., & Pedre-Piñeiro, A. M. (2017). Significance of l-carnitine for human health. *IUBMB Life*, *69*(8), 578–594. https://doi.org/10.1002/iub.1646.

Arduini, A., & Zammit, V. A. (2016). A tennis lesson: Sharp practice in the science behind the Sharapova case. *Postgraduate Medical Journal*, *92* (1090), 429–430. https://doi.org/10.1136/postgradmedj-2016-134124.

Beitnere, U., van Groen, T., Kumar, A., Jansone, B., Klusa, V., & Kadish, I. (2014). Mildronate improves cognition and reduces amyloid-beta pathology in transgenic Alzheimer's disease mice. *Journal of Neuroscience Research*, *92*(3), 338–346. https://doi.org/10.1002/jnr.23315.

Brand, A. H., & Perrimon, N. (1993). Targeted gene expression as a means of altering cell fates and generating dominant phenotypes. *Development*, *118*(2), 401–415.

Browne, S. E., Bowling, A. C., MacGarvey, U., Baik, M. J., Berger, S. C., Muquit, M. M. K., … Beal, M. F. (1997). Oxidative damage and metabolic dysfunction in Huntington's disease: Selective vulnerability of the basal ganglia. *Annals of Neurology*, *41*(5), 646–653. https://doi.org/10.1002/ana.410410514.

Cheng, M. L., Chang, K. H., Wu, Y. R., & Chen, C. M. (2016). Metabolic disturbances in plasma as biomarkers for Huntington's disease. *Journal of Nutritional Biochemistry*, *31*, 38–44. https://doi.org/10.1016/j.jnutbio.2015.12.001.

Chiang, M. C., Nicol, C. J., Cheng, Y. C., Lin, K. H., Yen, C. H., & Lin, C. H. (2016). Rosiglitazone activation of PPARgamma-dependent pathways is neuroprotective in human neural stem cells against amyloid-beta-induced mitochondrial dysfunction and oxidative stress. *Neurobiology of Aging*, *40*, 181–190. https://doi.org/10.1016/j.neurobiolaging.2016.01.132.

Cui, L., Jeong, H., Borovecki, F., Parkhurst, C. N., Tanese, N., & Krainc, D. (2006). Transcriptional repression of PGC-1alpha by mutant huntingtin leads to mitochondrial dysfunction and neurodegeneration. *Cell*, *127*(1), 59–69. https://doi.org/10.1016/j.cell.2006.09.015.

Dabrowska, A., Luis venero, J., Iwasawa, R., Hankir, M., Rahman, S., Boobis, A., & Hajji, N. (2016). Erratum: PGC-1alpha controls mitochondrial biogenesis and dynamics in lead-induced neurotoxicity. *Aging (Albany NY)*, *8*(4), 832. https://doi.org/10.18632/aging.100955.

Dambrova, M., & Liepinsh, E. (2016). Response to comment by Sergei V. Jargin: "Meldonium (Mildronate): Primum non nocere". *Pharmacological Research*, *114*, 295–296. https://doi.org/10.1016/j.phrs.2016.10.005.

Dambrova, M., Liepinsh, E., & Kalvinsh, I. (2002). Mildronate: Cardioprotective action through carnitine-lowering effect. *Trends in Cardiovascular Medicine*, *12*(6), 275–279. https://doi.org/Pii S1050-1738(02)00175-5. Doi 10.1016/S1050-1738(02)00175-5

Dambrova, M., Makrecka-Kuka, M., Vilskersts, R., Makarova, E., Kuka, J., & Liepinsh, E. (2016). Pharmacological effects of meldonium: Biochemical mechanisMs and biomarkers of cardiometabolic activity. *Pharmacological Research*, *113*, 771–780. https://doi.org/10.1016/j.phrs.2016.01.019.

Dickey, A. S., Sanchez, D. N., Arreola, M., Sampat, K. R., Fan, W., Arbez, N., … La Spada, A. R. (2017). PPARdelta activation by bexarotene promotes neuroprotection by restoring bioenergetic and quality control homeostasis. *Science Translational Medicine*, *9*(419), eaal2332. https://doi.org/10.1126/scitranslmed.aal2332.

Gershman, B., Puig, O., Hang, L., Peitzsch, R. M., Tatar, M., & Garofalo, R. S. (2007). High-resolution dynamics of the transcriptional response to nutrition in Drosophila: A key role for dFOXO. *Physiological Genomics*, *29*(1), 24–34. https://doi.org/10.1152/physiolgenomics.00061.2006.

Gines, S., Seong, I. S., Fossale, E., Ivanova, E., Trettel, F., Gusella, J. F., & MacDonald, M. E. (2003). Specific progressive cAMP reduction implicates energy deficit in presymptomatic Huntington's disease knock-in mice. *Human Molecular Genetics*, *12*(5), 497–508.

Graham, S. F., Kumar, P., Bahado-Singh, R. O., Robinson, A., Mann, D., & Green, B. D. (2016). Novel metabolite biomarkers of Huntington's disease as detected by high-resolution mass spectrometry. *Journal of Proteome Research*, *15*(5), 1592–1601. https://doi.org/10.1021/acs.jproteome.6b00049.

Guedes-Dias, P., Pinho, B. R., Soares, T. R., De proença, J., Duchen, M. R., & Oliveira, J. M. A. (2016). Mitochondrial dynamics and quality control in Huntington's disease. *Neurobiology of Disease*, *90*, 51–57. https://doi.org/10.1016/j.nbd.2015.09.008.

Guo, X., Sun, X., Hu, D., Wang, Y. J., Fujioka, H., Vyas, R., … Qi, X. (2016). VCP recruitment to mitochondria causes mitophagy impairment and neurodegeneration in models of Huntington's disease. *Nature Communications*, *7*, 12646. https://doi.org/10.1038/ncomms12646.

Helguera, P., Seiglie, J., Rodriguez, J., Hanna, M., Helguera, G., & Busciglio, J. (2013). Adaptive downregulation of mitochondrial function in down syndrome. *Cell Metabolism*, *17*(1), 132–140. https://doi.org/10.1016/j.cmet.2012.12.005.

Hughes, D. (2016). Meldonium and the prohibited list. *Australian Prescriber*, *39*(3), 102–102. https://doi.org/10.18773/austprescr.2016.032.

Isajevs, S., Isajeva, D., Beitnere, U., Jansone, B., Kalvinsh, I., & Klusa, V. (2011). Mildronate as a regulator of protein expression in a rat model of Parkinson's disease. *Medicina-Lithuania*, *47*(10), 552–559.

Jin, J., Albertz, J., Guo, Z., Peng, Q., Rudow, G., Troncoso, J. C., … Duan, W. (2013). Neuroprotective effects of PPAR-γ agonist rosiglitazone in N171-82Q mouse model of Huntington's disease. *Journal of Neurochemistry*, *125* (2013), 410–419. https://doi.org/10.1111/jnc.12190.

Johri, A., Calingasan, N. Y., Hennessey, T. M., Sharma, A., Yang, L., Wille, E., … Beal, M. F. (2012). Pharmacologic activation of mitochondrial biogenesis exerts widespread beneficial effects in a transgenic mouse model of Huntington's disease. *Human Molecular Genetics*, *21*, 1124–1137. https://doi.org/10.1093/hmg/ddr541.

Johri, A., Chandra, A., & Flint beal, M. (2013). PGC-1alpha, mitochondrial dysfunction, and Huntington's disease. *Free Radical Biology and Medicine*, *62*, 37–46. https://doi.org/10.1016/j.freeradbiomed.2013.04.016.

Kim, J., Moody, J. P., Edgerly, C. K., Bordiuk, O. L., Cormier, K., Smith, K., … Ferrante, R. J. (2010). Mitochondrial loss, dysfunction and altered dynamics in Huntington's disease. *Human Molecular Genetics*, *19*(20), 3919–3935. https://doi.org/10.1093/hmg/ddq306.

Kumar, A., Vaish, M., & Ratan, R. R. (2014). Transcriptional dysregulation in Huntington's disease: A failure of adaptive transcriptional homeostasis. *Drug Discovery Today*, *19*(7), 956–962. https://doi.org/10.1016/j.drudis.2014.03.016.

Li, X. J., Orr, A. L., & Li, S. (2010). Impaired mitochondrial trafficking in Huntington's disease. *Biochimica et Biophysica Acta (BBA)—Molecular Basis of Disease*, *1802*(1), 62–65. https://doi.org/10.1016/j.bbadis.2009.06.008.

Liepinsh, E., Vilskersts, R., Skapare, E., Svalbe, B., Kuka, J., Cirule, H., … Dambrova, M. (2008). Mildronate decreases carnitine availability and up-regulates glucose uptake and related gene expression in the mouse heart. *Life Sciences*, *83*(17-18), 613–619. https://doi.org/10.1016/j.lfs.2008.08.008.

Liu, C., & Lin, J. D. (2011). PGC-1 coactivators in the control of energy metabolism. *Acta Biochimca Biophysica Sinica (Shanghai)*, *43*(4), 248–257. https://doi.org/10.1093/abbs/gmr007.

McGill, J. K., & Beal, M. F. (2006). PGC-1alpha, a new therapeutic target in Huntington's disease? *Cell*, *127*(3), 465–468. https://doi.org/10.1016/j.cell.2006.10.023.

Mehrotra, A., Sood, A., & Sandhir, R. (2015). Mitochondrial modulators improve lipid composition and attenuate memory deficits in experimental model of Huntington's disease. *Molecular and Cellular Biochemistry*, *410*(1-2), 281–292. https://doi.org/10.1007/s11010-015-2561-5.

Merzetti, E. M., & Staveley, B. E. (2015). spargel, the PGC-1alpha homologue, in models of Parkinson disease in *Drosophila melanogaster*. *BMC Neuroscience*, *16*, 70. https://doi.org/10.1186/s12868-015-0210-2.

Mestre, T., Ferreira, J., Coelho, M. M., Rosa, M., & Sampaio, C. (2009). Therapeutic interventions for symptomatic treatment in Huntington's disease. *Cochrane Database of Systematic Reviews*, (3), CD006456. https://doi.org/10.1002/14651858.CD006456.pub2.

Mucerino, S., Di Salle, A., Alessio, N., Margarucci, S., Nicolai, R., Melone, M. A. B., … Peluso, G. (2017). Alterations in the carnitine cycle in a mouse model of Rett syndrome. *Scientific Reports*, *7*, 41824. https://doi.org/10.1038/srep41824.

Naia, L., Cunha-Oliveira, T., Rodrigues, J., Rosenstock, T. R., Oliveira, A., Ribeiro, M., … Rego, A. C. (2017). Histone deacetylase inhibitors protect against pyruvate dehydrogenase dysfunction in Huntington's disease. *Journal of Neuroscience*, *37*(10), 2776–2794. https://doi.org/10.1523/Jneurosci.2006-14.2016.

Ng, C. H., Basil, A. H., Hang, L., Tan, R., Goh, K. L., O'Neill, S., … Lim, K. L. (2017). Genetic or pharmacological activation of the Drosophila PGC-1alpha ortholog spargel rescues the disease phenotypes of genetic models of Parkinson's disease. *Neurobiology of Aging*, *55*, 33–37. https://doi.org/10.1016/j.neurobiolaging.2017.03.017.

Porter, C., Constantin-Teodosiu, D., Constantin, D., Leighton, B., Poucher, S. M., & Greenhaff, P. L. (2017). Muscle carnitine availability plays a central role in regulating fuel metabolism in the rodent. *Journal of Physiology*, *595*(17), 5765–5780. https://doi.org/10.1113/JP274415.

Pupure, J., Fernandes, M. A. S., Santos, M. S., Moreno, A. J. M., Kalvinsh, I., Klusa, V., & Oliveira, C. R. (2008). Mitochondria as the target for mildronate's protective effects in azidothymidine (AZT)-induced toxicity of isolated rat liver mitochondria. *Cell Biochemistry and Function*, *26*(5), 620–631. https://doi.org/10.1002/cbf.1486.

Quintanilla, R. A., Jin, Y. N., Fuenzalida, K., Bronfman, M., & Johnson., G. V. W. (2008). Rosiglitazone treatment prevents mitochondrial dysfunction in mutant huntingtin-expressing cells: Possible role of peroxisome proliferator-activated receptor-gamma (PPARgamma) in the pathogenesis of Huntington disease. *Journal of Biological Chemistry*, *283*, 25628–25637. https://doi.org/10.1074/jbc.M804291200.

Romero, E., Cha, G. H., Verstreken, P., Ly, C. V., Hughes, R. E., Bellen, H. J., & Botas, J. (2008). Suppression of neurodegeneration and increased neurotransmission caused by expanded full-length huntingtin accumulating in the cytoplasm. *Neuron*, *57*(1), 27–40. https://doi.org/10.1016/j.neuron.2007.11.025.

Rosenstock, T. R., Duarte, A. I., & Rego, A. C. (2010). Mitochondrial-associated metabolic changes and neurodegeneration in Huntington's disease–from clinical features to the bench. *Current Drug Targets*, *11*(10), 1218–1236.

Schmittgen, T. D., & Livak, K. J. (2008). Analyzing real-time PCR data by the comparative C(T) method. *Nature Protocols*, *3*, 1101–1108.

Schobersberger, W., Dünnwald, T., Gmeiner, G., & Blank, C. (2017). Story behind meldonium-from pharmacology to performance enhancement: A narrative review. *British Journal of Sports Medicine*, *51*(1), 22–25. https://doi.org/10.1136/bjsports-2016-096357.

Scialò, F., Sriram, A., Fernández-Ayala, D., Gubina, N., Lõhmus, M., Nelson, G., … Sanz, A. (2016). Mitochondrial ROS produced via reverse electron transport extend animal lifespan. *Cell Metabolism*, *23*(4), 725–734. https://doi.org/10.1016/j.cmet.2016.03.009.

Tanimura, T., Isono, K., Takamura, T., & Shimada, I. (1982). Genetic dimorphism in the taste sensitivity to trehalose in *Drosophila melanogaster*. *Journal of Comparative Physiology*, *147*(4), 433–437. https://doi.org/10.1007/bf00612007.

Tars, K., Leitans, J., Kazaks, A., Zelencova, D., Liepinsh, E., Kuka, J., … Pugovics, O. (2014). Targeting carnitine biosynthesis: Discovery of

new inhibitors against γ-butyrobetaine hydroxylase. *Journal of Medicinal Chemistry*, *57*(6), 2213–2236. https://doi.org/10.1021/jm401603e.

Thevis, M., Kuuranne, T., & Geyer, H. (2018). Annual banned-substance review: Analytical approaches in human sports drug testing. *Drug Testing and Analysis*, *10*(1), 9–27. https://doi.org/10.1002/dta.2336.

Trettel, F., Rigamonti, D., Hilditch-Maguire, P., Wheeler, V. C., Sharp, A. H., Persichetti, F., & MacDonald, M. E. (2000). Dominant phenotypes produced by the HD mutation in STHdh(Q111) striatal cells. *Human Molecular Genetics*, *9*(19), 2799–2809.

Tsunemi, T., Ashe, T. D., Morrison, B. E., Soriano, K. R., Au, J., Roque, R. A. V., … La Spada, A. R. (2012). PGC-1alpha rescues Huntington's disease proteotoxicity by preventing oxidative stress and promoting TFEB function. *Science Translational Medicine*, *4*(142), 142ra197. https://doi.org/10.1126/scitranslmed.3003799.

Venegas, V., Wang, J., Dimmock, D., & Wong, L. J. (2011). Real-time quantitative PCR analysis of mitochondrial DNA content. *Current Protocols In Human Genetics*, *68*, 19.7.1–19.7.12. https://doi.org/10.1002/0471142905.hg1907s68.

How to cite this article: Di Cristo F, Finicelli M, Digilio FA, et al. Meldonium improves Huntington's disease mitochondrial dysfunction by restoring peroxisome proliferator-activated receptor γ coactivator 1α expression. *J Cell Physiol*. 2018;1–14. https://doi.org/10.1002/jcp.27602

Chapter 10

Hydrogel Nanocomposite Systems: Characterization and Application in Drug-Delivery Systems

Raffaele Conte[1]

Adriana De Luise[1]

Anna Valentino[1]

Francesca Di Cristo[1]

Orsolina Petillo[1]

Francesco Riccitiello[2]

Anna Di Salle[1]

Anna Calarco[1]

Gianfranco Peluso[1]

[1]Institute of Agro-Environmental and Forest Biology (IBAF), Italian National Research Council (CNR), Naples, Italy

[2]University of Naples “Federico II”, Naples, Italy

1 Introduction

1.1 Drug Delivery and Nanotechnologies

Drug targeting to specific organs and tissues is one of the critical endeavors of the new century. The search for new drug-delivery approaches involves a multidisciplinary scientific program aimed to improve the therapeutic index and bioavailability with site-specific delivery [1,2]. These new delivery systems are engineered to reduce solubility problems, protect the drug from the external environment (e.g., photodegradation, pH changes), and control the release profile [3,4] to improve the efficacy of treatments and reduce toxicity and side effects [5]. All these devices must be biocompatible and, on these premises, the versatility and biodegradability of recently introduced polymers of both synthetic (e.g., poly(D,L-lactide-co-glycolide)) and natural origin (e.g., chitosan) constitute a leading approach to new dosage forms able to deliver a higher dose at site-specific organs while conferring controlled release and degradation of nontoxic products [6]. The use of nanotechnology for the engineering of drug-delivery systems rapidly produced commercially available products, leading to the emergence of the term “nanomedicine,” defined as the application of nanosized materials in developing new therapies. At this scale, materials display different physicochemical properties due to their small size, surface structure, and high surface area [7]. These properties allow nanoparticle systems to overcome the limitations of conventional formulations as they facilitate the intracellular uptake to specific cellular targets. The requirements for designing nanovectors are controlled particle size, surface charge, and controllable release of therapeutically active agents with a targeted and specific activity at a predetermined rate and time. For these systems, numerous biological applications are reported, such as cancer therapy; stabilization and protection of drug molecules, proteins, peptides, and DNA; analysis of environmental hazards; protein and gene delivery; self-regulated releasing devices; biorecognizable systems; and stimulus-controlled vectors [7]. Thus, nanotechnology has been adopted in several fields such as drug/gene delivery [8,9], imaging [10], and diagnostics [11]. Clinically, nano-drug-delivery systems are used for various routes of administration, including oral, nasal, transdermal, parenteral, pulmonary, and ocular, with an aim to overcome various membrane barriers. These nanometric entities are excellent platforms to incorporate drugs and deliver them to the desired action site without compromising their activity. In particular, nanovectors are used to transport products that have poor solubility or a short half-life, to solve many of the inherent problems of these molecules (e.g., stability, solubility, toxicity).

1.2 Hydrogels

The current direction of material research is aimed at fabricating engineered systems that can mimic or stimulate native tissue. In particular, the design of advanced biomaterials with controlled physical, chemical, electrical, and biological properties facilitates the formation of functional tissues [12,13] and holds enormous promise in treating organ failure resulting from injuries, aging, and diseases [14,15]. Among the various biomaterials, hydrogels

(HYGs) are particularly suitable as they can mimic the physical, chemical, electrical, and biological properties of most biological tissues [12,13,16]. Structurally, HYGs are three-dimensional polymeric networks with the tendency to absorb a large quantity of water without dissolving (up to 20- to 40-fold their dry weight). The formation of this distinctive three-dimensional network occurs through the crosslinking of the polymeric chains via physical interactions, covalent bonding, hydrogen bonding, and van der Waals interactions between specific functional groups such as –OH, $–CONH_2$, $–SO_3H$, –CONH, and –COOR. These unique physical properties result in the HYG casting into various sizes and shapes [1].

1.3 Hydrogel Classification

HYGs are classified on the basis of their route of synthesis, types of crosslinks, and structure. According to the route of synthesis, HYGs are divided into “homopolymer HYGs,” if made of one type of hydrophilic monomer; “copolymer HYGs,” if composed of two types of monomers; and “multipolymer HYGs” or “interpenetrating polymer networks,” if composed of three or more types of monomers [2]. The crosslink-based classification is in regard to the ionic charges present on the polymer network. “Anionic HYGs” are thermoassociative carboxymethyl pullulan HYGs [3], “cationic HYGs” refers to new thermosensitive HYGs of *N*-isopropylacrylamide (NIPAAm(ok)) and (3-acrylamidopropyl)trimethylammonium chloride [4], “neutral HYGs” are composed of miscible blends of water-insoluble polymers like poly(2,4,4-trimethylhexamethylene terephthalamide) [5], while “ampholytic HYGs” are HYGs based on acrylamide polymers [6]. Finally, the physical structure of the HYGs leads to classification as “amorphous HYGs,” if there are randomly arranged chains [7]; “semicrystalline HYGs,” if there are present regions of ordered macromolecular arrangement [8]; and “hydrogen-bonded” or “complexation” structures, if there exists a three-dimensional network linked by hydrogen bonds [9]. Table 10.1 recaps the classification of HYGs.

Table 10.1 Hydrogel Classification

Type of Classification	Name	Composition
Route of synthesis	Homopolymer hydrogels	One type of hydrophilic monomer
Route of synthesis	Copolymer hydrogels	Two types of monomers
Route of synthesis	Multipolymer hydrogels	Three or more types of monomers
Type of crosslink	Anionic hydrogels	Thermoassociative carboxymethyl pullulan hydrogels
Type of crosslink	Cationic hydrogels	Thermosensitive hydrogels of *N*-isopropylacrylamide and (3-acrylamidopropyl)trimethylammonium chloride
Type of crosslink	Neutral hydrogels	Miscible blends of water-insoluble polymers like poly(2,4,4-trimethylhexamethylene terephthalamide)
Type of crosslink	Ampholytic hydrogels	Acrylamide polymers
Physical structure	Amorphous hydrogels	Randomly arranged chains
Physical structure	Semicrystalline hydrogels	Regions of ordered macromolecular arrangement
Physical structure	Hydrogen-bonded or complexation structures	Three-dimensional network linked by hydrogen bonds

1.4 The Esigen(Exigence)ce of Hydrogel Nanocomposite Systems

HYGs have many applications, particularly in stem cell engineering, immunomodulation, and cancer research [17,18]. Most of these uses demand multiple functionalities of the HYG network and dynamic interactions of the HYG with the surrounding matrices [18]. For a better functionalization, a range of innovations in polymer chemistry, nanofabrication technologies, and biomolecular engineering lead to HYG networks with customized functionality and nanodimensions [19]. The growing interest in developing nanocomposite HYGs for various biomedical applications is shown by the sharp increase in the number of publications related to HYG nanocomposite systems (NC-HYGs) (Fig. 10.1).

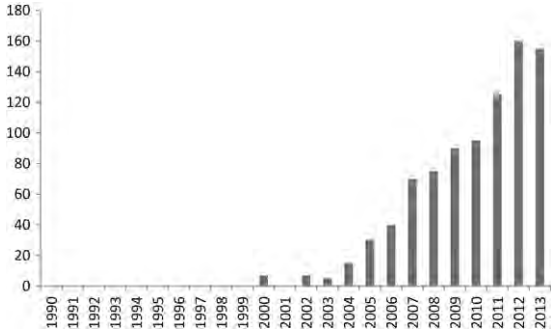

Figure 10.1 Number of publications related to nanocomposite hydrogels (data updated to 2013).

2 Hydrogel Nanocomposite Systems

NC-HYGs are the most recent advances (as of this writing) in HYG technology and are defined as crosslinked three-dimensional water-swollen networks in the presence of nanoparticles. The formation of these networks occurs through physical and chemical interactions in which the inclusion of nanoparticles adds unique properties like mechanical resistance, optical activity, thermal behavior, barrier resistance, etc. [10]. The extraordinary features introduced by NC-HYGs can overcome the limitations of conventional HYGs.

2.1 Materials Used for Hydrogel Nanocomposite Systems

A wide range of nanosized composites can be used to produce NC-HYGs. Practical examples are the clays in the smectite group (e.g., hectorite, montmorillonite), their modifications (e.g., by fluorination or addition of pyloric acid), synthetic mica [20,21], polyhedral oligomeric silsesquioxane [22,23], rigid polysiloxane [24], fibrillar attapulgite [25], and hydrotalcite [26].

Hectorite is a rare soft, greasy, white mineral with the chemical formula $Na_{0.3}(Mg,Li)_3Si_4O_{10}(OH)_2$ that occurs as an alteration product of clinoptilolite from volcanic ash [27]. Large deposits of hectorite are available, and this compound is mostly used in making cosmetics, thanks to its swelling properties.

Montmorillonite is a very soft phyllosilicate group of minerals that precipitate from water solutions as microscopic crystals and that have strong cation-exchange capacity due to the isomorphous substitution of magnesium for alumina in the central alumina plane. The individual crystals of montmorillonite clay are not tightly bound, causing the clay to swell. Thus, the water content of montmorillonite is variable and it increases greatly in volume under wet conditions. This swelling property makes montmorillonite useful as an anticaking agent in animal feed, in papermaking, and as a retention and drainage aid component for cosmetics and drugs. In particular, montmorillonite is effective as an adsorptive of heavy metals [28] and to treat contact dermatitis [29].

Mica comprises a group of sheet silicate minerals having nearly perfect basal cleavage. All are monoclinic, with a tendency toward pseudohexagonal crystals, and are similar in chemical composition, with the general formula $X_2Y_{4-6}Z_8O_{20}(OH,F)_4$, in which X is commonly potassium, sodium, or calcium; Y is alumina, magnesium, or iron; while Z is silica, alumina, iron, or titanium [30]. The commercially important micas are muscovite and phlogopite, which are used in a variety of applications because these sheets are chemically inert, dielectric, elastic, flexible, hydrophilic, insulating, lightweight, platey, reflective, refractive, and resilient, with a range in opacity from transparent to opaque. Micas are stable when exposed to electricity, light, moisture, and extreme temperatures and have superior electrical properties as insulators and dielectrics. These properties make them useful in drug-delivery applications.

Silsesquioxane comprises organosilicon compounds with the chemical formula $(RSiO_{3/2})_n$ (R=H, alkyl, aryl, or alkoxyl). Silsesquioxanes are colorless solids that adopt cagelike or polymeric structures with Si–O–Si linkages and tetrahedral Si vertices, which have attracted attention as precursors to ceramic materials and nanocomposites [31]. The silica core confers rigidity and thermal stability, while several substituents can be attached to the silica centers, forming an organic exterior [31]. In medicine, silsesquioxanes have been functionalized with biocidal quaternary ammonium groups to produce antimicrobial coatings that act as disinfectants, antiseptics, and antifoulants [32]. In particular, the small size of the silsesquioxane molecule (2–5 nm) produces a prominent antimicrobial efficacy due to the high charge density [32]. In addition, the silsesquioxane core in these hybrid materials provides an increased glass transition temperature, improved mechanical properties, higher use temperature, and lower flammability, leading to the production of medical devices resistant to microbial infections [33].

Polysiloxanes, or polymerized siloxanes, are polymers with a silicon–oxygen backbone and chemical formula $(R_2SiO)_n$, where R is usually a methyl, alkyl, or aryl group. Polysiloxanes have greater resistance to the effects of UV radiation than organic polymers containing a carbon–carbon backbone and are available in the form of oils, greases, rubbers, or plastics depending on molecular weight [34]. Moreover, they are flexible, chemically inert, permeable to gases, and water resistant, with a low glass transition temperature and low surface energy; thus, they are suitable for industrial and medical protective and maintenance coatings [35].

Attapulgite is a magnesium aluminum phyllosilicate with the formula $(Mg,Al)_2Si_4O_{10}(OH)\cdot 4(H_2O)$ that occurs in a type of clay soil common to the southeastern United States. Attapulgite forms gel structures in fresh and salt water by establishing a lattice structure of particles connected through hydrogen bonds [36]. Gel-grade, dry-processed attapulgite is used in a very wide range of applications for suspension, reinforcement, and binding, such as in paints, sealants, adhesives, tape-joint compound, catalysts, suspension fertilizers, wild-fire suppressants, foundry coatings, animal feed suspensions, and molecular sieve binders. In medicine, following oral administration, attapulgite physically binds to acids and toxic substances in the stomach and digestive tract and has an antidiarrheal effect by adsorbing the bacteria or germs that may be causing the diarrhea [37,38].

Hydrotalcite is a layered double hydroxide of the general formula $Mg_6Al_2CO_3(OH)_{16}\cdot 4(H_2O)$, with high water content. The layers of the structure stack, produce a three-layer rhombohedral structure or a two-layer hexagonal structure; also these two polytypes are often intergrown [39]. The carbonate anions that lie between the structural layers are weakly bound, so hydrotalcite has anion-exchange capabilities [39]. In medicine, hydrotalcite is used as an antacid or as a filler for dental restorations [40].

Graphene is an allotrope of carbon in a two-dimensional, atomic-scale, hexagonal lattice in which one atom forms each vertex. Thus, it can be considered as an indefinitely large aromatic molecule, with many unusual properties [41]. In fact, it is about 200 times stronger than steel. It efficiently conducts heat and electricity and is nearly transparent [41]. Moreover, it can be simply obtained in nanosized dimensions and included into HYGs.

Bioglasses are a broad category of substances, with different chemical compositions, which include SiO_2, CaO and P_2O_5, Na_2O, K_2O, MgO, Al_2O_3, CaF_2, and B_2O_3. The main bioactive glasses used clinically are the bioglass in the system Na_2O–CaO–SiO_2–P_2O_5, tricalcium phosphate $(Ca_3(PO_4)_2)$, crystalline oxyfluoroapatite $(Ca_{10}(PO_4)6O, F)$, and wollastonite $(CaSiO_3)$. These materials have useful thermal properties and are broadly used in the synthesis of drug-delivery systems [42].

Table 10.2 recaps the nanosized composites that are most used to produce NC-HYGs.

Table 10.2 Nanosized Composites Used to Produce Hydrogel Nanocomposite Systems

Name	Properties	Chemical Structure
Hectorite	Good swelling properties	$Na_{0.3}(Mg,Li)_3Si_4O_{10}(OH)_2$
Montmorillonite	Swelling property; strong cation-exchange capacity	$(Na,Ca)_{0,3}(Al,Mg)_2Si_4O_{10}(OH)_2\cdot n(H_2O)$
Mica	Chemically inert, dielectric, elastic, flexible, hydrophilic, insulating, lightweight, platey, reflective, refractive, resilient, and range in opacity from transparent to opaque	$X_2Y_{4-6}Z_8O_{20}(OH, F)_4$, where X is commonly potassium, sodium, or calcium; Y is alumina, magnesium, or iron; while Z is silica, alumina, iron, or titanium
Silsesquioxane	Rigidity and thermal stability	$(RSiO_{3/2})_n$, where R=H, alkyl, aryl, or alkoxyl
Polysiloxanes	Great resistance to UV radiation; flexible, chemically inert, permeable to gases, water resistant	$(R_2SiO)_n$, where R=methyl, alkyl, or aryl group
Attapulgite	Capacity to form gel structures in fresh and salt water	$(Mg,Al)_2Si_4O_{10}(OH)\cdot 4(H_2O)$
Bioglasses	Thermally active	Na_2O–CaO–SiO_2–P_2O_5
Graphene	Strong; conductor of heat and electricity; transparent	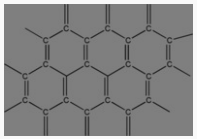

Regarding the network structure instead, water-soluble monomers containing amide groups, such as NIPAAm, *N,N*-dimethylacrylamide, and acrylamide, are the most effective, while other monomers (e.g., those containing carboxyl, sulfonyl, or hydroxyl groups) can be used as comonomers [43,44] or alone (forming less well performing NC-HYGs) [45].

Poly(*N*-isopropylacrylamide) (PNIPAAm) is a temperature-responsive polymer synthesized from NIPAAm via free radical polymerization, which forms a three-dimensional HYG when crosslinked with *N,N*-methylene-bis-acrylamide or *N,N*-cystamine-bis-acrylamide. When heated in water above 32°C, PNIPAAm undergoes a reversible lower critical solution temperature phase transition from a swollen hydrated state to a shrunken dehydrated state, losing about 90% of its volume. Because of these characteristics, PNIPAAm has been investigated for applications in tissue engineering [46,47] and controlled drug delivery [48,49]. In particular, PNIPAAm can be placed in a solution of bioactive molecules for drug penetration. Such loaded polymers can then be placed in vivo, where there is a rapid release of biomolecules, due to the initial gel collapse, followed by a slow release of biomolecules due to surface pore closure [50]. Examples of these drug-delivery systems include the intestinal delivery of human calcitonin [51], insulin [51], and ibuprofen [52].

Polyacrylamide is a polymer with the chemical structure –$CH_2CHCONH_2$– formed from acrylamide subunits. It can be synthesized as a simple linear-chain structure or in the crosslinked form, using *N*,*N*-methylene-bis-acrylamide. Polyacrylamide is highly water absorbent, forming a soft gel when hydrated. Such material is commonly used in manufacturing soft contact lenses, and as a thickener and suspending agent. More recently, it has been used as a subdermal filler for aesthetic facial surgery [53].

Polyamidoamine (PAMAM) is a class of dendrimer that is made of repetitively branched subunits of amide and amine functionality [54]. Like other dendrimers, PAMAMs have a spherelike shape with an internal molecular architecture consisting of treelike branching. PAMAM dendrimers exhibit great biocompatibility due to the combination of surface amines and interior amide bonds with properties similar to those of globular proteins [55]. The relative ease and low cost of synthesis of PAMAM dendrimers along with their biocompatibility, structural control, and functionalizability, have made PAMAMs viable candidates for applications in drug development, biochemistry, and nanotechnology [55–57].

Poly(glycerol-succinic acid) is a novel dendrimer composed of glycerol and succinic acid. It is composed entirely of building blocks known to be biocompatible with or degradable in vivo by natural metabolites and, because of this, is broadly used for drug-delivery systems [58].

Poly(ethylene glycol) (PEG) is a polyether compound with the chemical structure H–(O–CH_2–CH_2)$_n$–OH and with different molecular weights. These differences lead to different physical properties (e.g., viscosity, due to chain length effects), but with nearly identical chemical properties [59]. Different forms of PEG are also available, depending on the initiator used for the polymerization process [59]. In medicine, PEG is the basis of a number of laxatives and bowel preparations before surgery or colonoscopy. Moreover, it is used as an excipient in many pharmaceutical products and, when attached to various protein medications, it allows a slowed clearance of the carried protein from the blood [60].

Poly(amine-ester) is a polymer composed of ester covalently linked with amine. These are often synthesized has hyperbranched poly(amine–ester) (HPE) macromers with different degrees of terminal modification, to make injectable HYGs as multidrug-delivery systems. In fact, the aqueous solutions of these macromers are fast transformed into a HYG at body temperature with a low concentration (0.05 wt%) of ammonium persulfate [61]. Such polymers are readily functionalized, making them useful in a variety of applications.

Table 10.3 recaps the most-used monomers for network structures of NC-HYGs.

Table 10.3 Composites for the Network Structure of Hydrogel Nanocomposite Systems

Name	Properties	Chemical Structure
Poly(*N*-isopropylacrylamide)	Temperature responsive; reversible lower critical solution; temperature phase transition at 32°C	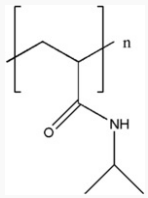
Polyacrylamide	Highly water absorbent	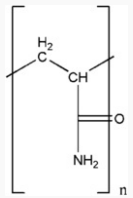
Polyamidoamine	Great biocompatibility; low cost of synthesis; structural control; functionalizability	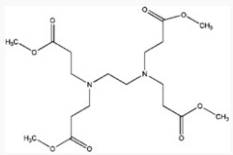
Poly(glycerol–succinic acid)	Highly biocompatible; highly biodegradable	

		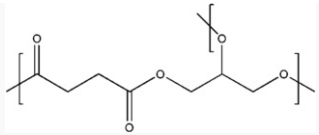
Poly(ethylene glycol)	Modulatable viscosity	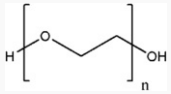
Poly(amine–ester)	Functionalizability	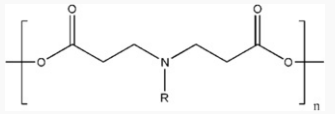

2.2 Synthetic Procedure

The synthetic procedure for NC gel formation consists of the in situ free radical polymerization of monomers in the presence of nanoparticles uniformly dispersed in the medium [62]. Nanoparticles are used as reinforcing agents and are also able to act as multifunctional crosslinkers [63–66] that can be used alone or together with an organic crosslinker to produce an NC-HYG [67]. Ideal nanoparticles must have a diameter of about 30 nm, while particles of larger sizes (e.g., >300 nm) are less effective probably because of insufficient exfoliation and moderate aggregation in aqueous solutions.

2.3 Structure

The network structure of an NC-HYG was proposed on the basis of analytical data from transmission electron microscopy (TEM), X-ray diffraction, thermogravimetric analysis, differential scanning calorimetry, and Fourier transform infrared spectroscopy measurements [62], and according to the observed mechanical, optical, and swelling properties of these materials [64,65]. The confirmed hypothesis affirms that nanoparticles disperse homogeneously in the polymer matrix [68] and act as multiple crosslinkers [69,70]. Moreover, the thermal fluctuations of the nanocomponents are largely suppressed upon network formation [71]. The crosslinker nature of nanoparticles was settled by rubber-elasticity theory and it was calculated that each nanoparticle has more than 100 crosslinking points [64,65]. The effective crosslink density was obtained by rheological measurements [72] and through the degree of equilibrium swelling (ES) with the Flory–Rehner theory [73]. In general, NC-HYGs have larger ES values compared with HYGs. The process of formation of the network structure was also studied by analyzing changes in viscosity, optical transparency, and X-ray diffraction [74], while the gelation mechanism was investigated by dynamic light scattering and small-angle neutron scattering (SANS) measurements. Interestingly, by contrast-variation SANS, it has been found that, often, there is a polymer layer surrounding the nanoparticles with a thickness of about 1 nm, irrespective of nanoparticle concentration [75]. Finally, TEM observations were useful to highlight the dispersion of the nanoparticles inside the polymer structure.

2.4 Shape

Since the synthetic procedure is quite simple and versatile, NC-HYGs can be prepared in many shapes by means of different molds [76]. In fact, huge blocks, sheets, thin films, rods, hollow tubes, spheres, bellows, and uneven sheets are broadly used to cast the medium composed of nanoparticles, monomers, and, eventually, organic crosslinkers. Also, microgels with dimensions of several hundred nanometers [77] and porous NC-HYGs have been prepared with the same technique [76]. The use of molds is particularly important in the engineering of drug-delivery devices capable of being implanted into the intended site of action for a local therapy.

Fig. 10.2 summarizes the synthetic procedure for NC-HYGs.

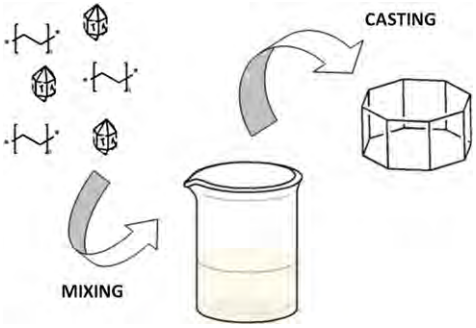

Figure 10.2 The mixing and casting procedure for hydrogel nanocomposite system creation.

3 Nanocomposite Hydrogel Properties

NC-HYGs withstand high levels of deformation, in the form of elongation and compression, bending, tearing, twisting, and knotting [64]. Moreover, they can be treated as rubbery materials and can tolerate all the conventional mechanical tests.

3.1 Tensile Properties

In general, an NC-HYG can be elongated to more than 1000% of its original length; also, the extensibility depends on the kind of nanoparticles and polymers used [64,78]. Moreover, NC-HYGs exhibit high time-dependent recovery from large strains [78], and this ability changes according to the nanoparticle/polymer system [79] and composition [78].

3.2 Compression

NC-HYGs generally withstand extensive forces of compression, in contrast to normal HYGs, which are readily broken into pieces under small strains. The compression resistance increases proportional to the nanoparticle concentration [78], due to the formation of the crosslinked network [67] composed of microcomplex structures consisting of nanoparticles with enhanced densities of chemical crosslinks.

3.3 Equilibrium Swelling

NC-HYGs generally exhibit a high degree of ES in water compared with normal HYGs [62,73]. This parameter depends on the kinds of nanoparticles and polymers used. In particular, in a fixed system, the ES decreases with increasing nanoparticles and polymer [65,73]. However, NC-HYGs have unusual behaviors, such as the appearance of a maximum in the swelling curve [80] and a clear increase in ES with the retention of high mechanical properties [81], which are explained by the rearrangement of the entangled polymer chains and nanoparticles during the course of swelling.

3.4 Stimulus Sensitivity

NC-HYGs are often engineered to be controlled by changes in the external temperature or pH or by electrostimulation. The thermosensitivity of an NC-HYG is a property that can be widely varied by altering the gel composition [82]. For example, thermosensitive NC-HYGs can be obtained by decreasing the concentration of nanoparticles to improve the thermal molecular motions of the polymeric chains attached to the nanoparticles' surface [73]. In contrast, the transition temperature of NC-HYGs does not depend on the concentration of the nanoparticles, but can be shifted toward lower or higher temperatures by adding, respectively, inorganic salts or cationic surfactants to the surrounding aqueous solution [64,73]. The sensitivity to pH depends on the monomer used for NC-HYG preparation. For example, a semiinterpenetrating network structure composed of linear poly(acrylic acid) is pH controlled owing to the variation in surface charge of the acrylic monomers at different proton concentrations [83]. Similarly, electrostimulation is effective only if the NC-HYG polymeric structure changes, applying different potentials, as in the case of linear carboxymethyl chitosan [84] and chitosan/clay gels [85].

3.5 Transparency

The transparency is a property that depends on the diffusion of the crosslinking regions inside the network structure. In fact, HYGs generally turn opaque with increasing crosslinker concentration owing to the inhomogeneous distribution of crosslink points, while NC-HYGs are generally transparent, regardless of the crosslink density [64,65]. These findings indicate that the network structure forms uniformly throughout the NC-HYG [68,75]. Moreover, a further loss of transmittance depends on the polymer used also if, NC-HYGs are not sensitive to the kind of polymer, except for a slight decrease at low [65] and very high nanoparticle concentration [78].

3.6 Optical Anisotropy

HYGs are normally amorphous (optically isotropic). NC-HYGs, instead, exhibit optical anisotropy when the nanoparticle concentration exceeds a critical value calculated for spontaneous nanoparticle aggregation [73]. Furthermore, the optical anisotropy of an NC-HYG changes uniquely on uniaxial deformation, regardless of the optical characteristics in the original HYG [86].

3.7 Sliding Frictional Behaviors

NC-HYGs respond in very different ways to kinetic friction, according to their wetting status. In fact, sliding frictional measurements have been conducted on the surface of NC-HYGs under different environmental conditions and loads [87]. In air, NC-HYGs exhibit a characteristic force profile with a maximum static force and a subsequent constant dynamic frictional force, both of which vary depending on the gel composition and on the load of the sliding plate. In contrast, under wet conditions, NC-HYGs have very low frictional forces and the dynamic frictional coefficient decreases with increasing load. This distinct change in frictional force with the surroundings is particularly observed in NC-HYGs with low nanoparticle concentration.

3.8 Water Contact Angles

HYGs, because of their hydrophilic nature, have very low contact angles for water. NC-HYGs, however, can have particular polymer–nanoparticle links that enhance hydrophobicity. In fact, Haraguchi et al. [88] have found that the surface of an NC-HYG consisting of a PNIPAAm/clay network exhibits extraordinarily high hydrophobicity and showed a maximum contact angle of 151. The high hydrophobicity of the NC-HYG is primarily attributed to the amphiphilicity of PNIPAAm and, more specifically, to the spontaneous alignment of *N*-isopropyl groups at the gel–air interface [88]. Moreover, the hydrophobicity of NC-HYGs is enhanced by the organization of the network structure, and the surface of an NC-HYG can exhibit reversible hydrophobic-to-hydrophilic changes depending on the surroundings (air or water) [88].

3.9 Porosity

Porous solid NC-HYGs have been obtained by freeze-drying NC-HYGs without the use of an added porogen [89]. Other methods to obtain porous NC-HYGs are the use of salts [90] or a mixture of calcium carbonate with sodium bicarbonate that creates porous structures due to the formation of carbon dioxide [91].

3.10 Cell Cultivation and Biocompatibility

Drug-delivery applications require biocompatible materials that do not prevent physiological cell growth. Thus, NC-HYGs were broadly studied for cell culturing and biocompatibility. For example, Haraguchi et al. [92] found that cells such as human dermal fibroblasts and human umbilical vein endothelial cells can be cultured to confluence on the surface of an NC-HYG consisting of a PNIPAAm/clay network, while the same cells hardly develop on normal HYGs. Moreover, the cultured cells can be detached as cell sheets without trypsin treatment, simply by decreasing the temperature to 20°C [93].

Table 10.4 compares the chemical–physical properties of NC-HYGs and normal hydrogels.

Table 10.4 Comparison of the Chemical–Physical Properties Between Hydrogel Nanocomposite Systems and Hydrogels

	Hydrogel Nanocomposite Systems	Hydrogels
Tensile properties	+	−
Compression	+	−
Equilibrium swelling	+	−
Thermosensitivity	−	+
pH sensitivity	=	=
Electrostimulation	=	=
Transparency	+	−
Optical anisotropy	+	−
Sliding frictional behavior	+	−

Water contact angle	+	−
Porosity	=	=
Biocompatibility	+	−

The comparison is between structures formed with the same monomers and crosslinkers at the same concentration. The only difference is the presence of nanoparticles.

4 Hydrogel Nanocomposite Applications in Drug Delivery

HYG nanocomposite systems are extensively used as drug-delivery systems thanks to the possibility of manipulating network design to develop systems with a desired release profile. In particular, the hydrophilicity and porosity of HYG networks can be controlled by the choice of monomer(s) and crosslinker [94], while the incorporation of nanomaterials in the HYG matrix allows additional control of the network properties. Various types of HYG nanocomposite systems have been developed in the past few years, and their swelling and drug release properties have been extensively studied. In many applications, in fact, drug-delivery systems are designed to release a drug at a constant rate for long periods of time. In other situations, instead, therapeutics such as peptides and hormones require pulsatile release to match their natural release profile in the body [95–98].

4.1 Nanocomposite Hydrogels From Carbon-Based Nanomaterials

Carbon-based nanomaterials are extensively used to incorporate multifunctionality (e.g., high mechanical, electrical conductivity, and optical properties) to the HYG [99]. Examples of materials used for carbon-based nanocomposite HYGs (carbon-NC-HYGs) for drug-delivery systems are graphene, buckminsterfullerene (C_{60}), and nanodiamonds [99,100]. Structurally, carbon-NC-HYGs are classified as multiwalled or single walled. Multiwalled carbon-NC-HYGs have two or more layers of polymeric network structures, while single-walled carbon-NC-HYGs are composed of a single network. In both these formations, the strong hydrophobic nature of carbon nanomaterials results in limited interaction with hydrophilic polymers of the nano-HYG. In particular, the strong π–π interactions between the carbon nanocomponents lead to the formation of aggregates. Several techniques were thus developed to enhance the dispersion of the carbon-based nanomaterials within the nanocomposite network. For example, various polar groups such as amines (–NH_2), hydroxyls (–OH), and carboxyls (–COOH) were linked to the surface of the nanocomponents to facilitate their dispersion [101]. Similarly, their solubility was improved by modifying their surface properties through the addition of single-stranded DNA, proteins, and surfactants. Another approach used to functionalize the surface of carbon-based nanomaterials was the grafting of polymer chains onto their surface [102]. This shielding approach was also aimed at enhancing the dispersion of carbon nanomaterials into the HYG and improving the physical interactions between these two components. An example of carbon-NC-HYGs that have been produced is carbon nanotubes with amyloid fibrils that were used to modify the surface of carbon nanostructures to generate fibrous HYGs with a significant decrease in the gelling concentration and enhanced polymer–nanotube interactions [103]. Similarly, Wang et al. [104] synthesized crosslinked HYGs with nano–graphite oxide (GO) sheets produced by chemical reaction. In fact, graphene sheets were treated with strong oxidizers to obtain GO to enhance the solubility of graphene under physiological conditions. GO interacts with hydrophilic polymers to form physically or covalently crosslinked networks [104]. These types of composites have high mechanical strength and excellent heat and electricity conductivity characteristics due to the presence of graphene. However, these examples show carbon nanoparticles used as physical fillers in the polymer networks and not covalently incorporated into the resulting materials. A new carbon-NC-HYG has carbon-based nanoparticles as the crosslinking agent chemically conjugated to the polymeric network. The covalent crosslinking between polymer and carbon nanoparticles enables the transfer of mechanical force within the crosslinked network, resulting in enhanced mechanical strength and toughness [105]. For example, Liu et al. [41] fabricated mechanically stiff and highly resilient nanocomposite HYGs by covalently conjugating GO sheets functionalized via radiation-induced peroxidation to polyacrylamide. These NC-HYGs had more than 900% and 500% increases in tensile strength and elongation compared with conventional polymeric HYGs [41]. All these devices are designed to retain hydrophilic drugs or small molecules in the HYG network and release them in a controlled manner. In particular, covalently crosslinked carbon-NC-HYGs have a prolonged drug release compared with carbon-NC-HYGs in which the carbon nanomaterials are simply dispersed into the network, owing to the improved organization of the structure. Table 10.5 recaps the types of nanocomposite HYGs from carbon-based materials.

Table 10.5 Nanocomposite Hydrogels From Carbon-Based Nanomaterials

Type	Characteristics	References
Fibrous hydrogel of carbon nanocomposites modified with amyloid fibrils	Decreased gelling concentration and enhanced polymer–nanotube interactions	[103]
Crosslinked hydrogels with nano–graphite oxide	High mechanical strength and excellent conduction of heat and electricity	[104]
Nanocomposite hydrogels with graphene oxide sheets conjugated to polyacrylamide	Broadly increased in tensile strength and elongation	[41]

4.2 Nanocomposite Hydrogels From Polymeric Nanoparticles

Nanocomposite HYGs made from polymeric nanoparticles such as dendrimers, hyperbranched polymers, liposomes, polymeric micelles, and core–shell polymeric particles have gained great attention in drug-delivery application due to their ability to entrap hydrophobic or hydrophilic drugs (e.g., drugs, proteins, and genes) [106]. Among these systems, particular attention was addressed to nanovectors with highly branched and spherical structure. This is because they display a multitude of functional groups on their periphery, resulting in higher reactivity and loading efficiency compared with the polymeric HYGs fabricated from linear polymers [107]. Many examples of nanocomposite HYGs from polymeric nanoparticles are available. Dendritic nanoparticles used to reinforce the HYG network via covalent or noncovalent interactions with the polymeric chains, in fact, were synthesized by Zhong and Yung [108]. These PAMAM nanoparticles were physically integrated within collagen scaffolds to improve the structural integrity and mechanical stiffness [108]. Moreover, the addition of PAMAM nanoparticles significantly improved human conjunctival fibroblast proliferation in collagen HYGs due to the increase in the stiffness of the nanocomposite network. The applications of these hybrid HYGs are envisioned in pharmaceutical and biomedical areas that require a porous structure with controlled drug release properties [109,110]. Similarly, a triblock copolymer made from poly(glycerol–succinic acid) dendrimers as terminal blocks and PEG as the linear core was evaluated for soft tissue engineering applications [111]. The stiffness of the HYG, the degradation properties, and the hydration kinetics of this device can be tailored by changing the dendrimer concentration. Such nanocomposite HYGs showed high stress-absorbing capacity and thus may be useful for cartilage tissue drug release. Interestingly, encapsulated chondrocytes retained a rounded morphology and showed a significant increase in the production of type II collagen and proteoglycans, due to the incorporation of the nanoparticles. Similarly, Zhang et al. [112] produced HYGs from HPE nanoparticles, to improve drug loading efficiency and set control over the release kinetics [112]. The periphery of the HPE nanoparticles was modified with photocrosslinkable moieties to form a covalently crosslinked network upon UV exposure. By controlling the crosslinking density, the authors could tune the physical properties of the resulting HYGs, including the microstructure and mechanical strength. These photocrosslinkable HYGs were able to encapsulate a hydrophobic drug within the inner cavities of the nanoparticles. A controlled drug release from the nanocomposite network was observed for more than a week, a result that is difficult to achieve when using conventional HYGs made from linear polymers [112]. Table 10.6 shows the types of nanocomposite HYGs from polymeric nanoparticles and their characteristics.

Table 10.6 Nanocomposite Hydrogels From Polymeric Nanoparticles

Type	Characteristics	References
Polyamidoamine nanoparticles physically integrated within collagen scaffolds	Improved structural integrity and mechanical stiffness; improved human conjunctival fibroblast proliferation	[108]
Triblock copolymer made from poly(glycerol–succinic acid) dendrimers and poly(ethylene glycol)	High stress-absorbing capacity; good polymeric support for encapsulated chondrocyte growth	[111]
Hydrogels from hyperbranched poly(amine–ester)	Improved drug-loading efficiency and control over the release kinetics; prolonged release kinetics	[112]

4.3 Nanocomposite Hydrogels From Inorganic Nanoparticles

A new generation of advanced biomaterials is obtained by combining inorganic nanoparticles with natural or synthetic polymers. These inorganic nanoparticles mainly consist of minerals that are already present in the body and are necessary for the normal functioning of human tissues [113]. For example, calcium is an important component of bone and plays a vital role in bone development and maintenance. Phosphate, together with intracellular calcium, promotes the deposition of a mineralized matrix of osteoblasts and prevents bone loss [113]. Silicon [113] and fluoride [114] play a key role in skeletal development due to the fact that they stimulate the osteogenic differentiation of human stem cells and also promote collagen type I synthesis. Other bioactive nanoparticles include hydroxyapatite (nHA), synthetic silicate nanoparticles, bioactive glasses, silica, calcium phosphate glass ceramic, and b-wollastonite [115]. Gaharwar et al. [116] synthesized HYGs with nHA incorporated into a PEG matrix to obtain highly elastomeric nanocomposite HYGs. Interestingly, the addition of nHA to the polymeric network imparted elastomeric properties, enhanced the mechanical strength, and improved the physiological stability of the nanocomposite networks [116]. Although the exact interactions between nHA and the polymeric network were not investigated, it was speculated that the nanoparticles, more than the physical, electrostatic, and ionic interactions, have an important role in the high toughness and elastomeric properties of the nanocomposite networks. Moreover, the addition of nHA resulted in enhanced cell adhesion compared with PEG HYGs [116]. Similar results were obtained when the same authors replaced nHA with silica nanospheres [117]. The new inorganic nanoparticles had enhanced mechanical properties and cell adhesion characteristics [117]. The higher mechanical strength of both these nanocomposite networks (PEG–nHA and PEG–silica) led to the utilization of these nanocomposite HYGs as injectable fillers for orthopedic applications with drug-delivery abilities [116,118]. Synthetic silicate nanoparticles, also known as nanoclays, improve the physical and mechanical properties of polymeric HYGs [119–122] owing to the high surface interactions between the polymers and the nanoparticles. Nanoclays are widely used to reinforce thermoplastic polymers to obtain hybrid structures with hierarchical structure, elastomeric properties, and self-healing characteristics [119,120]. Studies have shown that nanoclay induces osteogenic differentiation of human mesenchymal stem cells without the use of exogenous growth factors [123], triggering a series of events that follow the temporal pattern of osteogenic differentiation. In general, all these synthetic silicates can be processed to create devices such as controlled cell adhesion surfaces, antimicrobial films, injectable tissue repair matrices, bioactive fillers, or therapeutic agents for triggering specific cellular responses toward bone-related tissue engineering approaches and drug-delivery systems [116,122,124]. Gaharwar et al. [116,122] and Schexnailder et al. [125] created synthetic silicate nanoplatelets mixed

with linear and branched polymers that were mechanically strong and were used to create tissue-adhesive nanocomposite HYGs. These unique physical and chemical properties are attributed to the high noncovalent surface interactions of the silicate nanoparticles with the polymer chains that reversibly adsorb on the silicate surfaces [122]. Such systems showed shear thinning characteristics and could be used for minimally invasive therapies. Gaharwar et al. also synthesized HYGs with silicates physically crosslinked with polymers [118,126]. The addition of silicates improved the elongation of the polymeric HYGs by the formation of networks [118,126]. Other types of inorganic nanoparticles for nanocomposite HYG preparation are calcium phosphate, bioglasses, and b-wollastonite, which are incorporated into different synthetic and natural polymers to obtain bioactive nanocomposite HYGs with high mechanical strength [127]. The degradation products of these systems have favorable biological response, providing opportunities for their use in various biomedical applications. Table 10.7 recaps the synthesized nanocomposite HYGs containing inorganic nanoparticles.

Table 10.7 Nanocomposite Hydrogels From Inorganic Nanoparticles

Type	Characteristics	References
Hydrogels with hydroxyapatite incorporated into a poly(ethylene glycol) matrix	High elastomeric properties, enhanced mechanical strength, and improved physiological stability	[116]
Hydrogels with silica nanospheres incorporated into a poly(ethylene glycol) matrix	Enhanced mechanical properties and cell adhesion characteristics	[117]
Nanoclays into polymeric hydrogels	Elastomeric properties and self-healing characteristics; enhanced osteogenic differentiation of human mesenchymal stem cells	[119–122]
Synthetic silicate nanoplatelets mixed with linear and branched polymers	Mechanically strong and tissue adhesive; strong shear thinning characteristics	[116,122,125]
Silicates physically crosslinked with polymers	Good elongation	[118,126]
Calcium phosphate, bioglasses, and b-wollastonite incorporated into different synthetic and natural polymers	High mechanical strength; degradation products giving favorable biological response	[127]

4.4 Nanocomposite Hydrogels From Metal and Metal Oxide Nanoparticles

Many types of metallic nanoparticles are used to fabricate nanocomposite HYGs for biomedical applications, including gold (Au), silver (Ag), and other noble metals, while the most diffused metal oxide nanoparticles are iron oxide (Fe_3O_4, Fe_2O_3), titania (TiO_2), alumina, and zirconia [127]. Metal and metal oxide nanoparticles possess desired physical properties such as electrical conductivity (e.g., Au nanorods), magnetic properties (e.g., iron oxides), and antimicrobial properties (e.g., Ag nanoparticles). Thus, nanocomposite HYGs containing metal or metal oxide nanoparticles are extensively used as imaging agents, drug-delivery systems, conductive scaffolds, switchable electronics, actuators, and sensors and are also explored for biosensing, diagnostic, and bioactuation applications [127]. The interactions between the polymer and the metal/metal oxide nanoparticles are often weak. However, by functionalizing the nanoparticle surfaces, the interactions between the polymer and the nanoparticles can be enhanced [128,129]. Such enhanced interactions significantly influence the physical, chemical, and biological properties of the nanocomposite HYGs. For example, Au nanoparticles entrapped within a polymeric network consisting of hyaluronic acid and gelatin do not improve the mechanical properties [130], whereas when Au is thiol-functionalized, the Au nanoparticles crosslink with the polymeric network, increasing the stiffness of the HYG [130]. Moreover, the superior electrical and thermal conductivity of metallic nanoparticles, when embedded or entrapped within a polymeric network, leads to an enhanced thermoelectrical conductivity of the nanocomposite HYG [130]. Dvir et al. [131] incorporated Au nanowires within macroporous alginate HYGs to enhance the electrical conductivity of the polymeric network. Such conductive scaffolds were used to engineer tissues that required the propagation of electrical signals to facilitate the formation of functional tissues, such as neonatal rat cardiomyocytes seeded with the conductive HYG network that contract synchronously if electrically stimulated [131]. Moreover, the addition of Au nanowire to the alginate HYG showed a higher expression of cardiac markers (such as troponin I and connexin 43) in the seeded cardiac cells compared with the normal alginate HYGs [131]. Gaharwar et al. [132] covalently conjugated magnetic nanoparticles with biocompatible and thermoresponsive hydroxypropyl cellulose to obtain stimulus-responsive HYGs. When these hybrid HYGs are subjected to external magnetic fields, the magnetic nanoparticles entrapped within the HYG network generate heat. The increase in the temperature of surrounding matrix above the lower critical solution temperature of the polymer results in a coil-to-globule transition of the polymer chains. Such triggers can be used to release therapeutic agents or cells from the nanocomposite HYGs [132]. Price et al. [133] synthesized nanocomposite HYGs with nanophase alumina and titania incorporated within a polymeric matrix such as poly(L-lactic-co-glycolic acid), resulting in enhanced osteoblast adhesion and proliferation [133,134]. However, these nanoparticles have limited interactions with polymeric chains, resulting in no increase in the physical properties of the HYG network [133,134]. Pasqui et al. [135] functionalized the surface of titania with amine groups to facilitate covalent interactions between the nanoparticles and carboxymethyl cellulose. These hybrid nanocomposite HYGs were used to encapsulate cells for tissue engineering applications and for prolonged drug delivery. Table 10.8 shows the main types of nanocomposite HYGs from metal and metal oxide nanoparticles.

Table 10.8 Nanocomposite Hydrogels From Metal and Metal Oxide Nanoparticles

Type	Characteristics	References
Thiol-functionalized gold nanoparticles in a network of hyaluronic acid and gelatin	Increased stiffness and thermoelectrical conductivity	[130]
Gold nanowires within macroporous alginate hydrogels	Enhanced electrical conductivity	[131]
Covalently conjugated magnetic nanoparticles with biocompatible and thermoresponsive hydroxypropyl cellulose	Magnetic field–responsive hydrogels	[132]
Nanophase alumina and titania incorporated within poly(L-lactic-co-glycolic acid)	Enhanced osteoblast adhesion and proliferation	[133]
Titania nanoparticles functionalized with amine groups crosslinked with carboxymethyl cellulose	Good encapsulation abilities; prolonged release	[135]

4.5 Next Generation of Nanocomposite Hydrogels

The next generation of nanocomposite HYGs will be produced to better control some essential features such as stimulus responsiveness and biodegradation. The strategies that have been developed to design nanocomposite HYGs with multiple functionalities combine multiple phases within a nanocomposite HYG network and mimic the structure and properties of native tissues. Wang et al. [136] synthesized aliphatic ester dendrimers conjugated with a PEG spacer that can physically interact with inorganic nanoplatelets to form physically crosslinked HYGs. These crosslinked networks have self-healing characteristics, high mechanical strength, and adhesive properties. In another study, Skelton et al. [137] produced biomimetic adhesive nanocomposite HYGs by combining poly(acrylamide) (PAAm), silicate nanoplatelets, and dopamine methacrylamide (DMA). It was observed that the addition of DMA was necessary to enhance the stiffness and energy dissipation capability, to mimic the properties of elastomeric tissues. The chemically crosslinked network and the presence of DMA enhanced the interfacial interactions of silicate and PAAm [137]. Shin et al. [138] fabricated multicomponent nanocomposite HYGs from ferritin and poly(vinyl alcohol), using electrospinning and the ability of poly(vinyl alcohol) to swell in aqueous media. The addition of ferritin significantly enhanced the mechanical stiffness and reduced creep during the cyclic deformation of the nanocomposite HYGs [138]. These types of hybrid HYG networks can potentially be used to fabricate scaffolds for tissue engineering applications, in stimulus-responsive matrices for drug release, or as actuators [138]. Similarly, PNIPAAm nanoparticle-composed HYGs were used to design therapeutic devices for tissue engineering and drug-delivery applications [127,139]. PNIPAAm exhibits a negative swelling transition at 34°C. Such polymeric systems can be further decorated with appropriate nanoparticles to develop stimulus-responsive matrices. In particular, the type of nanoparticles embedded within the HYG networks determines the responsiveness to stimuli (e.g., mechanically adaptive, pH/enzyme/ion responsive, electrically stimulating, thermoresponsive, magnetic field responsive) [127,139]. Owens et al. [140] developed Au nanoparticles entrapped within a stimulus-responsive matrix to design therapeutic HYGs. Such a hybrid system was produced by encapsulating the PEG-functionalized Au nanoparticles within thermally responsive PAAm/poly(acrylic acid) (PAA). Au nanoparticles have the ability to absorb visible to near-infrared (530–1200 nm) wavelengths and thus can be used to generate heat locally. The local heating by the nanoparticles causes the swelling/deswelling of the polymeric network and results in the release of entrapped macromolecules. Thus, the covalently crosslinked PAAm/PAA interpenetrating polymer network can be used to deliver therapeutics using an external trigger for a range of biomedical and drug-delivery applications [140]. Nanocomposite HYGs are also emerging as a powerful technology to engineer tissues with spatiotemporal control of cells, molecular cues, and biophysical signals [141,142]. For example, photocrosslinked gelatin methacrylate–carbon nanotubes [143] and hyperbranched polyester [112] nanocomposite HYGs were developed to entrap cells in predefined geometries and cellular microenvironments to position the different types of cells within the HYG network to facilitate the formation of functional tissues. Langer and coworkers [144,145] embedded magnetic steel beads in an ethylene–vinyl polymer matrix in which the release of macromolecules was regulated by the application of a low-frequency oscillating magnetic field. The device containing insulin was implanted subcutaneously in diabetic rats and was demonstrated to effectively control glucose levels following an oscillating magnetic field [146]. Table 10.9 summarizes the most recent nanocomposite HYGs as of this writing.

Table 10.9 Next Generation of Nanocomposite Hydrogels

Type	Characteristics	References
Physically crosslinked hydrogels with inorganic nanoplatelets conjugating aliphatic ester dendrimers with PEG spacer	Self-healing, high mechanical strength and adhesive properties	[136]
Biomimetic nanocomposite hydrogels of polyacrylamide, silicate nanoplatelets, and dopamine methacrylamide	Enhanced stiffness and energy dissipation capability	[137]
Electrospun multicomponent nanocomposite hydrogels with ferritin and poly(vinyl alcohol)	Enhanced mechanical stiffness and reduced creep during the cyclic deformation of the nanocomposite hydrogels	[138]
PEG-functionalized gold nanoparticles within thermally responsive poly(acrylamide)/poly(acrylic acid)	UV-light sensitivity	[140]
Magnetic steel beads in an ethylene–vinyl polymer matrix	Regulation of the release by application of a low-frequency oscillating magnetic field	[144,145]

PEG, poly(ethylene glycol).

5 Conclusions and Future Perspectives

Nanocomposite HYGs are advanced biomaterials that can be potentially used for various biomedical and pharmaceutical applications. The utilization of these HYG networks includes sensors, actuators, scaffolds for stem cell engineering, regenerative medicine, and drug-delivery systems in the form of electrically conductive scaffolds, mechanically stiff and highly elastomeric networks, cell and tissue adhesive matrices, injectable matrices, and controlled drug-delivery depots. Compared with conventional polymeric HYGs, nanocomposite HYGs have superior physical, chemical, electrical, and biological properties. The improved performance of the nanocomposite HYG network is mainly attributed to the enhanced interactions between the polymer chains and the nanoparticles. In the future, however, the design of the next generation of nanocomposite HYGs will require not only close control over the physical, chemical, and electrical properties, but also the need to integrate suitable biological clues within the network. The synthesis and fabrication of such HYGs will focus on designing multicomponent networks able to incorporate multiple functionalities. In addition, future studies of nanocomposite HYGs will also be targeted at understanding the interactions between polymeric chains and nanoparticles at different length scales. Moreover, new fabrication technologies will also be devised to recapitulate the cellular microenvironment of native tissues within the nanocomposite HYGs.

References

[1] R. Haag and F. Kratz, Polymer therapeutics: concepts and applications, *Angew Chem Int Ed* **45** (8), 2006, 1198–1215.

[2] B. Semete, L. Booysen, Y. Lemmer, L. Kalombo, L. Katata, J. Verschoor and H.S. Swai, In vivo evaluation of the biodistribution and safety of PLGA nanoparticles as drug delivery systems, *Nanomed Nanotechnol Biol Med* **6** (5), 2010, 662–671.

[3] H.C. Korting and M. Schäfer-Korting, Carriers in the topical treatment of skin disease, In: M. Schäfer-Korting, (Ed), *Drug delivery,* 2010, Springer Berlin Heidelberg, Berlin, Heidelberg, 435–468.

[4] S. Wang, M. Tan, Z. Zhong, M. Chen and Y. Wang, Nanotechnologies for curcumin: an ancient puzzler meets modern solutions, *J Nanomater* **2011**, 2011, 8.

[5] J.R. Lattin, D.M. Belnap and W.G. Pitt, Formation of eLiposomes as a drug delivery vehicle, *Colloids Surf B Biointerfaces* **89**, 2012, 93–100.

[6] L.E. van Vlerken, Z. Duan, S.R. Little, M.V. Seiden and M.M. Amiji, Biodistribution and pharmacokinetic analysis of paclitaxel and ceramide administered in multifunctional polymer-blend nanoparticles in drug resistant breast cancer model, *Mol Pharm* **5** (4), 2008, 516–526.

[7] R. Conte, I.D. Luca, A.D. Luise, O. Petillo, A. Calarco and G. Peluso, New therapeutic potentials of nanosized phytomedicine, *J Nanosci Nanotechnol* **16** (8), 2016, 8176–8187.

[8] W. Geldenhuys, T. Mbimba, T. Bui, K. Harrison and V. Sutariya, Brain-targeted delivery of paclitaxel using glutathione-coated nanoparticles for brain cancers, *J Drug Target* **19** (9), 2011, 837–845.

[9] O. Taratula, O.B. Garbuzenko, P. Kirkpatrick, I. Pandya, R. Savla, V.P. Pozharov, H. He and T. Minko, Surface-engineered targeted PPI dendrimer for efficient intracellular and intratumoral siRNA delivery, *J Control Release* **140** (3), 2009, 284–293.

[10] V. Mody, R. Siwale, A. Singh and H. Mody, Introduction to metallic nanoparticles, *J Pharm Bioallied Sci* **2** (4), 2010, 282–289.

[11] D. Brambilla, B. Le Droumaguet, J. Nicolas, S.H. Hashemi, L.-P. Wu, S.M. Moghimi, P. Couvreur and K. Andrieux, Nanotechnologies for Alzheimer's disease: diagnosis, therapy, and safety issues, *Nanomed Nanotechnol Biol Med* **7** (5), 2011, 521–540.

[12] O.Z. Fisher, A. Khademhosseini, R. Langer and N.A. Peppas, Bioinspired materials for controlling stem cell fate, *Acc Chem Res* **43** (3), 2010, 419–428.

[13] B.V. Slaughter, S.S. Khurshid, O.Z. Fisher, A. Khademhosseini and N.A. Peppas, Hydrogels in regenerative medicine, *Adv Mater (Deerfield Beach Fla)* **21** (32–33), 2009, 3307–3329.

[14] A. Khademhosseini, J.P. Vacanti and R. Langer, Progress in tissue engineering, *Sci Am* **300** (5), 2009, 64–71.

[15] N.A. Peppas, J.Z. Hilt, A. Khademhosseini and R. Langer, Hydrogels in biology and medicine: from molecular principles to bionanotechnology, *Adv Mater* **18** (11), 2006, 1345–1360.

[16] A.M. Kloxin, C.J. Kloxin, C.N. Bowman and K.S. Anseth, Mechanical properties of cellularly responsive hydrogels and their experimental determination, *Adv Mater* **22** (31), 2010, 3484–3494.

[17] D.E. Discher, D.J. Mooney and P.W. Zandstra, Growth factors, matrices, and forces combine and control stem cells, *Science (New York NY)* **324** (5935), 2009, 1673–1677.

[18] M.W. Tibbitt and K.S. Anseth, Hydrogels as extracellular matrix mimics for 3D cell culture, *Biotechnol Bioeng* **103** (4), 2009, 655–663.

[19] N. Annabi, A. Tamayol, J.A. Uquillas, M. Akbari, L.E. Bertassoni, C. Cha, G. Camci-Unal, M.R. Dokmeci, N.A. Peppas and A. Khademhosseini, 25th anniversary article: rational design and applications of hydrogels in regenerative medicine, *Adv Mater (Deerfield Beach Fla)* **26** (1), 2014, 85–123.

[20] K. Haraguchi and H.-J. Li, Mechanical properties of nanocomposite hydrogels consisting of organic/inorganic networks and the effects of clay modification thereto, *J Netw Polym Jpn* **25** (1), 2004, 2–12.

[21] F. Bignotti, F. Lebon and I. Peroni, Effect of filler networking on the response of thermosensitive composite hydrogels, *Eur Polym J* **43** (5), 2007, 1996–2006.

[22] J. Mu and S. Zheng, Poly(*N*-isopropylacrylamide) nanocrosslinked by polyhedral oligomeric silsesquioxane: temperature-responsive behavior of hydrogels, *J Colloid Interface Sci* **307** (2), 2007, 377–385.

[23] K.-M. Kim and Y. Chujo, Organic-inorganic hybrid gels having functionalized silsesquioxanes, *J Mater Chem* **13** (6), 2003, 1384–1391.

[24] Y. Kaneko, K. Noguchi and J-i. Kadokawa, Synthesis of temperature-responsive organic-inorganic hybrid hydrogel by free-radical polymerization of methacrylamide using water-soluble rigid polysiloxane having acryamido side-chains as a cross-linking agent, **39**, 2007, 1078–1081.

[25] Y. Xiang, Z. Peng and D. Chen, A new polymer/clay nano-composite hydrogel with improved response rate and tensile mechanical properties, *Eur Polym J* **42** (9), 2006, 2125–2132.

[26] W.-F. Lee and Y.-C. Chen, Effect of intercalated hydrotalcite on swelling and mechanical behavior for poly(acrylic acid-co-*N*-isopropylacrylamide)/hydrotalcite nanocomposite hydrogels, *J Appl Polym Sci* **98** (4), 2005, 1572–1580.

[27] A. Benhammou, B. Tanouti, L. Nibou, A. Yaacoubi and J.-P. Bonnet, Mineralogical and physicochemical investigation of Mg-smectite from Jbel Ghassoul, Morocco, *Clay Clay Miner* **57** (2), 2009, 264–270.

[28] K.G. Bhattacharyya and S.S. Gupta, Adsorption of a few heavy metals on natural and modified kaolinite and montmorillonite: a review, *Adv Colloid Interface Sci* **140** (2), 2008, 114–131.

[29] J. Saary, R. Qureshi, V. Palda, J. DeKoven, M. Pratt, S. Skotnicki-Grant and L. Holness, A systematic review of contact dermatitis treatment and prevention, *J Am Acad Dermatol* **53** (5), 2005, 845.

[30] H.G. Hansma, Possible origin of life between mica sheets: does life imitate mica?, *J Biomol Struct Dynam* **31** (8), 2013, 888–895.

[31] D.B. Cordes, P.D. Lickiss and F. Rataboul, Recent developments in the chemistry of cubic polyhedral oligosilsesquioxanes, *Chem Rev* **110** (4), 2010, 2081–2173.

[32] G. Sauvet, W. Fortuniak, K. Kazmierski and J. Chojnowski, Amphiphilic block and statistical siloxane copolymers with antimicrobial activity, *J Polym Sci Part A Polym Chem* **41** (19), 2003, 2939–2948.

[33] P. Majumdar, J. He, E. Lee, A. Kallam, N. Gubbins, S.J. Stafslien, J. Daniels and B.J. Chisholm, Antimicrobial activity of polysiloxane coatings containing quaternary ammonium-functionalized polyhedral oligomeric silsesquioxane, *J Coat Technol Res* **7** (4), 2010, 455–467.

[34] K.E. Polmanteer and M.J. Hunter, Polymer composition versus low-temperature characteristics of polysiloxane elastomers, *J Appl Polym Sci* **1** (1), 1959, 3–10.

[35] G.D. Friends, J.B. Melpolder, J.F. Kunzler and J.S. Park, Polysiloxane composition with improved surface wetting characteristics and biomedical devices made thereof, Google Patents. 1987.

[36] S. Hénin and S. Caillère, Fibrous minerals, In: J.E. Gieseking, (Ed), *Soil components: vol. 2: inorganic components,* 1975, Springer Berlin Heidelberg, Berlin, Heidelberg, 335–349.

[37] J. Wolford, Attapulgite as a thixotropic suspending agent, 2007.

[38] A.J. Aguiar and J.E. Zelmer, Antacid preparations and means of producing the same, Google Patents. 1967.

[39] R.K. Allada, A. Navrotsky, H.T. Berbeco and W.H. Casey, Thermochemistry and aqueous solubilities of hydrotalcite-like solids, *Science (New York NY)* **296** (5568), 2002, 721–723.

[40] R. Conte, A.D. Lusie, O. Petillo, C. Rengo, F. Riccitiello, A. Di Salle, A. Calarco and G. Peluso, Biodegradable polymers for dental tissue engineering and regeneration, In: G. Rohman, (Ed), *Biodegradable polymers: recent developments and new perspectives,* 2017, IAPC, Zagreb.

[41] J. Liu, C. Chen, C. He, J. Zhao, X. Yang and H. Wang, Synthesis of graphene peroxide and its application in fabricating super extensible and highly resilient nanocomposite hydrogels, *ACS Nano* **6** (9), 2012, 8194–8202.

[42] S.M. Salman, S.N. Salama and H.A. Abo-Mosallam, The crystallization behaviour and bioactivity of wollastonite glass-ceramic based on Na_2O–K_2O–CaO–SiO_2–F glass system, *J Asian Ceram Soc* **3** (3), 2015, 255–261

[43] S. Kundakci, Ö.B. Üzüm and E. Karadağ, Swelling and dye sorption studies of acrylamide/2-acrylamido-2-methyl-1-propanesulfonic acid/bentonite highly swollen composite hydrogels, *React Funct Polym* **68** (2), 2008, 458–473.

[44] K. Xu, J. Wang, S. Xiang, Q. Chen, W. Zhang and P. Wang, Study on the synthesis and performance of hydrogels with ionic monomers and montmorillonite, *Appl Clay Sci* **38** (1), 2007, 139–145.

[45] S.H. Nair, K.C. Pawar, J.P. Jog and M.V. Badiger, Swelling and mechanical behavior of modified poly(vinyl alcohol)/laponite nanocomposite membranes, *J Appl Polym Sci* **103** (5), 2007, 2896–2903.

[46] H. Von Recum, A. Kikuchi, M. Okuhara, Y. Sakurai, T. Okano and K. Sung Wan, Retinal pigmented epithelium cultures on thermally responsive polymer porous substrates, *J Biomater Sci Polym Ed* **9** (11), 1998, 1241–1253.

[47] E.L. Lee and H.A. von Recum, Cell culture platform with mechanical conditioning and nondamaging cellular detachment, *J Biomed Mater Res Part A* **93** (2), 2010, 411–418.

[48] J.E. Chung, M. Yokoyama, M. Yamato, T. Aoyagi, Y. Sakurai and T. Okano, Thermo-responsive drug delivery from polymeric micelles constructed using block copolymers of poly(*N*-isopropylacrylamide) and poly(butylmethacrylate), *J Control Release* **62** (1–2), 1999, 115–127.

[49] H. Yan and K. Tsujii, Potential application of poly(*N*-isopropylacrylamide) gel containing polymeric micelles to drug delivery systems, *Colloids Surf B Biointerfaces* **46** (3), 2005, 142–146.

[50] A.S. Huffman, A. Afrassiabi and L.C. Dong, Thermally reversible hydrogels: II. Delivery and selective removal of substances from aqueous solutions, *J Control Release* **4** (3), 1986, 213–222.

[51] D. Schmaljohann, Thermo- and pH-responsive polymers in drug delivery, *Adv Drug Deliv Rev* **58** (15), 2006, 1655–1670.

[52] Z. Zhou, S. Zhu and D. Zhang, Grafting of thermo-responsive polymer inside mesoporous silica with large pore size using ATRP and investigation of its use in drug release, *J Mater Chem* **17** (23), 2007, 2428–2433.

[53] Y. Yagi, K. Kato, D. Murakami, K. Misaki and M. Ota, Utilization of aquamid as a filler for rhinoplasty in orientals, *Plast Reconstr Surg* **123** (1), 2009, 26e–28e.

[54] E. Abbasi, S.F. Aval, A. Akbarzadeh, M. Milani, H.T. Nasrabadi, S.W. Joo, Y. Hanifehpour, K. Nejati-Koshki and R. Pashaei-Asl, Dendrimers: synthesis, applications, and properties, *Nanoscale Res Lett* **9** (1), 2014, 247.

[55] R. Esfand and D.A. Tomalia, Poly(amidoamine) (PAMAM) dendrimers: from biomimicry to drug delivery and biomedical applications, *Drug Discov Today* **6** (8), 2001, 427–436.

[56] C.C. Lee, J.A. MacKay, J.M.J. Frechet and F.C. Szoka, Designing dendrimers for biological applications, *Nat Biotechnol* **23** (12), 2005, 1517–1526.

[57] D.A. Tomalia, L.A. Reyna and S. Svenson, Dendrimers as multi-purpose nanodevices for oncology drug delivery and diagnostic imaging, *Biochem Soc Trans* **35** (Pt 1), 2007, 61–67.

[58] M.A. Carnahan and M.W. Grinstaff, Synthesis and characterization of poly(glycerol−succinic acid) dendrimers, *Macromolecules* **34** (22), 2001, 7648–7655.

[59] J. Kahovec, Nomenclature of regular single- strand organic polymers (IUPAC Recommendations 2002), In: *Chemistry International – Newsmagazine for IUPAC* **vol. 25**, 2003, 20.

[60] A. Mero, O. Schiavon, G. Pasut, F.M. Veronese, E. Emilitri and P. Ferruti, A biodegradable polymeric carrier based on PEG for drug delivery, *J Bioact Compat Polym* **24** (3), 2009, 220–234.

[61] H. Zhang, C. Zhao, H. Cao, G. Wang, L. Song, G. Niu, H. Yang, J. Ma and S. Zhu, Hyperbranched poly(amine-ester) based hydrogels for controlled multi-drug release in combination chemotherapy, *Biomaterials* **31** (20), 2010, 5445–5454.

[62] K. Haraguchi and T. Takehisa, Nanocomposite hydrogels: a unique organic–inorganic network structure with extraordinary mechanical, optical, and swelling/de-swelling properties, *Adv Mater* **14** (16), 2002, 1120–1124.

[63] A. Okada and A. Usuki, Twenty years of polymer-clay nanocomposites, *Macromol Mater Eng* **291** (12), 2006, 1449–1476.

[64] K. Haraguchi, T. Takehisa and S. Fan, Effects of clay content on the properties of nanocomposite hydrogels composed of poly(*N*-isopropylacrylamide) and clay, *Macromolecules* **35** (27), 2002, 10162–10171.

[65] K. Haraguchi, R. Farnworth, A. Ohbayashi and T. Takehisa, Compositional effects on mechanical properties of nanocomposite hydrogels composed of poly(*N*,*N*-dimethylacrylamide) and clay, *Macromolecules* **36** (15), 2003, 5732–5741.

[66] K. Haraguchi, Nanocomposite hydrogels, *Curr Opin Solid State Mater Sci* **11** (3), 2007, 47–54.

[67] K. Haraguchi and L. Song, Microstructures formed in co-cross-linked networks and their relationships to the optical and mechanical properties of PNIPA/clay nanocomposite gels, *Macromolecules* **40** (15), 2007, 5526–5536.

[68] M. Shibayama, J. Suda, T. Karino, S. Okabe, T. Takehisa and K. Haraguchi, Structure and dynamics of poly(*N*-isopropylacrylamide)−clay nanocomposite gels, *Macromolecules* **37** (25), 2004, 9606–9612.

[69] M. Shibayama, T. Karino, S. Miyazaki, S. Okabe, T. Takehisa and K. Haraguchi, Small-angle neutron scattering study on uniaxially stretched poly(*N*-isopropylacrylamide)−clay nanocomposite gels, *Macromolecules* **38** (26), 2005, 10772–10781.

[70] J. Nie, B. Du and W. Oppermann, Swelling, elasticity, and spatial inhomogeneity of poly(*N*-isopropylacrylamide)/clay nanocomposite hydrogels, *Macromolecules* **38** (13), 2005, 5729–5736.

[71] J. Nie, B. Du and W. Oppermann, Dynamic fluctuations and spatial inhomogeneities in poly(*N*-isopropylacrylamide)/clay nanocomposite hydrogels studied by dynamic light scattering, *J Phys Chem B* **110** (23), 2006 11167–11175.

[72] O. Okay and W. Oppermann, Polyacrylamide−clay nanocomposite hydrogels: rheological and light scattering characterization, *Macromolecules* **40** (9), 2007, 3378–3387.

[73] K. Haraguchi, H.-J. Li, L. Song and K. Murata, Tunable optical and swelling/deswelling properties associated with control of the coil-to-globule transition of poly(*N*-isopropylacrylamide) in polymer−clay nanocomposite gels, *Macromolecules* **40** (19), 2007, 6973–6980.

[74] K. Haraguchi, H.-J. Li, K. Matsuda, T. Takehisa and E. Elliott, Mechanism of forming organic/inorganic network structures during in-situ free-radical polymerization in PNIPA−Clay nanocomposite hydrogels, *Macromolecules* **38** (8), 2005, 3482–3490.

[75] S. Miyazaki, H. Endo, T. Karino, K. Haraguchi and M. Shibayama, Gelation mechanism of poly(*N*-isopropylacrylamide)−clay nanocomposite gels, *Macromolecules* **40** (12), 2007, 4287–4295.

[76] K. Haraguchi, Nanocomposite gels: new advanced functional soft materials, *Macromol Symp* **256** (1), 2007, 120–130.

[77] Q. Zhang, L. Zha, J. Ma and B. Liang, A novel route to the preparation of poly(*N*-isopropylacrylamide) microgels by using inorganic clay as a cross-linker, *Macromol Rapid Commun* **28** (1), 2007, 116–120.

[78] K. Haraguchi and H.-J. Li, Mechanical properties and structure of polymer−clay nanocomposite gels with high clay content, *Macromolecules* **39** (5), 2006, 1898–1905.

[79] M. Zhu, Y. Liu, B. Sun, W. Zhang, X. Liu, H. Yu, Y. Zhang, D. Kuckling and H.-J.P. Adler, A novel highly resilient nanocomposite hydrogel with low hysteresis and ultrahigh elongation, *Macromol Rapid Commun* **27** (13), 2006, 1023–1028.

[80] V. Can, S. Abdurrahmanoglu and O. Okay, Unusual swelling behavior of polymer–clay nanocomposite hydrogels, *Polymer* **48** (17), 2007, 5016–5023.

[81] W. Zhang, Y. Liu, M. Zhu, Y. Zhang, X. Liu, H. Yu, Y. Jiang, Y. Chen, D. Kuckling and H.-J.P. Adler, Surprising conversion of nanocomposite hydrogels with high mechanical strength by posttreatment: from a low swelling ratio to an ultrahigh swelling ratio, *J Polym Sci Part A Polym Chem* **44** (22), 2006, 6640–6645.

[82] K. Haraguchi and H.-J. Li, Control of the coil-to-globule transition and ultrahigh mechanical properties of PNIPA in nanocomposite hydrogels, *Angew Chem Int Ed* **44** (40), 2005, 6500–6504.

[83] L. Song, M. Zhu, Y. Chen and K. Haraguchi, Temperature- and pH-sensitive nanocomposite gels with semi-interpenetrating organic/inorganic networks, *Macromol Chem Phys* **209** (15), 2008, 1564–1575.

[84] J. Ma, Y. Xu, Q. Zhang, L. Zha and B. Liang, Preparation and characterization of pH- and temperature-responsive semi-IPN hydrogels of carboxymethyl chitosan with poly (*N*-isopropyl acrylamide) crosslinked by clay, *Colloid Polym Sci* **285** (4), 2007, 479–484.

[85] K.H. Liu, T.Y. Liu, S.Y. Chen and D.M. Liu, Effect of clay content on electrostimulus deformation and volume recovery behavior of a clay-chitosan hybrid composite, *Acta Biomater* **3** (6), 2007, 919–926.

[86] K. Murata and K. Haraguchi, Optical anisotropy in polymer-clay nanocomposite hydrogel and its change on uniaxial deformation, *J Mater Chem* **17** (32), 2007, 3385–3388.

[87] K. Haraguchi and T. Takada, Characteristic sliding frictional behavior on the surface of nanocomposite hydrogels consisting of organic-inorganic network structure, *Macromol Chem Phys* **206** (15), 2005, 1530–1540.

[88] K. Haraguchi, H.-J. Li and N. Okumura, Hydrogels with hydrophobic surfaces: abnormally high contact angles for water on PNIPA nanocomposite hydrogels, *Macromolecules* **40** (7), 2007, 2299–2302.

[89] K. Haraguchi and K. Matsuda, Spontaneous formation of characteristic layered morphologies in porous nanocomposites prepared from nanocomposite hydrogels, *Chem Mater* **17** (5), 2005, 931–934.

[90] J. Kim, M.J. Yaszemski and L. Lu, Three-dimensional porous biodegradable polymeric scaffolds fabricated with biodegradable hydrogel porogens, *Tissue Eng Part C Methods* **15** (4), 2009, 583–594.

[91] M. Bhamidipati, A.M. Scurto and M.S. Detamore, The future of carbon dioxide for polymer processing in tissue engineering, *Tissue Eng Part B Rev* **19** (3), 2013, 221–232.

[92] K. Haraguchi, T. Takehisa and M. Ebato, Control of cell cultivation and cell sheet detachment on the surface of polymer/clay nanocomposite hydrogels, *Biomacromolecules* **7** (11), 2006, 3267–3275.

[93] K. Haraguchi and T. Takehisa, Novel manufacturing process of nanocomposite hydrogel for bio-applications, 2005, 119–126, (42231).

[94] C.C. Lin and A.T. Metters, Hydrogels in controlled release formulations: network design and mathematical modeling, *Adv Drug Deliv Rev* **58** (12–13), 2006, 1379–1408.

[95] A. Kikuchi and T. Okano, Pulsatile drug release control using hydrogels, *Adv Drug Deliv Rev* **54** (1), 2002, 53–77.

[96] J. Kost and R. Langer, Responsive polymeric delivery systems, *Adv Drug Deliv Rev* **46** (1–3), 2001, 125–148.

[97] S. Sershen and J. West, Implantable, polymeric systems for modulated drug delivery, *Adv Drug Deliv Rev* **54** (9), 2002, 1225–1235.

[98] T. Bussemer, I. Otto and R. Bodmeier, Pulsatile drug-delivery systems, *Crit Rev Ther Drug Carrier Syst* **18** (5), 2001, 433–458.

[99] C. Cha, S.R. Shin, N. Annabi, M.R. Dokmeci and A. Khademhosseini, Carbon-based nanomaterials: multi-functional materials for biomedical engineering, *ACS Nano* **7** (4), 2013, 2891–2897.

[100] S. Goenka, V. Sant and S. Sant, Graphene-based nanomaterials for drug delivery and tissue engineering, *J Control Release* **173**, 2014, 75–88.

[101] P.-C. Ma, N.A. Siddiqui, G. Marom and J.-K. Kim, Dispersion and functionalization of carbon nanotubes for polymer-based nanocomposites: a review, *Compos Part A Appl Sci Manuf* **41** (10), 2010, 1345–1367.

[102] T. Liu and S. Guo, Properties of polyurethane/carbon nanotube nanocomposites, In: *Polymer nanotube nanocomposites,* 2010, John Wiley & Sons, Inc., 141–176.

[103] C. Li and R. Mezzenga, Functionalization of multiwalled carbon nanotubes and their pH-responsive hydrogels with amyloid fibrils, *Langmuir* **28** (27), 2012, 10142–10146.

[104] E. Wang, M.S. Desai and S.-W. Lee, Light-controlled graphene-elastin composite hydrogel actuators, *Nano Lett* **13** (6), 2013, 2826–2830.

[105] S.J.V. Frankland, A. Caglar, D.W. Brenner and M. Griebel, Molecular simulation of the influence of chemical cross-links on the shear strength of carbon nanotube−polymer interfaces, *J Phys Chem B* **106** (12), 2002, 3046–3048.

[106] N. Joshi and M. Grinstaff, Applications of dendrimers in tissue engineering, *Curr Top Med Chem* **8** (14), 2008, 1225–1236.

[107] E.R. Gillies and J.M. Frechet, Dendrimers and dendritic polymers in drug delivery, *Drug Discov Today* **10** (1), 2005, 35–43.

[108] S. Zhong and L.Y. Yung, Enhanced biological stability of collagen with incorporation of PAMAM dendrimer, *J Biomed Mater Res Part A* **91** (1), 2009, 114–122.

[109] E. Oral and N.A. Peppas, Responsive and recognitive hydrogels using star polymers, *J Biomed Mater Res Part A* **68A** (3), 2004, 439–447.

[110] N.A. Peppas, Y. Huang, M. Torres-Lugo, J.H. Ward and J. Zhang, Physicochemical foundations and structural design of hydrogels in medicine and biology, *Annu Rev Biomed Eng* **2**, 2000, 9–29.

[111] S.H.M. Söntjens, D.L. Nettles, M.A. Carnahan, L.A. Setton and M.W. Grinstaff, Biodendrimer-based hydrogel scaffolds for cartilage tissue repair, *Biomacromolecules* **7** (1), 2006, 310–316.

[112] H. Zhang, A. Patel, A.K. Gaharwar, S.M. Mihaila, G. Iviglia, S. Mukundan, H. Bae, H. Yang and A. Khademhosseini, Hyperbranched polyester hydrogels with controlled drug release and cell adhesion properties, *Biomacromolecules* **14** (5), 2013, 1299–1310.

[113] A. Hoppe, N.S. Guldal and A.R. Boccaccini, A review of the biological response to ionic dissolution products from bioactive glasses and glass-ceramics, *Biomaterials* **32** (11), 2011, 2757–2774.

[114] A. Calarco, A. Di Salle, L. Tammaro, I. De Luca, S. Mucerino, O. Petillo, F. Riccitiello, V. Vittoria and G. Peluso, Long-term fluoride release from dental resins affects STRO-1+ cell behavior, *J Dent Res* **94** (8), 2015, 1099–1105.

[115] L.L. Hench and J.M. Polak, Third-generation biomedical materials, *Science (New York NY)* **295** (5557), 2002, 1014–1017.

[116] A.K. Gaharwar, S.A. Dammu, J.M. Canter, C.J. Wu and G. Schmidt, Highly extensible, tough, and elastomeric nanocomposite hydrogels from poly(ethylene glycol) and hydroxyapatite nanoparticles, *Biomacromolecules* **12** (5), 2011, 1641–1650.

[117] A.K. Gaharwar, C. Rivera, C.J. Wu, B.K. Chan and G. Schmidt, Photocrosslinked nanocomposite hydrogels from PEG and silica nanospheres: structural, mechanical and cell adhesion characteristics, *Mater Sci Eng C Mater Biol Appl* **33** (3), 2013, 1800–1807.

[118] A.K. Gaharwar, C.P. Rivera, C.J. Wu and G. Schmidt, Transparent, elastomeric and tough hydrogels from poly(ethylene glycol) and silicate nanoparticles, *Acta Biomater* **7** (12), 2011, 4139–4148.

[119] P. Bordes, E. Pollet and L. Avérous, Nano-biocomposites: biodegradable polyester/nanoclay systems, *Prog Polym Sci* **34** (2), 2009, 125–155.

[120] C.-J. Wu, A.K. Gaharwar, P.J. Schexnailder and G. Schmidt, Development of biomedical polymer-silicate nanocomposites: a materials science perspective, *Materials* **3** (5), 2010, 2986–3005.

[121] A.K. Gaharwar, P. Schexnailder, V. Kaul, O. Akkus, D. Zakharov, S. Seifert and G. Schmidt, Highly extensible bio-nanocomposite films with direction-dependent properties, *Adv Funct Mater* **20** (3), 2010, 429–436.

[122] A.K. Gaharwar, V. Kishore, C. Rivera, W. Bullock, C.J. Wu, O. Akkus and G. Schmidt, Physically crosslinked nanocomposites from silicate-crosslinked PEO: mechanical properties and osteogenic differentiation of human mesenchymal stem cells, *Macromol Biosci* **12** (6), 2012, 779–793.

[123] A.K. Gaharwar, S.M. Mihaila, A. Swami, A. Patel, S. Sant, R.L. Reis, A.P. Marques, M.E. Gomes and A. Khademhosseini, Bioactive silicate nanoplatelets for osteogenic differentiation of human mesenchymal stem cells, *Adv Mater (Deerfield Beach Fla)* **25** (24), 2013, 3329–3336.

[124] J.I. Dawson and R.O. Oreffo, Clay: new opportunities for tissue regeneration and biomaterial design, *Adv Mater (Deerfield Beach Fla)* **25** (30), 2013, 4069–4086.

[125] P.J. Schexnailder, A.K. Gaharwar, R.L. Bartlett Ii, B.L. Seal and G. Schmidt, Tuning cell adhesion by incorporation of charged silicate nanoparticles as cross-linkers to polyethylene oxide, *Macromol Biosci* **10** (12), 2010, 1416–1423.

[126] A.K. Gaharwar, P.J. Schexnailder, A. Dundigalla, J.D. White, C.R. Matos-Pérez, J.L. Cloud, S. Seifert, J.J. Wilker and G. Schmidt, Highly extensible bio-nanocomposite fibers, *Macromol Rapid Commun* **32** (1), 2011, 50–57.

[127] P. Schexnailder and G. Schmidt, Nanocomposite polymer hydrogels, *Colloid Polym Sci* **287** (1), 2009, 1–11.

[128] A.C. Balazs, T. Emrick and T.P. Russell, Nanoparticle polymer composites: where two small worlds meet, *Science (New York NY)* **314** (5802), 2006, 1107–1110.

[129] F. Caruso, Nanoengineering of particle surfaces, *Adv Mater* **13** (1), 2001, 11–22.

[130] A. Skardal, J. Zhang, L. McCoard, S. Oottamasathien and G.D. Prestwich, Dynamically crosslinked gold nanoparticle - hyaluronan hydrogels, *Adv Mater (Deerfield Beach Fla)* **22** (42), 2010, 4736–4740.

[131] T. Dvir, B.P. Timko, M.D. Brigham, S.R. Naik, S.S. Karajanagi, O. Levy, H. Jin, K.K. Parker, R. Langer and D.S. Kohane, Nanowired three-dimensional cardiac patches, *Nat Nanotechnol* **6** (11), 2011, 720–725.

[132] A.K. Gaharwar, J.E. Wong, D. Müller-Schulte, D. Bahadur and W. Richtering, Magnetic nanoparticles encapsulated within a thermoresponsive polymer, *J Nanosci Nanotechnol* **9** (9), 2009, 5355–5361.

[133] R.L. Price, L.G. Gutwein, L. Kaledin, F. Tepper and T.J. Webster, Osteoblast function on nanophase alumina materials: influence of chemistry, phase, and topography, *J Biomed Mater Res Part A* **67** (4), 2003,

1284–1293.

[134] T.J. Webster, R.W. Siegel and R. Bizios, Nanoceramic surface roughness enhances osteoblast and osteoclast functions for improved orthopaedic/dental implant efficacy, *Scr Mater* **44** (8), 2001, 1639–1642.

[135] D. Pasqui, A. Atrei, G. Giani, M. De Cagna and R. Barbucci, Metal oxide nanoparticles as cross-linkers in polymeric hybrid hydrogels, *Mater Lett* **65** (2), 2011, 392–395.

[136] Q. Wang, J.L. Mynar, M. Yoshida, E. Lee, M. Lee, K. Okuro, K. Kinbara and T. Aida, High-water-content mouldable hydrogels by mixing clay and a dendritic molecular binder, *Nature* **463** (7279), 2010, 339–343.

[137] S. Skelton, M. Bostwick, K. O'Connor, S. Konst, S. Casey and B.P. Lee, Biomimetic adhesive containing nanocomposite hydrogel with enhanced materials properties, *Soft Matter* **9** (14), 2013, 3825–3833.

[138] M.K. Shin, G.M. Spinks, S.R. Shin, S.I. Kim and S.J. Kim, Nanocomposite hydrogel with high toughness for bioactuators, *Adv Mater* **21** (17), 2009, 1712–1715.

[139] M.A. Stuart, W.T. Huck, J. Genzer, M. Muller, C. Ober, M. Stamm, G.B. Sukhorukov, I. Szleifer, V.V. Tsukruk, M. Urban, F. Winnik, S. Zauscher, I. Luzinov and S. Minko, Emerging applications of stimuli-responsiv polymer materials, *Nat Mater* **9** (2), 2010, 101–113.

[140] D.E. Owens, J.K. Eby, Y. Jian and N.A. Peppas, Temperature-responsive polymer–gold nanocomposites as intelligent therapeutic systems, *J Biomed Mater Res Part A* **83A** (3), 2007, 692–695.

[141] A. Khademhosseini and R. Langer, Microengineered hydrogels for tissue engineering, *Biomaterials* **28** (34), 2007, 5087–5092.

[142] A. Khademhosseini, R. Langer, J. Borenstein and J.P. Vacanti, Microscale technologies for tissue engineering and biology, *Proc Natl Acad Sci USA* **103** (8), 2006, 2480–2487.

[143] S.R. Shin, S.M. Jung, M. Zalabany, K. Kim, P. Zorlutuna, S.B. Kim, M. Nikkhah, M. Khabiry, M. Azize, J. Kong, K.-T. Wan, T. Palacios, M.R. Dokmeci, H. Bae, X. Tang and A. Khademhosseini, Carbon-nanotube-embedded hydrogel sheets for engineering cardiac constructs and bioactuators, *ACS Nano* **7** (3), 2013, 2369–2380.

[144] E.R. Edelman, J. Kost, H. Bobeck and R. Langer, Regulation of drug release from polymer matrices by oscillating magnetic fields, *J Biomed Mater Res* **19** (1), 1985, 67–83.

[145] D.S. Hsieh, R. Langer and J. Folkman, Magnetic modulation of release of macromolecules from polymers, *Proc Natl Acad Sci USA* **78** (3), 1981, 1863–1867.

[146] J. Kost, J. Wolfrum and R. Langer, Magnetically enhanced insulin release in diabetic rats, *J Biomed Mater Res* **21** (12), 1987, 1367–1373.

Abstract

The field of controlled drug delivery continues to be one of the key areas of research in pharmaceutics and medicine. In these studies, hydrogel nanocomposite systems (NC-HYGs) have been extensivel investigated because of their unique and tailorable properties. In fact, NC-HYGs mimic the native tissue microenvironment through their porous and hydrated molecular structure. Moreover, new reinforced polymeri hydrogels incorporating nanoparticles within the hydrogel network are being produced with the aim to improve the mechanical properties of the hydrogel and provide superior functionality, such as controlled release This chapter covers the most recent developments in the field of nanocomposite hydrogels with emphasis on biomedical and pharmaceutical applications. In particular, we will discuss definitions, synthesis characterization, and applications of hydrogel nanocomposites as drug-delivery systems. Moreover, future directions in designing more advanced nanocomposite hydrogels for biomedical and biotechnologica applications will be provided.

Keywords: Biomedical applications; Drug delivery; Nanocomposite hydrogels; Nanoparticles; Tissue engineering

Queries and Answers

Query: Please check the edits made to the chapter title.
Answer: ok

Query: Please check whether the first name and the last name of the authors are identified correctly.
Answer: ok

Query: The term “NIPAAm” is being used as the abbreviation for “*N*-isopropylacrylamide” to be consistent with other chapters.
Answer: ok

Query: Please note that colour shades present in all the tables. Those tables have been treated as normal table. Kindly check whether the all those tables should be appeared in color or not.
Answer: The grey scale is fine

Query: Please check the spelling of the word “Esigence” in section title “The Esigence of Hydrogel Nanocomposite Systems”.
Answer: Please write "Exigence"

Query: Please note that “Data updated to 2013” in the sentence “The growing interest…” has been removed as it is already present in Fig. 10.1 caption.
Answer: ok

Query: Kindly consider modifying the sentence “Moreover, a further loss…” for better clarity and readability.
Answer: Please change with " In particular NC-HYGs show a loss of transmittance only at low [65] and very high nanoparticle concentration [78]. "

Query: Please check the inserted year of publication for Refs. [2,11].
Answer: Both the references are fine

Query: Please confirm that given names and surnames have been identified correctly and are presented in the desired order and please carefully verify the spelling of all authors’ names.
Answer: Yes

Query: Figure 10.2 has the required resolution, but still it looks blurred. Please provide a better quality figure.
Answer: see attached

Perspective

EML4-ALK translocation identification in RNA exosomal cargo (*ExoALK*) in NSCLC patients: a novel role for liquid biopsy

Pablo Reclusa[1,2#], Jean-François Laes[3#], Umberto Malapelle[4], Anna Valentino[5], Danilo Rocco[6], Ignacio Gil-Bazo[7,8], Christian Rolfo[1,9]

[1]Phase I-Early Clinical Trials Unit, Oncology Department, Antwerp University Hospital (UZA) & Center for Oncological Research of Antwerp (CORE) Antwerp University, Antwerp, Belgium; [2]Department of Surgical, Oncological and Stomatological Disciplines, University of Palermo, Palermo, Italy; [3]OncoDNA SA, 6041 Gosselies, Belgium; [4]Department of Public Health, University of Naples Federico II, Naples, Italy; [5]Gene Expression and Molecular Genetics Laboratory, Institute of Biosciences and BioResources, National Council of Research, CNR, Naples, Italy; [6]Oncology Unit, A.O.R.N. Vincenzo Monaldi – Ospedale dei Colli, Naples, Italy; [7]Department of Oncology, Clínica Universidad de Navarra & Navarra Health Research Institute (IDISNA), Pamplona, Spain; [8]Centro de Investigación Biomédica en Red de Cáncer (CIBERONC), Madrid, Spain; [9]University of Maryland Marlene and Stewart Greenebaum Comprehensive Cancer Center, Baltimore, MD, USA

[#]These authors contributed equally to this work.

Correspondence to: Prof. Christian Rolfo, MD, PhD, MBA. University of Maryland Marlene and Stewart Greenebaum Comprehensive Cancer Center, Baltimore, MD, USA. Email: christian.rolfo@umm.edu.

Abstract: The introduction of druggable targets has significantly improved the outcomes of non-small cell lung cancer patients (NSCLC). *EML4-ALK* translocation represents 4–6% of the druggable alterations in NSCLC. With the approval of Crizotinib, first discovered drug for the *EML4-ALK* translocation, on first line treatment for patients with detected mutation meant a complete change on the treatment landscape. The current standard method for *EML4-ALK* identification is immunohistochemistry or FISH in a tumor biopsy. However, a big number of NSCLC patients have not tissue available for analysis and others are not suitable for biopsy due to their physical condition or the location of the tumor. Liquid biopsy seems the best alternative for identification in these patients that have no tissue available. Circulating free RNA has not been validated for the identification of this mutation. As a complementary tool, exosomes might represent a good tool for predictive biomarkers study, and due to their stability, they preserve the genetic material contained in them. Our group has described for the first time the translocation *EML4-ALK* in RNA isolated from exosomes derived from NSCLC patients using next generation sequencing.

Keywords: Exosomes; liquid biopsy; ALK translocation; non-small cell lung cancer (NSCLC); biomarkers

Submitted Oct 07, 2018. Accepted for publication Oct 17, 2018.
doi: 10.21037/tcr.2018.11.35
View this article at: http://dx.doi.org/10.21037/tcr.2018.11.35

Introduction

Lung cancer treatment landscape has completely changed in the last decade. The introduction of druggable targets in the therapeutic scenario gave the opportunity to significantly improve the outcomes in the most lethal malignant disease. *EML4-ALK* translocation represents a story of success in drug development. The discovery of the aberration in tumors of patients with lung cancer in 2007 (1) soon translated into a rapid approval of the first ALK tyrosine kinase inhibitor (TKI), crizotinib (2), and the subsequent early arrival of second and third generation TKIs, all happening in roughly a decade. The current standard for the identification of the target necessarily implies identification of rearrangement in the tumor tissue either by FISH or immunohistochemistry. Unfortunately, despite the efforts, a big number of non-small cell lung cancer (NSCLC) patients have no tissue available for determination. The isolation of ctDNA is a novel approach, but still not validated for *EML4-ALK* translocation (3,4). Exosomes, new members of the liquid biopsy family, carrying genetic material represent an important tool for biomarkers discovery (5). Our group has identified, for the first time, *EML4-ALK* translocation in exosomes (*ExoALK*), using a next generation sequencing technique.

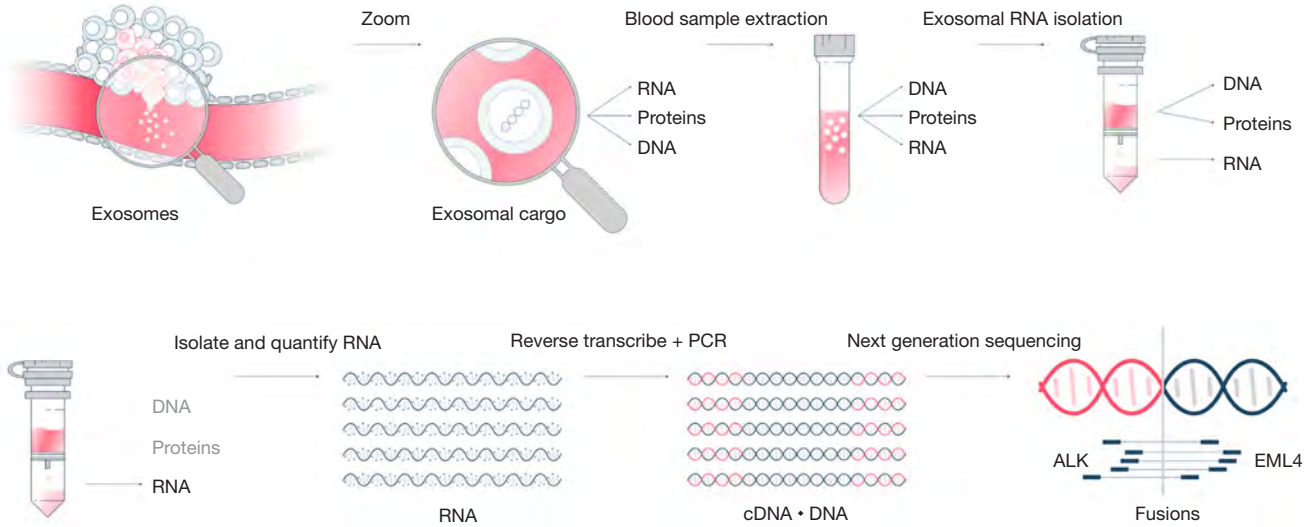

Figure 1 Schematic representation of *ExoALK* proof of concept study.

Material and methods

Patients selection

Patients with confirmed diagnosis of stage IIIB–IV NSCLC, naïve or under treatment with known *ALK* status were eligible for this proof of concept study. *EML4-ALK* translocation in tumor tissue was performed by FISH according to the clinical records of the patients. Patients gave their informed consent before the sample collection according to the institution regulation. Blood samples were collected only at a single point. Clinical data were collected from the electronic medical records. Samples and data from patients included in the study were provided by the Biobank of the University of Navarra (Reg#: B_0000612) and were processed following standard operating procedures approved by the Ethical and Scientific Committees. The trial was approved by the Antwerp University Hospital ethical committee n. 14/17/206.

Exosomal RNA isolation

The exosomal RNA cargo was extracted from 1 mL of plasma using ExoRNeasy Kit from QIAGEN with a modification of the original protocol to avoid loss of material and volume. This includes 3 centrifugations of 5' × 500 g, 15' × 3,000 g and 30' × 10,000 g instead of the filtration in 0.8 µM (*Figure 1*).

Next generation sequencing

The fusions were analyzed using the Ion Ampliseq RNA Fusion Lung Cancer panel (Thermo Fisher Scientific, Waltham, USA). The primers used for amplification were then partially digested by the Pfu enzyme. The product of digestion was ligated with corresponding barcoded adapters and purified using Ampure Beads (Agilent Genomics Inc). The product of purification was amplified for 5 more cycles and subsequently purified using Ampure Beads. Ten pM of each library was loaded into the IonChef system (Thermo Fisher Scientific, Waltham, USA) for the emulsion polymerase chain reaction (PCR) and then loaded in the chip.

The quality of the data was assessed using the Torrent suite software (Thermo Fisher Scientific, Waltham, USA) associated with the sequencing machine. The minimum read length for fusion detection was set to 50 bp (base pair). We consider that under this value the reads were too short to overlap targeted fusion breakpoint. In addition, to assess the detection quality, at least 20,000 reads were required per sample (*Figure 1*).

Results

A total of 19 patients with plasma samples were included in the study, 16 of them harboring *EML4-ALK* translocations in tissue. In 1 mL of plasma, the RNA concentration ranged

Table 1 Concordance between tissue and *ExoALK*

Exosomal RNA (*ExoALK*) (n=17)	Tissue (patients n=19)	
	Positive	Negative
Positive	9	0
Negative	5	3
Degraded RNA	2	–

Sensitivity =64%; Specificity =100%.

from 0.5 to 121 mg/mL. In total, 17 patients were finally eligible for extracellular vesicles analysis. In nine patients, we were able to identify the translocation in the exosomal RNA. The concordance between tissue and exosomes was 64% (9 out of 14 patients). All three patients being negative for the fusion gene in tissue resulted also negative in the *ExoALK* analysis, representing a specificity of 100% (*Table 1*). No correlation was found between the RNA yield and the type of sample or its clinical variables.

Discussion

Here we demonstrate for the first time that *EML4-ALK* translocation detection in exosomes of NSCLC patients is feasible, with a high sensitivity and specificity. The exosomal analysis represents an opportunity for patients therapeutic selection with a minimal invasive procedure, easy to perform and with an affordable cost. The development of new techniques with a direct detection of the fusion by capture instead of by amplification would be the key to improve the sensitivity of *ExoALK* in the future.

Acknowledgements

The authors acknowledge OncoDNA for the free research collaboration, Dr. Maxime Lienard from OncoDNA for the contribution in exosomal cargo analysis and Prof. Patrick Pauwels from Molecular Pathology Unit at Antwerp University Hospital for the data analysis. Human samples and data from patients included in the study were provided by Biobank@UZA (Antwerp, Belgium; ID: BE71030031000), the AORN Vincenzo Monaldi, Department of Oncology, Naples, Italy and were processed following standard operating procedures approved by the Ethical and Scientific Committees. We particularly acknowledge the patients for their participation and the Biobank of the University of Navarra (Reg#: B_0000612) for its collaboration. P Reclusa received a scholarship grant from University of Palermo.

Footnote

Conflicts of Interest: The authors have no conflicts of interest to declare.

References

1. Soda M, Choi YL, Enomoto M, et al. Identification of the transforming EML4-ALK fusion gene in non-small-cell lung cancer. Nature 2007;448:561-6.
2. Solomon BJ, Mok T, Kim DW, et al. First-line crizotinib versus chemotherapy in ALK-positive lung cancer. N Engl J Med 2014;371:2167-77.
3. Nilsson RJ, Karachaliou N, Berenguer J, et al. Rearranged EML4-ALK fusion transcripts sequester in circulating blood platelets and enable blood-based crizotinib response monitoring in non-small-cell lung cancer. Oncotarget 2016;7:1066-75.
4. Dagogo-Jack I, Brannon AR, Ferris LA, et al. Tracking the Evolution of Resistance to ALK Tyrosine Kinase Inhibitors Through Longitudinal Analysis of Circulating Tumor DNA. JCO Precis Oncol 2018;2018. doi: 10.1200/PO.17.00160.
5. Rolfo C, Castiglia M, Hong D, et al. Liquid biopsies in lung cancer: The new ambrosia of researchers. Biochim Biophys Acta 2014;1846:539-46.

Cite this article as: Reclusa P, Laes JF, Malapelle U, Valentino A, Rocco D, Gil-Bazo I, Rolfo C. *EML4-ALK* translocation identification in RNA exosomal cargo (*ExoALK*) in NSCLC patients: a novel role for liquid biopsy. Transl Cancer Res 2019;8(Suppl 1):S76-S78. doi: 10.21037/tcr.2018.11.35

Melone et al. *Cell Death and Disease* (2018)9:228
DOI 10.1038/s41419-018-0313-7

Cell Death & Disease

REVIEW ARTICLE Open Access

The carnitine system and cancer metabolic plasticity

Mariarosa Anna Beatrice Melone[1,2], Anna Valentino[1,3], Sabrina Margarucci[4], Umberto Galderisi[5], Antonio Giordano[2,6] and Gianfranco Peluso[3]

Abstract

Metabolic flexibility describes the ability of cells to respond or adapt its metabolism to support and enable rapid proliferation, continuous growth, and survival in hostile conditions. This dynamic character of the cellular metabolic network appears enhanced in cancer cells, in order to increase the adaptive phenotype and to maintain both viability and uncontrolled proliferation. Cancer cells can reprogram their metabolism to satisfy the energy as well as the biosynthetic intermediate request and to preserve their integrity from the harsh and hypoxic environment. Although several studies now recognize these reprogrammed activities as hallmarks of cancer, it remains unclear which are the pathways involved in regulating metabolic plasticity. Recent findings have suggested that carnitine system (CS) could be considered as a gridlock to finely trigger the metabolic flexibility of cancer cells. Indeed, the components of this system are involved in the bi-directional transport of acyl moieties from cytosol to mitochondria and vice versa, thus playing a fundamental role in tuning the switch between the glucose and fatty acid metabolism. Therefore, the CS regulation, at both enzymatic and epigenetic levels, plays a pivotal role in tumors, suggesting new druggable pathways for prevention and treatment of human cancer.

Facts

- Malignant cells are capable of creating an equilibrium between producing and consuming energy and metabolic intermediates synthesis to sustain growth and survival.
- Metabolic plasticity makes cancer cells more aggressive and able to metastasize. Oncogenic pathways, nutrient availability, and microenvironment influence cell metabolism.
- The carnitine system is a pivotal mediator in cancer metabolic plasticity, intertwining key pathways, factors, and metabolites that supply an energetic and biosynthetic demand for cancer cells.
- MiRnas and metabolic enzymes regulate metabolic plasticity through the carnitine system suggesting their use for developing new therapeutic strategies.

Open questions

- What is the role of the carnitine system in cancer metabolism rewiring?
- Is the carnitine system dysregulated in cancerogenesis?
- What is the purpose of epigenetics in the modulation of the expression of proteins belonging to the carnitine system?
- Is it possible to explore new anticancer treatment targeting component(s) of the carnitine system?

Correspondence: Antonio Giordano (antonio.giordano@unisi.it) or Gianfranco Peluso (gianfranco.peluso@ibaf.cnr.it)
[1]Department of Medical, Surgical, Neurological, Metabolic Sciences, and Aging, 2nd Division of Neurology, Center for Rare Diseases and InterUniversity Center for Research in Neurosciences, University of Campania "Luigi Vanvitelli", Naples, Italy
[2]Department of Biology, Sbarro Institute for Cancer Research and Molecular Medicine, Center for Biotechnology, College of Science and Technology, Temple University, Philadelphia, PA, USA
Full list of author information is available at the end of the article
These authors contributed equally: Melone Mariarosa Anna Beatrice and Valentino Anna.
Edited by A. Finazzi-Agrò

SPRINGER NATURE
CDDpress

Cancer cells must maintain metabolic homeostasis in a wide range of conditions, including harsh microenvironments in which cancer cells must continue to meet the high bio-energetic demand in order to undergo replication[1]. These cells achieve metabolic homeostasis by regulating the dynamics of nutrients present in the microenvironment, and the ability of cancer cells to utilize them to produce energy and to synthesize macromolecules. It is feasible that the capability of cancer cells to employ alternative nutrients in different environments is critical in supporting and affecting their survival. However, tumor cell metabolic plasticity is not just as the result of the metabolic dynamic impact changes induced by the microenvironment and fuel choices of cancer cells. Instead, it is more appropriate to envision metabolic plasticity regarding uptake of alternative metabolic substrates and promotion of metabolic rewiring as a built-in feature that has evolved to allow cancer cells to constantly adapt to changing intracellular- and extracellular metabolic conditions[2].

Intracellular metabolite concentrations have to fine-tune the signaling networks governing metabolic pathways independently of the environment to ensure a balance between the availability of nutrients and the cellular capacity to use them effectively. Metabolites, through post-translational modifications of metabolite-sensitive protein (i.e. acetylation, methylation or glycosylation), transduce the information on the cell metabolic status, and modulate the activities of signaling proteins, enzymes, and transcriptional regulators[3]. Therefore, it is necessary to understand how a variety of intrinsic and extrinsic factors are integrated to create the metabolic flexibility and to reduce the metabolic dependencies dictated by oncogenic signaling. In this review, we identify the carnitine system (CS) as a gridlock to finely trigger the cancer cells' metabolic plasticity. In this context, the CS regulation at both the enzyme and the gene level plays a pivotal role in the metabolic flux modulation of tumors, and scientists can target them for therapeutic purposes.

Nutrients and energy acquisition strategies in cancer cells metabolism

Cancer cells prioritize aerobic glycolysis (Warburg effect), as the primary fuel and convert excess pyruvate to lactate independently from oxygen availability[4]. In addition, glucose is considered to be the primary carbon source that contributes to the production of mitochondrial citrate in cancer cells. The citrate in excess of mitochondrial requirements is exported in the cytosol, converted into acetyl-CoA by ATP-citrate lyase (ACLY), and used for protein acetylation and lipogenesis. While the principles regulating glucose-dependence in cancer cells have been extensively reviewed, we still do not fully understand how cancer cells use many of the metabolic strategies to contribute to core metabolic functions in the presence of nutrients different from glucose. Indeed, in addition to glycolysis, cancer cells can carry out various metabolic strategies such as fatty acid oxidation (FAO)[2,5]. Recent studies have reported that lipids from neighboring adipose tissues, lipoproteins, lysophospholipids, and intracellular storage fat have the potential to maintain viability and growth of cancer cells[6–9]. Fatty acids can satisfactorily fuel cancer cells, since mitochondrial FAO produces much more ATP per mole than oxidation of other nutrients, such as glucose or amino acids. For example, prostate cancer and B-cell lymphomas promote FAO as the main source of energy production and express FAO enzymes at high levels, even under nutrient-replete conditions[10,11]. Again, autophagy and related processes enable tumor growth by sustaining oxidative phosphorylation[12]. Interestingly, the strong dependence of mitochondrial β-oxidation on autophagic and fatty acid (FA) catabolic processes makes some tumors more resistant to nutrient deprivation and environmental stressors[13].

A peculiarity of several tumors is to present simultaneously two metabolic pathways in opposite directions, such as fatty acid biosynthesis and FAO ("futile cycle"). This paradoxical condition fulfils two fundamental tasks: (a) it provides the biosynthesis of FA important for cancer propagation, while ensuring an important source of ATP and Nicotinamide adenine dinucleotide (NADH) by the catabolism of any FA excess; and (b) it might induce a dynamic switching behavior that is useful in triggering signaling pathway(s) able to overcome metabolic stress maintaining cellular energy homeostasis (i.e. AMP-activated protein kinase; AMPK)[14,15].

However, unlike glycolytic and lipogenic pathways, where specific metabolic enzymes such as hexokinase 2 and FAS are known to be deregulated by oncogene(s) or by inactivation of tumor suppressors[16,17], there is limited evidence for cancer-associated abnormal expression or activity of the enzymes directly involved in the FAO pathway. Regarding expression and activity, the knowledge about the regulation of carriers and enzymes that modulate β-oxidation in cancer cells is of extreme interest since their inhibition may significantly affect the tumorigenic potential even in the presence of compensatory metabolic pathways.

The carnitine system and its implication in cancer cells metabolic plasticity

The use of diet-derived or adipose tissue-released long-chain fatty acids as energy substrates requires about 25 different enzymes and transport proteins, which carry out fatty acids, import, them into mitochondria, and facilitate the β-oxidation steps. In particular, the mitochondrial inner membrane is impermeable to fatty acyl-CoA thioesters and, thus, the specialized CS, for transporting

fatty acids across mitochondrial membranes has evolved[18]. Components of the CS are both enzymes able to catalyze the acyl-CoA + carnitine ↔ CoA + acylcarnitines reaction and carrier(s) involved in the bi-directional transport of acyl moieties from cytosol to mitochondria and vice versa. Four components comprise this transporting system: the carnitine palmitoyltransferase 1 (CPT1) and 2 (CPT2), the carnitine-acylcarnitine translocase (CACT), and the carnitine acetyltransferase (CrAT) that close the carnitine cycle, allowing the export of the FAO-produced acetyl-CoA as acetyl-carnitine (Fig. 1).

Carnitine palmitoyl transferase family

Carnitine palmitoyltransferase 1A

CPT1A is present mostly in the colon, duodenum, liver, kidney, and small intestine, and its deficiency results in a rare autosomal recessive metabolic disorder of long-chain FAO[19]. The overexpression of CPT1A is often associated with tumor progression in several cancers such as breast, gastric, prostate, lymphoma, leukemia, ovarian, lung, and myeloma[20–23]. Several studies reported that inhibition/depletion of CPT1 leads to apoptosis and suppression of cancer cell proliferation, chemoresistance, and neovascularization[24–28]. It has been proposed that CPT1A contributes to cell survival, not only by increasing FAO[29] but also by stimulating histone acetylase activity in the nucleus[30]. CPT1A can also protect cells from apoptosis by clearing the cytoplasmic long-chain fatty acyl-CoA such as palmitoyl-CoA, and thus impede the production of "palmitate/palmitoyl-CoA/ceramide" involved in the apoptosis pathway activation[31]. Pharmacological inhibition of CPT1A results in impaired cancer cell proliferation in acute myeloid leukemia and intensive cytotoxicity in Burkitt's lymphoma[23,32]. Interestingly, the CPT1 inhibition decreases β-oxidation, which remarkably attenuates c-myc–mediated lymphomagenesis. This suggests a potential role of CPT1 in the pathogenesis of c-myc-driven cancer. In particular, Ricciardi et al. demonstrated in vitro the anti-leukemic activity of the novel CPT1A reversible inhibitor ST1326 on leukemia cell lines and primary cells obtained from patients with hematologic malignancies, which induces cell growth arrest,

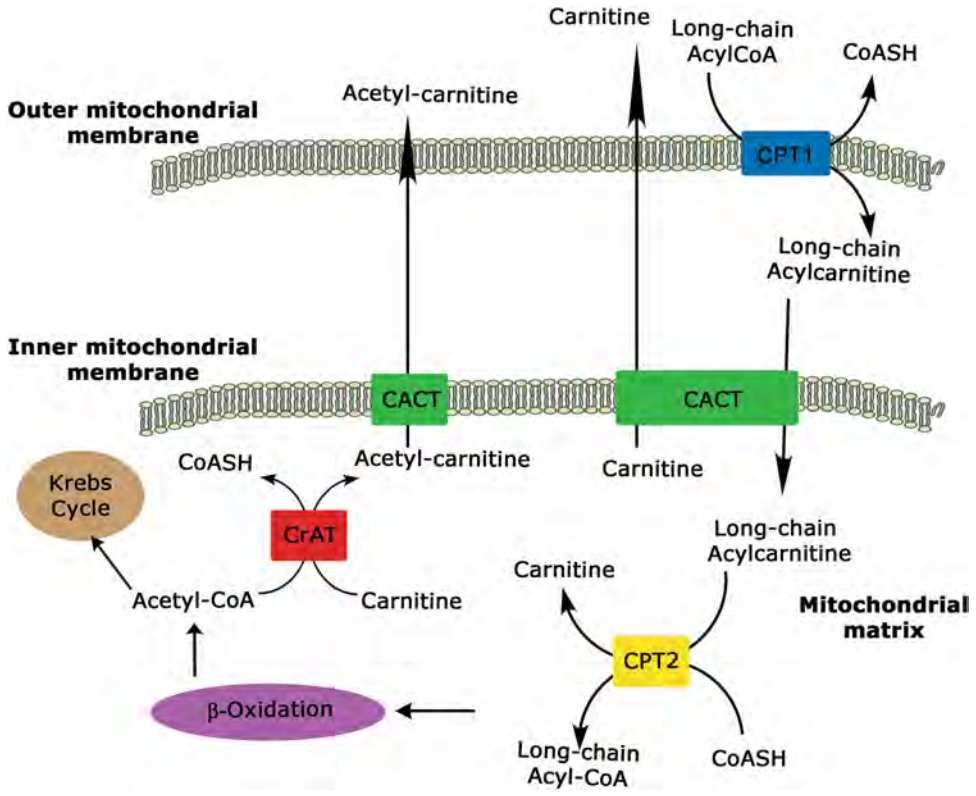

Fig. 1 Schematic view of carnitine system. The long-chain fatty acid-CoAs are converted into the carnitine derivatives by CPT1, located on the outer mitochondrial membrane of the contact sites. A specific carnitine-acylcarnitine translocase (CACT) catalyzes the mole-to-mole exchange of carnitine/acetylcarnitine and acylcarnitines promoting the import of the acylcarnitines through the mitochondrial membranes. In the mitochondrial matrix, long-chain acylcarnitines are reconverted to the respective long-chain acyl-CoAs by carnitine-palmitoyltransferase-2 (CPT2) and undergo β-oxidation to produce acetyl-CoAs. Finally, CrAT converts short-chain acetyl-CoAs to their membrane permeant acetylcarnitine counterparts, allowing CACT to export them from mitochondrion to cytoplasm

mitochondrial damage, and apoptosis[32]. Moreover, Pacilli et al. demonstrated that ST1326 inhibits FAO not only by blocking CPT1A but also by inhibiting CACT activity[23]. In addition, Shao et al. proved that most ovarian cancer cell lines express CPT1A highly and that its inactivation decreased cellular ATP levels, inducing cell cycle arrest at G0/G1[33]. Several studies highlight the role of CPT1A in prostate cancer. Indeed, Schlaepfer et al. showed that the blockage of CPT1A (with etomoxir) and the lipid synthesis/lipolysis (with orlistat) decreased the viability of the androgen-dependent prostate cell lines LNCaP, VCaP, and patient-derived prostate cancer cells[34]. These effects were associated with decreased androgen receptors, mTOR and AKT expression signaling, and increased caspase-3 activation[35]. The upregulated CPT1A expression and activity was also observed in PC3 and LNCaP malignant prostate cells (androgen independent and dependent cells) and human prostate cancer specimens[22]. This recent study identifies an miRNA that targets CPT1A as a potential biomarker for therapy. Upregulated expression of CPT1A has also been determined in breast cancer by an integrated genomic strategy based on the use of gene expression signatures of oncogenic pathway activity[20]. Moreover, Linher-Melville et al. showed that prolactin (PRL) increased the expression and the activity of CPT1A in breast cancer cells with respect to normal cells[29]. The authors suggest that inhibition of FAO may lead to an overall decrease in cancer cell survival, while an increase in CPT1 activity, such as the PRL-mediated response, may provide a supportive environment for malignant cells[36]. Malonyl-CoA, the product of acetyl-CoA carboxylases (ACC), inhibits CPT1A. ACC exists as two related enzymes, the cytosolic isoform ACC1 and the mitochondrion-anchored ACC2. Both enzymes catalyze ATP-dependent carboxylation of acetyl-CoA to form malonyl-CoA. ACC1 is thought to be the predominant isoform mediating fatty acid synthesis, whereas ACC2, the isoform located near CPT1, is the major regulator of CPT1 activity. ACC1 expression has been shown to be frequently upregulated in several tumor types[37], and have reported the expression and/or activation of ACC2 to be inhibited in a variety of cancers[38].

Carnitine palmitoyltransferase 1 B

Carnitine palmitoyltransferase 1 B (CPT1B) is expressed mainly in tissues characterized by high rates of FAO, such as muscle and brown adipose tissue. CPT1B is also expressed in minor quantities in the testis, spleen, duodenum, lymph node, and stomach. Although CPT1A and CPT1B exhibit considerable sequence similarity, the sensitivity of these two enzymes to their physiological inhibitor, malonyl-CoA, differs greatly (CPT1A has a ten-fold higher Ki for malonyl-CoA)[39,40]. CPT1B is involved in human colorectal cancer as determined by Yeh et al.[41]. By using a combined approach of Microarray-Bioinformatic technologies, the authors have revealed the overexpression of CPT1B in clinical tissue specimens of colorectal cancer, demonstrating a potential metabolic mechanism contributing to colorectal cancer. Moreover, recently, Kim et al., have demonstrated the deregulation of some carnitine-acylcarnitine metabolic pathway-associated genes, such as CPT1B, that results in an increased mortality in patients with muscle-invasive bladder cancer[42].

Carnitine palmitoyltransferase 1C

The brain-specific carnitine palmitoyltransferase 1C (CPT1C) displays high-affinity to bind malonyl-CoA, but its enzymatic activity cannot be observed using conventional assays[43]. Recent studies showed that CPT1C was localized both in the endoplasmic reticulum and mitochondria, but its presence in endoplasmic reticulum is predominant. CPT1C is involved in cellular energy-sensing pathways and has an important role in the hypothalamic regulation of energy homeostasis[44]. It has been reported that the CPT1C isoform is overexpressed in human tumor cells such as neuroblastoma, several sarcomas of soft-tissues and lung, and malignant peripheral nerve sheath tumors (associated with neurofibromatosis type 1)[45]. When CPT1C is upregulated, it increases FA consumption, and ATP production, facilitating tumor growth and survival[43]. Interestingly, depletion of CPT1C in mice led to delayed tumor development and a striking increase in survival[46,47]. Sanchez-Macedo et al. showed that p53 directly activated CPT1C transcription, conferring to tumor cells resistance[46]. A recent study indicates that CPT1C might be induced in the MCF-7 breast cancer cell line by the indirect action of activated 5′ AMP-activated protein kinase (AMPK)[48]. Moreover, Zaugg et al. showed that MCF-7 breast cancer cells constitutively overexpressing CPT1C displayed an increased FAO-dependent ATP production, and resistance to glucose deprivation or hypoxia[43]. Finally, a recent study revealed that peroxisome proliferator-activated receptor alpha (PPARα) upregulated the expression of CPT1C, in a p-53 independent way, modulating proliferation and senescence of tumor cells[49]. These findings suggest that CPT1C is a regulator of FA homeostasis in cancer cells and might be indirectly involved in the modulation of CPT1A activity through the lowering of cellular malonyl-CoA levels. Indeed, CPT1C binds to malonyl-CoA with the same affinity as CPT1A. Recently, in high-grade glioblastoma, Cirillo et al. showed an association between the expression of CPT1C and ZFP57, a zinc finger protein involved in gene imprinting[50]. Since a truncated form of CPT1C has been demonstrated in the nuclei of human diffuse gliomas, new perspectives are opening on the role of CPT1C expression in cancer cells[51].

Carnitine palmitoyltransferase 2

Compared to CPT1 isoforms, less is known about CPT2 deregulation in cancer; nevertheless, a recent study has reported that this enzyme could be considered as an independent prognostic factor in colorectal cancer patients[52]. Another study analyzed the expression of several enzymes involved in FA metabolism in the leukemia cells compared to normal cells. The results showed that leukemia cells presented a higher expression of most CPT isoforms, including CPT2. This suggests that chronic lymphocytic leukemia cells were highly active in de novo FA synthesis as well as in FA catabolism[53]. In addition, a recent paper correlates the phosphorylation state of Src with the expression and activity of CPT1A and CPT2 in triple-negative breast cancer (TNBC)[54]. It is well known that aberrant Src activation plays prominent roles in cancer formation and progression[55]. The authors determined by trans-mitochondrial cybrids and multiple OMICs approaches that TNBC exhibit high levels of ATP through FAO and activates Src oncoprotein through autophosphorylation. The inhibition of FAO by the knocking down of CPT1 and CPT2 significantly decreased the phosphorylation level of Src and the number of metastatic nodules, confirming the role of mitochondrial FAO and CPT genes in Src regulation and their significance in breast cancer metastasis.

Carnitine translocase and transferase components

Carnitine/AcylCarnitine translocase

Mitochondria import acylcarnitines through carnitine/acylcarnitine translocase (CACT) located in the inner mitochondrial membrane, which catalyzes a mole-to-mole exchange of carnitines/acetylcarnitines and acylcarnitines[56]. It has been demonstrated that, together with the regulation of CPT1 by malonyl-CoA, acetylation of CACT plays a crucial role in the control of the influx of fatty acyl units into mitochondria[57]. Peluso at al. hypothesized that in obesity-related insulin resistance (IR), skeletal muscle may decrease FAO because of decreased CACT activity[58]. Subsequently another work of the same research team analyzed the metabolic effects of CACT down-expression in human myocyte cells stably transfected with CACT antisense cDNA. This study revealed a complex metabolic situation determined by insulin and palmitate in CACT-deficient cells, and has provided insight into the functional interactions between CACT, CPT1, malonyl-CoA, and acetyl-carnitine[59]. To date, the correlation between CACT and cancer has received little attention, and only a few studies have reported a link between the altered expression of CACT and cancer. Kim et al. have demonstrated that in bladder cancer patients the expression of carnitine enzymes such as CACT has significantly deregulated in tumor tissues compared to normal bladder tissues[42]. Moreover, Valentino et al. demonstrated that in androgen-dependent and -independent prostate tumor cells as well as in human prostate cancer specimens, the over-expression and the increased activity of CACT is a hallmark of prostate cancer[22].

Carnitine *O*-acetyltransferase

Carnitine *O*-acetyltransferase (CrAT), located primarily in the mitochondrial matrix, catalyzes the addition or the removal of carnitine from medium- and short-chain acyl-CoA[60,61], facilitating the efflux of mitochondrial acetyl-CoA to the cytosol and buffering the intracellular pools of acetyl-CoA and carnitine. CrAT deficiency leads to accumulating acetyl-CoA, which exerts an allosteric inhibiting effect on pyruvate dehydrogenase (PDH), a rate-limiting enzyme for pyruvate entry into the Krebs cycle. This metabolic alteration has been associated with metabolic diseases or to insulin deficiency[62–64]. Interestingly, the CrAT activity is reduced during obesity and aging, leading to impaired glycemic control[65]. Studies in Crat knockout mice demonstrated that CrAT deficiency leads to abnormal fuel selection, which results in a perturbation of glucose homeostasis and suggest that deficits in CrAT activity might contribute to diet-induced metabolic inflexibility by exacerbating the Randle glucose-fatty acid cycle[66]. The higher CrAT amount determined both in prostate cancer cells (PC3 and LNCaP, androgen-dependent and androgen-independent, respectively) and prostate tumor biopsy by Valentino et al. highlight the importance of CrAT to contribute to maintaining a high metabolic plasticity of prostate cancers[22]. Finally, CrAT might play a fundamental role in histone acetylation in cancer cells. From a canonical point of view, ATP Citrate Lyase (ACL) produces acetyl-CoA from mitochondrion-derived citrate. Most of the acetyl-CoA produced by ACL originally derives from glucose or glutamine carbon. In addition to contributing to FA synthesis, acetyl-CoA can regulate cell growth by controlling the expression of genes involved in this process by histone acetylation. Alternatively, acetylcarnitine, produced in excess in mitochondria by CrAT, is transported into cytosol by CACT and enters the nucleus, where a nuclear CrAT converts the acetylcarnitine to acetyl-CoA[67], and it becomes a source of acetyl groups for histone acetylation. Therefore, besides citrate-derived acetyl-CoA by nuclear ATP-citrate lyase[68], the carnitine-mediated supply of acetyl groups is also an important source of acetyl-CoA for nuclear histone acetylation. Indeed, genetic deficiency of the translocase markedly reduced the mitochondrial acetylcarnitine-dependent nuclear histone acetylation, indicating the significance of the carnitine-dependent mitochondrial acetyl group contribution to histone acetylation.

Metabolic intermediates and carnitine system

Metabolic pathways are monitored and controlled by allosteric or post-translational regulation of enzymes that

catalyze specific biochemical reactions. Afterwards, alternative splicing, mRNA stability, translation, and protein degradation control the abundance of enzymes ("long-term regulation")[69]. In this view, nutrients, such as glucose or free fatty acids, provide intermediate metabolites the ability to interact directly with an enzyme (the metabolic sensor) that rules the rate limiting step of a metabolic process, thus regulating substrate preference. A case in point is the so-called "glucose-fatty acid cycle", a prime example of tightly coordinated cellular energy metabolism that provides a mechanistic reciprocal regulation of lipid and glucose oxidation to maintain cell homoeostasis and to avoid mitochondrial overloading. Interestingly, β-oxidation and aerobic glycolysis are connected to each other through cross-signaling in such a manner that beta-oxidation not only is compatible with ongoing aerobic glycolysis, but also it promotes the Warburg Effect. Indeed, the PDH complex, which decarboxylates glycolytically derived pyruvate to acetyl coenzyme A and links cytoplasmic glycolysis to the mitochondrial tricarboxylic acid (TCA) cycle, is modulated by reversible phosphorylation by PDH kinase (PDK). Nicotinamide adenine dinucleotide (NADH) and acetyl-CoA, two metabolic intermediates produced in the course of FAO, induce activation of PDK, which in turn phospho-inactivates the E1α subunit of the PDH complex, leading to lower rates of glucose oxidation and higher rates of lactate release[70]. Interestingly, multiple transcription factors, such as Myc, Wnt, and hypoxia inducible factors, can cause a transcriptional increase of one or more PDK isoforms in a cancer cell. A cross-talk between metabolic intermediates produced by aerobic glycolysis, and enzymes belonging to the carnitine cycle is also present in cancer cells. The relationship between lactate and cancer growth reflects the pleotropic actions of this molecule able to influence the metabolic phenotype of the cancer cells. A recent study has demonstrated that lactate-induced acidification of the microenvironment over a period of weeks induces a metabolic adaptation of the tumor cell population, promoting β-oxidation as a

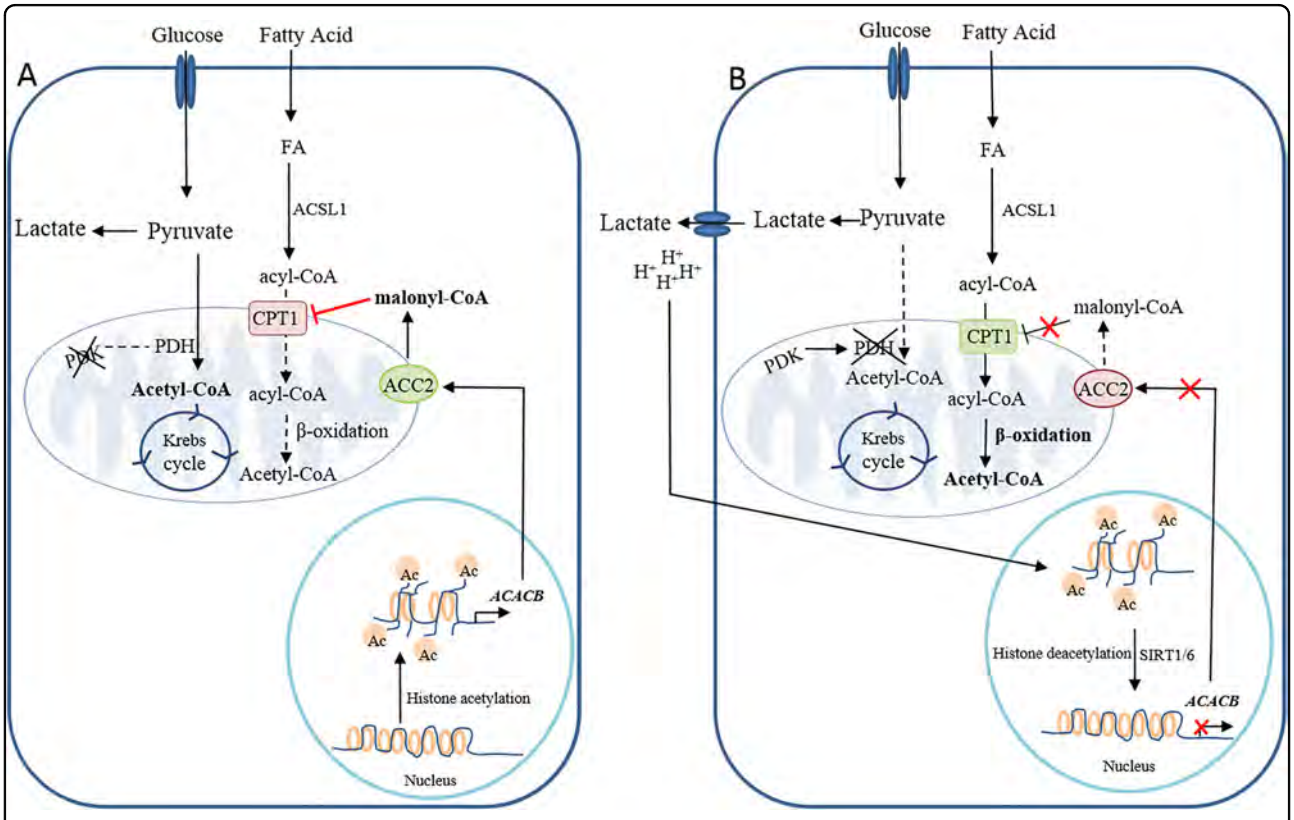

Fig. 2 Epigenetic ACC2 control modulates the reprogramming of fatty acid metabolism in cancer cells. a Epigenetic control of *ACACB* by histone acetylation induces an increased expression of both ACC2 and its catalytic product, malonyl-CoA, leading to the inhibition of CPT1A activity. On the contrary, **b** histone deacetylation by sirtuin(s) (SIRT1/6), also promoted by lactate-induced acidification of the microenvironment, leads to a decreased expression of *ACACB* and consequently enhances CPT1A activity. NADH and acetyl-CoA, two metabolic intermediates produced in the course of FAO, promote activation of PDK, which in turn phospho-inactivates the E1α subunit of the PDH complex, leading to lower rates of glucose oxidation and higher rates of lactate release

metabolic strategy (the Corbet−Feron Effect)[71]. In addition, cancer cells chronically exposed to an acidic pH reveal a downregulation of the mitochondrial ACC2 isoform, the enzyme that regulates CPT1 activity by malonyl-CoA synthesis. Therefore, only ACC1 isoform is expressed in tumor cells under acidosis to produce malonyl-CoA as a substrate for FA synthesis. Of interest, the down-expression of ACC2 results from an epigenetic process linked to histone deacetylation at the ACACB promoter by Sirtuin 1/6 that are activated by high cytosolic NAD^+ levels associated with enhanced FAO and reduced glucose metabolism.

The non-enzymatic mitochondrial protein hyperacetylation induced by the increased availability of mitochondrial acetyl-CoA avoids the risk associated with mitochondria overfeeding, restraining the activity of the respiratory complex I and modulating CACT activity. Indeed, it has been demonstrated that acetylation plays a key role in the control of CACT function that, together with the long-chain acyl-CoA dehydrogenase, contributes to β-oxidation regulation. CACT acetylation compromises its activity, causing a decrease in its transport function. This mechanism represents a control of the influx of fatty acyl units into mitochondria in response to the intramitochondrial acetyl-CoA level, in addition to the finely regulated mechanism of CPT1 by malonyl-CoA. CACT acetylation mechanism is in line with a dynamic post-translational protein control that could undergo an on/off switch induced by deacetylation/acetylation linked to the availability of acetyl-CoA[57].

Recently, it was found that FA-derived acetyl-CoA is a significant font of carbon for acetylation of certain histone lysine, even in the presence of glucose[72]. Again, CS might be fundamental not only to produce but also to transport acetyl-CoA from the mitochondria to the nucleus for supplying acetyl-CoA for histone acetylation. Acetylcarnitine synthetized in mitochondria by CrAT is transported out mitochondria by CACT and transformed back to acetyl-CoA by CrAT present in the nucleus. In this model CS assumes a mechanistic role by which FA are perceived and integrated into the epigenome.

All these considerations are schematized in Figs. 2 and 3.

Small-non-coding RNA (miRNAs) as a carnitine system regulator

Among all small non-coding RNAs, microRNAs (miRNAs) (Fig. 4), 18–25 nucleotides in length, are well characterized as post-transcriptional regulators of mRNAs[73,74] and are considered a potential source of biomarkers for many diseases, including cancer[75].

MiRNAs play important regulatory roles in a variety of biological processes such as cell proliferation, intercellular

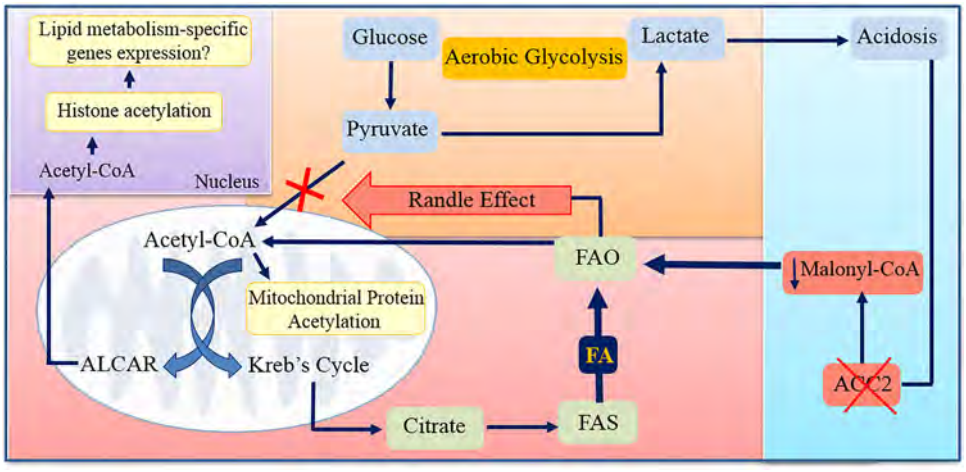

Fig. 3 The involvement of carnitine cycle in cancer cell metabolism. In cancer metabolism the aerobic glycolysis induces the conversion of the pyruvate (the end product of the glycolysis) into lactate (shown in orange) leading to the acidification of the microenvironment. The increased acidosis (shown in blue), in association with epigenetic mechanism(s), promotes the downregulation of the mitochondrial ACC2 isoform that in turn increases FAO (shown in red) via CPT1A upregulation. NADH and acetyl-CoA, produced in excess during FAO, promote the conversion of pyruvate into lactate through the inhibition of PDH by PDK (Randle effect). The increased availability of mitochondrial acetyl-CoA enhances the intramitochondrial non-enzymatic acetylation of proteins both of the Kreb's cycle and of the carnitine cycle, avoiding the risk associated with mitochondria overfeeding. In addition, the excess of acetyl-CoA is exported in the cytosol either as citrate or as acetyl L-carnitine (ALCAR). The citrate is converted into acetyl-CoA by ACLY for the synthesis of fatty acids that might be re-imported into the mitochondria for beta-oxidation (Futile Cycle). ALCAR, shuttled to the nucleus (shown in violet), can be used as source of acetyl groups for histone acetylation, probably contributing to lipid metabolism-specific gene expression

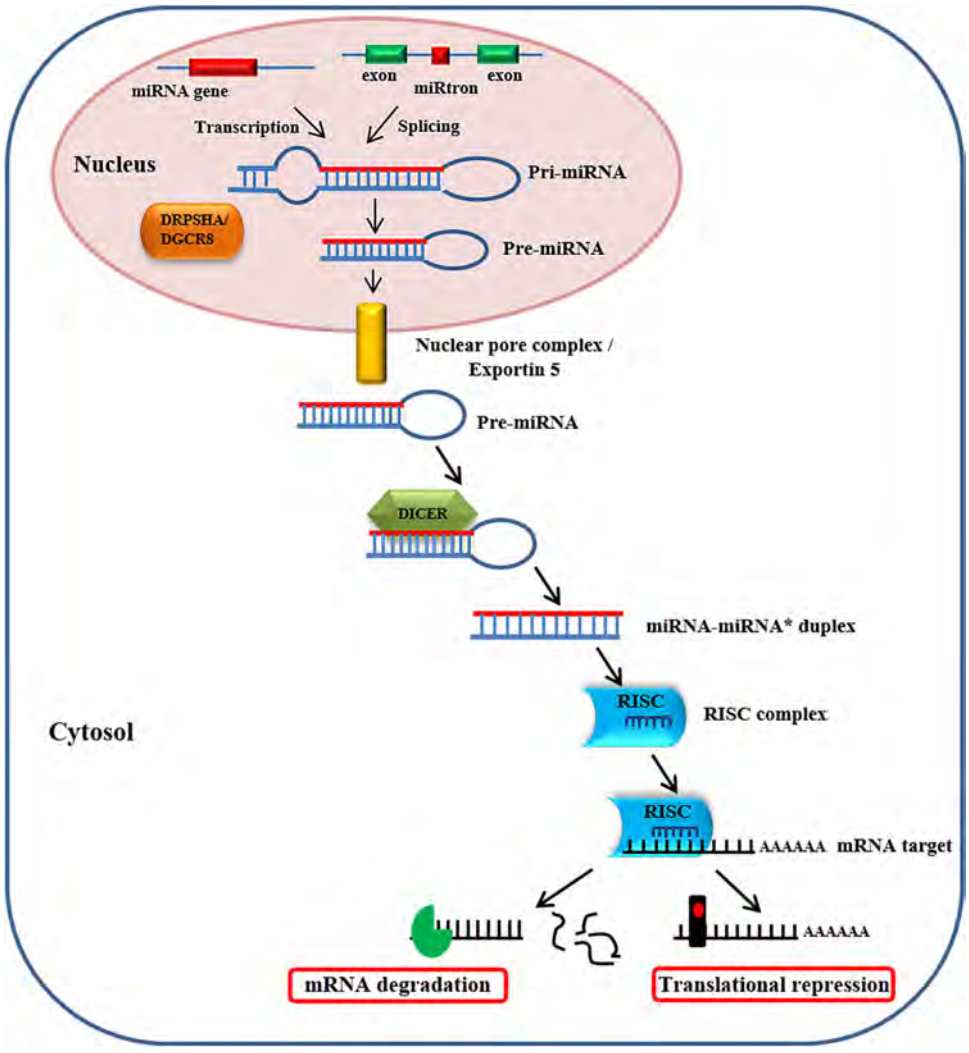

Fig. 4 miRNAs biogenesis and mechanism of action. MicroRNAs are transcribed by RNA polymerases II and III in pri-miRNAs, generating precursors that undergo a series of cleavage events to form mature microRNA. Drosha, the first nuclear ribonuclease III, recognizes pri-miRNA and cuts the double-stranded RNA freeing a pre-miRNA. Pre-miRNA hairpin is exported from the nucleus in a process involving the nucleocytoplasmic protein Exportin-5. In the cytoplasm, the pre-miRNA hairpin is cleaved by the RNase III enzyme Dicer in an miRNA duplex of 18–22 nt. Although either the duplex strands may potentially act as functional miRNAs, only one strand is usually incorporated into the RNA-induced silencing complex (RISC) where the miRNA and its mRNA target interact. Mature miRNA acts either by degrading the mRNA target or by inhibiting its translation

signaling, cell growth, cell death, cellular differentiation, apoptosis, and cancer metabolism[76–78]. Their expression profiles have been found to be tissue type-specific and frequently deregulated in various cancers[79]. MiRNAs have unique characteristics (i.e. stability, tissue specificity, easily detected and manipulated) that make them potential therapeutic targets for cancer treatment[80]. Emerging evidence demonstrates that miRNAs are critical regulators of lipid synthesis and FAO[81] resulting in defective cell metabolism and carcinogenesis[82] directly targeting key enzymes or transcription factors as oncogenes and tumor suppressors[81] as shown in Table 1.

MiR-122 was the first miRNA identified as tissue-specific, and it is the most abundant in liver involved in lipid metabolic reprogramming[83]. MiR-122 inhibition leads to decreased plasma cholesterol and triglyceride levels associated with altered lipids biosynthesis and increased FAO. Several genes involved in fatty acid synthesis and oxidation were altered in mice treated with anti-miR-122 including FAS, ACC1, and ACC2[84]. Furthermore, miR-122 silencing in high-fat-fed mice reduced hepatic steatosis, with a decrease in cholesterol synthesis and stimulation of FAO[85]. Recently, Iliopoulos et al. identified a new miRNA, miR-370, that has effects on lipid metabolism

Table 1 miRNAs involved in cancer metabolic plasticity

MiRNAs	Target	Reference
miR-122	Cholesterol biosynthesis	88–90
miR-370	Fatty acid oxidation, CPT1A	91
miR-378/378*	Lipid metabolism, CrAT	92, 93
miR-335	Lipid metabolism and adipogenesis	94
miR-205	Lipid metabolism	95
miR-143	Adipocyte differentiation	96
miR-27	Adipolysis	97
miR-33a/b	Cholesterol efflux and β-oxidation	98–100
miR-185	Lipogenesis and cholesterogenesis	101
miR-342	Lipogenesis and cholesterogenesis	101
miR-124	CPT1A	27
miR-129	CACT	27, 102

similar to miR-122. MiR-370 targets CPT1A reducing FAO. Particularly, the human hepatic cell line HepG2 transfection with miR-370 upregulates the expression of miR-122. This upregulation leads to an increased expression of lipogenic genes, including sterol regulatory element-binding proteins (SREBP1c) and diacylglycerol acyltransferase-2 (DGAT2), which suggests that miR-370 provides a further point of regulation of this pathway[86]. Interestingly, components of cholesterol efflux and fatty acid metabolism are regulated by miR-33a and miR-33b. These miRNAs reside in intronic regions within SREBP-1 and 2, the key transcriptional regulators of lipid metabolism[87], and control the expression of carnitine *O*-octanoyltransferase (CROT), CPT1A, hydroxyacyl coenzyme A (hydroxyacyl-CoA) dehydrogenase subunit beta (HADHB), and AMPK, targeting their 3′ UTR[88]. Another important miRNA regulating cell metabolism is miR-378/378*, embedded within gene encoding peroxisome proliferator-activated receptor gamma coactivator 1-beta (PGC-1β), a transcriptional regulator of oxidative energy metabolism. In breast cancer cells, a high level of miR-378* induces the metabolic shift from an oxidative to a glycolytic bioenergetics pathway by inhibiting the expression of two PGC-1β partners, ERRγ (estrogen-related receptor gamma) and GABPA (GA binding protein transcription factor, alpha subunit). This leads to a reduction in TCA cycle gene expression and oxygen consumption as well as an increase in lactate production and cell proliferation[89]. Targets of miR-378 are also CRAT; indeed, it has been shown that mice genetically lacking miR-378 and miR-378* are resistant to high-fat-diet-induced obesity and display enhanced mitochondrial FA metabolism and elevated oxidative capacity of insulin-target tissue[90]. Moreover, Valentino et al. have demonstrated that the downregulation of hsa-miR-124-3p, hsa-miR-129-5p, and hsa-miR-378 induces an increase in both expression and activity of CPT1A, CACT, and CrAT in malignant prostate cells[22]. In addition, the analysis of human prostate cancer and prostate control specimens confirmed the aberrant expression of miR-124-3p, miR-129-5p, and miR-378 in primary tumors. Forced expression of the above-mentioned miRNAs affected tumorigenic properties, (i.e. proliferation, migration, and invasion), in PC3 and LNCaP cells regardless of their hormone sensitivity. MiR-143, miR-27, miR-335, miR-14, and miR-205 have been recently associated with lipid metabolism and adipocyte differentiation[91]. MiR-27a inhibits the expression of several lipid metabolic genes, including SREBP1-2, FASN, and PPARα/γ, by reducing lipid synthesis and increasing lipid secretion from cells[92]. The expression of MiR-335 is modulated by lipid loading, resulting in overexpression in liver and adipose tissue of obese mice[93]. However, the role of miR-335 in triggering lipid metabolism still remains unknown. Another miRNA implicated in the regulation of lipid metabolism is miR-14. Zu et al., indeed, demonstrated in *Drosophila melanogaster* that the deletion of miR-14 increased the levels of triacylglycerol and diacylglycerol while its overexpression resulted in the converse effect[94]. Recently, it has been found that miR-205 deregulates lipid metabolism in hepatocellular carcinoma by targeting acyl-CoA synthetase ACSL1, a lipid metabolism enzyme in liver[95]. Furthermore, in prostate cancer cells, miR-185 and miR-342 control lipogenesis and cholesterogenesis by reducing the expression of SREBP-1/2 and downregulating their targeted genes, including fatty acid synthase[96]. The function of miRNAs on lipid metabolic plasticity reveals molecular strategies aimed to control metabolic flux by miRNAs in cancerogenesis, thus lighting up one of miRNAs therapeutic aspect[97] (Fig. 5).

Concluding remarks

Cancer metabolic plasticity allows tumor cells to survive in the face of adverse environmental conditions. Metabolites involved in metabolic plasticity must be able to fluctuate in response to internal or external perturbations. Therefore, identifying regulatory nodes within the metabolic network is challenging due to its complex structure. Although today several studies have investigated the mechanism involved in metabolic plasticity, but key pathway has not been identified which could be considered a unique target for cancer therapy. We critically review how cancer cells control the metabolic regulatory mechanisms. Therefore, we have emphasized the crucial role of the CS and its fine-tuned regulation, which is both enzymatic- and miRNA-dependent, as the primary factor in metabolic cancer flexibility.

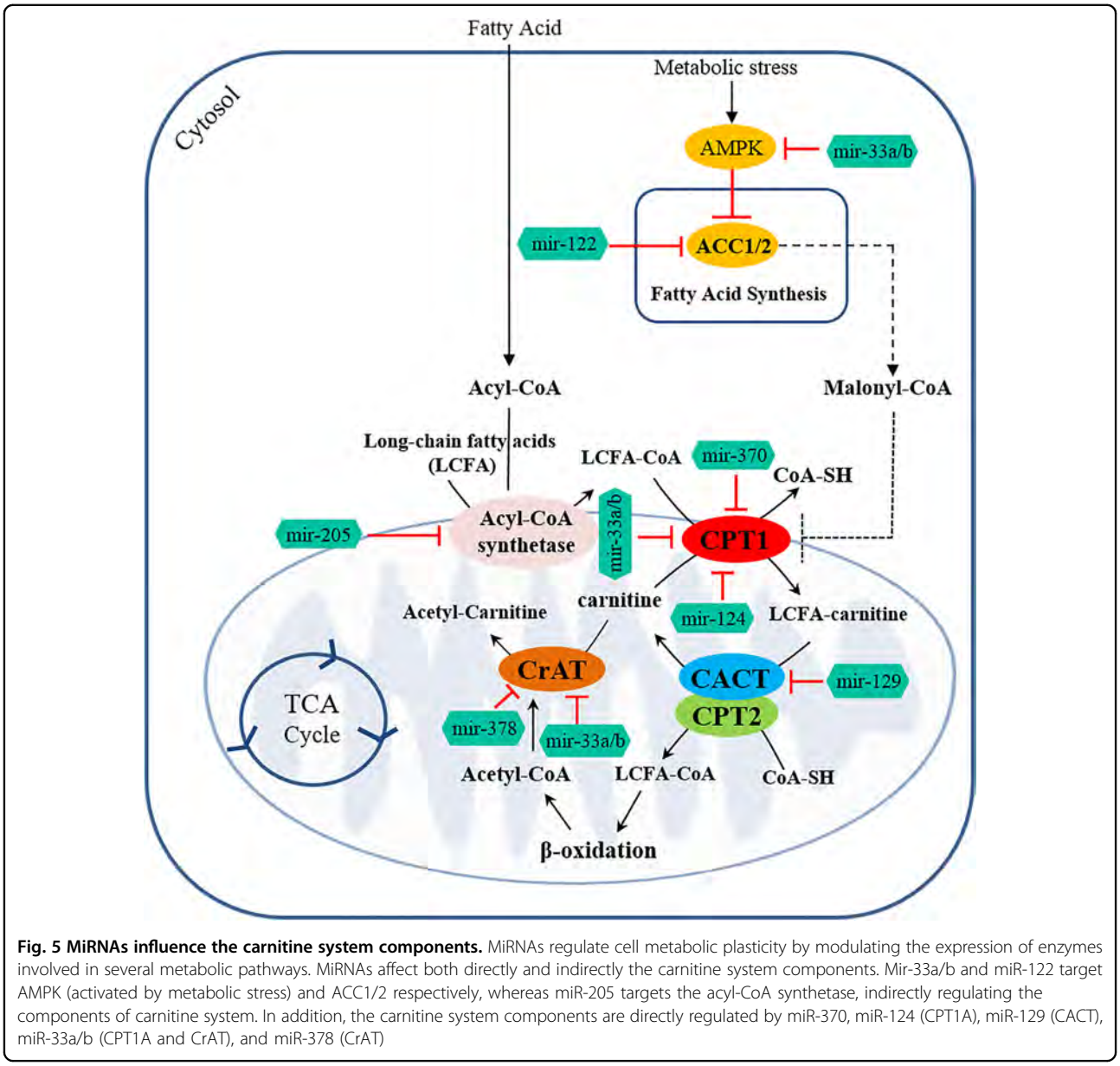

Fig. 5 MiRNAs influence the carnitine system components. MiRNAs regulate cell metabolic plasticity by modulating the expression of enzymes involved in several metabolic pathways. MiRNAs affect both directly and indirectly the carnitine system components. Mir-33a/b and miR-122 target AMPK (activated by metabolic stress) and ACC1/2 respectively, whereas miR-205 targets the acyl-CoA synthetase, indirectly regulating the components of carnitine system. In addition, the carnitine system components are directly regulated by miR-370, miR-124 (CPT1A), miR-129 (CACT), miR-33a/b (CPT1A and CrAT), and miR-378 (CrAT)

Acknowledgements
This work was supported by Ministero dell'Istruzione, dell'Università e della Ricerca of Italy, Progetto PON—'Ricerca e Competitività 2007–2013'—PON01_01802: Sviluppo di molecole capaci di modulare vie metaboliche intracellulari redoxsensibili per la prevenzione e la cura di patologie infettive, tumorali, neurodegenerative e loro delivery mediante piattaforme nano tecnologiche', and PON01_02512: 'Ricerca e sviluppo di bioregolatori attivi sui meccanismi epigenetici dei processi infiammatori nelle malattie croniche e degenerative'.

Author details
[1]Department of Medical, Surgical, Neurological, Metabolic Sciences, and Aging, 2nd Division of Neurology, Center for Rare Diseases and InterUniversity Center for Research in Neurosciences, University of Campania "Luigi Vanvitelli", Naples, Italy. [2]Department of Biology, Sbarro Institute for Cancer Research and Molecular Medicine, Center for Biotechnology, College of Science and Technology, Temple University, Philadelphia, PA, USA. [3]Institute of Agro-Environmental and Forest Biology, National Research Council, IBAF-CNR, Naples, Italy. [4]Institute of Bioscience and BioResources, IBBR- CNR, Naples, Italy. [5]Department of Experimental Medicine, Biotechnology and Molecular Biology Section, University of Campania "Luigi Vanvitelli", Naples, Italy. [6]Department of Medicine, Surgery and Neuroscience, University of Siena, Siena, Italy

Conflict of interest
The authors declare that they have no conflict of interest.

Received: 5 December 2017 Revised: 9 January 2018 Accepted: 11 January 2018
Published online: 14 February 2018

References

1. Goodpaster, B. H. & Sparks, L. M. Metabolic flexibility in health and disease. *Cell Metab.* **25**, 1027–1036 (2017).
2. Quail, D. & Joyce, J. Microenvironmental regulation of tumor progression and metastasis. *Nat. Med.* **19**, 1423–1437 (2013).
3. Pavlova, N. N. & Thompson, C. B. The emerging hallmarks of cancer metabolism. *Cell Metab.* **23**, 27–47 (2016).
4. Martinez-Reyes, I. et al. TCA cycle and mitochondrial membrane potential are necessary for diverse biological functions. *Mol. Cell* **61**, 199–209 (2016).
5. Gao, X., Reid, M. A., Kong, M. & Locasale, J. W. Metabolic interactions with cancer epigenetics. *Mol. Asp. Med.* **54**, 50–57 (2016).
6. Nieman, K. M. et al. Adipocytes promote ovarian cancer metastasis and provide energy for rapid tumor growth. *Nat. Med.* **17**, 1498–U207 (2011).
7. Rios, M. et al. Lipoprotein internalisation induced by oncogenic AMPK activation is essential to maintain glioblastoma cell growth. *Eur. J. Cancer* **50**, 3187–3197 (2014).
8. Kamphorst, J. J. et al. Hypoxic and Ras-transformed cells support growth by scavenging unsaturated fatty acids from lysophospholipids. *Proc. Natl. Acad. Sci. USA* **110**, 8882–8887 (2013).
9. Nomura, D. K. et al. Monoacylglycerol lipase regulates a fatty acid network that promotes cancer pathogenesis. *Cell* **140**, 49–61 (2010).
10. Caro, P. et al. Metabolic signatures uncover distinct targets in molecular subsets of diffuse large B cell lymphoma. *Cancer Cell* **22**, 547–560 (2012).
11. Wu, X., Daniels, G., Lee, P. & Monaco, M. E. Lipid metabolism in prostate cancer. *Am. J. Clin. Exp. Urol.* **2**, 111–120 (2014).
12. Yang, S. et al. Pancreatic cancers require autophagy for tumor growth. *Genes Dev.* **25**, 717–729 (2011).
13. Viale, A. et al. Oncogene ablation-resistant pancreatic cancer cells depend on mitochondrial function. *Nature* **514**, 628–632 (2014).
14. Samoilov, M., Plyasunov, S. & Arkin, A. P. Stochastic amplification and signaling in enzymatic futile cycles through noise-induced bistability with oscillations. *Proc. Natl. Acad. Sci. USA* **102**, 2310–2315 (2005).
15. Hardie, D. G. & Pan, D. A. Regulation of fatty acid synthesis and oxidation by the AMP-activated protein kinase. *Biochem. Soc. Trans.* **30**(Pt 6), 1064–1070 (2002).
16. Alvarez, J. V. et al. Oncogene pathway activation in mammary tumors dictates FDG-PET uptake. *Cancer Res.* **74**, 7583–7598 (2014).
17. Yoon, S. et al. Up-regulation of acetyl-CoA carboxylase alpha and fatty acid synthase by human epidermal growth factor receptor 2 at the translational level in breast cancer cells. *J. Biol. Chem.* **282**, 26122–26131 (2007).
18. Bastin, J. Regulation of mitochondrial fatty acid beta-oxidation in human: what can we learn from inborn fatty acid beta-oxidation deficiencies? *Biochimie* **96**, 113–120 (2014).
19. Longo, N., Amat di San Filippo, C. & Pasquali, M. Disorders of carnitine transport and the carnitine cycle. *Am. J. Med. Genet. C. Semin. Med. Genet.* **142C**, 77–85 (2006).
20. Gatza, M. L., Silva, G. O., Parker, J. S., Fan, C. & Perou, C. M. An integrated genomics approach identifies drivers of proliferation in luminal-subtype human breast cancer. *Nat. Genet.* **46**, 1051–1059 (2014).
21. Li, S. et al. High metastaticgastric and breast cancer cells consume oleic acid in an AMPK dependent manner. *PLoS ONE* **9**, e97330 (2014).
22. Valentino, A. et al. Deregulation of MicroRNAs mediated control of carnitine cycle in prostate cancer: molecular basis and pathophysiological consequences. *Oncogene* **36**, 6030–6040 (2017).
23. Pacilli, A. et al. Carnitine-acyltransferase system inhibition, cancer cell death, and prevention of Myc-induced lymphomagenesis. *J. Natl. Cancer Inst.* **105**, 489–498 (2013).
24. Li, J. et al. Inhibition of lipolysis by mercaptoacetate and etomoxir specifically sensitize drug-resistant lung adenocarcinoma cell to paclitaxel. *PLoS ONE* **8**, e74623 (2013).
25. Tung, S. et al. PPARalpha and fatty acid oxidation mediate glucocorticoid resistance in chronic lymphocytic leukemia. *Blood* **122**, 969–980 (2013).
26. Schoors, S. et al. Fatty acid carbon is essential for dNTP synthesis in endothelial cells (vol 520, pg 192, 2015). *Nature* **526**, 144 (2015).
27. Patella, F. et al. Proteomics-based metabolic modeling reveals that fatty acid oxidation (FAO) controls endothelial cell (EC) permeability. *Mol. Cell Proteom.* **14**, 621–634 (2015).
28. Giordano, A. et al. tBid induces alterations of mitochondrial fatty acid oxidation flux by malonyl-CoA-independent inhibition of carnitine palmitoyltransferase-1. *Cell Death Differ.* **12**, 603–613 (2005).
29. Linher-Melville, K. et al. Establishing a relationship between prolactin and altered fatty acid β-oxidation via carnitine palmitoyl transferase 1 in breast cancer cells. *BMC Cancer* **11**, 56 (2011).
30. Mazzarelli, P. et al. Carnitine palmitoyltransferase I in human carcinomas: a novel role in histone deacetylation? *Cancer Biol. Ther.* **6**, 1606–1613 (2007).
31. Grosch, S., Schiffmann, S. & Geisslinger, G. Chain length-specific properties of ceramides. *Prog. Lipid Res.* **51**, 50–62 (2012).
32. Ricciardi, M. R. et al. Targeting the leukemia cell metabolism by the CPT1a inhibition: functional preclinical effects in leukemias. *Blood* **126**, 1925–1929 (2015).
33. Shao, H. J. et al. Carnitine palmitoyltransferase 1A functions to repress FoxO transcription factors to allow cell cycle progression in ovarian cancer. *Oncotarget* **7**, 3832–3846 (2016).
34. Schlaepfer, I. R. et al. Lipid catabolism via CPT1 as a therapeutic target for prostate cancer. *Mol. Cancer Ther.* **13**, 2361–2371 (2014).
35. Schlaepfer, I. R. et al. Inhibition of lipid oxidation increases glucose metabolism and enhances 2-deoxy-2-[(18)F]fluoro-d-glucose uptake in prostate cancer mouse xenografts. *Mol. Imaging Biol.: MIB: Off. Publ. Acad. Mol. Imaging* **17**, 529–538 (2015).
36. Pucci, S. et al. Carnitine palmitoyl transferase-1A (CPT1A): a new tumor specific target in human breast cancer. *Oncotarget* **7**, 19982–19996 (2016).
37. Svensson, R. U. et al. Inhibition of acetyl-CoA carboxylase suppresses fatty acid synthesis and tumor growth of non-small-cell lung cancer in preclinical models. *Nat. Med.* **22**, 1108–1119 (2016).
38. German, N. J. et al. PHD3 loss in cancer enables metabolic reliance on fatty acid oxidation via deactivation of ACC2. *Mol. Cell* **63**, 1006–1020 (2016).
39. Casals, N. et al. Carnitine palmitoyltransferase 1C: from cognition to cancer. *Prog. Lipid Res.* **61**, 134–148 (2016).
40. McGarry, J. D. & Brown, N. F. The mitochondrial carnitine palmitoyltransferase system. From concept to molecular analysis. *Eur. J. Biochem.* **244**, 1–14 (1997).
41. Yeh, C. S. et al. Fatty acid metabolism pathway play an important role in carcinogenesis of human colorectal cancers by Microarray-Bioinformatics analysis. *Cancer Lett.* **233**, 297–308 (2006).
42. Kim, W. T. et al. Metabolic pathway signatures associated with urinary metabolite biomarkers differentiate bladder cancer patients from healthy controls. *Yonsei Med. J.* **57**, 865–871 (2016).
43. Zaugg, K. et al. Carnitine palmitoyltransferase 1C promotes cell survival and tumor growth under conditions of metabolic stress. *Genes Dev.* **25**, 1041–1051 (2011).
44. Lohse, I., Reilly, P. & Zaugg, K. The CPT1C 5′ UTR contains a repressing upstream open reading frame that is regulated by cellular energy availability and AMPK. *PLos ONE6* **6**, e21486 (2011).
45. Reilly, P. T. & Mak, T. W. Molecular pathways: tumor cells co-opt the brain-specific metabolism gene CPT1C to promote survival. *Clin. Cancer Res.* **18**, 5850–5855 (2012).
46. Sanchez-Macedo, N. et al. Depletion of the novel p53-target gene carnitine palmitoyltransferase 1C delays tumor growth in the neurofibromatosis type I tumor model. *Cell Death Differ.* **20**, 659–668 (2013).
47. Carrasco, P. et al. Ceramide levels regulated by carnitine palmitoyltransferase 1C control dendritic spine maturation and cognition. *J. Biol. Chem.* **287**, 21224–21232 (2012).
48. Wu, Y., Sarkissyan, M., Mcghee, E., Lee, S. & Vadgama, J. V. Combined inhibition of glycolysis and AMPK induces synergistic breast cancer cell killing. *Breast Cancer Res. Tr.* **151**, 529–539 (2015).
49. Chen, Y. et al. PPARalpha regulates tumor cell proliferation and senescence via a novel target gene carnitine palmitoyltransferase 1C. *Carcinogenesis* **38**, 474–483 (2017).
50. Cirillo, A. et al. High grade glioblastoma is associated with aberrant expression of ZFP57, a protein involved in gene imprinting, and of CPT1A and CPT1C that regulate fatty acid metabolism. *Cancer Biol. Ther.* **15**, 735–741 (2014).
51. Wakamiya, T. et al. Elevated expression of fatty acid synthase and nuclear localization of carnitine palmitoyltransferase 1C are common among human gliomas. *Neuropathol.: Off. J. Jpn. Soc. Neuropathol.* **34**, 465–474 (2014).
52. Guo, H. L. et al. Integrated transcriptomic analysis of distance-related field cancerization in rectal cancer patients. *Oncotarget* **8**, 61107–61117 (2017).
53. Liu, P. P. et al. Elimination of chronic lymphocytic leukemia cells in stromal microenvironment by targeting CPT with an antiangina drug perhexiline. *Oncogene* **35**, 5663–5673 (2016).

54. Park, J. H. et al. Fatty acid oxidation-driven Src links mitochondrial energy reprogramming and oncogenic properties in triple-negative breast cancer. *Cell Rep.* **14**, 2154–2165 (2016).
55. Aleshin, A. & Finn, R. S. SRC: a century of science brought to the clinic. *Neoplasia* **12**, 599–607 (2010).
56. Ramsay, R. R., Gandour, R. D. & van der Leij, F. R. Molecular enzymology of carnitine transfer and transport. *Biochim. Biophys. Acta* **1546**, 21–43 (2001).
57. Giangregorio, N., Tonazzi, A., Console, L. & Indiveri, C. Post-translational modification by acetylation regulates the mitochondrial carnitine/acylcarnitine transport protein. *Mol. Cell. Biochem.* **426**, 65–73 (2017).
58. Peluso, G. et al. Decreased mitochondrial carnitine translocase in skeletal muscles impairs utilization of fatty acids in insulin-resistant patients. *Front. Biosci.* **7**, A109–A116 (2002).
59. Peluso, G. et al. Differential carnitine/acylcarnitine translocase expression defines distinct metabolic signatures in skeletal muscle cells. *J. Cell. Physiol.* **203**, 439–446 (2005).
60. Houten, S. M. & Wanders, R. J. A. A general introduction to the biochemistry of mitochondrial fatty acid beta-oxidation. *J. Inherit. Metab. Dis.* **33**, 469–477 (2010).
61. Pieklik, J. R. & Guynn, R. W. Equilibrium constants of the reactions of choline acetyltransferase, carnitine acetyltransferase, and acetylcholinesterase under physiological conditions. *J. Biol. Chem.* **250**, 4445–4450 (1975).
62. Muoio, D. M. Metabolic inflexibility: when mitochondrial indecision leads to metabolic gridlock. *Cell* **159**, 1253–1262 (2014).
63. Seiler, S. E. et al. Obesity and lipid stress inhibit carnitine acetyltransferase activity. *J. Lipid Res.* **55**, 635–644 (2014).
64. Seiler, S. E. et al. Carnitine acetyltransferase mitigates metabolic inertia and muscle fatigue during exercise. *Cell Metab.* **22**, 65–76 (2015).
65. Noland, R. C. et al. Carnitine insufficiency caused by aging and overnutrition compromises mitochondrial performance and metabolic control. *J. Biol. Chem.* **284**, 22840–22852 (2009).
66. Muoio, D. M. et al. Muscle-specific deletion of carnitine acetyltransferase compromises glucose tolerance and metabolic flexibility. *Cell. Metab.* **15**, 764–777 (2012).
67. Madiraju, P., Pande, S. V., Prentki, M. & Madiraju, S. R. Mitochondrial acetylcarnitine provides acetyl groups for nuclear histone acetylation. *Epigenetics* **4**, 399–403 (2009).
68. Wellen, K. E. et al. ATP-citrate lyase links cellular metabolism to histone acetylation. *Science* **324**, 1076–1080 (2009).
69. Boroughs, L. K. & DeBerardinis, R. J. Metabolic pathways promoting cancer cell survival and growth. *Nat. Cell Biol.* **17**, 351–359 (2015).
70. Holness, M. J. & Sugden, M. C. Regulation of pyruvate dehydrogenase complex activity by reversible phosphorylation. *Biochem. Soc. Trans.* **31**, 1143–1151 (2003). (Pt 6).
71. Corbet, C. et al. Acidosis drives the reprogramming of fatty acid metabolism in cancer cells through changes in mitochondrial and histone acetylation. *Cell Metab.* **24**, 311–323 (2016).
72. McDonnell, E. et al. Lipids reprogram metabolism to become a major carbon source for histone acetylation. *Cell Rep.* **17**, 1463–1472 (2016).
73. Krol, J., Loedige, I. & Filipowicz, W. The widespread regulation of microRNA biogenesis, function and decay. *Nat. Rev. Genet.* **11**, 597–610 (2010).
74. Garzon, R., Marcucci, G. & Croce, C. M. Targeting microRNAs in cancer: rationale, strategies and challenges. *Nat. Rev. Drug Discov.* **9**, 775–789 (2010).
75. Li, Z. H. & Rana, T. M. Therapeutic targeting of microRNAs: current status and future challenges. *Nat. Rev. Drug Discov.* **13**, 622–638 (2014).
76. Bartel, D. P. MicroRNAs: genomics, biogenesis, mechanism, and function (Reprinted from *Cell* 116, 281–297 (2004)). *Cell* **131**, 11–29 (2007).
77. He, L. & Hannon, G. J. MicroRNAs: Small RNAs with a big role in gene regulation (vol 5, pg 522 2004). *Nat. Rev. Genet.* **5**, 522 (2004). -+.
78. Ambros, V. The functions of animal microRNAs. *Nature* **431**, 350–355 (2004).
79. Volinia, S. et al. A microRNA expression signature of human solid tumors defines cancer gene targets. *Proc. Natl. Acad. Sci. USA* **103**, 2257–2261 (2006).
80. Zhang, B. H. & Farwell, M. A. microRNAs: a new emerging class of players for disease diagnostics and gene therapy. *J. Cell. Mol. Med.* **12**, 3–21 (2008).
81. Rottiers, V. & Naar, A. M. MicroRNAs in metabolism and metabolic disorders. *Nat. Rev. Mol. Cell Biol.* **13**, 239–250 (2012).
82. Chen, B. et al. Roles of microRNA on cancer cell metabolism. *J. Transl. Med.* **10**, 228 (2012).
83. Lagos-Quintana, M. et al. Identification of tissue-specific microRNAs from mouse. *Curr. Biol.* **12**, 735–739 (2002).
84. Elmen, J. et al. LNA-mediated microRNA silencing in non-human primates. *Nature* **452**, 896–U10 (2008).
85. Esau, C. et al. miR-122 regulation of lipid metabolism revealed by in vivo antisense targeting. *Cell Metab.* **3**, 87–98 (2006).
86. Iliopoulos, D., Drosatos, K., Hiyama, Y., Goldberg, I. J. & Zannis, V. I. MicroRNA-370 controls the expression of microRNA-122 and Cpt1alpha and affects lipid metabolism. *J. Lipid Res.* **51**, 1513–1523 (2010).
87. Najafi-Shoushtari, S. H. et al. MicroRNA-33 and the SREBP Host Genes Cooperate to Control Cholesterol Homeostasis. *Science* **328**, 1566–1569 (2010).
88. Rayner, K. J. et al. MiR-33 contributes to the regulation of cholesterol homeostasis. *Science* **328**, 1570–1573 (2010).
89. Eichner, L. J. et al. miR-378(*) mediates metabolic shift in breast cancer cells via the PGC-1beta/ERRgamma transcriptional pathway. *Cell Metab.* **12**, 352–361 (2010).
90. Carrer, M. et al. Control of mitochondrial metabolism and systemic energy homeostasis by microRNAs 378 and 378*. *Proc. Natl. Acad. Sci. USA* **109**, 15330–15335 (2012).
91. Esau, C. et al. MicroRNA-143 regulates adipocyte differentiation. *J. Biol. Chem.* **279**, 52361–52365 (2004).
92. Shirasaki, T. et al. MicroRNA-27a regulates lipid metabolism and inhibits hepatitis C virus replication in human hepatoma cells. *J. Virol.* **87**, 5270–5286 (2013).
93. Nakanishi, N. et al. The up-regulation of microRNA-335 is associated with lipid metabolism in liver and white adipose tissue of genetically obese mice. *Biochem. Biophys. Res. Commun.* **385**, 492–496 (2009).
94. Xu, P. Z., Vernooy, S. Y., Guo, M. & Hay, B. A. The Drosophila microRNA mir-14 suppresses cell death and is required for normal fat metabolism. *Curr. Biol.* **13**, 790–795 (2003).
95. Cui, M. et al. MiR-205 modulates abnormal lipid metabolism of hepatoma cells via targeting acyl-CoA synthetase long-chain family member 1 (ACSL1) mRNA. *Biochem. Biophys. Res. Commun.* **444**, 270–275 (2014).
96. Menendez, J. A., Decker, J. P. & Lupu, R. In support of fatty acid synthase (FAS) as a metabolic oncogene: Extracellular acidosis acts in an epigenetic fashion activating FAS gene expression in cancer cells. *J. Cell. Biochem.* **94**, 1–4 (2005).
97. Fernandez-Hernando, C., Suarez, Y., Rayner, K. J. & Moore, K. J. MicroRNAs in lipid metabolism. *Curr. Opin. Lipidol.* **22**, 86–92 (2011).
98. Esser, V. et al. Inhibitors of mitochondrial carnitine palmitoyltransferase-I limit the action of proteases on the enzyme—isolation and partial amino-acid-analysis of a truncated form of the rat-liver isozyme. *J. Biol. Chem.* **268**, 5810–5816 (1993).
99. Yamazaki, N., Shinohara, Y., Shima, A. & Terada, H. High expression of a novel carnitine palmitoyltransferase-I like protein in rat brown adipose-tissue and heart—isolation and characterization of its Cdna clone. *FEBS Lett.* **363**, 41–45 (1995).
100. Ramsay, R. R., Gandour, R. D. & van der Leij, F. R. Molecular enzymology of carnitine transfer and transport. *Bba-Protein Struct. M.* **1546**, 21–43 (2001).
101. Bonnefont, J. P. et al. Carnitine palmitoyltransferases 1 and 2: biochemical, molecular and medical aspects. *Mol. Asp. Med.* **25**, 495–520 (2004).
102. Jogl, G., Hsiao, Y. S. & Tong, L. Structure and function of carnitine acyltransferases. *Ann. NY Acad. Sci.* **1033**, 17–29 (2004).

Oncogene (2017), 1–11

www.nature.com/onc

ORIGINAL ARTICLE

Deregulation of MicroRNAs mediated control of carnitine cycle in prostate cancer: molecular basis and pathophysiological consequences

A Valentino[1], A Calarco[1], A Di Salle[1], M Finicelli[2], S Crispi[2], RA Calogero[3], F Riccardo[3], A Sciarra[4], A Gentilucci[4], U Galderisi[5], S Margarucci[2] and G Peluso[1]

Cancer cells reprogram their metabolism to maintain both viability and uncontrolled proliferation. Although an interplay between the genetic, epigenetic and metabolic rewiring in cancer is beginning to emerge, it remains unclear how this metabolic plasticity occurs. Here, we report that in prostate cancer cells (PCCs) microRNAs (miRNAs) greatly contribute to deregulation of mitochondrial fatty acid (FA) oxidation via carnitine system modulation. We provide evidence that the downregulation of hsa-miR-124-3p, hsa-miR-129-5p and hsa-miR-378 induced an increase in both expression and activity of CPT1A, CACT and CrAT in malignant prostate cells. Moreover, the analysis of human prostate cancer and prostate control specimens confirmed the aberrant expression of miR-124-3p, miR-129-5p and miR-378 in primary tumors. Forced expression of the miRNAs mentioned above affected tumorigenic properties, such as proliferation, migration and invasion, in PC3 and LNCaP cells regardless of their hormone sensitivity. CPT1A, CACT and CrAT overexpression allow PCCs to be more prone on FA utilization than normal prostate cells, also in the presence of high pyruvate concentration. Finally, the simultaneous increase of CPT1A, CACT and CrAT is fundamental for PCCs to sustain FA oxidation in the presence of heavy lipid load on prostate cancer mitochondria. Indeed, the downregulation of only one of these proteins reduces PCCs metabolic flexibility with the accumulation of FA-intermediate metabolites in the mitochondria. Together, our data implicate carnitine cycle as a primary regulator of adaptive metabolic reprogramming in PCCs and suggest new potential druggable pathways for prevention and treatment of prostate cancer.

Oncogene advance online publication, 3 July 2017; doi:10.1038/onc.2017.216

INTRODUCTION

Cancer cells reprogram their metabolic pathways, including glycolysis, the Krebs cycle and fatty acid (FA) metabolism, to satisfy their need to proliferate, survive and metastasize.[1–3] This altered metabolism is a common denominator among heterogenic malignant cells and has been identified as one of the hallmarks of cancer.

Tumor cells proliferation is supported by aerobic glycolysis in which pyruvate is transformed into lactate independently of the presence of oxygen (Warburg effect), and not by fatty acid oxidation (FAO), the primary source of energy production in normal cells.

Additional metabolic peculiarities of tumor cells are the high rate of glutamine oxidation and the increase of FA synthesis. This reorganization of cancer metabolism is fundamental to satisfy the energy as well as the biosynthetic intermediate request of proliferating cells and to preserve the integrity of the cells from the harsh and hypoxic environment.[4–7]

However, although FA synthesis is within a clear metabolic framework, the extent of the role of FA catabolism, as the energy and materials sources for cancer proliferation, is still being deciphered.

A particularly intriguing example of how FAs have potential to fuel tumor cells occurs with prostate cancer. The metabolism of the normal prostate cells is changed greatly upon transformation.[8–10]

The normal prostate cells have a truncated Krebs cycle where the neo-synthesized citrate is a secretory product rather than an intermediate of metabolism. Thus, in the prostate, the ATP production derives via aerobic glycolysis, with less dependence on aerobic oxidation.

An increase in oxidative phosphorylation is a requirement for the progression of the prostate tumor, and so a continuous supply of acetyl-CoA is required to ensure citrate oxidation via the Krebs cycle.[11,12] As prostate cancer cells (PCCs) exhibit a low rate of glycolysis, FAO serves as the main source of acetyl-CoA, and by extension, ATP (Figure 1).[13–15]

The need for lipids of prostate neoplastic tissue can be satisfied by several mechanisms.[16] The uptake of circulating lipids and the transfer of FA from stromal adipocytes to PCCs increase *de novo* synthesis of lipids and phospholipids, and accumulation of cholesteryl ester as cytosolic lipid droplets.[16] Unlike this metabolic reprogramming, alterations in lipid-associated pathways encountered in prostate cancer remain ill-defined.

FAs used as energy substrate require ~25 different enzymes and transport proteins, which carry out the cellular uptake and activation of FAs, their translocation into the mitochondrial matrix, and their β-oxidation. In particular, the mitochondrial inner

[1]Institute of Agro-environmental and Forest Biology, National Research Council, IBAF – CNR, Naples, Italy; [2]Institute of Bioscience and BioResources – CNR, Naples, Italy; [3]Department of Molecular Biotechnology and Health Sciences, Laboratory of Immunology, University of Turin, Turin, Italy; [4]Prostate Cancer Unit, Department Urology, University 'Sapienza', Policlinico Umberto I, Rome, Italy and [5]Department of Experimental Medicine, Biotechnology and Molecular Biology Section, University of Campania 'Luigi Vanvitelli', Naples, Italy. Correspondence: Professor G Peluso, Institute of Agro-environmental and Forest Biology, National Research Council, IBAF – CNR, via P. Castellino,111, Naples, Italy. E-mail: gianfranco.peluso@ibaf.cnr.it
Received 21 October 2016; revised 9 May 2017; accepted 17 May 2017

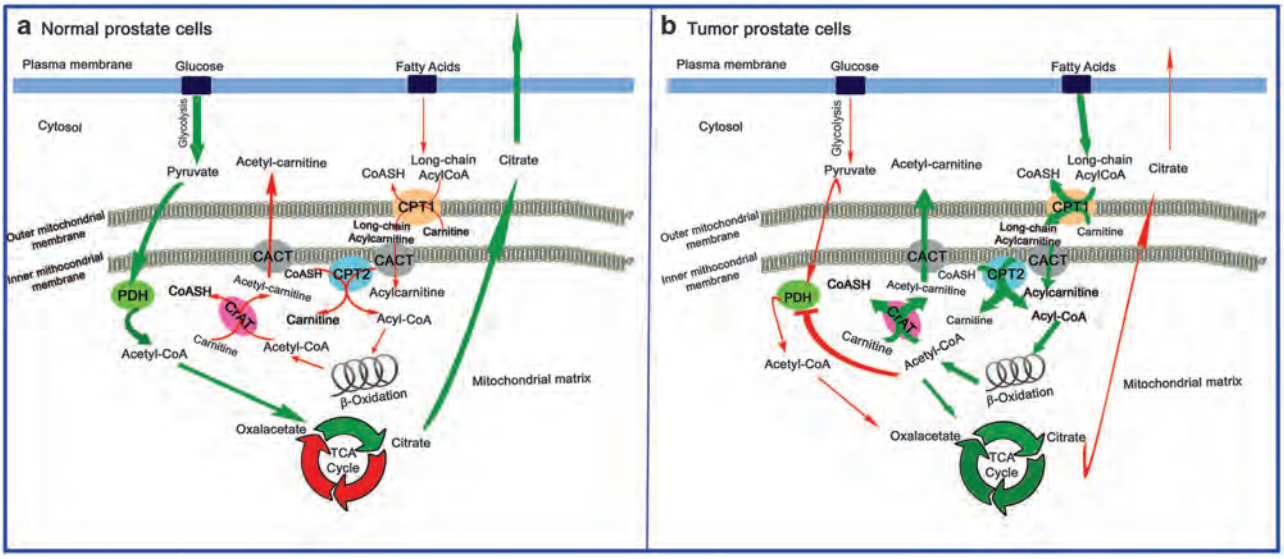

Figure 1. Schematic representation of metabolic differences between normal and cancer prostate cells. (**a**) In normal prostate cells, ATP is obtained mainly via glycolytic pathway and citrate is an end-product of glucose metabolism, rather than an utilizable intermediate. The truncated Krebs cycle allows to synthesize citrate from acetyl-CoA and oxaloacetate and to export citrate from the mitochondria to the cytosol by the mitochondrial citrate transporter. (**b**) In cancer prostate cells, FAO is the dominant bioenergetic pathway, and the carnitine cycle regulates the FA mitochondrial import/export, and the intra-mitochondrial acyl-CoA pools. Three components of the carnitine system (CPT1, CACT and CrAT) are upregulated in prostate cancer cells and work closely together to ensure mitochondrial FA supply and to avoid the mitochondrial side effects of FA overloading (that is, intra-mitochondrial accumulation of FAO intermediates). The intra-mitochondrial acetyl-CoA increase, imposed by the heavy lipid load, allosterically inhibits PDH that catalyzes the rate-limiting oxidative decarboxylation of pyruvate into acetyl-CoA. (FAO, fatty acid oxidation; FA, fatty acid; PDH, pyruvate dehydrogenase complex; CPT1, carnitine-palmitoyltransferase-1; CACT, carnitine-acylcarnitine translocase; CrAT, carnitine acetyltransferase. Green arrows: dominant metabolic pathway).

membrane is impermeable to fatty acyl-CoA thioesters and, thus, a specific system for transporting FAs across mitochondrial membranes has evolved.[17] The most important limiting steps of beta-oxidation is represented by a group of four carnitine acyltransferases, which govern FA mitochondrial import/export and regulate intra-mitochondrial acyl-CoA pools.[18]

It is known that the transport of long-chain FAs across the mitochondrial membrane depends on a complicated mechanism regulated by the carnitine system. Components of the carnitine systems are both enzymes able to catalyze the acyl-CoA +carnitine ↔ CoA+acylcarnitines reaction and carrier(s) involved in the bi-directional transport of acyl moieties from cytosol to mitochondria and *vice-versa*. The long-chain FA-CoA are converted into the carnitine derivatives by carnitine-palmitoyltransferase-1 (CPT1), an integral protein located on the outer mitochondrial membrane of the contact sites.[19] Acylcarnitines are transported into the mitochondrial matrix by carnitine-acylcarnitine translocase (CACT), that also exports by-products of FAO, such as acetylcarnitines, from mitochondria to cytosol.[20] In the mitochondrial matrix, long-chain acylcarnitines are reconverted to the respective long-chain acyl-CoAs by carnitine-palmitoyltransferase-2 (CPT2).[19] Finally, the enzyme carnitine acetyltransferase (CrAT) catalyzes the addition or the removal of carnitine from acetyl-CoA, promoting the efflux of two carbon acetyl units from mitochondria to cytosol and buffering the intra-mitochondrial pools of acetyl-CoA.[21] Despite the important role that the carnitine system can play in cancer cell metabolism, little is known about the expression level of each and every component of the system in cancer cells. Also, only scattered information is available about the epigenetic control of carnitine system related-gene expression in tumors, although there is evidence that microRNAs (miRNAs) can modulate the expression of CPT1 or CACT in normal cells undergoing metabolic stress condition (Figure 1).[22–25]

In the present study, we examined, in three prostate cell lines, PNT2 (prostate control cells), LNCaP (androgen-dependent PCCs) and PC3 (androgen-independent PCCs), the expression and biological significance of all the components of the carnitine system. We first demonstrated that malignant prostate cells increase both expression and activity of some components of the carnitine system, specifically CPT1A, CACT and CrAT. Next, we provided, for the first time, evidence that the overexpression of these proteins is regulated by the concordant decrease of specific miRNAs (hsa-miR-124-3p, hsa-miR-129-5p and hsa-miR-378) in both LNCaP and PC3 cells, regardless of their hormone sensitivity. Of interest, we demonstrated that control of the carnitine system by miRNAs is present also in prostate tissue specimens obtained from patients suffering from prostate cancer.

Our results give oncogenic relevance to the carnitine system and underline the biological role of the carnitine cycle in the maintenance of cancer metabolic flexibility. Therefore, the evaluation of CPT1A/CACT/CrAT proteins could provide additional predictive markers over conventional analysis in prostate cancer. Finally, these findings may suggest new druggable pathways for prevention and treatment of prostate cancer.

RESULTS

Carnitine system in prostate cells

Enhanced mitochondrial β-oxidation of FAs, such as palmitate, has been linked to tumor promotion in prostate cancer.[13,14,26] Indeed, we observed higher oxidation rate of palmitate in PC3 cells than in PNT2 cells, supporting that PCCs promote FAO as the dominant pathway to meet tumor bioenergetic requirements (Figure 2a).

To investigate whether increased β-oxidation was related to an increased flux of FAs into the mitochondria via changes in key carrier levels, we analyzed the expression (both at mRNA and protein levels) as well as the activity of CPT1, CPT2, CACT and CrAT.

As shown in Figure 2b, mRNA expression levels of *CPT1A*, *CACT* and *CRAT* were significantly upregulated in PC3 respect to PNT2

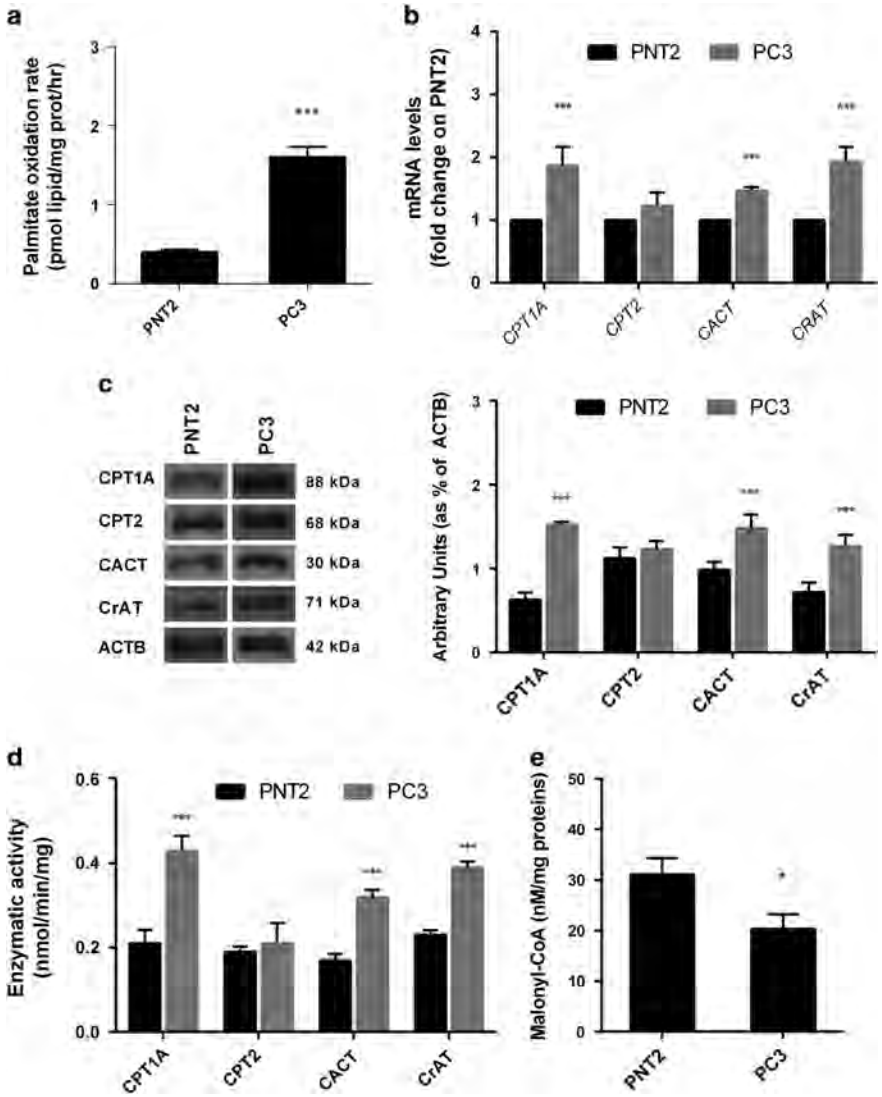

Figure 2. FAO and carnitine system analysis in PNT2 and PC3 cells. (**a**) Palmitate oxidation determined as [$^{14}CO_2$] production was measured in mitochondrial-enriched fractions. All values were normalized to the mitochondrial protein content and data expressed as mean ± s.d. ($n = 3$). (**b**) *CPT1A, CPT2, CACT* and *CRAT* mRNA levels were determined by quantitative real-time PCR and normalized to the housekeeping β-actin (*ACTB*). The comparative cycle threshold (CT) method ($2^{-\Delta\Delta CT}$) was applied to calculate relative differences in PCR results. (**c**) Western blot analysis of CPT1A, CPT2, CACT, CrAT and ACTB. Densitometric analyses were performed using Quantity One 1-D analysis software (BioRad, Italy). (**d**) The enzymatic activities were determined in mitochondria as described in materials and methods section and normalized for the mitochondrial protein contents. (**e**) Malonyl-CoA level was measured in PNT2, and PC3 cells and values were normalized to total protein content. The bars represent the means ± s.d. ($n = 6$). Statistically significant variations: $^*P < 0.05$, $^{**}P < 0.01$, $^{***}P < 0.005$ versus PNT2.

cells ($P < 0.05$), whereas no statistically significant difference was observed for *CPT2* expression. Western blot analysis confirmed that CPT1A, CACT and CrAT proteins were markedly more expressed in tumor cell lines than in normal prostate cell line (Figure 2c).

To evaluate whether the observed increased expression of CPT1A, CACT and CrAT could be consistent with a gain of function of these proteins, enzyme activities were assayed. As showed in Figure 2d, we demonstrated that the activities of CPT1A, CACT and CrAT were markedly higher in PC3 mitochondria than in control PNT2 mitochondria.

To sustain an enhanced FAO, PCCs have to maintain a low level of malonyl-CoA, the CPT1A physiological allosteric inhibitor. Therefore, we analyzed the malonyl-CoA concentration in all cell lines and demonstrated that the amount of malonyl-CoA was significantly lower ($P < 0.05$) in malignant cells than in PNT2 cells (Figure 2e).

miRNAs expression in prostate cell lines

Recent studies highlighted the pivotal role of miRNAs in the finely post-transcriptional adjustment of enzymes involved in metabolic reprogramming of cancer cells.[27,28] Our preliminary examination of the miRNAs content in malignant and normal prostate cells with Small RNA App (CORE App in Illumina BaseSpace cloud), showed a very different overall content of RNA fragments (Supplementary Figure S1a) corroborated by the differential expression analysis. In particular, DESeq2 detected a total of 417 miRNAs differentially expressed using as threshold $|\log2(PC3/PNT2)| \geqslant 1$ and FDR $\leqslant 0.1$ (Supplementary Figure S1b).[29] A more rigorous analysis, $|\log2(PC3/PNT2)| \geqslant 3.5$, *P*-value $\leqslant 10^{-5}$ and FDR $\leqslant 0.1$, revealed a total of 80 miRNAs differentially expressed in the PC3 compared with PNT2, including 32 miRNAs upregulated and 48 miRNAs downregulated (Supplementary Table S2).

Then, we selected three specific miRNAs (hsa-miR-129-5p, hsa-miR-124-3p and hsa-miR-378) identified by miRNA target

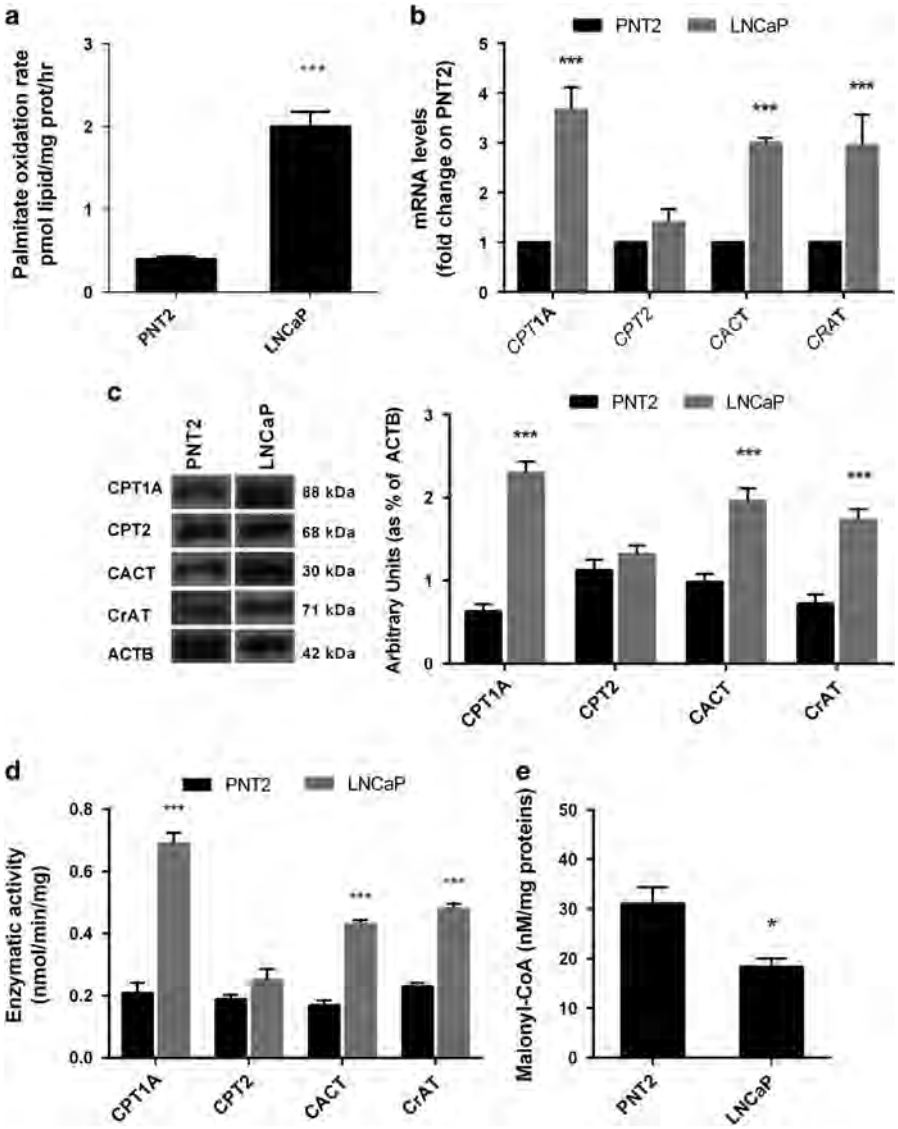

Figure 3. FAO and carnitine system analysis in LNCaP cells. (**a**) Palmitate oxidation determined as [$^{14}CO_2$] production was measured in mitochondrial-enriched fractions. All values were normalized to the mitochondrial protein content and data expressed as mean ± s.d. ($n = 3$). (**b**) *CPT1A, CPT2, CACT* and *CRAT* mRNA levels were determined by quantitative real-time PCR and normalized to the housekeeping β-actin (*ACTB*). The comparative cycle threshold (CT) method ($2^{-\Delta\Delta CT}$) was applied to calculate relative differences in PCR results. (**c**) Western blot analysis of CPT1A, CPT2, CACT, CrAT and ACTB. Densitometric analyses were performed using Quantity One 1-D analysis software (BioRad, Italy). (**d**) The enzymatic activities were determined in mitochondria as described in materials and methods section and normalized for the mitochondrial protein contents. (**e**) Malonyl-CoA level was measured in PNT2, and LNCaP cells and values were normalized to total protein content. The bars represent the means ± s.d. ($n = 6$). Statistically significant variations: $^*P < 0.05$, $^{**}P < 0.01$, $^{***}P < 0.005$ versus PNT2.

prediction algorithms as possible intermediaries in the regulation of carnitine cycle proteins. Web-based tools identified *CACT* as a target of hsa-miR-129-5p (downregulated by 4.9-fold in PC3 respect to PNT2), *CPT1A* as a target of hsa-miR-124-3p (downregulated by 3.5-fold) and *CRAT* as a target of hsa-miR-378 (downregulated by 3.5-fold). Indeed, sequence analysis revealed that the 3′-untranslated region (UTRs) of *CACT*, *CPT1A* and *CRAT* contain the putative binding site for the identified miRNAs (Supplementary Figure S2).

CPT1A, CACT and CrAT are direct targets of hsa-miR-124-3p, hsa-miR-129-5p and hsa-miR-378

To determine whether the carnitine system deregulation was a common signature in prostate cancers, we analyze the palmitate oxidation rate and the expression both at the transcriptional and translational level of CPT1A, CACT and CRAT in LNCaP, a well-known model of androgen-dependent PCC line. As shown in Figure 3, LNCaP exhibited, respect to PNT2, a markedly upregulation of CPT1A, CACT and CrAT at mRNA (Figure 3b) and protein levels (Figure 3c) and an increased β-oxidation (Figure 3a). Functional assays and malonyl-CoA determination corroborated these results showing an overall increase in enzymatic activity (Figure 3d) and a decrease of malonyl-CoA concentration (Figure 3e).

Next, to validate miRNAs sequencing in both the androgen-independent (PC3) and androgen-dependent (LNCaP) prostate tumor cells, the endogenous levels of identified miRNAs were analyzed by TaqMan-based quantitative real-time PCR (qPCR). Consistent with bioinformatic analysis, a statistically significant downregulation of hsa-miR-129-5p, hsa-miR-124-3p and hsa-miR-378 was evident in both tumor cells compared with PNT2 (Figure 4a).

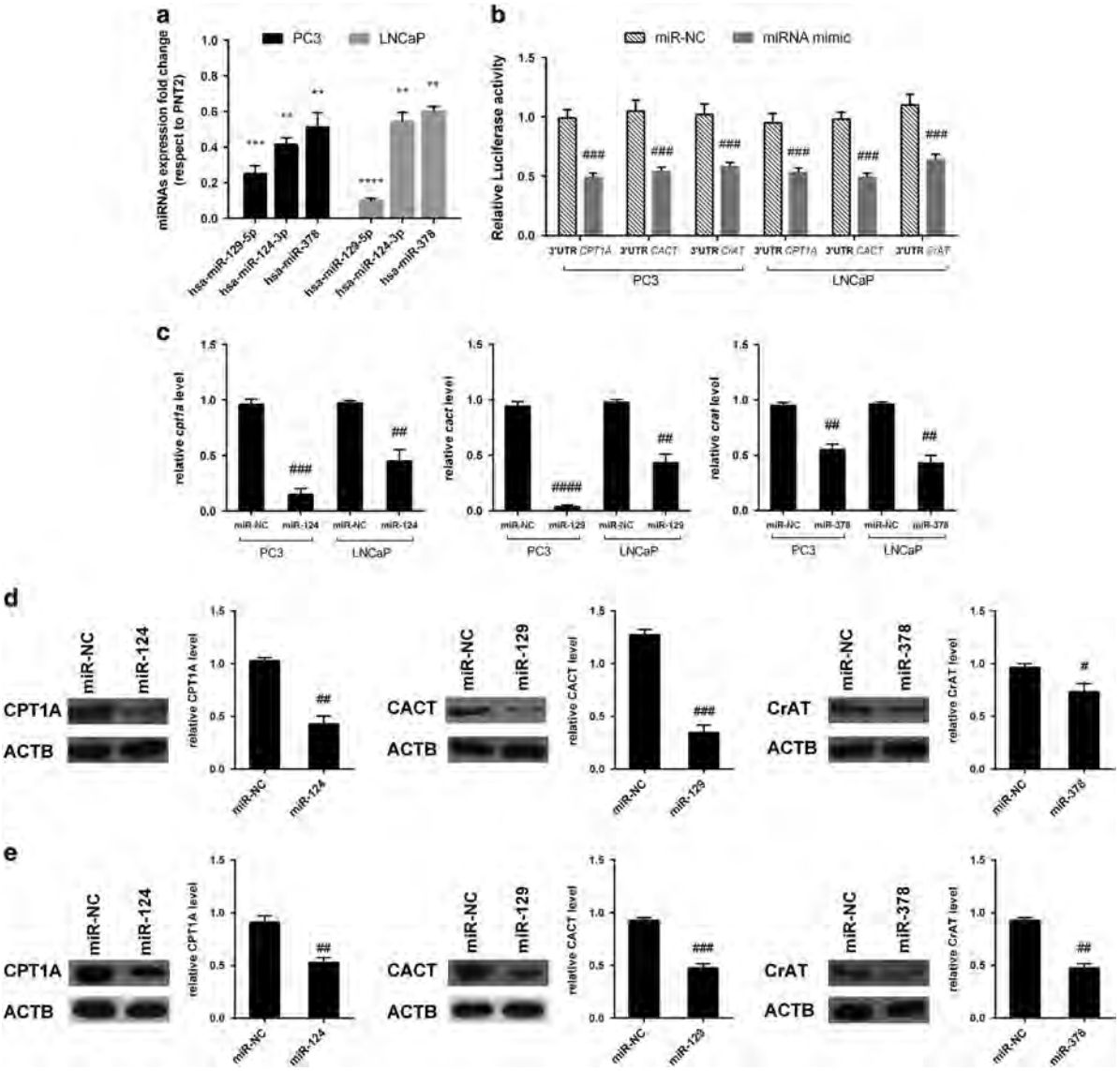

Figure 4. Validation of CPT1A, CACT and CrAT as targets of miR-124, miR-129 and miR-378 in PC3 and LNCaP cells. (**a**) qPCR validation of differentially expressed miRNAs in PC3 and LNCaP respect to PNT2. Detection of miRNAs was performed by TaqMan qPCR miRNA assay and normalized to RNU6B. The comparative cycle threshold (CT) method ($2^{-\Delta\Delta CT}$) was applied to calculate relative differences in PCR results. (**b**) Luciferase reporter assays. PC3 and LNCaP cells were transfected with 3′-UTR-reporter constructs together with miRNA mimics. miR-NC was used as negative control, and the results were normalized to *Renilla* luciferase activity. (**c**) MiRNA targets levels were detected in PC3 and LNCaP cells by qPCR and normalized to *ACTB*. The comparative cycle threshold (CT) method (2-ΔΔCT) was applied to calculate relative differences in PCR results. Western blot analysis of CPT1A, CACT and CrAT proteins was performed on total protein fraction of PC3 (**d**) and LNCaP (**e**). The protein expression was normalized to the housekeeping protein ACTB. The bars represent the means ± s.d. ($n = 6$). Statistically significant variations: $^{**}P < 0.01$, $^{***}P < 0.005$, $^{****}P < 0.001$ versus PNT2; $^{\#}P < 0.05$, $^{\#\#}P < 0.01$, $^{\#\#\#}P < 0.005$, $^{\#\#\#\#}P < 0.001$ miRNAs versus miR-NC.

To verify if hsa-miR-129-5p, hsa-miR-124-3p and hsa-miR-378 directly bind with 3′ UTRs of *CACT*, *CPT1A* and *CRAT*, luciferase reporter assay was carried out. Each corresponding 3′-UTR sequence, inserted into a luciferase reporter plasmid, was co-transfected with miR-124, miR-129 or miR-378 into PC3 and LNCaP cells (Figure 4b). Our results demonstrated that the identified miRNAs significantly ($P < 0.005$) inhibited the activity of firefly luciferase confirming that *CPT1A*, *CACT* or *CRAT* mRNAs are direct the target of the corresponding miRNAs. Next, the effect of miRNA mimics overexpression on the mRNA and protein levels of identified targets was examined. The qPCR (Figure 4c) and western blot (Figures 4d and e) analyses showed that miR-129, miR-124 or miR-378 markedly suppressed the mRNA and protein expression levels of CPT1A, CACT or CrAT, in comparison with miR-NC. Taken together, these findings suggest that hsa-miR-124-3p, hsa-miR-129-5p and hsa-miR-378 are involved in modulating, at the post-transcriptional level, the expression of CPT1A, CACT and CrAT in both PCC lines.

Anti-tumorigenic effects of identified miRNAs in PCCs

To evaluate the tumorigenic potential of PCCs overexpressing miR-124, miR-129 or miR-378, the proliferative cell rate, and the cell migration and invasive ability were analyzed on PC3, and LNCaP transfected with miRNA mimics as well as miR-NC (Figures 5 and 6). The MTT proliferation test demonstrated that overexpression of each miRNA mimics was able to decrease

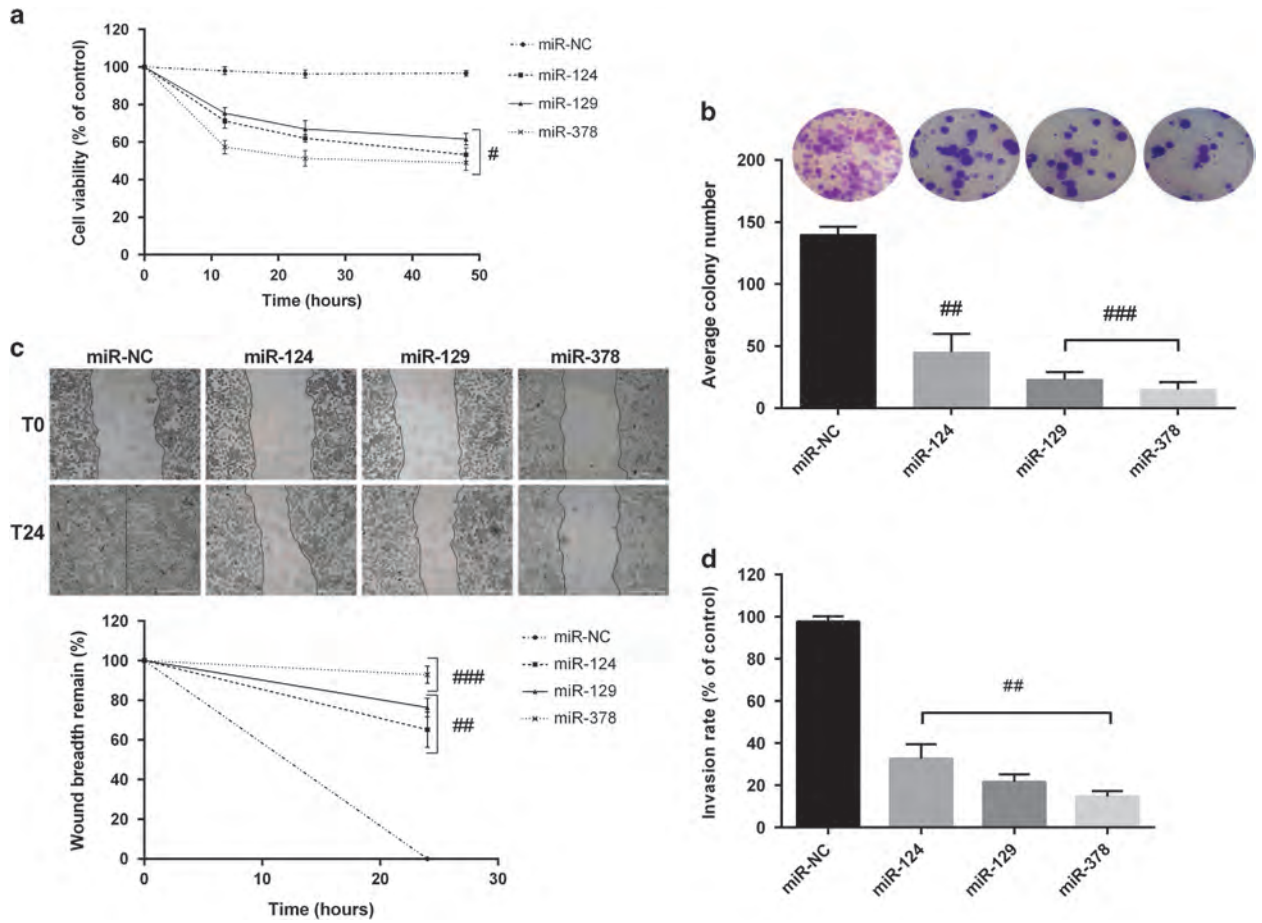

Figure 5. Influence of forced expression of miR-124, miR-129 and miR-378 on PC3 proliferation, migration and invasion. (**a**) Cell proliferation of PC3 cells was determined by MTT assay after 12, 24 and 48 h. (**b**) Colony formation assay was performed after 14 days of culture. For quantification colonies with at least 50 cells were considered. Representative micrographs were obtained using phase contrast microscope after staining with crystal violet. (**c**) Wound-healing assay was performed on transfected PC3 cells, and the wound closure rate was measured by detecting the closure distance after 24 h. Representative micrographs of the cell migration (up) and quantification (down) from three independent experiments were presented. (**d**) Transwell invasion assay with Matrigel was performed in mimics or miR-NC transfected PC3 cells after 24 h. Five random fields in each well were counted under a microscope. The bars represent the means ± s.d. ($n = 6$). Statistically significant variations: $^{\#}P < 0.05$, $^{\#\#}P < 0.01$, $^{\#\#\#}P < 0.005$ miRNAs versus miR-NC.

significantly ($P < 0.05$) PC3 and LNCaP cell growth (Figures 5a and 6a). The colony formation assay, which reflects the self-renewal ability of transfected cells, also showed that the gain of function of miR-124, miR-129 or miR-378 reduced prostate cancer colony formation (Figures 5b and 6b).

As assessed by a wound-healing assay (Figure 5c), the migration capability of PC3 cells was significantly inhibited by the over-expression of miR-124 (65%, $P < 0.01$), miR-129 (75%, $P < 0.01$) and miR-378 (93%, $P < 0.005$). Moreover, the number of PC3 cells crossed Matrigel was markedly decreased by 85–70% compared with the control cells (Figure 5d).

Similarly, forced expression of miR-124, miR-129 or miR-378 in LNCaP cells negatively modulate migration and invasion (Figures 6c and d). In particular, the wound gap was >93%, and the number of cells migrating to the lower chamber decreased by >80% after each miRNA mimics transfection in comparison with miR-NC transfection. To further validate the regulatory role of miRNAs on the identified targets expression, rescue experiments were performed in both cell lines. The transient transfection of exogenous CPT1A, CACT or CrAT lacking their 3'UTR with each mimic, rescued tumorigenic potential of PCCs (Supplementary Figure S3 and S4) confirming the regulatory role of miRNAs on the identified targets expression.

Overexpression of miR-124, miR-129 and miR-378 modulates mitochondrial FA flux modifying intracellular acylcarnitine contents

Tumor cells can rapidly switch between fat and glucose oxidation exhibiting a metabolic flexibility in response to nutrients availabilities.[30] These raises the question of whether upregulated carnitine cycle is responsive to fluctuations in the nutrient state. As shown in Figures 7a and b, PC3 and LNCaP cancer cells exhibited, also in the presence of pyruvate concentration up to 0.2 mM, a significant increase of [1-^{14}C]palmitate oxidation when compared with PNT2 control cells.

Next, to provide an index of how the PCCs metabolically respond to carnitine cycle perturbation induced by overexpression of each miRNA, the evaluation of both ASAC (acid-soluble, short and medium chains) and AIAC (acid-insoluble, long-chains) acylcarnitines content in miRNAs transfected PC3 and LNCaP cells was determined (Figures 7c and d). Forced expression of miR-129 or miR-378 induced a significant increase ($P < 0.005$) in AIAC content in both cancer cell lines respect to miR-NC transfected cells. On the contrary, the downregulation of CPT1A expression by miR-124, limiting the conversion of long-chain acyl-CoA moieties to long-chain acylcarnitine, led to a significant decrease ($P < 0.005$) in AIAC content. Moreover, miR-124 and miR-129 overexpressing cells did not exhibit any significant difference in

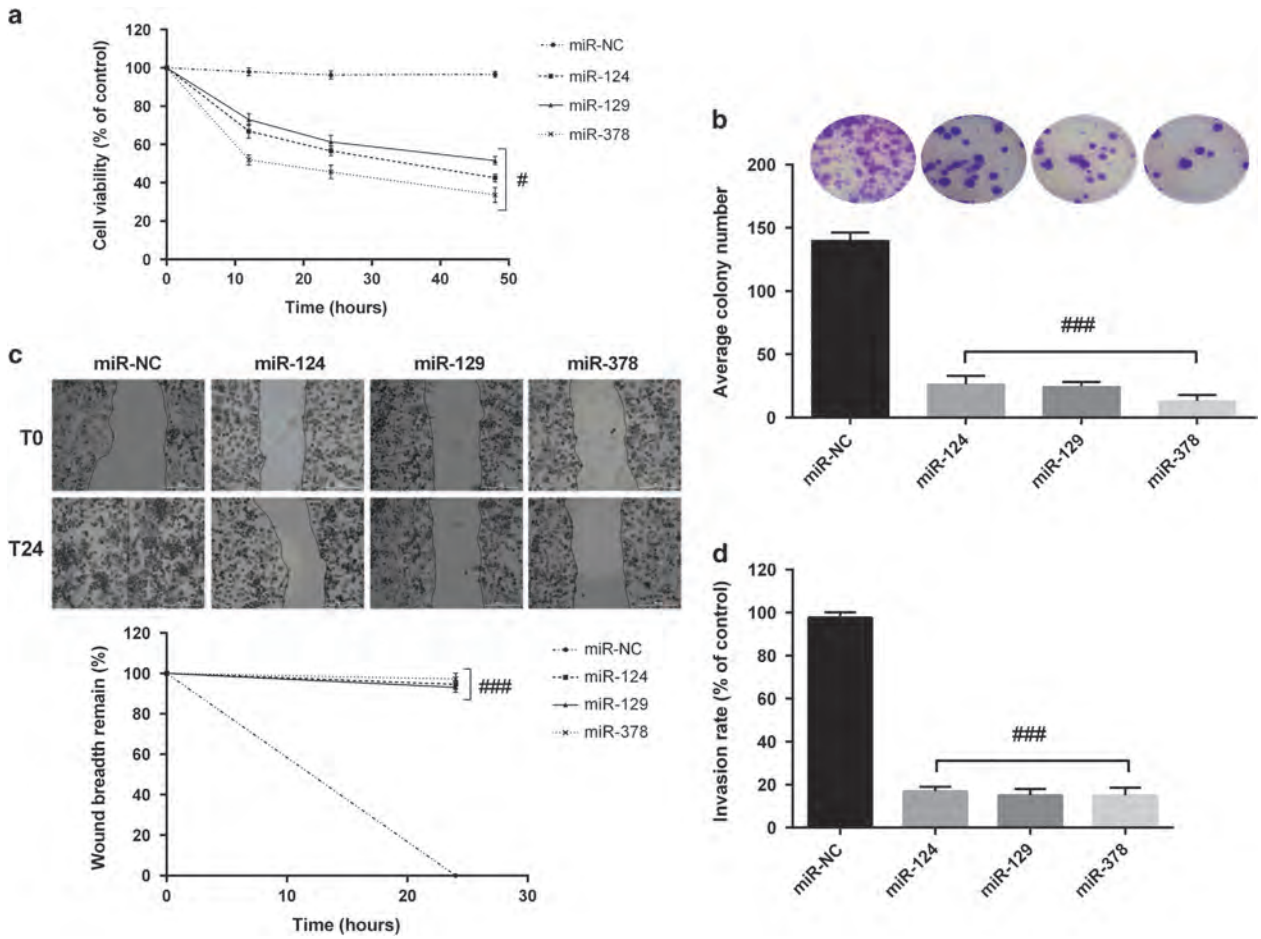

Figure 6. Influence of forced expression of miR-124, miR-129 and miR-378 on LNCaP proliferation, migration and invasion. (**a**) Cell proliferation of LNCaP cells was determined by MTT assay after 12, 24 and 48 h. (**b**) Colony formation assay was performed after 14 days of culture. For quantification colonies with at least 50 cells were considered. Representative micrographs were obtained using phase contrast microscope after staining with crystal violet. (**c**) Wound-healing assay was performed on transfected LNCaP cells, and the wound closure rate was measured by detecting the closure distance after 24 h. Representative micrographs of the cell migration (up) and quantification (down) from three independent experiments were presented. (**d**) Transwell invasion assay with Matrigel was performed in mimics or miR-NC transfected LNCaP cells after 24 h. Five random fields in each well were counted under a microscope. The bars represent the means ± s.d. ($n = 6$). Statistically significant variations: $^{\#}P < 0.05$, $^{\#\#}P < 0.01$, $^{\#\#\#}P < 0.005$ miRNAs versus miR-NC.

ASAC content in comparison with control miR-NC transfected cells, while the transfection with miR-378 led to a relevant ASAC reduction.

Taken together, these results suggest that the FA addiction of PC3 and LNCaP cells is conferred by the constitutive upregulation of the carnitine cycle, and that inhibition of CPT1A, CACT or CrAT expression blocks the ability of PCCs to completely metabolize lipid substrates, leading to abnormal cell acylcarnitine profiles.

miRNAs overexpression in tissue specimens of prostate cancer

Owing to the highly heterogeneous nature of prostate cancer, a laser capture microdissection microscope was used on 30 FFPE prostatectomy. Laser capture microdissection allows to determine the densest region of tumor and capture as much tumor RNA as possible enriching for malignant glands and avoiding contamination with stromal tissue or non-malignant glands. The expression of the identified miRNAs and their targets in laser capture samples was analyzed by qPCR. As shown in Figures 8a–c, a significantly decreased expression ($P < 0.001$) of hsa-miR-129-5p, hsa-miR-124-3p and hsa-miR-378 was observed in all of the tumor samples compared with normal controls, demonstrating the same down-regulation identified in PCCs. Moreover, *CPT1A*, *CACT* and *CRAT* expression levels (Figure 8d-f) were significantly ($P < 0.001$) upregulated in all the tumor samples respect to controls.

DISCUSSION

The complex molecular events that govern FA metabolic pathway (s) during prostate cancerogenesis are largely unknown. Here, we report that in PCCs, hsa-miR-129-5p, hsa-miR-124-3p and hsa-miR-378 downregulation greatly contribute to deregulation of mitochondrial FAO. We clarify how miRNAs perturbation of carnitine cycle promotes a novel metabolic adaptation of PCC to support cancer development and progression.

In the last few years, systematic profiles detailing the miRNA expression in prostate cancer vs normal prostate cells have demonstrated both up- and downregulated miRNA patterns.[31–33] However, the results of these studies were highly contradictory, and their discrepancies may be explained by differences in tissue selection, RNA and the platforms used for the detection.[34] Moreover, Gill *et al.*[35] highlighted the need for seeking an accurate link between miRNAs and prostate cancer through an understanding of the signaling pathways that these miRNAs control, to identify therapeutically attractive molecular targets.

At our knowledge, only one paper has analyzed the regulation of lipogenesis and cholesterogenesis by miRNA in prostate tumor

cells, while no information is available in the scientific literature about the epigenetic control of FAO-associated genes in prostate cancer.[36]

For the first time, we demonstrated that hsa-miR-124-3p, hsa-miR-129-5p and hsa-miR-378 regulated CPT1A, CACT and CrAT expression in PCCs, regardless of their hormone sensitivity.

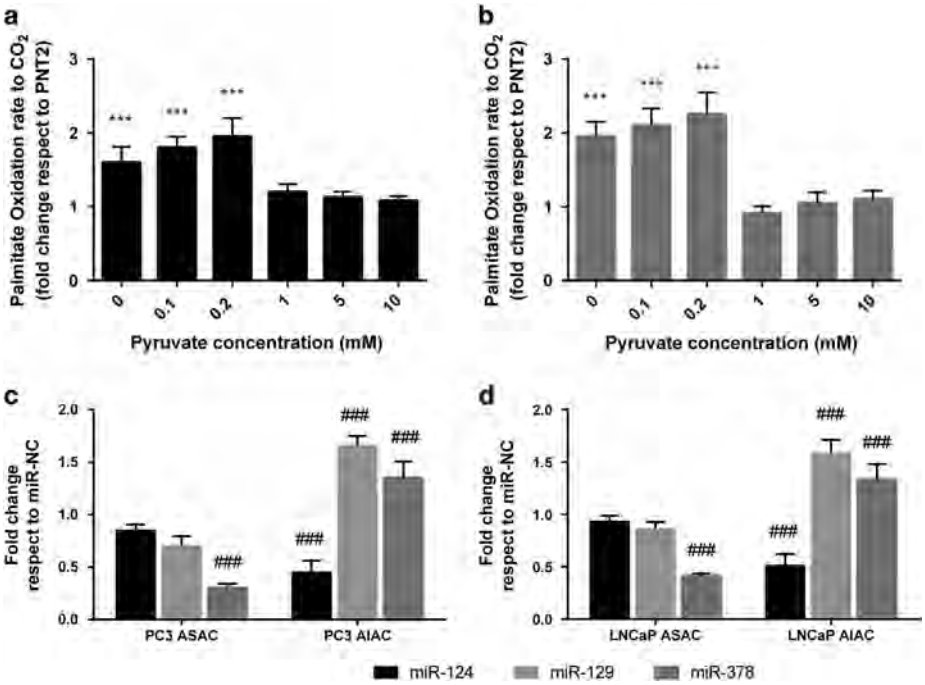

Figure 7. Evaluation of prostate cancer cell FA metabolism. The [1-^{14}C]palmitate oxidation rate in PC3 (**a**) or LNCaP (**b**) cells was measured in the presence of different concentration of pyruvate (0–10 mM). All values were normalized to the mitochondrial protein content, and results are reported as fold change respect to PNT2 oxidation rates. Acid-soluble (ASAC) and acid-insoluble (AIAC) acylcarnitines content was determined by the radioisotopic method in transfected PC3 (**c**) and LNCaP (**d**) cells. Results are reported as fold change respect to miR-NC transfected cells. The bars represent the means ± s.d. ($n = 6$). Statistically significant variations: ***$P < 0.005$ versus PNT2; $^{###}P < 0.005$ miRNAs versus miR-NC.

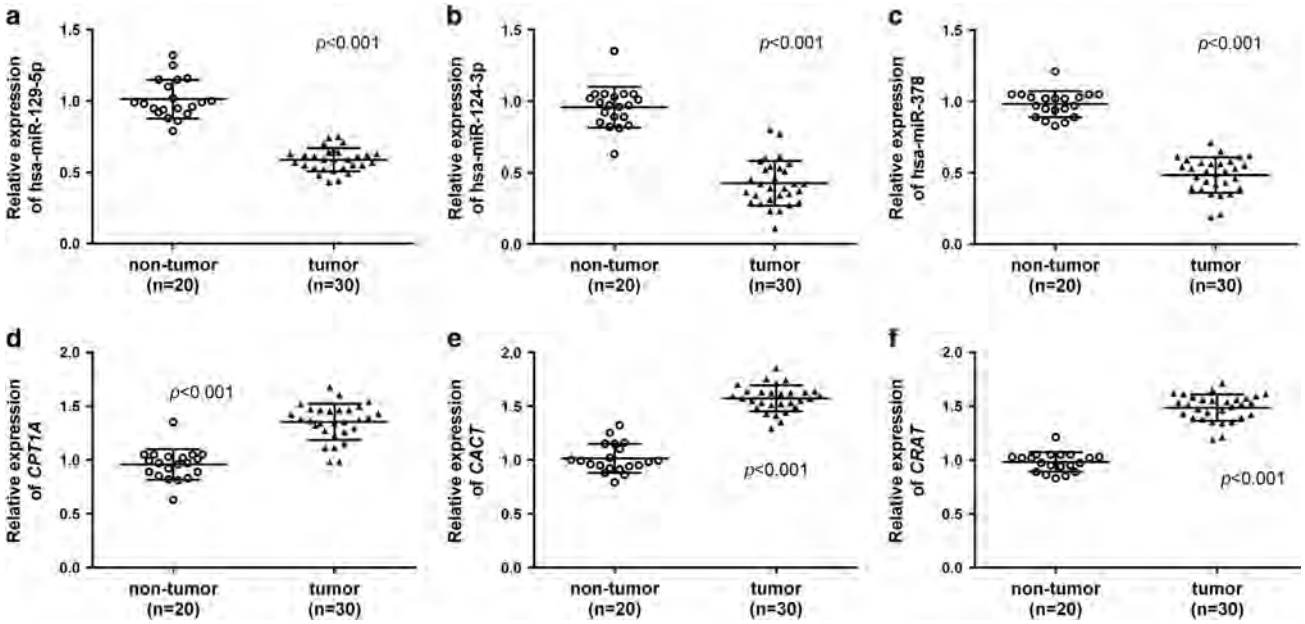

Figure 8. Expression of identified miRNAs in laser capture samples of prostate cancer. (**a**) hsa-miR-129-5p, (**b**) hsa-miR-124-3p and (**c**) hsa-miR-378 expression levels were detected in 30 formalin-fixed-paraffin-embedded (FFPE) prostatectomy tissue and in 20 FFPE normal epithelial tissue samples after LCM. Detection of miRNAs was performed by TaqMan qPCR miRNA assay and normalized to RNU6B. The relative differences were calculated using the $2^{-\Delta Ct}$ method. (**d**) *CPT1A*, (**e**) *CACT* and (**f**) *CRAT* mRNA levels were determined by quantitative real-time PCR and normalized to the housekeeping β-actin (ACTB). The comparative cycle threshold (CT) method (2-ΔΔCT) was applied to calculate relative differences in PCR results. The bars represent the means ± s.d.

miR-124 is known to function as a tumor suppressor in many cancers.[37,38] Shi *et al*.[39] demonstrated that miR-124 downregulation was a hallmark of malignant prostatic cells, and could contribute to the pathogenesis of prostate cancer. Our study suggests a new fundamental role for miR-124 in modulating CPT1A expression in PCCs. This overexpression, associated with an increased activity of CPT1A seems to be apparently in contrast with the lipogenic activity normally exacerbated in prostate cancer. In general, FA synthesis and FAO are mutually exclusive metabolic pathways, under the control of malonyl-CoA, an intermediate in FA synthesis. Malonyl-CoA acts as an allosteric inhibitor of CPT1 preventing FA biosynthesis and FAO from occurring simultaneously.[40] Surprisingly, we demonstrated that the amount of malonyl-CoA was extremely low in PCCs, indicating that the high rate of FA synthesis keeps a low level of malonyl-CoA. Thus, the overexpression of CPT1A, together with the loss of allosteric inhibition by malonyl-CoA, imposes a heavy lipid load on prostate cancer mitochondria.

miR-129-5p is deregulated in several tumors, such as laryngeal cancer, neuroendocrine tumors, gastric cancer and medullary thyroid carcinoma.[41–44] Ma *et al*.[45] reported that low miR-129-5p expression was strongly correlated with cancer invasion, recurrence and poor survival in hepatocellular carcinoma. Here we identified CACT as a novel target of miR-129-5p in prostate cancer.

CACT overexpression coordinates both the import of acylcarnitines inside the mitochondrial matrix in exchange of free carnitine, contributing to the increased FAO and the export of excess FAO intermediates as carnitine derivatives, thus avoiding intramitochondrial accumulation of acyl units.[46]

Recent findings have reported that in breast cancer cells the expression of miRNA-378 results in a shift from aerobic oxidative metabolism to glycolytic metabolism in the presence of available oxygen (Warburg effect) as represented by an increase in lactate levels and a reduction in oxygen consumption.[47] Thus, miRNA-378 counterbalances the metabolic actions of PGC-1β that orchestrates cellular programs of oxidative metabolism, by regulating the biogenesis of mitochondria and controlling the enzymes involved in oxidative phosphorylation.[48] Interestingly, it was found that CrAT is repressed by miR-378.[49] As CrAT decreases acetyl-CoA and regenerates free CoA, chronic inhibition of CrAT expression by miRNA-378 has the potential to raise the mitochondrial acetyl-CoA/CoA ratio to a level that promotes pyruvate dehydrogenase phosphorylation inhibiting glucose oxidation.[50] Conversely, in our study, we demonstrate that in PCCs miRNA-378 was downregulated leading to a concomitant increase of CrAT. Such high amounts of CrAT, which essentially siphons acetyl-CoA from the TCA cycle, are not in contrast with the FA-dependent metabolism of PCCs. Besides, the conversion of short-chain acyl-CoAs to their acylcarnitine counterparts by CrAT permits a CACT-dependent export of acyl moieties from mitochondria to cytosol avoiding both accumulations of FA-intermediate metabolites in the mitochondria and perturbation of FAO.[51]

A mechanistic explanation of these results might be that the induced overexpression of CPT1A, CACT and CrAT, the key players of carnitine cycle, contribute to maintaining a high metabolic flexibility of PCCs. We also demonstrated that forcing miR-124-3p, miR-129-5p or miR-378 expression in PCCs significantly decreased migration, proliferation and invasion of transfected cells. Our evaluation of acylcarnitines content and palmitate oxidation degree in cancer cells has provided a measure of how PC3 and LNCaP metabolically respond to carnitine cycle perturbation induced by overexpression of each miRNA.

Finally, we analyzed human prostate cancer samples and prostate control specimens, and we confirmed that the aberrant expression of miR-124-3p, miR-129-5p and miR-378 as well as CPT1A, CACT and CrAT overexpression were present also in primary tumors. Together, our data implicate carnitine cycle as a primary regulator of adaptive metabolic reprogramming in PCCs and suggest new potential druggable pathways for prevention and treatment of prostate cancer.

MATERIALS AND METHODS

For details, see Supplementary Materials and Methods.

Materials

The human CPT1A, CACT and CRAT sequences cloned in the pCMV6-XL5 expression vector with or without their 3′ UTR were purchased from OriGene Technologies (Rockville, MD, USA). All chemical reagents were of analytical grade or higher and were from Sigma-Aldrich (Milan, Italy).

Cell culture

The human prostate adenocarcinoma cell lines (PC3 and LNCaP), and the immortalized non-cancerous prostate epithelial cell line (PNT2),[52,53] were purchased from the European Collection of Cell Cultures (ECACC, UK) and tested for mycoplasma contamination. Cells were grown according to the manufacturer's instructions (with an approximate population doubling time of 31 h for PC3 and 38 h for LNCaP) and used within 2–4 months.

Malonyl-CoA measurement

Malonyl-CoA concentration was quantified in whole-cell lysates from PNT2, PC3 and LNCaP cells and analyzed by enzyme-linked immunosorbent assay as reported by Fritz *et al*.[54]

Enzymatic determinations

CPT1A activity was assayed in prostate cell mitochondria as the incorporation of radiolabeled carnitine into acylcarnitine in the presence or absence of malonyl-CoA according to Giordano *et al*.[55] and Priore *et al*.[56] CPT1A activity insensitive to 100 mmol/l malonyl-CoA was always subtracted from the experimentally determined CPT1A activity. CACT activity was assayed according to Peluso *et al*. and IJlst *et al*.[57,58] CrAT activity was determined as described by Muoio *et al*.[59] Enzymatic activities were determined in at least three different experiments.

RNA isolation, reverse transcription and qPCR

Total RNA (mRNA and miRNAs) was extracted from cells using QIAzol reagent (Qiagen, Milan, Italy) according to the manufacturer's instructions. qPCR and data collection were performed on 7900HT Fast Real-time PCR System (Applied Biosystems, Milan, Italy).

miRNAs transient transfection

Cells were transfected by Lipofectamine RNAiMAX (Invitrogen, Milan, Italy) following manufacturer's protocol. hsa-miR-129-5p, hsa-miR-124-3p, hsa-miR-378 mirVana miRNA mimics (Ambion, Milan, Italy) and mirVana miRNA mimic negative control #1 (miR mimic NC, Ambion) were purchased from Applied Biosystems. For convenience, hsa-miR-129-5p, hsa-miR-124-3p, hsa-miR-378 mimic and the negative control were hereafter referred to as miR-124, miR-129, miR-378 and miR-NC, respectively. Forced expression of mimics was confirmed by qPCR, and transfected cells were used in further analyses. For rescue experiments, PC3 and LNCaP cells were co-transfected with 10 pmole of mimics and 50 ng of each vector.

Luciferase assay

The pEZX-MT06 target reporter vectors containing full length of CPT1A 3'UTR, CACT 3'UTR and CrAT 3'UTR inserted downstream of the firefly luciferase sequence, were purchased from GeneCopoeia (Rockville, MD, USA). Twenty-four hours before transfection, 1.5×10^4 cells were plated in a 96-well plate. Ten pmoles of miR-124, miR-129, miR-378 or miR-NC were transfected into cells together with 100 ng of pEZX-MT MT06 clones by Lipofectamine RNAiMAX. Luciferase assay was performed 24 h after transfection by the Luc-Pair Luciferase Assay Kit (GeneCopoeia). Sample firefly luciferase expression was normalized against *Renilla* luciferase activity.

Cell proliferation and Colony forming assay

Following transfection, cell proliferation at 0, 12, 24 and 48 h was determined by MTT assay following manufacturer's protocol (Sigma-Aldrich). A microplate reader (Cytation3, ASHI) was used to measure the absorbance of each well at 570 nm.

For colony formation assay, cells were counted, seeded in six-well plates (in triplicate) at a density of 500 cells/well and incubated at 37 °C in a 5% CO_2 humidified incubator. The culture medium was replaced every 3days. After 14 days in culture, cells were stained with crystal violet and counted. Colonies with at least 50 cells were considered for quantification. Representative plates were photographed using phase contrast microscope (Leica, Milan, Italy).

Cell migration and invasion assays

Approximately 1×10^5 cells were plated in two-well Lab-Tek Chamber Slide (Sigma-Aldrich). After overnight incubation, cells were transfected with mimics or miR-NC. Wounds were created in confluent cells using a 200 µl pipette tip. Any free-floating cells or debris were removed by rinsing cells several times with media, and the speed of wound closure was monitored after 24 h by measuring the distance of the wound from 0 h. Each experiment was conducted in triplicate, and representative scrape lines were photographed using phase contrast microscope (Leica).

For the invasion assays, after 24 h transfection, 1×10^5 cells were seeded onto the transwell migration chambers in serum-free media (8 µm pore size; Millipore, Milan, Italy). The membrane in the upper chamber was coated overnight with 1 mg/ml BD Matrigel Matrix (BD Biosciences, Milan, Italy). After 24 h, the non-invading cells were clear out with a cotton-tipped swab, and the cells at the bottom of the insert were stained with May-Grunwald-Giemsa (Sigma-Aldrich). Stained cells were counted under a microscope (Leica) at ×200 magnification of five random fields in each well. At least three independent experiments were performed.

Western blotting

Polyacrylamide gel electrophoresis was carried out, in triplicate, according to standard procedures using 30 µg of total cell lysates. Membranes were probed with the specific primary antibodies followed by secondary antibodies conjugated with horseradish peroxidase. The bands were quantified densitometrically using Quantity One 1-D analysis software (BioRad, Milan, Italy).

Energy substrate oxidation

Acid-soluble acylcarnitines and acid-insoluble acylcarnitines were measured by a radioisotope method as described by Brass & Hoppel[60] in transfected cells after 24 h of treatment with [^{14}C]carnitine.

Palmitate oxidation was determined as the capture of $^{14}CO_2$ from palmitate ([1-^{14}C]palmitate at 0.5 µCi/ml, 150 µM). The reaction mixture contained 100 sucrose mM, 10 mM Tris/HCl, 80 mM KCl, 1 mM $MgCl_2$, 2 mM L-carnitine, 0.1 mM malate, 2 mM ATP, 50 µM CoA, 1 mM dithiothreitol, 0.2 mM ethylenediaminetetraacetic acid and 0.5% bovine serum albumin. Reactions were performed for 60 min at 30 °C after addition of enriched mitochondrial fraction. One hundred µl of 2 M sulfuric acid was added to terminate the reaction, and the radioactivity of CO_2 (trapped in 200 µl of 1 M NaOH) was determined by liquid scintillation counting.

For the analysis of palmitate oxidation dependence from pyruvate, palmitate oxidation was determined as aforementioned in the presence of 0-10mM cold pyruvate, as described by Kim *et al.*[61]

Laser capture microdissection and RNA extraction

This study included 30 patients diagnosed with organ-confined disease (pT2), no lymph node involvement (N0), no metastasis (M0) and Gleason score >6 (3+3), who underwent a radical retropubic prostatectomy at the Prostate Unit, Department of Urology, Policlinico Umberto I, University Sapienza (Rome, Italy). Written informed consent was obtained from all of the patients before the study, and the protocol was approved by the internal ethical committee. The stage and the grade of all the cases were classified according to OMS 2004, and the 1997 UICC TNM, respectively.

The freshly collected tissues were formalin-fixed-paraffin-embedded and reviewed by an expert pathologist with the primary goal of determining the densest region of the tumor. Tumor sections cut at 5 microns were lightly stained with hematoxylin and eosin before microdissection with a laser capture microdissection microscope (Arcturus Laser Capture Microdissection, Applied Biosystems). RNA extraction was performed using the Qiagen AllPrep DNA/RNA FFPE Kit (Qiagen) as described by Shahabi *et al.*[62]

Statistical analysis

All quantitative data were presented as the mean ± s.d. Each experiment was performed at least six times. Statistical significance was evaluated using a *t*-test or one-way analysis of variance, followed by Bonferroni's test for multiple comparisons to determine statistical differences between groups. All the data were analyzed with the GraphPad Prism version 5.01 statistical software package (GraphPad, La Jolla, CA, USA).

CONFLICT OF INTEREST

The authors declare no conflict of interest.

ACKNOWLEDGEMENTS

This work was supported from Ministero dell'Istruzione, dell'Università e della Ricerca of Italy, Progetto PON – 'Ricerca e Competitività 2007–2013'—PON01_01802: 'Sviluppo di molecole capaci di modulare vie metaboliche intracellulari redox-sensibili per la prevenzione e la cura di patologie infettive, tumorali, neurodegenerative e loro delivery mediante piattaforme nano tecnologiche', and PON01_02512: 'Ricerca e sviluppo di bioregolatori attivi sui meccanismi epigenetici dei processi infiammatori nelle malattie croniche e degenerative'. Precis: this study reports the critical role of specific miRNAs (hsa-miR-124-3p, hsa-miR-129-5p and hsa-miR-378) to sustain prostate cancer metabolic flexibility via modulation of CPT1A, CACT and CrAT expression.

AUTHOR CONTRIBUTIONS

Conception and design: G Peluso, A Valentino, A Calarco, A Di Salle. Development of methodology: A Valentino, M Finicelli, S Margarucci, A Calarco, A Di Salle, RA Calogero. Acquisition of data (provided animals, acquired and managed patients, provided facilities, etc.): A Sciarra, A Gentilucci. Analysis and interpretation of data (for example, statistical analysis, biostatistics, computational analysis): S Crispi, RA Calogero, A Valentino. Writing, review and/or revision of the manuscript: A Valentino, A Calarco, A Di Salle, U Galderisi, G Peluso. Study supervision: U Galderisi, G Peluso.

REFERENCES

1 Dang CV, Semenza GL. Oncogenic alterations of metabolism. *Trends Biochem Sci* 1999; **24**: 68–72.
2 Dang CV. Links between metabolism and cancer. *Genes Dev* 2012; **26**: 877–890.
3 Modica-Napolitano JS, Singh KK. Mitochondrial dysfunction in cancer. *Mitochondrion* 2004; **4**: 755–762.
4 DeBerardinis RJ, Mancuso A, Daikhin E, Nissim I, Yudkoff M, Wehrli S *et al.* Beyond aerobic glycolysis: Transformed cells can engage in glutamine metabolism that exceeds the requirement for protein and nucleotide synthesis. *Proc Natl Acad Sci* 2007; **104**: 19345–19350.
5 Semenza GL. HIF-1: upstream and downstream of cancer metabolism. *Curr Opin Genet Dev* 2010; **20**: 51–56.
6 Shanware NP, Mullen AR, DeBerardinis RJ, Abraham RT. Glutamine: pleiotropic roles in tumor growth and stress resistance. *J Mol Med (Berl)* 2011; **89**: 229–236.
7 DeBerardinis RJ. Is cancer a disease of abnormal cellular metabolism? New angles on an old idea. *Genet Med* 2008; **10**: 767–777.
8 McDunn JE, Li Z, Adam KP, Neri BP, Wolfert RL, Milburn MV *et al.* Metabolomic signatures of aggressive prostate cancer. *Prostate* 2013; **73**: 1547–1560.
9 Sreekumar A, Poisson LM, Rajendiran TM, Khan AP, Cao Q, Yu J *et al.* Metabolomic profiles delineate potential role for sarcosine in prostate cancer progression. *Nature* 2009; **457**: 910–914.
10 Teahan O, Bevan CL, Waxman J, Keun HC. Metabolic signatures of malignant progression in prostate epithelial cells. *Int J Biochem Cell Biol* 2011; **43**: 1002–1009.
11 Costello LC, Franklin RB. The intermediary metabolism of the prostate: a key to understanding the pathogenesis and progression of prostate malignancy. *Oncology* 2000; **59**: 269–282.
12 Costello LC, Franklin RB. 'Why do tumour cells glycolyse?': from glycolysis through citrate to lipogenesis. *Mol Cell Biochem* 2005; **280**: 1–8.
13 Liu Y. Fatty acid oxidation is a dominant bioenergetic pathway in prostate cancer. *Prostate Cancer Prostatic Dis* 2006; **9**: 230–234.

14 Liu Y, Zuckier LS, Ghesani NV. Dominant uptake of fatty acid over glucose by prostate cells: a potential new diagnostic and therapeutic approach. *Anticancer Res* 2010; **30**: 369–374.
15 Schlaepfer IR, Glode LM, Hitz CA, Pac CT, Boyle KE, Maroni P *et al.* Inhibition of lipid oxidation increases glucose metabolism and enhances 2-Deoxy-2-[(18)F] Fluoro-D-glucose uptake in prostate cancer mouse xenografts. *Mol Imaging Biol* 2015; **17**: 529–538.
16 Wu X, Daniels G, Lee P, Monaco ME. Lipid metabolism in prostate cancer. *Am J Clin Exp Urol* 2014; **2**: 111–120.
17 Bastin J. Regulation of mitochondrial fatty acid beta-oxidation in human: what can we learn from inborn fatty acid beta-oxidation deficiencies? *Biochimie* 2014; **96**: 113–120.
18 Foster DW. The role of the carnitine system in human metabolism. *Ann N Y Acad Sci* 2004; **1033**: 1–16.
19 Bonnefont JP, Djouadi F, Prip-Buus C, Gobin S, Munnich A, Bastin J. Carnitine palmitoyltransferases 1 and 2: biochemical, molecular and medical aspects. *Mol Aspects Med* 2004; **25**: 495–520.
20 Ramsay RR, Gandour RD, van der Leij FR. Molecular enzymology of carnitine transfer and transport. *Biochim Biophys Acta* 2001; **1546**: 21–43.
21 Jogl G, Hsiao YS, Tong L. Structure and function of carnitine acyltransferases. *Ann N Y Acad Sci* 2004; **1033**: 17–29.
22 Calin GA, Croce CM. MicroRNA signatures in human cancers. *Nat Rev Cancer* 2006; **6**: 857–866.
23 Khanmi K, Ignacimuthu S, Paulraj MG. MicroRNA in prostate cancer. *Clin Chim Acta* 2015; **451**: 154–160.
24 Kurisetty VV, Lakshmanaswamy R, Damodaran C. Pathogenic and therapeutic role of miRNAs in breast cancer. *Front Biosci (Landmark Ed)* 2014; **19**: 1–11.
25 Liu X, Chen X, Yu X, Tao Y, Bode AM, Dong Z *et al.* Regulation of microRNAs by epigenetics and their interplay involved in cancer. *J Exp Clin Cancer Res* 2013; **32**: 96.
26 Price DT, Coleman RE, Liao RP, Robertson CN, Polascik TJ, DeGrado TR. Comparison of [18 F]fluorocholine and [18 F]fluorodeoxyglucose for positron emission tomography of androgen dependent and androgen independent prostate cancer. *J Urol* 2002; **168**: 273–280.
27 Arora A, Singh S, Bhatt AN, Pandey S, Sandhir R, Dwarakanath BS. Interplay Between Metabolism and Oncogenic Process: Role of microRNAs. *Transl Oncogenomics* 2015; **7**: 11–27.
28 Pinweha P, Rattanapornsompong K, Charoensawan V, Jitrapakdee S. MicroRNAs and oncogenic transcriptional regulatory networks controlling metabolic reprogramming in cancers. *Comput Struct Biotechnol J* 2016; **14**: 223–233.
29 Love MI, Huber W, Anders S. Moderated estimation of fold change and dispersion for RNA-seq data with DESeq2. *Genome Biol* 2014; **15**: 550.
30 Cardenas-Navia LI, Mace D, Richardson RA, Wilson DF, Shan S, Dewhirst MW. The pervasive presence of fluctuating oxygenation in tumors. *Cancer Res* 2008; **68**: 5812–5819.
31 Ambs S, Prueitt RL, Yi M, Hudson RS, Howe TM, Petrocca F *et al.* Genomic profiling of microRNA and messenger RNA reveals deregulated microRNA expression in prostate cancer. *Cancer Res* 2008; **68**: 6162–6170.
32 Porkka KP, Pfeiffer MJ, Waltering KK, Vessella RL, Tammela TL, Visakorpi T. MicroRNA expression profiling in prostate cancer. *Cancer Res* 2007; **67**: 6130–6135.
33 Song C, Chen H, Wang T, Zhang W, Ru G, Lang J. Expression profile analysis of microRNAs in prostate cancer by next-generation sequencing. *Prostate* 2015; **75**: 500–516.
34 Schaefer A, Jung M, Kristiansen G, Lein M, Schrader M, Miller K *et al.* MicroRNAs and cancer: current state and future perspectives in urologic oncology. *Urol Oncol* 2010; **28**: 4–13.
35 Gill BS, Alex JM, Navgeet, Kumar S. Missing link between microRNA and prostate cancer. *Tumour Biol* 2016; **37**: 5683–5704.
36 Li X, Chen YT, Josson S, Mukhopadhyay NK, Kim J, Freeman MR *et al.* MicroRNA-185 and 342 inhibit tumorigenicity and induce apoptosis through blockade of the SREBP metabolic pathway in prostate cancer cells. *PLoS One* 2013; **8**: e70987.
37 Dong P, Ihira K, Xiong Y, Watari H, Hanley SJ, Yamada T *et al.* Reactivation of epigenetically silenced miR-124 reverses the epithelial-to-mesenchymal transition and inhibits invasion in endometrial cancer cells via the direct repression of IQGAP1 expression. *Oncotarget* 2016; **7**: 20260–20270.
38 Wang X, Liu Y, Liu X, Yang J, Teng G, Zhang L *et al.* MiR-124 inhibits cell proliferation, migration and invasion by directly targeting SOX9 in lung adenocarcinoma. *Oncol Rep* 2016; **35**: 3115–3121.
39 Shi XB, Ma AH, Xue L, Li M, Nguyen HG, Yang JC *et al.* miR-124 and Androgen Receptor Signaling Inhibitors Repress Prostate Cancer Growth by Downregulating Androgen Receptor Splice Variants, EZH2, and Src. *Cancer Res* 2015; **75**: 5309–5317.
40 Eaton S. Control of mitochondrial beta-oxidation flux. *Prog Lipid Res* 2002; **41**: 197–239.
41 Shen N, Huang X, Li J. Upregulation of miR-129-5p affects laryngeal cancer cell proliferation, invasiveness, and migration by affecting STAT3 expression. *Tumour Biol* 2016; **37**: 1789–1796.
42 Dossing KB, Binderup T, Kaczkowski B, Jacobsen A, Rossing M, Winther O *et al.* Down-Regulation of miR-129-5p and the let-7 Family in Neuroendocrine Tumors and Metastases Leads to Up-Regulation of Their Targets Egr1, G3bp1, Hmga2 and Bach1. *Genes (Basel)* 2015; **6**: 1–21.
43 Shen R, Pan S, Qi S, Lin X, Cheng S. Epigenetic repression of microRNA-129-2 leads to overexpression of SOX4 in gastric cancer. *Biochem Biophys Res Commun* 2010; **394**: 1047–1052.
44 Duan L, Hao X, Liu Z, Zhang Y, Zhang G. MiR-129-5p is down-regulated and involved in the growth, apoptosis and migration of medullary thyroid carcinoma cells through targeting RET. *FEBS Lett* 2014; **588**: 1644–1651.
45 Ma N, Chen F, Shen SL, Chen W, Chen LZ, Su Q *et al.* MicroRNA-129-5p inhibits hepatocellular carcinoma cell metastasis and invasion via targeting ETS1. *Biochem Biophys Res Commun* 2015; **461**: 618–623.
46 Palmieri F, Pierri CL. Mitochondrial metabolite transport. *Essays Biochem* 2010; **47**: 37–52.
47 Eichner LJ, Perry MC, Dufour CR, Bertos N, Park M, St-Pierre J *et al.* miR-378(*) mediates metabolic shift in breast cancer cells via the PGC-1beta/ERRgamma transcriptional pathway. *Cell Metab* 2010; **12**: 352–361.
48 Riehle C, Abel ED. PGC-1 proteins and heart failure. *Trends Cardiovasc Med* 2012; **22**: 98–105.
49 Carrer M, Liu N, Grueter CE, Williams AH, Frisard MI, Hulver MW *et al.* Control of mitochondrial metabolism and systemic energy homeostasis by microRNAs 378 and 378*. *Proc Natl Acad Sci USA* 2012; **109**: 15330–15335.
50 Lu J, Tan M, Cai Q. The Warburg effect in tumor progression: mitochondrial oxidative metabolism as an anti-metastasis mechanism. *Cancer Lett* 2015; **356**: 156–164.
51 Schlaepfer IR, Rider L, Rodrigues LU, Gijon MA, Pac CT, Romero L *et al.* Lipid catabolism via CPT1 as a therapeutic target for prostate cancer. *Mol Cancer Ther* 2014; **13**: 2361–2371.
52 Johnson IR, Parkinson-Lawrence EJ, Butler LM, Brooks DA. Prostate cell lines as models for biomarker discovery: performance of current markers and the search for new biomarkers. *Prostate* 2014; **74**: 547–560.
53 Berthon P, Cussenot O, Hopwood L, Leduc A, Maitland N. Functional expression of sv40 in normal human prostatic epithelial and fibroblastic cells - differentiation pattern of nontumorigenic cell-lines. *Int J Oncol* 1995; **6**: 333–343.
54 Fritz V, Benfodda Z, Henriquet C, Hure S, Cristol JP, Michel F *et al.* Metabolic intervention on lipid synthesis converging pathways abrogates prostate cancer growth. *Oncogene* 2013; **32**: 5101–5110.
55 Giordano A, Calvani M, Petillo O, Grippo P, Tuccillo F, Melone MA *et al.* tBid induces alterations of mitochondrial fatty acid oxidation flux by malonyl-CoA-independent inhibition of carnitine palmitoyltransferase-1. *Cell Death Differ* 2005; **12**: 603–613.
56 Priore P, Giudetti AM, Natali F, Gnoni GV, Geelen MJ. Metabolism and short-term metabolic effects of conjugated linoleic acids in rat hepatocytes. *Biochim Biophys Acta* 2007; **1771**: 1299–1307.
57 Peluso G, Petillo O, Margarucci S, Mingrone G, Greco AV, Indiveri C *et al.* Decreased mitochondrial carnitine translocase in skeletal muscles impairs utilization of fatty acids in insulin-resistant patients. *Front Biosci* 2002; **7**: a109–a116.
58 IJlst L, van Roermund CW, Iacobazzi V, Oostheim W, Ruiter JP, Williams JC *et al.* Functional analysis of mutant human carnitine acylcarnitine translocases in yeast. *Biochem Biophys Res Commun* 2001; **280**: 700–706.
59 Muoio DM, Noland RC, Kovalik JP, Seiler SE, Davies MN, DeBalsi KL *et al.* Muscle-specific deletion of carnitine acetyltransferase compromises glucose tolerance and metabolic flexibility. *Cell Metab* 2012; **15**: 764–777.
60 Brass EP, Hoppel CL. Relationship between acid-soluble carnitine and coenzyme A pools in vivo. *Biochem J* 1980; **190**: 495–504.
61 Kim JY, Hickner RC, Cortright RL, Dohm GL, Houmard JA. Lipid oxidation is reduced in obese human skeletal muscle. *Am J Physiol Endocrinol Metab* 2000; **279**: E1039–E1044.
62 Shahabi A, Lewinger JP, Ren J, April C, Sherrod AE, Hacia JG *et al.* Novel gene expression signature predictive of clinical recurrence after radical prostatectomy in early stage prostate cancer patients. *Prostate* 2016; **76**: 1239–1256.

Supplementary Information accompanies this paper on the Oncogene website (http://www.nature.com/onc)

Clin Transl Oncol
DOI 10.1007/s12094-016-1599-5

REVIEW ARTICLE

Exosomal microRNAs in liquid biopsies: future biomarkers for prostate cancer

A. Valentino[1,2,3] · P. Reclusa[1,2] · R. Sirera[1,2,4] · M. Giallombardo[1,2] · C. Camps[5,6] · P. Pauwels[2,7] · S. Crispi[3] · C. Rolfo[1,2]

Received: 8 September 2016 / Accepted: 12 December 2016

Abstract Prostate cancer is the second most diagnosed cancer in males in the world. Plasma quantification of prostate-specific antigen substantially improved the early detection of prostate cancer, but still lacks the required specificity. Clinical management of prostate cancer needs advances in the development of new non-invasive biomarkers, ameliorating current diagnosis and prognosis and guiding therapeutic decisions. microRNAs (miRNAs) are a class of small non-coding RNAs that regulate gene expression at the post-transcriptional level. These miRNAs are expressed in the cells and are also present in cell-derived extracellular vesicles such as exosomes. Exosomes have been shown to act as mediators for cell to cell communication because of the regulatory functions of their content. High levels of exosomes are found in several body fluids from cancer patients and could be a potential source of non-invasive biomarkers. In this review, we summarize the diagnostic and prognostic utility of exosomal miRNAs in prostate cancer.

Keywords Prostate cancer · MiRNAs · Exosome · Biomarker · Liquid biopsies

A. Valentino and P. Reclusa contributed equally.

✉ C. Rolfo
christian.rolfo@uza.be

1 Phase I-Early Clinical Trials Unit, Oncology Department, Antwerp University Hospital, Wilrijkstraat 10, 2650 Edegem, Belgium

2 Center for Oncological Research (CORE), Antwerp University, Antwerp, Belgium

3 Gene Expression and Molecular Genetics Laboratory, Institute of Biosciences and BioResources, National Center for Research, CNR, Naples, Italy

4 Department of Biotechnology, Universitat Politecnica de Valencia, Valencia, Spain

5 Medical Oncology Department, Hospital General Universitario de Valencia, Valencia, Spain

6 Department of Medicine, Universitat de València, Valencia, Spain

7 Molecular Pathology Unit, Antwerp University Hospital, Antwerp, Belgium

Prostate cancer

Prostate cancer is the most commonly diagnosed male malignancy and the second leading cause of cancer-related death in males in the western world [1, 2]. Malignant transformation of prostate epithelial cells and progression to carcinoma are likely to result from a complex series of events under both genetic and environmental influences [3, 4]. Prostate cancer develops mainly in aged men, the inherited risk of prostate cancer is as high as 60% [5] and some predisposing genes have been identified [6–8]. Other risk factors include race, a diet rich in fat, and obesity [3]. A better understanding of the genetic and biologic mechanisms that determine why some prostate carcinomas remain silent while others cause serious, even life-threatening illness are needed [5].

In the early stages, the disease locally confined to the prostate, is hormone or androgen-dependent and can be managed by surgical intervention or radiation treatment [4]. In the case of advanced prostate cancer, androgen deprivation therapy initially reduce tumor burden and circulating prostate-specific antigen (PSA), but unfortunately the disease relapse in most cases [9]. Advanced prostate cancer can present metastasis in the lung, pleura, liver and bone, with a great impact in patient morbidity and

Published online: 04 January 2017

mortality despite aggressive therapy [10]. Currently, prognostic markers are serum levels of PSA, Gleason score and pathological stage [11]. PSA is secreted by prostate cancer cells and can be found in blood, but has a low specificity as biomarker because its level can also be elevated for non-cancerous reasons [12, 13] or even diminished in metastatic disease [14]. These tests do not distinguish exactly the aggressiveness of the tumor or the potential metastatic capacity, so prostate biopsy, an invasive procedure, remains the only definitive diagnostic test for prostate cancer. But the implementation of novel state-of-the-art techniques such as the analysis of exosomal content of microRNAs (miRNAs) might be a promising candidate for the diagnosis and disease stratification of prostate cancer.

miRNA biogenesis, functions and implications in cancer

miRNAs are endogenous, small, from 18 to 25 nucleotides and non-coding RNAs widely found in both animals and plants that regulate post-transcriptionally gene expression. These small RNAs down-regulate gene expression by binding a region in the 3′ untranslated region (3′UTR) of their messenger RNA (mRNA) targets [15–17]. If the miRNA completely binds the sequence of their mRNA, the mRNA degradation is induced, while by contrast when miRNA bind incompletely, translational repression is induced [18]. miRNAs genes are transcribed by RNA polymerase II into long primary miRNAs (pri-miRNAs). These pri-miRNAs are processed in the nucleus into 70–80 nucleotide precursor miRNAs (pre-miRNAs) by the RNase III enzyme Drosha [19] and its cofactor DGCR8. Then pre-miRNA is actively transported from the nucleus to the cytoplasm by Exportin 5/Ran-GTP complex where is processed by the enzyme Dicer in the cytoplasm. Dicer is an RNase III endonuclease that cleaves the pre-miRNA into the mature miRNA that become stably associated with the RNA-induced silenced complex (RISC), forming the miRISC. The miRISC inhibits the target genes by repressing translation initiation, inducing deadenylation of mRNA, and thereby inducing ribosomes to drop off prematurely and promoting mRNA degradation by Argonaute, one of its essential catalytic components [20] (Fig. 1). miRNAs can target hundreds of transcripts, and more than one miRNA can converge on a single target transcript, thus the potential regulatory scenario of miRNAs is enormous. In this regard, miRNAs expression profiles have been found to be tissue type-specific and play important regulatory roles in a variety of biological process, such as cell proliferation, intercellular signaling, cell growth, cell death, cellular differentiation, apoptosis and metabolism control [21]. miRNA expression in tumor has been found to be up or down-regulated compared with normal tissue supporting their complex dual role either as oncogene (oncomir) or tumor suppressor gene [22]. For instance miRNA-125b has been shown to be an oncomir in prostate cancer but can also act as a tumor suppressor in ovarian and breast cancer [23]. Not only miRNAs are deregulated in cancer but also the enzymes involved in their biogenesis and processing. For example, Dicer is up-regulated during prostate cancer progression and its levels correlate with clinical stage, lymph node status and Gleason score [24]. miRNAs can be detected in a small volume samples from most body fluids, including serum, plasma, urine, saliva and are known to circulate in a highly stable cell free form [25]. Their stability, ease detection using a range of techniques, including miRNA cloning, microarray, quantitative PCR and next generation sequencing, make it feasible to identify and confirm abnormal miRNA expression in most human malignances [26]. These characteristics, together with its association with neoplastic disease progression, make miRNA an ideal tumor biomarker either in the tissue or in body fluids [20].

Exosomes and prostasomes

Exosomes are nano-sized (40–100 nm) extracellular vesicles (EV) derived from multivesicular bodies (MVB). Cells use exosomes to exchange of proteins, lipids and nucleic acids [27], therefore are important mediator for cell to cell communication, and indeed are considered to play a fundamental role in many physiological and pathological processes [28]. Exosomes are either released from normal or neoplastic cells and are present in the blood plasma, amniotic fluids, malignant ascites [29], breast milk [30] and other body fluids such as urine [31]. Exosomes contain mRNA, miRNAs and DNA so the transfer of this sort of information and oncogenic signaling to the tumor microenvironment let the modulation of tumor progression, proliferation angiogenic switch, the formation of the metastatic niche [32] and even the suppression of immune responses [33] (Fig. 2).

Several molecules or pathways are involved in the biogenesis of MVBs, such as the ESCRT machinery (endosomal sorting complexes required for transport), certain lipids (such as ceramide) and the tetraspanins [34]. MVBs can be either fused with lysosomes or with the plasma membrane, which allows the release of their content to the extracellular compartment [35]. Exosomes then will interact with recipient target cells via different mechanisms such as plasma membrane fusion and transport (RAB11, RAB27 and RAB35) or adhesion to corresponding receptors [36, 37]. Unfortunately, the mechanism that regulates

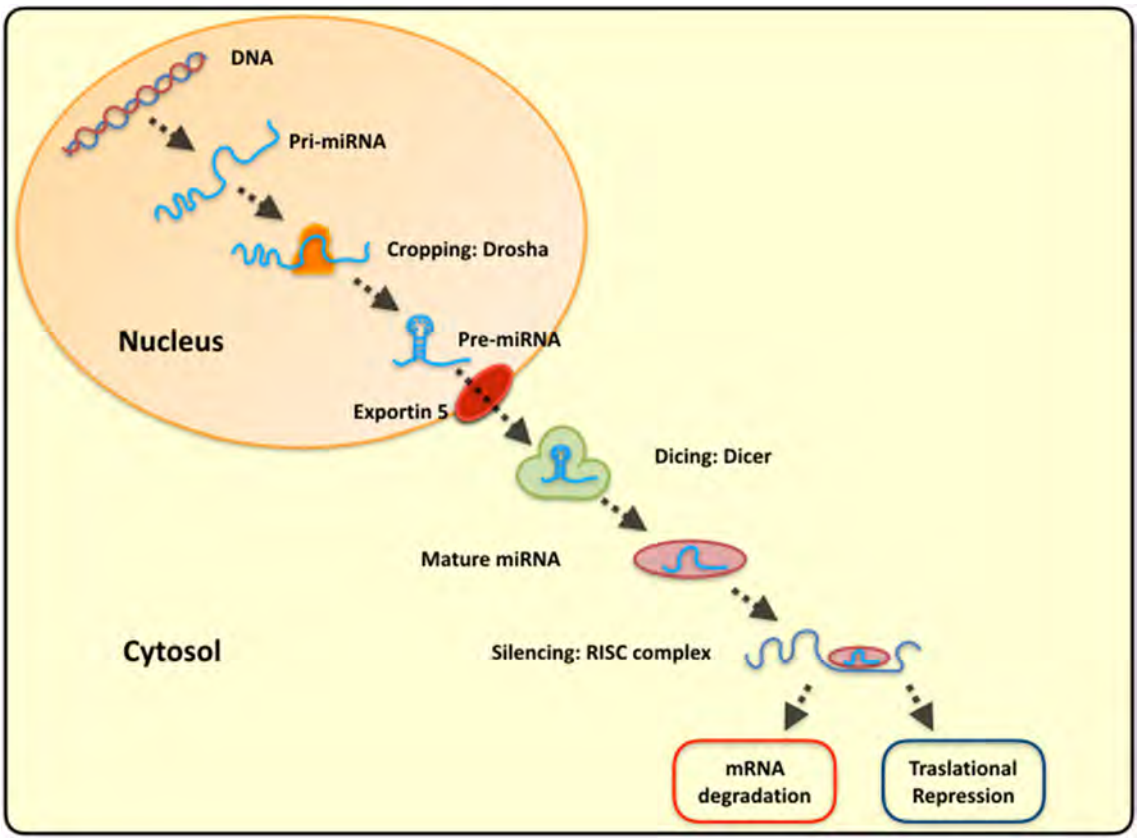

Fig. 1 miRNA biogenesis and mechanism of action

the exosomes release and uptake is still unknown. There are different ways to isolate exosomes either from tissue culture or form body fluids as sucrose density-gradient, ultracentrifugation [38] or by means of antibodies against exosomal markers, such as CD9, CD81, CD63 [39]. Recently, nanomembrane ultrafiltration concentrator and ExoQuick reagent are used as an effective and proven alternative to ultracentrifugation as well as a modified exosome precipitation method offers also a quick and scalable for exosomes isolation [40].

EVs, matching in size to vesicles from the prostate epithelium, now are known as prostasomes, found inside the 'storage vesicles' within prostate epithelial cells [41].

Prostasomes are microvesicles (50–500 nm) present in prostate secretions, produced by prostatic ductal epithelial cells and normal component of seminal fluid [42].

In prostasomes term, there are several populations: one with a small size type equivalent to exosomes, and released by prostate cells because of multivesicular endosomes with the plasma membrane, and other type equivalent to microvesicles with large size and derived by direct shedding of plasma membrane [43].

Prostasomes play a role as antioxidant factors in semen by interacting with polymorphonuclear neutrophils and inhibiting NADPH oxidase activity, and thus can act as antibacterial agents [44]. Interesting component have similarly been found in prostasomes isolated from human semen, such as prostatic acid phosphatase (PAP), PSA, prostate-specific transglutaminase and prostate stem cell antigen (PSCA) which are also markers for prostate cancer [45]. Prostasome have also a peculiar lipid composition with high levels of sphingomyelin, cholesterol, and glycosphingolipids [46] and in addition have also been reported to contain chromosomal DNA, mRNA and miRNA [47]. The protein content on prostasome surface is also very relevant as the presence of complement inhibitory proteins such as CD46 and CD59 that confer resistance to complement dependent cytotoxicity [48]. Prostasomes are not only secret by normal prostatic cells but also by neoplastic cells that export prostasomes to the extracellular environment, participating in tumor proliferation and metastasis [49]. Prostasome levels are reportedly increased in prostate cancer patients and these levels are associated with the disease aggressiveness [50]. The development of future isolation techniques for prostasomes found in biological fluids will let to get better insight in the identification and analysis of the protein, lipid and nucleic acids content of them and the potential utility for the diagnosis and prognosis of prostate cancer.

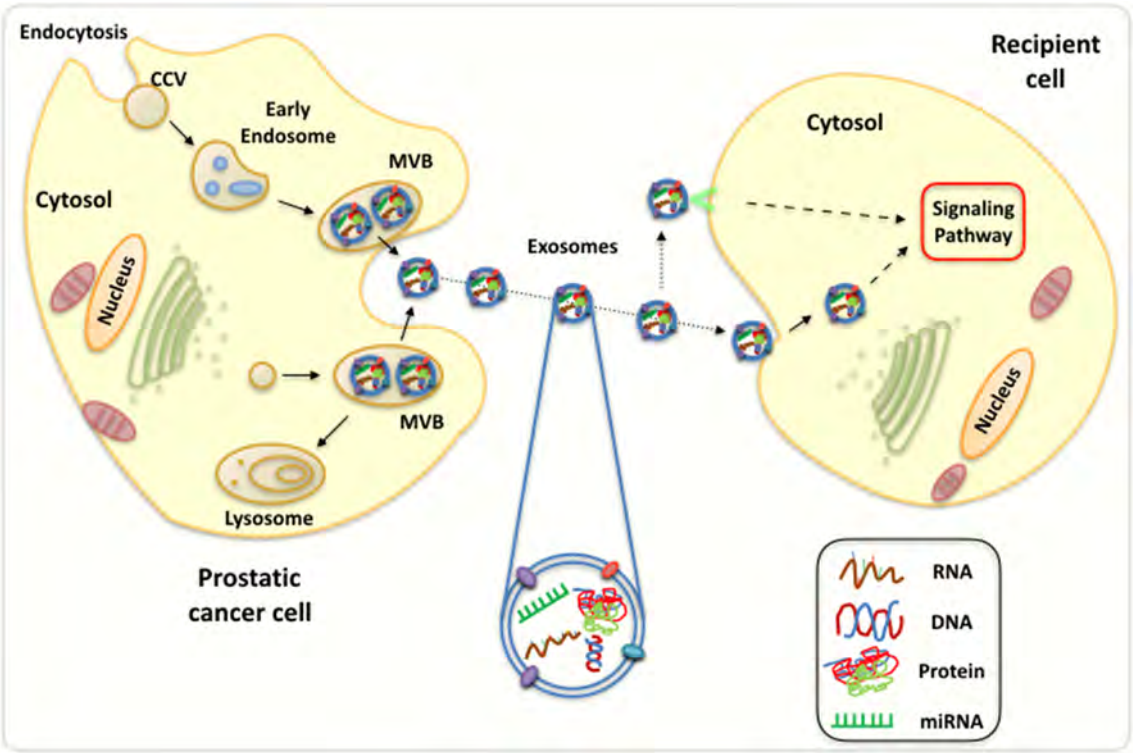

Fig. 2 Exosomes promote cell–cell communication playing an important role in gene regulation due to their ability to transport cancer-promoting material such as miRNAs

Exosomal miRNAs in prostate cancer

miRNAs are expressed not only in cells and present in biological fluids, but can be found also in cell-derived extracellular vesicles such as exosomes [51]. In fact, RNA sequencing analysis of plasma-derived exosomes revealed that miRNAs are the most abundant exosomal RNA species [52]. The miRNA content of extracellular vesicles reflects the miRNA expression profile of the cells they originated from [53]. For example, Brase et al. screened more 60 exosomal miRNAs identifying mir-375 and mir-141 as appropriate markers for prostate cancer [54]. This miRNAs content in exosomes could be considered as a potential novel biomarker for prostate cancer that may be used to diagnose but also to predict the disease stage [55, 56]. This is currently needed because the blood level of the gold standard marker for prostate cancer, PSA, do not always correlate with disease stage and aggressiveness of the malignancy [57]. For example, miR-21 is significantly elevated in the early stage, but not in advanced prostate cancer [58] and miR-16 is up-regulated in plasma of metastatic prostate cancer patients, but down-regulated in primary or metastatic prostate cancer tissues [59]. Additionally, other miRNAs have been reported to be detected in blood exosomes in metastatic prostate cancer patients [60–63]. MiRNAs have identified deregulated in plasma and serum microvesicles in prostate cancer patients compared with healthy control [64] and were also associated with the stage of the disease, the Gleason score and lymph node metastasis. For instance, Lodes et al. found 15 miRNAs (miR-16, -92a, -103, -107, -197, -34b, -328, -485-3p, -486-5p, -92b, -574-3p, -636, -640, -766, -885-5p) over-expressed in serum from stage 3 and 4 prostate cancer patients compared with healthy controls [65]. Furthermore, Mahn et al., found miR-26a, miR-195, and let-7i to be up-regulated in patients with prostate cancer compared with patients affected by benign prostatic hyperplasia [66]. Therefore, the different expression of specific miRNAs in liquid biopsies might be useful for a correct diagnosis. Another source where to investigate neoplastic abnormalities in prostate cancer with clinical value is the urine as its composition reflects the alterations in urogenital system [67].

An investigation of the proteome of urinary exosomes identified 246 proteins differentially expressed in prostate cancer patients compared to healthy male controls being the majority of these proteins up-regulated in exosomes from prostate cancer patients with high sensitivity and specificity [68]. A urinary 3-gene expression assay in exosomes has demonstrated an improved identification of patients with higher-grade prostate cancer among men with elevated PSA reduce the number of unnecessary biopsies

Table 1 miRNAs deregulated in prostate cancer compared to healthy controls

MiRNAs deregulated in prostate cancer	Source	Potential target genes	References
Let-7i, mir-16, mir-24, mir-26a, mir-26b, mir-34b, mir-92b, mir-93, mir-103, mir-106a, mir-141, mir-195, mir-197, mir-223, mir-298, mir-328, mir-346, mir-375, mir-1290	Serum	MAPK, p53, WNT5A EZH2,LARP1,AKT, SOX2,PDCD10,SPAG9,SOCS5, MBNL1, MTPN, E2F2, MYC, MCM7, BCL2, PLAG1, ACSL3, HMGA1, EGF2, BCOX1, AKT,ITGA3/ ITGB1,p21	Hessvik et al. [61], Moltzahn et al. [72], Lodes et al. [73]
Let-7e, let-7c, mir-20a, mir-21, mir-30c, mir-130b, mir-145, mir-1811a-2*, mir-221, mir-301a, mir-326, mir331-3p, mir-432, mir-574-3p, mir-622, mir-625*, mir-1285, mir-2110, mir-141, mir-1290	Plasma	HMGA2, IGF1R, AR, ABL2, PDCD4, TGFβ, BCL9, MMP2, SOX2, SENP1, Bmi1, SIRT1, IRF2, RAB1A, HECTD2, NDRG2, DOHH, ERBB-2, WNT5A, EZH2, LARP1	Shen et al. [74], Huang et al. [52]
mir-107, mir-574-3p, mir-141-5p, mir-21-5p, mir-34a, mir-483-5p	Urine	WNT5A, EZH2, LARP1, PDCD4, p57Kip2, SIRT1, CD44, WNT/TCF7, AR, Notch-1, c-Myc	Nina Pettersen Hessvik et al. [61], Samsonov et al. [71]
mir-141, mir-21	Saliva	MAPK, WNT5A, EZH2, LARP1, PDCD4, FBXO11, p57Kip2, TGFBR2, MARCKS	Hizir et al. [58]
mir-141,mir-9, mir-200b,mir-21,mir-221,mir-16,mir-92a, mir-103,mir-107, mir-197, mir-92b,mir-574-3p,mir-885-5p,mir-298,mir-26a,mir-1274a,mir-106a,mir-26b,mir-30b,c,d, mir-24, let-7a,c,e,i, miR-1285,mir-20a,mir-107,mir-130b,mir-301a,mir-331-3p,mir-625,mir-485-3p,mir-874,mir-155,mir-181a-2, mir-326, mir-762, mir-185, mir-151 and mir-149	Metastatic cell line (PC3)	IGFR1, TCR, GH, STAT, MAPK, PRLR, TGFβ, BCL2, ERG, PDGF-D, Bmi, TGFBR2, p57kip2, MARCKS, Bmi, SIRT1, IRF2, SOCS3, HECTD2, RAB14, DVL2, PDCD10, PI3 K, AKT3, WNT5A, ULK2, BCL9, CDKN1B/p27, E2F2, CCND2, AR, ABL2, CX43, MMP2, NDRG2, DOHH, ERBB-2, ANXA7, DAX1, SREBP, CASZ1, IL1RAPL1, SOX17, N4BP1, ARHGDIA	Hessvik et al. [75], Alireza Ahadi et al. [51]
Let-7a, b,c, mir-149, mir-762, mir-30b-3p, mir-20a,b, mir-17-5p, mir-18a-5p, mir-106-5p, mir-93-5p,	Metastatic cell line (VCaP)	KRAS, E2F2, CCND2, IGF1R, RPS2, AR, c-MYC, ABL2, CX43, TIMP3, p300/CBP, RE-1, KEGG	Alireza Ahadi et al. [51]
Let-7a, b,c,d,e,i, mir-17, mir-18a, mir-20a, mir-93, mir-106b, mir-149	Metastatic cell line (LNCaP)	KRAS, E2F2, CCND2, IGF1R, RPS2, AR, c-MYC, BPX3, ABL2, CX43, TIMP3, p300/CBP, RE-1, PTEN, ZBTB4, p21, CASP7, SDC-1	Alireza Ahadi et al. [51]

[69]. In a proof-of-concept study analyzing the transcriptome in tumor exosomes isolated from the urine of patients with prostate cancer, revealed biomarkers, with potential for monitoring cancer patients. If it could expand to include not only mRNAs but also miRNAs it will help to classify the tumor phenotype, its severity and the tumor response to treatment [70]. Additional studies have demonstrated alteration of certain specifics miRNAs, such as mir-107, mir-574-3p and mir-483-5p, found in the urine of men with prostate cancer compared with healthy controls [70]. In metastatic prostate cancer, miR-141 is enriched in exosomes found in cells obtained by urine sediments, as well as in parallel tissue samples, suggesting the diagnostic and prognostic potential of miR-141 for prostate cancer [71]. As shown in Table 1, there are several deregulated miRNAs in different liquid biopsy (serum, plasma, urine, saliva and cells) of prostate cancer. Regarding other important factors, it has been observed that the miRNAs content of exosomes plays a role in docetaxel resistance. mir-34a that was significantly decreased in prostate cancer versus normal tissues as well as in urine, regulates BCL-2 and may in part, regulate the response to docetaxel [76, 77].

Conclusion

There is still limited knowledge about the biological roles of exosomal miRNAs in prostate cancer. The development of new exosome isolations methods and the incorporation of high-throughput technologies as next generation sequencing (NGS) for miRNA analysis will change dramatically the scenario. The scientific community will advance in the use of plasma or urine exosomal miRNAs as source for new prostate cancer biomarkers substituting progressively invasive procedures as biopsy or serum PSA. This challenge of blood-based assays may represent the needed association between basic and clinical research, driving definitively the outbreak of personalized medicine in prostate cancer.

Acknowledgements The authors would like to thank Dr. Rodolfo Mauceri for the artwork of the figures illustrating this review.

Compliance with ethical standards

Conflict of interest The authors declare that they have no conflict of interest.

References

1. Damber JE, Aus G. Prostate cancer. Lancet. 2008;371(9625):1710–21.
2. Siegel RL, Miller KD, Jemal A. Cancer statistics, 2016. CA Cancer J Clin. 2016;66(1):7–30.
3. Wright ME, Chang SC, Schatzkin A, Albanes D, Kipnis V, Mouw T, et al. Prospective study of adiposity and weight change in relation to prostate cancer incidence and mortality. Cancer. 2007;109(4):675–84.
4. Mellado B, Codony J, Ribal MJ, Visa L, Gascón P. Molecular biology of androgen-independent prostate cancer: the role of the androgen receptor pathway. Clin Transl Oncol. 2009;11(1):5–10.
5. Ruijter E, van de Kaa C, Miller G, Ruiter D, Debruyne F, Schalken J. Molecular genetics and epidemiology of prostate carcinoma. Endocr Rev. 1999;20(1):22–45.
6. Kopper L, Tímár J. Genomics of prostate cancer: is there anything to "translate"? Pathol Oncol Res. 2005;11(4):197–203.
7. Brinkmann AO, Kuiper GG, Ris-Stalpers C, van Rooij HC, Romalo G, Trifiro M, et al. Androgen receptor abnormalities. J Steroid Biochem Mol Biol. 1991;40(1–3):349–52.
8. Cansino Alcaide JR, Martínez-Piñeiro L. Molecular biology in prostate cancer. Clin Transl Oncol. 2006;8(3):148–52.
9. Taplin ME, Bubley GJ, Shuster TD, Frantz ME, Spooner AE, Ogata GK, et al. Mutation of the androgen-receptor gene in metastatic androgen-independent prostate cancer. N Engl J Med. 1995;332(21):1393–8.
10. Heise M, Haus O. Hereditary prostate cancer. Postepy Hig Med Dosw (Online). 2014;68:653–65.
11. Hosseini-Beheshti E, Pham S, Adomat H, Li N, Tomlinson Guns ES. Exosomes as biomarker enriched microvesicles: characterization of exosomal proteins derived from a panel of prostate cell lines with distinct AR phenotypes. Mol Cell Proteomics. 2012;11(10):863–85.
12. Heidenreich A, Bastian PJ, Bellmunt J, Bolla M, Joniau S, van der Kwast T, et al. EAU guidelines on prostate cancer. part 1: screening, diagnosis, and local treatment with curative intent-update 2013. Eur Urol. 2014;65(1):124–37.
13. Watahiki A, Macfarlane RJ, Gleave ME, Crea F, Wang Y, Helgason CD, et al. Plasma miRNAs as biomarkers to identify patients with castration-resistant metastatic prostate cancer. Int J Mol Sci. 2013;14(4):7757–70.
14. Ruiz-Martín I, Rodríguez-Sánchez CA, Ocaña-Fernández A, del Valle-Zapico J, Soto de Prado-Otero D, Cruz-Hernández JJ. Metastatic prostate cancer with a normal prostate-specific antigen level. Clin Transl Oncol. 2005;7(9):412–3.
15. Tarhan F, Orçun A, Küçükercan I, Camursoy N, Kuyumcuoğlu U. Effect of prostatic massage on serum complexed prostate-specific antigen levels. Urology. 2005;66(6):1234–8.
16. Krol J, Loedige I, Filipowicz W. The widespread regulation of microRNA biogenesis, function and decay. Nat Rev Genet. 2010;11(9):597–610.
17. Garzon R, Marcucci G, Croce CM. Targeting microRNAs in cancer: rationale, strategies and challenges. Nat Rev Drug Discov. 2010;9(10):775–89.
18. Dykxhoorn DM. MicroRNAs and metastasis: little RNAs go a long way. Cancer Res. 2010;70(16):6401–6.
19. Denli AM, Tops BB, Plasterk RH, Ketting RF, Hannon GJ. Processing of primary microRNAs by the Microprocessor complex. Nature. 2004;432(7014):231–5.
20. Heneghan HM, Miller N, Kerin MJ. MiRNAs as biomarkers and therapeutic targets in cancer. Curr Opin Pharmacol. 2010;10(5):543–50.
21. Volinia S, Calin GA, Liu CG, Ambs S, Cimmino A, Petrocca F, et al. A microRNA expression signature of human solid tumors defines cancer gene targets. Proc Natl Acad Sci USA. 2006;103(7):2257–61.
22. Lu J, Getz G, Miska EA, Alvarez-Saavedra E, Lamb J, Peck D, et al. MicroRNA expression profiles classify human cancers. Nature. 2005;435(7043):834–8.
23. Budd WT, Seashols-Williams SJ, Clark GC, Weaver D, Calvert V, Petricoin E, et al. Dual action of miR-125b as a tumor suppressor and OncomiR-22 promotes prostate cancer tumorigenesis. PLoS ONE. 2015;10(11):e0142373.
24. Chiosea S, Jelezcova E, Chandran U, Acquafondata M, McHale T, Sobol RW, et al. Up-regulation of dicer, a component of the MicroRNA machinery, in prostate adenocarcinoma. Am J Pathol. 2006;169(5):1812–20.
25. Cortez MA, Bueso-Ramos C, Ferdin J, Lopez-Berestein G, Sood AK, Calin GA. MicroRNAs in body fluids–the mix of hormones and biomarkers. Nat Rev Clin Oncol. 2011;8(8):467–77.
26. Metias SM, Lianidou E, Yousef GM. MicroRNAs in clinical oncology: at the crossroads between promises and problems. J Clin Pathol. 2009;62(9):771–6.
27. Raposo G, Stoorvogel W. Extracellular vesicles: exosomes, microvesicles, and friends. J Cell Biol. 2013;200(4):373–83.
28. Théry C, Boussac M, Véron P, Ricciardi-Castagnoli P, Raposo G, Garin J, et al. Proteomic analysis of dendritic cell-derived exosomes: a secreted subcellular compartment distinct from apoptotic vesicles. J Immunol. 2001;166(12):7309–18.
29. Andre F, Schartz NE, Movassagh M, Flament C, Pautier P, Morice P, et al. Malignant effusions and immunogenic tumour-derived exosomes. Lancet. 2002;360(9329):295–305.
30. Taylor DD, Gercel-Taylor C. MicroRNA signatures of tumor-derived exosomes as diagnostic biomarkers of ovarian cancer. Gynecol Oncol. 2008;110(1):13–21.
31. Gonzales PA, Zhou H, Pisitkun T, Wang NS, Star RA, Knepper MA, et al. Isolation and purification of exosomes in urine. Methods Mol Biol. 2010;641:89–99.
32. Simons M, Raposo G. Exosomes–vesicular carriers for intercellular communication. Curr Opin Cell Biol. 2009;21(4):575–81.
33. Keller S, Sanderson MP, Stoeck A, Altevogt P. Exosomes: from biogenesis and secretion to biological function. Immunol Lett. 2006;107(2):102–8.
34. Schmidt O, Teis D. The ESCRT machinery. Curr Biol. 2012;22(4):R116–20.
35. Kowal J, Tkach M, Théry C. Biogenesis and secretion of exosomes. Curr Opin Cell Biol. 2014;29:116–25.
36. Lakkaraju A, Rodriguez-Boulan E. Itinerant exosomes: emerging roles in cell and tissue polarity. Trends Cell Biol. 2008;18(5):199–209.
37. Stenmark H. Rab GTPases as coordinators of vesicle traffic. Nat Rev Mol Cell Biol. 2009;10(8):513–25.
38. Greening DW, Xu R, Ji H, Tauro BJ, Simpson RJ. A protocol for exosome isolation and characterization: evaluation of ultracentrifugation, density-gradient separation, and immunoaffinity capture methods. Methods Mol Biol. 2015;1295:179–209.
39. Gould SJ, Raposo G. As we wait: coping with an imperfect nomenclature for extracellular vesicles. J Extracell Vesicles. 2013;2:20389. doi:10.3402/jev.v2i0.20389.
40. Kanchi Ravi R, Khosroheidari M, DiStefano JK. A modified precipitation method to isolate urinary exosomes. J Vis Exp. 2015;95:51158. doi:10.3791/51158 **PubMed PMID: 25651044**.
41. Ronquist G, Brody I, Gottfries A, Stegmayr B. An Mg^{2+} and Ca^{2+}-stimulated adenosine triphosphatase in human prostatic fluid: part I. Andrologia. 1978;10:261–72.
42. Burden HP, Holmes CH, Persad R, Whittington K. Prostasomes—their effects on human male reproduction and fertility. Hum Reprod Update. 2006;12(3):283–92.
43. Aalberts M, Stout TA, Stoorvogel W. Prostasomes: extracellular vesicles from the prostate. Reproduction. 2013;147(1):R1–14. doi:10.1530/REP-13-0358 **Review. PubMed PMID: 24149515**.
44. Carlsson L, Påhlson C, Bergquist M, Ronquist G, Stridsberg M. Antibacterial activity of human prostasomes. Prostate. 2000;44(4):279–86.
45. Bjartell A, Montironi R, Berney DM, Egevad L. Tumour markers in prostate cancer II: diagnostic and prognostic cellular biomarkers. Acta Oncol. 2011;50(Suppl 1):76–84.
46. Brouwers JF, Aalberts M, Jansen JW, van Niel G, Wauben MH, Stout TA, et al. Distinct lipid compositions of two types of human prostasomes. Proteomics. 2013;13(10–11):1660–6.
47. Li H, Huang S, Guo C, Guan H, Xiong C. Cell-free seminal mRNA and microRNA exist in different forms. PLoS ONE. 2012;7(4):e34566.
48. Babiker AA, Nilsson B, Ronquist G, Carlsson L, Ekdahl KN. Transfer of functional prostasomal CD59 of metastatic prostatic cancer cell origin protects cells against complement attack. Prostate. 2005;62(2):105–14.
49. Sahlén G, Ahlander A, Frost A, Ronquist G, Norlén BJ, Nilsson BO. Prostasomes are secreted from poorly differentiated cells of prostate cancer metastases. Prostate. 2004;61(3):291–7.
50. Tavoosidana G, Ronquist G, Darmanis S, Yan J, Carlsson L, Wu D, et al. Multiple recognition assay reveals prostasomes as promising plasma biomarkers for prostate cancer. Proc Natl Acad Sci USA. 2011;108(21):8809–14.
51. Ahadi A, Brennan S, Kennedy PJ, Hutvagner G, Tran N. Long non-coding RNAs harboring miRNA seed regions are enriched in prostate cancer exosomes. Sci Rep. 2016;6:24922.
52. Huang X, Yuan T, Tschannen M, Sun Z, Jacob H, Du M, et al. Characterization of human plasma-derived exosomal RNAs by deep sequencing. BMC Genom. 2013;14:319.
53. Skog J, Würdinger T, van Rijn S, Meijer DH, Gainche L, Sena-Esteves M, et al. Glioblastoma microvesicles transport RNA and proteins that promote tumour growth and provide diagnostic biomarkers. Nat Cell Biol. 2008;10(12):1470–6.
54. Brase JC, Johannes M, Schlomm T, Fälth M, Haese A, Steuber T, et al. Circulating miRNAs are correlated with tumor progression in prostate cancer. Int J Cancer. 2011;128(3):608–16.
55. Casanova-Salas I, Rubio-Briones J, Fernández-Serra A, López-Guerrero JA. miRNAs as biomarkers in prostate cancer. Clin Transl Oncol. 2012;14(11):803–11.
56. Endzeliņš E, Melne V, Kalniņa Z, Lietuvietis V, Riekstiņa U, Llorente A, et al. Diagnostic, prognostic and predictive value of cell-free miRNAs in prostate cancer: a systematic review. Mol Cancer. 2016;15(1):41.
57. Shariat SF, Semjonow A, Lilja H, Savage C, Vickers AJ, Bjartell A. Tumor markers in prostate cancer I: blood-based markers. Acta Oncol. 2011;50(Suppl 1):61–75.
58. Hizir MS, Balcioglu M, Rana M, Robertson NM, Yigit MV. Simultaneous detection of circulating oncomiRs from body fluids for prostate cancer staging using nanographene oxide. ACS Appl Mater Interfaces. 2014;6(17):14772–8.
59. Bonci D, Coppola V, Musumeci M, Addario A, Giuffrida R, Memeo L, et al. The miR-15a-miR-16-1 cluster controls prostate cancer by targeting multiple oncogenic activities. Nat Med. 2008;14(11):1271–7.
60. Li Z, Ma YY, Wang J, Zeng XF, Li R, Kang W, et al. Exosomal microRNA-141 is upregulated in the serum of prostate cancer patients. Onco Targets Ther. 2016;9:139–48.

61. Hessvik NP, Sandvig K, Llorente A. Exosomal miRNAs as Biomarkers for prostate cancer. Front Genet. 2013;4:36.
62. Gallo A, Tandon M, Alevizos I, Illei GG. The majority of microRNAs detectable in serum and saliva is concentrated in exosomes. PLoS ONE. 2012;7(3):e30679.
63. Bonci D, Coppola V, Patrizii M, Addario A, Cannistraci A, Francescangeli F, et al. A microRNA code for prostate cancer metastasis. Oncogene. 2016;35(9):1180–92.
64. Bryant RJ, Pawlowski T, Catto JW, Marsden G, Vessella RL, Rhees B, et al. Changes in circulating microRNA levels associated with prostate cancer. Br J Cancer. 2012;106(4):768–74.
65. Lodes MJ, Caraballo M, Suciu D, Munro S, Kumar A, Anderson B. Detection of cancer with serum miRNAs on an oligonucleotide microarray. PLoS One. 2009; 4(7):e6229.
66. Circulating microRNAs (miRNA) in serum of patients with prostate cancer. Mahn R, Heukamp LC, Rogenhofer S, von Ruecker A, Müller SC, Ellinger J. Urology. 2011; 77(5):1265.e9-16.
67. Motamedinia P, Scott AN, Bate KL, Sadeghi N, Salazar G, Shapiro E, et al. Urine exosomes for non-invasive assessment of gene expression and mutations of prostate cancer. PLoS ONE. 2016;11(5):e0154507.
68. Øverbye A, Skotland T, Koehler CJ, Thiede B, Seierstad T, Berge V, et al. Identification of prostate cancer biomarkers in urinary exosomes. Oncotarget. 2015;6(30):30357–76.
69. McKiernan J, Donovan MJ, O'Neill V, Bentink S, Noerholm M, Belzer S, et al. A novel urine exosome gene expression assay to predict high-grade prostate cancer at initial biopsy. JAMA Oncol. 2016;2(7):882–9.
70. Nilsson J, Skog J, Nordstrand A, Baranov V, Mincheva-Nilsson L, Breakefield XO, et al. Prostate cancer-derived urine exosomes: a novel approach to biomarkers for prostate cancer. Br J Cancer. 2009;100(10):1603–7.
71. Samsonov R, Shtam T, Burdakov V, Glotov A, Tsyrlina E, Berstein L, et al. Lectin-induced agglutination method of urinary exosomes isolation followed by mi-RNA analysis: application for prostate cancer diagnostic. Prostate. 2016;76(1):68–79.
72. Moltzahn F, Olshen AB, Baehner L, Peek A, Fong L, Stöppler H, et al. Microfluidic-based multiplex qRT-PCR identifies diagnostic and prognostic microRNA signatures in the sera of prostate cancer patients. Cancer Res. 2011;71(2):550–60.
73. Lodes MJ, Caraballo M, Suciu D, Munro S, Kumar A, Anderson B. Detection of cancer with serum miRNAs on an oligonucleotide microarray. PLoS ONE. 2009;4(7):e6229.
74. Shen MM, Abate-Shen C. Molecular genetics of prostate cancer: new prospects for old challenges. Genes Dev. 2010;24(18):1967–2000.
75. Hessvik NP, Phuyal S, Brech A, Sandvig K, Llorente A. Profiling of microRNAs in exosomes released from PC-3 prostate cancer cells. Biochim Biophys Acta. 2012;1819(11–12):1154–63.
76. Corcoran C, Rani S, O'Driscoll L. miR-34a is an intracellular and exosomal predictive biomarker for response to docetaxel with clinical relevance to prostate cancer progression. Prostate. 2014;74(13):1320–34.
77. Fujita Y, Kojima K, Hamada N, Ohhashi R, Akao Y, Nozawa Y, et al. Effects of miR-34a on cell growth and chemoresistance in prostate cancer PC3 cells. Biochem Biophys Res Commun. 2008;377(1):114–9.

DE GRUYTER

Volume 2, Issue 4 (Apr 2017) Previous Article

Recent advances in “bioartificial polymeric materials” based nanovectors

Raffaele Conte / Ilenia De Luca / Anna Valentino / Anna Di Salle / Anna Calarco / Francesco Riccitiello / Gianfranco Peluso

Published Online: 2017-04-25 | **DOI:** https://doi.org/10.1515/psr-2016-0131

FREE ACCESS

Abstract

This chapter analyzes the advantages of the use of bioartificial polymers as carriers and the main strategies used for their design. Despite the enormous progresses in this field, more studies are required for the fully evaluation of these nanovectors in complex organisms and for the characterization of the pharmacodynamic and pharmacokinetic of the loaded drugs. Moreover, progresses in polymer chemistry are introducing a wide range of functionalities in the bioartificial polymeric material (BPM) nanostructures leading to a second generation of bioartificial polymer therapeutics based on novel and heterogeneous architectures with higher molecular weight and predictable structures, in order to achieve greater multivalency and increased loading capacity. Therefore, research on bioartificial polymeric nanovectors is an “on-going” field capable of attracting medical interest.

Keywords: chitosan; doxorubicin; nanofibers; poly(ethylene glycol)

1 Introduction

1.1 Bioartificial polymeric materials

“Bioartificial polymeric materials” (BPMs) are a class of polymeric composites based on the blend between synthetic and natural polymers, designed to produce new materials combining the biocompatibility of the biological components with the physical and mechanical features of the synthetics [1–3].These materials are engineered for different applications such as biodegradable delivery systems, leak proof membranes, systems of proteins purification, dialysis membranes, wound dressing, artificial skin, cardiovascular devices, nerve guide channels, implantable devices, bone graft substitutes [4–6] and have an enormous repercussion in the human life quality [7]. Table 1summarizes the main applications of these materials (Table 1).

Tab.

Table 1:

Uses of bioartificial polymeric materials.

1.1.1 Natural polymers for BPMs

Natural polymers are macromolecules produced by living organisms (e.g. plants, mammals, crustaceans) with structural or functional purposes. The main classes of natural polymers are polynucleotides, polypeptides and polysaccharides [8]. Polynucleotides act as carriers of the genetic information, polypeptides function as structural materials or catalysts, polysaccharides are components of membranes and enhance intracellular communication [9]. Natural polymers are broadly used as advanced materials for the production of fibers, adhesives, coatings, gels, thermoplastics, resins, etc. and most of them have medical applications [9, 10]. (Table 2). These polymers possess several inherent advantages such as bioactivity, the ability to present receptor-binding ligands to cells, susceptibility to cell-triggered proteolytic degradation and natural remodeling. However, their immunogenicity, variability in purity across groups, complex structure, strength inadequacies and difficulty in controlling material degradability limit their utilization [11].

Tab.

Table 2:

Natural polymers used for bioartificial polymeric materials.

1.1.2 Synthetic polymers for BPMs

Synthetic polymers are petroleum-based products produced by chemical reactions. These materials are important components of BPMs thanks to their inert nature, high resistance of chemical linkages to hydrolytic and oxidative degradation and ability to tailor mechanical properties. Synthetic polymers contribute to the efficient functioning of devices providing mechanical support to implants such as articulating surfaces and scaffolds (e.g. knee and hip implants), protective coatings to improve blood compatibility, electrically stimulating devices (e.g. pacemakers, heart valves), catheters and dialysis tubing, vascular grafts and implantable drug delivery systems (e.g. drug eluting coatings on vascular stents). The main classes of synthetic polymers used in BPMs include poly(olefins), poly(urethanes), poly(carbonates), poly(siloxanes), poly(amides), poly(ethers), poly(sulfones) and poly(esters) [12–15]. Table 3summarizes their chemical structures and general properties (Table 3).

Tab.

Table 3:

Synthetic polymers used for bioartificial polymeric materials.

1.2 Nanotechnology and medicine

Nanotechnology (NT) is the science of manipulating matter at the atomic or molecular scale and holds the promise of providing significant improvements in the technologies intended to enhance human well-being and protect the environment [15]. NT is often regarded as a product of the latter part of the twentieth century but it influenced human evolution from the earliest civilization. Indeed, the ancient Greeks used permanent hair-dying recipes composed of 5 nm lead sulfide crystals and European medieval artists colored stained glass using metal nanoparticles. Modern NT, started in 1959 when physicist Richard Feynman recognized the possibility to build machines able to manufacture objects with atomic precision and explained that, at the nanoscale, surface phenomena dominate the behavior of the objects [16]. The term NT, however, was introduced in 1974 by Norio Taniguchi referring to the “production technology to get the extra-high accuracy and ultra-fine dimensions” [17]. Practical application of NT started with the description of the molecular manufacturing [18] and the invention of the scanning tunneling microscope (STM) that allowed the first direct manipulation of individual atoms [17]. Nowadays, NT is a dynamic field where over 50,000 articles published annually and more than 2,500 patents filed [19].

Nanomedicine, an offshoot of NT, uses nano-sized tools for the diagnosis, prevention and treatment of diseases (Figure 1). Applicative examples are biosensors, implantable devices, prostheses components and drug delivery platforms. This chapter focuses on the delivery of therapeutic substances through bioartificial polymeric nanovectors, a novel and interesting aspect of nanomedicine.

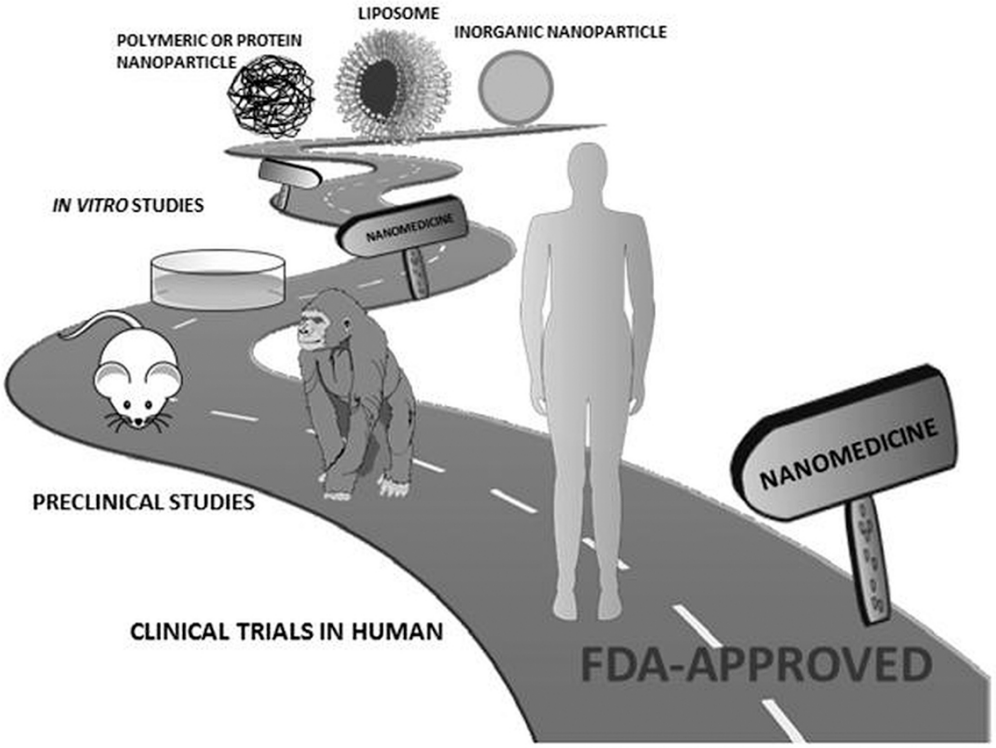

Figure 1:

Nanovectors direction to the FDA approval.

2 Bioartificial polymeric nanovectors

Drug delivery is the method of administering pharmaceutical compounds to achieve therapeutic effects in humans or animals [20]. The delivery vehicles are films, plasters, gels and polymeric-based nanovectors. Among these, nano-sized delivery systems have a significant role in the alteration of bioavailability, pharmacokinetic and pharmacodynamic properties of drug molecules thanks to their favorable chemical-physical characteristics due to the reduced dimensions, their ability of delivering therapeutic agents directly into the intended site of action and their capability to overcome tight junction membrane barriers (e.g. blood brain barrier and blood-ocular-barrier) [21–24]. Nanovectors are particularly useful to transport drugs that have poor solubility or a short half-life and have numerous biological applications such as cancer therapy, stabilization and protection of molecules, proteins, peptides and DNA, analysis of environmental hazards, protein and gene delivery, action as self-regulated devices bio-recognizable systems and stimuli-controlled vectors [25–27].

BPMs are widely used as nano-sized drug delivery systems due to the synthetically controllable size, surface charge and morphology, solubility, mechanical properties and pharmacokinetic [24, 28–30]. Bioartificial polymeric nanovectors are targeted to the biological substrate using three different mechanisms: active targeting, passive targeting and endocytosis. Active targeting is an internalization method that uses receptors, surface ligands, antigen-antibody combinations or aptamers to enter targeted tissues or cells. Passive targeting takes advantage of nanosystems’ physicochemical properties (e.g. small size, surface functionalization, morphology) to accumulate in target tissues. In particular, the nanovehicles are able to enter into the cells through van der Waals forces, electrostatic charges, steric interactions or interfacial tension based on the pathophysiological characteristics of the tissues (e.g. extravasation of nanovectors through the “leaky” endothelium of tumor tissue). Finally, endocytosis, the major route for nanomedicines, allows transport of nanodelivery systems across cell membrane and is generally classified into phagocytosis and pinocytosis [31–34]. The synthesis of BPM nanovectors

depends on the polymeric units of the material and follows top down or bottom up approaches. “Top down” approach refers to the reduction of a bulk material to get nano-sized particle, while “bottom up” allows the build of nanoparticles starting from the monomers [35]. The technique used greatly impacts the physical, chemical and biological properties of the produced vehicles and influences their size, shape and surface chemistry [36–38]. However, clinical utilization of BPM-based nanovectors is still at the early stages and the commercialized vehicles are mainly composed of synthetic polymers. Table 4summarizes the marketed polymeric nanovectors for drug delivery applications (Table 4).

Tab.

Table 4:

Commercialized polymeric nanovectors for drug delivery applications.

2.1 Nanospheres and Nanocapsules

Nanospheres (NSs) and nanocapsules (NCs) are nano-sized vectors composed of amphiphilic copolymers structured with hydrophobic chains forming the inner part of the particles and hydrophilic portions on the surface. NSs have homogeneous solid matrices [39] while NCs exhibit a core-shell structure in which the drug is confined to a reservoir or within a cavity surrounded by a polymer membrane [40]. Both NSs and NCs allow the fine tuning of their properties through surface functionalization, the use of different shell materials and with the regulation of their size [41–43]. Poly-lactic acid (PLA), poly-glycolic acid (PGA), poly-lactic-co-glycolic acid (PLGA), poly ε-caprolactone (PCL), chitosan (CS) and polyethylene glycol (PEG) are the main materials used for the synthesis of these systems due to their wide biocompatibility and biodegradability [44–48]. NS drugs are dissolved, entrapped, encapsulated, chemically bound or adsorbed to the constituent polymer matrix [49, 50] while NCs carry the active substance in the core, or on their surfaces or absorbed in the polymeric membrane [51–53]. The use of NSs and NCs is an attractive strategy for the vectorization of a variety of active substances such as antineoplastics, antiinflammatories, immunosuppressants, antigens, hormones, antivirals, antibacterials, antifungals, diuretics, antipneumocystics and vitamins. Moreover, these systems are useful to mask unpleasant tastes, to provide controlled release properties, to protect vulnerable molecules from degradation and to increase the therapeutic efficacy of active molecules [54, 55]. Finally, NSs and NCs have high intracellular uptake and require a low amount of polymer for each particle, resulting in high drug loading [46, 49]. NSs and NCs have common preparation techniques that are classified into two general categories depending on the starting material. The use of monomers requires emulsion polymerization, interfacial polymerization or ionic gelation methods. Differently, for preformed polymers, nanoparticle preparation is achieved through emulsification/solvent evaporation, emulsification/solvent diffusion, salting out, dialysis and nanoprecipitation. The emulsion polymerization method is carried out using organic or aqueous solvents as continuous phase [46]. Surfactants or protective soluble polymers are used to prevent aggregation in the early stages of the polymerization. The polymerization process starts using an initiator molecule (ion or free radical), or activating the monomer with high-energy radiations. Incorporation of active principles is obtained dissolving the substance in the same phase of the monomers. The interfacial polymerization is a process with a similar mechanism that involves the dissolution of two reactive agents into two phases (i.e., continuous- and dispersed-phase), with the reaction that takes place at the interface of the two liquids [56]. Interfacial polymerization permits to modulate the formation of NSs or NCs using different eluents. In fact, to promote NC formation, aprotic solvents are used, while protic liquids induce the formation of NSs [57]. Incorporation of active principles is obtained dissolving the drug into the dispersed phase. Ionic gelation permits the preparation of polymeric nanoparticles using biodegradable hydrophilic polymers such as CS, gelatin and sodium alginate. This method requires the mixture of two aqueous phases, one containing the hydrophilic polymer and the other a crosslinker (e.g. poly-anion sodium tripolyphosphate). The positive groups of the polymer interact with negative charged crosslinkers to form nano-sized vectors [58]. Drug is added in the same phase of the hydrophilic polymer [58]. Emulsification/solvent evaporation is a method that requires the preparation of the polymer solution in lipophilic volatile solvent with a subsequent formation of an emulsion, adding water and stabilizers. The lipophilic solvent diffuses through the emulsion and its evaporation lead to the formation of a nanoparticle suspension. High-speed homogenization or sonication is utilized to improve the diffusion, while the solvent evaporation is favored by continuous magnetic stirring at room temperature or under reduced pressure. The solidified nanoparticles are collected by centrifugation and washed with distilled water to remove additives [59]. Drug loading is carried dispersing the substance in the volatile solvent. Similarly, in the emulsification/solvent diffusion method, the encapsulating polymer is dissolved in a partially water soluble eluent and saturated with water to ensure the diffusion. Subsequently, the polymer-water saturated solvent phase is emulsified in an aqueous solution containing stabilizers, leading to the solvent diffusion to the external phase and to the formation of nanovectors. Drug loading is achieved dissolving the substance in the polymer phase [46]. Salting out is a modification of the emulsification/solvent diffusion in which polymer and drug are initially solubilized in the volatile solvent which is emulsified into an aqueous gel containing salting-out agents (e.g. electrolytes, such as magnesium chloride, calcium chloride, and magnesium acetate, or non-electrolytes such as sucrose) and colloidal stabilizers (e.g. polyvinylpyrrolidone or hydroxyethylcellulose). This oil/water emulsion is diluted with aqueous solutions to enhance the diffusion. The salting out agents improve the encapsulation efficiency of the drug [46]. In the dialysis methodology, the polymer is dissolved in an organic solvent and placed inside a dialysis tube. Dialysis is performed against a non-solvent miscible with the lipophilic eluent. The progressive aggregation of polymer and the formation of nanoparticles is the consequence of the displacement of the organic solvent inside the membrane [59]. Drug incorporation is obtained adding the active principle in the same eluent of the polymer. Finally, in the nanoprecipitation method, the polymer is solubilized in a water-miscible solvent and is injected into a stirred aqueous solution containing a surfactant. The stirring causes a fast diffusion of the solvent and the polymer deposition on the interface between the water and the organic eluent, leading to the instantaneous formation of a colloidal suspension [60]. The aqueous solution must be a non-solvent of the polymer [61]. Drug encapsulation is achieved solubilizing the drug into the organic solvent [61]. A schematic representation of the described preparation techniques is available in Figure 2. Bioartificial polymers are widely studied as components of NSs and NCs. Such systems are described by Bellotti et al. as composed of butyl methacrylate, poly(ethylene glycol) methyl ether methacrylate, 2-(dimethylamino) ethyl methacrylate crosslinked with trimethylolpropane trimethacrylate and functionalized with folic acid on their surface in order to specific target enclosed anticancer drug to cancer cells [62]. The antitumor activity is the subject of research of several other authors. For example, Cui et al. formed ionically assembled nanoparticles from poly(ionic liquid-co-N-isopropylacrylamide) with deoxycholic acid through electrostatic interactions. These nanoparticles exhibit dual-responsive properties based on pH and thermal environment conditions with practical applications as drug

delivery carriers, as shown by the encapsulation of doxorubicin. In particular, low pH and high temperature provoke structural collapse of the ionically assembled nanoparticle and the release of doxorubicin. In fact, 80 % of drug molecules are released within 48 h at pH 5.2, 43 °C, but only 30 % of doxorubicin is released within 48 h at 37 °C and pH 7.4 [63]. Bahadur et al. designed nanoparticles formed by poly(2-(pyridin-2-yldisulfanyl)ethyl acrylate) conjugated with PEG and cyclo(Arg-Gly-Asp-d-Phe-Cys) peptide. These nanovectors are loaded with doxorubicin. The size of the vehicle is 50.13 ± 0.5 nm in PBS. Such vectors are stable in physiological condition and release doxorubicin with the trigger of acidic pH and redox potential. Moreover, these acrylate-based nanoparticles show a two-phase release kinetics, providing both loading and maintenance doses for cancer therapy. The conjugation with the peptide enhances the cellular uptake and nuclear localization. In fact, these vectors exhibit significantly higher anticancer efficacy compared to that of free doxorubicin at concentrations higher than 5 μM [64]. Barick et al. synthesized glycine functionalized magnetite (Fe_3O_4) nanoparticles by Michael addition/amidation reaction. These nanocarriers have average size of about 10 nm and are resistant to protein adsorption in physiological medium. Moreover, the terminal amino acids on the shell of the magnetic nanocarriers allow outer functionalization and potential conjugation with drug molecules. The encapsulation of doxorubicin as model drug revealed high loading affinity, sustained release profile, magnetic-field-induced heating and substantial cellular internalization. Moreover, the enhanced toxicity to tumor cells using a local magnetic field suggests their potential for combination therapy involving hyperthermia and chemotherapy [65]. Similarly, Zhao et al. produced arginine–glycine–aspartic acid-modified Fe_3O_4 nanoparticles to control the delivery and release of doxorubicin. The conjugation of these targeted magnetite nanoparticles with the drug is *via* acid-labile imine bond. Such linkage gives magnetic control, specific targeting and pH-responsivity to the nanocarriers. The cell toxicity assays indicate higher anticancer activity of these pH-sensitive magnetic nanocarriers compared to free doxorubicin and increased cytotoxicity consequent to the conjugation with arginine–glycine–aspartic acid peptides [66]. Cheng et al. developed nanoparticles of carboxy-terminated poly(d,L-lactide-co-glycolide)-block-poly(ethylene glycol) conjugated with A10 RNA aptamers, able to bind the prostate specific membrane antigens. Such nanoparticles deliver docetaxel and paclitaxel to tumor cells. These nanovectors are evaluated in a xenograft mouse model of prostate cancer. The surface functionalization with A10 aptamers significantly enhances the delivery to tumors [67]. Patil et al. synthesized copolymer PLA–PEG nanoparticles functionalized with biotin or folic acid and incorporating paclitaxel, by solvent polymerization technique. The addiction of the ligands significantly enhances nanoparticles accumulation in tumor cells *in vitro* and results in improved efficacy of in a mouse xenograft tumor model [68]. Farokhzad et al. synthesized a bioconjugate composed of PLA-block-PEG copolymer and aptamers for targeted delivery to prostate cancer cells. These nanovectors encapsulate the model drug rhodamine labeled with dextran. Such nanoparticles present carboxylic acid groups on the particle surface, useful for functionalization and for covalent conjugation with amine-modified aptamers. Moreover, the coating of PEG enhances circulating half-life and decreases the uptake into non-targeted cells. The bioconjugation with RNA aptamers permits the targeting on prostate LNCaP epithelial cells [69]. Schiffelers et al. produced self-assembling nanoparticles with siRNA and polyethyleneimine PEGylated with an Arg-Gly-Asp (RGD) peptide ligand attached at the distal end of the PEG. These nanovectors deliver siRNA inhibiting vascular endothelial growth factor receptor-2 expression into tumor neovasculature expressing integrins. Intravenous administration of this system into tumor-bearing mice results in selective tumor uptake, siRNA sequence-specific inhibition of protein expression within the tumor and reduction of both tumor angiogenesis and growth rate [70]. Cho et al. synthesized retinoic acid loaded poly(L-lactic acid) nanoparticles coated with galactose-carrying polymer for hepatocyte-specific targeting using galactose ligands as recognition signals to asialoglycoprotein receptors. The authors study the effects of released retinoic acid on morphology and DNA synthesis of hepatocytes. Such drugs modify *in vitro* shapes of hepatocytes. Moreover, fluorescence and confocal laser microscopic studies confirm the positive influence of galactose-carrying polymers coating on nanoparticles internalization [71] Soppimath et al. synthesized core-shell nanoparticles, self-assembled from the amphiphilic tercopolymer poly(N-isopropylacrylamide-co-N,N-dimethylacrylamide-co-10-undecenoic acid) in which 10-undecenoic acid is employed as hydrophobic and pH-sensitive segment. The temperature responsiveness of the core-shell nanoparticles is triggered by a change in the environmental pH. The shell of these nanoparticles is composed of amine groups able to conjugate biological signals for specific affinities to certain cell types. Such nanoparticles, loaded with doxorubicin, are stable in PBS at 37 °C but precipitate in acidic environment, triggering the release of the enclosed drug molecules [72]. Shu et al. produced crosslinked hollow polyelectrolyte NCs composed of cysteamine conjugated CS and dextran sulfate by adsorption on β-cyclodextrin functionalized silica spheres. These NCs have enhanced physical stability against acidic pH conditions and decrease the loss of protein caused by the gastric cavity and the release of drugs in the intracellular environment after glutathione reduction. Bovine serum albumin (BSA) used as model drug exhibits spherical morphology, dimension of 120 nm, with a good polydispersion index and sustained release without the initial burst [73]. The cited vehicles are summarized in Table 5.

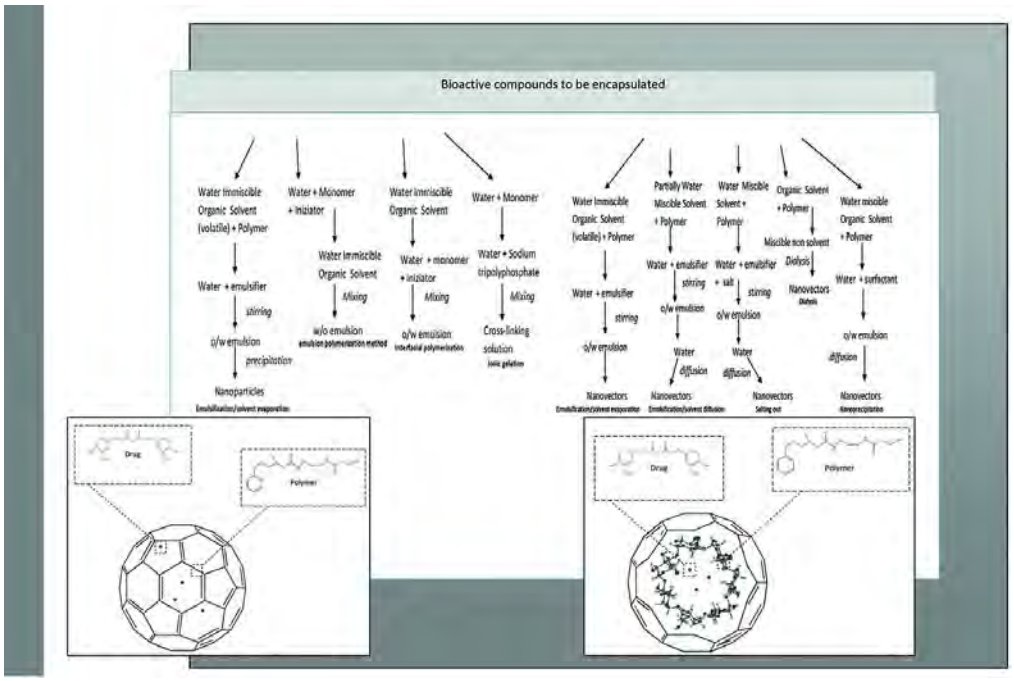

Figure 2:

Schematic representation and manufacturing methods of nanospheres –left- and nanocapsules –right.

Tab.

Table 5:

Bioartificial polymeric nanospheres and nanocapsules.

2.2 Nanohydrogels and nanoaggregates

Nanohydrogels (NHYs) are nano-sized networks of polymer chains able to incorporate H_2O in their structure. Usually, NHYs are macromolecular hydrocolloids with numerous hydrophilic functional groups [74]. Their composition ranges from linear water-soluble polymers to water insoluble molecules that act as swellable networks stabilized by crosslinking agents. In general, these substances have high molecular weight (5000–10000 Da) and cannot cross-biological membranes. Further, they include cellulosic components like sodium carboxymethyl cellulose or polyanion bioadhesives like polyacrylic acid. These nanovectors are classified on the basis of the presence or absence of electrical charge located on the crosslinked chains. In fact, they are grouped as nonionic, anionic, cationic, amphoteric electrolytes or zwitterions. The surface charge regulates the adhesivity. For example NHYs, due to their capability of forming strong non-covalent bonds with the mucin, have prolonged ocular residence time and reduced dosing frequency [75]. Production of hydrogels requires the simple preparation of polymer solutions in low or intermediate concentrations and the formation of crosslinks for the prevention of the dissolution. Many crosslinking methods are currently available for hydrogel synthesis. Generally, physically crosslinked gels are those whereas physical interactions exist between polymer chains (e.g. hydrogen bonds, amphiphilic graft) while chemically crosslinked hydrogels are synthesized with covalent bonds (e.g. crosslink with aldehydes, free radical polymerization). The nanodimensions are usually obtained with sonication [76]. The medical application of nano-sized hydrogels is limited by the difficult administration of an accurate dose of active principle due to the variable release of gelified systems [75]. Nanoaggregates (NAGs) are colloidal carriers formed from amphiphilic block copolymers. In some cases, further molecules act as crosslinker agents. NAGs possess inherent properties such as high loading efficiency and *in vivo* stability. These vehicles are able to provide site-specific drug delivery via either a passive or active targeting mechanisms. NAGs are suitable for encapsulation of poorly water-soluble drugs by covalent conjugation as well as physical encapsulation. Active transport is achieved by conjugating a drug with vectors or ligands that bind specific receptors [77]. The synthesis of NHYs and NAGs is summarized in Figure 3. The use of bioartificial materials for the preparation of NHYs and NAGs is a novel research interest. Despite of this, a number of papers are available in literature. For example, CS-poly (acrylamide-co-methacrylic acid) hydrogels were synthesized by Ullah et al. They use different coupling agents (3-dimethylaminopropyl)-3-ethylcarbodimide hydrochloride and 3-aminopropyltriethoxysilane) and the functionalization with phenylboronic acid, a glucose sensing moiety, to design multifunctional NHYs with enhanced glucose sensitivity, stability, drug loading and release profile. Moreover, the authors study the glucose-induced volume phase transition and release profile at physiological conditions of the model drug Alizarin Red (a compound with 1,2-diol structure, similar to insulin) in order to find potential application in self-regulated insulin delivery with enhanced sensitivity toward glucose [78]. Jaiswal et al. synthesized poly *N*-isopropylacrylamide – CS-based NHYs encapsulating iron oxide (Fe_3O_4) magnetic nanoparticles through free radical polymerization of the acrylate in presence of CS. These NHSs are spherical shaped with size ranging from 50 nm to 200 nm on the base of the feed ratios of CS. The encapsulation of Fe_3O_4 nanoparticles into poly *N*-isopropylacrylamide–CS based NHYs is confirmed by transmission electron microscopy. This system shows optimal magnetization, good specific absorption rate and excellent cytocompatibility, finding potential applications in hyperthermia treatment of cancer and targeted drug delivery [79]. Yoon et al. produced self-assembled NAGs co-encapsulating doxorubicin and oligonucleotides through the conjugation of four-arm poly(ethylene glycol) with doxorubicin and anti-bcl-2 oligonucleotides. These conjugates are hydrophobically self-assembled into NAGs in aqueous solutions. Elemental scanning of the products reveals a core-shell structure with the drug located at the core of the vectors and the genetic materials at the shell. Analysis by dynamic light scattering and electron microscopy proves the complete disappearance of the particles under reducing conditions and the liberation of oligonucleotides at low pH. *In vitro* studies confirm the uptake of drug and oligonucleotides in cells treated with

NAGs [80]. Table 6recaps the described nanovectors (Table 6).

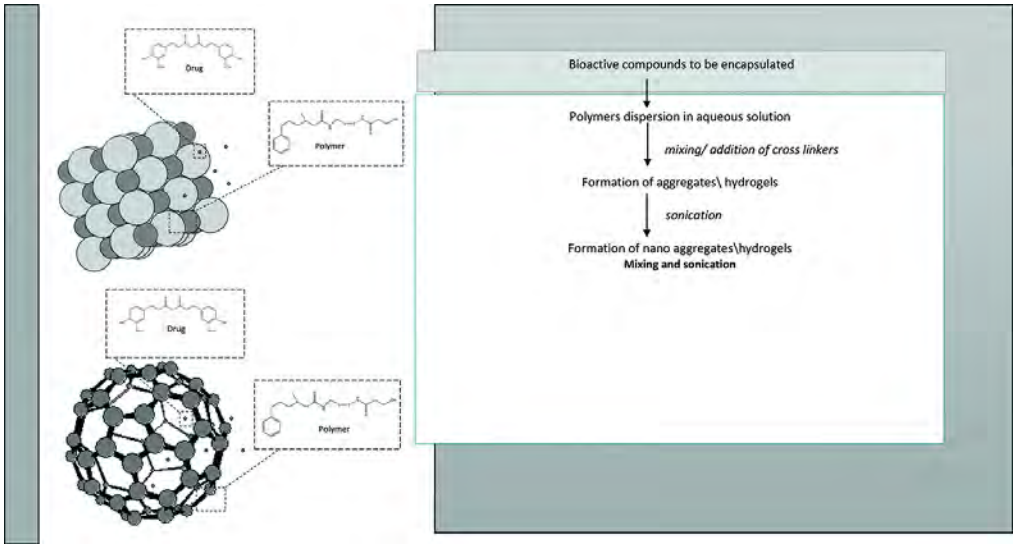

Figure 3:

Schematic representation and manufacturing methods of nanoaggregates –top- and nanohydrogels –bottom.

Tab.

Table 6:

Bioartificial polymeric nanohydrogels and nanoaggregates.

2.3 Micelles (MCs) and solid lipid nanoparticles (SLNs)

Micelles (MCs) are colloidal dispersions belonging to a large family of systems consisting of particulate matter (the “dispersed phase”), distributed within a continuous phase (the “dispersion medium”), usually constituted by water. MCs form spontaneously at certain concentration (critical micelle concentration) and temperature (critical micelle temperature) values from amphiphilic or surface active agents. Usually, these vehicles have particle size ranging between 5 and 100 nm [81, 82]. Regarding the structure, the hydrophobic fragments of amphiphilic molecules form the core of MCs, while hydrophilic fragments the shells. The formation of MCs is driven by the decrease of free energy in the system because of the removal of hydrophobic fragments from the continuous phase, and the re-establishing of hydrogen bond network in water. Moreover, additional energy results from the formation of van der Waals bonds between hydrophobic blocks in the core of the formed MCs [83]. MCs possess high stability both *in vitro* and *in vivo*, good biocompatibility and are able to solubilize a broad variety of poorly soluble pharmaceuticals through the interaction of the lipophilic substances with their hydrophobic core [84]. Many of these drug-loaded vehicles are currently at different stages of preclinical and clinical trials [85]. Micellar nano-drug delivery systems have increased water solubility, improved bioavailability, reduction of toxicity, enhanced permeability across the physiological barriers, substantial changes in drug biodistribution, extended blood half-life and protection from degradation [86]. Moreover, MCs have spontaneous interstitial penetration into the body compartments with leaky vasculature (tumors and infarcts) [87]. Active targeting of MCs is obtained through surface chemical attachment of driving molecules [88]. MCs are prepared simply dissolving the amphiphiles in water. These vectors are thermodynamically stabilized against disassembly if the amphiphilic concentration remains above the CMC. While, upon dilution below the CMC, MCs disassemble with a rate depending on the structure of the amphiphiles and on the interactions between the chains [89]. The encapsulation of molecules is obtained dissolving the substance into the micellar solution [89]. A further method of MCs preparation, useful to encapsulate non-water soluble molecules, is the thin-film hydration method. The amphiphilic copolymer and the lipophilic drug are dissolved in organic solvent. Then, the apolar eluent is removed to get the drug-containing lipid membrane. This film is resuspended in a polar solvent for nano-MCs self-assembly. The driving force of this process is the hydrophobic effect between the non-polar segments of the polymers. The hydrophobic effect also plays an important role in the drug encapsulation, stabilizing the intermolecular interaction between the substance and the hydrophobic segment [90]. SLNs are colloidal carrier systems, generally spherical in shape, composed of a high melting point lipids, as a solid core, coated by aqueous surfactants. The core lipids are fatty acids, acylglycerols and waxes, whereas phospholipids, sphingomyelins, bile salts and sterols are utilized as stabilizers [91]. SLNs are useful for the delivery of poor water soluble drugs [92]. The particle diameters are in the range of 10–1000 nm. SLNs are characterized by high biocompatibility, high bioavailability, physical stability, protection of incorporated labile drugs from degradation, excellent tolerability, prevention of problems related with multiple routs of administration, avoidance of the use of organic solvents during the preparation, formation of films over the skin showing occlusive properties and absence of problems concerning large-scale production and sterilization [93, 94]. However, common disadvantages of SLNs are particle growth, unpredictable gelation tendency, uncertain diffusion of the drug within the lipid matrix of the vector, unexpected dynamics of polymorphic transitions and inherent low incorporation rate due to the crystalline structure of the solid lipid [95, 96]. SLNs are prepared through homogenization, solvent-evaporation, microemulsion and film-ultrasound dispersion techniques. In the homogenization method, the homogenizers push a liquid with high pressure (100–2000 bar) through a narrow gap. The high shear stress and cavitation forces disrupt the particles down to the submicron range. This technique is carried in hot or cold conditions. Hot homogenization requires temperatures above the melting point of the lipid and necessitates the preparation of a pre-emulsion of the drug loaded lipid melt with the aqueous emulsifier. Higher temperatures result in lower particle sizes. In cold conditions, the drug containing lipid melt is cooled and dispersed into a cold surfactant solution. This pre-suspension is homogenized at or below room temperature, breaking the lipids in solid nanoparticles. In the solvent-evaporation method, the lipids are dissolved in a water-immiscible organic solvent that is emulsified in an aqueous solvent. The nanoparticles

dispersion is obtained upon evaporation of the eluent that leads to lipid precipitation. The microemulsion technique is operated stirring a mixture of low melting fatty acids, emulsifiers and water, at 65–70 °C. This hot liquid is dispersed in cold water (2–3 °C) under stirring. The high-temperature gradient facilitates rapid lipid crystallization and prevent aggregation. Finally, in the film-ultrasound dispersion method, the lipid and the drug are put into suitable organic solution that is evaporated to form a lipid film. The following addition of an aqueous solvent results in an emulsion that is sonicated giving SLNs with uniform particle size [97]. A recap of the production methods for both MCs and SLNs is available in Figure 4. Bioartificial polymers are widely used in the preparation of both these vesicular systems. For example, Zhang et al. used the core crosslinking method to generate MCs able to increase curcumin delivery to HeLa cells (immortalized cancer cells) *in vitro* and improve tumor accumulation *in vivo*. These MCs are designed with folic acid-PEG as the hydrophilic unit, pyridyldisulfide as the crosslinkable and hydrophobic unit, and disulfide bond as the crosslinker. Such nanovectors show spherical shape with a diameter of 91.2 nm and high encapsulation efficiency. Cytotoxicity effectiveness is demonstrated by the high cellular uptake and the positive *in vitro* antitumor studies. The linkage with folate targets the curcumin against cancer cells and enhances the *in vivo* efficacy of these MCs [98]. Similarly, Lee et al. produced pH-sensitive polymeric MCs composed of poly(l-histidine), PEG and poly(L-lactic acid) block copolymers with folate conjugation, delivering adriamycin. These MCs are investigated for pH-dependent drug release, folate receptor-mediated internalization and cytotoxicity using MCF-7 cells (human breast adenocarcinoma cell line) *in vitro*. These nanovectors show accelerated drug release only at acidic pH. Moreover, the conjugation with folic acid enhances tumor cell kill due to folate receptor-mediated tumor uptake [99]. Li et al. reported linear PEG and dendritic cholic acids block copolymers MCs stabilized with boronate esters at the core–shell interface for efficient anticancer drug delivery. Such system is loaded with paclitaxel to assess its capacity to retain the encapsulated drug under physiological conditions and release the payload when triggered by the lower pH value of the tumor environment or by the presence of competitive diols (e.g. mannitol). This nanovector shows minimal premature drug release at physiological glucose level and physiological pH values in blood circulation and simple activation at the acidic tumor microenvironment or by the additional intravenous administration of mannitol as an on-demand triggering agent [100]. Paclitaxel-loaded mixed polymeric MCs consisting of poly(ethylene glycol) distearoyl phosphoethanolamine conjugates, solid triglycerides and cationic lipofectin lipids were prepared by Wang et al. Optimized MCs have average size of about 100 nm, and zeta-potential of about −6 mV. Such vehicles are stable when stored at 4°C or at room temperature. Release of paclitaxel starts at 37 °C and, approximately, 16 % of the drug is dispensed in 72 h. *In vitro* anticancer effects of the nanovectors are evaluated using human mammary adenocarcinoma (BT-20) and human ovarian carcinoma (A2780) cell lines. The results show enhanced anti-cancer activity due to the ability of the MCs to escape from endosomes and enter the cytoplasm of BT-20 and A2780 cancer cells [101]. Lee et al. developed paclitaxel-loaded sterically stabilized SLNs for parenteral administration. These nanovectors, prepared using the hot homogenization method, are composed of trimyristin as a solid lipid core and egg phosphatidylcholine and pegylated phospholipid as stabilizers. The particles are spherical in shape, with sizes and zeta potentials of around 200 nm and −38 mV. Paclitaxel is loaded to the solid cores at a w/w ratio of 6 % with high encapsulation efficiency. *In vitro* drug release studies show a slow sustained release and high cytotoxicity on OVCAR-3 human ovarian cancer cell line and MCF-7 breast cancer cell line [102]. Gao et al. prepared poly(ethylene glycol)/phosphatidyl ethanolamine (PEG−PE) conjugates for the solubilization and delivery of various poorly soluble anticancer drugs such as m-porphyrin, tamoxifen and taxol. These MCs are stable and have the size of 10 to 40 nm [103]. Wong et al. investigated the in vivo efficacy, unwanted toxicity and loco-regional distribution of doxorubicin-loaded polymer-lipid hybrid nanoparticles formulation in a murine solid tumor model after intratumoral injection. These SLNs are prepared by dispersing the drug in stearic acid and tristearin, with subsequent addition of the hydrolyzed polymers of epoxidized soybean oil to enhance doxorubicin incorporation into the lipids. This formulation is injected intratumorally in murine solid tumors of approximately 0.3 g. *In vivo*, SLNs-treated tumors develop substantially larger central necrotic regions compared to the untreated tumors, with minimal systemic toxicity [104]. Kukowska-Latallo et al. produced polyamidoamine dendritic polymers conjugated to folic acid as targeting agent for methotrexate. These conjugates are injected intravenous into immunodeficient mice bearing human KB tumors overexpressing the folic acid receptors, resulting in high internalization into the tumor cells [105]. Table 7acts as a recap of the described nanosystems.

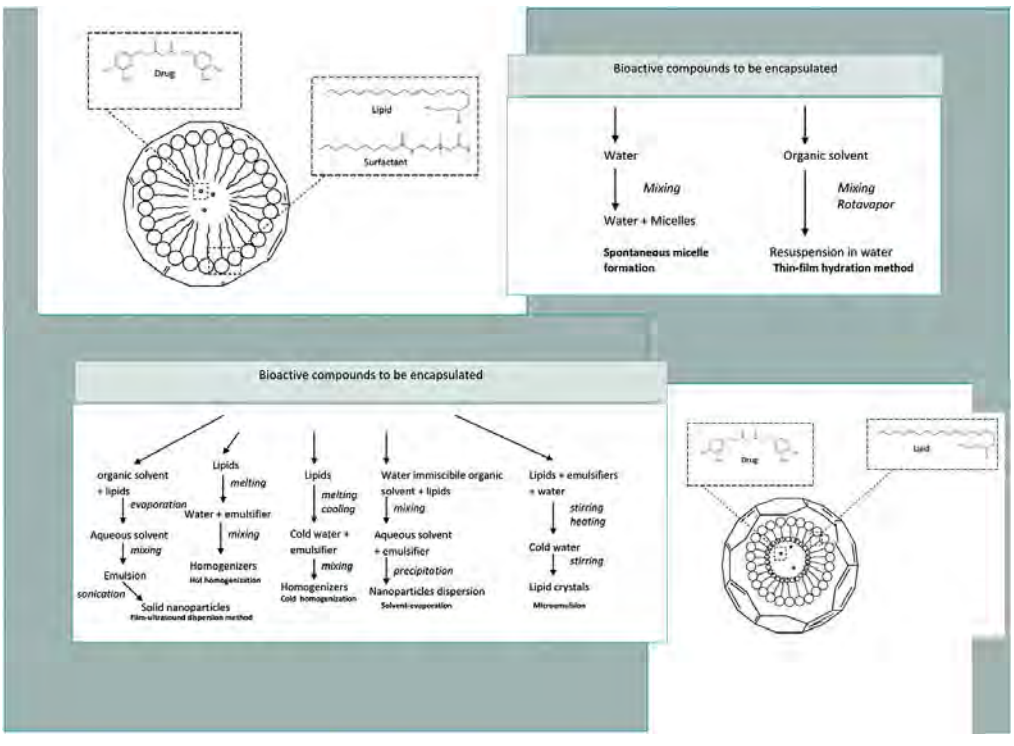

Figure 4:

Schematic representation and manufacturing methods of micelles –left- and solid lipid nanoparticles –right.

Tab.

Table 7:

Bioartificial polymeric micelles and solid lipid nanoparticles.

2.4 Nanofibers

Nanofibers (NFs) are fibers with diameters less than 100 nanometers that exhibit special properties due to the extremely high surface to weight ratio, low density, high pore volume and tight pore size [106]. These properties make NFs suitable for applications ranging from medical (e.g. drug delivery systems) to industrial and high-tech fields (e.g. aerospace, capacitors, transistors, battery separators, energy storage, fuel cells) [106]. In nanomedicine, NFs are widely used due to their similarity to the extracellular matrix (ECM), the possibility to use several materials for their synthesis (in fact, natural and synthetic polymers along with several solvent systems are effectively used to create NFs) and the possibility to change their architecture in regard to porosity, diameter, mechanical properties, structure arrangement and structure functionalization [107]. The synthetic techniques for NFs are self-assembly, phase separation and electrospinning. All of these techniques require the preparation of a homogeneous drug–polymer solution that is loaded in the electrospinning machine (electrospinning technique), is simply mixed (self-assembly method) or is treated to obtain gelation and freeze-drying (phase separation) (Figure 5) [106, 107]. Research about NFs as drug delivery systems is at the early stage of exploration and most of the works focus on the sustained release profiles of model drugs (e.g. small molecules, herbs, proteins, DNA, genes and vaccines) using biodegradable hydrophilic, hydrophobic or amphiphilic polymers and, recently, BPMs [108]. Zhang et al. reported degradable heparin-poly (ε-caprolactone) fiber mats fabricated by electrospinning. The highly sulfated heparin heteropolymer remains homogenous in the spinning solution and is distributed throughout the fabricated polymers. The NFs release heparin for 14 days with a diffusionally controlled kinetics over this period. The drug retains its biological properties and functionality [109]. Chew et al. investigated the encapsulation of human β-nerve growth factor (NGF), stabilized in BSA carrier proteins, in a copolymer of ε-caprolactone and ethyl ethylene phosphate. The proteins are randomly dispersed throughout the electrospun fibrous mesh in an aggregated form. The sustained release of NGF by diffusion is detectable for at least 3 months and the bioactivity of the drug is retained throughout this period [110]. Feng et al. produced CS polyethylene oxide NFs with uniform diameter of 112 nm and the potential modulation of CS viscosity and surface tension through the use of different CS molecular weight and polyethylene oxide quantities. These vehicles exhibit excellent biocompatibility with hepatocytes [111]. Similarly, Bhattarai et al. reported that CS\polyethylene oxide nanofibrous scaffolds promote the attachment of human osteoblast and chondrocytes, maintaining their characteristic morphology and viability. This matrix is of particular interest for tissue engineering, drug delivery and tissue remodeling [112]. Moreover, Subramanyan et al. prepared CS\polyethylene oxide NFs for cartilage tissue engineering. These scaffolds are used for cell attach and deliver of growth factors [113]. Park et al. produced chitin/poly glycolic acid NFs with BSA coating to improve human epidermal fibroblasts attach and spread [114]. Shalumon et al. developed bioactive and biocompatible NFs composed of carboxymethyl cellulose\polyvinyl alcohol blend. Such nanomaterials are tested for cytotoxicity and cell attachment, resulting in a safe application for tissue engineering and drug delivery [115]. Nanofibrous scaffold of CS\polyvinyl alcohol and carboxyethylchitosan\polyvinyl alcohol are also prepared by Zhou et al. These materials, tested on L929 fibroblast culture, have good cell attachment and growth [116]. CS hydroxyapatite nanofibrous scaffolds are reported by Yang et al. This nanomaterial significantly stimulates the bone forming ability due to the excellent osteoconductivity of hydroxyapatite [117]. Finally, Junkasem et al. described the fabrication of α-chitin whisker-reinforced poly(vinyl alcohol) NFs by electrospinning. The α-chitin whiskers are prepared from α-chitin flakes by acid hydrolysis. Such vectors exhibit average length and width of about 549 and 31 nm, respectively. The incorporation of the chitin whiskers within the poly(vinyl alcohol) is verified by infrared spectroscopy and thermogravimetry, resulting in an increased Young’s modulus of the bioartificial polymer of about 4–8 times compared to the unmodified poly(vinyl alcohol) [118]. Table 8summarizes the described bioartificial polymeric NFs (Table 8).

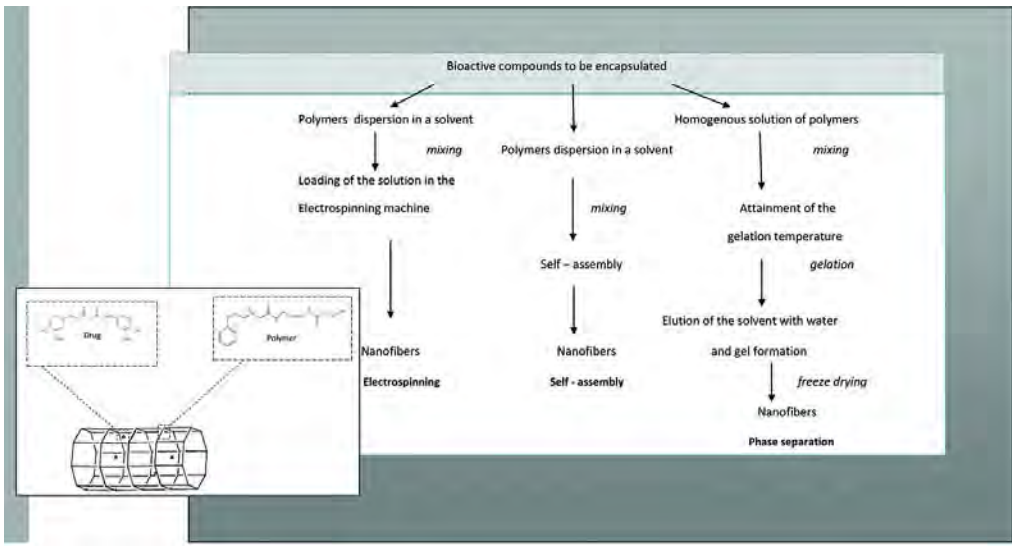

Figure 5:

Schematic representation and manufacturing methods of nanofibers.

Tab.

Table 8:

Bioartificial polymeric nanofibers.

3 Conclusion

This chapter analyzes the advantages of the use of bioartificial polymers as carriers and the main strategies used for their design. Despite the enormous progresses in this field, more studies are required for the fully evaluation of these nanovectors in complex organisms and for the characterization of the pharmacodynamic and pharmacokinetic of the loaded drugs. Moreover, progresses in polymer chemistry are introducing a wide range of functionalities in the BPM nanostructures leading to a second generation of bioartificial polymer therapeutics based on novel and heterogeneous architectures with higher molecular weight and predictable structures, in order to achieve greater multivalency and increased loading capacity. Therefore, research on bioartificial polymeric nanovectors is an “on-going” field capable of attracting medical interest.

Acknowledgment

This work was supported by Progetto PON—“Ricerca e Competitività 2007–2013”—PON01_01802: “Sviluppo di molecole capaci di modulare vie metaboliche intracellulari redox-sensibili per la prevenzione e la cura di patologie infettive, tumorali, neurodegenerative e loro delivery mediante piattaforme nano tecnologiche”, PON01_02512: “Ricerca e sviluppo di bioregolatori attivi sui meccanismi epigenetici dei processi infiammatori nelle malattie croniche e degenerative”, PON03_00106: “Materiali Avanzati per la Ricerca ed il comparto Agroalimentare, Laboratorio Pubblico-Privato, MAReA” and PRIN 2012 (prot. 201288JKYY): “Nanotecnologie per variare i programmi di sviluppo osseo nella parete vasale per la prevenzione e trattamento delle patologie associate alla calcificazione ectopica arteriosa”.

Acknowledgment

This article is also available in: Tylkowski, Polymer Engineering. De Gruyter (2017), isbn 978–3–11–046828–1.

References

1. Lazzeri L. Trends in polymer science. Cambridge, UK: Elsevier Trends Journals, 1996.
2. Barbani N, Lazzeri L, Lelli L, et al. Physical and biological stability of dehydro-thermally crosslinked collagen—Poly(vinyl alcohol) blends. J Mater Science Mater Med. 1994;5:882–886.
3. Cascone MG. Dynamic–mechanical properties of bioartificial polymeric materials. Polym Int. 1997;43:55–69.
4. Williams DF. On the nature of biomaterials. Biomaterials. 2009;30:5897–5909.
5. Ratner BD, Bryant SJ. Biomaterials: where we have been and where we are going. Annu Rev Biomed Eng. 2004;6:41–75.
6. Scotchford CA, Cascone MG, Downes S, Giusti P. Osteoblast responses to collagen-PVA bioartificial polymers in vitro: the effects of cross-linking method and collagen content. Biomaterials. 1998;19:1–11.
7. Langer R, Tirrell DA. Designing materials for biology and medicine. Nature. 2004;428:487–492.
8. Joyce Y, Wong JD. Biomaterials. Boca Raton, FL: CRC Press, 2007.
9. Long Y. Biodegradable polymer blends and composites from renewable resources. New Jersey, USA: John Wiley & Sons, 2009.
10. Sionkowska A. Natural polymers as components of blends for biomedical applications. In: Severian Dumitriu VP, editors. Polymeric biomaterials: structure and function Vol. 1. Boca Raton, FL: CRC Press, 2013.
11. Parthasarathy M, Sethuraman S. Hierarchical characterization of biomedical polymers. In: Laurencin CT, Deng M, editors. Natural and synthetic biomedical polymers. Oxford, UK: Elsevier, 2014:33–42.
12. Martina M, Hutmacher DW. Biodegradable polymers applied in tissue engineering research: a review. Polym Int. 2007;56:145–157.
13. Nair LS, Laurencin CT. Biodegradable polymers as biomaterials. Prog Polym Sci. 2007;32:762–798.
14. Ulery BD, Nair LS, Laurencin CT. Biomedical applications of biodegradable polymers. J Polymer Sci B Polymer Phys. 2011;49:832–864.
15. Place ES, George JH, Williams CK, Stevens MM. Synthetic polymer scaffolds for tissue engineering. Chem Soc Rev. 2009;38:1139–1151.
16. Bostrom A, Löfstedt RE. Nanotechnology risk communication past and prologue. Risk Anal Off Publ Soc Risk Anal. 2010;30:1645–1662.
17. Koodali RT, Klabunde KJ. Nanotechnology: fundamental principles and applications. In: Kent AJ, editors. Handbook of industrial chemistry and biotechnology. Boston, MA: Springer US, 2012:249–263.
18. Drexler KE. Engines of creation. London, UK: Fourth Estate, 1996.
19. Huang C, Notten A, Rasters N. Nanoscience and technology publications and patents: a review of social science studies and search strategies. J Technol Transfer. 2010;36:145–172.
20. Jain KK. Drug delivery systems – an overview. In: Jain KK, editor. Drug delivery systems. Totowa, NJ: Humana Press, 2008:1–50.
21. Davies AG, Thompson JM. Advances in nanoengineering: electronics, materials and assembly. London, UK: Imperial College Press, 2007.
22. Mansur HS. Quantum dots and nanocomposites. Wiley Interdiscip Rev Nanomed Nanobiotechnol. 2010;2:113–129.
23. Arzt E, Gorb S, Spolenak R. From micro to nano contacts in biological attachment devices. Proc Natl Acad Sci. 2003;100:10603–10606.

24. Soppimath KS, Aminabhavi TM, Kulkarni AR, Rudzinski WE. Biodegradable polymeric nanoparticles as drug delivery devices. J Controlled Release Off J Controlled Release Soc. 2001;70:1–20.
25. Takeuchi H, Yamamoto H, Kawashima Y. Mucoadhesive nanoparticulate systems for peptide drug delivery. Adv Drug Deliv Rev. 2001;47:39–54.
26. Panyam J, Labhasetwar V. Biodegradable nanoparticles for drug and gene delivery to cells and tissue. Adv Drug Deliv Rev. 2003;55:329–347.
27. Cao X, Lai S, Lee LJ. Design of a self-regulated drug delivery device. Biomed Microdevices. 2001;3:109–117.
28. Cheng CJ, Tietjen GT, Saucier-Sawyer JK, Saltzman WM. A holistic approach to targeting disease with polymeric nanoparticles. Nat Rev Drug Discov. 2015;14:239–247.
29. Faraji AH, Wipf P. Nanoparticles in cellular drug delivery. Bioorg Med Chem. 2009;17:2950–2962.
30. Doshi N, Mitragotri S. Designer biomaterials for nanomedicine. Adv Funct Mater. 2009;19:3843–3854.
31. Kamaly N, Xiao Z, Valencia PM, Radovic-Moreno AF, Farokhzad OC. Targeted polymeric therapeutic nanoparticles: design, development and clinical translation. Chem Soc Rev. 2012;41:2971–3010.
32. Kumari A, Yadav SK, Yadav SC. Biodegradable polymeric nanoparticles based drug delivery systems. Colloids Surf, B. 2010;75:1–18.
33. Champion JA, Mitragotri S. Role of target geometry in phagocytosis. Proc Natl Acad Sci USA. 2006;103:4930–4934.
34. Sahoo B, Devi KS, Banerjee R, Maiti TK, Pramanik P, Dhara D. Thermal and pH responsive polymer-tethered multifunctional magnetic nanoparticles for targeted delivery of anticancer drug. ACS Appl Mater Interfaces. 2013;5:3884–3893.
35. Nagavarma BV, Yadav HK, Ayaz A, Vasudha LS, Shivakumar HG. Different techniques for preparation of polymeric nanoparticles- A review. Asian J Pharm Clin Res. 2012;5:16–23.
36. Dutta RK, Sharma PK, Kobayashi H, Pandey AC. Functionalized biocompatible nanoparticles for site-specific imaging and therapeutics. In: Kunugi S, Yamaoka T, editors. Polymers in nanomedicine. Berlin, Germany: Springer Berlin Heidelberg, 2012:233–275.
37. Albanese A, Tang PS, Chan WC. The effect of nanoparticle size, shape, and surface chemistry on biological systems. Annu Rev Biomed Eng. 2012;14:1–16.
38. Li YP, Pei YY, Zhang XY, Gu Z, Zhou Z, Yuan W, et al. PEGylated PLGA nanoparticles as protein carriers: synthesis, preparation and biodistribution in rats. J Controlled Release. 2001;71:203–211.
39. Amit Singh GG, Sharma PK. Nanospheres: a novel approach for targeted drug delivery system. Int J Pharm Sci Rev Res. 2010;5:84–88.
40. Anton N, Benoit JP, Saulnier P. Design and production of nanoparticles formulated from nano-emulsion templates-a review. J Controlled Release Off J Controlled Release Soc. 2008;128:185–199.
41. Storm G, Belliot SO, Daemen T, Lasic DD. Surface modification of nanoparticles to oppose uptake by the mononuclear phagocyte system. Adv Drug Deliv Rev. 1995;17:31–48.
42. Scherrmann JM, Temsamani J. The use of pep: tran’s vectors for the delivery of drugs into the central nervous system. Int Congress Ser. 2005;1277:199–211.
43. Sarti S, Bordi F. Polymeric hollow micro and nanospheres for biotechnological applications: a focused review. Mater Lett. 2013;109:134–139.
44. Shive MS, Anderson JM. Biodegradation and biocompatibility of PLA and PLGA microspheres. Adv Drug Deliv Rev. 1997;28:5–24.
45. Yow HN, Routh AF. Formation of liquid core–polymer shell microcapsules. Soft Matter. 2006;2:940–949.
46. Pinto Reis C, Neufeld RJ, Ribeiro AJ, Veiga F. Nanoencapsulation I. Methods for preparation of drug-loaded polymeric nanoparticles. Nanomed Nanotechnol Biol Med. 2006;2:8–21.
47. Galindo-Rodriguez S, Allemann E, Fessi H, Doelker E. Physicochemical parameters associated with nanoparticle formation in the salting-out, emulsification-diffusion, and nanoprecipitation methods. Pharm Res. 2004;21:1428–1439.
48. Prabhakar VT, Yadav A, Ratan R. Magic magic bullets - nanocapsules in future medicine. Int J Pharma Sci. 2013;3:303–308.
49. Guterres SS, Alves MP, Pohlmann AR. Polymeric nanoparticles, nanospheres and nanocapsules, for cutaneous applications. Drug Target Insights. 2007;2:147–157.
50. Moghimi SM, Hunter AC, Murray JC. Long-circulating and target-specific nanoparticles: theory to practice. Pharmacol Rev. 2001;53:283–318.
51. Khoee S, Yaghoobian M. An investigation into the role of surfactants in controlling particle size of polymeric nanocapsules containing penicillin-G in double emulsion. Eur J Med Chem. 2009;44:2392–2399.
52. Radtchenko I, Sukhorukov G, Mohwald H. A novel method for encapsulation of poorly water-soluble drugs: precipitation in polyelectrolyte multilayer shells. Int J Pharm. 2002;242:219–223.
53. Mora-Huertas CE, Fessi H, Elaissari A. Polymer-based nanocapsules for drug delivery. Int J Pharm. 2010;385:113–142.

54. Whelan J. Nanocapsules for controlled drug delivery. Drug Discovery Today. 2001;6:1183–1184.
55. Barratt GM. Therapeutic applications of colloidal drug carriers. Pharm Sci Technolo Today. 2000;3:163–171.
56. Karode SK, Kulkarni SS, Suresh AK, Mashelkar RA. New insights into kinetics and thermodynamics of interfacial polymerization. Chem Eng Sci. 1998;53:2649–2663.
57. Puglisi G, Fresta M, Giammona G, Ventura CA. Influence of the preparation conditions on poly(ethylcyanoacrylate) nanocapsule formation. Int J Pharm. 1995;125:283–287.
58. Dustgani A, Farahani EV, Imani M. Preparation of chitosan nanoparticles loaded by dexamethasone sodium phosphate. Iran J Pharm Sci. 2008;4:111–114.
59. Rao JP, Geckeler KE. Polymer nanoparticles: preparation techniques and size-control parameters. Prog Polym Sci. 2011;36:887–913.
60. Quintanar-Guerrero D, Allémann E, Fessi H, Doelker E. Preparation techniques and mechanisms of formation of biodegradable nanoparticles from preformed polymers. Drug Dev Ind Pharm. 1998;24:1113–1128.
61. Vauthier C, Dubernet C, Fattal E, Pinto-Alphandary H, Couvreur P. Poly(alkylcyanoacrylates) as biodegradable materials for biomedical applications. Adv Drug Deliv Rev. 2003;55:519–548.
62. Bellotti E, Barbani N, Cascone MG, Cristallini C. Development and characterization of new intelligent nanoparticles for drug targeting. In: R. Alessandro, editor Biocompatible materials for medicine. Mantova, Italy: Universitas Studiorum, 2014:187–190.
63. Cui W, Lu X, Cui K, Niu L, Wei Y, Lu Q. Dual-responsive controlled drug delivery based on ionically assembled nanoparticles. Langmuir ACS J Surf Colloids. 2012;28:9413–9420.
64. Remant Bahadur KC, Thapa B, Xu P. pH and redox dual responsive nanoparticle for nuclear targeted drug delivery. Mol Pharm. 2012;9:2719–2729.
65. Barick KC, Singh S, Jadhav NV, Bahadur D, Pandey BN, Hassan PA. pH-responsive peptide mimic shell cross-linked magnetic nanocarriers for combination therapy. Adv Funct Mater. 2012;22:4975–4984.
66. Zhao Z, Huang D, Yin Z, Chi X, Wang X, Gao J. Magnetite nanoparticles as smart carriers to manipulate the cytotoxicity of anticancer drugs: magnetic control and pH-responsive release. J Mater Chem. 2012;22:15717–15725.
67. Cheng J, Teply BA, Sherifi I, Sung J, Luther G, Gu FX, et al. Formulation of functionalized PLGA-PEG nanoparticles for in vivo targeted drug delivery. Biomaterials. 2007;28:869–876.
68. Patil YB, Toti US, Khdair A, Ma L, Panyam J. Single-step surface functionalization of polymeric nanoparticles for targeted drug delivery. Biomaterials. 2009;30:859–866.
69. Farokhzad OC, Jon S, Khademhosseini A, Tran TN, Lavan DA, Langer R. Nanoparticle-aptamer nanoparticle-aptamer bioconjugates: a new approach for targeting prostate cancer cells. Cancer Res. 2004;64:7668–7672.
70. Schiffelers RM, Ansari A, Xu J, Zhou Q, Tang Q, Storm G, et al. Cancer siRNA therapy by tumor selective delivery with ligand-targeted sterically stabilized nanoparticle. Nucleic Acids Res. 2004;32:e149.
71. Cho CS, Cho KY, Park IK, Kim SH, Sasagawa T, Uchiyama M, et al. Receptor-mediated delivery of all trans-retinoic acid to hepatocyte using poly(L-lactic acid) nanoparticles coated with galactose-carrying polystyrene. J Controlled Release Off J Controlled Release Soc. 2001;77:7–15.
72. Soppimath KS, Tan DC, Yang YY. pH-triggered thermally responsive polymer core–shell nanoparticles for drug delivery. Adv Mater. 2005;17:318–323.
73. Shu S, Zhang X, Wu Z, Wang Z, Li C. Gradient cross-linked biodegradable polyelectrolyte nanocapsules for intracellular protein drug delivery. Biomaterials. 2010;31:6039–6049.
74. Robinson JR, Mlynek GM. Bioadhesive and phase-change polymers for ocular drug delivery. Adv Drug Deliv Rev. 1995;16:45–50.
75. Gurtler F, Gurny R. Patent literature review of ophthalmic inserts. Drug Dev Ind Pharm. 1995;21:1–18.
76. Ahmed EM. Hydrogel: preparation, characterization, and applications: a review. J Adv Res. 2015;6:105–121.
77. Sharma VK, Jain A, Soni V. Nano-aggregates: emerging delivery tools for tumor therapy. Crit Rev Ther Drug Carrier Syst. 2013;30:535–563.
78. Ullah F, Othman MB, Javed F, Ahmad Z, Akil HM, Rasib SZ. Functional properties of chitosan built nanohydrogel with enhanced glucose-sensitivity. Int J Biol Macromol. 2016;83:376–384.
79. Jaiswal MK, Banerjee R, Pradhan P, Bahadur D. Thermal behavior of magnetically modalized poly(N-isopropylacrylamide)-chitosan based nanohydrogel. Colloids Surf, B. 2010;81:185–194.
80. Yoon S, Kim WJ, Yoo HS. Dual-responsive breakdown of nanostructures with high doxorubicin payload for apoptotic anticancer therapy. Small (Weinheim an Der Bergstrasse, Germany). 2013;9:284–293.
81. Tanford C. The hydrophobic effect: formation of micelles and biological membranes, 2nd ed Somerset, NJ: John Wiley & Sons, 1980.
82. Ruckenstein E, Nagarajan R. Critical micelle concentration. Transition point for micellar size distribution. J Phys Chem. 1975;79:2622–2626.
83. Jones M, Leroux J. Polymeric micelles – a new generation of colloidal drug carriers. Eur J Pharm Biopharm.

1999;48:101–111.

84. Torchilin VP. Micellar nanocarriers: pharmaceutical perspectives. Pharm Res. 2007;24:1–16.
85. Cabral H, Kataoka K. Progress of drug-loaded polymeric micelles into clinical studies. J Controlled Release Off J Controlled Release Soc. 2014;190:465–476.
86. Torchilin VP. Structure and design of polymeric surfactant-based drug delivery systems. J Controlled Release Off J Controlled Release Soc. 2001;73:137–172.
87. Gabizon AA. Liposome circulation time and tumor targeting: implications for cancer chemotherapy. Adv Drug Deliv Rev. 1995;16:285–294.
88. Torchilin VP. Targeted polymeric micelles for delivery of poorly soluble drugs. Cell Mol Life Sci CMLS. 2004;61:2549–2559.
89. Allen C, Maysinger D, Eisenberg A. Nano-engineering block copolymer aggregates for drug delivery. Colloids Surf, B. 1999;16:3–27.
90. Ai X, Zhong L, Niu H, He Z. Thin-film hydration preparation method and stability test of DOX-loaded disulfide-linked polyethylene glycol 5000-lysine-di-tocopherol succinate nanomicelles. Asian J Pharm Sci. 2014;9:244–250.
91. Wissing SA, Muller RH. A novel sunscreen system based on tocopherol acetate incorporated into solid lipid nanoparticles. Int J Cosmet Sci. 2001;23:233–243.
92. Schwarz C, Mehnert W, Lucks JS, Müller RH. Solid lipid nanoparticles (SLN) for controlled drug delivery. I. Production, characterization and sterilization. J Controlled Release. 1994;30:83–96.
93. Muller RH, Mader K, Gohla S. Solid lipid nanoparticles (SLN) for controlled drug delivery - a review of the state of the art. Eur J Pharmaceutics Biopharm. 2000;50:161–177.
94. Muller RH, Radtke M, Wissing SA. Solid lipid nanoparticles (SLN) and nanostructured lipid carriers (NLC) in cosmetic and dermatological preparations. Adv Drug Deliv Rev. 2002;54 Suppl 1 S131–S155.
95. Attama AA, Muller-Goymann CC. Effect of beeswax modification on the lipid matrix and solid lipid nanoparticle crystallinity. Colloids and Surf, A. 2008;315:189–195.
96. Parhi R, Suresh P. Preparation and characterization of solid lipid nanoparticles-a review. Curr Drug Discov Technol. 2012;9:2–16.
97. Ekambaram P, Hasan Sathali AA, Priyanka K. Solid lipid nanoparticles: a review. Scientific Rev Chem Communications. 2012;2:80–102.
98. Zhang Y, Zhou J, Yang C, Weiwei W, Liping C, Fan H, et al. Folic acid-targeted disulfide-based cross-linking micelle for enhanced drug encapsulation stability and site-specific drug delivery against tumors. Int J Nanomed. 2016;11:1119–1130.
99. Lee ES, Na K, Bae YH. Polymeric micelle for tumor pH and folate-mediated targeting. J Controlled Release. 2003;91:103–113.
100. Li Y, Xiao W, Xiao K, Berti L, Juntao L, Tseng HP, et al. Well-defined, reversible boronate crosslinked nanocarriers for targeted drug delivery in response to acidic ph values and cis-diols. Angew Chem Int Ed. 2012;51:2864–2869.
101. Wang J, Mongayt D, Torchilin VP. Polymeric micelles for delivery of poorly soluble drugs: preparation and anticancer activity in vitro of paclitaxel incorporated into mixed micelles based on poly(ethylene glycol) -lipid conjugate and positively charged lipids. J Drug Target. 2005;13:73–80.
102. Lee MK, Lim SJ, Kim CK. Preparation, characterization and in vitro cytotoxicity of paclitaxel-loaded sterically stabilized solid lipid nanoparticles. Biomaterials. 2007;28:2137–2146.
103. Gao Z, Lukyanov AN, Singhal A, Torchilin VP. Diacyllipid-polymer micelles as nanocarriers for poorly soluble anticancer drugs. Nano Lett. 2002;2:979–982.
104. Wong HL, Rauth AM, Bendayan R, Wu XY. In vivo evaluation of a new polymer-lipid hybrid nanoparticle (PLN) formulation of doxorubicin in a murine solid tumor model. Eur J Pharm Biopharm Off J Arbeitsgemeinschaft Fur Pharmazeutische Verfahrenstechnik Ev. 2007;65:300–308.
105. Kukowska-Latallo JF, Candido KA, Cao Z, Nigavekar SS, Majoros IJ, Thomas TP, et al. Nanoparticle targeting of anticancer drug improves therapeutic response in animal model of human epithelial cancer. Cancer Res. 2005;65:5317–5324.
106. Pisignano D. Structural and surface properties of polymer nanofibers and their applications. In: Dario Pisignano, editor. Polymer nanofibers: building blocks for nanotechnology. Cambridge, UK: The Royal Society of Chemistry, 2013:189–235.
107. Pham QP, Sharma U, Mikos AG. Electrospinning of polymeric nanofibers for tissue engineering applications: a review. Tissue Eng. 2006;12:1197–1211.
108. Huang ZM, Zhang YZ, Kotaki M, Ramakrishna S. A review on polymer nanofibers by electrospinning and their applications in nanocomposites. Compos Sci Technol. 2003;63:2223–2253.
109. Yu DG, Zhu LM, White K, Branford-White C. Electrospun nanofiber-based drug delivery systems. Health. 2009;01:67–75.
110. Chew SY, Wen J, Yim EK, Leong KW. Sustained release of proteins from electrospun biodegradable fibers. Biomacromolecules. 2005;6:2017–2024.

111. Feng ZQ, Leach MK, Chu XH, Wang YC, Tian T, Shi XL, et al. Electrospun chitosan nanofibers for hepatocyte culture. J Biomed Nanotechnol. 2010;6:658–666.

112. Bhattarai N, Edmondson D, Veiseh O, Matsen FA, Zhang M. Electrospun chitosan-based nanofibers and their cellular compatibility. Biomaterials. 2005;26:6176–6184.

113. Subramanian A, Vu D, Larsen GF, Lin HY. Preparation and evaluation of the electrospun chitosan/PEO fibers for potential applications in cartilage tissue engineering. J Biomater Sci Polym Ed. 2005;16:861–873.

114. Park KE, Kang HK, Lee SJ, Min BM, Park WH. Biomimetic nanofibrous scaffolds: preparation and characterization of PGA/chitin blend nanofibers. Biomacromolecules. 2006;7:635–643.

115. Shalumon KT, Binulal NS, Selvamurugan N, Naira SV, Menona D, Furuikeb T, et al. Electrospinning of carboxymethyl chitin/poly(vinyl alcohol) nanofibrous scaffolds for tissue engineering applications. Carbohydr Polym. 2009;77:863–869.

116. Zhou Y, Yang D, Chen X, Xu Q, Lu F, Nie J. Electrospun water-soluble carboxyethyl chitosan/poly(vinyl alcohol) nanofibrous membrane as potential wound dressing for skin regeneration. Biomacromolecules. 2008;9:349–354.

117. Yang D, Jin Y, Zhou Y, Ma G, Chen X, Lu F, et al. In situ mineralization of hydroxyapatite on electrospun chitosan-based nanofibrous scaffolds. Macromol Biosci. 2008;8:239–246.

118. Junkasem J, Rujiravanit R, Supaphol P. Fabrication of α-chitin whisker-reinforced poly(vinyl alcohol) nanocomposite nanofibres by electrospinning. Nanotechnology. 2006;17:4519–4528.

Review Article

Exosomes genetic cargo in lung cancer: a truly Pandora's box

Pablo Reclusa[1], Rafael Sirera[2], Antonio Araujo[3], Marco Giallombardo[1], Anna Valentino[1], Laure Sorber[4], Ignacio Gil Bazo[5], Patrick Pauwels[4], Christian Rolfo[1]

[1]Phase I- Early Clinical trials Unit, Oncology Department & Center for Oncological Research (CORE) Antwerp University Hospital, Antwerp, Belgium; [2]Department of Biotechnology, Politechnic University of Valencia Hospitality Centre of Oporto, Valencia, Spain; [3]Department of Medical Oncology, Centro Hospitalar do Porto, Porto, Portugal; [4]Molecular Pathology Unit, Antwerp University Hospital & Center for Oncological Research (CORE) Antwerp University Hospital, Antwerp, Belgium; [5]Department of Medical Oncology, University of Navarra, Pamplona, Spain

Contributions: (I) Conception and design: P Reclusa, C Rolfo; (II) Administrative support: R Sirera, A Araujo, IG Bazo, P Pauwels, C Rolfo; (III) Provision of study materials or patients: P Reclusa, M Giallombardo, L Sorber, C Rolfo; (IV) Collection and assembly of data: P Reclusa, R Sirera, A Valentino, C Rolfo; (V) Data analysis and interpretation: P Reclusa, R Sirera, A Valentino, C Rolfo; (VI) Manuscript writing: All authors; (VII) Final approval of manuscript: All authors.

Correspondence to: Prof./Dr. Christian Rolfo. Head of Phase I - Early Clinical Trials Unit, Antwerp University Hospital, Wilrijkstraat 10, 2650 Edegem, Antwerp, Belgium. Email: christian.rolfo@uza.be.

Abstract: Lung cancer is a highly lethal disease. Targeted therapies have been developed in last years, however survival rates are not improving due to the delay in the diagnosis, making biomarkers one of the most interesting fields of study in cancer. Liquid biopsy has raised as an alternative to tissue biopsy due to improvements in analytical techniques for circulating tumor cells (CTCs), cell free DNA and exosomes. Among all, exosomes have raised as one of the most promising tools to understand the tumor due to their stability in the blood and their similarity to the cells of origin. In the last years, different alterations have been described inside the exosomes derived from non-small cell lung cancer (NSCLC) cells mirroring the processes inside these tumoral cells, such as *EGFR* mutation, translocations or microRNA (miRNA) deregulation. All these studies have opened the window to a new world of possibilities in the study of tumor biomarkers.

Keywords: Non-small cell lung cancer (NSCLC); exosomes; ncRNAs; liquid biopsy

Submitted Jul 06, 2016. Accepted for publication Sep 18, 2016.
doi: 10.21037/tlcr.2016.10.06
View this article at: http://dx.doi.org/10.21037/tlcr.2016.10.06

Biomarkers of non-small cell lung cancer (NSCLC)

Lung cancer is the second most common cancer and the leading cause of cancer death for both men and women besides the important therapeutic achievements, the global disease control rate is still low. Other factors that can contribute to this unsuccessful scenario is the delay in the early detection, including also the absence of reliable biomarkers (1) and new drugs to fulfill an unmet medical need, specifically in NSCLC.

Biomarkers play a crucial role in medicine, as indicators of normal or pathological processes or as tools to assess pharmacological responses to therapeutic interventions or as a prognostic and predictive aid to elucidate the risk of recurrence and progression and the possibilities of treatments effectiveness (2). For this reason, biomarkers have become one of the most studies aspects in cancer (3).

The introduction of molecular biology in oncology, and mainly in NSCLC, made possible to identify drugable targets, for example *EGFR* mutation and *ALK* translocations among others. In this personalize treatment era, tissue became one of the most important treasure in the diagnosis and recurrence of the disease. Unfortunately, the amount of material is a big issue in lung cancer, due to the impossibility to reach the tumor. At this point, new tools have to be discovered in order to reveal the molecular information of the tumor. In this regards liquid biopsy has become a more and more important instrument in cancer

research and in the clinic.

Liquid biopsy

Nowadays important efforts in molecular profiling of the tumors are allowing to develop new technology that permits to analyze the tumor characteristics in peripheral blood. Accordingly, the liquid biopsy refers to the analysis of components that can be isolated and analyzed from a blood sample as, circulating tumor cells (CTCs), cell free circulating DNA (circulating tumor DNA, ctDNA) and exosomes (a part of the secreted micro-vesicles) (4-6). In this regard, CTCs have been demonstrated to be good predictors for risk of metastatic progression, to monitor the response of an undergoing treatment, or to identify new targets and resistance mechanisms (7). On the other hand, ctDNA the most used component of the liquid biopsies is now being studied as possible biomarker and prognostic factor in cancer, although it is still difficult to standardize (8-11).

Nevertheless, the ultimate techniques developed in the field of sequencing and DNA amplification such as next generation sequencing (NGS) and digital droplet PCR (ddPCR) are transforming the molecular profiling of the tumor in a fast, easy, reliable and affordable manner (12-15).

Exosomes

Exosomes are the last frontier in liquid biopsies. Exosomes are spherical nano-size vesicles with a diameter between 30 to 100 nm and with a well delimited round morphology by electron microscopy that are released by exocytosis from multivesicular bodies of late endosome (16). They are exocytosed in a constitutive manner by any cell in both physiological and pathological condition and can be found in several body fluids like urine, saliva, amniotic liquid or blood (17,18). Exosome's composition may reflect that of the parental cells, so the study of cancer derived exosomes (DEX) are an important non-invasive surrogate of the tumor. Additionally, as exosomes are linked to cell-secretion pathway, they carry some common proteins independent of the cells of origin that allow the development of robust exosomes-isolation techniques. These proteins are well known exosomes markers, such as ALIX, CD9, CD63, CD81, HSP70 and TSG-101, among others (19).

Several methods are used to extract exosomes with no clear winner. The principal methods to isolate the exosomes are ultracentrifugation, sucrose density-gradient ultracentrifugation, exosome immunoprecipitation and the isolation using commercial kits (20).

Inside the exosomes

Exosomes contain a wide variety of components such as single-stranded RNA, long non-coding RNA (lncRNA), microRNA (miRNA), proteins and lipids. Recently also double-stranded DNA has also been found inside the exosomes giving a new chance for exosomes to become the principal diagnostic tool (21) (*Figure 1*).

Since their discovery, the amount of information about his microvesicles has raised considerably, and a 'microvesicle content database' has been created to facilitate the access to all the newly discovered components (http://www.microvesicles.org). Currently (June 2016) this database contained 92,897 proteins, 27,642 mRNA, 4,936 miRNAs and 584 lipids based on a total of 538 studies. Although many of these proteins are common to all cell types, some others are privative for a certain cell alteration or tumorogenic process and can be useful for the identification of the origin of these vesicles and thus can be an adequate biomarker to get more information from the tumor of origin. In addition the study of the lipids is interesting due to their role in the internalization process of exosomes and to the bioactive function of some of them such as prostaglandins and leukotrienes (22).

Additionally, Valadi *et al*. described for the first time the presence of miRNAs inside (23) exosomes. miRNAs are short single-stranded and non-coding RNA molecules that act regulating gene expression as oncogenic or tumor suppressor function. They are involved in progression, cellular differentiation, apoptosis or cell signaling.

Exosomes biology

Although exosomes can be released directly from the plasma membrane (24), most of them are derived from the endosomal compartment as a part of the endocytic machinery (25). A very important part of the exosomes formation is controlled for the mechanism of endosomal sorting complex required for transport (ESCRT), which is the responsible for the accumulation and sorting of molecules in the endocytic machinery. In tumor cells, where ESCRT is significantly altered, the protein profile inside the exosomes and the amount of exosomes released can be modified (26,27). Once exosomes are released from the cells other cells can capture these vesicles as a physiological response to the endocytic machinery fusing them either with

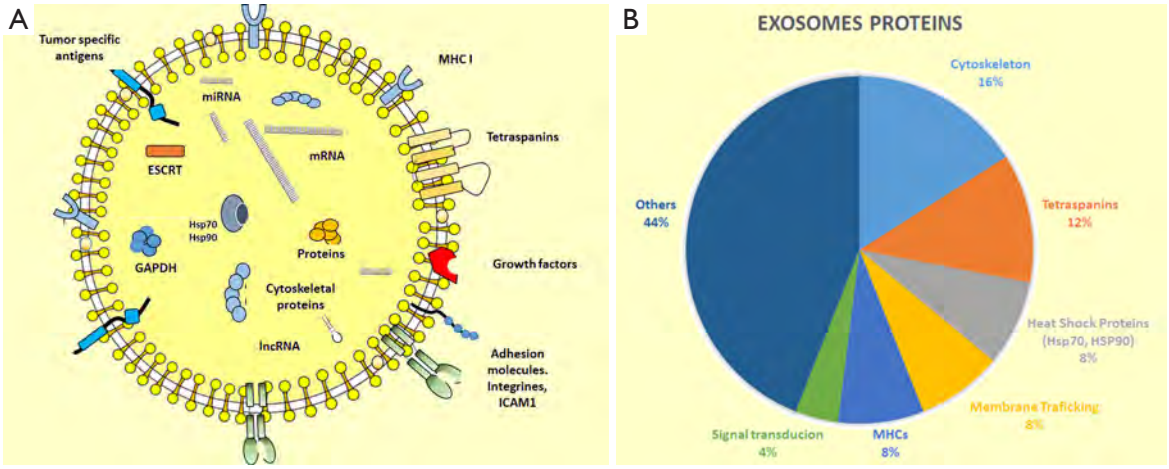

Figure 1 Exosomes cargo. (A) Schematic picture of the content of an exosome; (B) diagram the principal proteins of the exosomes.

the plasma membrane or with lysosomes. If the exosomes fuse with lysosomes, their content will be degraded by proteolytic enzymes (28), but in contrast if the exosomes fuse with the plasma membrane, their content is released into the cytoplasm of the cell (29) being able to modify in a autocrine or paracrine manner the target cell behavior. This exosome's uptake has reveal that they have a very important role in cell to cell communication or crosstalk (30,31) and three principal mechanisms governing this process have been described up to date (32). The first one, common to all type of vesicles is endocytosis, including pinocytosis, clathrin-mediated endocytosis, phagocytosis and others (30,33-35). A second mechanism is by direct binding of both cell and exosome membranes (36), leading to membranes fusion. Exosomes contain an enormous amount of surface proteins such as leptins, immunoglobulins, integrins and tetraspanins that are involved in their function, motility and internalization into the cells (34,37). The third mechanism is linked to ligand-receptor interaction that is the effect of the interplay of specific proteins in the exosome and the target cell surface (32). In this regard, tumor metastasis is not produced to random organs but to determine organs in each case and exosomes contribute to prepare the pre-metastatic niche. For example, integrin profiling in exosomes could be a feasible tool to identify possible organotropic metastasis before they have been produced (38).

Exosomes and cancer

In recent years, more and more studies are ongoing with regard to the function of exosomes and their application for tumor detection and treatment and several reports have demonstrated that exosomes can play pleiotropic roles affecting pivotal aspects of tumor development and growth (*Figure 2*). For instance, exosomes derived from prostate tumor cells act in a paracrine fashion inducing a reprogramming of cell metabolism and enhancing of cell proliferation (39). The fusion gene *TMPRSS2:ERG* and *EGFR*, both related with advanced prostate have been described inside the exosomes (40,41). Cells from renal carcinoma are able to release exosomes containing some miRNAs and other RNAs that transform normal endothelial cells into an activated angiogenic phenotype, and directing towards lung cancer metastasis (42). In other studies it has been demonstrated that exosomes derived from highly metastatic melanoma cells promote the pre-metastatic niche formation through the education of the bone marrow and by reprogramming its progenitor cells to a pro-vasculogenic phenotype (43). On the other hand, another described role of exosomes in breast cancer and multiple myeloma is the ability to promote drug resistance through horizontal transfer (44,45). Exosomes are also involved in the creation of a pro-inflammatory microenvironment that promotes tumor growth by means of immunological proteins such as MHC-II, CD40 and CD40L. In breast cancer exosomes containing 27-Hydroxycholesterol (27-OHC), a lipid associated with proliferation and metastasis in estrogen receptor positive (ER+) tumor cells, open a new window to understand how exosomes genesis is achieved and its correlation with the content of the cells of origin (46). Other studies performed in exosomes derived from ovarian cancer cell lines show that exosomes can carry functional

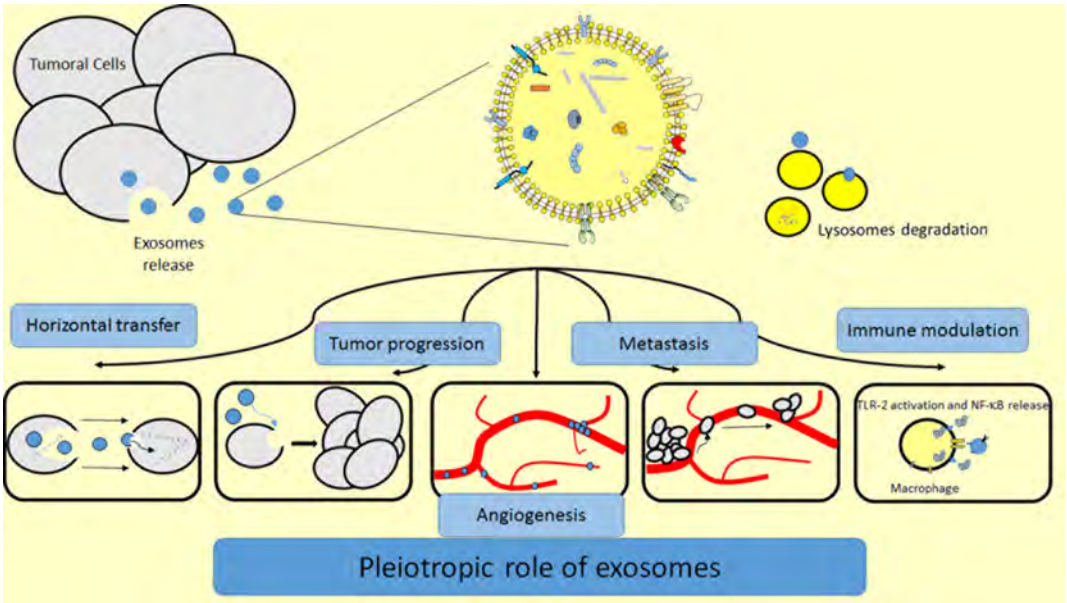

Figure 2 Pleiotropic roles of tumor derived exosomes (DEX).

proteins that reprogram cell metabolism of the cell enhancing the pentose phosphate pathway that is crucial for resisting oxidant injury and favors tumor survival (47-49). Many miRNAs profiles have been identified in cancer-related exosomes. The oncogenic miRNA-21, upregulated in exosomes released by chronic myelogenous leukemia after Curcumin treatment, has been one of the most studied miRNA (50). Moreover, miRNA-21 has been found to be upregulated in different types of tumors such as esophageal squamous cell carcinoma (51) or glioblastoma (52), and its levels correlated with tumor progression and aggressiveness. miR-21 has also been described to be elevated in pancreatic carcinoma but no correlation was found with the stage of the disease (53). In ovarian cancer a profile of eight miRNAs (miR-21, miR-141, miR-200a, miR-200c, miR-200b, miR-203, miR-205 and miR-214) in both tumor cells and tumor exosomes has been already analyzed in a large cohort of 467 patients. The results revealed that levels of the miRNAs were different from those measured in benign disease, and the same miRNAs were undetectable in healthy donors (54).

Exosomes in NSCLC

As it was mentioned before, exosomes contain overexpressed or mutated proteins in the same proportion as the primary tumors. Therefore, in the specific case of exosomes obtained from NSCLC patients, EGFR (55), K-ras, claudins and other proteins can be analyzed. Recently, the translocation *ALK-EML4* has also been identifying inside the exosomes (56). Al-Nedawi *et al*. demonstrated that exosomes carrying *EGFR* were able to interact with endothelial cells activating both MAPK and Akt pathways, resulting on an overexpression of VEGF and an augmentation of the vascularity of the tumor (57).

Many non-coding RNAs (ncRNAs) have been described in NSCLC, being involved in various processes of cancer formation and evolution (58,59) (*Table 1*). Rabinowits *et al*. carried one of the first studies concerning the possibility of using exosomes as a source of genetic material derived from the tumor comparing the miRNA content between the exosomes and the tumoral cells from patients with NSCLC and with healthy donors. Although the study revealed no differences between both compartments (72) it opened a window for tumor molecular identification. In a proof of concept, in a small cohort of patients with diagnosed NSCLC and a group of healthy donors, Rolfo *et al*. demonstrated the upregulation of two miRNA related with the EGFR pathway, 30b and 30c (60).

In a study that included 28 NSCLC patients, 365 miRNAs were analyzed and the level of let-7f and miR-30e-3p in were found to be associated with poor outcome. The authors also found that patients with more advanced stage of disease and lymph node metastases had higher exosome related miR-20b levels (62). miRNA-373 and miRNA-512

Table 1 Principal miRNAs detected in NSCLC, their principal molecule of pathway targeted and its function (if known)

Non-coding RNA	Molecule or pathway targeted	Clinical relevance	References
miRNA			
miR-30b; miR-30c	EGFR pathway	—	(60)
miR-373; miR-512	RelA and PIK3CA RNAs; TEAD4	Silenced. Upregulation results in tumor suppressor effects	(61)
miR-30e-3p; let-7f	—	Advanced non-resectable tumors	(62)
miR-20b	—	Metastasis in lymphatic nodes	(62)
miR-29a-3p; miR-150-5p	—	Toxicity in response to radiotherapy	(63)
miR-208a	p21	Tumor progression. Resistance to radiotherapy	(64)
miR-1246	DR5	Tumor progression. Resistance to radiotherapy	(65)
miR-302b	TGFbRII	Downregulated. Tumor suppressor. Blocks cell proliferation and migration	(66)
miR-221-3p	EGFR	Upregulation. Better clinical outcome	(67)
miR-222-3p	EGFR	Upregulation. Better clinical outcome	(67)
miR-1228	—	Endogenous control	(67-69)
lncRNAs			
HOTAIR	p21	Resistance to cisplatin	(70,71)

miRNAs, microRNA; NSCLC, non-small cell lung cancer; lncRNAs, long non-coding RNA; HOTAIR, exosomal non-coding RNA.

are tumor suppressor miRNA that are silenced in the tumor and whose reactivation produces a restriction of the growth and invasiveness of the tumor. Studying exosomes it has been demonstrated that the downregulation of these two miRNAs is associated with as a poor prognosis in NSCLC patients and that therapy that affects epigenetic status led to re-expression of both miRNAs which, on one side, augmented cisplatin-induced apoptosis while, on the other side inhibited cell migration (61). Other miRNAs present in the exosomes have been identified as possible biomarkers in response to certain treatments. miR-29a-3p and miR-150-5p were shown to decrease with increasing radiation dose so, and therefore identified as a reproducible circulating biomarkers that correlated with delivered radiotherapy dose (63). In another example, miR-208a and miR-1246 through the binding to p21 and DR5 mRNAs respectively, have been reported to promote tumor progression and resistance to radiotherapy (64,65). Also miR-302b has been described to block the cell proliferation and cell migration through interaction with its target, the mRNA of TGFβRII (66). Finally, our group recently described recently a correlation between the overexpression of miR-221-3p and 222-3p, both related with EGFR status, and a good clinical outcome in patients under osimertinib treatment (67). In addition to miRNAs, other ncRNAs have been identified inside the tumor-DEX, such as lncRNAs; non-coding RNA molecules with more than 200 bp with either tumor suppressor or oncogenic functions. However, the study of ncRNAs is less extended due to a lower general knowledge in the field and the lack of known function of many lncRNAs. In this regard, some lncRNAs have been described and studied in lung cancer but it has not been elucidated if are also present in exosomes. A good example of this is HOTAIR a largely studied onco-lncRNA related with resistance to cisplatin in NSCLC through p21 that has been also related with proliferation, migration and invasion (70,71).

Exosomes have been considered also as possible vehicles for the selective and directed administration of drugs. In lung cancer two clinical trials were planned, a Phase I trial in which DEX immunotherapy were used, and a Phase II in which DEXs vaccination with exosomes carrying IL-15Ra and NKG2D in association with cyclophosphamide after platinum-based chemotherapy. The main objective of both studies was to measure the toxicity and they had positive results, concluding that DEXs are able to activate the adaptive and the innate immune system (68,73).

Discussion

Thanks to the lipid bilayer that makes the cargo very stable, exosomes allow the analysis of genetic material in order to identify the tumor of origin, mutations and possible resistances for the treatments, among others. However, some methodological issues are still focus of debate and

need better implementations. For the moment, there are no standardized methods to extract exosomes. The most used protocol relies in ultracentrifugation in sucrose gradient, a step that is complicated to implement in the clinical setting due to the lack of expertise in the field of many laboratories. Some companies have started the development of user friendly and reproducible kits to improve the time, the quality and the yield of exosome extraction.

Some other controversial issues remain in exosome research. One of the key factors for exosome production and function is the cell or tissue microenvironment. For the *in vitro* analysis, most of the studies are performed in completely artificial monolayer of cultured tumor cells. To avoid this spatial problem Villasante *et al.* have recently published a technique based in a three dimensional tumor model to bypass the effect of culture microenvironment in tumor exosomes production (69).

In quantitative studies, another important problem is still the absence of endogenous control for exosomal miRNA titration. Some groups have described the miR-1228 as a good endogenous control in several investigations (67,74,75), but definitively, more studies are needed to validate this finding..

In conclusion, liquid biopsies have become a reality in lung cancer. The learning curve for oncologists includes CTCs and the current hot topic, circulating free DNA. Exosomes are still an area of research but they are likely to be implemented in the clinical practice in the near future, opening a new window in the cancer prediction, prognosis and treatment. Although more efforts are required in order standarize exosome isolation and analysis so that they can be implemented in the clinical setting, step by step we understand more of the exosome-related physiologic processes and their impact in carcinogenesis. The main point about exosomes is their pleiotropic role in cancer, not only as biomarkers but also as a sort of "Pandora box" that contains the "instructions" for migration and aggressiveness of the tumor and information about druggable targets. We are only in the beginning of the long, promising history of this new component of the liquid biopsy family.

Acknowledgements

None.

Footnote

Conflicts of Interest: The authors have no conflicts of interest to declare.

References

1. Siegel RL, Miller KD, Jemal A. Cancer statistics, 2016. CA Cancer J Clin 2016;66:7-30.
2. Sturgeon CM, Duffy MJ, Stenman UH, et al. National Academy of Clinical Biochemistry laboratory medicine practice guidelines for use of tumor markers in testicular, prostate, colorectal, breast, and ovarian cancers. Clin Chem 2008;54:e11-79.
3. Biomarkers Definitions Working Group. Biomarkers and surrogate endpoints: preferred definitions and conceptual framework. Clin Pharmacol Ther 2001;69:89-95.
4. Yap TA, Lorente D, Omlin A, et al. Circulating tumor cells: a multifunctional biomarker. Clin Cancer Res 2014;20:2553-68.
5. Mäbert K, Cojoc M, Peitzsch C, et al. Cancer biomarker discovery: current status and future perspectives. Int J Radiat Biol 2014;90:659-77.
6. Kosaka N, Iguchi H, Ochiya T. Circulating microRNA in body fluid: a new potential biomarker for cancer diagnosis and prognosis. Cancer Sci 2010;101:2087-92.
7. Alix-Panabières C, Pantel K. Circulating tumor cells: liquid biopsy of cancer. Clin Chem 2013;59:110-8.
8. Yanagita M, Redig AJ, Paweletz CP, et al. A prospective evaluation of circulating tumor cells and cell-free DNA in EGFR mutant non-small cell lung cancer patients treated with erlotinib on a phase II trial. Clin Cancer Res 2016. [Epub ahead of print].
9. Jansen MP, Martens JW, Helmijr JC, et al. Cell-free DNA mutations as biomarkers in breast cancer patients receiving tamoxifen. Oncotarget 2016. [Epub ahead of print].
10. Hadano N, Murakami Y, Uemura K, et al. Prognostic value of circulating tumour DNA in patients undergoing curative resection for pancreatic cancer. Br J Cancer 2016;115:59-65.
11. Camps C, Jantus-Lewintre E, Cabrera A, et al. The identification of KRAS mutations at codon 12 in plasma DNA is not a prognostic factor in advanced non-small cell lung cancer patients. Lung Cancer 2011;72:365-9.
12. Castéra L, Krieger S, Rousselin A, et al. Next-generation sequencing for the diagnosis of hereditary breast and ovarian cancer using genomic capture targeting multiple candidate genes. Eur J Hum Genet 2014;22:1305-13.
13. Hortobagyi GN, Piccart-Gebhart MJ, Rugo HS, et al. Correlation of molecular alterations with efficacy of everolimus in hormone receptor–positive, HER2-negative

advanced breast cancer: Results from BOLERO-2. J Clin Oncol 2013;31:abstr LBA509.
14. Chen WW, Balaj L, Liau LM, et al. BEAMing and Droplet Digital PCR Analysis of Mutant IDH1 mRNA in Glioma Patient Serum and Cerebrospinal Fluid Extracellular Vesicles. Mol Ther Nucleic Acids 2013;2:e109.
15. Oxnard GR, Paweletz CP, Kuang Y, et al. Noninvasive detection of response and resistance in EGFR-mutant lung cancer using quantitative next-generation genotyping of cell-free plasma DNA. Clin Cancer Res 2014;20:1698-705.
16. Kalra H, Simpson RJ, Ji H, et al. Vesiclepedia: a compendium for extracellular vesicles with continuous community annotation. PLoS Biol 2012;10:e1001450.
17. Conde-Vancells J, Rodriguez-Suarez E, Embade N, et al. Characterization and comprehensive proteome profiling of exosomes secreted by hepatocytes. J Proteome Res 2008;7:5157-66.
18. Mathivanan S, Simpson RJ. ExoCarta: A compendium of exosomal proteins and RNA. Proteomics 2009;9:4997-5000.
19. Théry C, Ostrowski M, Segura E. Membrane vesicles as conveyors of immune responses. Nat Rev Immunol 2009;9:581-93.
20. Théry C, Amigorena S, Raposo G, et al. Isolation and characterization of exosomes from cell culture supernatants and biological fluids. Curr Protoc Cell Biol 2006;Chapter 3:Unit 3.22.
21. Thakur BK, Zhang H, Becker A, et al. Double-stranded DNA in exosomes: a novel biomarker in cancer detection. Cell Res 2014;24:766-9.
22. Record M, Carayon K, Poirot M, et al. Exosomes as new vesicular lipid transporters involved in cell-cell communication and various pathophysiologies. Biochim Biophys Acta 2014;1841:108-20.
23. Valadi H, Ekström K, Bossios A, et al. Exosome-mediated transfer of mRNAs and microRNAs is a novel mechanism of genetic exchange between cells. Nat Cell Biol 2007;9:654-9.
24. Booth AM, Fang Y, Fallon JK, et al. Exosomes and HIV Gag bud from endosome-like domains of the T cell plasma membrane. J Cell Biol 2006;172:923-35.
25. Morvan J, Rinaldi B, Friant S. Pkh1/2-dependent phosphorylation of Vps27 regulates ESCRT-I recruitment to endosomes. Mol Biol Cell 2012;23:4054-64.
26. Kowal J, Tkach M, Théry C. Biogenesis and secretion of exosomes. Curr Opin Cell Biol 2014;29:116-25.
27. Colombo M, Moita C, van Niel G, et al. Analysis of ESCRT functions in exosome biogenesis, composition and secretion highlights the heterogeneity of extracellular vesicles. J Cell Sci 2013;126:5553-65.
28. Sahu R, Kaushik S, Clement CC, et al. Microautophagy of cytosolic proteins by late endosomes. Dev Cell 2011;20:131-9.
29. Mittelbrunn M, Sánchez-Madrid F. Intercellular communication: diverse structures for exchange of genetic information. Nat Rev Mol Cell Biol 2012;13:328-35.
30. Fitzner D, Schnaars M, van Rossum D, et al. Selective transfer of exosomes from oligodendrocytes to microglia by macropinocytosis. J Cell Sci 2011;124:447-58.
31. Atay S, Gercel-Taylor C, Taylor DD. Human trophoblast-derived exosomal fibronectin induces pro-inflammatory IL-1β production by macrophages. Am J Reprod Immunol 2011;66:259-69.
32. Mulcahy LA, Pink RC, Carter DR. Routes and mechanisms of extracellular vesicle uptake. J Extracell Vesicles 2014;3.
33. Feng D, Zhao WL, Ye YY, et al. Cellular internalization of exosomes occurs through phagocytosis. Traffic 2010;11:675-87.
34. Escrevente C, Keller S, Altevogt P, et al. Interaction and uptake of exosomes by ovarian cancer cells. BMC Cancer 2011;11:108.
35. Stephens L, Ellson C, Hawkins P. Roles of PI3Ks in leukocyte chemotaxis and phagocytosis. Curr Opin Cell Biol 2002;14:203-13.
36. Parolini I, Federici C, Raggi C, et al. Microenvironmental pH is a key factor for exosome traffic in tumor cells. J Biol Chem 2009;284:34211-22.
37. Christianson HC, Svensson KJ, van Kuppevelt TH, et al. Cancer cell exosomes depend on cell-surface heparan sulfate proteoglycans for their internalization and functional activity. Proc Natl Acad Sci U S A 2013;110:17380-5.
38. Hoshino A, Costa-Silva B, Shen TL, et al. Tumour exosome integrins determine organotropic metastasis. Nature 2015;527:329-35.
39. Zhao H, Yang L, Baddour J, et al. Tumor microenvironment derived exosomes pleiotropically modulate cancer cell metabolism. Elife 2016;5:e10250.
40. Kharmate G, Hosseini-Beheshti E, Caradec J, et al. Epidermal Growth Factor Receptor in Prostate Cancer Derived Exosomes. PLoS One 2016;11:e0154967.
41. Nilsson J, Skog J, Nordstrand A, et al. Prostate cancer-derived urine exosomes: a novel approach to biomarkers for prostate cancer. Br J Cancer 2009;100:1603-7.
42. Grange C, Tapparo M, Collino F, et al. Microvesicles released from human renal cancer stem cells stimulate

angiogenesis and formation of lung premetastatic niche. Cancer Res 2011;71:5346-56.
43. Peinado H, Alečković M, Lavotshkin S, et al. Melanoma exosomes educate bone marrow progenitor cells toward a pro-metastatic phenotype through MET. Nat Med 2012;18:883-91.
44. Ambudkar SV, Sauna ZE, Gottesman MM, et al. A novel way to spread drug resistance in tumor cells: functional intercellular transfer of P-glycoprotein (ABCB1). Trends Pharmacol Sci 2005;26:385-7.
45. Wang J, Hendrix A, Hernot S, et al. Bone marrow stromal cell-derived exosomes as communicators in drug resistance in multiple myeloma cells. Blood 2014;124:555-66.
46. Roberg-Larsen H, Lund K, Seterdal KE, et al. Mass spectrometric detection of 27-hydroxycholesterol in breast cancer exosomes. J Steroid Biochem Mol Biol 2016. [Epub ahead of print].
47. Yi H, Zheng X, Song J, et al. Exosomes mediated pentose phosphate pathway in ovarian cancer metastasis: a proteomics analysis. Int J Clin Exp Pathol 2015;8:15719-28.
48. D'Alessandro A, Amelio I, Berkers CR, et al. Metabolic effect of TAp63alpha: enhanced glycolysis and pentose phosphate pathway, resulting in increased antioxidant defense. Oncotarget 2014;5:7722-33.
49. Jiang P, Du W, Wu M. Regulation of the pentose phosphate pathway in cancer. Protein Cell 2014;5:592-602.
50. Taverna S, Giallombardo M, Pucci M, et al. Curcumin inhibits in vitro and in vivo chronic myelogenous leukemia cells growth: a possible role for exosomal disposal of miR-21. Oncotarget 2015;6:21918-33.
51. Tanaka Y, Kamohara H, Kinoshita K, et al. Clinical impact of serum exosomal microRNA-21 as a clinical biomarker in human esophageal squamous cell carcinoma. Cancer 2013;119:1159-67.
52. Skog J, Würdinger T, van Rijn S, et al. Glioblastoma microvesicles transport RNA and proteins that promote tumour growth and provide diagnostic biomarkers. Nat Cell Biol 2008;10:1470-6.
53. Que R, Ding G, Chen J, et al. Analysis of serum exosomal microRNAs and clinicopathologic features of patients with pancreatic adenocarcinoma. World J Surg Oncol 2013;11:219.
54. Taylor DD, Gercel-Taylor C. MicroRNA signatures of tumor-derived exosomes as diagnostic biomarkers of ovarian cancer. Gynecol Oncol 2008;110:13-21.
55. Krug AK, Karlovich C, Koestler T, et al. Abstract B136: Plasma EGFR mutation detection using a combined exosomal RNA and circulating tumor DNA approach in patients with acquired resistance to first-generation EGFR-TKIs. Am Assoc Cancer Res 2016;14:B136.
56. Brinkmann K, Enderle D, Koestler T, et al. Abstract 545: Plasma-based diagnostics for detection of EML4-ALK fusion transcripts in NSCLC patients. Cancer Res 2015;75:545.
57. Al-Nedawi K, Meehan B, Kerbel RS, et al. Endothelial expression of autocrine VEGF upon the uptake of tumor-derived microvesicles containing oncogenic EGFR. Proc Natl Acad Sci U S A 2009;106:3794-9.
58. Usó M, Jantus-Lewintre E, Sirera R, et al. miRNA detection methods and clinical implications in lung cancer. Future Oncol 2014;10:2279-92.
59. Giallombardo M, Chacártegui Borrás J, Castiglia M, et al. Exosomal miRNA Analysis in Non-small Cell Lung Cancer (NSCLC) Patients' Plasma Through qPCR: A Feasible Liquid Biopsy Tool. J Vis Exp 2016;(111).
60. Rolfo C, Chacartegui J, Giallombardo M, et al. 71P Exosomes isolated in plasma of non-small cell lung cancer patients contain microRNA related to the EGFR pathway: Proof of concept. J Thorac Oncol 2016;11:S85.
61. Adi Harel S, Bossel Ben-Moshe N, Aylon Y, et al. Reactivation of epigenetically silenced miR-512 and miR-373 sensitizes lung cancer cells to cisplatin and restricts tumor growth. Cell Death Differ 2015;22:1328-40.
62. Silva J, García V, Zaballos Á, et al. Vesicle-related microRNAs in plasma of nonsmall cell lung cancer patients and correlation with survival. Eur Respir J 2011;37:617-23.
63. Dinh T-KT, Fendler W, Chalubinska-Fendler J, et al. Circulating miR-29a and miR-150 correlate with delivered dose during thoracic radiation therapy for non-small cell lung cancer. Radiat Oncol 2016;11:61.
64. Yuan D, Xu J, Wang J, et al. Extracellular miR-1246 promotes lung cancer cell proliferation and enhances radioresistance by directly targeting DR5. Oncotarget 2016;7:32707-22.
65. Tang Y, Cui Y, Li Z, et al. Radiation-induced miR-208a increases the proliferation and radioresistance by targeting p21 in human lung cancer cells. J Exp Clin Cancer Res 2016;35:7.
66. Li J, Yu J, Zhang H, et al. Exosomes-Derived MiR-302b Suppresses Lung Cancer Cell Proliferation and Migration via TGFβRII Inhibition. Cell Physiol Biochem 2016;38:1715-26.
67. Giallombardo M, Jorge Chacartegui J, Reclusa P, et al. Follow up analysis by exosomal miRNAs in EGFR mutated non-small cell lung cancer (NSCLC) patients

during osimertinib (AZD9291) treatment: A potential prognostic biomarker tool. J Clin Oncol 2016;34:abstr e23035.
68. Morse MA, Garst J, Osada T, et al. A phase I study of dexosome immunotherapy in patients with advanced non-small cell lung cancer. J Transl Med 2005;3:9.
69. Villasante A, Marturano-Kruik A, Ambati SR, et al. Recapitulating the Size and Cargo of Tumor Exosomes in a Tissue-Engineered Model. Theranostics 2016;6:1119-30.
70. Ono H, Motoi N, Nagano H, et al. Long noncoding RNA HOTAIR is relevant to cellular proliferation, invasiveness, and clinical relapse in small-cell lung cancer. Cancer Med 2014;3:632-42.
71. Liu Z, Sun M, Lu K, et al. The long noncoding RNA HOTAIR contributes to cisplatin resistance of human lung adenocarcinoma cells via downregualtion of p21(WAF1/CIP1) expression. PLoS One 2013;8:e77293.
72. Rabinowits G, Gerçel-Taylor C, Day JM, et al. Exosomal microRNA: a diagnostic marker for lung cancer. Clin Lung Cancer 2009;10:42-6.
73. Viaud S, Thery C, Ploix S, et al. Dendritic cell-derived exosomes for cancer immunotherapy: what's next? Cancer Res 2010;70:1281-5.
74. Rolfo CD, Giallombardo M, Castiglia M, et al. Exosomes isolation and characterization in non small cell lung carcinoma patients: Proof of concept study. J Clin Oncol 2015;33:abstr 11101.
75. Hu J, Wang Z, Liao BY, et al. Human miR-1228 as a stable endogenous control for the quantification of circulating microRNAs in cancer patients. Int J cancer 2014;135:1187-94.

Cite this article as: Reclusa P, Sirera R, Araujo A, Giallombardo M, Valentino A, Sorber L, Bazo IG, Pauwels P, Rolfo C. Exosomes genetic cargo in lung cancer: a truly Pandora's box. 2016;5(5):483-491. doi: 10.21037/tlcr.2016.10.06

CTM Cancer Translational Medicine

Cancer Transl Med 2017;3(2):53–7
doi: 10.4103/2395-3977.202226

Mini Review

Circulating MicroRNAs and Long Noncoding RNAs: Liquid Biomarkers in Thoracic Cancers

Pablo Reclusa[1], Anna Valentino[1], Rafael Sirera[1,2], Martin Frederik Dietrich[3], Luis Estuardo Raez[3], Christian Rolfo[1]

[1]Department of Oncology, Phase I - Early Clinical Trials Unit, Antwerp University Hospital, Center for Oncological Research, Antwerp University, Antwerp, Belgium; [2]Department of Biotechnology, Universitat Politecnica de Valencia, Valencia, Spain; [3]Department of Thoracic Oncology, Memorial Cancer Institute, Pembroke Pines, FL, USA

Address for correspondence: Prof. Christian Rolfo, Phase I - Early Clinical Trials Unit, Antwerp University Hospital, Wilrijkstraat 10, 2650 Edegem, Belgium. E-mail: christian.rolfo@uza.be

Received August 01, 2016; Accepted December 22, 2016

Thoracic cancers are the leading causes of cancer-related deaths worldwide. Recent advances in genome and transcriptome analysis have allowed for the identification of numerous classes of noncoding RNAs (ncRNAs) that play important roles either in a biological process or human disease. microRNAs (miRNAs) are small, 19–22 nucleotides, ncRNAs that regulate posttranscriptional gene expression by binding to the 3′ untranslated region (3′UTR) of their target mRNA. Conversely, long noncoding RNAs (lncRNAs) are a novel class of transcripts longer than 200 nucleotides that do not encode any proteins. Some lncRNAs can interact with miRNAs and act as repressors, impeding them to bind to their protein-coding targets. There is cumulative evidence that these ncRNAs contribute to the tumorigenic process regulating cell growth, apoptosis, and metastasis, and may serve as biomarkers in various types of tumors. In this review, we have summarized the important role of ncRNAs as promising biomarkers in liquid biopsy for the diagnosis and prognosis of thoracic malignancies such as lung cancer, mesothelioma, and thymoma.

Key words: Liquid biopsy, long noncoding RNA, microRNA, thoracic cancers

INTRODUCTION

While it is estimated that more than 70% of the human genome is transcribed into primary RNA, approximately, only 2% of human DNA encodes for proteins. A particular family of RNA, noncoding RNAs (ncRNAs), can be divided into two major groups according to their transcript lengths: (1) the long noncoding RNAs (lncRNAs) which are longer than 200 bp, and (2) small ncRNAs, which are shorter than 200 bp.[1] In this second group, there are: (a) the piwi-interacting RNAs, which is the largest class of small ncRNAs molecules expressed in animal cells and involved in epigenetic and posttranscriptional gene silencing; (b) the small nucleolar RNAs, which guide chemical modifications of other RNAs; and (c) the microRNAs (miRNAs), which also function in the posttranscriptional regulation of gene expression. Small ncRNAs are implicated in the regulation of genome expression; they play important roles in a wide range of biological processes, including modulation of cellular development, differentiation, apoptosis, and carcinogenesis.[2]

NONCODING RNA

The miRNAs are described as a subgroup of small ncRNAs (19–24 nucleotides) that regulate targets at a posttranscriptional level [Figure 1]. They either inhibit mRNA translation or facilitate mRNA destruction by base pairing to partially complementary sites predominately in the untranslated region of the messenger.[3] miRNA networks are highly conserved among species, and contribute to the regulation of several cellular functions, including cellular proliferation and differentiation, apoptosis, signal transduction, organ development, and immune response.[4] miRNAs are transcribed by RNA polymerase II and cleaved by RNase III (Drosha) to a pre-miRNA of about 70–90 nucleotides. This pre-miRNA is exported from the nucleus into the cytoplasm by exportin 5 and cleaved again by Dicer, another RNase. This yields a mature miRNA of about 18–21 nucleotides which can bind target mRNAs to form RNA-induced silencing complex, leading to translation, inhibition,

How to cite this article: Reclusa P, Valentino A, Sirera R, Dietrich MF, Raez LE, Rolfo C. Circulating micrornas and long noncoding rnas: Liquid biomarkers in thoracic cancers. *Cancer Transl Med* 2017;3(2):53-7.

or mRNA degradation [Figure 2].[5] In addition, miRNAs have several interesting characteristics such as stability, tissue specificity, easy detection, and manipulation. Most cancers have deregulated miRNAs, which represent potential diagnostic and therapeutic targets,[6] and can be used to assess the effect of chemotherapy.[7]

lncRNAs are mainly located in the nucleus, where they are transcribed by the RNA polymerase II. They interact with nucleic acids and proteins, participating in the epigenetic regulation of gene expression and guiding chromatin-modifying complexes.[8,9] In addition, they can interact with splicing regulatory proteins in the cytoplasm to affect the alternative splicing of mRNA, and interact with translational factors to influence the stability of mRNAs.[10] It has also been demonstrated that lncRNAs sequester miRNA molecules and prevent them from binding their targets.[11,12] Only a fraction of the lncRNAs have been characterized experimentally. The LNCipedia 4.0 (http://www.lncipedia.org/), is a database that contains 118,777 human annotated lncRNAs with information about secondary structures, protein coding potential and miRNA binding sites.[13] Cancer-associated lncRNAs may serve as diagnostic or predictive biomarkers of cancer, and in the future might also help to provide new therapeutic strategies.[14] Both lncRNA and miRNA are considered potential cancer biomarkers with potential clinical therapeutic applications.[15]

NONCODING RNAS IN LIQUID BIOPSY

Biopsy is still the current source for tumor information, however, information about tumor location, size, and heterogeneity are not easy to obtain. To rid this problem, liquid biopsy has become one of the most promising tools for the identification, prediction and prognosis of tumors.[16] Some potential advantages of liquid biopsy are its minimal invasiveness and the vast amount of information that can be obtained from unconventional sources such as urine, saliva, or the blood. Three main components have been studied in regards to liquid biopsy: (1) circulating tumor cells, (2) exosomes, and (3) circulating tumor nucleic acids, including circulating tumor DNA and circulating tumor RNA (ctRNA), which comprises lncRNAs and miRNA.[16,17] In general, RNA is a very labile molecule with a short half-life in standard conditions. However, different reports demonstrate unconventional stability levels of RNA in the blood and after incubation at room temperature for 24 h or incubation with RNase A for 3 h.[17-19] The reason for this stability is the association of ctRNA with other components in the liquid biopsy such as lipids, phospholipids, apoptotic bodies, or DNA in nucleosomes.[20-23]

In the last years, due to advances in different techniques, the detection of this circulating ncRNAs with a low yield has improved dramatically,[19,24,25] making it possible to get crucial information through microarrays or deep-sequencing (DeepSeq) with a small amount of material. The real time quantitative polymerase chain reaction is still the most used method to analyze these molecules due to its specificity and affordability,[26-29] providing a feasible tool in a clinical setting [Figure 3].

NONCODING RNAS IN LIQUID BIOPSY FROM LUNG CANCER PATIENTS

Circulating ncRNAs have been shown to play a crucial role in tumor initiation, progression and metastasis. It is known that tumorigenesis is frequently associated with an over-expression

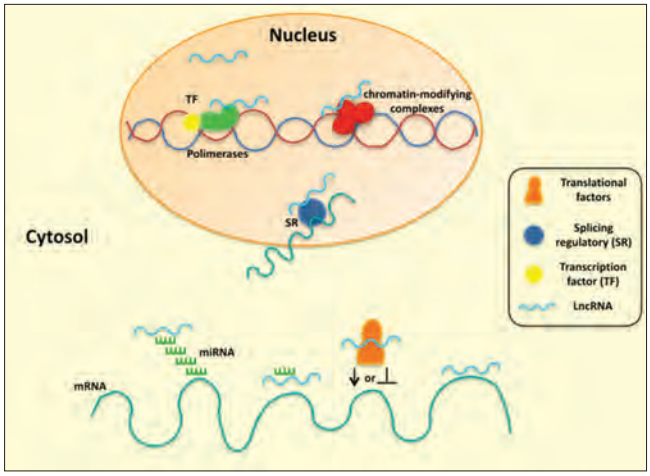

Figure 1. Non-coding RNA mechanisms of action

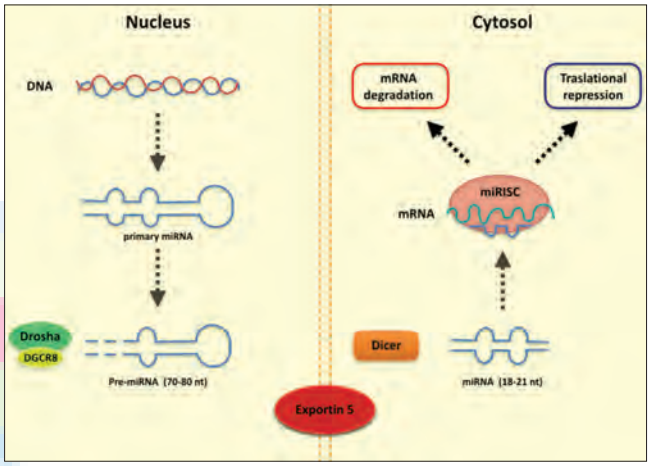

Figure 2. MicroRNA biogenesis and mechanism of action

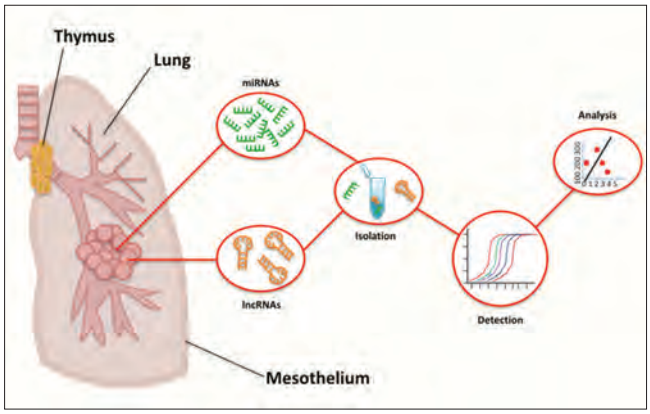

Figure 3. LncRNAs and microRNAs as biomarkers and therapeutic targets in thoracic

of oncogenes, as well as a down-regulation of tumor-suppressor genes. ncRNAs can act as either oncogenes or tumor-suppressor genes, and several studies in lung cancer patients have found them to be deregulated in the tissue and in the plasma. miRNAs in liquid biopsy have several advantages such as tissue specific expression and relatively easy detection, thus they may be considered as potential biomarkers for diagnosis, prognosis, and personalized therapy.

MicroRNAs

The present data suggest the potential value of miRNAs as diagnostic blood-based markers for early detection of lung cancer. miR-21 was the first miRNA with oncogenic function found in serum and plasma significantly higher in nonsmall cell lung cancer patients than in healthy controls.[30] Furthermore, plasma levels of miR-155, miR-197, and miR-182 were significantly increased in plasma of lung cancer patients with stage I compared to controls with high specificity and sensitivity.[31] Powrózek *et al.*[32] investigated the role of miR-944 and miR-3662 as biomarkers and described a higher expression profile in lung cancer patients. Conversely, other studies have indicated that miR-361-3p, miR-625[29], and miR-375[33] were significantly decreased in serum of NSCLC patients compared to benign disease and healthy individuals. In addition, miR-625 was lower in serum from smoking patients compared with nonsmoking patients.[29] Expanding the analytical capability of miRNAs, a set of 6 miRNAs (miR-429, miR-205, miR-200b, miR-203, miR-125b, and miR-34b) have been found significantly higher in the serum of NSCLC patients in early stages with a high sensitivity and specificity.[34] In this regard, Geng *et al.*[35] tested 12 candidate miRNAs in plasma samples of both lung cancer patients and controls and found that all miRNAs were up-regulated but only 5 (miR-20a, miR-223, miR-21, miR-221, and miR-145) resulted significantly increased in the early stage of NSCLC patients compared to healthy controls. These miRNAs showed better diagnostic value in smokers relative to nonsmokers.[35] Several other studies have analyzed the potential diagnostic role of miRNAs in different types of biological samples such as sputum and pleural effusion in lung cancer. In particular, miR-21 and miR-210 were found to be the most deregulated miRNAs in sputum of NSCLC patients, whereas miR-30d, miR-24, and miR-26a were higher in malignant effusions compared to normal effusions.[36]

Regarding the association with clinically relevant pathological variables in NSCLC patients, miR-21 expression was not related to age, sex, smoking status, pathology, lymph node metastasis, but it was associated with pathological TMN stage.[30] In addition, miR-145 and miR-146 augmented circulating levels failed to associate with pathological characteristics of the patients,[37] while serum miR-125b were associated with clinical stages, lymph node, epidermal growth factor receptor mutation and smoking status in NSCLC patients.[38] Other studies have shown that plasma levels of let-7c and miR-152 are related with pathological features such as histological classification, differentiation status, lymph node metastasis and stage.[39] miRNAs expression profiles can be evaluated after surgery, in fact, let-7c and miR-152 in the postoperative plasmas are significantly increased compared to the preoperative plasmas as well as miR-361-3p is up-regulated after surgery.[40] While contrarily, other studies have demonstrated that miR-205 is selectively found in exosomes and its levels decrease after lung cancer removal.[41] Petriella *et al.*[42] confirmed that several miRNAs can be deregulated in both serum and tissues. miR-486-5p has a higher expression in tumor serum than in tumor tissues, whereas miR-29c* showed a lower expression in tumor tissues than in tumor serum. These studies may suggest the need to monitor both serum and tissues samples to search for altered expression of specific miRNAs in NSCLC patients.[42] Circulating miR-142-3p and miR-29b have been found up-regulated in lung adenocarcinomas[43] and associated with the risk of recurrence. Patients with metastatic NSCLC presented with lower levels of miR-375 than those with nonmetastatic disease. In addition, low expression of miR-375 in plasma was an independent predictor of poor prognosis for NSCLC patients,[33] and high miR-142-3p serum levels may be valuable to predict a worse response in patients who received adjuvant therapy.[43]

Long-noncoding RNAs

Despite efforts in the field, not many lncRNAs have been described in liquid biopsies from lung cancer patients. One of the most studies is MALAT1, which binds to unmethylated Polycomb 2 protein, promoting the relocation of growth control genes in response to mitogenic signals.[44] It seems that MALAT1 enhances the metastatic capacity of the tumor because it has been described that patients with metastatic lung cancer have higher MALAT1 levels in peripheral blood than those without metastasis.[28]

Recently, a study analyzing a microarray of more than 800 deregulated lncRNAs in the plasma of 11 lung cancer patients and 9 healthy controls has allowed further validation of three lncRNAs: RP11-397D12, AC0074031, and ERICH1-AS1.[27] A similar study, where 21 lncRNAs were examined in the blood of 20 lung cancer patients and 20 healthy donors, found three different lncRNA signatures: SPRY-IT1, ANRIL, and NEAT1. This study was eventually validated with a larger cohort of fifty lung cancer patients and fifty healthy donors.[45]

NONCODING RNA IN LIQUID BIOPSY FROM MALIGNANT PLEURAL MESOTHELIOMA AND THYMOMA PATIENTS

Malignant pleural mesothelioma (MPM) and thymoma are two cancers with a very low prevalence in both genders, making the material available for the studies limited. However, in recent years, the feasibility of studying different aspects of liquid biopsy has permitted the discovery of some new aspects about miRNAs from both mesothelioma and thymoma tumors. Until now, no lncRNAs have been analyzed in liquid biopsy from these tumors.

One of the biggest studies in liquid biopsy was carried by Gayosso-Gómez *et al.*,[26] in which a wide screen of miRNAs was analyzed in serum from 11 MPM patients, 36 adenocarcinoma NSCLC patients and 45 healthy donors. After DeepSeq and both computational and differential expression analysis, they found three miRNAs related to the p38 pathway: miR-1271, miR-96-5p, and miR-409-5p differentially upregulated. p38 downregulation is associated with cell proliferation and tumorigenesis.[46] In other publications, miR-126 has been described to be highly downregulated in serum samples from patients with MPM compared to NSCLC patients and healthy donors.[47,48] miR-625-3p was the first miRNA described to be significantly upregulated in patients with MPM, compared to healthy donors.[49] The degree of methylation of miR-34b/c plays a key role in the pathogenesis of MPM, and correlates with the presence of MPM compared to benign asbestos pleurisy and healthy donors. In addition, it also correlates with the stage of MPM.[50]

The aberrant lncRNAs implicated in thymoma development still remain unknown, and only one study has been carried out measuring miRNAs in liquid biopsy. miR-21-5p and miR-148a-3p were significantly up-regulated in plasma from thymoma and thymic carcinoma patients, compared to healthy donors. Furthermore, the expression levels of these on co-miRNAs

appeared significantly reduced during follow-up, emphasizing their potential role as biomarkers not only for diagnosis but also to evaluate complete resection and response to treatment.[51] Clearly, more studies are required to identify and validate new ncRNA as diagnostic, prognostic, and therapeutic biomarkers, however, due to new technology, there may be more information in the coming years.

CONCLUSION

Deregulated transcriptional profiles found in tumors suggest that ncRNAs may represent effective biomarkers in thoracic tumors with diagnostic, prognostic, and predictive utility. Based on the development of studies related to cfDNA, preliminary consideration has been given to ncRNA as a feasible tool for daily clinical practice. In our opinion, analysis of ncRNA will soon be used to diagnose, predict and improve treatment of patients. Exosomes are arising as a very promising tool to improve the quality of life of patients through better diagnosis and prediction of their disease. They could also potentially replace traditionally invasive biopsies from daily clinical practice due to their better protection of genetic material and their high representation of cellular cargo. However, since there are still unknown aspects in regards to exosome production and interaction, more work still needs to be performed in the field of exosome research.

In recent years, research in ncRNA has been on the rise, and 140,000 ncRNAs have been described, including miRNAs and lncRNAs, many of which are currently being studied in different tumors. Many ncRNAs have already been detected with promising characteristics, however, validation of these profiles must be performed to bring ncRNAs to the clinical setting. The scientific community is making a huge effort to detect new useful molecules in cancer. In our opinion, in the future years, liquid biopsy will become a necessary complement to the tissue analysis both with cfDNA and exosomes.

Financial support and sponsorship

Nil.

Conflicts of interest

There are no conflicts of interest.

REFERENCES

1. Volders PJ, Helsens K, Wang X, Menten B, Martens L, Gevaert K, Vandesompele J, Mestdagh P. LNCipedia: a database for annotated human lncRNA transcript sequences and structures. *Nucleic Acids Res* 2013; 41: D246–51.
2. Batista PJ, Chang HY. Long noncoding RNAs: cellular address codes in development and disease. *Cell* 2013; 152 (6): 1298–307.
3. Lu J, Getz G, Miska EA, Alvarez-Saavedra E, Lamb J, Peck D, Sweet-Cordero A, Ebert BL, Mak RH, Ferrando AA, Downing JR, Jacks T, Horvitz HR, Golub TR. MicroRNA expression profiles classify human cancers. *Nature* 2005; 435 (7043): 834–8.
4. Kim VN, Han J, Siomi MC. Biogenesis of small RNAs in animals. *Nat Rev Mol Cell Biol* 2006; 10 (2): 126–39.
5. Bartel DP. MicroRNAs: genomics, biogenesis, mechanism, and function. *Cell* 2004; 116 (2): 281–97.
6. Vencken SF, Greene CM, McKiernan PJ. Non-coding RNA as lung disease biomarkers. *Thorax* 2015; 70 (5): 501–3.
7. Ouyang M, Li Y, Ye S, Ma J, Lu L, Lv W, Chang G, Li X, Li Q, Wang S, Wang W. MicroRNA profiling implies new markers of chemoresistance of triple-negative breast cancer. *PLoS One* 2014; 9 (5): e96228.
8. Kung JT, Colognori D, Lee JT. Long noncoding RNAs: past, present, and future. *Genetics* 2013; 193 (3): 651–69.
9. Derrien T, Johnson R, Bussotti G, Tanzer A, Djebali S, Tilgner H, Guernec G, Martin D, Merkel A, Knowles DG, Lagarde J, Veeravalli L, Ruan X, Ruan Y, Lassmann T, Carninci P, Brown JB, Lipovich L, Gonzalez JM, Thomas M, Davis CA, Shiekhattar R, Gingeras TR, Hubbard TJ, Notredame C, Harrow J, Guigó R. The GENCODE v7 catalog of human long noncoding RNAs: analysis of their gene structure, evolution, and expression. *Genome Res* 2012; 22 (9): 1775–89.
10. Sang H, Liu H, Xiong P, Zhu M. Long non-coding RNA functions in lung cancer. *Tumour Biol* 2015; 36 (6): 4027–37.
11. Tay Y, Rinn J, Pandolfi PP. The multilayered complexity of ceRNA crosstalk and competition. *Nature* 2014; 505 (7483): 344–52.
12. Cesana M, Cacchiarelli D, Legnini I, Santini T, Sthandier O, Chinappi M, Tramontano A, Bozzoni I. A long noncoding RNA controls muscle differentiation by functioning as a competing endogenous RNA. *Cell* 2011; 147 (2): 358–69.
13. Volders PJ, Verheggen K, Menschaert G, Vandepoele K, Martens L, Vandesompele J, Mestdagh P. An update on LNCipedia: a database for annotated human lncRNA sequences. *Nucleic Acids Res* 2015; 43 (8): 4363–4.
14. Shi X, Sun M, Liu H, Yao Y, Song Y. Long non-coding RNAs: a new frontier in the study of human diseases. *Cancer Lett* 2013; 339 (2): 159–66.
15. Seto AG. The road toward microRNA therapeutics. *Int J Biochem Cell Biol* 2010; 42 (8): 1298–305.
16. Rolfo C, Castiglia M, Hong D, Alessandro R, Mertens I, Baggerman G, Zwaenepoel K, Gil-Bazo I, Passiglia F, Carreca AP, Taverna S, Vento R, Santini D, Peeters M, Russo A, Pauwels P. Liquid biopsies in lung cancer: the new ambrosia of researchers. *Biochim Biophys Acta* 2014; 1846 (2): 539–46.
17. Wong BC, Lo YM. Plasma RNA integrity analysis: methodology and validation. *Ann N Y Acad Sci* 2006; 1075: 174–8.
18. Schmidt B, Engel E, Carstensen T, Weickmann S, John M, Witt C, Fleischhacker M. Quantification of free RNA in serum and bronchial lavage: a new diagnostic tool in lung cancer detection? *Lung Cancer* 2005; 48 (1): 145–7.
19. Zhou X, Yin C, Dang Y, Ye F, Zhang G. Identification of the long non-coding RNA H19 in plasma as a novel biomarker for diagnosis of gastric cancer. *Sci Rep* 2015; 5: 11516.
20. Rosi A, Guidoni L, Luciani AM, Mariutti G, Viti V. RNA-lipid complexes released from the plasma membrane of human colon carcinoma cells. *Cancer Lett* 1988; 39 (2): 153–60.
21. Halicka HD, Bedner E, Darzynkiewicz Z. Segregation of RNA and separate packaging of DNA and RNA in apoptotic bodies during apoptosis. *Exp Cell Res* 2000; 260 (2): 248–56.
22. Sisco KL. Is RNA in serum bound to nucleoprotein complexes? *Clin Chem* 2001; 47 (9): 1744–5.
23. Tsui NB, Ng EK, Lo YM. Stability of endogenous and added RNA in blood specimens, serum, and plasma. *Clin Chem* 2002; 48 (10): 1647–53.
24. Arita T, Ichikawa D, Konishi H, Komatsu S, Shiozaki A, Shoda K, Kawaguchi T, Hirajima S, Nagata H, Kubota T, Fujiwara H, Okamoto K, Otsuji E. Circulating long non-coding RNAs in plasma of patients with gastric cancer. *Anticancer Res* 2013; 33 (8): 3185–93.
25. Isin M, Ozgur E, Cetin G, Erten N, Aktan M, Gezer U, Dalay N. Investigation of circulating lncRNAs in B-cell neoplasms. *Clin Chim Acta* 2014; 431: 255–9.
26. Gayosso-Gómez LV, Zárraga-Granados G, Paredes-Garcia P, Falfán-Valencia R, Vazquez-Manríquez ME, Martinez-Barrera LM, Castillo-Gonzalez P, Rumbo-Nava U, Guevara-Gutierrez R, Rivera-Bravo B, Ramirez-Venegas A, Sansores R, Negrete-Garcia MC, Ortiz-Quintero B. Identification of circulating miRNAs profiles that distinguish malignant pleural mesothelioma from lung adenocarcinoma. *EXCLI J* 2014; 13: 740–50.

27. Tang Q, Ni Z, Cheng Z, Xu J, Yu H, Yin P. Three circulating long non-coding RNAs act as biomarkers for predicting NSCLC. *Cell Physiol Biochem* 2015; 37 (3): 1002–9.
28. Guo F, Yu F, Wang J, Li Y, Li Y, Li Z, Zhou Q. Expression of MALAT1 in the peripheral whole blood of patients with lung cancer. *Biomed Rep* 2015; 3 (3): 309–12.
29. Roth C, Stückrath I, Pantel K, Izbicki JR, Tachezy M, Schwarzenbach H. Low levels of cell-free circulating miR-361-3p and miR-625* as blood-based markers for discriminating malignant from benign lung tumors. *PLoS One* 2012; 7 (6): e38248.
30. Wei J, Gao W, Zhu CJ, Liu YQ, Mei Z, Cheng T, Shu YQ. Identification of plasma microRNA-21 as a biomarker for early detection and chemosensitivity of non-small cell lung cancer. *Chin J Cancer* 2011; 30 (6): 407–14.
31. Zheng D, Haddadin S, Wang Y, Gu LQ, Perry MC, Freter CE, Wang MX. Plasma microRNAs as novel biomarkers for early detection of lung cancer. *Int J Clin Exp Pathol* 2011; 4 (6): 575–86.
32. Powrózek T, Krawczyk P, Kowalski DM, Winiarczyk K, Olszyna-Serementa M, Milanowski J. Plasma circulating microRNA-944 and microRNA-3662 as potential histologic type-specific early lung cancer biomarkers. *Transl Res* 2015; 166 (4): 315–23.
33. Yu H, Jiang L, Sun C, Li Guo L, Lin M, Huang J, Zhu L. Decreased circulating miR-375: a potential biomarker for patients with non-small-cell lung cancer. *Gene* 2014; 534 (1): 60–5.
34. Halvorsen AR, Bjaanæs M, LeBlanc M, Holm AM, Bolstad N, Rubio L, Peñalver JC, Cervera J, Mojarrieta JC, López-Guerrero JA, Brustugun OT, Helland Å. A unique set of 6 circulating microRNAs for early detection of non-small cell lung cancer. *Oncotarget* 2016; 7 (24): 37250–9.
35. Geng Q, Fan T, Zhang B, Wang W, Xu Y, Hu H. Five microRNAs in plasma as novel biomarkers for screening of early-stage non-small cell lung cancer. *Respir Res* 2014; 15: 149.
36. Xiao YF, Yong X, Fan YH, Lü MH, Yang SM, Hu CJ. microRNA detection in feces, sputum, pleural effusion and urine: novel tools for cancer screening (Review). *Oncol Rep* 2013; 30 (2): 535–44.
37. Wang X, Zhang Y, Fu Y, Zhang J, Yin L, Pu Y, Liang G. MicroRNA-125b may function as an oncogene in lung cancer cells. *Mol Med Rep* 2015; 11 (5): 3880–7.
38. Zhao Q, Cao J, Wu YC, Liu X, Han J, Huang XC, Jiang LH, Hou XX, Mao WM, Ling ZQ. Circulating miRNAs is a potential marker for gefitinib sensitivity and correlation with EGFR mutational status in human lung cancers. *Am J Cancer Res* 2015; 5 (5): 1692–705.
39. Dou H, Wang Y, Su G, Zhao S. Decreased plasma let-7c and miR-152 as noninvasive biomarker for non-small-cell lung cancer. *Int J Clin Exp Med* 2015; 8 (6): 9291–8.
40. Zhao C, Lu F, Chen H, Zhao F, Zhu Z, Zhao X, Chen H. Clinical significance of circulating miRNA detection in lung cancer. *Med Oncol* 2016; 33 (5): 41.
41. Aushev VN, Zborovskaya IB, Laktionov KK, Girard N, Cros MP, Herceg Z, Krutovskikh V. Comparisons of microRNA patterns in plasma before and after tumor removal reveal new biomarkers of lung squamous cell carcinoma. *PLoS One* 2013; 8 (10): e78649.
42. Petriella D, De Summa S, Lacalamita R, Galetta D, Catino A, Logroscino AF, Palumbo O, Carella M, Zito FA, Simone G, Tommasi S. miRNA profiling in serum and tissue samples to assess noninvasive biomarkers for NSCLC clinical outcome. *Tumour Biol* 2016; 37 (4): 5503–13.
43. Kaduthanam S, Gade S, Meister M, Brase JC, Johannes M, Dienemann H, Warth A, Schnabel PA, Herth FJ, Sültmann H, Muley T, Kuner R. Serum miR-142-3p is associated with early relapse in operable lung adenocarcinoma patients. *Lung Cancer* 2013; 80 (2): 223–7.
44. Yang L, Lin C, Liu W, Zhang J, Ohgi KA, Grinstein JD, Dorrestein PC, Rosenfeld MG. ncRNA- and Pc2 methylation-dependent gene relocation between nuclear structures mediates gene activation programs. *Cell* 2011; 147 (4): 773–88.
45. Hu X, Bao J, Wang Z, Zhang Z, Gu P, Tao F, Cui D, Jiang W. The plasma lncRNA acting as fingerprint in non-small-cell lung cancer. *Tumour Biol* 2016; 37 (3): 3497–504.
46. MacNeil AJ, Jiao SC, McEachern LA, Yang YJ, Dennis A, Yu H, Xu Z, Marshall JS, Lin TJ. MAPK kinase 3 is a tumor suppressor with reduced copy number in breast cancer. *Cancer Res* 2014; 74 (1): 162–72.
47. Tomasetti M, Staffolani S, Nocchi L, Neuzil J, Strafella E, Manzella N, Mariotti L, Bracci M, Valentino M, Amati M, Santarelli L. Clinical significance of circulating miR-126 quantification in malignant mesothelioma patients. *Clin Biochem* 2012; 45 (7–8): 575–81.
48. Panou V, Vyberg M, Weinreich UM, Meristoudis C, Falkmer UG, Røe OD. The established and future biomarkers of malignant pleural mesothelioma. *Cancer Treat Rev* 2015; 41 (6): 486–95.
49. Kirschner MB, Cheng YY, Badrian B, Kao SC, Creaney J, Edelman JJ, Armstrong NJ, Vallely MP, Musk AW, Robinson BW, McCaughan BC, Klebe S, Mutsaers SE, van Zandwijk N, Reid G. Increased circulating miR-625-3p: a potential biomarker for patients with malignant pleural mesothelioma. *J Thorac Oncol* 2012; 7 (7): 1184–91.
50. Muraoka T, Soh J, Toyooka S, Aoe K, Fujimoto N, Hashida S, Maki Y, Tanaka N, Shien K, Furukawa M, Yamamoto H, Asano H, Tsukuda K, Kishimoto T, Otsuki T, Miyoshi S. The degree of microRNA-34b/c methylation in serum-circulating DNA is associated with malignant pleural mesothelioma. *Lung Cancer* 2013; 82 (3): 485–90.
51. Bellissimo T, Russo E, Ganci F, Vico C, Sacconi A, Longo F, Vitolo D, Anile M, Disio D, Marino M, Blandino G, Venuta F, Fazi F. Circulating miR-21-5p and miR-148a-3p as emerging non-invasive biomarkers in thymic epithelial tumors. *Cancer Biol Ther* 2016; 17 (1): 79–82.

Biomolecular Research & Therapeutics

Conte et al., J Biomol Res Ther 2016, 5:2
http://dx.doi.org/10.4172/2167-7956.1000139

Review Article Open Access

Polyphenols Nanoencapsulation for Therapeutic Applications

Conte R[1], Calarco A[2], Napoletano A[2], Valentino A[2], Margarucci S[2], Di Cristo F[2], Di Salle A[2]* and Peluso G[2]

[1]*Institute for Polymers, Composites and Biomaterials - National Research Council, Pozzuoli, Italy*
[2]*Institute of Bioscience and BioResources - National Research Council, Naples, Italy*

Abstract

Natural polyphenols are valuable compounds present in plants, fruits, legumes, chocolate, tea, wine and marine organisms possessing scavenging properties towards radical oxygen species. These abilities make polyphenols interesting either for the treatment of various diseases like inflammation and cancer or for anti-ageing purposes in cosmetic formulations. Unfortunately, such compounds lack in long-term stability, are very sensitive to light, and often present a low water solubility and poor bioavailability. To overcome these limitations and enhance polyphenols therapeutic applications, nanotechnology-based delivery systems have been developed, and among all, nanoencapsulation represented a promising strategy. This review described a recent overview of physicochemical nanoencapsulated polyphenols focusing on the most representative molecules such as resveratrol, quercetin, epigallocatechin-3-gallate, and curcumin.

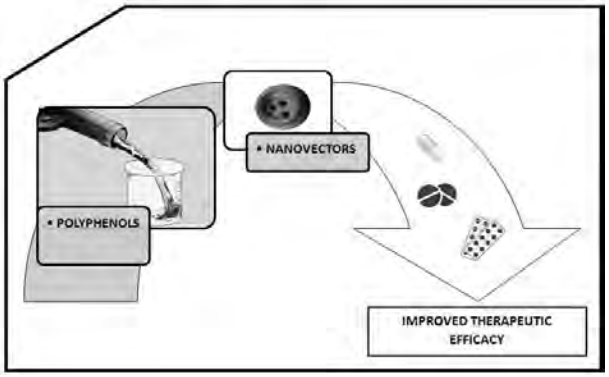

Keywords: Nanotechnology; Polyphenols; Drug delivery; Bioavailability

Introduction

Polyphenols (PPH) are a large family of ubiquitous and varied molecules in the form of secondary metabolites of all vascular plants and several marine organisms. These natural compounds range from simple molecules to complex structures that have in common the presence of benzenic cycles bearing one or several hydroxy functions. These active principles play an important role in growth, reproduction, resistance to pathogens, predators and diseases [1]. In particular, these phytochemicals contribute importantly to the color and organoleptic properties of plants while, in the case of marine organisms, they act in the antioxidative response of microalgae and cyanobacteria against UV exposure [2]. Indeed, Klejdus et al. [2] showed that several classes of flavonoids, such as isoflavones, flavanones, flavonols and dihydrochalcones are found in microalgae and cyanobacteria despite of the fact that these organisms are evolutionary more primitive than terrestrial plants [2]. In medicine, polyphenols contribute to the promotion of health and reduction in the risk of common chronic diseases [3] (Figure 1).

Several studies show an inverse correlation between the consumption of polyphenols and the risk of major illness such as cancer, cardiovascular diseases, type 2 diabetes mellitus, neurodegenerative diseases and osteoporosis [4]. Such relationship is due to the PPH activity as potent effectors of biologic processes associated with the pathogenesis of human diseases. These effects also result from the ability of PPH to interact with proteins, enzymes, and membrane receptors modulating their activity in a specific way [5]. Among their properties, the strong free radical scavenging action mainly due to PPH ability to donate hydrogen atoms or electrons is probably the most studied [6,7]. Antioxidant effect of polyphenols can be achieved by several mechanisms of action such as molecular complexation with pro-oxidant proteins, chelation of metal ions or direct trapping of Reactive Oxygen Species (ROS). Moreover, polyphenols are recognized also for their ability to beneficially affect inflammation (e.g. by edema inhibition), to upregulate detoxification pathways or to modulate cell-signal transduction [8,9]. While PPH appear to have a dynamic interaction with gut microbiota, their efficacy in promoting health and reducing the risk of chronic diseases is dependent on their systemic bioavailability and metabolism. Generally, polyphenols have low bioavailability due to many intrinsic and extrinsic factors, including their chemical structure and molecular weight, low hydrosolubility, low stability in the gastrointestinal environment, extensive phase II metabolism and rapid elimination [10,11]. As a consequence, clinical applications of

***Corresponding author:** Di Salle A, Institute of Bioscience and Bio Resources, Naples, Italy, Tel: +39-0816132569; E-mail: anna.disalle@ibbr.cnr.it

Received March 09, 2016; **Accepted** April 28, 2016; **Published** May 06, 2016

Citation: Conte R, Calarco A, Napoletano A, Valentino A, Margarucci S, et al. (2016) Polyphenols Nanoencapsulation for Therapeutic Applications. J Biomol Res Ther 5: 139. doi:10.4172/2167-7956.1000139

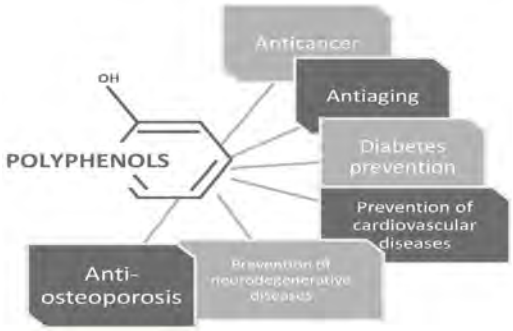

Figure 1: A schematic representation of therapeutic effects of Polyphenols.

PPH are limited. To avoid these drawbacks, nanodelivery systems able to maintain the structural integrity of the bioactive molecules have been developed [12-14]. Numerous nanoencapsulation methods have been developed based on physical (e.g. spray drying), physicochemical (e.g. ionic gelation, hydrophobic interactions, etc.) and chemical (e.g. *in situ* polymerization) principles. This review highlights the recent progress in the strategies for physicochemical nanoencapsulation of epigallocatechin-3-gallate, resveratrol, quercetin, ellagitannin, ellagic acid, phlorotannins, oleuropein, hydroxytyrosol and curcumin chosen as most representative examples of polyphenols molecules.

Classification of Polyphenols

Thousands of polyphenolic compounds have grouped together in various classes, depending to the basic chemical skeleton variations, such as degrees of oxidation, hydroxylation, methylation, glycosylation and the possible connections to other molecules (Table 1 and Figure 2). A simple sorting divides polyphenols in four classes: flavonoids (including the subclasses anthocyanidins, catechins, flavones, flavonols, flavanones and isoflavones), coumarins, stilbenes and tannins, although other constituents, like chalcones and lignans exhibit polyphenolic structures. Flavonoids are C15 compounds with the structure C6-C3-C6 in which two benzene rings are linked together by a group of three carbons. The arrangement of the C3 group determines how the compounds are classified. Typical flavonoids have A-, B- and C-ring typically depicted with the A-ring on the left-hand side.

The A-ring originates from the condensation of three malonyl-CoA molecules, and the B-ring originates from *p*-coumaroyl-CoA. The A-ring in most of flavonoids is either meta-dihydroxylated or meta-trihydroxylated. Substituents on A- and B- ring, along with the arrangement of the ring C-, differentiate the anthocyanidins, catechins, flavones, flavonols, flavanones and isoflavones. Coumarins, having C6-C3 skeleton with an oxygen heterocycle as part of the C3-unit, include isocoumarins, with a similar structure but reversed position of the oxygen and carbonyl groups within the oxygen heterocycle. Stilbenes, with a C6-C2-C6 structure, chemically are diarylethene, featured with a central ethane double bond substituted with phenyl groups on each carbon atoms of the double bond. Tannins comprise a group of compounds with a wide diversity in structure that is characterized by the ability to bind and precipitate proteins and to form complex molecules. Typically, these molecules require at least 12 hydroxyl groups and five phenyl groups to function as protein binders. Tannins are classified in three subgroups: condensed tannins, hydrolysable tannins and complex tannins, according to the type of linkage between simple units [15].

Polyphenols Bioavailability and the use of Nano Vectors

Polyphenols low bioavailability is mainly due to the low absorption in the human gastrointestinal (GI) tract following consumption, extensive biotransformation within the gut and rapid clearance from the body (Figure 3) [16]. In particular, many PPH are available as glycosylated compounds, and this form diminish their diffusion across barriers in the GI tract [10]. Other polyphenols cannot be absorbed from enterocytes because they are unstable in the acidic condition of the stomach and in the alkaline status of the small intestine [17]. Moreover, PPH are extensively transformed via phase II pathways, predominately methylation, glucuronidation and sulfation in the enterocytes of the small intestine, and then further metabolized in the liver, facilitating their quick excretion [10]. A number of strategies have been used to increase the chemical stability or permeability of these species. These approaches usually rely upon the addition of chemical additives such as reducing agents to maintain the structure, the use of dissolving agents to increase solubility [18], the interaction with inhibitors of phase I and/or II enzymes to escape biotransformation [19], the addition of complementary ingredients such as lipids or protein [20], the conjugation with promoiety groups [21]. More recently, encapsulation in nanovectors such as cyclodextrins, matrix systems, solid dispersions and liposomes has emerged as a novel strategy to improve poyphenols delivery, distribution and bioactivity [22]. Such systems differ for the internal structure (core-shell-like or matrix) and the physical state of the encapsulated active substances. Moreover, the effective use of nanoparticles as drug delivery systems require polyphenol encapsulation efficiency (EE) of, at least, sixty per cent (the percentage of drug entrapment efficiency is calculated according to the formula: Experimental drug loading/Theoretical drug loading x100).

Systems used for Nanoencapsulation

Nanotechnology is a science involving the formation of particles with diameters ranging from 1 to 1000 nm and for which the end product exhibits properties or phenomena attributable to its dimensions [12]. Nowadays, nanoencapsulation is an effective approach to improve solubility, minimize degradation process, reduce toxicity, and

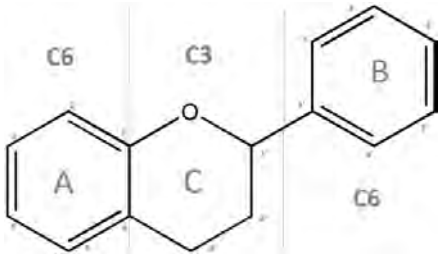

Figure 2: Basic chemical skeleton of typical Polyphenols.

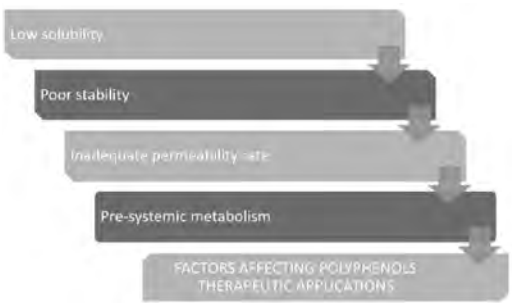

Figure 3: Factors affecting Polyphenols therapeutic applications.

Polyphenols	Chemical Structure	Examples	Sources (List is not Exhaustive)
Flavonols	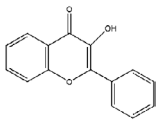	Myricetin, Quercetin, Kaempferol	Onions, broccoli, blueberries, red wine, tea
Flavones	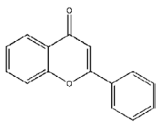	Aspigenin, Luteolin, Tangeretin, Nobiletin	Parsley, celery, millet, wheat, skin of citrus
Flavanones	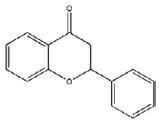	Hesperetin, Naringenin, Eriodictyol	Grapefruit, orange, lemon, tomatoes, mint
Isoflavones	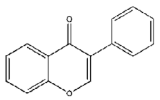	Genistein, Daidzein, Glycitein	Leguminous plants, soya
Flavanols (Catechins)	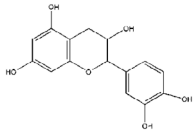	Catechin, Epicatechin	Apricot, cherry, grape, peach, apple, green and black tea, red wine, cider
Anthocyanins	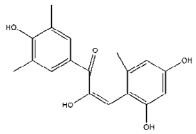	Cyanidin, Pelargonidin, Delphinidin, Petunidin	Red wine, aubergines, cabbage, beans, onions, radishes, fruit in general
Coumarins	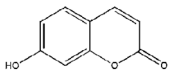	Ombelliferone, Aesculetin, Scopoletin	Tonka bean, chestnut, Melilotus officinalis, Angelica officinalis
Isocoumarins	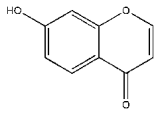	Isocoumarin	Tonka bean, chestnut, Melilotus officinalis, Angelica officinalis
Stilbenes	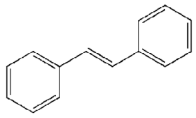	Resveratrol	Wine
Tannins	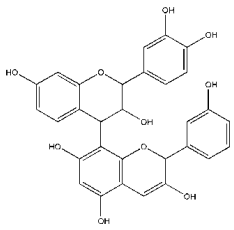	Ellagitannin, Ellagic acid and Phlorotannins	Plants (pomegranate) and brown algae

Table 1: Main classes of Polyphenols with structures and sources.

control the active absorption and biological response of polyphenols. Nanoencapsulation refers to several methods based on chemical, physical, and physiochemical principles. Chemical nanoencapsulation (e.g. interfacial and *in situ* polymerization methods) requires the polymerization of monomers at the interface of two immiscible substances through the addition of a cross-linker in the external phase [23]. Physical processes (e.g. air-suspension method, pan coating, spray drying, spray congealing, micro-orifice system, etc.) involve the interaction of the vector material with the molecules to be encapsulated when both are aerosolized or atomized [24]. Finally, physiochemical processes (e.g. coacervation, phase separation, complex emulsion, meltable dispersion and nanoprecipitation) form stable nanometer size drug nanosuspensions or nanoparticles through particle size reduction approaches [25]. The process versatility combined with the ability to increase loading capacities, persistence at the target sites and permeation and retention effect, make physiochemical methods interesting approaches to enhance PPH pharmacologic action [13,14,26]. Recently, several studies analyze nanoparticle-mediated delivery of polyphenols, based on biodegradable and biocompatible polymers able to encapsulate polyphenols in nanostructures such as cyclodextrins, nanospheres, nanocapsules, solid lipid nanoparticles, liposomes and micelles (Figure 4) [27-46].

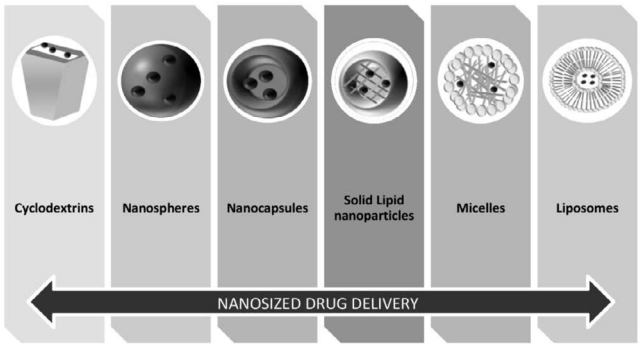

Figure 4: Schematic representation of nano-sized delivery systems for Polyphenols.

Cyclodextrins (CD) are a group of structurally related natural products formed during bacterial digestion of cellulose. They are structured as cyclic oligosaccharides consisting of (α-1,4)-linked α-D-glucopyranose units with lipophilic central cavity and hydrophilic outer surface. Specifically, the hydroxyl functions are orientated to the exterior and the central cavity is lined by the skeletal carbons and ethereal oxygens of the glucose residues. The natural α-, β- and γ- cyclodextrins (αCD, βCD and γCD) consist of six, seven, and eight glucopyranose units, respectively. These molecules have a limited aqueous solubility [27]. Effective NanoDDS are obtained using water-soluble cyclodextrin derivatives such as hydroxypropyl βCD and γCD, randomly methylated β-cyclodextrin (RMβCD), and sulfobutylether β-cyclodextrin sodium salt (SBEβCD) [28]. CD form complexes with molecules through inclusion into the CD cavity via van der Waals connections, hydrophobic interactions or hydrogen bonds. This complexation is enhanced when CD and drug have opposite charge and the temperature is low [29,30]. Another type of nanosized vectors are nanospheres (NS), structured with hydrophobic chains forming the inner part of the spheres and hydrophilic portions oriented on the surface. These NanoDDS have homogeneous solid matrices in which the polymer chains arrange in a "frozen" state phase-separated from the bulk solution [31]. Nanospheres allow a fine tuning of their properties through the use of different shell materials such as Poly-lactic acid (PLA), Poly-glycolic acid (PGA), Poly-lactic-co-glycolic acid (PLGA), poly ε-caprolactone (PCL), Chitosan (CS), Polyethylene glycol (PEG) and Eudragit (anionic copolymers based on methacrylic acid and methyl methacrylate). These polymers are widely used for the preparation of NS due to their biocompatibility and biodegradability [32]. Drugs are dissolved, entrapped, encapsulated, chemically bound or adsorbed to the constituent polymer matrix in order to be effectively delivered to the site of action [33]. Nanocapsules (NC) have similar composition but exhibit a core-shell structure in which the drug is confined within a cavity surrounded by a polymer membrane [34]. Nanocapsules can carry the active substance also on their surfaces or imbibed into the layer [35]. The cavity contains the active substances both in liquid or solid form [36]. Solid Lipid nanoparticles (SLNs) are vectors composed of high melting point lipids, as solid core, coated by aqueous surfactants. Examples of core lipids are fatty acids, acylglycerols and waxes, whereas phospholipids, sphingomyelins, bile salts and sterols are utilized as stabilizers [37]. SLNs have high biocompatibility, high bioavailability, physical stability, protection abilities of incorporated labile drugs from degradation, excellent tolerability, prevention of problems related with multiple routes of administration, avoidance of the use of organic solvents during the preparation and absence of problems concerning large scale production and sterilization [38,39]. However, common disadvantages of SLNs are particle growth, unpredictable gelation tendency, uncertain diffusion of the drug within the lipid matrix of the vector and unexpected dynamics of polymorphic transitions [40]. Liposomes (LS) are drug delivery systems that form spontaneously by hydration of lipid powder in aqueous medium produced from cholesterols, non-toxic surfactants, sphingolipids, glycolipids, long chain fatty acids and membrane proteins [41]. Liposomes have particle sizes ranging from 30 nm to several micrometers and consist of one or more lamellaes (phospholipidic bilayer membranes) surrounding aqueous units where the polar head groups are oriented in the pathway of the interior and exterior aqueous phases [42]. Self-aggregation of polar lipids is not limited to conventional bilayer structures, but they may self-assemble into various types of colloidal particles depending on molecular shape, temperature, and dispersion conditions [43]. Micelles (MC) are colloidal dispersions, with particle size ranging between 5 to 100 nm that form spontaneously at certain concentration and temperature values from amphiphilic agents. MC formation is driven by the decrease of free energy in the system because of the removal of hydrophobic fragments from the continuous phase, and the re-establishing of hydrogen bond network in water. Moreover, additional energy results from the formation of Van der Waals bonds between hydrophobic blocks in the core of the formed micelles. Hydrophobic fragments of amphiphilic molecules form the core of micelles, while hydrophilic portions the shells [44]. MC possesses high stability, good biocompatibility, and is able to solubilize a broad variety of poorly soluble pharmaceuticals [45]. Examples of amphiphilic agents used to form MC are Pluronic (Plu), Poly (ethylene glycol) (PEG), Poly (D,L-lactide-co-glycolide) (PLGA) and Polycaprolactone (PCL) [46].

Nanoparticles as Potential Delivery Systems of Polyphenols

Epigallocatechin-3-gallate (EGCG)

Epigallocatechin-3-gallate is a water-soluble flavanol found predominately in green tea leaves (*Camellia sinensis*) (Figure 5) that acts in the prevention of some forms of cancer, cardiovascular diseases, type 2 diabetes mellitus and osteoporosis. Epigallocatechin-3-gallate is highly susceptible to degradation in the intestinal milieu and via oxidative processes. Efforts to promote the intake, enhance the stability, and increase bioavailability of EGCG are directed to incorporate this flavanol into nanosized delivery vectors (Table 2).

Siddiqui et al. [47] reported the encapsulation of EGCG in poly (L-lactide)-poly (ethylene glycol), (PLA-PEG) nanoparticles and assessed its efficacy against human prostate cancer (PC3) cells both *in*

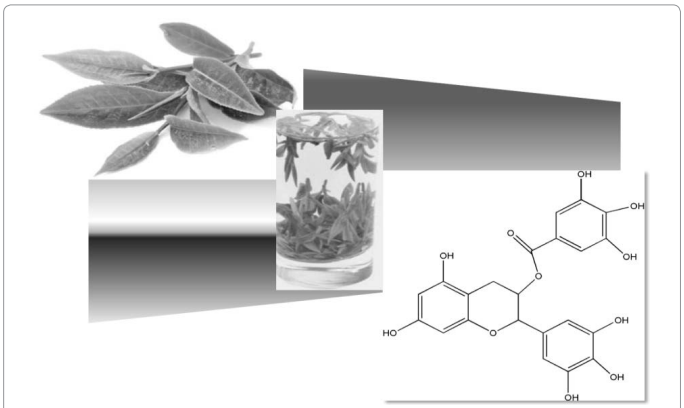

Figure 5: Epigallocatechin-3-gallate (EGCG) structure and natural derivation.

Nanovectors	Type of Delivery Systems	References
Polyester nanoparticles	Poly(L-lactide)-poly(ethylene glycol), (PLA-PEG) nanoparticles	[47]
	PLGA-PEG nanoparticles functionalized with the prostate-specific membrane antigen (PSMA) inhibitor on the surface	[49]
	PLGA biodegradable nanoparticles	[50]
Serum albumin nanoparticles	Bovine serum albumin (BSA) nanoparticles	[48]
Carbohydrate matrix	Carbohydrate matrix composed of maltodextrin (60%) and gum arabic (40%)	[51]
	Gelatin nanoparticles	[52]
	Chitosan nanoparticles	[53,54]

Table 2: Nano delivery systems for epigallocatechin gallate.

vitro and *in vivo*. The results showed that encapsulated EGCG retained its biological effectiveness with an over 10-fold dose advantage form exerting its efficacy in the inhibition of PC3 proliferation. Moreover, PLA-PEG nanoparticles were biocompatible and permitted the control of the time and rate of polymer degradation. Epigallocatechin-3-gallate was also incorporated in bovine serum albumin (BSA) nanoparticles (with a mean particle size of 200 nm) and their effect evaluated against PC3 cells [48]. In this work, PC3 cells lethality was positively correlated with the nanoparticles uptake amount. The specific targeting to prostate cancer cells was obtained also with Poly (lactide-co-glycolide)-Poly(ethylene glycol) (PLGA-PEG) nanoparticles encapsulating EGCG and functionalized with the prostate-specific membrane antigen (PSMA) inhibitor [49]. Other PLGA-based nanovectors for EGCG were synthesized by Italia et al. [50] with a loading efficiency of 70 % and high antioxidant efficiency *in vivo*. These nanoparticles, given by oral administration, acted 3 times more quickly of solutions of free epigallocatechin-3-gallate administered parenterally. A further nanosized delivery systems encapsulating epigallocatechin gallate is constituted by carbohydrate matrix composed of maltodextrin (60%) and gum arabic (40%) with EE of 85% [51]. These particles were able to inhibit steps of the tumorigenesis process. Smith et al. [52] immobilized EGCG on lipid-coated nanoparticles with a bioavailability, after encapsulation, increased twice-fold compared to that of the free form. Epigallocatechin gallate inside the membrane preserved its antioxidant activity and blocked the production of hepatocyte growth factor (HGF) from cancer cell lines MBA-MD-231. On these bases were prepared also gelatin nanoparticles loaded with EGCG with an interesting inhibitory effect on HGF-induced cell scattering [53]. Finally, epigallocatechin-3-gallate was encapsulated into chitosan nanoparticles (sizing 165 nm and exhibiting a zeta potential of 33 mV) by Dube et al. [54] in order to evaluate the ability of chitosan tripolyphosphate nanoparticles to increase EGCG stability and bioavailability. They found that EGCG-chitosan nanoparticles incubated in alkaline solution took more time to degrade to 50% of the initial level, compared to pure epigallocatechin. Moreover, Dube et al. found that chitosan tripolyphosphate EGCG exhibited a 1.8-fold greater absorption rate than the same dose of free EGCG in *ex vivo* mice experiments and that chitosan NP increased the relative oral bioavailability by 1.5-fold compared to the same dose of free EGCG in an *in vivo* absorption experiment on mice [55].

Quercetin (QC)

Quercetin is a semi-lipophilic flavonol ubiquitous in plants (Figure 6). In medicine, dietary supplementation of QC is promoted for prevention and treatment of cancer and this active principle is now largely utilized as a nutritional supplement and as a phytochemical remedy for a variety of diseases like diabetes, obesity, circulatory dysfunction, inflammation and mood disorders. Quercetin has a strong antioxidant activity which potentially enables it to quench free radicals from forming resonance-stabilized phenoxyl radicals but, like most flavonoids, it is extensively transformed via phase II metabolism for elimination from the body [56]. Nanosized vectors encapsulating quercetin were developed to improve its oral bioavailability and to enhance its antioxidant and anti-inflammatory action (Table 3).

Li et al. [57] reported the synthesis of solid lipid nanoparticles of 155 nm of size composed of soya lecithin, Tween-80 and PEG that encapsulate QC, with EE of 91%. These nanoparticles were able to increase the relative oral bioavailability of quercetin by 5.7 fold as compared to the free form. Lipid-coated Nano capsules were reported by Barras et al. [58], with a solubility 100 times higher respect to free quercetin, stable for more than ten weeks and with no degradation product being detected. Wu et al. [59] prepared nanosized QC delivery systems with aminoalkyl methacrylate copolymers sized 82 nm and with encapsulation efficiency of 99%. They resulted in a *in vitro* radical scavenging activity of quercetin nanoparticles toward di(phenyl)-(2,4,6-trinitrophenyl)iminoazanium (DPPH) radicals and superoxide anion enhanced by 883- and 1377- fold as compared to the free form. However, in recent years, an increasing number of works reported the synthesis of PLGA nanoparticles able to encapsulate QC. Indeed, Pool et al. [60] reported that quercetin encapsulated within PLGA displayed a more potent antioxidant action against peroxyl radical-induced lipid peroxidation and a greater capacity for chelating activity toward transient metals than free QC. Ghosh et al. [61] evaluated the antioxidant activity of a single pre-treatment of quercetin encapsulated into PLGA nanoparticles, administered orally to female rats, in the protection against injury from ROS produced in liver and brain tissue subsequent to a subcutaneous injection of arsenite. QC-PLGA nanoparticles provided full protection against the arsenite induced ROS injury, while free quercetin was ineffective. The same group

Nanovectors	Type of Delivery Systems	References
Solid lipid nanoparticles	SLNs composed of soya lecithin, Tween-80 and PEG	[57]
	Lipid-coated nanocapsules	[58]
Acrylic nanoparticles	Aminoalkyl methacrylate copolymers nanoparticles	[59]
Polyester nanoparticles	PLGA nanoparticles	[60-63]
	PLA nanoparticles	[64]
	Eudragit-polyvinilalchool nanoparticles	[59]
Cyclodextrines	2-(hydroxy-propyl)-β-cyclodextrines (HP-β-CD)	[65]

Table 3: Nano delivery systems for Quercetin.

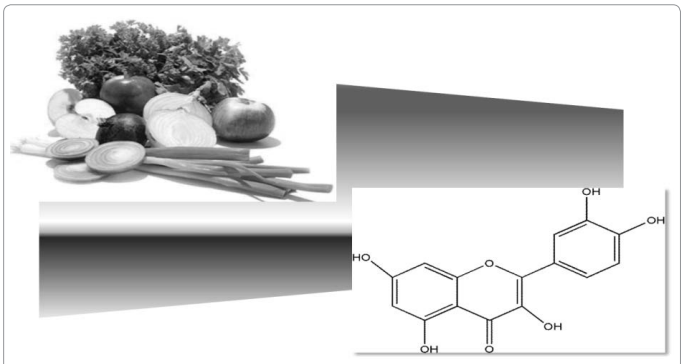

Figure 6: Quercetin structure and natural derivation.

reported a synergy between QC and meso-2,3-dimercaptosuccinic acid (a hydrophilic arsenic chelator), encapsulated together into PLGA nanoparticles, in the protection against arsenic induced damages [62]. In a rat model, Chakraborty et al. [63] examined the potency of a single dose of quercetin-PLGA nanoparticles administered orally prior to alcohol induced gastric ulcer in the protection against oxidative damages, demonstrating that QC-PLGA nanoparticles prevented 90 % of alcohol-induced ulceration as compared to the 20% of the free quercetin. QC encapsulated into PLA nanoparticles had increased antioxidant activity along with a slow and total release after 72 h, useful for potential therapeutic applications [64]. Similarly, Wu et al. [59] synthesized Eudragit-polyvinilalchool quercetin-loaded nanoparticles with particle size of 85 nm, good polydispersity, drug loading of around 99% and enhanced antioxidant activity. Lastly, QC and myricetin in 2-(hydroxy-propyl)-β-cyclodextrines (HP-β-CD) had improved bioavailability [65].

Resveratrol (RE)

Resveratrol, chemically known as 3,5,4'-trihydroxystilbene, is a naturally occurring polyphenol produced by a wide variety of plants in response to injury, UV Irradiation, ozone exposure and fungal attack (Figure 7) [66]. This polyphenol is an antioxidant [67], anti-inflammatory [68], anticancer [69], cell cycle inhibitor [70], anti-aging [68], neuroprotector [71] and cardioprotector [72] agent with application in the treatment of obesity and diabetes [73]. Moreover, it is used to stabilize polyester films for packaging and potential biomedical applications [74]. However, resveratrol has rapid and extensive metabolism [75] that affects its body distribution and bioavailability. Further, there is a significant person-to-person variability in drug absorption and metabolic processes depending on the hepatic function and on the metabolic activity of the local intestinal microflora [76]. To overcome these problems, in the recent years, several nano-drug delivery systems were synthesized (Table 4).

A good example is the liposomal formulation containing RE, with a good encapsulation efficiency of around 70% [77]. PEG-PCL resveratrol nanoparticles had enhanced loading efficiency and higher cytotoxicity to malignant glioma cells, compared with free resveratrol, and a good cellular uptake occurring by endocytosis [78]. Singh and Pai [79] reported sustained release of trans-resveratrol from orally administered PLGA nanoparticles (drug encapsulation efficiency more than 78%, with a particle size of about 170 nm). RE was detected in the rat plasma for up to 4 days with higher concentration in the systemic circulation and in the organs rich in mononuclear phagocyte system. The same authors encapsulated resveratrol in Eudragit RL 100 nanoparticles with a drug incorporation efficiency of 84% and the

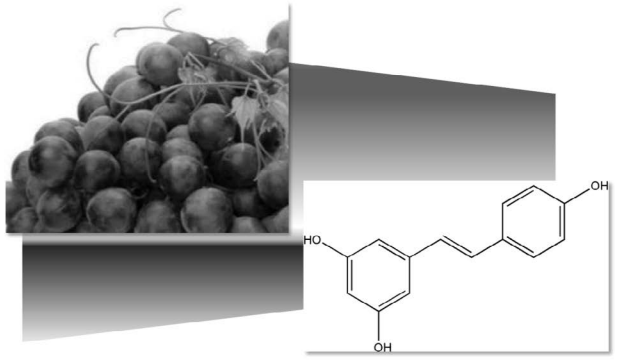

Figure 7: Resveratrol structure and natural derivation.

Nanovectors	Type of Delivery Systems	References
Liposomes	Cholesterol, dicetyl phosphate and lecithin liposomes	[77]
	Soy phosphatidylcholine liposomes	[43]
	Liposomal resveratrol formulation for intravenous administration	[84]
	Proliposomal formulation containing distearoyl phosphatidyl choline (DSPC)	[85]
Polyester nanoparticles	PEG-PCL nanoparticles	[78]
	PLGA nanoparticles	[79]
	Eudragit RL 100 nanoparticles	[80]
Carbohydrate matrix	Carboxymethyl chitosan nanoparticles	[81]
Solid Lipid nanoparticles	Stearic acid and Phospholipon® 90G SLNs	[39]
	Cetyl palmitate and polysorbate 60 SLNs	[40]
	Glyceryl behenate-based solid lipid nanoparticles	[83]
Micelles	PCL-PEG micelles	[86]
Cyclodextrins	Cyclodextrins based nanosponges	[87]

Table 4: Nano delivery systems for Resveratrol.

average size 180 nm. The *in vivo* studies of these vectors, in a rat model, showed that nanoparticles exhibited prolonged plasma levels up to 16 h, maintaining drug levels in the liver, spleen, heart, lungs, kidney and brain up to 24 h in comparison with free drug being cleared within 6 h [80]. Zu et al. [81] reported carboxymethyl chitosan nanoparticles as potential carrier for resveratrol. These nanoparticles (sized 155 nm and showing an encapsulation efficiency of 44%) improved the solubility of resveratrol, thereby greatly affecting the antioxidant activity of the drug. *In vivo* biodistribution study indicated higher body localization of drug loaded carboxymethyl chitosan nanoparticles, in comparison to free resveratrol solution in phosphate buffered saline (PBS) [81]. Additionally, were synthesized resveratrol loaded Solid Lipid nanoparticles with a controlled release profile, due to an initial burst release of 40% caused by the active principle associated with the particle shell, and a subsequent prolonged release of the drug located in the lipid matrix. In this system, the efficiency of the cellular uptake depended on the molecular interactions with the biological membrane organization, lipid rafts and the actin cytoskeleton invaginations for the receptor mediated entrance. Moreover, SLNs were able to carry RE to the nuclear target site [82]. Resveratrol loaded SLNs were also prepared by Pandita et al. [39] with a drug incorporation efficiency of 89% and average diameter of 134 nm. The drug delivery system showed prolonged release *in vitro* up to 120 h in a Wistar rat model, enhancing plasma bioavailability compared to free drug suspension. Other resveratrol-SLNs were produced using Polysorbate 60 as surfactant, with an entrapment efficiency of 70% and the particle size ranged between 150 and 250 nm: the drug release in simulated gastric fluid (SGF) was of 8% at 3 h [40]. Jose et al. [83] checked the brain targeting ability of glyceryl behenate-based solid lipid nanoparticles to utilize the potent anticancer properties of resveratrol. The *in vivo* biodistribution study using Wistar rats demonstrated that these SLNs significantly increased the brain concentration of RE. Moreover, these DDS had lower distribution to other tissues, proving the targeting abilities of this system. Resveratrol loaded soy phosphatidylcholine liposomes were synthesized by Pando et al. [43] to investigate the *ex vivo* percutaneous absorption of RE. Results indicated high cutaneous accumulation and low transdermal delivery of the drug. Moreover, Coimbra et al. [84] designed liposomal resveratrol formulation for

intravenous administration. The encapsulation process gave protection against trans–cis isomerization, with 70% trans-resveratrol still present after 16 min of UV light exposure compared to 10% when resveratrol is exposed in its free form. In addition, *in vivo*, intravenous injection of 5 mg/kg body weight of resveratrol in nude BALB/c female mice with subcutaneous head and neck squamous cell carcinoma led to a significant reduction in tumor volume [84]. Basavaraj et al. [85] produced resveratrol-loaded proliposomal formulation with entrapment efficiency of 20–23% and zeta potential of −22 mV containing distearoyl phosphatidyl choline (DSPC) with or without cholesterol. Faster drug release was observed in formulation without cholesterol and the release increased as the amount of DSPC in the formulation was enhanced. Lu et al. [86] produced resveratrol loaded micelles in which polycaprolactone (PCL) constituted the hydrophobic core and poly (ethylene glycol) (PEG) was the hydrophilic shell of micelles. This system showed a protective effect on adrenal gland PC12 cells against superoxide-induced damage during the phenomenon of oxidative stress. Finally, cyclodextrins-resveratrol complexes were used to increase the concentration of the polyphenol in aqueous solution, while maintaining its biological activity. For example, spherical CD-based nanosponges showed increasing solubility and stability, together with good drug encapsulation efficiency, compared to free RE [87].

Ellagitannin (ET), Ellagic acid (EAC) and Phlorotannins (PHT)

Ellagitannin, Ellagic acid and Phlorotannins are examples of the phenolic class of tannins, widely diffused in plant and marine organisms (Figure 8). In fact, ET and EAC are most present in the pomegranate (*Punica granatum*), a fruit-bearing shrub that originated in the region from Iran to northern India, while phlorotannins are isolated from algae. Ellagitannin and Ellagic acid decrease heart disease risk factors, affect LDL oxidation, macrophage oxidative status, foam cell formation [88,89] provoke the reduction of systolic blood pressure by inhibiting serum angiotensin-converting enzyme [90] and prevent cancer. These tannins show free-radical scavenging properties [91,92] and selectively inhibit the growth of breast, prostate, colon, lung tumors, and skin cancer [93,94]. Similar properties are found in phlorotannins, present in brown algae, formed by the polymerization of phloroglucinol. Specifically, the phlorotannins eckol, phlorofucofuroeckol A, dieckol and 8,8'-bieckol are isolated from the Laminariaceous brown algae *Eisenia bicyclis* (Kjellman) Setchell, *Ecklonia cava* Kjellman and *Ecklonia kurome* Okamura [95]. All these tannins have limited therapeutic applications due to low water solubility, inadequate permeability [96], poor absorption and instability [97]. Nanosized drug delivery systems mask the active substances inside the nanoparticulate network, thus preventing degradation and increasing bioavailability (Table 5).

For example, gelatin nanoparticles incorporating partially purified pomegranate (PPE) ellagitannins showed a good loading efficiency and the capacity of inducing a late stage of apoptosis and necrosis in the human promyelocytic leukemia cells (HL-60) [98]. Similar results were obtained with Chitosan nanoparticles containing ellagic acid [99] and with Ellagic acid-loaded PLGA nanoparticles [100]. In particular, Ellagic acid-Chitosan nanoparticles were spherical shaped with an average particle size of 176 nm, showing a drug-encapsulation and loading-efficiency of 94% and 33%, respectively. The *in vitro* drug release profile in the PBS medium showed sustained release of EAC from chitosan nanoparticles. Further, the therapeutic efficacy of Ellagic acid-Chitosan nanoparticles in human oral cancer cell line (KB) exhibited significant cytotoxicity in KB cells in a dose-dependent manner with a very low IC50 value compared to the free EAC [99]. Ellagic acid-loaded PLGA nanoparticles had a rapid initial release of EAC in pH 7.4 phosphate buffer, followed by a slower sustained release [100]. Further, the authors tested the influence of the stabilizers DMAB and PVA on the size, loading efficacy, release kinetics in PBS, stability, cytotoxic activities and *in situ* intestinal permeability of these nanoparticles [100]. Same study was conducted also on PLGA-PCL ellagic acid nanoparticles [101]. Both resulted on improved tannin bioavailability with potential therapeutic application due to the oral administration of smaller quantity of nanoparticles, compared to the free drug. Shirode et al. [102] synthesized poly (D,L-lactic-*co*-glycolic acid)–poly(ethylene glycol) (PLGA–PEG) nanoparticles, with an average diameter of 150-200 nm, loaded with pomegranate extract or with the individual polyphenol components (e.g. punicalagin or ellagic acid). Synthetized nanoparticles showed a 2- to 12-fold enhanced antiproliferative effect on MCF-7 and Hs578T breast cancer cells compared to free extracts [102]. Similarly, brown algal phlorotannins were encapsulated in lecithin unilamellar vesicles prepared by the extrusion method. These nanovectors maintained their activity on lipid peroxidation inhibition and radical scavenging activities and presented the advantage of the improved stability [95].

Oleuropein (OR) and Hydroxytyrosol (HYT)

Oleuropein and Hydroxytyrosol are phenolic compounds naturally present in olive fruits and leaves (Figure 9) [103]. Indeed, olive leaf extracts are rich in oleuropein, demethyloleuropein, oleuroside, verbascoside, non-glycosidic secoiridoids and ligstrosides as well as several flavonoids and biflavonoids. Also olive oil vegetation water (or olive mill waste water), obtained by centrifugation or sedimentation of the olive oil, contains these organic polyphenols. Such compounds have several pharmacological properties, including antioxidant, anti-inflammatory, anti-atherogenic, anticancer, antimicrobial, antiviral and cardioprotective effects. Oleuropein and hydroxytyrosol exhibit similar free radical-scavenger ability, but with different action mechanisms. *In vitro* studies, in a model system consisting of dipalmitoylphosphatidylcholine/linoleic acid unilamellar vesicles (DPPC/LA LUVs) and a water-soluble azo compound as a free radical generator (LP–LUV test) [104] revealed that hydroxytyrosol can serve

Nanovectors	Type of Delivery Systems	References
Carbohydrate matrix	Gelatin nanoparticles incorporating partially purified pomegranate (PPE) ellagitannins	[98]
	Chitosan nanoparticles	[99]
Polyester nanoparticles	PLGA nanoparticles	[100]
	PLGA-PCL nanoparticles	[101]
	PLGA–PEG nanoparticles	[102]
Liposomes	Lecithin unilamellar vesicles	[95]

Table 5: Nano delivery systems for Tannins.

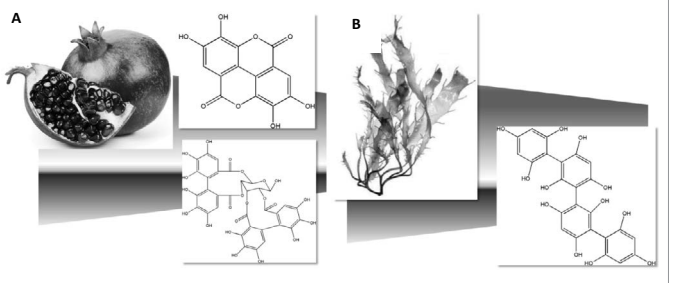

Figure 8: (A) Ellagic acid (up), Ellagitannin (down) and (B) Phlorotannin structures with their natural derivation.

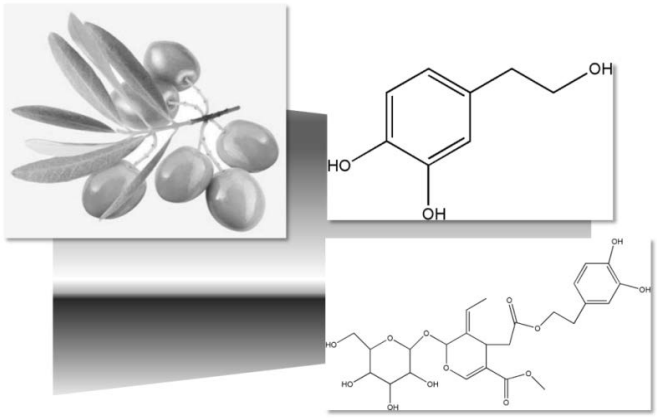

Figure 9: Hydroxytyrosol (up) and Oleuropein (down) structures and natural derivation.

as scavenger of aqueous peroxyl radicals near the membrane surface, while oleuropein acts also as a scavenger of chain-propagating lipid peroxyl radicals within the membranes. The pharmacologic activity of these active principles is enhanced by the use of nanotechnology as reported in Table 6.

Haghighi et al. [105] developed oleuropein-magnetic bovine serum albumin (BSA) nanoparticles with an initial burst and a sustained release. Hussain et al. [106] administered chitosan co-loaded hydrocortisone (HC) and hydroxytyrosol nanoparticles to provide additional anti-inflammatory and antioxidant benefits in the treatment of atopic dermatitis (AD). The co-loaded nanoparticles showed different particle sizes, zeta potentials, loading efficiencies, and morphology, when the pH of the chitosan solution was increased from 3.0 to 7.0. Moreover, they significantly increased the permeation of the drugs and showed higher epidermal and dermal accumulation of HC compared to commercial hydrocortisone formulations. *In vivo* studies resulted in the efficient control of transepidermal water loss, intensity of erythema and dermatitis index [106]. Similarly, a patent by Katas used [107] hydrocortisone and hydroxytyrosol loaded chitosan nanoparticles as local treatment of atopic dermatitis. Such nanovectors gave reduced side effects, increased efficiency of delivery, antibacterial properties and enhanced transepidermal penetration. Moreover, Siddique et al. [108] produced HC-HT co-loaded chitosan nanoparticles (HC–HT CSNPs) of 235 nm in size and with zeta potential +39.2 mV incorporated into aqueous cream (vehicle) to treat atopic dermatitis. This formulation was investigated *in vivo*, in albino Wistar rats, for acute dermal toxicity, dermal irritation and repeated dose toxicity. The results proved that HC–HT CS nanoparticles did not cause neither skin irritation, nor adverse-effect with respect to body weight, organ weight, feed consumption, blood hematological and biochemical, urinalysis, and histopathological parameters, when the HC–HT CS were used for 28 days at a dose of 1000 mg/body surface area per day. This study demonstrated that nanoencapsulation significantly reduced the toxic effects of HC. Qingxia Guan et al. [109] investigated the therapeutic efficiency of monomethoxy polyethylene glycol-poly (lactic co-glycolic acid) (mPEG-PLGA) nanoparticles co-loaded with syringopicroside and hydroxytyrosol prepared using a nanoprecipitation method. In particular, they analyzed the parameters of *in vivo* pharmacokinetics, biodistribution, fluorescence, endomicroscopy and cellular uptake. This vector (92 nm with a narrow polydispersity and a negative zeta potential of -24.5 mV) showed an encapsulation efficiency of ~ 33% and drug loading of 12%, that allows persisting drug plasma concentrations while the nanoparticles moved gradually into the cell, thereby increasing the available quantity. The *in vitro* effect resulted in the liver hepatocellular carcinoma (HepG2.2.15) cells proliferation inhibition [109]. Olive leaf extract containing oleuropein and hydroxytyrosol was encapsulated in β-CD, increasing the water solubility and antioxidant capacity of the encapsulated polyphenols [110]. Similarly, López-García et al. [111] studied the complexation of hydroxytyrosol with β-CD or HP-β-CD. Only β-CD appeared to be very strong photo-protectors of polyphenolic compounds subjected to ultraviolet radiation (λ=254 nm). Finally, Mohammadi et al. showed that water/oil/water emulsion with whey protein concentrate (WPC) and pectin complexes of olive leaf phenolic compounds result in a high stability and controlled release of the encapsulated compounds [112].

Curcumin (CU)

Curcumin is the principal polyphenol of the curcuminoid class of the Indian spice *Curcuma Longa* Linn., a plant typically grown and used in Southeast Asia (Figure 10) [113]. Curcumin lowers cholesterol, reduces platelet aggregation, inhibits the proliferation of cancer cells and improves digestion by increasing the flow of bile from the gallbladder [114]. Moreover, it has immunomodulatory, antiangiogenic and neuroprotective actions, antioxidant and anti-inflammatory abilities and the capacity to modulate the activity of several key transcription factors, cytokines, growth factors, kinases and other enzymes [115]. The activity of CU is correlated with the inhibition of the inducible nuclear factor kappa B (NF-kB) activation, and the suppression of cancer cell proliferation [116]. In addition, the clinical efficacy for rheumatoid arthritis, psoriasis, and postoperative inflammation of Curcumin is due to the reduction of NF-kB, cyclooxygenase 2 (COX2) and proinflammatory cytokines [117]. However, the pharmacological potential of CU is hampered by its low solubility, bioavailability, and stability [118]. In fact, Curcumin is sparingly soluble in water at

Nanovectors	Type of Delivery Systems	References
Serum albumin nanoparticles	Magnetic bovine serum albumin (BSA) nanoparticles	[105]
Carbohydrate matrix	Chitosan nanoparticles	[106]
	Chitosan nanoparticles incorporated into an aqueous cream	[107,108]
Polyester nanoparticles	mPEG-PLGA nanoparticles	[109]
Cyclodextrins	β-CD	[110]
	HP-β-CD	[111]
Micelles	whey protein concentrate (WPC) and pectin complexes	[112]

Table 6: Nano delivery systems for Oleuropein and Hydroxytyrosol.

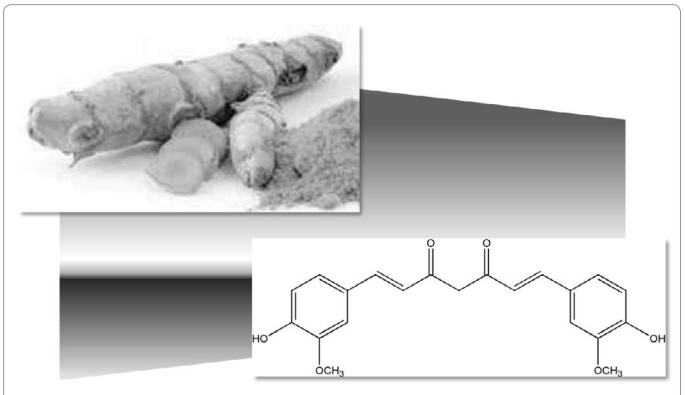

Figure 10: Curcumin structure and natural derivation.

acidic or neutral pH and slightly soluble under alkali conditions. For another CU is unstable in the gut and trace amounts of curcumin that pass through the gastrointestinal tract are rapidly degraded [118]. Nanotechnology permits to enhance the bioavailability of CU through the encapsulation of the drug in the hydrophobic domains of various types of nanovectors (Table 7).

β-Cyclodextrin-curcumin (CD-CUR) nanovectors inhibited telomerase gene expression in breast cancer cells. CD-CUR lowered the gene expression of telomerase more than free curcumin in breast cancer cells (T47D) in a time and dose dependent manner [119]. Similarly, Human Serum Albumin (HSA) possessed two affinity sites for curcumin [120] and literature studies revealed that Curcumin-HSA complexes had greater therapeutic effect than free CU, with no observable toxicity [121]. Self-assembled micelles containing Curcumin spontaneously formed in aqueous phase using Pluronic (Plu), poly(ethylene glycol) (PEG), Poly (D,L-lactide-co-glycolide) (PLGA), or polycaprolactone (PCL) with improved drug stability [44,122]. For example, Chen et al. [44] formulated curcumin in polyethylene glycol (PEG)-derivatized FTS (S-trans, trans-farnesylthiosalicylic acid)-based nanomicellar system. This nanovector had small size of around 20 nm. The nanomicellar curcumin demonstrated enhanced cytotoxicity towards several cancer cell lines *in vitro*. Moreover, intravenous application of curcumin-loaded micelles led to a significantly more effective inhibition of tumor growth in a syngeneic mouse breast cancer model (4T1.2) than free Curcumin. Similarly, Alizadeh et al. [123] synthesized diblock copolymer micelles made of oleoyl chloride and methoxy polyethylene glycol 2000 effective in inhibiting mammary and hepatocellular carcinoma cells proliferation *in vitro*. Moreover, tumor growth in micelles-treated mice was significantly suppressed and/or almost completely stopped at the end of the treatment [123]. Also, polymeric nanoparticles were structurally effective for embedding the water-insoluble curcumin. As the micelles, the most commonly used polymers included polylactic acid, polyglycolic acid, copolymer lactic acid/glycolic acid, polyethylene glycol, chitosan or a blend of these

Nanovectors	Type of Delivery Systems	References
Cyclodextrins	β-Cyclodextrin	[119]
Serum albumin nanoparticles	Human Serum Albumin nanoparticles	[120,121]
Micelles	Polyethylene glycol (PEG)-derivatized FTS (S-*trans*, *trans*-farnesylthiosalicylic acid)-based nanomicellar system	[44]
	Pluronic	[122]
	Diblock Copolymer Micelles made of oleoyl chloride and methoxy polyethylene glycol 2000	[123]
Carbohydrate matrix	Chitosan–starch (BDMCA–CS) nanocomposite	[124]
Polyester nanoparticles	PLGA nanoparticles	[125]
	Poly-(allylamine hydrochloride) (PAH), poly-(sodium 4-styrenesulfonate) (PSS) and chitosan nanocapsules	[126]
Liposomes	Diacyl phosphocholine liposomes	[127,128]
	Flexible liposomes	[129]
Solid Lipid nanoparticles	Dioctyl sodium sulfosuccinate and Poloxamer 188 SLNs	[130]
	Transferrin-mediated solid lipid nanoparticles	[37,38]

Table 7: Nano delivery systems for Curcumin.

[124]. For example, bis-demethoxy curcumin analog loaded Chitosan–starch (BDMCA–CS) nanocomposite particles were developed by Subramanian et al. [125] by ionic gelation method. The entrapment efficiency and drug loading capacity were high and the *in vitro*-drug release showed a slow and sustained diffusion controlled release of the drug. Curcumin loaded PLGA nanoparticles; described by Verderio et al. [126] released intracellularly CU in a time and dose dependent manner at low drug concentration, yielding cell proliferation inhibition by G2/M cell arrest. Poly-(allylamine hydrochloride) (PAH), poly-(sodium 4-styrenesulfonate) (PSS) and chitosan nanocapsules loaded with curcumin were fabricated by Goethals et al. around a solid core/mesoporus (SC/MS) structure. These nanovectors resulted in high cytotoxicity in breast cancer MCF-7 cells due to effective curcumin loading and low particle aggregation [127]. Examples of liposomal delivery systems of CU were Diacyl phosphocholine liposomes and coated or uncoated flexible liposomal systems. Diacyl phosphocholine nanovectors had six molecules of phosphatidylcholine binding one molecule of Curcumin [128]. The drug was inserted into the membrane in a transbilayer orientation, anchored by hydrogen bonding to the phosphate group of phospholipids [129], increasing drug bioavailability. Similarly, Silica-coated flexible liposomes loaded with curcumin (CUR-SLNs) and curcumin-loaded flexible liposomes (CUR-FLs) without silica-coatings had higher bioavailability compared to that of free curcumin suspensions [130]. Other particularly suitable nanocarriers were Solid-lipid nanoparticles: Tiyaboonchai et al. [131] used Dioctyl sodium sulfosuccinate and Poloxamer 188 SLNs in a microemulsion technique to produce drug delivery systems sized less than 450 nm and showing up to 70% incorporation efficiency of curcuminoids. The same type of nanovectors were developed for the treatment of Alzheimer's disease by Kakkar and Kaur [37], and further improved by Mulik et al. [38], demonstrating how transferrin-mediated solid lipid nanoparticles containing curcumin had significant increases in apoptosis, cytotoxicity, ROS, and cellular uptake compared to a curcumin solubilized surfactant solutions and curcumin-loaded solid lipid nanoparticles, in breast cancer.

Conclusion

Polyphenols are among the most powerful active compounds synthesized by plants and marine organisms, and show a unique combination of chemical, biological and physiological activities. However, their limited stability and/or solubility, often combined with a poor bioavailability, have to be resolved in order to make these compounds able to answer growing demands in human health. In this review, the results of recent studies implementing various delivery techniques applied to polyphenolic compounds confirmed that nanoencapsulation is an interesting means to improve their activity. The various reported research revealed that physicochemical nanoencapsulation provided a significant protection against drastic conditions such as oxidation and thermal degradation, thereby contributing to increase the shelf life of the active ingredients. Furthermore, nanoparticles are also able to control the release, change the physical properties of the initial material, and improve the bioavailability of the polyphenolic compound. Future developments must be aimed to complete the characterization of absorption, distribution, metabolism and elimination behavior of nanosized systems carrying the polyphenols in order to potentiate their therapeutic applications.

Acknowledgement

We thank Dr. Orsolina Petillo for editing the manuscript and for administrative assistance. This work was supported by Progetto PON—"Ricerca e Competitività

2007–2013"—PON01_01802: "Sviluppo di molecole capaci di modulare vie metaboliche intracellulari redox-sensibili per la prevenzione e la cura di patologie infettive, tumorali, neurodegenerative e loro delivery mediante piattaforme nano tecnologiche", PON01_02512: "Ricerca e sviluppo di bioregolatori attivi sui meccanismi epigenetici dei processi infiammatori nelle malattie croniche e degenerative", PON03_00106: "Materiali Avanzati per la Ricerca ed il comparto Agroalimentare, Laboratorio Pubblico-Privato, MAReA" and PRIN 2012 (prot. 201288JKYY): "Nanotecnologie per variare i programmi di sviluppo osseo nella parete vasale per la prevenzione e trattamento delle patologie associate alla calcificazione ectopica arteriosa".

References

1. Beckman C (2000) Phenolic-storing cells: Keys to programmed cell death and periderm formation in wilt disease resistance and in general defense responses in plants? Physiological and Molecular Plant Pathology 57: 101-110.
2. Klejdus B, Lojková L, Plaza M, Snóblová M, Stěrbová D (2010) Hyphenated technique for the extraction and determination of isoflavones in algae: ultrasound-assisted supercritical fluid extraction followed by fast chromatography with tandem mass spectrometry. J Chromatogr A 1217: 7956-7965.
3. Liu RH (2003) Health benefits of fruit and vegetables are from additive and synergistic combinations of phytochemicals. Am J Clin Nutr 78: 517S-520S.
4. Pandey KB, Rizvi SI (2009) Plant polyphenols as dietary antioxidants in human health and disease. Oxid Med Cell Longev 2: 270-278.
5. McManus JP, Davis KG, Beart JE, Gaffney SH, Lilley TH, et al. (1985) Polyphenol interactions. Part 1. Introduction; some observations on the reversible complexation of polyphenols with proteins and polysaccharides. J. Chem. Soc Perkin 2: 1429–1438.
6. Perron NR, Brumaghim JL (2009) A review of the antioxidant mechanisms of polyphenol compounds related to iron binding. Cell Biochem Biophys 53: 75-100.
7. Kim HS, Quon MJ, Kim JA (2014) New insights into the mechanisms of polyphenols beyond antioxidant properties; lessons from the green tea polyphenol, epigallocatechin 3-gallate. Redox Biol 2: 187-195.
8. Nijveldt RJ, van Nood E, van Hoorn DE, Boelens PG, van Norren K, et al. (2001) Flavonoids: a review of probable mechanisms of action and potential applications. Am J Clin Nutr 74: 418-425.
9. Fraga CG, Galleano M, Verstraeten SV, Oteiza PI (2010) Basic biochemical mechanisms behind the health benefits of polyphenols. Mol Aspects Med 31: 435-445.
10. Scalbert A, Williamson G (2000) Dietary intake and bioavailability of polyphenols. J Nutr 130: 2073S-85S.
11. D'Archivio M, Filesi C, Varì R, Scazzocchio B, Masella R (2010) Bioavailability of the polyphenols: status and controversies. Int J Mol Sci 11: 1321-1342.
12. Etheridge ML, Campbell SA, Erdman AG, Christy LH, Susan MW, et al. (2013) The big picture on nanomedicine: the state of investigational and approved nanomedicine products. Nanomedicine: Nanotechnology, Biology, and Medicine 9: 1-14.
13. Acosta E (2009) Bioavailability of nanoparticles in nutrient and nutraceutical delivery. Current Opinion in Colloid and Interface Science 14: 3-15.
14. Nair HB, Sung B, Yadav VR, Kannappan R, Chaturvedi MM, et al. (2010) Delivery of antiinflammatory nutraceuticals by nanoparticles for the prevention and treatment of cancer. Biochem Pharmacol 80: 1833-1843.
15. Grotewold E (2005) The Science of Flavonoids, Springer, New York, NY, pp: 274.
16. Milbury PE, Vita JA, Blumberg JB (2010) Anthocyanins are bioavailable in humans following an acute dose of cranberry juice. J Nutr 140: 1099-1104.
17. Bermudez-Soto M, Tomas-Barberan F, Garcia-Conesa M (2007) Stability of polyphenols in chokeberry (Aronia melanocarpa) subjected to *in vitro* gastric and pancreatic digestion. Food Chemistry 102: 865–874.
18. Ader P, Wessmann A, Wolffram S (2000) Bioavailability and metabolism of the flavonol quercetin in the pig. Free Radic Biol Med 28: 1056-1067.
19. Brand W, Padilla B, van Bladeren PJ, Williamson G, Rietjens IM (2010) The effect of co-administered flavonoids on the metabolism of hesperetin and the disposition of its metabolites in Caco-2 cell monolayers. Mol Nutr Food Res 54: 851-860.
20. Lesser S, Cermak R, Wolffram S (2004) Bioavailability of quercetin in pigs is influenced by the dietary fat content. J Nutr 134: 1508-1511.
21. Lam W, Kazi A, Kuhn D, Chow LMC, Chan ASC, et al. (2004) A potential pro-drug for a green tea polyphenol proteasome inhibitor: evaluation of the peracetate ester of (-)epigallocatechin gallate [(-)-EGCG]. Bioorganic and Medicinal Chemistry 12: 5587–5593.
22. Musthaba SM, Baboota S, Ahmed S, Ahuja A, Ali J (2009) Status of novel drug delivery technology for phytotherapeutics. Expert Opin Drug Deliv 6: 625-637.
23. Pinto Reis C, Neufeld RJ, Ribeiro AJ, Veiga F (2006) Nanoencapsulation I. Methods for preparation of drug-loaded polymeric nanoparticles. Nanomedicine 2: 8-21.
24. Wais U, Jackson AW, He T, Zhang H (2016) Nanoformulation and encapsulation approaches for poorly water-soluble drug nanoparticles. Nanoscale 8: 1746-1769.
25. Merisko-Liversidge E, Liversidge GG (2011) Nanosizing for oral and parenteral drug delivery: a perspective on formulating poorly-water soluble compounds using wet media milling technology. Adv Drug Deliv Rev 63: 427-440.
26. Groneberg DA, Giersig M, Welte T, Pison U (2006) Nanoparticle-based diagnosis and therapy. Curr Drug Targets 7: 643-648.
27. Szejtli J (1998) Introduction and General Overview of Cyclodextrin Chemistry. Chem Rev 98: 1743-1754.
28. Eastburn SD, Tao BY (1994) Applications of modified cyclodextrins. Biotechnol Adv 12: 325-339.
29. Stella VJ, He Q (2008) Cyclodextrins. Toxicol Pathol 36: 30-42.
30. Tros de Ilarduya MC, Martín C, Goñi MM, Martínez-Ohárriz MC (1998) Solubilization and interaction of sulindac with beta-cyclodextrin in the solid state and in aqueous solution. Drug Dev Ind Pharm 24: 301-306.
31. Singh A, Garg G, Sharma PK (2010) Nanospheres: A Novel Approach For Targeted Drug Delivery System. International Journal of Pharmaceutical Sciences Review and Research 5: 84-88.
32. Shive MS, Anderson JM (1997) Biodegradation and biocompatibility of PLA and PLGA microspheres. Adv Drug Deliv Rev 28: 5-24.
33. Guterres SS, Alves MP, Pohlmann AR (2007) Polymeric nanoparticles, nanospheres and nanocapsules, for cutaneous applications. Drug Target Insights 2: 147-157.
34. Anton N, Benoit JP, Saulnier P (2008) Design and production of nanoparticles formulated from nano-emulsion templates-a review. J Control Release 128: 185-199.
35. Khoee S, Yaghoobian M (2009) An investigation into the role of surfactants in controlling particle size of polymeric nanocapsules containing penicillin-G in double emulsion. Eur J Med Chem 44: 2392-2399.
36. Radtchenko I, Sukhorukov G, Möhwald H (2002) A novel method for encapsulation of poorly water-soluble drugs: precipitation in polyelectrolyte multilayer shells. Int J Pharm 242: 219-223.
37. Kakkar V, Kaur IP (2011) Evaluating potential of curcumin loaded solid lipid nanoparticles in aluminium induced behavioural, biochemical and histopathological alterations in mice brain. Food Chem Toxicol 49: 2906-2913.
38. Mulik RS, Mönkkönen J, Juvonen RO, Mahadik KR, Paradkar AR (2010) Transferrin mediated solid lipid nanoparticles containing curcumin: enhanced *in vitro* anticancer activity by induction of apoptosis. Int J Pharm 398: 190-203.
39. Pandita D, Kumar S, Poonia N, Lather V (2014) Solid lipid nanoparticles enhance oral bioavailability of resveratrol, a natural polyphenol. Food Research International 62: 1165-1174.
40. Neves AR, Lúcio M, Martins S, Lima JL, Reis S (2013) Novel resveratrol nanodelivery systems based on lipid nanoparticles to enhance its oral bioavailability. Int J Nanomedicine 8: 177-187.
41. Li L, Braiteh FS, Kurzrock R (2005) Liposome-encapsulated curcumin: *in vitro* and *in vivo* effects on proliferation, apoptosis, signaling, and angiogenesis. Cancer 104: 1322-1331.
42. Li L, Ahmed B, Mehta K, Kurzrock R (2007) Liposomal curcumin with and without oxaliplatin: effects on cell growth, apoptosis and angiogenesis in colorectal cancer. Mol Cancer Ther 6: 1276-1282.
43. Pando D, Caddeo C, Manconi M, Fadda AM, Pazos C (2013) Nanodesign of olein vesicles for the topical delivery of the antioxidant resveratrol. J Pharm Pharmacol 65: 1158-1167.
44. Chen Y, Zhang X, Lu J, Huang Y, Li J, et al. (2014) Targeted delivery of curcumin to tumors via PEG-derivatized FTS-based micellar system. AAPS J 16: 600-608.

45. Amit Singh GG, Sharma PK (2010) Nanospheres: A novel approach for targeted drug delivery system. International Journal of Pharmaceutical Sciences Review and Research 5: 84-88.

46. Yow HN, Routh AF (2006) Formation of liquid core–polymer shell microcapsules. Soft Matter 2: 940-949.

47. Siddiqui IA, Adhami VM, Bharali DJ, Hafeez BB, Asim M, et al. (2009) Introducing nanochemoprevention as a novel approach for cancer control: Proof of principle with green tea polyphenol epigallocatechin-3-gallate. Cancer Research 69: 1712-1716.

48. Zu YG, Yuan S, Zhao XH, Zhang Y, Zhang XN, et al. (2009) [Preparation, activity and targeting ability evaluation *in vitro* on folate mediated epigallocatechin-3-gallate albumin nanoparticles]. Yao Xue Xue Bao 44: 525-531.

49. Sanna V, Pintus G, Roggio AM, Punzoni S, Posadino AM, et al. (2011) Targeted biocompatible nanoparticles for the delivery of (-)-epigallocatechin 3-gallate to prostate cancer cells. J Med Chem 54: 1321-1332.

50. Italia JL, Datta P, Ankola DD, Kumar MNVR (2008) Nanoparticles enhance per oral bioavailability of poorly available molecules: Epigallocatechin gallate nanoparticles ameliorates cyclosporine induced nephrotoxicity in rats at three times lower dose than oral solution. Journal of biomedical nanotechnology 4: 304–312.

51. Rocha S, Generalov R, Pereira MDC, Peres I, Juzenas P, et al. (2011) Epigallocatechin gallate-loaded polysaccharide nanoparticles for prostate cancer chemoprevention. Nanomedicine 6: 79–87.

52. Smith A, Giunta B, Bickford PC, Fountain M, Tan J, et al. (2010) Nanolipidic particles improve the bioavailability and a-secretase inducing ability of epigallocatechin-3-gallate (EGCG) for the treatment of Alzheimer's disease. International Journal of Pharmaceutics 389: 207–212.

53. Shutava TG, Balkundi SS, Vangala P, Steffan JJ, Bigelow RL, et al. (2009) Layer-by-Layer-Coated Gelatin Nanoparticles as a Vehicle for Delivery of Natural Polyphenols. ACS Nano 3: 1877-1885.

54. Dube A, Ng K, Nicolazzo J, Larson I (2010) Effective use of reducing agents and nanoparticle encapsulation in stabilizing catechins in alkaline solution. Food Chemistry 122: 662–667.

55. Dube A, Nicolazzo JA, Larson I (2010) Chitosan nanoparticles enhance the intestinal absorption of the green tea catechins (+)-catechin and (-)-epigallocatechin gallate. Eur J Pharm Sci 41: 219-225.

56. D'Andrea G (2015) Quercetin: A flavonol with multifaceted therapeutic applications? Fitoterapia 106: 256-271.

57. Li H, Zhao X, Ma Y, Zhai G, Li L, et al. (2009) Enhancement of gastrointestinal absorption of quercetin by solid lipid nanoparticles. J Control Release 133: 238-244.

58. Barras A, Mezzetti A, Richard A, Lazzaroni S, Roux S, et al. (2009) Formulation and characterization of polyphenol-loaded lipid nanocapsules. Int J Pharm 379: 270-277.

59. Wu TH, Yen FL, Lin LT, Tsai TR, Lin CC, et al. (2008) Preparation, physicochemical characterization, and antioxidant effects of quercetin nanoparticles. Int J Pharm 346: 160-168.

60. Pool H, Quintanar D, de Dios Figueroa J (2012) Antioxidant effects of quercetin and catechin encapsulated into PLGA nanoparticles. Journal of Nanomaterials 1-12.

61. Ghosh A, Mandal AK, Sarkar S, Panda S, Das N (2009) Nanoencapsulation of quercetin enhances its dietary efficacy in combating arsenic-induced oxidative damage in liver and brain of rats. Life Sci 84: 75-80.

62. Ghosh S, Dungdung SR, Chowdhury ST, Mandal AK, Sarkar S, et al. (2011) Encapsulation of the flavonoid quercetin with an arsenic chelator into nanocapsules enables the simultaneous delivery of hydrophobic and hydrophilic drugs with a synergistic effect against chronic arsenic accumulation and oxidative stress. Free Radic Biol Med 51: 1893-1902.

63. Chakraborty S, Stalin S, Das N, Choudhury ST, Ghosh S, et al. (2012) The use of nano-quercetin to arrest mitochondrial damage and MMP-9 upregulation during prevention of gastric inflammation induced by ethanol in rat. Biomaterials 33: 2991-3001.

64. Kumari A, Yadav SK, Pakade YB, Singh B, Yadav SC (2010) Development of biodegradable nanoparticles for delivery of quercetin. Colloids Surf B Biointerfaces 80: 184-192.

65. Mercader-Ros MT, Lucas-Abellán C, Fortea MI, Gabaldón JA, Núñez-Delicado E (2010) Effect of HP-ß-cyclodextrins complexation on the antioxidant activity of flavonols. Food Chemistry 118: 769-773.

66. Goswami SK, Das DK (2009) Resveratrol and chemoprevention. Cancer Lett 284: 1-6.

67. de la Lastra CA, Villegas I (2007) Resveratrol as an antioxidant and pro-oxidant agent: mechanisms and clinical implications. Biochem Soc Trans 35: 1156-1160.

68. de la Lastra CA, Villegas I (2005) Resveratrol as an anti-inflammatory and anti-aging agent: mechanisms and clinical implications. Mol Nutr Food Res 49: 405-430.

69. Ulrich S, Wolter F, Stein JM (2005) Molecular mechanisms of the chemopreventive effects of resveratrol and its analogs in carcinogenesis. Mol Nutr Food Res 49: 452-461.

70. Joe AK, Liu H, Suzui M, Vural ME, Xiao D, et al. (2002) Resveratrol induces growth inhibition, S-phase arrest, apoptosis, and changes in biomarker expression in several human cancer cell lines. Clin Cancer Res 8: 893-903.

71. Bastianetto S, Zheng WH, Quirion R (2000) Neuroprotective abilities of resveratrol and other red wine constituents against nitric oxide-related toxicity in cultured hippocampal neurons. Br J Pharmacol 131: 711-720.

72. Bradamante S, Barenghi L, Villa A (2004) Cardiovascular protective effects of resveratrol. Cardiovasc Drug Rev 22: 169-188.

73. Baur JA, Pearson KJ, Price NL, Jamieson HA, Lerin C, et al. (2006) Resveratrol improves health and survival of mice on a high-calorie diet. Nature 444: 337-342.

74. Agustin-Salazar S, Gamez-Meza N, Medina-Juàrez LA, Soto-Valdez H, Cerruti P (2014) From nutraceutics to materials: effect of resveratrol on the stability of polylactide. ACS Sustainable Chemistry and Engineering 2: 1534–1542.

75. Walle T, Hsieh F, DeLegge MH, Oatis JE Jr, Walle UK (2004) High absorption but very low bioavailability of oral resveratrol in humans. Drug Metab Dispos 32: 1377-1382.

76. Vitaglione P, Sforza S, Galaverna G, Ghidini C, Caporaso N, et al. (2005) Bioavailability of trans-resveratrol from red wine in humans. Mol Nutr Food Res 49: 495-504.

77. Caddeo C, Teskac K, Sinico C, Kristl J (2008) Effect of resveratrol incorporated in liposomes on proliferation and UV-B protection of cells. Int J Pharm 363: 183-191.

78. Junfei Shao XL, Lu X, Jiang C, Hu Y, Li Q, et al. (2009) Enhanced growth inhibition effect of Resveratrol incorporated into biodegradable nanoparticles against glioma cells is mediated by the induction of intracellular reactive oxygen species levels. Colloids and Surfaces B: Biointerfaces 72: 40-47.

79. Singh G, Pai RS (2014) Optimized PLGA nanoparticle platform for orally dosed trans-resveratrol with enhanced bioavailability potential. Expert Opin Drug Deliv 11: 647-659.

80. Singh G, Pai RS (2014) *In-vitro/in-vivo* characterization of trans-resveratrol-loaded nanoparticulate drug delivery system for oral administration. J Pharm Pharmacol 66: 1062-1076.

81. Zu Y, Zhang Y, Wang W, Zhao X, Han X, et al. (2016) Preparation and *in vitro/in vivo* evaluation of resveratrol-loaded carboxymethyl chitosan nanoparticles. Drug Deliv 23: 981-991.

82. Teskac K, Kristl J (2010) The evidence for solid lipid nanoparticles mediated cell uptake of resveratrol. Int J Pharm 390: 61-69.

83. Jose S, Anju SS, Cinu TA, Aleykutty NA, Thomas S, et al. (2014) *In vivo* pharmacokinetics and biodistribution of resveratrol-loaded solid lipid nanoparticles for brain delivery. Int J Pharm 474: 6-13.

84. Coimbra M, Isacchi B, van Bloois L, Torano JS, Ket A, et al. (2011) Improving solubility and chemical stability of natural compounds for medicinal use by incorporation into liposomes. Int J Pharm 416: 433-442.

85. Basavaraj S, Betageri GV (2014) Improved oral delivery of resveratrol using proliposomal formulation: investigation of various factors contributing to prolonged absorption of unmetabolized resveratrol. Expert Opin Drug Deliv 11: 493-503.

86. Lu X, Ji C, Xu H, Li X, Ding H, et al. (2009) Resveratrol-loaded polymeric micelles protect cells from Abeta-induced oxidative stress. Int J Pharm 375: 89-96.

87. Ansari KA, Vavia PR, Trotta F, Cavalli R (2011) Cyclodextrin-based nanosponges for delivery of resveratrol: *in vitro* characterisation, stability, cytotoxicity and permeation study. AAPS PharmSciTech 12: 279-286.

88. Aviram M, Rosenblat M, Gaitini D, Nitecki S, Hoffman A, et al. (2004) Pomegranate juice consumption for 3 years by patients with carotid artery stenosis reduces common carotid intima-media thickness, blood pressure and LDL oxidation. Clin Nutr 23: 423-433.

89. Esmaillzadeh A, Tahbaz F, Gaieni I, Alavi-Majd H, Azadbakht L (2004) Concentrated pomegranate juice improves lipid profiles in diabetic patients with hyperlipidemia. J Med Food 7: 305-308.

90. Aviram M, Dornfeld L (2001) Pomegranate juice consumption inhibits serum angiotensin converting enzyme activity and reduces systolic blood pressure. Atherosclerosis 158: 195-198.

91. Kulkarni AP, Mahal HS, Kapoor S, Aradhya SM (2007) In vitro studies on the binding, antioxidant and cytotoxic actions of punicalagin. J Agric Food Chem 55: 1491-1500.

92. Mertens-Talcott SU, Jilma-Stohlawetz P, Rios J, Hingorani L, Derendorf H (2006) Absorption, metabolism, and antioxidant effects of pomegranate (*Punica granatum* l.) polyphenols after ingestion of a standardized extract in healthy human volunteers. J Agric Food Chem 54: 8956-8961.

93. Kim ND, Mehta R, Yu W, Neeman I, Livney T, et al. (2002) Chemopreventive and adjuvant therapeutic potential of pomegranate (*Punica granatum*) for human breast cancer. Breast Cancer Res Treat 71: 203-217.

94. Albrecht M, Jiang W, Kumi-Diaka J, Lansky EP, Gommersall LM, et al. (2004) Pomegranate extracts potently suppress proliferation, xenograft growth, and invasion of human prostate cancer cells. J Med Food 7: 274-283.

95. Shibata T, Ishimaru K, Kawaguchi S, Yoshikawa H, Hama Y (2008) Antioxidant activities of phlorotannins isolated from Japanese Laminariaceae. Journal of Applied Phycology 20: 705-711.

96. Bala I, Bhardwaj V, Hariharan S, Kumar MN (2006) Analytical methods for assay of ellagic acid and its solubility studies. J Pharm Biomed Anal 40: 206-210.

97. Lei F, Xing DM, Xiang L, Zhao YN, Wang W, et al. (2003) Pharmacokinetic study of ellagic acid in rat after oral administration of pomegranate leaf extract. J Chromatogr B Analyt Technol Biomed Life Sci 796: 189-194.

98. Li Z, Percival SS, Bonard S, Gu L (2011) Fabrication of nanoparticles using partially purified pomegranate ellagitannins and gelatin and their apoptotic effects. Mol Nutr Food Res 55: 1096-1103.

99. Arulmozhi V, Pandian K, Mirunalini S (2013) Ellagic acid encapsulated chitosan nanoparticles for drug delivery system in human oral cancer cell line (KB). Colloids Surf B Biointerfaces 110: 313-320.

100. Bala I, Bhardwaj V, Hariharan S, Kharade SV, Roy N, et al. (2006) Sustained release nanoparticulate formulation containing antioxidant-ellagic acid as potential prophylaxis system for oral administration. J Drug Target 14: 27-34.

101. Sonaje K, Italia JL, Sharma G, Bhardwaj V, Tikoo K, et al. (2007) Development of biodegradable nanoparticles for oral delivery of ellagic acid and evaluation of their antioxidant efficacy against cyclosporine A-induced nephrotoxicity in rats. Pharm Res 24: 899-908.

102. Shirode AB, Bharali DJ, Nallanthighal S, Coon JK, Mousa SA, et al. (2015) Nanoencapsulation of pomegranate bioactive compounds for breast cancer chemoprevention. Int J Nanomedicine 10: 475-484.

103. D'Andria R, Di Salle A, Petillo O, Sorrentino G, Peluso G (2013) Nutraceutical, cosmetic, health products derived from olive. Present and future of the Mediterranean olive sector. Options méditerranéennes SERIES A: Mediterranean Seminars, CIHEAM.

104. Saija A, Trombetta D, Tomaino A, Lo Cascio R, Princi P, et al. (1998) *In vitro* evaluation of the antioxidant activity and biomembrane interaction of the plant phenols oleuropein and hydroxytyrosol. International Journal of Pharmaceutics 166: 123-133.

105. Haghighi SM, Ebrahimpourmoghaddam S, Purkhosrow A, Mohammadi S, Nekooein AA, et al. (2012) Magnetic Bovine Serum Albumin-based nanoparticles as potential controlled release drug delivery systems. Proceedings of the 4th International Conference on Nanostructures (ICNS4), Kish Island, I.R. Iran.

106. Hussain Z, Katas H, Amin MCI, Kumolosasi E, Buang F, et al. (2013) Self-assembled polymeric nanoparticles for percutaneous co-delivery of hydrocortisone/hydroxytyrosol: An *ex vivo* and *in vivo* study using an NC/Nga mouse model. International Journal of Pharmaceutics 444: 109–119.

107. Katas H, Amin MCI, Sahudin S, Buang F (2013) Chitosan-based skin-targeted nanoparticle drug delivery system and method.

108. Siddique MI, Katas S, Amin MCI, Ng SF, Zulfakar MH, et al. (2015) Minimization of Local and Systemic Adverse Effects of Topical Glucocorticoids by Nanoencapsulation: *In Vivo* Safety of Hydrocortisone–Hydroxytyrosol Loaded Chitosan Nanoparticles. Journal of Pharmaceutical Sciences 104: 4276-4286.

109. Guan Q, Sun S, Li X, Lv S, Xu T, et al. (2016) Preparation, *in vitro* and *in vivo* evaluation of mPEG-PLGA nanoparticles co-loaded with syringopicroside and hydroxytyrosol. J Mater Sci Mater Med 27: 24.

110. Mourtzinos I, Salta F, Yannakopoulou K, Chiou A, Karathanos VT (2007) Encapsulation of olive leaf extract in beta-cyclodextrin. J Agric Food Chem 55: 8088-8094.

111. López-García MA, López O, Maya I, Fernández-Bolaños JG (2010) Complexation of hydroxytyrosol with ß-cyclodextrins. An efficient photoprotection. Tetrahedron 66: 8006–8011.

112. Mohammadi A, Jafari SM, Assadpour E, Faridi Esfanjani A (2016) Nano-encapsulation of olive leaf phenolic compounds through WPC-pectin complexes and evaluating their release rate. Int J Biol Macromol 82: 816-822.

113. Yadav VR, Aggarwal BB (2011) Curcumin: a component of the golden spice, targets multiple angiogenic pathways. Cancer Biol Ther 11: 236-241.

114. Rasyid A, Rahman AR, Jaalam K, Lelo A (2002) Effect of different curcumin dosages on human gall bladder. Asia Pac J Clin Nutr 11: 314-318.

115. Menon VP, Sudheer AR (2007) Antioxidant and anti-inflammatory properties of curcumin. Adv Exp Med Biol 595: 105-125.

116. Bhattacharyya S, Mandal D, Sen GS, Pal S, Banerjee S, et al. (2007) Tumor-induced oxidative stress perturbs nuclear factor-kappaB activity-augmenting tumor necrosis factor-alpha-mediated T-cell death: protection by curcumin. Cancer Res 67: 362-370.

117. Jurenka JS (2009) Anti-inflammatory properties of curcumin, a major constituent of *Curcuma longa*: a review of preclinical and clinical research. Alternative Medicine Review 14: 141-153.

118. Anand P, Kunnumakkara AB, Newman RA, Aggarwal BB (2007) Bioavailability of curcumin: problems and promises. Mol Pharm 4: 807-818.

119. Kazemi-Lomedasht F, Rami A, Zarghami N (2013) Comparison of inhibitory effect of curcumin nanoparticles and free curcumin in human telomerase reverse transcriptase gene expression in breast cancer. Adv Pharm Bull 3: 127-130.

120. Pulla Reddy AC, Sudharshan E, Appu Rao AG, Lokesh BR (1999) Interaction of curcumin with human serum albumin--a spectroscopic study. Lipids 34: 1025-1029.

121. Kim TH, Jiang HH, Youn YS, Park CW, Tak KK, et al. (2011) Preparation and characterization of water-soluble albumin-bound curcumin nanoparticles with improved antitumor activity. Int J Pharm 403: 285-291.

122. Sahu A, Kasoju N, Goswami P, Bora U (2011) Encapsulation of curcumin in Pluronic block copolymer micelles for drug delivery applications. J Biomater Appl 25: 619-639.

123. Alizadeh AM, Sadeghizadeh M, Najafi F, Ardestani SK, Erfani-Moghadam V, et al. (2015) Encapsulation of curcumin in diblock copolymer micelles for cancer therapy. Biomed Res Int 2015: 824746.

124. Mayol L, Serri C, Menale C, Crispi S, Piccolo MT, et al. (2015) Curcumin loaded PLGA-poloxamer blend nanoparticles induce cell cycle arrest in mesothelioma cells. Eur J Pharm Biopharm 93: 37-45.

125. Subramanian SB, Francis AP, Devasena T (2014) Chitosan-starch nanocomposite particles as a drug carrier for the delivery of bis-desmethoxy curcumin analog. Carbohydr Polym 114: 170-178.

126. Verderio P, Bonetti P, Colombo M, Pandolfi L, Prosperi D (2013) Intracellular drug release from curcumin-loaded PLGA nanoparticles induces G2/M block in breast cancer cells. Biomacromolecules 14: 672-682.

127. Goethals EC, Shukla R, Mistry V, Bhargava SK, Bansal V (2013) Role of the templating approach in influencing the suitability of polymeric nanocapsules for drug delivery: LbL *vs.* SC/MS. Langmuir. 29: 12212–12219.

128. Began G, Sudharshan E, Udaya Sankar K, Appu Rao AG (1999) Interaction of curcumin with phosphatidylcholine: A spectrofluorometric study. Journal of agricultural and food chemistry 47: 4992-4997.

129. Barry J, Fritz M, Brender JR, Smith PE, Lee DK, et al. (2009) Determining the effects of lipophilic drugs on membrane structure by solid-state NMR spectroscopy: the case of the antioxidant curcumin. Journal of the American Chemical Society 131: 4490-4498.

130. Li C, Zhang Y, Su T, Feng L, Long Y, et al. (2012) Silica-coated flexible liposomes as a nanohybrid delivery system for enhanced oral bioavailability of curcumin. International Journal of Nanomedicine 7: 5995-6002.

131. Tiyaboonchai W, Tungpradit W, Plianbangchang P (2007) Formulation and characterization of curcuminoids loaded solid lipid nanoparticles. International Journal of Pharmaceutics 337: 299-306.

Citation: Conte R, Calarco A, Napoletano A, Valentino A, Margarucci S, et al. (2016) Polyphenols Nanoencapsulation for Therapeutic Applications. J Biomol Res Ther 5: 139. doi:10.4172/2167-7956.1000139

cancer biology & therapy

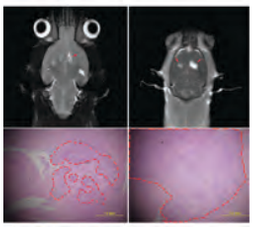

Cancer Biology & Therapy

ISSN: 1538-4047 (Print) 1555-8576 (Online) Journal homepage: http://www.tandfonline.com/loi/kcbt20

c-Myc modulation: a key role in melanoma drug response

Annalisa Fico, Daniela Alfano, Anna Valentino, Valeria Vasta, Ernesta Cavalcanti, Salvatore Travali, Eduardo J Patriarca & Emilia Caputo

To cite this article: Annalisa Fico, Daniela Alfano, Anna Valentino, Valeria Vasta, Ernesta Cavalcanti, Salvatore Travali, Eduardo J Patriarca & Emilia Caputo (2015) c-Myc modulation: a key role in melanoma drug response, Cancer Biology & Therapy, 16:9, 1375-1386, DOI: 10.1080/15384047.2015.1030546

To link to this article: http://dx.doi.org/10.1080/15384047.2015.1030546

RESEARCH PAPER

Cancer Biology & Therapy 16:9, 1375–1386; September 2015; © 2015 Taylor and Francis Group, LLC

c-Myc modulation: a key role in melanoma drug response

Annalisa Fico[1,#], Daniela Alfano[1,#], Anna Valentino[1], Valeria Vasta[2], Ernesta Cavalcanti[3], Salvatore Travali[2], Eduardo J Patriarca[1], and Emilia Caputo[1,2,*]

[1]Institute of Genetics and Biophysics; A Buzzati-Traverso; Naples, Italy; [2]Università degli Studi di Catania; Dipartimento di Scienze Bio-Mediche; Catania, Italy; [3]Istituto Nazionale Tumori Fondazione G Pascale; Naples, Italy

[#]These authors equally contributed to this work.

Keywords: B-RAF mutations, cancer therapy, chemotherapy, c-myc modulation, melanoma drug resistance, PP2A activity

Abbreviations: NSAIDs, Non-Steroidal Anti-Inflammatory Drugs; H_2O_2, Hydrogen Peroxide; OA, Okadaic Acid; PP2A, serine/threonine-protein phosphatase 2A 65 kDa regulatory subunit A α isoform

Understanding molecular mechanisms involved in melanoma resistance to drugs is a big challenge. Experimental evidences suggested a correlation between mutational status in B-RAF and melanoma cell susceptibility to drugs, such as paclitaxel, doxorubicin and temozolomide, which generate an accumulation of hydrogen peroxide (H_2O_2) in the cells. We investigated the survival phenotype and the protein level of c-myc, a B-RAF target molecule, in melanoma cells, carrying a different mutational status in B-RAF, upon paclitaxel, doxorubicin and H_2O_2 treatment. For the first time, we reported c-myc modulation is critical for melanoma drug response. It appeared drug-specific and post-transcriptionally driven through PP2A; in correlation, cell pre-treatment with okadaic acid (OA), a specific PP2A inhibitor, as well as PP2A silencing of melanoma cells, was able to increase melanoma cell drug-sensitivity and c-myc protein level. This is relevant for designing efficacious therapeutic strategies in melanoma.

Introduction

Melanoma is the most aggressive form of skin cancer,[1] and metastatic melanomas are usually resistant to current therapies, with a median survival rate of 6 months.[2] The modest antitumor activity of the single chemotherapeutic agents led to the investigation of combinations of these agents to improve outcomes in melanoma patients.[3,4] Cancer cells, however, differ in their susceptibility to chemotherapy, and a detailed understanding of the molecular mechanisms associated with the resistance to chemotherapy is critical for development of efficient therapeutic strategies.

Previous experimental evidences suggested a correlation between the mutational status in B-RAF and the melanoma susceptibility to chemotherapeutic drugs,[5] such as paclitaxel and doxorubicin [6-18], which are able to generate an accumulation of hydrogen peroxide (H_2O_2) in the cells. In particular, melanoma cell lines wild-type in B-RAF (SK23Mel, WM266Mel) have been reported more resistant to paclitaxel and doxorubicin[5] compared to the ones mutated in B-RAF (A375, SKMel 13, SKMel19, M14).

Here, we analyzed the molecules associated to the different behavior of 3 different melanoma cell lines, known as A375, 526 and SK23Mel upon their exposure to paclitaxel[3,4] doxorubicin and temozolomide. These cell lines were derived from patients with metastatic melanoma, but they were different in the B-RAF mutational status.[19,20] As previously reported, the single nucleotide mutation resulting in substitution of glutamic acid for valine (BRAFV600E: nucleotide 1799 T>A; codon GTG>GAG) in B-RAF is one among the most representative BRAF mutations observed in melanoma.[21,22] We used B-RAF mutated in homozygous (i.e. A375 cell line), B-RAF mutated in heterozygous (i.e., 526 cell line) and B-RAF wild-type melanoma cells (i.e. SK23Mel cell line).

In order to investigate the molecules involved in the different drug susceptibility, we examined c-myc protein level at different drug exposure times, since this is involved in the RAS-RAF-MEK-ERK protein kinase pathway. We examined the functional role of c-myc in the different susceptibility observed to drug exposure of all 3 melanoma cell lines and successively we expanded the study to more melanoma cell lines.

Results

A375, 526 and SK23Mel cell survival after exposure to paclitaxel, H_2O_2 and doxorubicin

Here, we investigated the behavior of A375 melanoma cell line, carrying a homozygous V600E mutation in B-RAF, after

*Correspondence to: Emilia Caputo; Email: emilia.caputo@igb.cnr.it
Submitted: 12/15/2014; Revised: 02/18/2015; Accepted: 03/08/2015
http://dx.doi.org/10.1080/15384047.2015.1030546

exposure to paclitaxel and we compared it to the one observed in 526 with a B-RAF V600E mutation in heterozygous and in SK23Mel cells, wild-type in B-RAF (Table S1 in *Supplementary Data*). To this end, all 3 cell lines were treated with paclitaxel at different concentrations for 24 hours and survival cell percentage was measured, as described in Materials and Methods. As shown in **Fig. 1A and S**, we found a cell survival percentage value of 35%, 56%, and 60% in A375, 526 and in SK23-Mel cells, respectively, upon a treatment with 45 nM paclitaxel for 24 hours.

It has been reported that hydrogen peroxide (H_2O_2) plays an important role in drug-induced cancer cell death[6,7,9,10] and that, H_2O_2 is accumulated in the cells following treatment with paclitaxel drug.[7] Here, we investigated the behavior of A375, 526 and SK23Mel melanoma cells line, after exposure to H_2O_2. As shown in **Fig. 1B and 1S**, we found a A375 cell survival percentage value of about 41% upon a treatment with 0.5 mM H_2O_2 for 24 hours *vs*. 526 and SK23Mel cell survival percentage value of about 68 and 71%, respectively, upon same treatment conditions. This finding suggested that A375 were more sensitive than 526 and SK23Mel melanoma cells to H_2O_2 treatment.

Since doxorubicin has been reported as another drug able to generate an accumulation of H_2O_2 in the cells,[9] we analyzed the A375, 526 and SK23Mel cell survival phenotype upon exposure to this chemotherapeutic agent. We measured a A375 lower survival cell percentage compared to the 526 and SK23Mel ones upon doxorubicin treatment (**Fig. 1C, 1S**), comparable to the one observed after H_2O_2 exposure (A375 survival percentage value of about 27% *versus* 53% and 58% of 526 and SK23Mel survival percentage value, respectively at doxorubicin concentration of 2.5μM for 24 hours). All together these data supported a strict correlation between B-RAF mutational status and susceptibility to chemotherapeutic drugs.

c-Myc analysis in melanoma cells after H_2O_2 exposure

In order to investigate the molecular mechanisms underlining the different melanoma cell line sensitivity to drugs, we examined the level of c-myc protein in all melanoma cell lines upon H_2O_2 treatment, since it is one of the target molecules in the RAS-RAF-MEK-ERK protein kinase pathway. We observed that while c-myc protein was up-regulated in A375 cells upon H_2O_2

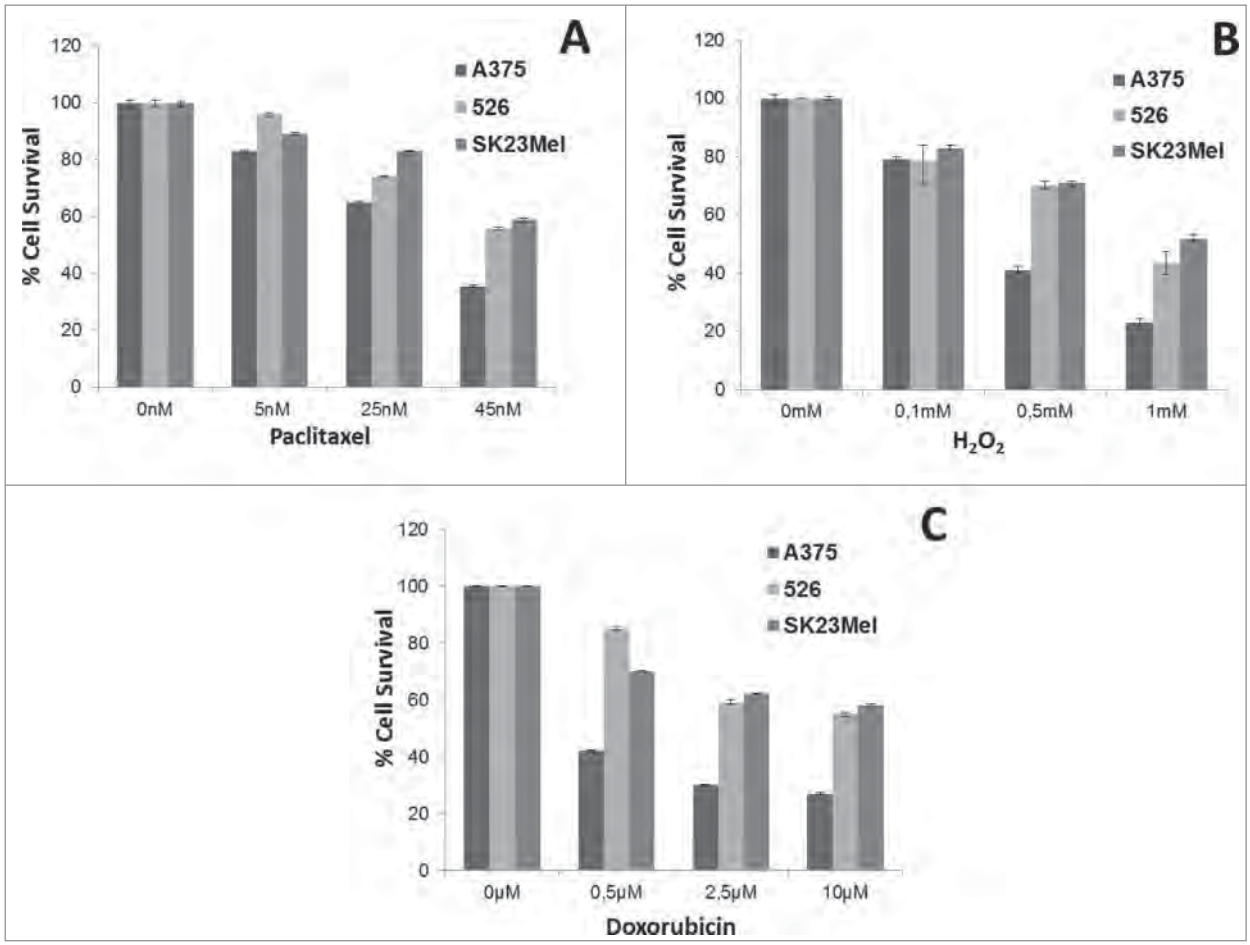

Figure 1. ell viability analysis of A375, 526 and SK23Mel melanoma cells upon paclitaxel (**A**), H_2O_2 (**B**) and doxorubicin (**C**) exposure at 24 hours with different indicated drug concentrations. Results represent the means (percentage values) of 3 independent experiments performed in triplicate. The error bars show 95% confidence intervals.

exposure, it was found down-regulated in 526 and it was stable in SK23Mel cells (**Fig. 2**). The same pattern of c-myc expression was observed upon paclitaxel and doxorubicin treatment in all cell lines examined (data not shown). This finding suggested that the c-myc regulation could play an important role in the sensitivity of these cells to the tested drugs.

To gain insight into the functional role of c-myc in the different susceptibility observed in these melanoma cells to H_2O_2 and drugs exposure, c-myc expression was either enhanced and or silenced by pDNA4-to/Myc/IRES and by means of small interfering RNA technology (siRNA), respectively as described in Materials and Methods. Then, we examined the c-myc

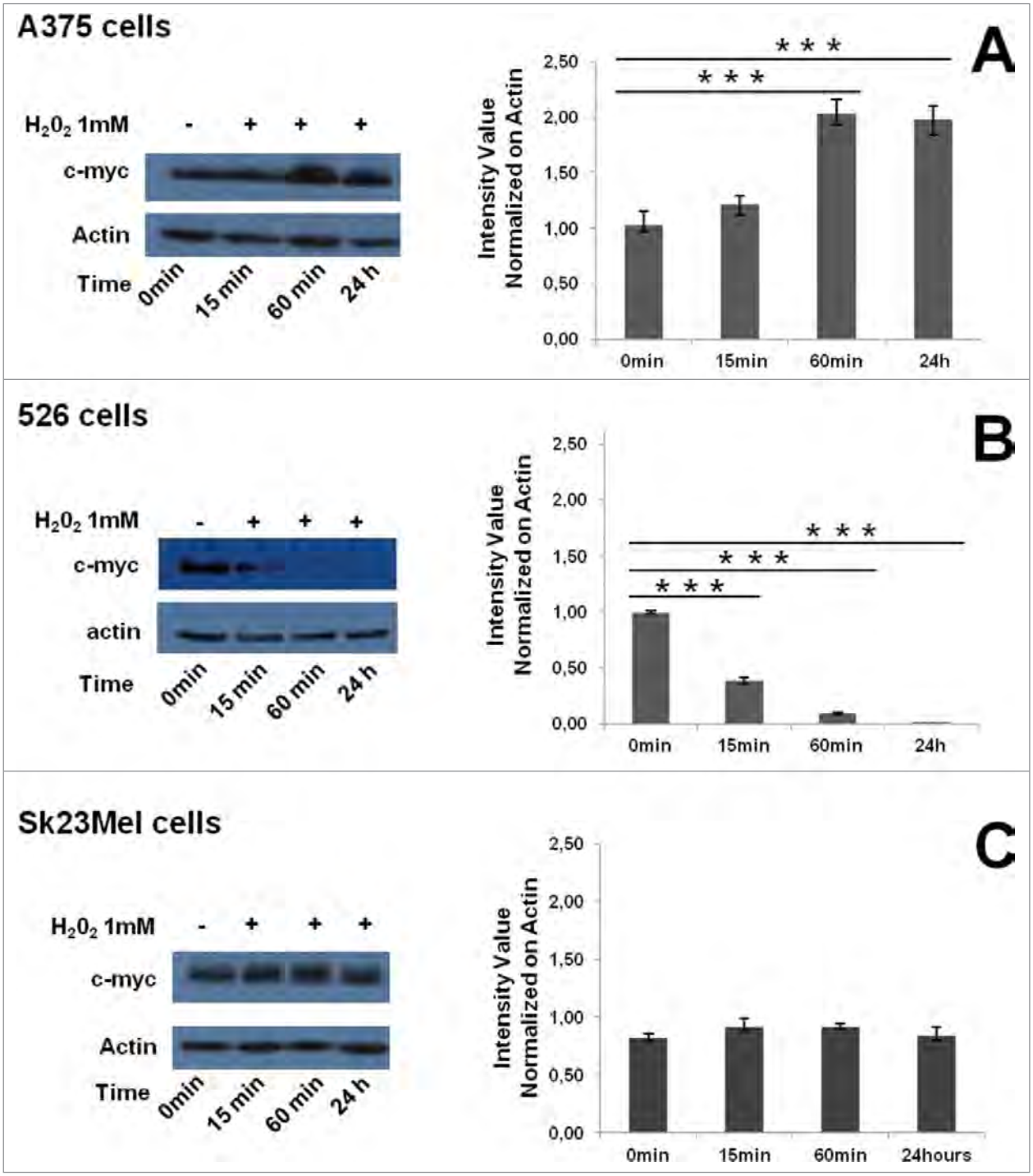

Figure 2. Western blot analysis of c-myc in A375 (**A**), 526 (**B**) and SK23Mel (**C**) melanoma cells upon H_2O_2 treatment (1 mM) at 15, 60 minutes and 24 hours. Actin was used as a loading control. The intensity of protein expression was quantified by scanning densitometry. Results represent the means (± s.e.m.) of 3 independent experiments performed in triplicate. P-value was determined by using t-test and value ≤0,001 was indicated (***).

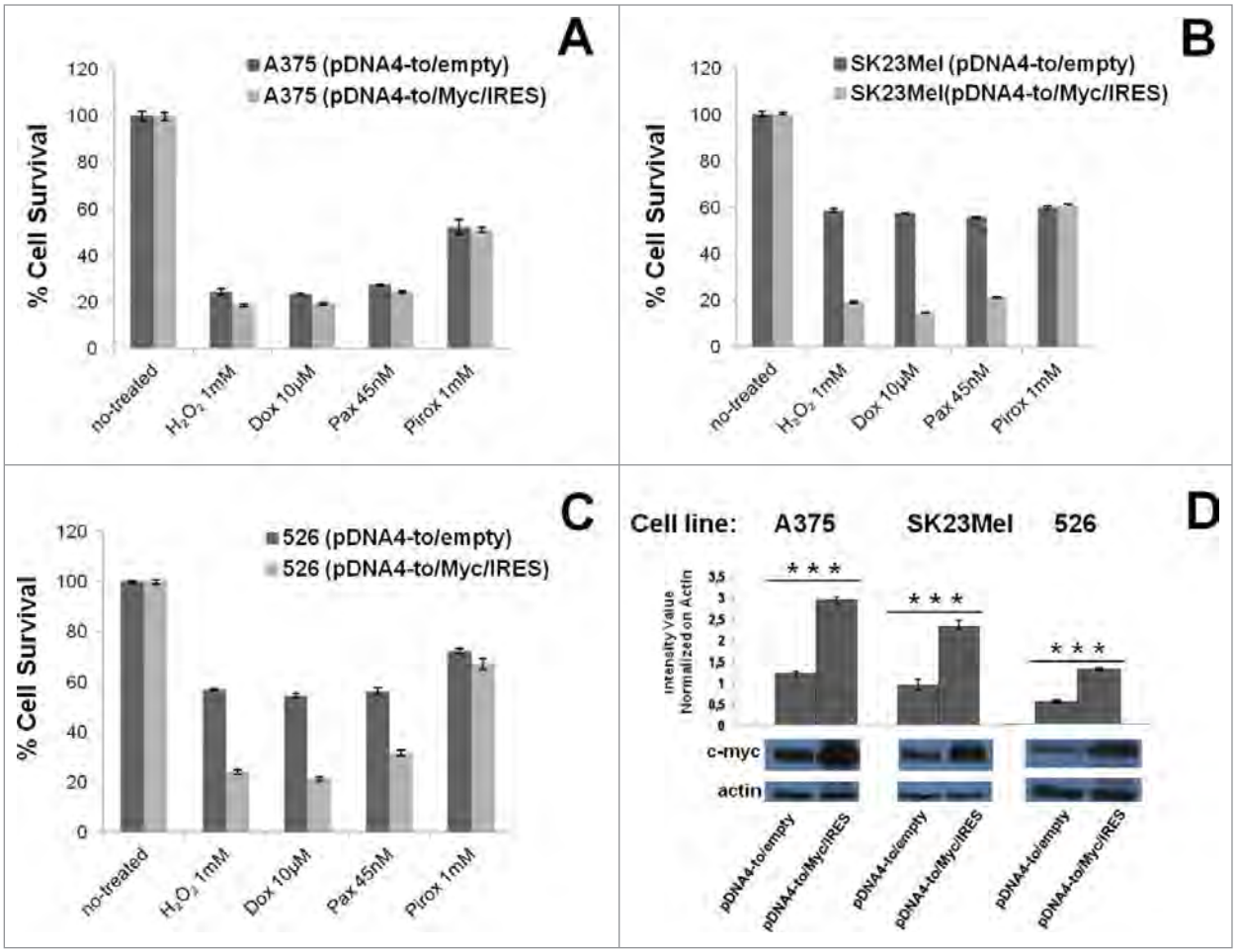

Figure 3. Cell viability analysis of A375 (**A**), SK23Mel (**B**) and 526 (**C**) melanoma cells, previously c-myc enhanced and then subjected to H_2O_2, doxorubicin (Dox), paclitaxel (Pax) and piroxicam (Pirox) treatment. Results represent the means (± s.e.m.) of 3 independent experiments performed in triplicate. Cell survival percentage value was also reported. c-myc expression levels were examined by western blot (**D**). Actin was used as a loading control. The intensity of protein expression was quantified by scanning densitometry. Results represent the means (± s.e.m.) of 3 independent experiments performed in triplicate. P-value was determined by using t-test and value ≤0,001 was indicated (***).

enhancing and silencing effects on the cell survival upon paclitaxel, doxorubicin and H_2O_2 exposure. The enhancing of c-myc protein in A375 cells decreased furthermore their survival phenotype percentage, when the cells were treated with the various chemotherapeutic agents (**Fig. 3A**). The same effect was more pronounced in SK23Mel cells (**Fig. 3B**) and in 526 cells (**Fig. 3C**). Enhancing was confirmed analyzing c-myc protein levels by western blot as shown in **Figure 3D**. Conversely, the c-myc silencing induced a major survival of A375 cells (**Fig. 4A**). The same was observed for SK23Mel and 526 melanoma cells, although at lower levels (**Fig. 4B, C**). Silencing was confirmed analyzing c-myc protein levels by western blot, as shown in **Figure 4D**. This finding supported the idea that c-myc is a key player in the different survival phenotype of A375 compared to the 526 and SK23Mel melanoma cells upon H_2O_2, paclitaxel and doxorubicin exposure. The effect appeared to be H_2O_2 specific, since the different level of expression of c-myc did not affect the survival phenotype of all cell lines after treatment with piroxicam, a non-steroidal anti-inflammatory drug (NSAIDs) with anti-neoplastic effects,[23,24] which does not trigger H_2O_2 accumulation.

Modulation of c-myc in melanoma cells upon H_2O_2, paclitaxel and doxorubicin exposure

In order to investigate if the different c-myc protein levels found in the cells upon H_2O_2 and drug exposure were resulting from the different transcript levels, we examined the level of c-myc mRNA in all melanoma cell lines after exposure to H_2O_2, paclitaxel and doxorubicin. We observed an increase of c-myc mRNA levels in 526 and SK23Mel cell lines upon the 3 different treatments, while it was found similar between untreated and treated A375 cells (**Fig. 5**), suggesting that c-myc modulation was not transcriptionally driven.

Furthermore, we investigated if c-myc modulation was PP2A dependent. It has been reported that PP2A is a protein

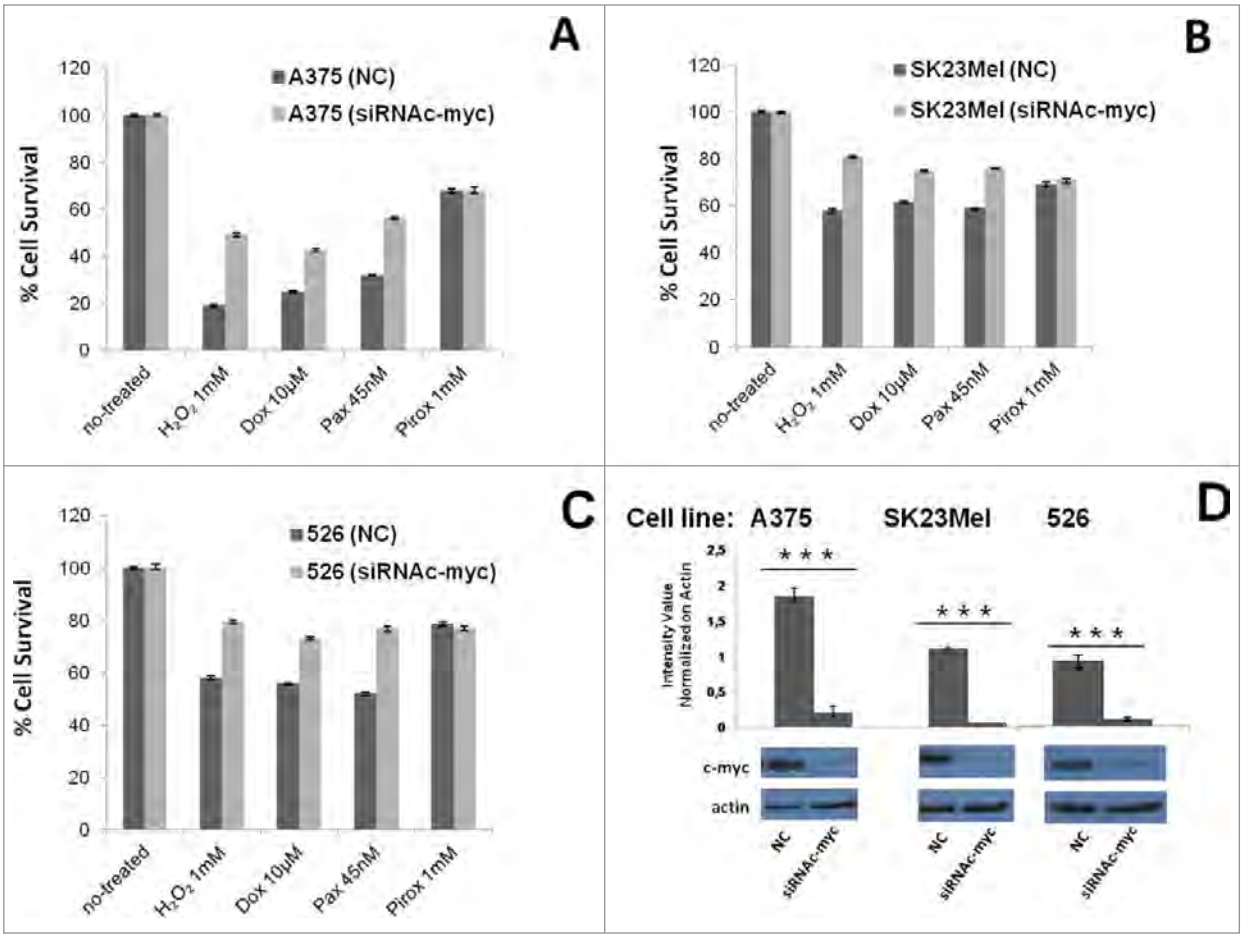

Figure 4. Cell viability analysis of A375 (**A**), SK23Mel (**B**) and 526 (**C**) melanoma cells, previously c-myc silenced and then subjected to H_2O_2, doxorubicin, paclitaxel and piroxicam treatment. Results represent the means (± s.e.m.) of 3 independent experiments performed in triplicate. Cell survival percentage value was also reported. c-myc expression levels were examined by western blot (**D**). Actin was used as a loading control. The intensity of protein expression was quantified by scanning densitometry. Results represent the means (± s.e.m.) of 3 independent experiments performed in triplicate. P-value was determined by using t-test and value ≤0,001 was indicated (***). NC indicated negative control as described in Materials and Methods.

phosphatase 2A (PP2A) that plays a prominent role in controlling accumulation of the proto-oncoprotein c-Myc. The PP2A phosphatase mediates its effects on c-Myc by de-phosphorylating a conserved residue, Ser 62, that normally stabilizes c-Myc, and in this way, PP2A enhances c-Myc ubiquitin-mediated degradation.[25,26]

Here, we investigated the PP2A protein level in all melanoma cell lines by western blot at different time of H_2O_2 treatment (**Fig. 6**). We found that there was a consistent reduction of PP2A protein already at time point of 15 minutes of about 50% compared to the initial level value before the treatment in A375 cells. It continues to decrease until about 25% of the initial value at 60 minutes of treatment. Conversely, the level of PP2A protein was found stable in SK23Mel cells, while in 526 cells it was increased of about 1,5-fold, 2,0-fold and 2,5-fold after 15, 60 minutes and 24 hours, respectively compared to time 0 of treatment. The same pattern of PP2A expression was observed upon paclitaxel and doxorubicin treatment in all cell lines examined (data not shown). This finding suggested that c-myc modulation was PP2A dependent.

H_2O_2, paclitaxel and doxorubicin susceptibility analysis of melanoma cells upon PP2A inhibition and knockdown

In order to validate that c-myc modulation was PP2A dependent, all cell lines were pre-treated with okadaic acid (OA) at 2nM for 60 minutes,[27] and then they were exposed to H_2O_2, paclitaxel and doxorubicin for 24 hours and their survival phenotype was examined. We observed that the only treatment with OA reduced the survived cell number of a value about 10% in all the cell lines analyzed compared to the same cells not-treated with OA (**Fig. 7**). In particular, we observed that the OA pre-treatment increased the A375 and SK23Mel sensitivity to H_2O_2 reducing the number of survived cells of about 11% and 16%, respectively (**Fig. 7A**). The effect was more pronounced in 526 melanoma cells, where a number of survived cells of about 26% was observed. At the same way, the OA pre-treatment increased the cell sensitivity to paclitaxel and doxorubicin treatment. A reduction of survived cell number was observed in A375 (about 15% and 17% upon paclitaxel and doxorubicin treatment, respectively), in 526 (about 13% and 12% upon paclitaxel and doxorubicin treatment, respectively) and in SK23Mel (about

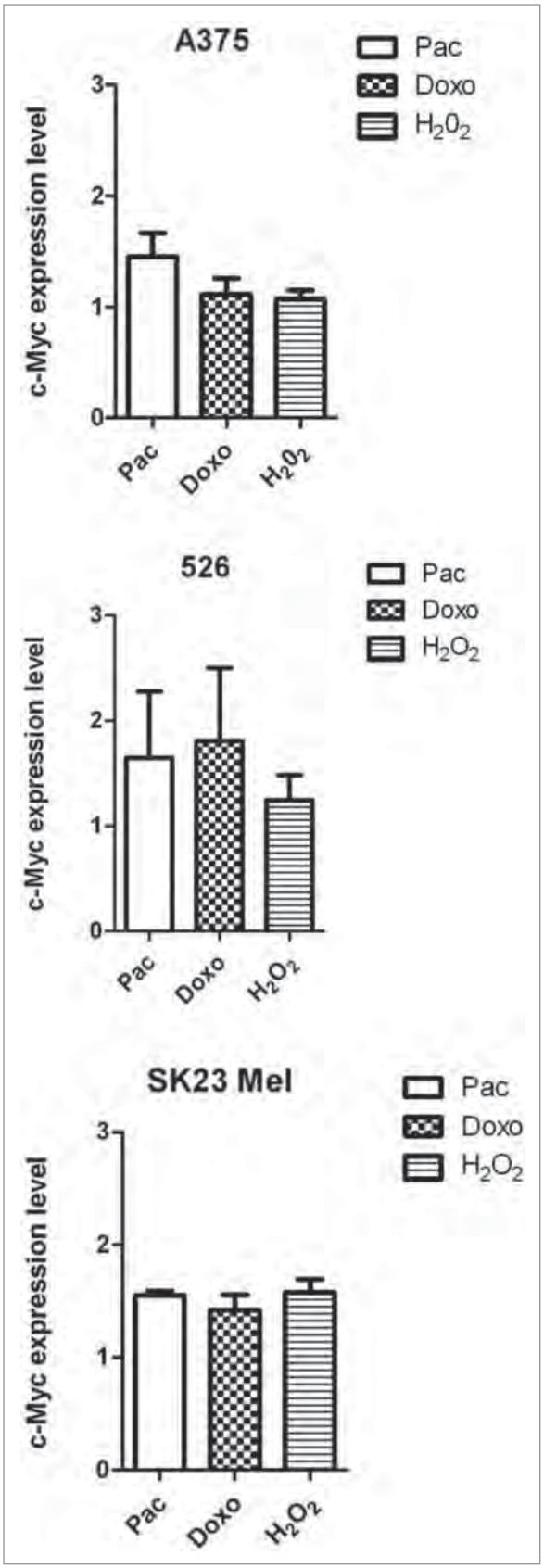

19% upon paclitaxel and doxorubicin treatment) as shown in **Fig. 7B, C**. In addition, we analyzed c-myc protein level in 526 cells OA pretreated and then treated with H_2O_2 for 24hours (**Fig. 7D**, lane 3) and we did not detect a c-myc protein level reduction as the one observed after the only H_2O_2 treatment without OA pre-treatment (**Fig. 7D**, lane 4), supporting that c-myc modulation was dependent from PP2A activity. Furthermore, we silenced PP2A in 526 melanoma cells and we examined the cell sensitivity to H_2O_2 treatment. We observed that when the PP2A protein level, upon PP2A silencing, was reduced of about 30%, c-myc protein level was increased of about 58% (**Fig. 7E**). In addition, an increase of melanoma cell sensitivity to H_2O_2 was observed upon PP2A knockdown. In fact the cell survival percentage value was about 25% in PP2A silenced cells compared to the 58% measured in melanoma control cells, as shown in **Fig. 7E**.

Cell survival analysis of more melanoma cell lines after exposure to H_2O_2 and paclitaxel with and without PP2A inhibition

In order to validate the molecular mechanisms responsible of the different melanoma cell line sensitivity to drugs, we analyzed the survival phenotype of more melanoma cell lines (MALME-3M, SKMel 5, M257) by measuring survival cell percentage, as described in Materials and Methods.

We found a MALME-3M lower survival cell percentage compared to the SKMel5 and M257 upon H_2O_2 and paclitaxel treatment (**Fig. 8A and B**). We also investigated the effect of OA pre-treatment on the sensitivity to different drugs examined. As shown in **Fig. 8A and B**, we observed that the OA pre-treatment increased the cell sensitivity to the different treatments in all 3 melanoma cell lines. We also analyzed the PP2A and c-myc protein level in all 3 melanoma cell lines upon exposure to H_2O_2 at 0.5 mM concentration for 24 hours. We observed a decrease of PP2A and increase of c-myc protein level in MALME-3M melanoma cells upon treatment. On the contrary, PP2A protein level increased while c-myc decreased in SKMel-5 cells. No significant change in c-myc and PP2A was detected in M257 cells (**Fig. 8C**).

Cell survival analysis of melanoma cell lines after exposure to temozolomide

We expand our analysis by exposing melanoma cells to another drug, that works by generating an accumulation of H_2O_2 in the cells: temozolomide. This drug is one among the chemotherapeutic agents used for melanoma treatment. All melanoma cells were

Figure 5. C-Myc expression level in melanoma cell lines, indicated in each panel, treated with paclitaxel (Pac, 45 nM), doxorubicin (Doxo, 10 μM) and H_2O_2 (1 mM) at 24 hours. Results represent the means (± s.e.m.) of 3 independent experiments performed in triplicate. Statistical analysis was done as indicated in Material and Methods. No significantly differences were found among the treatments ($P > 0.05$) in all examined cell lines.

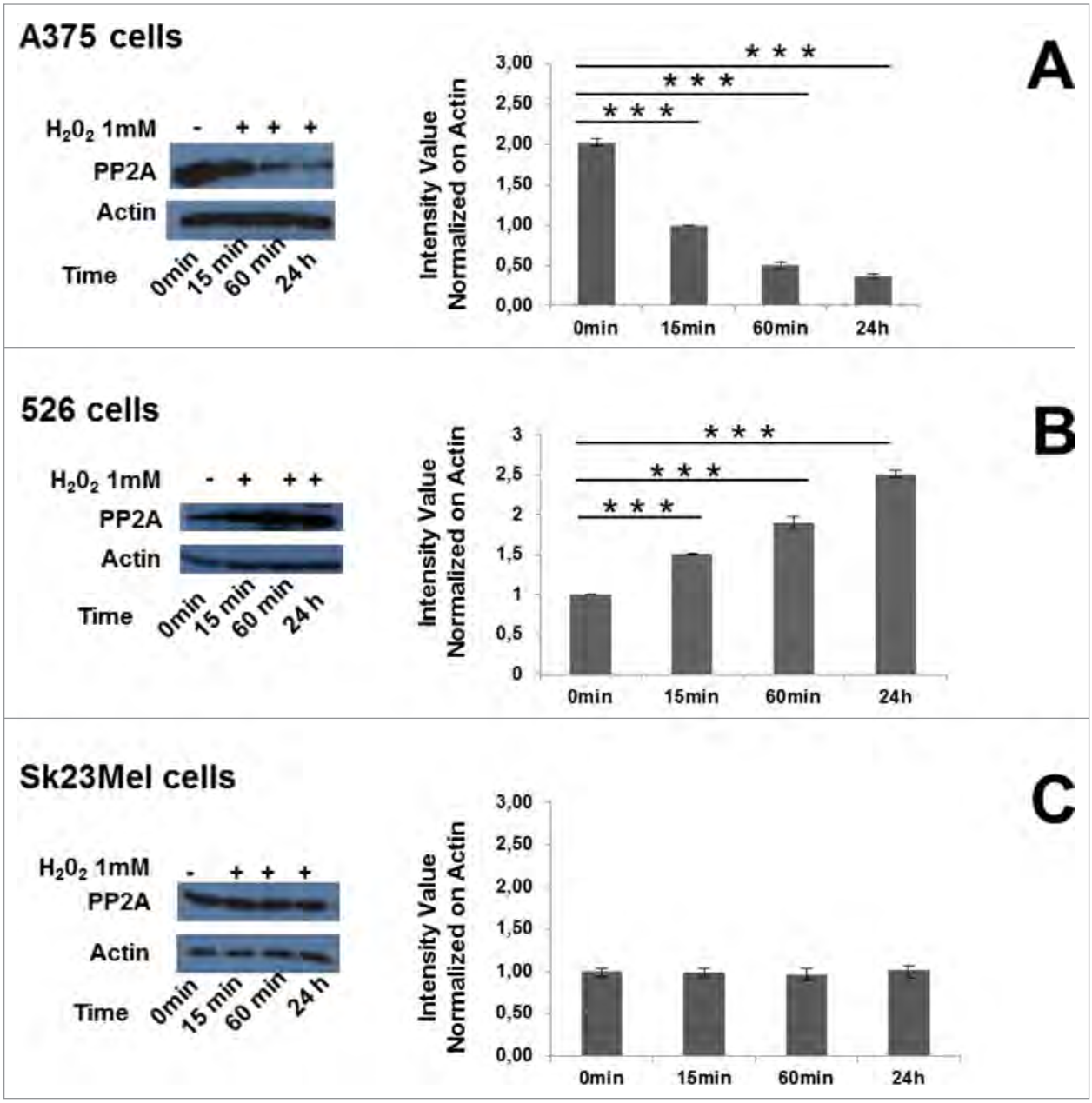

Figure 6. Western blot analysis of PP2A in melanoma cells upon H_2O_2 treatment (1 mM) at 15, 60 minutes and 24 hours. Actin was used as a loading control. The intensity of protein expression was quantified by scanning densitometry. Results represent the means (± s.e.m.) of 3 independent experiments performed in triplicate. P-value was determined by using t-test and value ≤0,001 was indicated (***).

treated with different concentrations of temozolomide and the survival cell percentage was measured. We found a A375 lower survival cell percentage compared to the 526, SKMel23, SKMel5 and M257 upon temozolomide treatment (**Fig. 8D**), as observed upon treatment of these cells with paclitaxel and doxorubicin.

Discussion

The identification of specific resistance patterns and a better understanding of the drug resistance mechanisms is a big challenge and it is critical for therapeutic success in melanoma patients. Recently novel biological therapeutic strategies to cure melanoma have been developed such as the one targeting B-RAF(V600E) mutated protein.[28] This targeted therapy has a short- term success in metastatic melanoma patients, since they are able to develop a resistance to this drug,[29] and it cannot be used for melanoma patients without BRAF mutation (50% of melanoma patients). Alternative therapeutics have been developed recently, providing encouraging results for melanoma treatment.[3,4,30] In particular, paclitaxel drug in randomized clinical studies for metastatic

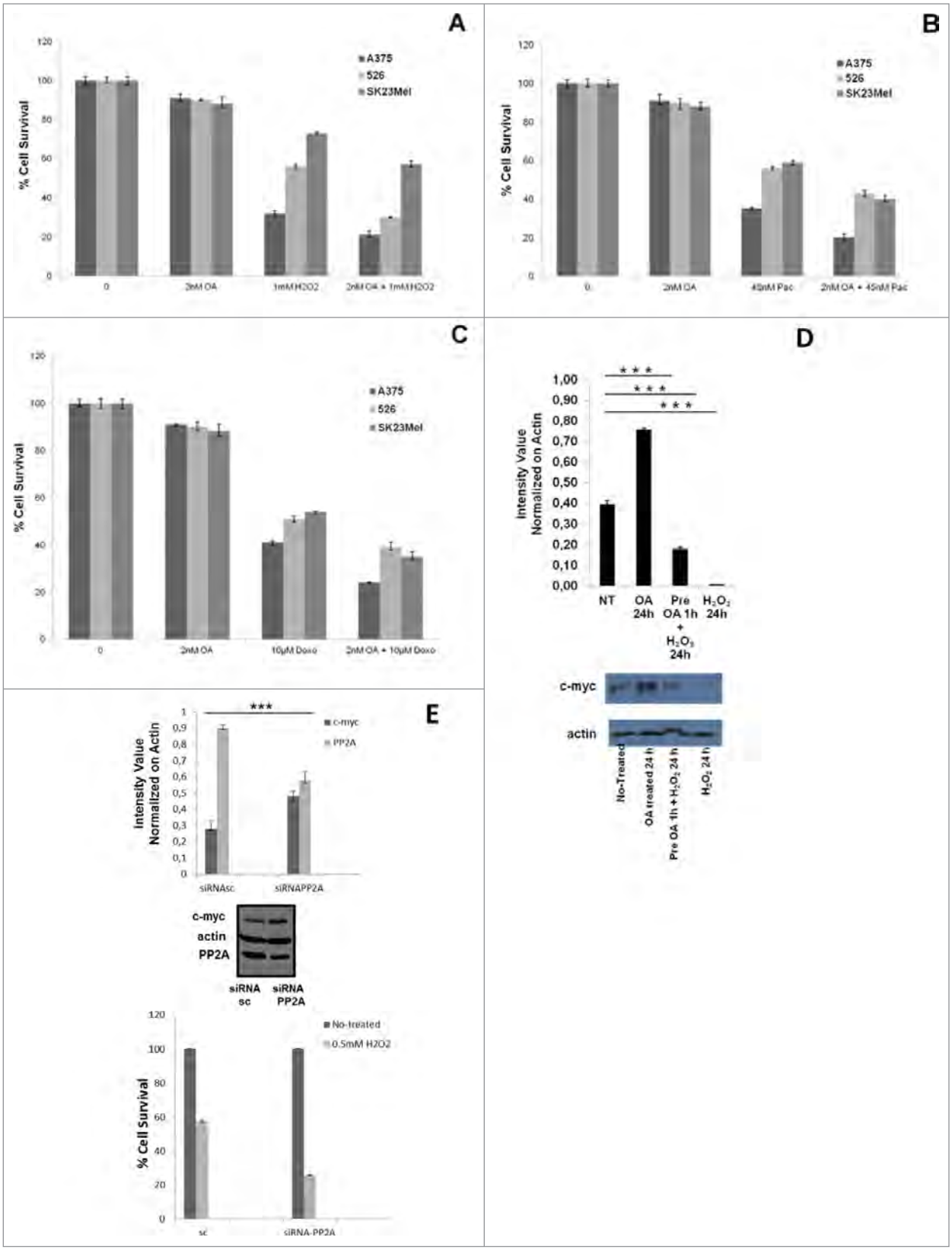

Figure 7. For figure legend, see page 1383.

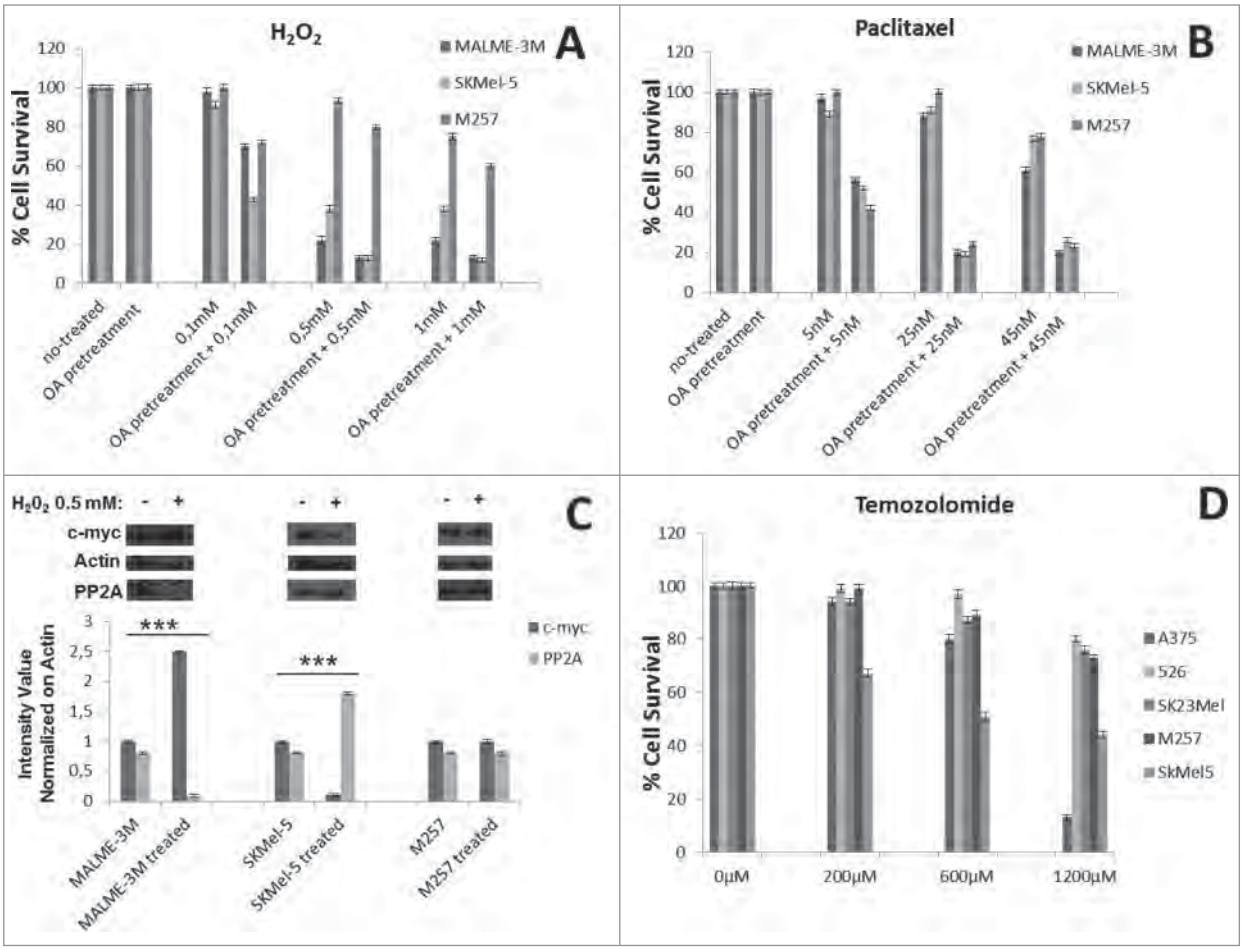

Figure 8. Cell viability analysis of MALME-3M, SKMel-5 and M257 melanoma cells pre-treated with OA (2 nM) for 60 minutes and then exposed to H_2O_2 (**A**) and paclitaxel (**B**) for 24 hours with indicated drug concentrations. Results represent the means (percentage values) of 3 independent experiments performed in triplicate. The error bars show 95% confidence intervals. Western blot analysis of PP2A and c-myc in MALME-3M, SKMel-5 and M257 melanoma cells (**C**) exposed to H_2O_2 (0.5 mM) at 24 hours. Actin was used as a loading control. The intensity of protein expression was quantified by scanning densitometry. Results represent the means (± s.e.m.) of 3 independent experiments performed in triplicate. P-value was determined by using t-test and value ≤0,001 was indicated (***). Cell viability analysis of A375, 526, SK23Mel, M257, SKMel5 melanoma cells upon temozolomide (**D**) exposure at 72 hours with different indicated drug concentrations. Results represent the means (percentage values) of 3 independent experiments performed in triplicate. The error bars show 95% confidence intervals.

melanoma patients independently from their B-RAF mutational status has been tested. In this study the drug has been conjugated to albumin since it has been demonstrated that paclitaxel in this form is prevalently delivered at the tumor sites, since only this form, and not paclitaxel, is able to bind SPARC (secreted protein acidic and rich in cysteine), a protein highly expressed on malignant melanocytes.[31] In this way, this drug can be used at lower concentrations during the treatment, reducing the side effects of this drug in the patients.[3,4]

Several experimental evidences suggested a correlation between the mutational status in B-RAF and the melanoma cell susceptibility to drugs able to generate an accumulation of hydrogen peroxide (H_2O_2) in the cells, such as paclitaxel and doxorubicin. Here, we investigated the molecular mechanisms underlining the resistance to both drugs of human melanoma cell lines, carrying a different mutational status in BRAF. Interestingly, we found that c-myc, a target molecule of RAS-RAF-MEK-ERK protein kinase pathway, was modulated during the different treatments with paclitaxel and doxorubicin drugs as well as upon

Figure 7. (See previous page). Cell viability analysis of A375, 526 and SK23Mel melanoma cells pre-treated with OA (2 nM) for 60 minutes and then exposed to H_2O_2 (**A**), paclitaxel (**B**) and doxorubicin (**C**) for 24 hours with indicated drug concentrations. Results represent the means (percentage values) of 3 independent experiments performed in triplicate. The error bars show 95% confidence intervals. Western blot analysis of c-myc in 526 (**D**) melanoma cells pre-treated with OA (2 nM) for 60 minutes and then exposed to H_2O_2 (1 mM) at 24 hours. Western blot analysis of PP2A and c-myc in 526 (**E**) melanoma cells after PP2A silencing and then exposed to H_2O_2 (0.5 mM) at 24 hours. Actin was used as a loading control. The intensity of protein expression was quantified by scanning densitometry. Results represent the means (± s.e.m.) of 3 independent experiments performed in triplicate. P-value was determined by using t-test and value ≤0,001 was indicated (***).

exposure of the cells to H_2O_2. In particular, we demonstrated by silencing and enhancing c-myc expression, the key role of this molecule in response to these drugs in melanoma. We showed that this molecular event was specifically associated to drugs able to induce an accumulation of H_2O_2 in the tumor cells, since the use of piroxicam was ineffective on c-myc modulation.

Furthermore, we observed that c-myc modulation was not transcriptional driven, since we found no c-myc mRNA level changed upon treatment with drugs as well as with H_2O_2. Interestingly, it was the role of PP2A in this modulation. We observed that the inactivation of this phosphatase was able to increase the sensitivity to all drugs tested in all melanoma cell lines, independently to their mutational status in B-RAF. These data suggest the possibility to modulate c-myc in order to increase the efficacies of the therapies based on paclitaxel or similar drugs. Interestingly, the study by Park et al., where correlative analysis between the expression of some genes and sensitiveness to different drugs have been performed on 60 cancer cell lines (NCI60). They observed a positive correlation between paclitaxel sensitivity and c-myc protein level, further strengthen our data.[5] However, the significance of this correlation was noticeable decreased, when the analysis was restricted to only the melanoma cell lines, enclosed in NCI60, considering that the melanoma cell line number was only 9, too small to generate statistically meaningful data. These findings suggested how the generation of a significant number of paired sensitive/resistant melanoma cell lines will be critical in future in order to elucidate the molecular mechanisms underlying drug resistance in melanoma.

Conflicting results have been reported on the role of c-myc in cell response to chemotherapeutic agents. Indeed, Pastorino et al. reported an increasing of therapeutic effects by treating melanoma with targeted combination of c-myc antisense and doxorubicin, in contrast with our data, most probably due to the different cellular models investigated.[32] On the contrary, our data support the role of c-myc as positive modulator of cell sensitivity to paclitaxel and doxorubicin, as recently described by Frenzel et al. in human neuroblastoma and B-cell lines.[33,34] This opens several possibilities and so it became critical for designing novel therapeutic strategies in melanoma. At the same way, PP2A inhibitors have been reported as potential anti-cancer agents.[35] However, their potentiality in melanoma treatment has not been tested, yet.

Furthermore, it has been reported that c-Myc regulates the transcription of several ABC transporter genes.[36] These molecules are able to efflux cytotoxic drugs, affecting the resistance of cancer cells to apoptosis in the context of treatment. However, several reports provide evidence that ABC transporters might also promote cell survival independently of cytotoxic drug efflux, suggesting together with our findings that further experiments are needed to address this issue in melanoma.

Materials and Methods

Reagents

Paclitaxel and doxorubicin were kindly provided from Drs. PA Ascierto and E. Irollo from National Cancer Institute of Naples, Italy. Okadaic Acid was purchased from Cell Signaling Technology, Inc. All other chemicals were molecular biology grade from Sigma.

Cell lines

Three cell lines were enclosed in this study. A375, 526 and SK23Mel melanoma cell lines were kindly provided by Dr. F. M. Marincola and Dr. M. Bettinotti, (NIH, Bethesda, USA), while MALME-3M, SKMel-5 and M257 melanoma cell lines were provided by Dr. PA Ascierto and Dr. P. Pirozzi, (Cancer National Institute, Naples, Italy). The melanoma cell lines were cultured in RPMI 1640 medium (Invitrogen-Gibco, Paisley, UK), supplemented with 3 mM L-glutamine (Invitrogen-Gibco, Paisley, UK), 2% penicillin/streptomycin, and 10% FBS. The cell cultures were incubated at 37°C in a humidified 5% CO2 atmosphere. Cells were harvested at 80% confluence and protein extraction was performed for further examination.

Cell lysate preparation

The cultured cells were harvested, washed with PBS, and lysed in a lysis buffer [1% Nonidet P-40, 150 mmol/L NaCl, 10 mmol/L Tris (pH 7.4), 1 mmol/L EDTA, 1 mmol/L EGTA (pH 8), 0.2 mmol/L sodium orthovanadate, 0.2 mmol/L phenylmethylsulfonyl fluoride] for 30 minutes at 4°C with constant agitation. The cell lysates were then subjected to a centrifugation (16,000 × *g* at 4°C) for 15 minutes to remove insoluble materials. The protein concentrations of supernatants were measured by Bradford assay.

Western Blot Analysis

Western blot analysis was performed according to standard procedures using a rabbit polyclonal antibody against actin (dilution 1/10,000; Abcam, Cambridge, UK), a rabbit monoclonal antibody against c-myc (dilution 1/10,000; Abcam, Cambridge, UK), a mouse monoclonal antibody against PP2A (diluted 1/1,000, Upstate Cell Signaling, Lake Placid, NY). The visualization was done by horseradish-labeled anti-rabbit and anti-mouse antibodies (Cell Signaling Technology, Danvers, MA) and the ECL chemiluminescence detection system (Amersham Pharmacia Biotech, Piscataway, NJ, USA). The image analysis of the detected bands after western blot was performed by Image J software.

CyQuant Assay

The monitoring of the cell number following the drug treatment was performed by using CyQuant Cell Proliferation Assay Kit, according to the procedure provided from the manufacture (Invitrogen, Paisley, UK).

siRNA and transfection

The sequences of c-myc siRNA were unique to their intended targets, based on BLAST searches. The sequences of the small interfering RNA (siRNA) oligonucleotides for c-myc (5′-CGUCCAAGCAGAGGAGCAA(dT)-3′, sense strand; 5′-UUGCUCCUCUGCUUGGACG(dT)-3′) and the universal negative control were purchased from Sigma-Aldrich. Briefly, 1*10 cells/

well were seeded into 6-well plates and incubated with the transfection complexes (75 mM siRNA and 10μl of Lipofectamine RNAiMAX, Invitrogen). For the c-myc over-expression, the plasmid pDNA4-to/Myc/IRES and the empty vector as control were kindly provided by Dr. I. Iaccarino (IGB-CNR, Naples, Italy). A transient transfection was performed on 1*105 cells/well for each experimental condition, by using 10 μl Lipofectamine 2000 (Invitrogen) and 2,5 μg of plasmid. The cells were analyzed 48 hours post-transfection. For knockdown PP2A cells were transfected with small interfering RNA (siRNA) oligonucleotides (PP2A-Cα siRNA) against the catalytic subunit of the specific phosphatase (Santa Cruz Biotechnology, Inc., CA, USA) using Lipofectamine RNAiMAX reagent (Invitrogen) according to the manufacturer's instructions. Cells were treated with the indicated conditions and analyzed 48 hours post-transfection.

Real-Time qRT-PCR

Expression levels of c-Myc was analyzed by quantitative real-time PCR analysis using total RNA (300 ng) from cell lines treated, with paclitaxel, doxorubicin or H_2O_2. Untreated cells were used as control. RNA was converted to cDNA using High-Capacity cDNA Reverse transcription kit (Applied Biosystems, Life Technologies, Grand Island, CA) underconditions described by the supplier. Gene specific primers for c-Myc (Forward 5′ CACCACCAGCAGCGACTCT, Reverse 5′ TTCCACA-GAAACAACATCGATTTC) was designed using Primer Express 2.0 software (Applied Biosystems). Actin β was used as internal control. Experiments were performed in triplicates. Quantitative PCRs were done on an ABI PRISM 7900HT Sequence Detection System (Applied Biosystems). The entire procedure for qRT-PCR analysis—primer design, reactions, amplicon specificity and determination of gene target expression levels—was performed as previously described.[36] Statistical analysis of the c-Myc expression levels were performed using GraphPad Prism 5.0® statistical software (GraphPad Software Inc., La Jolla, CA). Paired *t* test was used for comparison of 2 paired groups. Multiple comparisons were performed by the repeated measures ANOVA test with the Bonferroni correction for multiple.

Disclosure of Potential Conflicts of Interest

No potential conflicts of interest were disclosed.

Acknowledgments

We are grateful to Dr. Paolo A Ascierto, Dr. Elena Irollo, Dr. Stefania Crispi, Dr. Stefania Comes and Dr. Nicola Laprano for their critical comments. Gennaro Andolfi, Pasquale Barba and Gabriele Di Napoli for their excellent technical assistance. We are grateful to Anna Maria Aliperti for her assistance in the editing of the manuscript.

Funding

This work was supported by a sub-grant (1 R21DK070192-01) from NIH NIDDK to E.C. and by grants from Medical Research in Italy (RBNE08HM7T-003) to E.J.P. A.V. was supported by BIAM EPI-FORM "Ricerca e Competitività" 2007–2013.

References

1. Gray-Schopfer V, Wellbrock C, Marais R. Melanoma biology and new targeted therapy. Nature 2007; 445:851-7; PMID:17314971; http://dx.doi.org/10.1038/nature05661
2. Korn EL, Liu PY, Lee SJ, Chapman JA, Niedzwiecki D, Suman VJ, Moon J, Sondak VK, Atkins MB, Eisenhauer EA, et al. Meta-analysis of phase II cooperative group trials in metastatic stage IV melanoma to determine progression-free and overall survival benchmarks for future phase II trials. J. Clin Oncol 2008; 26: 527-34; PMID:18235113; http://dx.doi.org/10.1200/JCO.2007.12.7837
3. Kottschade LA, Suman VJ, Perez DG, McWilliams RR, Kaur JS, Amatruda TT 3rd, Geoffroy FJ, Gross HM, Cohen PA, Jaslowski AJ, et al. A randomized phase 2 study of temozolomide and bevacizumab or nab-paclitaxel, carboplatin, and bevacizumab in patients with unresectable stage IV melanoma : a North Central Cancer Treatment Group study, N0775. Cancer 2013; 119:586-92; PMID:22915053; http://dx.doi.org/10.1002/cncr.27760
4. Ott PA, Chang J, Madden K, Kannan R, Muren C, Escano C, Cheng X, Shao Y, Mendoza S, Gandhi A, et al. Oblimersen in combination with temozolomide and albumin-bound paclitaxel in patients with advanced melanoma: a phase I trial. Cancer Chemother Pharmacol 2013; 71:183-91; PMID:23064957; http://dx.doi.org/10.1007/s00280-012-1995-7
5. Park, ES, Rabinovsky R, Carey M, Hennessy BT, Agarwal R, Liu W, Ju Z, Deng W, Lu Y, Woo HG, et al. Integrative analysis of proteomic signatures, mutations, and drug responsiveness in the NCI 60 cancer cell line set. Mol Cancer Ther 2010; 9:257-67; PMID:20124458; http://dx.doi.org/10.1158/1535-7163.MCT-09-0743
6. Alexandre J, Batteux F, Nicco C, Chéreau C, Laurent A, Guillevin L, Weill B, Goldwasser F. Accumulation of hydrogen peroxide is an early and crucial step for paclitaxel induced cancer cell death both in vitro and in vivo. Int J Cancer 2006; 119:41-8; PMID:16450384; http://dx.doi.org/10.1002/ijc.21685
7. Alexandre J, Hu Y, Lu W, Pelicano H, Huang P. Novel action of paclitaxel against cancer cells: bystander effect mediated by reactive oxygen species. Cancer Res 2007; 67:3512-17; PMID:17440056; http://dx.doi.org/10.1158/0008-5472.CAN-06-3914
8. Jing Y, Dai J, Chalmers-Redman RM, Tatton WG, Waxman S. Arsenic trioxide selectively induces acute promyelocytic leukemia cell apoptosis via a hydrogen peroxide-dependent pathway. Blood 1999; 94:2102-11; PMID:10477740
9. Mizutani H, Taa-Oikawa S, Hiraku Y, Kojima M., Kawanishi S. Mechanism of apoptosis induced by doxorubicin through the generation of hydrogen peroxide. Life Sci 2005; 76:1439-53; PMID:15680309; http://dx.doi.org/10.1016/j.lfs.2004.05.040
10. Ubezio P, Civoli F. Flow cytometric detection of hydrogen peroxide production induced by doxorubicin in cancer cells. Free Radic Biol Med 1994; 16:509-16; PMID:8005536; http://dx.doi.org/10.1016/0891-5849(94)90129-5
11. Ikeda K, Kajiwara K, Tanabe E, Tokumaru S, Kishida E, Masuzawa Y, Kojo S. Involvement of hydrogen peroxide and hydroxyl radical in chemically induced apoptosis of HL-60 cells. Biochem Pharmacol 1999; 57:1361-5; PMID:10353256; http://dx.doi.org/10.1016/S0006-2952(99)00055-6
12. Fang J, Nakamura H, Iyer AK. Tumor-targeted induction of oxystress for cancer therapy. J Drug Target 2007; 15:475-86; PMID:17671894; http://dx.doi.org/10.1080/10611860701498286
13. Simizu S, Takada M, Umezawa K, Imoto M. Requirement of caspase-3(-like) protease-mediated hydrogen peroxide production for apoptosis induced by various anticancer drugs. J Biol Chem 1998; 273:26900-7; PMID:9756937; http://dx.doi.org/10.1074/jbc.273.41.26900
14. Gorman A, McGowan A, Cotter TG. Role of peroxide and superoxide anion during tumour cell apoptosis. FEBS Lett 1997; 404:27-33; PMID:9074631; http://dx.doi.org/10.1016/S0014-5793(97)00069-0
15. Ling YH, Liebes L, Zou Y, Perez-Soler R. Reactive oxygen species generation and mitochondrial dysfunction in the apoptotic response to Bortezomib, a novel proteasome inhibitor, in human H460 non-small cell lung cancer cells. J Biol Chem 2003; 278:33714-23; PMID:12821677; http://dx.doi.org/10.1074/jbc.M302559200
16. Pérez-Galán P, Roué G, Villamor N, Montserrat E, Campo E, Colomer D. The proteasome inhibitor bortezomib induces apoptosis in mantle-cell lymphoma through generation of ROS and Noxa activation independent of p53 status. Blood 2006; 107:257-64; PMID:16166592; http://dx.doi.org/10.1182/blood-2005-05-2091
17. Renschler MF. The emerging role of reactive oxygen species in cancer therapy. Eur J Cancer 2004; 40:1934-40; PMID:15315800
18. Doroshow JH. Role of hydrogen peroxide and hydroxyl radical formation in the killing of Ehrlich tumor cells by anticancer quinones. Proc Natl Acad Sci U S A

1986; 83:4514-8; PMID:3086887; http://dx.doi.org/10.1073/pnas.83.12.4514
19. Chang LF, Karin M. Mammalian MAP kinase signalling cascades. Nature 2001; 410:37-40; PMID:11242034; http://dx.doi.org/10.1038/35065000
20. Davies H, Bignell GR, Cox C, Stephens P, Edkins S, Clegg S, Teague J, Woffendin H, Garnett MJ, Bottomley W, et al. Mutations of the BRAF gene in human cancer. Nature 2002; 417:949-54; PMID:12068308; http://dx.doi.org/10.1038/nature00766
21. Wan PT, Garnett MJ, Roe SM, Lee S, Niculescu-Duvaz D, Good VM, Jones CM, Marshall CJ, Springer CJ, Barford D, et al. Mechanism of activation of the RAF-ERK signaling pathway by oncogenic mutations of B-RAF. Cell 2004; 116:855-67; PMID:15035987; http://dx.doi.org/10.1016/S0092-8674(04)00215-6
22. Michaloglou C, Vredeveld LC, Mooi WJ, Peeper DS. BRAF(E600) in benign and malignant human tumours. Oncogene 2008; 27:877-95; PMID:17724477; http://dx.doi.org/10.1038/sj.onc.1210704
23. Farah AE, Rosenberg F. Potential therapeutic applications of aspirin and other cyclo-oxygenase inhibitors. Br J Clin Pharmacol 1980; 10(Suppl 2): 261S-278S; PMID:6776977; http://dx.doi.org/10.1111/j.1365-2125.1980.tb01809.x
24. Mazhar D, Ang R, Waxman J. COX inhibitors and breast cancer. Br J Cancer 2006; 94:346-50.
25. Kamemura K, Hayes BK, Comer FI, Hart GW. Dynamic interplay between O-glycosylation and O-phosphorylation of nucleocytoplasmic proteins: alternative glycosylation/phosphorylation of THR-58, a known mutational hot spot of c-Myc in lymphomas, is regulated by mitogens. J Biol Chem 2008; 277:19229-35; PMID:11904304
26. Arnold HK, Sears RC. Protein Phosphatase 2A Regulatory Subunit B56a Associates with c-Myc and Negatively Regulates c-Myc Accumulation. Mol Cell Biol 2006; 26:2832-44; PMID:16537924; http://dx.doi.org/10.1128/MCB.26.7.2832-2844.2006
27. Cohen P. An improved procedure for identifying and quantitating protein phosphatases in mammalian tissues. FEBS Lett 1989; 250:596-600; PMID:2546812
28. Menzies AM, Long GV, Murali R. Dabrafenib and its potential for the treatment of metastatic melanoma. Drug Design, Dev Therapy 2012; 6:391-405; PMID:23251089
29. Chapman PB, Hauschild A, Robert C, Haanen JB, Ascierto P, Larkin J, Dummer R, Garbe C, Testori A, Maio M, et al. Improved survival with vemurafenib in melanoma with BRAF V600E mutation. N Engl J Med 2011; 364:2507-2516; PMID:21639808; http://dx.doi.org/10.1056/NEJMoa1103782
30. Caputo E, Miceli R, Motti ML, Taté R, Fratangelo F, Botti G, Mozzillo N, Carriero MV, Cavalcanti E, Palmieri G, et al. AurkA inhibitors enhance the effects of B-RAF and MEK inhibitors in melanoma treatment. J Transl Med 2014; 12:216; PMID:25074438
31. Ledda F, Bravo AI, Adris S, Bover L, Mordoh J, Podhajcer OL. The expression of the secreted protein acidic and rich in cysteine (SPARC) is associated with the neoplastic progression of human melanoma. J Invest Dermatol 1997; 108:210-4; PMID:9008236; http://dx.doi.org/10.1111/1523-1747.ep12334263
32. Pastorino F, Mumbengegwi DR, Ribatti D, Ponzoni M, Allen TM. Increase of therapeutic effects by treating melanoma with targeted combinations of c-myc antisense and doxorubicin. J Controlled Release 2008; 126:85-94; PMID:18166243; http://dx.doi.org/10.1016/j.jconrel.2007.11.010
33. Frenzel A, Zirath H, Vita M, Albihn A, Henriksson MA. Identification of cytotoxic drugs that selectively target tumor cells with MYC overexpression. Plos One 2011; 6: e27988; PMID:22132187
34. Liu D, Liu X, Xing M. Activities of multiple cancer-related pathways are associated with BRAF mutation and predict the resistance to BRAF/MEK inhibitors in melanoma cells. Cell Cycle 2014; 13:208-19; PMID:24200969; http://dx.doi.org/10.4161/cc.26971
35. Han X, Xu B, Beevers CS, Odaka Y, Chen L, Liu L, Luo Y, Zhou H, Chen W, Shen T, Huang S. Curcumin inhibits protein phosphatases 2A and 5, leading to activation of mitogen-activated protein kinases and death in tumor cells. Carcinogenesis 2012; 33:868-75; PMID:22298641; http://dx.doi.org/10.1093/carcin/bgs029
36. Crispi S, Calogero RA, Santini M, Mellone P, Vincenzi B, Citro G, Vicidomini G, Fasano S, Meccariello R, Cobellis G, et al. Global gene expression profiling of human pleural mesotheliomas: identification of matrix metalloproteinase 14 (MMP-14) as potential tumour target. PLoS One 2009; 4: e7016; PMID:19753302
37. Porro A, Iraci N, Soverini S, Diolaiti D, Gherardi S, Terragna C, Durante S, Valli E, Kalebic T, Bernardoni R, et al. c-MYC oncoprotein dictates transcriptional profiles of ATP-binding cassette transporter genes in chronic myelogenous leukemia CD34+ hematopoietic progenitor cells. Mol Cancer Res 2011; 9:1054-66; PMID:21693596; http://dx.doi.org/10.1158/1541-7786.MCR-10-0510

Cancer Letters 357 (2015) 286–296

Contents lists available at ScienceDirect

Cancer Letters

journal homepage: www.elsevier.com/locate/canlet

Original Articles

Ran signaling in melanoma: Implications for the development of alternative therapeutic strategies

Emilia Caputo [a,b,*], Ena Wang [c,d], Anna Valentino [a], Stefania Crispi [a,e], Valeria De Giorgi [c], Annalisa Fico [a], Bartolomea Ficili [b], Mariaelena Capone [f], AnnaMaria Anniciello [f], Ernesta Cavalcanti [f], Gerardo Botti [f], Nicola Mozzillo [f], Paolo A. Ascierto [f], Francesco M. Marincola [c,d], Salvatore Travali [b]

[a] *Institute of Genetics and Biophysics –I.G.B. A. Buzzati-Traverso– CNR, Naples I-80131, Italy*
[b] *Dipartimento di Scienze Biomediche, Università degli Studi di Catania, Catania I-95124, Italy*
[c] *Infectious Disease and Immunogenetics Section (IDIS), Department of Transfusion Medicine (DTM), Clinical Center (CC), Center for Human Immunology (CHI), National Institutes of Health (NIH), Bethesda, MD, United States*
[d] *Sidra Medical and Research Center, Doha, Qatar*
[e] *Institute of Biosciences and BioResources-IBB, CNR, Naples I-8013, Italy*
[f] *Istituto Nazionale Tumori Fondazione G. Pascale, Naples I-80131, Italy*

ARTICLE INFO

Article history:
Received 12 June 2014
Received in revised form 29 October 2014
Accepted 15 November 2014

Keywords:
Targeted therapy
Aurora kinase A in melanoma
Gene expression
Pathway analysis
Ran signaling

ABSTRACT

We performed a comparative study between two human metastatic melanoma cell lines (A375 and 526), and melanocytes (FOM78) by gene expression profiling and pathway analysis, using Gene Set Enrichment Analysis (GSEA) and Ingenuity Pathway Analysis (IPA) software. Genes involved in Ran signaling were significantly over-represented ($p \leq 0.001$) and up-regulated in melanoma cells. A melanoma-associated molecular pathway was identified, where Ran, Aurora Kinase A (AurkA) and TERT were up-regulated, while c-myc and PTEN were down-regulated. A consistent high Ran and AurkA gene expression was detected in about 48% and 53%, respectively, of 113 tissue samples from metastatic melanoma patients. AurkA down-regulation was observed in melanoma cells, by Ran knockdown, suggesting AurkA protein is a Ran downstream target. Furthermore, AurkA inhibition, by exposure of melanoma cells to MLN8054, a specific AurKA inhibitor, induced apoptosis in both melanoma cell lines and molecular alterations in the IPA-identified molecular pathway. These alterations differed between cell lines, with an up-regulation of c-myc protein level observed in 526 cells and a slight reduction seen in A375 cells. Moreover, Ran silencing did not affect the A375 invasive capability, while it was enhanced in 526 cells, suggesting that Ran knockdown, by AurkA down-regulation, resulted in a Ran-independent enhanced melanoma cell invasion. Finally, AurK A inhibition induced a PTEN up-regulation and its action was independent of B-RAF mutational status. These findings provide insights relevant for the development of novel therapeutic strategies as well as for a better understanding of mechanisms underlying therapy resistance in melanoma.

Introduction

The most aggressive form of skin cancer is melanoma, the incidence of which has dramatically increased worldwide [1]. Metastatic malignant melanoma has a very poor prognosis, with a median survival time of approximately 6 months [2]. Several of the molecular mechanisms associated with melanoma origin and progression have now been identified. For instance, the mitogen-activated protein kinase (MAPK) pathway is constitutively activated in melanoma cells, while it is only weakly activated by growth factors released from the local microenvironment in melanocytes, leading to an insufficient stimulus to induce proliferation under physiological conditions [3]. Activating mutations in N-Ras have been identified in 15–20% of all melanomas [4,5], while mutations in B-RAF have been observed in about 60% of melanomas, with V600E accounting for over 80% of all mutations. The BRAF (V600E) protein has markedly increased catalytic activity for its substrates and constitutively activates the RAS–RAF–MEK–ERK pathway [5,6]. However, MAPK pathway activation alone is insufficient for melanoma progression and it has been shown that full transformation only occurs with concurrent activation of the PI3K–AKT pathway following PTEN suppression [7].

Abbreviations: AurkA, aurora kinase A; MM, metastatic melanoma; IPA, Ingenuity Pathway Analysis; GSEA, Gene Set Enrichment Analysis; FDR, false discovery rate.

* Corresponding author. Tel.: +39 081 6132307; fax: +39 081 6132706.
E-mail address: emilia.caputo@igb.cnr.it (E. Caputo).

http://dx.doi.org/10.1016/j.canlet.2014.11.033
0304-3835/

Understanding the complex regulation of these pathways and the role of novel altered pathways may lead to improvements in the rational development of targeted therapies. In this study, we applied a network identification analysis, based on gene expression profiles and protein–protein interaction networks, to characterize and compare two different melanoma cell lines, A375 and 526 [8] and the melanocyte cell line, FOM78 [9] as control. Gene expression was also investigated in 113 tissue samples derived from metastatic melanoma patients.

Materials and methods

Cell lines

Human melanoma cell lines A375 and 526 and melanocyte FOM78 [9] were kindly provided by Dr. M. Bettinotti (NIH, Bethesda, MD, USA). Melanoma cell lines were cultured in RPMI 1640 medium (Invitrogen-Gibco, Monza MB, Italy), supplemented with 3 mM L-glutamine (Invitrogen-Gibco), 2% penicillin/streptomycin, and 10% FBS. Melanocytes were cultured in MGM-4 cell medium (Euroclone, Milan, Italy). All cultures were incubated at 37 °C in a humidified 5% CO_2 atmosphere.

Gene expression analysis

Total RNA was isolated from cultured cell lines using the RNeasy Mini Kit (Qiagen, Hilden, Germany). Total RNA quality and integrity was evaluated on the Agilent 2100 Bioanalyzer (Agilent Technologies, Santa Clara, CA, USA) and concentration was measured using a NanoDrop 1000 spectrophotometer (Thermo Scientific, Wilmington, DE, USA). Two rounds of RNA amplification were performed as previously described [10,11] and 6 μg of amplified χRNA was labeled with Cy5 while reference samples derived from peripheral blood mononuclear cells (PBMC) pooled from six normal donors were amplified in the same fashion and labeled with Cy3 using a ULS αRNA Fluorescent Labeling kit (Kreatech, Amsterdam, The Netherlands). A 36k whole transcriptome expression array was fabricated using human Array-Ready Oligo Set (AROS™ V4.0, Operon, Cologne, Germany) at the Infectious Disease and Immunogenetics Section (NIH, Bethesda, MD, USA). Hybridization was carried at 42 °C for 18–24 hours and the arrays were then washed, scanned and analyzed using BRB array software (http://linus.nci.nih.gov/BRB-ArrayTools.html) [12]. Genes with intensity <100 in both channels, spots size <20 um were excluded. Genes with intensity <100 in one channel only were adjusted to 100. After median normalization over the whole array, data were stringently filtered to remove genes with missing values in more than 40% of the experiments and genes with less than 1.5-fold change in either direction from the median value in less than 20% of the entire array experiments.

Pathway analysis

Ingenuity Pathway Analysis (IPA7.0, Ingenuity System®, http://www.ingenuity.com/) was used to functionally annotate differentially expressed genes from the cell lines analyzed and to identify potential networks each with a specific score, corresponding to the probabilistic fit between the networks and a list of biological functions stored in the Ingenuity Pathways Knowledge Base, a proprietary manually curated database.

GSEA analysis

Gene Set Enrichment Analysis (GSEA, http://www.broadinstitute.org/gsea/index.jsp) was used to assess whether an *a priori* defined set of genes showed statistically significant concordant differences between two phenotypes (melanoma cells vs. melanocytes). The primary result of the GSEA is the enrichment score (ES), which reflects the degree to which a gene set is overrepresented at the top or bottom of a ranked list of genes. Normalized log2 intensities were used in the analysis against a computational gene set defined by mining large collections of cancer-oriented microarray data (C4 computational gene sets, Molecular Signatures Database v4.0).

Quantitative real-time polymerase chain reaction (qRT-PCR) analysis

Total RNA (300 ng) from melanocyte and melanoma cell lines was converted to cDNA using High-Capacity cDNA Reverse transcription kit (Applied Biosystems, Life Technologies, Grand Island, CA, USA). Primers for the selected genes (AURKA: Forward 5′-CACCTTCGGCATCCTAATATTCTT-3', Reverse 5′-GGGCATTTGCCAATTCTGTT-3′; MYC Forward 5′-CACCACCAGCAGCGACTCT-3′, Reverse 5′-TTCCACAGAAACAACATCGATTTC-3′; PTEN Forward 5′-GGAGATATCAAGAGGATGGATTCG-3′, Reverse 5′-CAGGAAATCCCATAGCAATAATGTT-3′; RAN Forward 5′ TTGGTGATGGTGGTACTGGA-3′, Reverse 5′-GGAGAGCAGTTGTCTGAGCA-3′; RCC1 Forward 5′-TGCAGGTGCAGCTGGATGT-3′, Reverse 5′-CATCACCAAGTGGTCGTTTCC-3′; TERT Forward 5′-GGCGACATGGAGAACAAGCT-3′, Reverse 5′-CCAACAAGAAATCATCCACCAAA-3′) were designed using Primer Express 2.0 software (Applied Biosystems). Actinβ was used as internal control (Forward 5′-TTCTACAATGAGCTGCGTGTG-3′ and Reverse 5′-GGGGTGTTGAAGGTCTCAAA-3′). Experiments were performed in triplicate. Quantitative real-time polymerase chain reaction (qRT-PCR) was done on an ABI PRISM 7900HT Sequence Detection System (Applied Biosystems). The entire procedure for qRT-PCR analysis (primer design, reactions, amplicon specificity and determination of gene target expression levels) was performed as previously described [13].

Protein extracts

Cells were lysed in lysis buffer (1% Nonidet P-40, 150 mmol/L NaCl, 10 mmol/L Tris (pH 7.4), 1 mmol/L EDTA, 1 mmol/L EGTA [pH 8], 0.2 mmol/L sodium orthovanadate, 0.2 mmol/L phenylmethylsulfonyl fluoride) for 30 minutes at 4 °C with constant agitation. Insoluble material was removed by centrifugation (16000 × *g* at 4 °C) for 15 minutes and the total protein concentration was determined in the supernatant by Bradford assay.

Western blot analysis

Western blot was performed according to standard procedures. Mouse monoclonal antibodies against p53 (DO-1; diluted 1:1000; Santa Cruz Biotechnology, Inc, Dallas, TX, USA), rabbit monoclonal to c-Myc (1:5000, Abcam, Cambridge, UK), rabbit polyclonal to telomerase reverse transcriptase (diluted 1:1000; Abcam), rabbit polyclonal antibodies against PARP (diluted 1:1000, Cell Signaling Technology, Danvers, MA, USA), phospho-MEK1/2 (Ser217/221) (diluted 1:1000, Cell Signaling Technology), MEK1/2 (diluted 1:1000, Cell Signaling Technology), Aurora Kinase A (diluted 1:100; Abcam), Ran (diluted 1:500; Abcam) and β-actin (diluted 1:1,000, Cell Signaling Technology) were used. Detection was achieved by HRP-conjugated anti-mouse (1:10,000; Cell Signaling Technology) or HRP-conjugated anti-rabbit (1:1,000,000; Cell Signaling Technology) antibodies. Immune complexes were visualized by an enhanced chemiluminescence system (ECL Advance™, Amersham Pharmacia Biotech, Piscataway, NJ, USA). Actin was used as a loading control. The image analysis was performed by ImageJ software (http://rsbweb.nih.gov/ij/). Results represent the means (±SEM) of three independent experiments performed in triplicate. *P*-value was determined by using t-test and value ≤0.005 was indicated, in the figure, with the symbol: ***.

Gene expression analysis on melanoma tissues

Total RNA from 113 melanoma metastases from patients treated at the Surgery Branch, NCI, was extracted using miRNeasy minikit (Qiagen). RNA quality and quantity were estimated using Nanodrop (Thermo Scientific) and Agilent 2100 Bioanalyzer (Agilent Technologies). First- and second-strand cDNA were synthesized from 300 ng of total RNA according to the manufacturer's instructions (Ambion WT Expression Kit). cDNAs were fragmented, biotinylated, and hybridized to the GeneChip Human Gene 1.0 ST Arrays (Affymetrix WT Terminal Labeling Kit, Affymetrix, Santa Clara, CA, USA). The arrays were washed and stained on a GeneChip Fluidics Station 450 (Affymetrix); scanning was carried out with the GeneChip Scanner 3000 and image analysis with the Affymetrix GeneChip Command Console Scan Control. Expression data were normalized, background-corrected, and summarized using the RNA algorithm at the http://www.partek.com/ website. Data were log-transformed (base 2) for subsequent statistical analysis. Cluster analysis was performed using Cluster and TreeView software (Stanford University, Stanford, CA, USA).

Small interfering RNA transfection

Ran gene silencing by small interfering RNA (siRNA) was carried out with control no-targeted and two independent Ran-directed siRNA oligonucleotides (s11769 and s11767, Ambion, Carlsbad, CA) using Lipofectamine RNAiMAX reagent (Invitrogen, Paisley, UK), according to the manufacturer's instructions. Briefly, 1×10^5 cells/well were seeded into six-well plates and incubated with the transfection complexes (75 mM siRNAs and 10 μl of Lipofectamine RNAiMAX, Invitrogen). Cells were analyzed 48 hours post-transfection.

Invasion assays

An invasion assay was performed in a 24-well transwell chamber, by using a BD BioCoat Matrigel invasion chamber (BD Bioscience, Bedford, MA,USA), according to the manufacturer's instructions. Briefly, equal numbers of cells (2.5×10^4 cells/well) in RPMI 1640 medium complemented with 1% FCS were added to the upper compartment of the chamber. As a chemoattractant, the lower compartment contained RPMI 1640 medium supplemented with 10% FCS. After 18 hours at 37 °C in a 5% CO_2 incubator, the Matrigel coating on the upper surface of the filter was wiped off using a cotton swab. Cells that migrated through the filters were fixed, stained, photographed, and counted (4 random fields/insert, 10×) in the light microscope on ten randomly selected fields. The mean number of cells was calculated per field. Three sets of experiments were carried out, each in triplicate. The statistical significance of the results was calculated using the ANOVA procedure. The data were considered to be significant when $P < 0.05$.

Drug treatment

Cells were treated with medium containing the specific Aurora kinase A (AurkA) inhibitor MLN8054 (Selleck, Munich, Germany) at different concentrations for 72 hours and with B-RAF inhibitor (GSK2118436) (kindly provided by GlaxoSmithKline, London, UK) at a concentration of 30 nM in all experiments. Cells treated with DMSO (0.2%) were used as the vehicle control. Cell number evaluation, following drug treatment was performed using a CyQuant Cell Proliferation Assay Kit (Invitrogen). Results represented the means (percentage values) of three independent experiments performed in triplicate.

p53 mutational analysis

Genomic DNA was extracted from cells by QIAamp DNA mini kit (Qiagen) and was used as template for amplification of p53 exons 5–8. The primers were: exon 4 forward: 5′-GACCTGGTCCTCTGACTGCT-3′ and reverse: 5′-ATACGGCCAGGCATTGAAG-3′; exon 5–6 forward: 5′-AGGAGGTGCTTAGCGATGT-3′, reverse: 5′-CACT GACAACCACCCTTAAC-3′; exon 7 forward: 5′-CAGAGCGAGATTCCATCTCA-3′, reverse: 5′-ATGTGATGAGAGGTGGATGG-3′; exon 8 forward: 5′-GGAGTAGATGGAGCCTGGTT-3′, reverse: 5′-ATCTGAGGCATAACTGCACC-3′. PCR product sequence analysis was performed in both directions using the same primers and the BigDye Terminator Cycle Sequencing Kit (Applied Biosystems) using an ABI PRISM 310 genetic analyzer (Applied Biosystems). All sequences were confirmed in a second PCR-sequencing reaction.

Statistical analysis

Statistical analysis was performed using GraphPad Prism 5.0® statistical software (GraphPad Software Inc., La Jolla, CA, USA). Paired t-test was used for comparison of two paired groups. Multiple comparisons were performed by the repeated measures ANOVA test with the Bonferroni correction. Dot plot, reporting gene intensity values obtained from gene expression analysis, was generated across all samples examined, by using Partek Genomics Suite software.

Results

Gene profiling and network analysis of melanoma cell lines and melanocytes

The transcriptional datasets of the human melanoma cell lines A375 and 526 were functionally classified through an Ingenuity Pathways Analysis (IPA) Core Analysis (IPA7.0, Ingenuity System®) and compared with that of the melanocytes, FOM78. IPA is a web-delivered application that allows the identification of functional relationships between differentially expressed genes. For each probe set, IPA generates a metadata file, containing information on how to map the given dataset onto molecules associated with specific disease, cellular functions and canonical pathways. Thus, it is possible to obtain indications on the cellular processes, characterizing melanoma cell lines and genes potentially involved in disease development. We examined deregulated genes for molecular, cellular function and canonical pathways for both melanoma cell lines, A375 and 526, and melanocytes, with complete lists reported in Appendix: Supplementary Table S1.

All the deregulated genes (approximately 1800) obtained from the microarray data were analyzed with IPA Core Analysis. IPA associates molecules under analysis with known biological functions and diseases. The link between a category and the associated molecules is defined by a p-value. In general the more molecules involved the more likely the association is not due to random chance, and thus the more significant is the p-value. We found EEIF2 Signaling, Ran Signaling, Cell Cycle Control of Chromosomal Replication and Pyrimidine Metabolism as the top four categories among the known canonical pathways enriched within the set of differentially expressed genes (Fig. 1A). The canonical pathways are displayed along the x-axis, while the y-axis displays the -log of p-value, calculated by Fisher's exact test right-tailed. The majority of the genes, belonging to these categories, showed an opposite expression between the melanocyte and melanoma samples, as a result of being specifically up-regulated in the two melanoma cell lines compared to control (Fig. 1B). In particular, genes involving Ran signaling were significantly over-represented ($p \leq 0.001$) and up-regulated in both melanoma cell lines (Fig. 1C).

To further confirm the IPA pathway analysis results, we performed a GSEA based on c4 computational gene sets, defined by mining large collections of cancer-oriented microarray data (Appendix: Supplementary Table S2). Using the gene list reported in Appendix: Supplementary Table S1, we found 80/92 gene sets up-regulated in phenotype MEL; 56 gene sets were significant at a false discovery rate (FDR) < 25%; 22 gene sets were significantly enriched at nominal p-value < 1%; and 45 gene sets were significantly enriched at nominal p-value < 5%. Enrichment of genes involved in Ran signaling was observed in the melanoma cell lines compared with melanocytes, supporting the IPA findings.

Interestingly, molecules involved in the Ran signaling pathway have been previously reported to be differentially expressed in many human cancers, such as colon adenocarcinoma, prostate adenocarcinoma, renal cell carcinoma, breast adenocarcinoma, lung carcinoma and bladder transitional cell carcinoma [14]. Moreover, Ran overexpression in stably transfected cells has been reported to trigger an oncogenic transformation indicating that Ran up-regulation is involved in the loss of cellular growth control [15]. Here, we found RanBP1 and RCC1 molecules up-regulated in both melanoma cell lines (Fig. 1C).

Functional connections among Ran and genes in microarray dataset

In order to identify functional connections among Ran members and other genes present in our dataset, IPA pathway analysis was performed to correlate molecules that met different criteria (type of molecules, tissues and cells, diseases etc.) starting from molecules of interest. AurkA, c-myc, PTEN (Phosphatase and Tensin homolog on chromosome TEN) and TERT (Telomerase Reverse Transcriptase) genes were connected by a functional relationship (Fig. 2).

To independently validate the transcriptional signatures obtained from microarray analysis, we analyzed the expression of these genes using qRT-PCR and Western blot. The qRT-PCR data confirmed the expression values detected by microarray for all genes (Table 1) present in the pathway (Fig. 2). InWestern blot analysis, a high level of expression of AurkA and Ran was observed in both melanoma cell lines compared to melanocytes (Fig. 3A).

Both Ran and AurkA gene expression was also investigated in 113 tissue samples derived from metastatic melanoma patients. We detected Ran in about 48% and AurkA in about 53% of samples (Fig. 3B). A strong correlation was observed between expressions of the two genes, which is expected given that AurKA is a Ran effector molecule [16].

To further confirm AurkA as one of downstream targets of Ran signaling in melanoma, Ran expression was silenced by means of small interfering RNA technology (siRNA), as described in Materials and Methods. Then, the Ran silencing effects on the AurkA expression, on cell survival and on invasion capability of both melanoma cell lines were examined. We observed a reduction in AurkA expression in both melanoma cell lines upon Ran silencing (Fig. 3C). A reduction of cell proliferation was also detected in Ran silenced A375 and 526 cells compared to the non-silenced ones (Fig. 3D).

This finding may be the result of a cancer cell mitosis reduction, as previously reported [14]. Ran silencing was confirmed analyzing Ran protein levels by western blot, as showed in Fig. 3C.

We also examined the effect of Ran silencing on the invasive capability of these melanoma cell lines. Using an invasion assay, enhanced invasive ability of 526 melanoma cells was observed compared with A375 after Ran blocking (Fig. 3E). This finding is in contrast with data previously reported [17,18], and suggests Ran

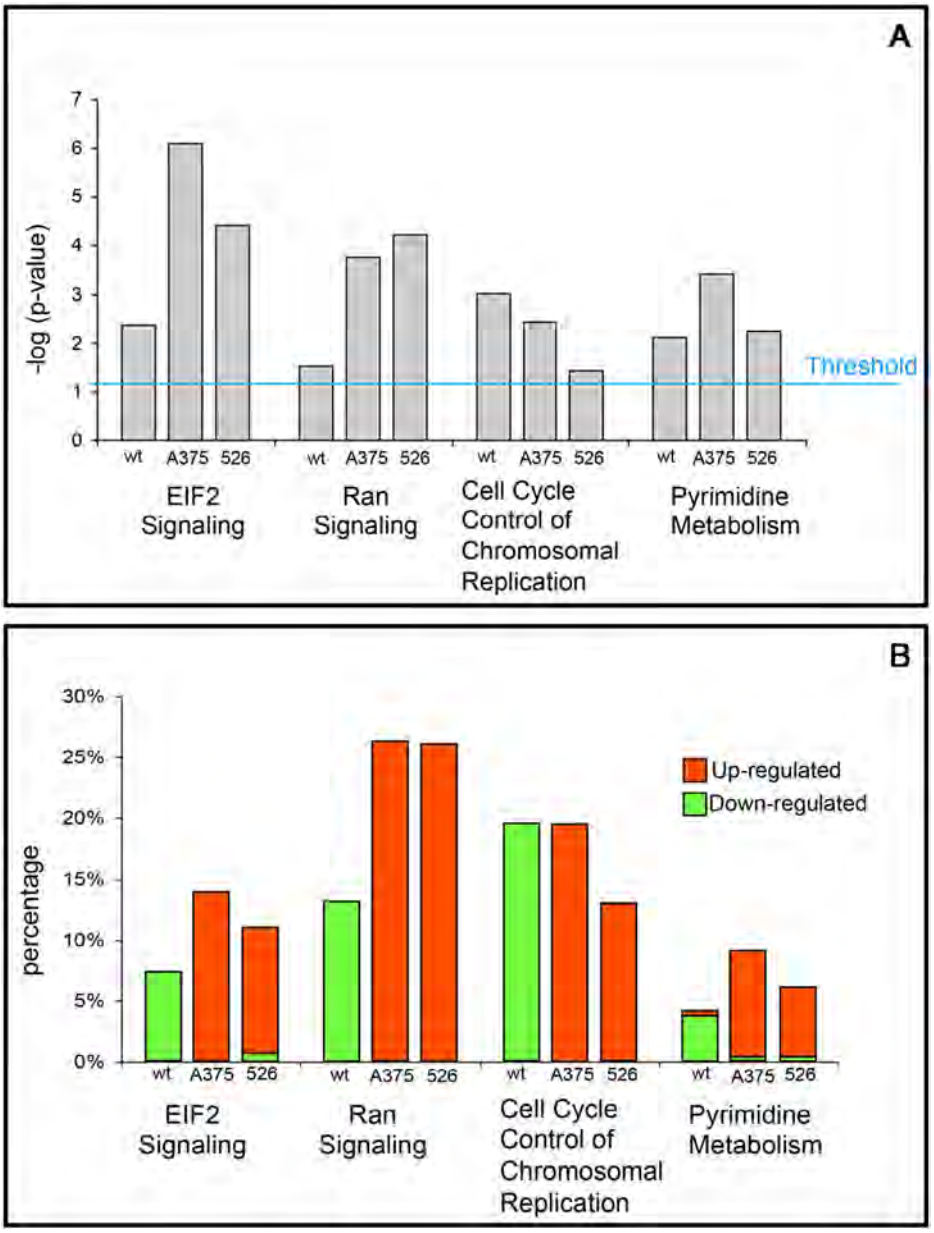

Fig. 1. The most significant canonical pathways across the melanocyte (FOM78) and two melanoma cell lines (A375, 526), detected by Ingenuity. (A). Details of the number of up-regulated or down-regulated molecules in each canonical pathway for all the analyzed cell lines (B). IPA Ran signaling canonical pathway with the relative gene expression (red up-regulated; green down-regulated) in melanocytes and melanoma cell lines. The analysis showed that most of examined genes had a strong association with EIF2 Signaling, Ran Signaling, Cell Cycle Control of Chromosomal Replication and Pyrimidine Metabolism (C). The shape of the node indicated the function of the protein. The line denotes binding between two proteins, while the line with an arrow indicates an 'action on' of a molecule. A dotted line was used to indicate an indirect action. (For interpretation of the references to color in this figure legend, the reader is referred to the web version of this article.)

independent mechanisms are involved in the invasive capability of melanoma cells.

Other genes included in the pathway with an opposite expression in melanocyte and melanoma cells were found associated with melanoma aggressiveness. In particular, the loss of PTEN has been related to the E- to N-cadherin profile switching, described during melanoma progression [19]. TERT expression up-regulation has been previously reported to be related to mutations in the promoter region, causing an increase of its activity. It has also been described in familiar and sporadic melanomas [20] and its amplification has been observed to be associated with poor outcome in acral lentiginous melanoma [21].

Exposure of melanoma cells to MLN8054, a specific AurkA inhibitor

AurkA inhibition has been shown to limit tumor growth, impair mitosis and induce senescence in melanoma, suggesting a potential therapeutic role [22]. Recently, we demonstrated the antitumor effects of an Aurk A inhibitor, as single agent and/or in various combinations with B-RAF and MEK inhibitors in a B-RAF (V600E) mutated human melanoma cell line (A375) and a three-dimensional (3D) human skin reconstruction model [23].

Both melanoma cell lines, expressing high levels of AurkA, were exposed to the AurkA inhibitor MLN8054 at different concentrations for 72 hours. As shown in Fig. 4A, both cell lines had an

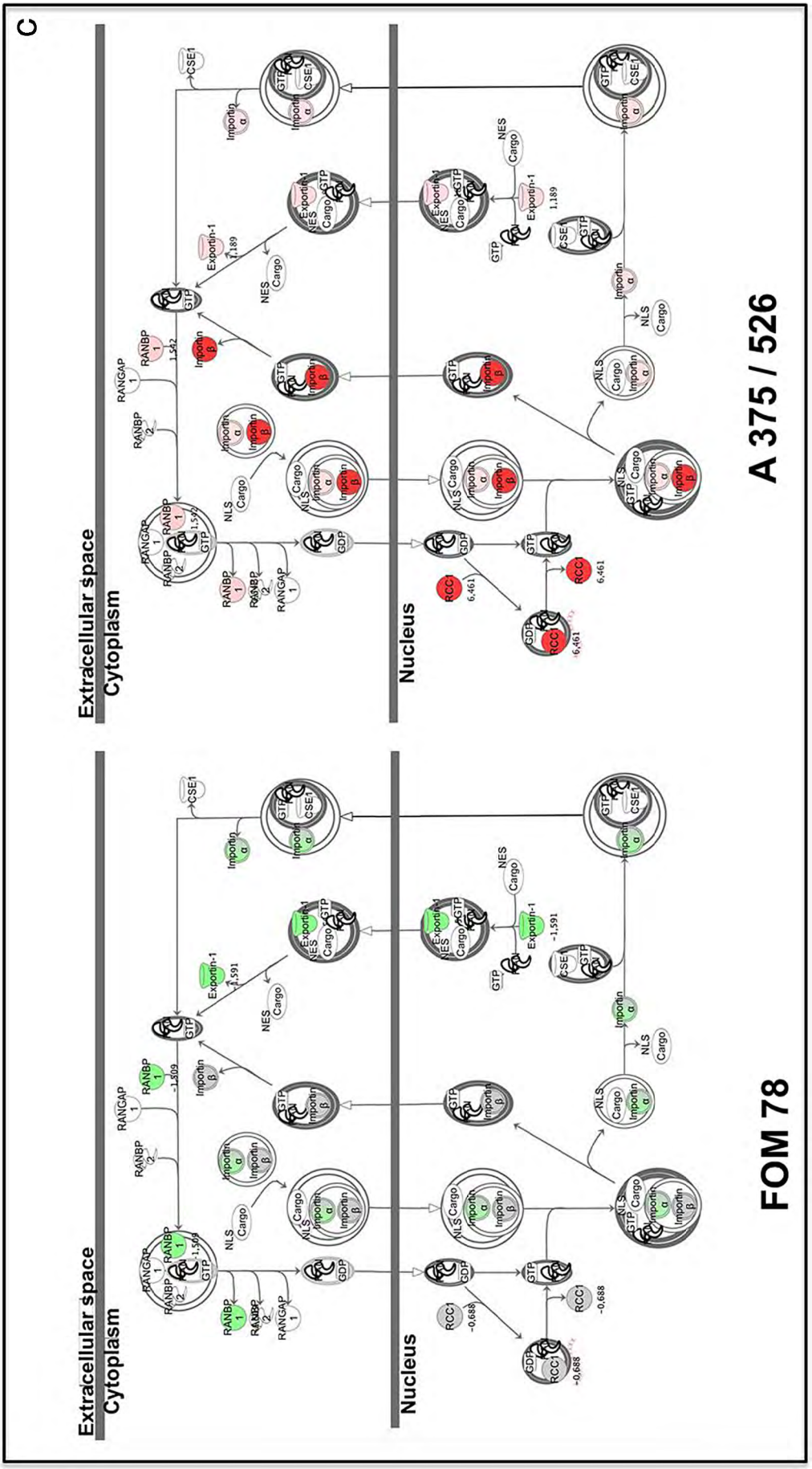

Fig. 1. (*continued*)

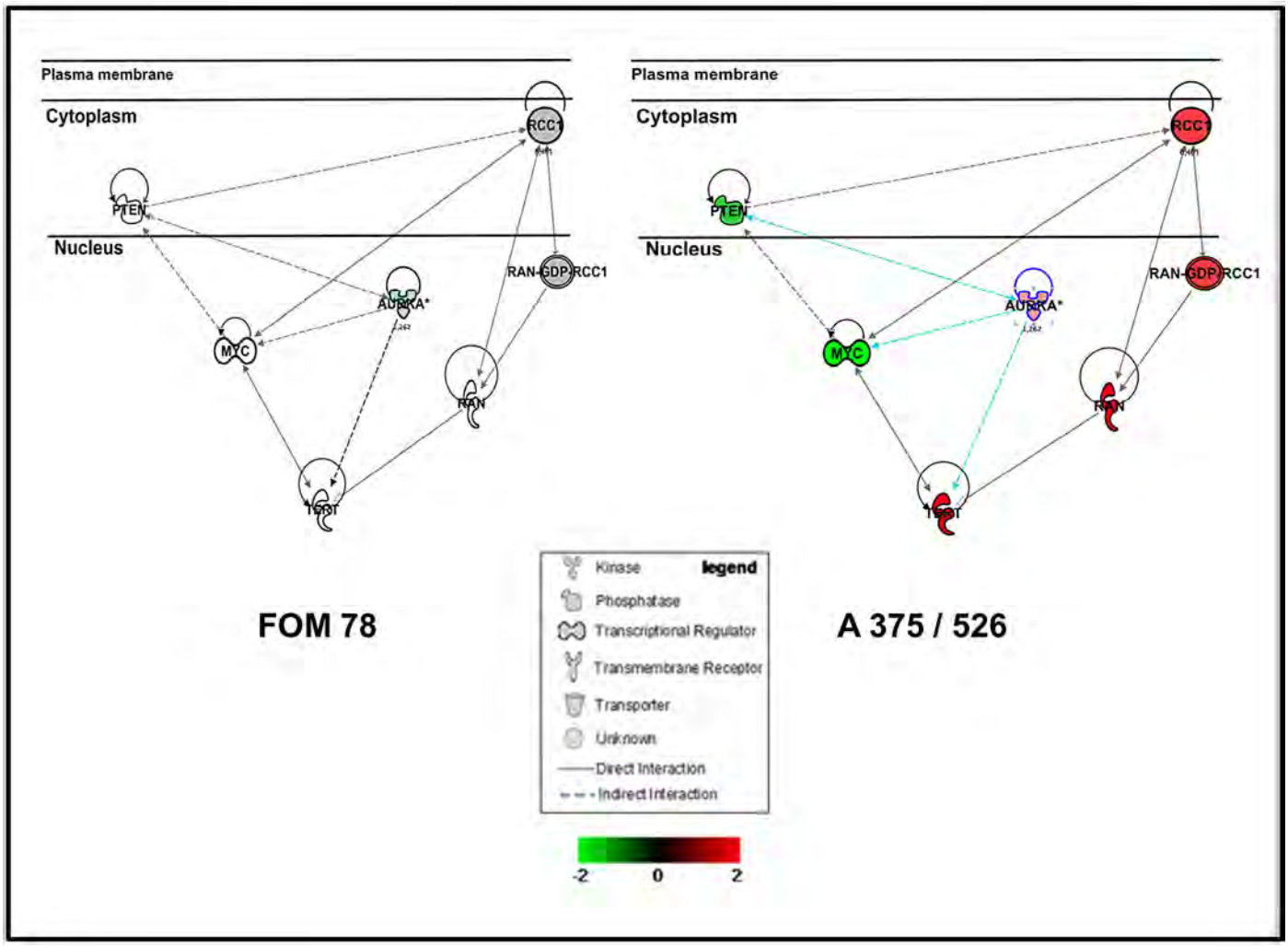

Fig. 2. IPA functional pathway analysis. AurKA functional relationship with other differentially expressed genes observed in melanocytes (FOM78) and in melanoma cell lines (A375 and 526). For each gene the relationship and the expression (red up-regulated; green down-regulated) are shown. Arrows indicate the direction of the relationship. (For interpretation of the references to color in this figure legend, the reader is referred to the web version of this article.)

approximately 60% survival on exposure to MLN8054 at 1 μM concentration. To further investigate the cytotoxic effect of MLN8054 on melanoma cells, we investigated PARP cleavage by Western blot. A PARP cleavage in both cell lines exposed to MLN8054 at 1 μM concentration was seen, although the timing was different, being observed at 24 hours in A375 cells and 48 hours in 526 cells (Fig. 4B). This finding suggested that both melanoma cell types were induced to undergo apoptosis following exposure to MLN8054.

To confirm that MLN8054 was inhibiting AurkA protein, we analyzed p53 protein level, a downstream target molecule of AurkA. p53 has been reported to be phosphorylated by AurkA, leading to its ubiquitination and proteolysis [24]. As expected, p53 protein level was increased at 72 hours in both cell lines exposed to MLN8054 (Fig. 4C). We also analyzed p53 DNA sequence, identifying a single base pair substitution at codon 72 in the exon 4. This substitution is responsible for one amino acidic residue change from Pro (CCC) to Arg (CGC) in heterozygosis in the A375 cell line. No mutations in the p53 gene were observed in the 526 cell line.

Since both melanoma cell lines carried the B-RAF V600E mutation, we also tested if AurkA inhibitor had a cytotoxic effect in SK23Mel, a B-RAF wild-type melanoma cell line. We found that MLN8054 action was independent of B-RAF mutational status (Fig. 4D), suggesting its potential in all melanomas over-expressing AurkA irrespective of B-RAF status.

Table 1
Gene validation by RT-PCR primer sequences.

Gene	Description	Fold change		q-PCR	
		A375	*526*	*A375*	*526*
AURKA	Aurora kinase A	1951	1262	3320	4679
MYC	v-myc myelocytomatosis viral oncogene homolog (avian)	–4569	–10,053	–4832	–6209
PTEN	Phosphatase and tensin homolog	–2288	–1080	–2453	–1873
RAN	RAN, member RAS oncogene family	7545	5045	10,560	7453
RCC1	Regulator of chromosome condensation 1	6563	6461	6870	5904
TERT	Telomerase reverse transcriptase	7359	5306	8402	6004

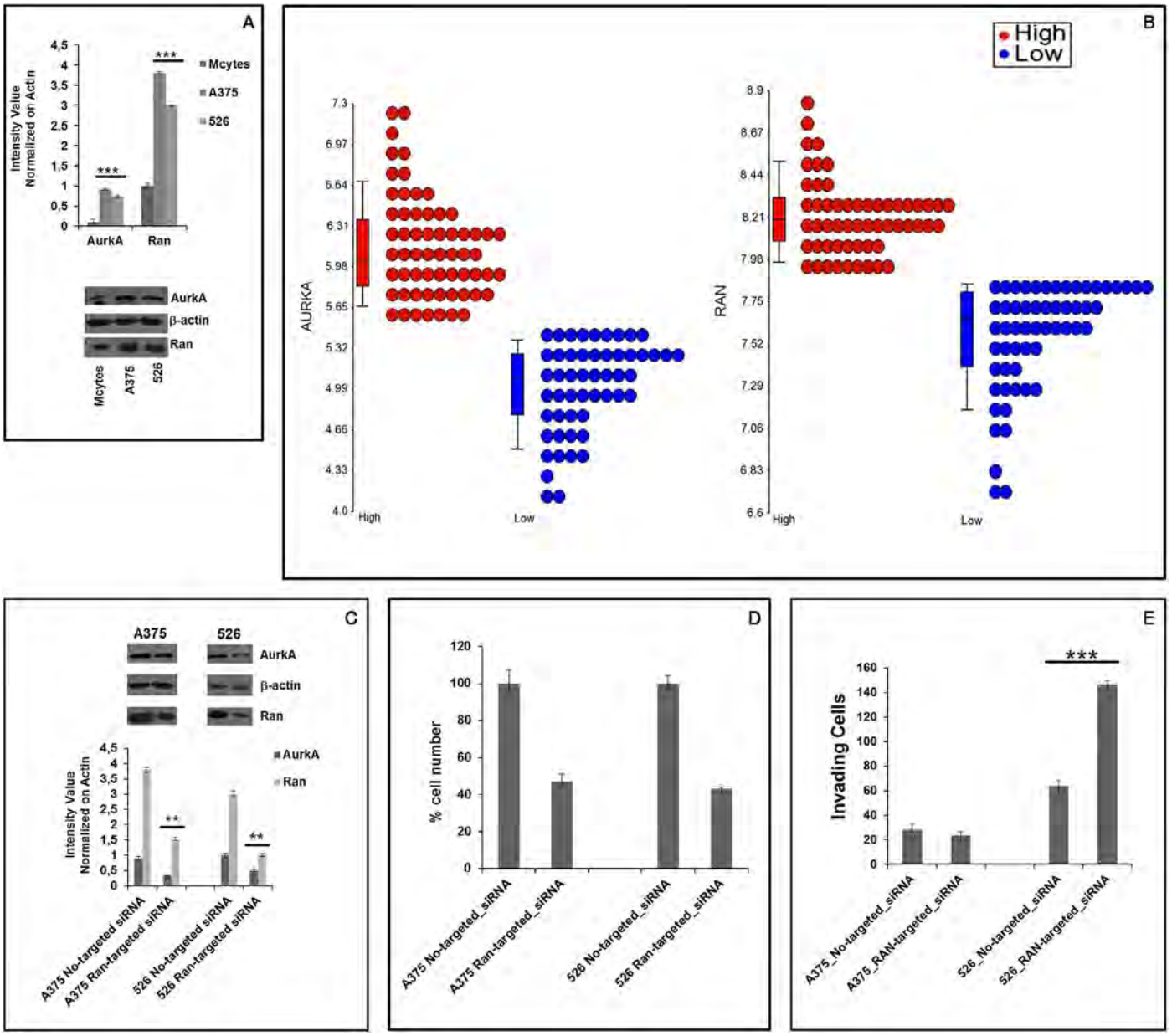

Fig. 3. Western blot analysis of AurkA and Ran in melanoma cells and melanocytes (A); dot plot showing differential distribution of AurkA and Ran gene intensities across 113 melanoma tissue samples. High intensities red dots, low intensities blue dots (B). Western blot analysis of AurkA and Ran expression in melanoma cells after Ran silencing (C). Melanoma cell proliferation analysis after Ran silencing (D). Invasive capability analysis of melanoma cell lines after Ran silencing. The percentages of invading (t = 16 hours) cells were calculated as reported in Materials and Methods. The pictures highlight the differences in cell number between control no-targeted and Ran-directed siRNA oligonucleotides melanoma transfected cells, able to invade to the lower surface of transwells (E). (For interpretation of the references to color in this figure legend, the reader is referred to the web version of this article.)

Since the V600E mutations in B-RAF are known to activate MEK, we also monitored MEK activation upon B-RAF inhibition by treating B-RAF mutated and wild-type melanoma cell lines with a B-RAF inhibitor. A decrease in the activated MEK1/2 protein level in both B-RAF-mutated melanoma cell lines exposed to B-RAF inhibitor was observed, while MEK activation was not altered in B-RAF wild-type melanoma cells (Fig. 4E).

Molecular pathway analysis of melanoma cells exposed to MLN8054

To investigate the effect of MLN8054 on the expression of genes involved in the above described molecular pathway, we analyzed c-myc, PTEN, AurkA, TERT and RCC1 molecules by Western blot and/or qRT-PCR. An increased c-myc protein level was observed in 526 melanoma cells, while a slight reduction was noted in A375 cells (Fig. 5A). It has previously been demonstrated that c-myc is involved in cancer cell invasion ability [25]. Our findings suggest that Ran knockdown was not sufficient to inhibit cell invasion in melanoma cells since the signaling triggered by Ran silencing through the AurkA down-regulation resulted in a stable and/or increased c-myc protein level in A375 and 526 melanoma cell lines, respectively, suggesting a c-myc-dependent and Ran-independent invasion mechanism in melanoma. In addition, an increased PTEN level was observed in both cell lines, with reduced AurkA and TERT mRNA level in 526 melanoma cells only, as shown in Fig. 5B. A decrease in TERT protein level was also observed in 526 melanoma cells by western blot, while no significant change was found in A375 cells (Fig. 5C).

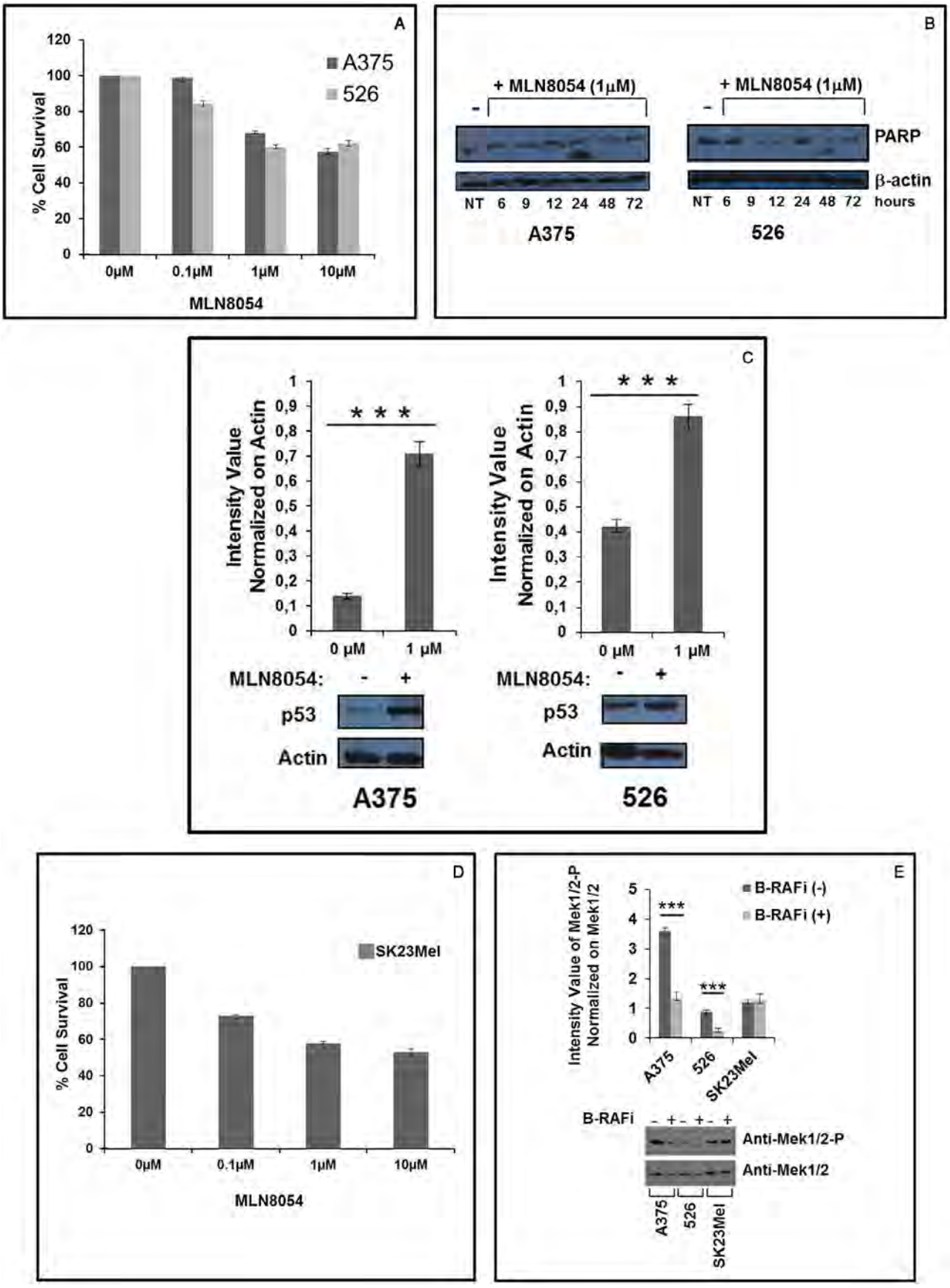

Fig. 4. Melanoma cell analysis on exposure to MLN8054. Cell viability analysis of A375 and 526 melanoma cells treated with MLN8054 (A). Western blot analysis of PARP (B) and of p53 (C) in melanoma cells upon MLN8054 treatment. *** indicates *P*-value ≤0.005. Cell viability analysis of SK23-Mel cells treated with MLN8054 (D). MEK activation analysis of melanoma cells, carrying and not-carrying B-RAF (V600E) mutation, upon treatment with B-RAF inhibitor (E).

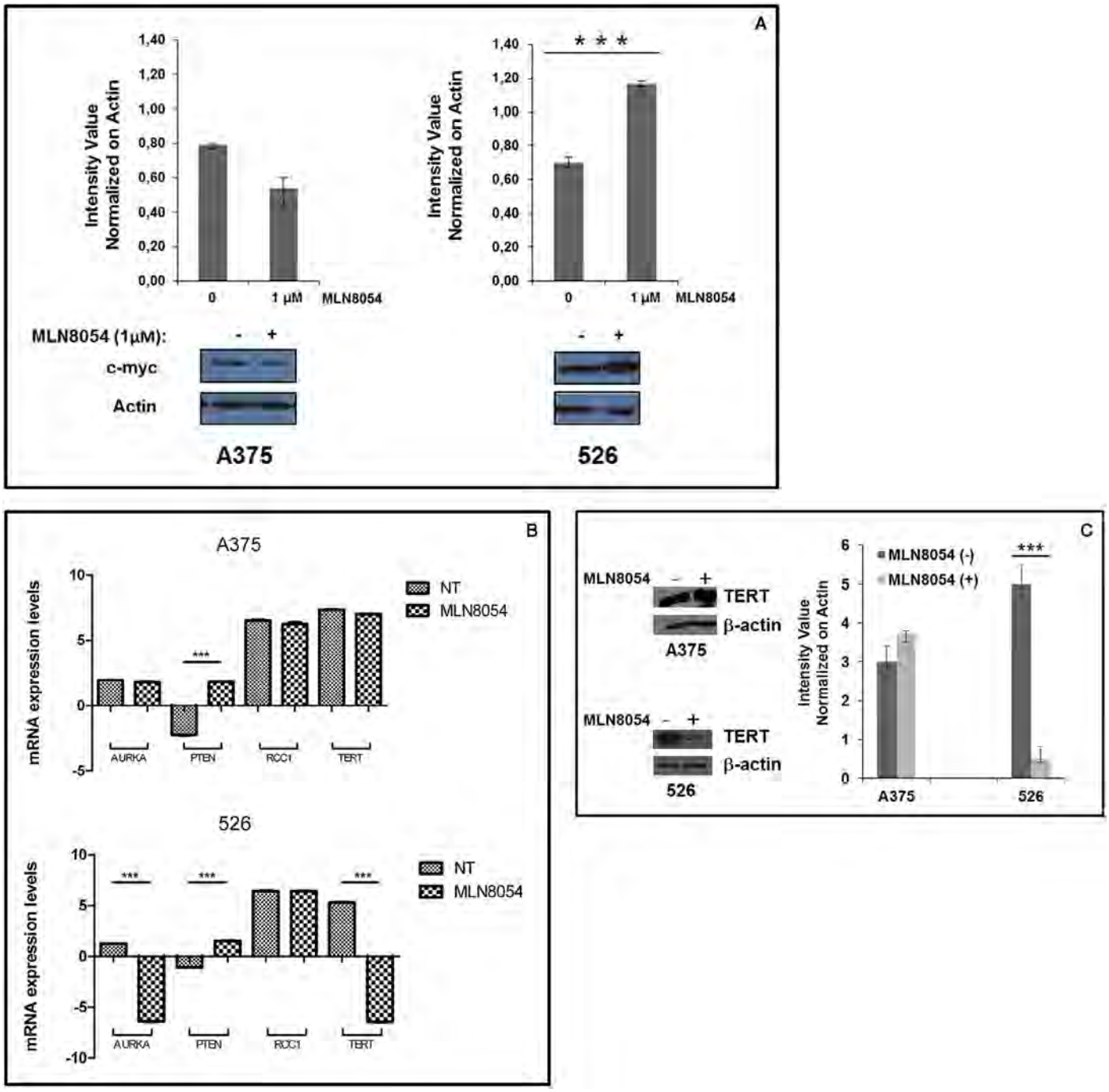

Fig. 5. AurkA, PTEN, c-myc, RCC1 and TERT analysis in melanoma cells on exposure to MLN8054 and MLN8054 cytotoxic effect on B-RAF wild-type melanoma cell line. Western blot analysis of c-myc in melanoma cells on exposure to MLN8054 (A). mRNA expression levels of AurkA, PTEN, RCC1 and TERT genes in A375 and 526 cells non-treated (NT) and MLN8054 Treated (MLN8054) (B). TERT protein level analysis in melanoma cells on exposure to MLN8054 (C).

These data suggest that, although MLN8054 showed a similar cytotoxic effect on both melanoma cell lines, the molecular mechanisms, underlining the cellular response to the treatment were different and dependent on the heterogeneity of cancer cells.

Discussion

Melanoma is characterized by chemo-resistance, aggressive clinical behavior and high metastatic spreading. Understanding the biological differences between normal and cancer cells is critical for the study of this malignancy since it will help enable the design of therapies that selectively kill cancer cells without toxicity to normal cells.

In this study, we described the molecular characterization of two melanoma cell lines with a melanocyte cell line as control, through the use of a combination of microarray and GSEA/IPA software analysis. Both of the melanoma cell lines, A375 and 526, have been reported to be positive for HLA-A2 phenotype but differ in the expression of the melanoma-associated antigens (MAAs), MART-1/Melan A and PMel 17/gp100, with 526 cells showing high expression of both MAAs compared to the A375 cells [8]. These melanoma cells were characterized for their B-RAF mutational status, with a

homozygous mutation in A375 cells and a heterozygous mutation in 526 cells detected at the V600E site (data not shown), although this is not concordant with a previously published report [26].

Gene expression analysis with IPA software provided interesting data on the potential proteins and molecular pathways associated with melanoma. Genes involved in the Ran signaling pathway were significantly over-represented and over-expressed in both melanoma cell lines compared with melanocytes. The GTPase Ran protein is one of the four key components (CRM1/Exportin 1, RAN/RAN-GTPase, RANGAP1, and RANBP1) of the nucleocytoplasmic transport machinery [27–29]. In melanoma, a deregulation of nucleocytoplasmic transport has recently been reported with a consequent Erk cellular mislocalization, leading to an Erk aberrant cytoplasmic/prosurvival activity [27]. Interestingly, all the other nucleocytoplasmic transport component genes included in our dataset were found to be up-regulated in both melanoma cell lines. This finding confirms a deregulation of nucleocytoplasmic transport in melanoma, supporting an additional mechanism of enhanced cytoplasmic accumulation of several proteins that is adopted by cancer cells to achieve proliferative potential [30].

In addition, Ran plays a direct role in mitosis, by promoting bipolar spindle assembly [31] through a group of effector proteins, including several microtubule-associated proteins (TPX2, NuMA, NuSAP and HURP), kinesin 5 and AurkA [32]. Interestingly, in addition to over-expression of AurkA, a kinesin family member (KIF 1B) was also observed to be over-expressed in melanoma cell lines. AurkA is one member of a serine/threonine kinase family, which comprises three elements (AurK A, B, and C) that are essential components of the mitotic pathway [32]; they ensure the proper chromosome assembly, the formation of the mitotic spindle, and cytokinesis. Over-expression of these kinases has been observed in several tumor types, including colon, breast, prostate, pancreas, thyroid, and head and neck, and is associated with advanced clinical stage and poor prognosis [33–36].

We demonstrated that components of the mitotic pathways, Ran and AurkA, were highly expressed in tissue specimens deriving from patients with metastatic melanoma. Ran was detected in about 48% and AurkA in 53% of the 113 tissue samples analyzed. As expected, given that AurkA is a Ran effector, the two genes showed a coordinated expression in melanoma tissue samples, assessed through mRNA profiling. The molecular pathway built by the IPA software tool, where Ran and AurkA were involved, also showed functional connections with c-myc, PTEN and TERT; c-myc and PTEN were down-regulated while TERT was up-regulated in both melanoma cell lines compared to melanocytes [21]. PTEN allele loss has previously been reported in at least 58% of melanoma metastases [37].

AurkA alone is not a potent inducer of cellular transformation and additional oncogenic events, such as Ras activation, which are needed to reveal the oncogenic potential of the cells. However, evidence of its deregulated expression in tumorigenesis and its established role in mitosis suggests that inhibiting these kinases may constitute the basis for the development of powerful anti-cancer strategies in many tumors, including melanoma [38]. Several small-molecules have already been developed as AurkA inhibitors [38–40] and we recently demonstrated the potential of AurkA inhibitors in the treatment of melanoma [23].

We also found that melanoma cells had a PARP cleavage following exposure to the AurkA inhibitor, MLN8054, suggesting apoptosis in both cell lines, although the timings were different. Treatment of melanoma cell lines with AurkA inhibitors has previously been reported to induce an up-regulation of its downstream target p53 [24], indicating that these inhibitors could regulate cancer cell survival in a p53-dependent manner, although the reduced cell viability that we observed in SK23Mel, a homozygous p53-mutant strain, upon exposure to MLN8054 did not exclude a p53-independent cell death regulation.

Changes in mRNA level of genes involved in the above identified pathway were studied upon MLN8054 exposure. A significant PTEN up-regulation was detected in both melanoma cell lines, suggesting that it may inhibit proliferation following AKT inactivation [41,42]. However, further experiments need to be performed in other melanoma cells to address this issue and the involvement of other molecular pathways, e.g. NF-kB, cannot be excluded [43].

More interestingly, down-regulation of AurkA and TERT mRNAs was observed in 526 melanoma cells but not in A375, suggesting different molecular mechanisms triggered by MLN8054 exposure in the different cell types. Exposure to MLN8054 also resulted in increased c-myc protein level in 526 melanoma cells and a slight reduction in A375 cells, suggesting AurkA inhibition may interfere with MAPK molecular signaling in A375 melanoma cells only. Ran silencing induced AurkA down-regulation as well as reduced proliferation of both melanoma cell lines, supporting the potential role of Ran and AurkA as targets for melanoma treatment as previously reported ([14], [23], [44]). Ran silencing also induced increased invasive capability in the 526 melanoma cell lines but not in A375 cells. This finding is in contrast with data previously reported [17,18], and suggests a secondary role for Ran in the invasive properties of melanoma. It has been recently reported that c-myc plays a key role in enhancing the invasive capability of hepatocellular carcinoma cells [25], suggesting that the increase of the 526 cell invasive capability was Ran-independent and may be c-myc-dependent, although further experiments are needed to address this issue.

Finally, the finding that SK23Mel, a B-RAF wild-type melanoma cell line, was sensitive to treatment with AurKA inhibitor suggested its possible role in the treatment of melanoma without B-RAF mutations. Our data showed the potential of AurkA and of the components of the nucleocytoplasmic transport machinery as targets for personalized therapy in melanoma. This finding, if confirmed, could result in a further possible option for personalized therapy in melanoma, alongside treatments targeting BRAF [45] and c-KIT [46]. These targeted therapies offer an alternative to conventional chemotherapy, which has been disappointingly ineffective [47,48]. Our findings highlight the need for larger studies involving other melanoma cell lines that could lead to the identification of genes and pathways involved in the clinical progression of disease and the discovery of new markers for early diagnosis, helping to transform care through a personalized approach.

Acknowledgments

The authors wish to thank Dr. E.J. Patriarca for his critical comments. AV was supported by BIAM EPI-FORM “Ricerca e Competitività” 2007–2013. This work was supported by a subgrant (1 R21DK070192-01) to EC from NIH NIDDK.

Conflict of interest

All authors have disclosed no financial competing interests. PAA has/had a consultant/advisory role for Bristol Myers-Squibb, Roche-Genentech, Merck Sharp & Dohme, GlaxoSmithKline, Ventana, and Novartis. He received research funds from Bristol Myers-Squibb, Roche-Genentech, and Ventana. He also received honoraria from Bristol Myers-Squibb, Roche-Genentech, and GlaxoSmithKline.

Appendix: Supplementary material

Supplementary data to this article can be found online at doi:10.1016/j.canlet.2014.11.033.

References

[1] A. Jemal, R. Siegel, E. Ward, Y. Hao, J. Xu, M.J. Thun, Cancer statistics, CA Cancer J. Clin. 59 (2009) 225–249.
[2] E.L. Korn, P.Y. Liu, S.J. Lee, J.A. Chapman, D. Niedzwiecki, V.J. Suman, et al., Meta-analysis of phase II cooperative group trials in metastatic stage IV melanoma to determine progression-free and overall survival benchmarks for future phase II trials, J. Clin. Oncol. 26 (2008) 527–534.
[3] C. Cohen, A. Zavala-Pompa, J.H. Sequeira, M. Shoji, D.G. Sexton, G. Cotsonis, et al., Mitogen-activated protein kinase activation is an early event in melanoma progression, Clin. Cancer Res. 8 (2002) 3728–3733.
[4] M.S. Brose, P. Volpe, M. Feldman, M. Kumar, I. Rishi, R. Gerrero, et al., BRAF and RAS mutations in human lung cancer and melanoma, Cancer Res. 62 (2002) 6997–7000.
[5] H. Davies, G.R. Bignell, C. Cox, P. Stephens, S. Edkins, S. Clegg, et al., Mutations of the BRAF gene in human cancer, Nature 417 (2002) 949–954.
[6] P.T. Wan, M.J. Garnett, S.M. Roe, S. Lee, D. Niculescu-Duvaz, V.M. Good, et al., Mechanism of activation of the RAF-ERK signaling pathway by oncogenic mutations of B-RAF, Cell 116 (2004) 855–867.
[7] D. Dankort, D.P. Curley, R.A. Cartlidge, B. Nelson, A.N. Karnezis, W.E. Damsky Jr., et al., Braf(V600E) cooperates with Pten loss to induce metastatic melanoma, Nat. Genet. 41 (2009) 544–552.
[8] J.N. Cormier, M.C. Panelli, J.A. Hackett, M.P. Bettinotti, A. Mixon, J. Wunderlich, et al., Natural variation of the expression of HLA and endogenous antigen modulates CTL recognition in an in vitro melanoma model, Int. J. Cancer 80 (1999) 781–790.
[9] M. Herlyn, J. Thurin, G. Balaban, J.L. Bennicelli, D. Herlyn, D.E. Elder, et al., Characteristics of cultured human melanocytes isolated from different stages of tumor progression, Cancer Res. 45 (1985) 5670–5676.
[10] E. Wang, L. Miller, G.A. Ohnmacht, E. Liu, F.M. Marincola, High fidelity mRNA amplification for gene profiling using cDNA microarrays, Nat. Biotechnol. 17 (2000) 457–459.
[11] E. Wang, RNA amplification for successful gene profiling analysis, J. Transl. Med. 3 (2005) 28.
[12] R. Simon, A. Lam, M.C. Li, M. Ngan, S. Menenzes, Y. Zhao, Analysis of gene expression data using BRB-array tools, Cancer Inform. 2 (2007) 11–17.
[13] S. Crispi, R.A. Calogero, M. Santini, P. Mellone, B. Vincenzi, G. Citro, et al., Global gene expression profiling of human pleural mesotheliomas: identification of matrix metalloproteinase 14 (MMP-14) as potential tumour target, PLoS ONE 4 (2009) e7016.
[14] F. Xia, C.W. Lee, D.C. Altieri, Tumor cell dependence on Ran-GTP-directed mitosis, Cancer Res. 68 (2008) 1826–1833.
[15] T.K. Ly, J. Wang, R. Pereira, K.S. Rojas, X. Peng, Q. Feng, et al., Activation of the Ran GTPase is subject to growth factor regulation and can give rise to cellular transformation, J. Biol. Chem. 285 (2010) 5815–5826.
[16] R.V. Silverman-Gavrila, A. Wilde, Ran is required before metaphase for spindle assembly and chromosome alignment and after metaphase for chromosome segregation and spindle midbody organization, Mol. Biol. Cell 17 (2006) 2069–2080.
[17] H.-F. Yuen, V.-K. Gunasekharan, K.-K. Chan, S.-D. Zhang, A. Platt-Higgins, K. Gately, et al., RanGtPase: a candidate for Myc-mediated cancer progression, J. Natl. Cancer Inst. 105 (2013) 475–488.
[18] L. Deng, Y. Shang, S. Guo, C. Liu, L. Zhou, Y. Sun, et al., Ran GTPase protein promotes metastasis and invasion in pancreatic cancer by deregulating the expression of AR and CXCR4, Cancer Biol. Ther. 15 (2014) 1087–1093.
[19] L. Hao, J.R. Ha, P. Kuzel, E. Garcia, S. Persad, Cadherin switch from E- to N-cadherin in melanoma progression is regulated by the PI3K/PTEN pathway through Twist and Snail, Br. J. Dermatol. 166 (2012) 1184–1197.
[20] S. Horn, A. Figl, P.S. Rachakonda, C. Fischer, A. Sucker, A. Gast, et al., TERT promoter mutations in familial and sporadic melanoma, Science 339 (2013) 959–961.
[21] A. Diaz, J.A. Puig-Butillé, C. Muñoz, D. Costa, A. Díez, A. Garcia-Herrera, et al., TERT gene amplification is associated with poor outcome in acral lentiginous melanoma, J. Am. Acad. Dermatol. 71 (2014) 839–841.
[22] Y. Liu, O.E. Hawkins, Y. Su, A.E. Vilgelm, T. Sobolik, Y.M. Thu, et al., Targeting aurora kinases limits tumour growth through DNA damage-mediated senescence and blockade of NF-κB impairs this drug-induced senescence, EMBO Mol. Med. 5 (2013) 149–166.
[23] E. Caputo, R. Miceli, M.L. Motti, R. Taté, F. Fratangelo, G. Botti, et al., AurkA inhibitors enhance the effects of B-RAF and MEK inhibitors in melanoma treatment, J. Transl. Med. 12 (2014) 216.
[24] H. Katayama, K. Sasai, H. Kawai, Z.M. Yuan, J. Bondaruk, F. Suzuki, et al., Phosphorylation by aurora kinase A induces Mdm2-mediated destabilization and inhibition of p53, Nat. Genet. 36 (2004) 55–62.
[25] Y. Zhao, W. Jian, W. Gao, Y.-X. Zheng, Y.-K. Wang, Z.-Q. Zhou, et al., RNAi silencing of c-Myc inhibits cell migration, invasion, and proliferation in HepG human hepatocellular carcinoma cell line: c-Myc silencing in hepatocellular carcinoma cell, Cancer Cell Int. 13 (2013) 23.
[26] H. Sumimoto, M. Miyagishi, H. Miyoshi, S. Yamagata, A. Shimizu, K. Taira, et al., Inhibition of growth and invasive ability of melanoma by inactivation of mutated BRAF with lentivirus-mediated RNA interference, Oncogene 23 (2004) 6031–6039.
[27] G. Pathria, C. Wagner, S.N. Wagner, Inhibition of CRM1-mediated nucleocytoplasmic transport: triggering human melanoma cell apoptosis by perturbing multiple cellular pathways, J. Invest. Dermatol. 132 (2012) 2780–2790.
[28] W.Y. Huang, L. Yue, W.S. Qiu, L.W. Wang, X.H. Zhou, Y.J. Sun, Prognostic value of CRM1 in pancreas cancer, Clin. Invest. Med. 32 (2009) E315.
[29] P.J. van der Watt, C.P. Maske, D.T. Hendricks, M.I. Parker, L. Denny, D. Govender, et al., The Karyopherin proteins, Crm1 and Karyopherin beta1, are overexpressed in cervical cancer and are critical for cancer cell survival and proliferation, Int. J. Cancer 124 (2009) 1829–1840.
[30] J.G. Turner, D.M. Sullivan, CRM1-mediated nuclear export of proteins and drug resistance in cancer, Curr. Med. Chem. 15 (2008) 2648–2655.
[31] O.J. Gruss, R.E. Carazo-Salas, C.A. Schatz, G. Guarguaglini, J. Kast, M. Wilm, et al., Ran induces spindle assembly by reversing the inhibitory effect of importin alpha on TPX2 activity, Cell 104 (2001) 83–93.
[32] G. Vader, S.M. Lens, The Aurora kinase family in cell division and cancer, Biochim. Biophys. Acta 1786 (2008) 60–72.
[33] H.T. Xu, L. Ma, F.J. Qi, Y. Liu, J.H. Yu, S.D. Dai, et al., Expression of serine threonine kinase 15 is associated with poor differentiation in lung squamous cell carcinoma and adenocarcinoma, Pathol. Int. 56 (2006) 375–380.
[34] R. Reiter, P. Gais, U. Jütting, M.K. Steuer-Vogt, A. Pickhard, K. Bink, et al., Aurora kinase A messenger RNA overexpression is correlated with tumor progression and shortened survival in head and neck squamous cell carcinoma, Clin. Cancer Res. 12 (2006) 5136–5141.
[35] N. Nishida, T. Nagasaka, K. Kashiwagi, C.R. Boland, A. Goel, High copy amplification of the Aurora-A gene is associated with chromosomal instability phenotype in human colorectal cancers, Cancer Biol. Ther. 6 (2007) 525–533.
[36] Y. Nadler, R.L. Camp, C. Schwartz, D.L. Rimm, H.M. Kluger, Y. Kluger, Expression of Aurora A (but not Aurora B) is predictive of survival in breast cancer, Clin. Cancer Res. 14 (2008) 4455–4462.
[37] A. Birck, V. Ahrenkiel, J. Zeuthen, K. Hou-Jensen, P. Guldberg, Mutation and allelic loss of the PTEN/MMAC1 gene in primary and metastatic melanoma biopsies, J. Invest. Dermatol. 114 (2000) 277–280.
[38] O. Gautschi, P.C. Mack, A.M. Davies, P.N. Lara Jr., D.R. Gandara, Aurora kinase inhibitors: a new class of targeted drugs in cancer, Clin. Lung Cancer 8 (2006) 93–98 Review.
[39] T. Marumoto, S. Honda, T. Hara, M. Nitta, T. Hirota, E. Kohmura, et al., Aurora-A kinase maintains the fidelity of early and late mitotic events in HeLa cells, J. Biol. Chem. 278 (2003) 51786–51795.
[40] W. He, M.G. Zhang, X.J. Wang, S. Zhong, Y. Shao, Y. Zhu, et al., AURKA suppression induces DU145 apoptosis and sensitizes DU145 to docetaxel treatment, Am. J. Transl. Res. 5 (2013) 359–367.
[41] B.D. Manning, L.C. Cantley, AKT/PKB signaling: navigating downstream, Cell 129 (2007) 1261–1274.
[42] L. Salmena, A. Carracedo, P.P. Pandolfi, Tenets of PTEN tumor suppression, Cell 133 (2008) 403–414.
[43] H. Akca, A. Demiray, O. Tokgun, J. Yokota, Invasiveness and anchorage independent growth ability augmented by PTEN inactivation through the PI3K/AKT/NFkB pathway in lung cancer cells, Lung Cancer 73 (2011) 302–309.
[44] M.P. Simula, M.D. Marin, L. Caggiari, V. De Re, R. Cannizzaro, V. Canzonieri, Ran-GTP control of tumor cell mitosis. Cancer Res. 69 (2009) 1240.
[45] K.T. Flaherty, I. Puzanov, K.B. Kim, A. Ribas, G.A. McArthur, J.A. Sosman, et al., Inhibition of mutated, activated BRAF in metastatic melanoma, N. Engl. J. Med. 363 (2010) 809–819.
[46] R.D. Carvajal, P.B. Chapman, J.D. Wolchok, L. Cane, J.B. Teitcher, J. Lutzky, et al., A phase II study of imatinib mesylate (IM) for patients with advanced melanoma harboring somatic alterations of KIT, J. Clin. Oncol. 27 (2009) 15s.
[47] P.A. Ascierto, H.Z. Streicher, M. Sznol, Melanoma: a model for testing new agents in combination therapies, J. Transl. Med. 8 (2010) 38.
[48] U. McDermott, J. Settleman, Personalized cancer therapy with selective kinase inhibitors: an emerging paradigm in medical oncology, J. Clin. Oncol. 27 (2009) 5650–5659.

BMC Medical Genomics

RESEARCH ARTICLE Open Access

Validation of microarray data in human lymphoblasts shows a role of the ubiquitin-proteasome system and NF-*k*B in the pathogenesis of Down syndrome

Barbara Granese[1†], Iris Scala[1†], Carmen Spatuzza[2], Anna Valentino[1], Marcella Coletta[1], Rosa Anna Vacca[3], Pasquale De Luca[4] and Generoso Andria[1*]

Abstract

Background: Down syndrome (DS) is a complex disorder caused by the trisomy of either the entire, or a critical region of chromosome 21 (21q22.1-22.3). Despite representing the most common cause of mental retardation, the molecular bases of the syndrome are still largely unknown.

Methods: To better understand the pathogenesis of DS, we analyzed the genome-wide transcription profiles of lymphoblastoid cell lines (LCLs) from six DS and six euploid individuals and investigated differential gene expression and pathway deregulation associated with trisomy 21. Connectivity map and PASS-assisted exploration were used to identify compounds whose molecular signatures counteracted those of DS lymphoblasts and to predict their therapeutic potential. An experimental validation in DS LCLs and fetal fibroblasts was performed for the most deregulated GO categories, i.e. the ubiquitin mediated proteolysis and the NF-*k*B cascade.

Results: We show, for the first time, that the level of protein ubiquitination is reduced in human DS cell lines and that proteasome activity is increased in both basal conditions and oxidative microenvironment. We also provide the first evidence that NF-*k*B transcription levels, a paradigm of gene expression control by ubiquitin-mediated degradation, is impaired in DS due to reduced I*k*B-alfa ubiquitination, increased NF-*k*B inhibitor (I*k*B-alfa) and reduced p65 nuclear fraction. Finally, the DSCR1/DYRK1A/NFAT genes were analysed. In human DS LCLs, we confirmed the presence of increased protein levels of DSCR1 and DYRK1A, and showed that the levels of the transcription factor NFATc2 were decreased in DS along with a reduction of its nuclear translocation upon induction of calcium fluxes.

Conclusions: The present work offers new perspectives to better understand the pathogenesis of DS and suggests a rationale for innovative approaches to treat some pathological conditions associated to DS.

Keywords: Down syndrome, Trisomy 21, Expression, Ubiquitin-proteasome system, NF-*k*B

Background

Down syndrome (DS) (MIM 190685) is a human complex disorder caused by the trisomy of either the entire, or a critical region of chromosome (chr) 21 (21q22.1-22.3). DS phenotypes are often variable. Intellectual disability and hypotonia are the hallmarks of the syndrome, while a wealth of distinct clinical manifestations, including congenital malformations, increased incidence of cancer, immune and endocrine abnormalities occur only in subsets of DS subjects. DS is also characterized by premature aging and dementia with neurological features that mimic those found in Alzheimer's disease. The underlying molecular mechanisms of DS are largely unknown. Several genome-wide expression studies have been performed both in mouse and human trisomic tissues. While DS mice models have unravelled a generalized overexpression of triplicated genes [1-4], the analysis of human DS tissues

* Correspondence: andria@unina.it
†Equal contributors
[1]Department of Pediatrics, Federico II University, Naples 80131, Italy
Full list of author information is available at the end of the article

showed contradictory results. In fact, some studies reported the selective over-expression of a limited subset of chr 21 genes [5-9], and others described subtle upregulations of chr 21 genes associated to a secondary, generalized and more extreme transcriptional deregulation of genes mapping on other chromosomes [10-15]. An additional level of complexity comes from the observation that gene expression differs extensively among unaffected individuals [16-19], including the expression of a number of chr 21 genes [20,21]. Therefore, some authors suggested to regard as poor candidates for DS pathogenesis those genes with high expression variation among controls and as reliable candidates those genes over-expressed in DS and tightly regulated in euploid cells [21-23]. Gene expression studies failed to provide definitive results; however, evidence in human DS cells point to the presence of abnormalities of extracellular matrix, of mitochondrial function and other metabolic pathways, including purine metabolism, in fetal specimens [5,11,13], and changes in transcriptional regulation, oxidative stress and immune-related genes in adult tissues [6,12,14,24,25]. Recently, the effect of single chr 21 genes on the trisomic trancriptome was established by comparing the genome-wide expression from mouse ES cells, engineered to host the whole human chr 21, with those overexpressing only single chr 21 genes. A subset of genes, including Runx1, Erg, Nrip, Olig2, PdxK and Aire, produced the strongest transcriptional response when overexpressed [26]. More recently, Vilardell et al. [27] performed a meta-analysis from 45 publicly available DS data sets, from both human and mouse transcriptome and proteome. The identified biological functions were mainly related to nervous system development, neurodegenerative disorders (e.g. Huntington's disease, Alzheimer's disease and Parkinson's disease) and defects in synapsis function (e.g. axon guidance, NGF signalling). Seventy distinct transcription factors, including RelA, NFATc1, NFATc2 and NFATc3, were identified as being affected by dosage imbalance.

Besides genome-wide expression analysis, few studies attempted to identify selected gene networks associated to specific DS features and to characterize molecular and biochemical functions disrupted in DS. In mice, Arron et al. [28] found that two critical chr 21 genes (DYRK1A and DSCR1, also known as RCAN1) act synergistically to control the nuclear localization of NFAT family of transcription factors and that knock-out mice for NFATc1, NFATc2, NFATc3 and NFATc4 display cardiovascular, neurological, skeletal and immune phenotypes strikingly similar to DS. In addition, DSCR1 promotes neurotoxicity [29] and attenuates the inflammatory response by stabilizing I*k*B-alfa [30]. The extra copy of DYRK1A in DS has been also associated to early onset of Alzheimer's disease [31] and to defective neuronal development mediated by the reduction of REST, a key regulator of pluripotency and neuronal differentiation [32]. DSCR1/NFAT pathway was also associated with neuronal susceptibility to oxidative stress [33], a biochemical feature of DS. Finally, a limited number of functional studies in human DS cells have unravelled a disruption of mitochondrial function as a pathogenetic trigger [34-37].

In this study we analyzed the genome-wide transcription profile of lymphoblastoid cell lines (LCLs) from DS and control subjects to investigate differential gene expression and pathway deregulation associated with trisomy 21. This cellular model has been widely used to analyze the expression profiles of chr 21 genes [21,23,38] as well as of other diseases including cancer [39-41] and neurodegenerative disorders [42,43]. Diseased versus control and intra-group comparisons were used to analyze the gene expression levels of chr 21 genes. The experimental validation focused on the most deregulated gene ontology (GO) categories to confirm their imbalance in DS, i.e. the ubiquitin mediated proteolysis and the NF-*k*B cascade. Interestingly, these two celullar processes are closely interconnected since I*k*B-alfa, the key modulator of NF-*k*B, can be regarded as a model protein of regulation of signal transduction by the ubiquitin-proteasome system (UPS). Moreover, both the ubiquitin mediated proteolysis and the I*k*B/NF-*k*B signal transduction interact with and regulate DSCR1 [44]. In mice, DSCR1 and DYRK1A act synergistically to prevent the nuclear occupancy of NFAT [28], a family of transcription factors activated by calcium fluxes. Finally, DSCR1 is ubiquitinated and degraded by both the proteasome and the autophagy-lysosome pathways [45]. As these pathways are interconnected and individually can cause immune response derangement, neurodegenerative diseases, premature aging and delay of cell growth, all main features of DS, our experimental validation focused on UPS, NF-*k*B and DYRK1A/DSCR1/NFAT genes. In human LCLs and fetal fibroblasts, we provide the first evidence that the level of protein ubiquitination is reduced in DS and that proteasome activity is increased in both basal conditions and oxidative microenvironment. In addition, we first show that the NF-*k*B transcriptional activity is impaired in DS due to reduced I*k*B-alfa ubiquitination, increased NF-*k*B inhibitor (I*k*B-alfa) cytosolic levels and reduced p65 nuclear fraction. Finally, the investigation of DSCR1/DYRK1A/NFAT genes, linked to the pathogenesis of DS in animal studies, confirmed increased protein levels of DSCR1 and DYRK1A and showed reduced levels of NFATc2 and decreased NFATc2 nuclear translocation upon calcium flows induction, adding new evidence to a transcriptional regulation deficit in DS.

Methods

Cell culture

LCLs were generated from peripheral blood samples of six karyotypically confirmed full trisomy 21 children and six age-matched controls (5 ± 1 year-old) recruited at the Department of Pediatrics, Federico II University of Naples. The study was performed in accordance with the principles of the Helsinki Declaration and was approved by the Federico II University Ethics Committee 'Carlo Romano'. The parents of all subjects gave written informed consent before participation. Lymphocytes were isolated by ficoll-hypaque (Gibco) and resuspended in 17% FBS-RPMI-1640 and equal volume of supernatant from overgrown B95.8 cell cultures in presence of 10 μg/ml of cyclosporine (Sandimmune Oral Suspension). Cells were grown in 17% FBS-RPMI-1640 (Cambrex) supplemented with 5000 U/ml penicillin-streptomycin, 2 mM glutamine (Gibco) and 0.16 mg/ml gentamicin, in a 37°C, 5% CO_2 incubator.

Fibroblasts from two DS and two control fetuses, spontaneously aborted at a gestational age between 14 and 19 weeks, were obtained from the Galliera Genetic Bank (Galliera Hospitals, Genova, Italy) in agreement with ethical guidelines stated in the TGB Network Charter and upon written informed consent. Cells were cultured at 37°C in D-MEM medium (Gibco) supplemented with 17% FBS, 5000U/ml penicillin-streptomycin, 2 mM glutamine (Gibco), in a 37°C, 5% CO_2 incubator. For functional analyses, sub-confluent cultures with comparable number of culture passages (5–15) and growth rate were used. Each aliquot of LCLs was maintained in culture for no longer than 3 months (less than 160 'population doubling levels') [46]. To exclude the possibility of chromosomal rearrangements (other than full trisomy 21) during culturing, LCLs were karyotyped before microarray analysis and before each experimental validation.

Cell treatment

Calcium flows were induced with 10 ng/ml PMA and 1 mg/ml Ionomycin (Sigma) for 4 hours at 37°C. For the proteasome blocking, cells were treated with 40 μM MG132 (Calbiochem) for 6 hours at 37°C for western blot experiments and 100 μM MG-132 for 2 hours for proteasome assay. Oxidative stress was induced with 0.1 mM H_2O_2 for 30 minutes and recoveries were observed 1, 2 and 4 hours after cell refreshing with RPMI without H_2O_2. Phospho-I*k*B-alfa was analyzed after cell treatment with 40 μM MG132 for 30 minutes and incubation with 0.3 μM Calyculin A for an additional 30 minutes [47].

RNA extraction and microarray hybridization procedure

RNAs from six DS and six control LCLs were independently hybridized on the Affymetrix HU133 plus 2.0 oligonucleotide array (Affymetrix, Santa Clara, CA), which allows the analysis of over 47,000 human transcripts including 38,500 well-characterized human genes. Total RNAs were obtained using TRIzol reagent (Gibco/BRL Life Technologies, Inc., Gaithersburg, MD) and used to prepare biotinylated target cRNA, according to the Affymetrix procedures. Quality and amount of starting RNA were confirmed using spectrophotometry and agarose gel electrophoresis. Purification of PolyA + mRNA from total RNA was performed with the Oligotex mRNA Kit (QIAGEN GmbH, Hilden, Germany): 1 μg of mRNA was used to generate first-strand cDNA by using a T7-linked oligo(dT) primer; after second strand synthesis, in-vitro transcription was performed with biotinylated UTP and CTP using the Enzo BioArray High Yield RNA Transcript Labeling Kit (Enzo Diagnostics, Farmingdale, NY). The target cRNA generated from each sample was processed according to the manufacturer's procedures. Fragmentation of biotinylated cRNA, washing and staining were done according to the instructions provided by Affymetrix.

Experimental design

The experimental design was a diseased versus control comparison. To assess the expression variation of chr 21 genes among DS and control samples, we focused our analysis on the variability of all chr 21 transcripts present on the array with FC ≥ 1.2 (n = 167), irrespective of the statistical analysis that excludes *'a priori'* variable genes. Gene variability was assessed by the CV, calculated as the ratio between standard deviation and mean expression levels for each gene among samples [22]. Arbitrary cut-offs were set at 0.2 and 0.5 and transcripts were divided into three classes: CV ≤ 0.2, corresponding to the tightly regulated genes; 0.2 < CV < 0.5, corresponding to genes with little variation; CV ≥ 0.5, corresponding to highly variable genes.

Data acquisition and processing

After scanning, array images were assessed by eye to confirm scanner alignment and the absence of significant bubbles or scratches on the chip surface. 3'/5' ratios for GAPDH and beta-actin were confirmed to be within acceptable limits (0.70–1.64), and BioB spike controls were found to be present on all chips, with BioC, BioD and CreX also present in increasing intensity. Array scanning data (CEL files) were processed using the RMA algorithm [48]. GeneSpring software (Silicon Genetics, Redwood City, CA) was used for data mining. Raw expression data were normalized per gene by dividing each measurement for each gene by the median of that gene's measurements in the corresponding control non-trisomic samples. Normalized data were log-transformed. To reduce the noise and the variability induced by several

sources including the manufacturing processes and the experimental procedures [49], expression data were pre-filtered and genes were considered suitable for differential evaluation if called present in at least 4 out of 6 samples. Microarray data were submitted to ArrayExpress (http://www.ebi.ac.uk/arrayexpress/) database (accession n. E-MTAB-1238). Statistical evaluation was performed by Welch t-test, corrected with Benjamini-Hochberg FDR algorithm and filtered for fold-changes in DS vs controls ≥ 1.2. Statistical significance was assessed at 0.05 and, for a further analysis, at 0.01. Supervised classification of samples was performed using hierarchical clustering (GeneSpring software).

Bioinformatics data analyses

GO and pathway analyses of gene lists were performed using David Bioinformatics software (http://david.abcc.ncifcrf.gov/) [50]. For GO functional class scoring, a modified Fisher exact test (EASE score) was used and the statistical significance was set at p-value < 0.05. The fold enrichment (FE) value was used as a measure of the magnitude of enrichment. To compare results and to highlight more reliable GO classes, a second web-based software was used, the Gene Ontology Tree Machine (GOTM) [51]. To identify compounds with molecular signatures that might mitigate the effects of trisomy 21, Connectivity Map build 0.2 was used. The database contains 564 expression profiles representing the effects of 164 compounds on 4 cancer cell lines, using the Affymetrix U133 microarrays [52]. Because the U133 plus 2.0 array contains a greater number of probe-sets, the Connectivity Map analysis was performed using only the probe-sets common to both arrays. A list of perturbagens, hypothetically connected (positively and negatively) with the signature of interest was generated according to the permutation p. Perturbagenes with negative enrichment scores (< −0.7) were considered connected to the reversal or repression of the biological state encoded in the query signature. Perturbagens with enrichment scores < −0.7 and p-value < 0.05 were entered in the PASSonline software (Prediction of Activity Spectra for Substances) [53,54] in order to estimate their predicted activity. The current version of PASS available online (http://www.pharmaexpert.ru/passonline/index.php) predicts around 3750 pharmacological effects, biochemical mechanisms of action, specific toxicities and metabolic terms on the basis of structural formulae of drug-like substances with average accuracy ~ 95%. The predicted activity spectrum of a compound is estimated as probable activity (Pa) and probable inactivity (Pi) and only activities with Pa > Pi are considered. When Pa > 0.7, there is a high chance to confirm the activity experimentally, while if 0.5 < Pa < 0.7, the probability is lower but there is more than 50% chance for the compound to be a novel therapeutic molecule. Only compounds with Pa > 0.5 were considered here as potential therapeutic molecules.

Quantitative Real-Time PCR

Single stranded cDNA was synthesized with random hexamer primers starting from 2 μg of total RNA using the High Capacity cDNA Archive Kit (Applied Biosystems). Real-time PCR was performed using 2 μl of cDNA and TaqMan Universal PCR MasterMix 2X on the Applied Biosystems 7300, according to the manufacturer's procedures. PCR reactions were performed in triplicate. Beta-2-microglobulin and ring finger protein 111 (RNF111) housekeeping genes were chosen as reference genes [55,56].

Protein extraction

Total protein extraction was carried out by cell incubation with the Tropix lysis solution (Applied Biosystems) supplemented with 0.1 M DTT in the presence of protease inhibitor cocktail 1X (Sigma). To better visualize protein-linked ubiquitins, lysis solution was supplemented with 5 mM manganese and 50 μM MG132 according to Mimnaugh and Neckers [57]. Cytoplasmic and nuclear fractions were obtained by celLytic NucLEAR Extraction kit (Sigma).

Immunoprecipitation

Immunoprecipitation was carried out incubating 500 μg – 1 mg cytoplasmic extracts with specific antibodies at 4°C for 2 hours. Dynabeads Protein G (Invitrogen) were added to the mixture and the incubation was continued for other 2 hours. Proteins complexed with antibody - Dynabeads Protein G were immunoprecipitated and washed for three times with the use of a magnet, and finally eluted by boiling in SDS sample buffer for 10 minutes.

Western blot analysis

Protein extracts (25–45 μg) were separated by 7-10% SDS-PAGE and then transferred on PVDF membrane (Millipore). Membranes were then blocked for 1 hour in 5% milk-1X PBS-0.1% Tween-20 (T-PBS) and then incubated from 4 hours to overnight with dilutions of specific primary antibodies: 1:1000 anti-NFATc1 (H-110), 1:100 anti-NFATc2 (4G6-G5), 1:1000 anti-NFATc3 (M-75), 1:1000 anti-NFATc4 (H-74), 1:2500 anti-DYRK1A (H-143) (SantaCruz); 1:1000 anti-DSCR1 (N-20) (SIGMA); 1:2000 anti-NF-*k*B p65 (Upstate); 1:1000 anti-NF-*k*B p50 (Upstate); 1:1500 anti-I*k*B-alfa (L35A5), 1:1000 anti-pI*k*B-alfa (Ser32/36), 1:1000 anti-ubiquitin (P4D1) (CellSignaling). 1:2000 anti-α-Tubulin (SIGMA) and 1:1000 Histone H1 (SPM 256) (SantaCruz) were used to normalize the levels of total, cytosolic and nuclear proteins. As secondary antibodies, 1:5000 anti-mouse, 1:2000 anti-rabbit and 1:2000 anti-goat IgG horseradish peroxidase conjugated

(GE-Healthcare) were used and the specific bands were visualized by ECL plus reaction (GE-Healthcare).

Luciferase assay

To test NF-*k*B transcriptional activity, LCLs from DS subjects and controls were plated in 24-well plates at density of $5x10^5$ cells/well and transfected, 24 hours later, with pNF-*k*B-Luc (Path Detect NF-*k*B Cis-Reporting System, Stratagene) and pSV-β-Gal plasmid by using Turbofect Transfection Reagent (Fermentas), according to the manufacturer's instruction. Forty-eight hours post-transfection, cells were harvested and processed to evaluate the luciferase and β-galactosidase activities by using Dual Light Luciferase System (Tropix, Bedford, MA, USA) in a bioluminometer (TECAN, Infinite 200). Experiments were performed in triplicate and repeated independently twice. The ratio of firefly luciferase activity to β-galactosidase activity was expressed as relative light units (RLU).

Luminescent proteasome assay

To individually measure the chymotrypsin-, trypsin- and caspase-like proteasome activities in cultured cells, the Proteasome-Glo™ 3 substrates Cell-Based Assay (Promega) was used. LCLs were plated in 96-well plates at concentration of $2x10^4$/well and incubated at 37°C overnight. The day after, cells were treated with 100 μM MG132 for 2 hours (inhibitor control) and 0.1 mM H_2O_2 for 30 minutes (test treatment) before adding the three specific proteasome substrates: Such-LLVY-Glow™ Substrate for the Chymotrypsin-Like activity, Z-LRR-Glow™ Substrate for the Trypsin-Like activity and Z-nLPnLD-Glo™ Substrate for the Caspase-Like activity. Luminescence for each sample, performed in duplicate and in two separate experiments, was read after 15 minutes in a plate-reading luminometer (TECAN, Infinite 200).

Statistical analysis

Data were reported as means ± S.E. Statistical analysis was performed with SPSS 13.0 software and the student's t-test was used for the statistical significance (two-tailed, $p < 0.05$) of differences between means of DS and control subjects. To validate the microarray data, the average expression ratios (DS/controls) of both array and qRT-PCR were subjected to Pearson's correlation analysis.

Results

Supervised analysis of pooled data of DS and control samples

For the analysis of differentially expressed genes, six DS LCLs were compared to six control samples. A first list of 3,416 differentially expressed genes was generated by using a corrected p-value cut-off of 0.05. Of these, 1,051 (30.7%) were up-regulated and 2,368 (69.3%) were down-regulated, with a gene expression variation ranging from 0.67 to 3.04. No chr 21 gene resulted down-regulated. A second list of genes was then generated by using a corrected p-value cut-off of 0.01. In this case, a total of 406 transcripts resulted significantly either up-regulated (n = 71; 17.5%) or down-regulated (n = 335; 82.5%) (Additional file 1A). Supervised hierarchical clustering of both the 4,490 and the 406 transcripts clearly distinguished between DS and control samples (Additional file 1B, C).

Chr 21 expression profiles

Two hundred-twenty genes out of 449 genes annotated on chr 21 (NCBI RefSeq 37.2) were detected in this microarray analysis. Among these, 59 known genes (13.1% of total chr 21 annotated genes) resulted differentially expressed in DS vs controls ($p < 0.05$, $FC \geq 1.2$), with FC ranging from 1.20 to 2.57 and a mean DS/control ratio of 1.36 ± 0.2. A graphic view of the differentially expressed chr 21 genes is illustrated in Figure 1, that shows how a substantial number of triplicated genes escapes the gene-dosage rule. To identify functional categories associated with the trisomic genes, the list of chr 21 deregulated genes was submitted to a GO analysis. Results indicated '*ATPase activity coupled to transmembrane movement of substances*' (p = 0.005, FE 11.3),'*cofactor metabolic process*' (p = 0.029, FE 5.8), '*regulation of cholesterol biosynthetic process*' (p = 0.031, FE 62.2) and '*oxidative phosphorylation'* (p = 0.04, FE 9.2) as the major enriched categories (Table 1). The analysis of the same genes, performed using KEGG database, showed Parkinson's (p = 0.01, FE 8.3), Alzheimer's (p = 0.02, FE 6.1) and Huntington's (p = 0.03, FE 5.5) diseases as the most deregulated biological pathways (Table 2).

Analysis of chr 21 gene expression variability among DS and controls

To assess the expression variation of chr 21 genes among DS and control samples, we focused the analysis on the variability of all chr 21 transcripts present on the array with $FC \geq 1.2$ (n = 167). Among controls, 77 transcripts (46.1%) had $CV \leq 0.2$, 74 (44.3%) had $0.2 < CV < 0.5$ and 16 (9,6%) had $CV \geq 0.5$. Among DS samples, 110 transcripts (65.9%) had $CV \leq 0.2$, 48 (28.7%) had $0.2 < CV < 0.5$ and 9 (5.4%) had $CV \geq 0.5$ (Table 3). Fifty-five transcripts were tightly regulated in both DS and controls and among them, notably, mitochondrial-related genes (ATP5O, ATP5J and NDUFV3), SOD1, DYRK1A and cell-cycle related genes (Additional file 2). GO analysis of this gene subset revealed the enrichment of the following categories: '*Cofactor metabolic process*' (p = 0.007, FE 9.4), *'ATPase activity, coupled to movement of substances'* (p = 0.0018; FE 15.9), *'oxidative phosphorylation*'

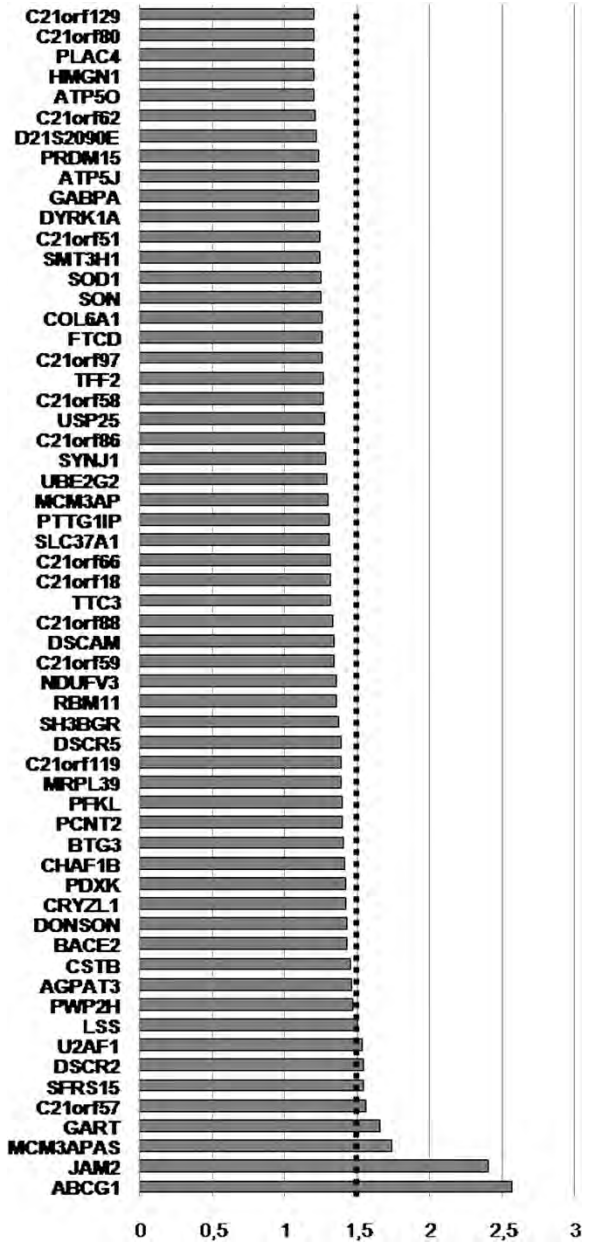

Figure 1 Average up-regulation ratios of chromosome 21 differentially expressed genes ($p < 0.05$).

(p = 0.016, FE 14.9), *'mitochondrial proton-transporting ATP synthase complex, coupling factor F(o)'* (p = 0.016, FE 120.4), *'regulation of cholesterol biosynthetic process'* (p = 0.019, FE 100.3) (Table 4). KEGG database showed the enrichment of *'oxidative phosphorylation'* (p = 0.03, FE 9.9) besides Parkinson's, Huntington's and Alzheimer's diseases (Table 5). Neither GO enriched categories nor KEGG pathways were associated to the 22 transcripts tightly regulated in controls (CV ≤ 0.2) and with little variation in DS (0.2 < CV < 0.5).

Table 1 Enriched GO categories of chromosome 21 up-regulated genes

GO term	Genes	%*	p-value	FE
ATPase activity, coupled to transmembrane movement of substances	ATP5O	6.2	0.005	11.3
	ATP5J			
	ABCG1			
Cofactor metabolic process	SOD1	6.2	0.029	5.8
	FTCD			
	PDXK			
	CRYZL1			
Regulation of cholesterol biosynthetic process	ABCG1	3.1	0.031	62.2
	SOD1			
Oxidative phosphorylation	ATP5O	4.7	0.04	9.2
	ATP5J			
	NDUFV3			

FE fold enrichment, *% of genes in category.

Genome-wide expression analysis, functional classes and pathway perturbation

GO functional class scoring was performed by comparing the list of the 406 differentially expressed genes to the complete list of genes spotted on the array.

Our analysis revealed a down-regulation of the biological processes related to ubiquitin metabolism; cell signalling, with a particular enrichment for the NF-*k*B cascade; cell cycle; protein localization; regulation of gene expression (Table 6). Among up-regulated categories, the most disrupted were those related to developmental processes and to transport and localization, with a strong enrichment of calcium ion transport (Table 7).

Table 2 Enriched pathways of chromosome 21 up-regulated genes

Pathway term	Genes	%	p-value	FE
Parkinson's disease	ATP5O	6.2	0.010	8.3
	ATP5J			
	NDUFV3			
	UBC6/7			
Alzheimer's disease	ATP5O	6.2	0.023	6.1
	ATP5J			
	NDUFV3			
	BACE			
Huntington's disease	ATP5O	6.2	0.030	5.5
	ATP5J			
	NDUFV3			
	SOD1			

FE fold enrichment.

Table 3 Chromosome 21 transcripts sorted by the coefficient of variation in both DS and control samples

		DS samples			
		CV ≤ 0.2	0.2 < CV < 0.5	CV ≥ 0.5	TOTAL
Controls	CV ≤ 0.2	55	22	0	77
	0.2 < CV < 0.5	49	19	6	74
	CV ≥ 0.5	6	7	3	16
	TOTAL	110	48	9	167

CV coefficient of variation, *DS* Down syndrome.

Pathway analysis identified ubiquitin-mediated proteolysis as the pathway mostly influenced by trisomy 21 (p = 2.9E-5; FE 4.8). Among genes involved in the ubiquitin-dependent proteolysis, a number of E2-conjugating enzymes (UBE2A, UBE2B, UBE2H), E3-ligases (UBE3A, ITCH, SMURF2, F-box proteins, MIB1) and deubiquitinating enzymes (USP1, USP2, USP8, USP12, USP15, USP28, USP32, USP33, USP34, USP38, USP47) resulted down-regulated. Microarray data were validated by qRT-PCR on 11 differentially expressed genes with different functions and by comparing their average expression ratios (DS/controls) with those of the array (Additional file 3).

Selection of possible therapeutic compounds

Connectivity map and PASS-assisted exploration were used to identify compounds whose molecular signatures counteracted those of DS lymphoblasts and to predict their therapeutic potential, respectively. We found 17 compounds with enrichment score < −0.7 (Additional file 4). Among these, adiphenine, eticlopride and vigabatrin display a predicted proteasome ATPase inhibitor activity (Pa score 0.72, 0.65 and 0.59, respectively). Adiphenine also displays a putative ubiquitin thiolesterase inhibitor and a proteasome endopeptidase complex inhibitor activity (Pa score 0.58 and 0.56, respectively). Finally, oxybenzone display a free radical scavenger activity (Pa 0.79).

Table 4 GO categories of the 55 chromosome 21 transcripts tightly regulated in DS and controls (CV ≤ 0.2)

GO term	Genes	%*	p-value	FE
Cofactor metabolic process	SOD1	9.5	0.0077	9.4
	FTCD			
	PDXK			
	CRYZL1			
ATPase activity, coupled to transmembrane movement of substances	ATP5O	9.5	0.0018	15.9
	ATP5J			
	ABCG1			
Oxidative phosphorylation	ATP5O	7.1	0.016	14.9
	ATP5J			
	NDUFV3			
Mitochondrial proton-transporting ATP synthase complex, coupling factor F(o)	ATP5O	4.8	0.016	120.4
	ATP5J			
Regulation of cholesterol biosynthetic process	ABCG1	4.8	0.019	100.3
	SOD1			

FE fold enrichment, *% of genes in category.

Table 5 Enriched pathways of the 55 chromosome 21 transcripts tightly regulated in DS and controls (CV ≤ 0.2)

Pathway term	Genes	%	p-value	FE
Parkinson's disease	ATP5O	9.5	0.002	13.8
	ATP5J			
	NDUFV3			
	UBC6/7			
Huntington's disease	ATP5O	9.5	0.0062	9.2
	ATP5J			
	NDUFV3			
	SOD1			
Oxidative phosphorylation	ATP5O	7.1	0.03	9.9
	ATP5J			
	NDUFV3			
Alzheimer's disease	ATP5O	7.1	0.049	7.6
	ATP5J			
	NDUFV3			

FE, fold enrichment.

Validation of some significantly deregulated GO categories

Protein ubiquitination and proteasome activity

Ubiquitinated protein levels were measured by Western blot with or without proteasome block by MG132. Results in both LCLs and fetal fibroblasts showed a reduction of the ubiquitination state in DS resting cells and an increase following MG132 treatment (Figure 2A, B).

As chronic oxidative stress (OS) is a feature of DS and a defective response to OS is known to occur in DS with accumulation of protein damage [58], ubiquitinated protein levels were also measured after incubation with 0.1 mM H_2O_2. DS cells showed a trend to increase ubiquitin-bound proteins after OS induction. After H_2O_2 withdrawal, DS cells showed a more efficient recovery in the first two hours compared to controls (Figure 3). As the increase of ubiquitination following proteasome blocking suggested a possible involvement of the proteasome, the three proteasome activities were tested in LCLs before and after incubation with H_2O_2. Proteasome activity assay revealed a significant increase in the trypsin-like and in the chymotrypsin-like activities (p < 0.01) in DS subjects,

Table 6 Enriched GO categories of down-regulated genes (p < 0.01), sorted by p-value

Biological process	GO term	N. of genes	%*	p-value	FE
Ubiquitin metabolism	ubiquitin-dependent protein catabolic process	16	5.4	5.2E-6	4.3
	modification-dependent protein catabolic process	25	8.5	1.4E-5	2.7
	proteolysis involved in cellular protein catabolic process	25	8.5	2.9E-5	2.6
	ligase activity	17	5.8	0.001	2.6
	proteolysis	29	9.8	0.009	1.6
	ubiquitin-protein ligase activity	8	2.7	0.013	3.2
	proteasomal ubiquitin-dependent protein catabolic process	6	2.0	0.025	3.6
Cell signalling	positive regulation of I-*k*B kinase/NF-*k*B cascade	9	3.1	0.0002	5.5
	positive regulation of protein kinase cascade	10	3.4	0.0024	3.5
	positive regulation of signal transduction	12	4.1	0.01	2.4
Protein localization	establishment of protein localization	25	8.5	0.002	2.0
Cell cycle	mitotic cell cycle	14	4.7	0.008	2.3
	cell cycle phase	15	5.1	0.009	2.2
	M phase of mitotic cell cycle	10	3.4	0.013	2.7
	mitosis	9	3.1	0.031	2.4
	nuclear division	9	3.1	0.031	2.4
	interphase	6	2.0	0.033	3.3
Regulation of gene expression	gene expression	62	21.0	0.022	1.3
	mRNA processing	12	4.1	0.023	2.2
	RNA splicing	11	3.7	0.024	2.3
Vescicle related	ER to Golgi vesicle-mediated transport	4	1.4	0.033	5.6

FE fold enrichment, *% of genes in category.

both in basal and OS conditions, while no differences were observed for the caspase-like activity (Figure 4).

IkB-alfa/NF-kB

NF-*k*B is finely regulated by a complex network of gene products and post-translational modifications. To demonstrate if a NF-*k*B defect occurs in DS, we choose to analyse the down-stream product of the NF-*k*B cascade, i.e. the behaviour of p50/p65 and of its inhibitors in DS cell lines. Levels of p50, p65, I*k*B-alfa and phospho-I*k*B-alfa proteins were assessed by Western blot using specific antibodies in DS and control samples. Results showed a significant reduction of p65 levels in the nuclear fractions and a significant increase of I*k*B-alfa in the cytosolic fractions of DS subjects, in both the dephosphorylated and phosphorylated forms (Figure 5A, B, C). No difference was observed for NF-*k*B p50 subunit levels (data not shown). Luciferase assay confirmed a significant reduction of NF-*k*B transcriptional activity in DS LCLs ($p < 0.05$) (Figure 5D). Immunoprecipitation of I*k*B-alfa in cytosolic fractions and subsequent Western blot with specific anti-ubiquitin antibody showed a reduction of the ubiquitinated levels of this inhibitor under basal conditions in DS fractions (Figure 6A). Ubiquitination levels returned similar to controls after proteasome blocking (Figure 6B).

Table 7 Enriched GO categories of the up-regulated genes (p < 0.01), sorted by p-value

Biological process	GO term	N. of genes	%*	p-value	FE
Transport and localization	calcium ion transport	5	8.3	0.001	10.6
	transmembrane transport	7	11.7	0.01	3.7
	metal ion transport	6	10.0	0.016	3.9
	localization	17	28.3	0.022	1.7
	cation transport	6	10.0	0.032	3.3
	transport	15	25.0	0.034	1.7
	ion transport	7	11.7	0.035	2.8
	establishment of localization	15	25.0	0.037	1.7
Development	cellular developmental process	14	23.3	0.002	2.5
	anatomical structure development	17	28.3	0.004	2.0
	cell differentiation	13	21.7	0.005	2.4
	system development	16	26.7	0.005	2.1
	multicellular organismal development	17	28.3	0.015	1.8
	organ development	12	20.0	0.021	2.1

FE fold enrichment, *% of genes in category.

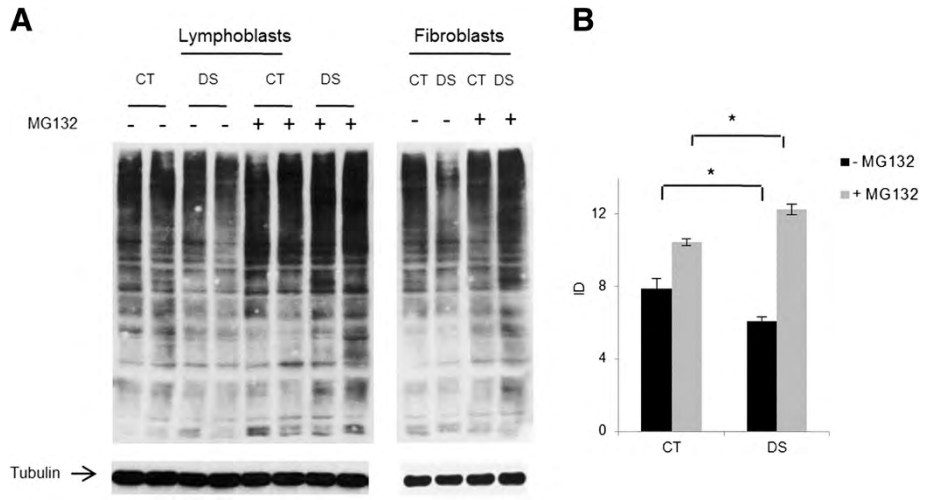

Figure 2 Western blot analysis of total ubiquitin-bound protein levels. A) Western blot performed on lymphoblasts and fetal fibroblasts in basal conditions and following proteasome blocking (40 μM MG132 for six hours). **B**) Histograms show the average protein ubiquitination of lymphoblasts derived from two controls and two DS subjects, normalized on tubulin levels. * $p < 0.05$.

DYRK1A/DSCR1/NFAT genes

DYRK1A, DSCR1 and the members of the NFAT transcription factors were evaluated by RT-PCR and Western blot. We observed a significant upregulation of DYRK1A, DSCR1 and NFATc4 (about 2-fold increase) and a down-regulation of NFATc2 (69% reduction) and NFATc1 (49% reduction) expression profiles in DS LCLs compared to controls (Figure 7A). No difference was observed for NFATc3. At protein level, we confirmed the significant reduction of NFATc2 and the increase of DYRK1A and DSCR1 (Figure 7B) while no difference was observed for NFATc1 and NFATc4 (data not shown). To assess NFAT nuclear translocation, Western blot experiments were performed upon induction of calcium fluxes through PMA/ionomycin. Results showed a reduction of NFATc2 nuclear levels following stimulation, suggesting the presence of mechanisms acting to inhibit its translocation (Figure 8).

Finally, soluble DSCR1 protein levels were investigated before and after proteasome blocking. Results showed a reduction of soluble DSCR1 levels in both samples after MG132 treatment, with a more marked effect in DS

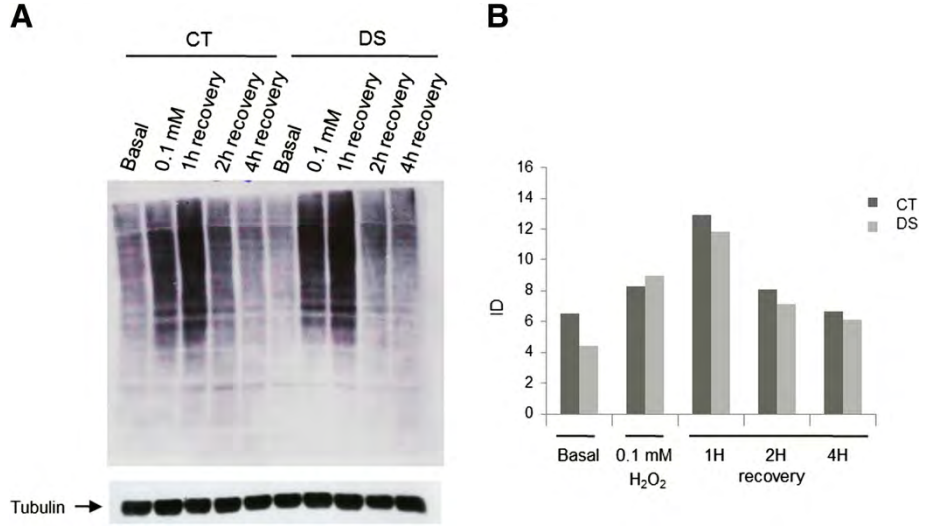

Figure 3 Ubiquitin-bound proteins in LCLs from a DS and a control subject in basal and OS conditions. A) Western blot analysis of ubiquitin-bound proteins in lymphoblasts from a DS and a control subject in basal conditions, under oxidative stress (0,1 mM H_2O_2 for 30 minutes) and after 1, 2 and 4 hours of recovery. **B**) relative densitometry.

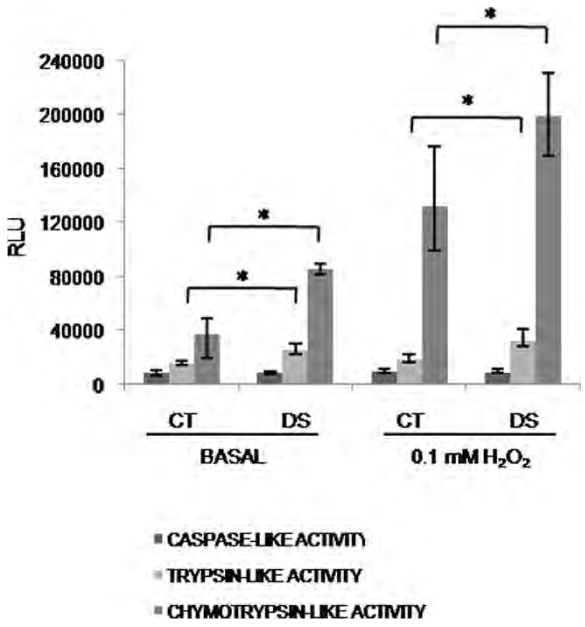

Figure 4 Proteasome activity assay from LCLs, in basal conditions and after treatment with 0,1 mM H_2O_2 for 30 minutes. Histograms show the average of the activities of DS subjects (n = 3) versus controls (n = 3), evaluated in duplicate and repeated twice. * *p < 0.05*.

subjects where the DSCR1 levels became comparable to controls (Figure 9).

Discussion

In spite of the great efforts made to analyze the effects of dosage imbalance at molecular level, the pathogenesis of DS is still unclear. So far, expression studies performed with distinct approaches led to inconclusive results, thus underlining the importance of integrating microarray data with functional validation of selected pathways.

The present study was aimed at analyzing gene expression profiles in LCLs from DS and controls to identify genes and metabolic pathways involved in DS pathogenesis, with an emphasis toward chr 21 genes. To select reliable GO classes, two distinct web-based softwares working on different statistic algorithms (DavidBioinformatics and GOTM) were used. These GO classes where further analysed to provide experimental evidence of their disruption in DS.

Despite some inherent limitations, the utility of LCLs is increasingly recognized in both genetic and functional studies [59]. Considering the similarity of the expression and regulation of certain genes between LCLs and neurons, LCLs have been used as surrogate cells in studies of neurological disorders as in the case of Parkinson's disease [60,61] and Alzheimer's disease [62]. LCLs have also been successfully used to study mitochondrial and organellar dysfunction as in the case of autophagy in juvenile neuronal ceroid lipofuscinosis [63]. Beside the present study, LCLs have been used in expression studies of chr 21 genes in three previous works [21,23,38] where it was demonstrated that the variance on gene expression levels due to culture conditions is extremely low in this cell model [21]. Moreover, Merla et al., [64] established six independent LCLs for the same individual and compared expression levels for 25 chr 21 genes finding a strong correlation ranging from 0.8 to 0.92. In this study, to maximize the quality of LCLs, each aliquot of LCLs was maintained in culture for no longer than 3 months (less than 160 'population doubling levels') and cells were karyotyped before microarray analysis and before each experimental validation to exclude the possibility of chromosomal rearrangements (other than full trisomy 21).

Overexpression of chr 21 genes

Our results showed a significant up-regulation of a subset of 59 chr 21 genes ($p < 0.05$) with a mean DS/control ratio of 1.36 ± 0.2. This confirms that most trisomic genes escape the predicted gene-dosage rule of 1.5-fold increase and underscores the existence of complex and unravelled mechanisms of transcriptional regulation [65]. In the present study, GO analysis of the overexpressed chr 21 genes indicated ATPase activity coupled to transmembrane movement of substances and oxidative phosphorylation as the major enriched categories. This result is in agreement with previous gene expression studies in fetal DS cerebral cortex, heart and trophoblasts [5,7,13,15] in which the most consistently disregulated chr 21 genes were those involved in mitochondrial function related metabolic pathways, such as ATP5O and ATP5J (encoding two mitochondrial ATP synthase subunits), NDUFV3 (subunit of NADH dehydrogenase), and SOD1 (involved in antioxidant defense system). Mitochondrial dysfunction has been proposed in the pathogenesis of DS for years. In particular, deficit of oxidative phosphorylation due to a deregulation of the mitochondrial respiratory chain complexes I, III and V [34,35,66-68], increased levels of the Krebs cycle enzymes (aconitase and NADP-linked isocitrate dehydrogenase) [69] and impaired mtDNA repair systems [70] were described in human DS cells. In isolated mitochondria from DS mice cortex, a decreased membrane potential and ATP content and selective defects in Complex-I mediated respiration were also found [71]. Furthermore, a close relationship between mitochondrial abnormalities and oxidative damage has been described in DS brains and fibroblasts [72]. Mitochondrial dysfunctions can result either in decreased ATP levels, or in increased ROS production [35,73]. Mitochondrial dysfunction was also described in neurodegenerative diseases such as Alzheimer's, Parkinson's and Huntington's diseases

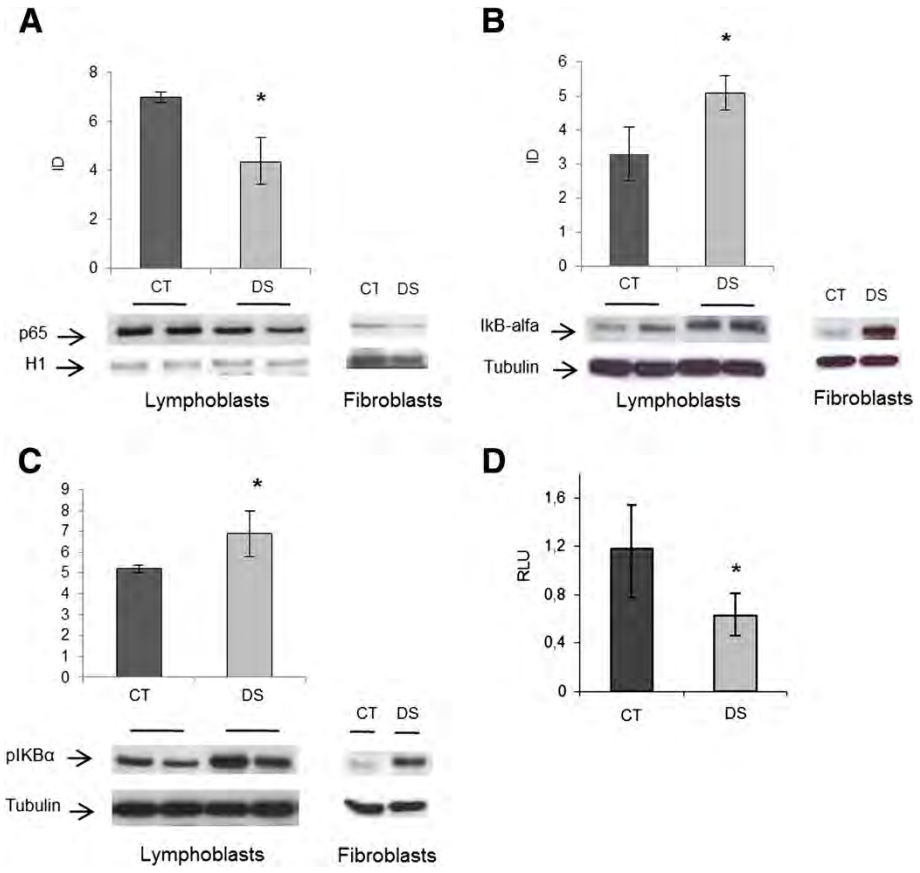

Figure 5 NF-kB p65, IkB-alfa and phospho-IkB-alfa in LCLs and fibroblats and relative densitometry. A) Western blot of NF-*k*B p65 nuclear levels and **B-C**) I*k*B-alfa and phospho-I*k*B-alfa cytosolic levels LCLs and relative densitometry. p65, I*k*B-alfa and phospho-I*k*B-alfa protein levels in fetal fibroblasts from one DS subject and one control are shown as well. As internal controls, tubulin and H1 histone were used for cytosolic and nuclear marker proteins, respectively. **D**) NF-*k*B Luciferase assay in lymphoblasts. Histograms show the average of the activity, expressed as relative light units (RLU), of DS subjects (n = 3) versus controls (n = 3) normalized on the average of the b-galactosidase activity. Experiments were performed in triplicate and repeated twice. * $p < 0.05$.

and in the normal aging processes [73-77]. Interestingly, when the trisomic genes, upregulated in the present gene expression study, were submitted to pathway analysis, Alzheimer's, Parkinson's and Huntington's diseases were identified as the most deregulated, in agreement with the meta-analysis from heterogeneous human and mouse DS data sets [27]. Finally, when only the amplified chr 21 genes tightly regulated in DS and in control subjects were submitted to *in silico* analysis, the same categories and pathways were identified. Taken together, these findings suggest that genes directly or indirectly involved in the oxidative phosphorylation, ATPase activity and, in general, in mitochondrial function, may have a role in the pathogenesis of DS phenotypes.

Genome-wide deregulation and pathway perturbation induced by trisomy 21

The genome-wide expression analysis revealed that 30.7% and 17.5% of genes were up-regulated at $p < 0.05$ and $p < 0.01$, respectively. A low percentage of up-regulated genes was also reported in two previous studies on LCLs, showing that 29% and 39% of genes were up-regulated, respectively [21,23]. In this study, genes involved in ubiquitin metabolism, cell signalling (with a particular enrichment of NF-*k*B cascade), cell cycle, protein localization and regulation of gene expression were down-regulated, and genes involved in developmental processes and calcium ion transport were up-regulated. The latter results are in agreement with previous genome-wide studies that reported the impairment of GO categories associated to developmental processes, both in fetal and adult DS biomaterials [9,14], as well as of calcium/potassium signalling on cell-free mRNA from amniotic fluid [78].

At mRNA level, while the ubiquitin pathway was reported as deregulated in DS trophoblasts and in rRNA-depleted samples from DS endothelial progenitor cells (EPCs) [15,79], NF-*k*B cascade, linked to the

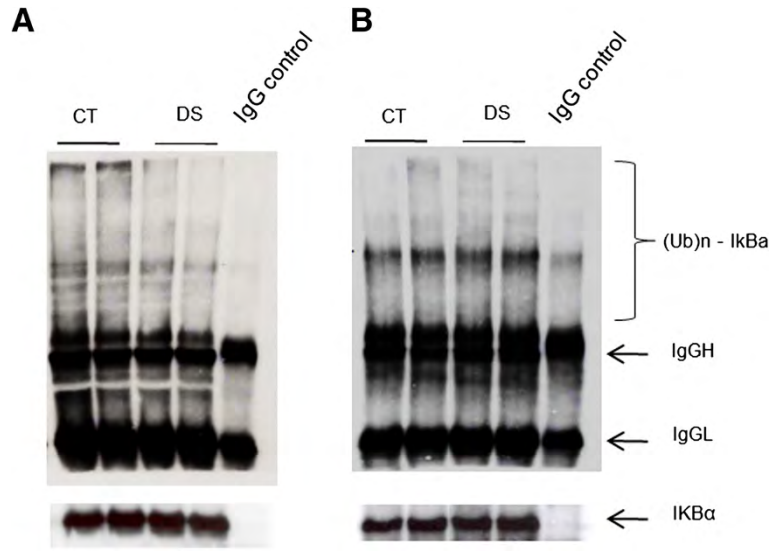

Figure 6 Ubiquitination of I*k*B-alfa in basal conditions (A) and after proteasome blocking with 40 μM MG132 for six hours (B). Cytoplasmic extracts were immunoprecipitated for I*k*B-alfa and then analyzed by western blot using an antibody against ubiquitin. IgG H and IgG L indicate immunoglobulin heavy and light chains in the immunoprecipitates that cross-react with the secondary antibody.

ubiquitn-mediated proteolysis, was found down-regulated in the present study for the first time. The close relation between the ubiquitin-mediated proteolysis and NF-*k*B and their relevance to a wealth of human disorders make these two pathways attractive candidates for DS pathogenesis.

The ubiquitin-dependent proteolysis

The UPS is the major proteolytic pathway used by eukaryotic cells to metabolize proteins [80]. Proteins to be degraded are covalently linked to a polyubiquitin chain by three different enzymes and then targeted to the 26S proteasome where are disassembled in small peptides, amino acids and ubiquitin monomers. UPS is known to metabolize misfolded, oxidized and damaged proteins, but also proteins involved in signal transduction, cell cycle regulation, differentiation and development, cellular response to stress, regulation of the immune and inflammatory response. A link between protein synthesis and degradation by UPS has been proposed [81]. Hence, derangements in this system, that can be associated to loss of function (mutation in an ubiquitin system enzyme or target substrate) or gain of function (abnormal or accelerated degradation of the target protein) could underlie, directly or indirectly, the pathogenesis of many diseases, including some features belonging to the DS spectrum. In particular, accumulation of ubiquitin conjugates and/or inclusion bodies

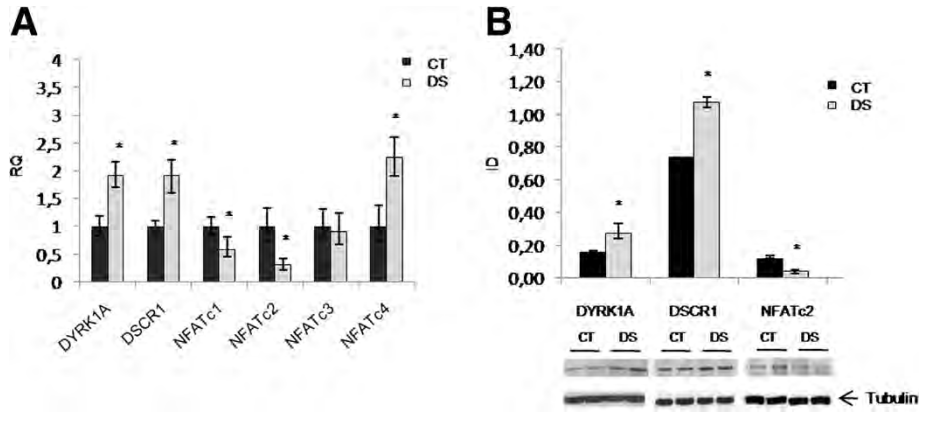

Figure 7 Analysis of DYRK1A, DSCR1 and NFATc1-4 gene products in LCLs. A) Relative quantification. Histograms show mRNA levels of pools of DS subjects (n = 3) versus controls (n = 3). All data are expressed relatively to control subjects, to which is assigned a value of 1-fold (1x). **B)** Western blot of total protein levels. * $p < 0.05$.

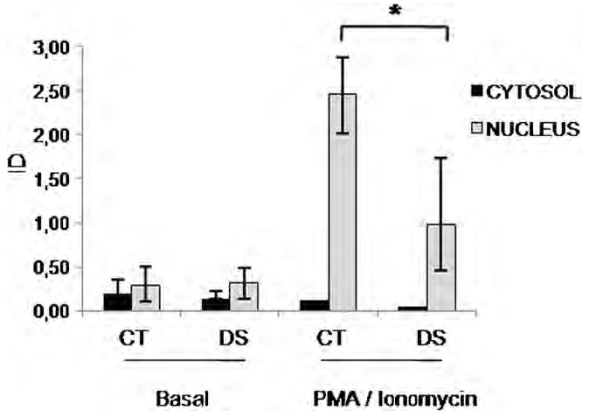

Figure 8 Analysis of activation and nuclear translocation of NFATc2, induced by PMA/Ionomycin. As internal controls, tubulin and H1 histone were used for cytosolic and nuclear marker proteins, respectively. * $p < 0.05$.

associated with ubiquitins have been reported in a broad array of chronic neurodegenerative diseases, such as the neurofibrillary tangles of Alzheimer's disease (AD), brain stem Lewy bodies (LBs) in Parkinson's disease (PD) and intracellular bodies in Huntington's disease [82]. In these cases, an involvement of the UPS was suggested [83-85]. So far, no data were available on the ubiquitination status and proteasome activity in human DS. By means of a protein screen by SDS-page, a study showed an increase of the proteasome zeta chain, an alpha subunit of the 20S proteasome, and of isopeptidase T, a deubiquitinating enzyme, in fetal DS brain [86]. More recently, a study on the cerebellum of Ts65Dn mice showed a reduction of the proteasome chymotrypsin-like activity and an increase of ubiquitinated proteins [87], results possibly ascribable to

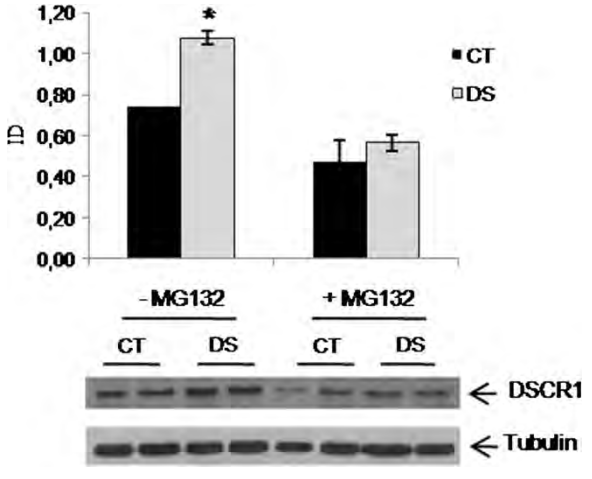

Figure 9 Western blot analysis of DSCR1 protein levels in basal conditions and following proteasome blocking with 40 μM MG132 for six hours in lymphoblasts from 2 DS and 2 control subjects. * $p < 0.05$.

the increased levels of beta-amyloid found in Ts65Dn mice brains [88].

The present study in human cell lines shows for the first time that, under basal conditions, there is a reduction of ubiquitinated protein levels in DS. This observation may either depend on defective ubiquitin-protein ligase activity (as suggested by microarray data) or on increased proteasome function, as demonstrated by the increase of two out of the three proteasome activities. Under OS, we observed an increase of ubiquitinated proteins in DS compared to the control sample. In the recovery period, ubiquitinated proteins were efficiently cleared in DS, probably due to the observed increase of the proteasome activities during OS. Previous studies have shown that chronic OS is a feature of DS [35,36,71,89-92]. Increased protein damage has also been shown in DS [58]. These observations may explain the increased proteasome activity, the accumulation of Ub-bound proteins after proteasome blocking with MG132 and, at least in part, the reduction of ubiquitin-bound proteins. These findings offer a new perspective to study this system in association to relevant DS pathological features, such as neurodegeneration, autoimmune disorders and predisposition to cancer.

I*k*B-alfa/NF-*k*B

The UPS is implicated in numerous cellular processes including activation of transcription factors such as NF-*k*B. The NF-*k*B family of transcription factors is critical in the development and maintenance of the immune system. Five NF-*k*B subunits exist and the most abundant and active form is a heterodimer composed of p50 and p65. Generally, this heterodimer is sequestered in the cytosol by one of the I*k*B inhibitors, most commonly I*k*B-alfa and is activated only upon I*k*B phosphorylation and subsequent proteasome mediated degradation [47]. Since this transcription factor is connected to a wide array of immune and inflammatory disorders, along with cell apoptosis and delay of cell growth, disruption of its pathway could play an important role in DS pathogenesis. In the present study, the GO analysis showed a down-regulation of the NF-*k*B cascade. Our experimental data provide the first evidence of a reduction of the NF-*k*B p65 subunit in DS nuclear fractions and of a significant reduction of its transcriptional activity. Along with this observation, cytosolic I*k*B-alfa levels were increased, in both the phosphorylated and dephosphorylated form. Ubiquitin-bound I*k*B-alfa was however reduced. These results, in agreement with the data of the total protein ubiquitination state, may be due to proteasome hyperfunction or to a defect of specific ubiquitin ligases activities, such as F-box proteins, or the recently described MIB1 [93], downregulated in this microarray experiment. As NF-*k*B signalling is

deeply modulated by ubiquitination at several levels [94,95], further studies on the regulation of NF-*k*B by ubiquitination in DS may add new clues to the pathogenesis of DS.

An additional level of interest comes from recent evidence of an interplay between NF-*k*B and NFAT pathway. In fact, NF-*k*B-inducing kinase interacts with and specifically phosphorylates the C-terminal region of DSCR1 in immortalized hippocampal cells as well as in primary cortical neurons, increasing DSCR1 protein stability and blocking its proteasomal degradation [44]. This could lead to an increase in soluble and insoluble DSCR1 levels that are cytotoxic [29]. Moreover, DSCR1 overexpression stabilizes I*k*B-alfa and decreases the steady-state activity of NF-*k*B, thus inhibiting the induction of genes involved in the inflammatory response [30].

The role of DYRK1A/DSCR1/NFAT genes in DS

The nuclear factors of activated T cells (NF-ATs) are a family of transcription factors that transduce calcium signals in the immune, cardiac, muscular, and nervous systems [96]. Like their distant relatives, the Rel family, which includes NF-*k*B, NFATs are located in the cytoplasm of resting cells and are activated for nuclear translocation [97]. Calcium signalling activates calcineurin and induces the movement of NFAT proteins into the nucleus, where they cooperate with other proteins to form complexes on DNA. As DYRK1A and DSCR1 regulate NFAT nuclear translocation, in the present study the DYRK1A/DSCR1/NFAT genes were analysed. DYRK1A at both RNA and protein levels resulted significantly overexpressed in DS. The same result was obtained for DSCR1, while a reduction of NFATc2 was observed at mRNA and protein level in DS resting cells. Reduction of NFATc2 was also observed in the nuclear fractions of DS after calcium flows stimulation. Together with the reduced NF-*k*B activity, this observation suggests the presence of a transcriptional regulation deficit in DS.

Conclusions

Results from the present microarray analysis in human LCLs show that the UPS functioning is impaired in DS. Among genes contributing to the ubiquitin mediated proteolysis and represented on the array, a number of E2-conjugating enzymes (such as UBE2A, UBE2B, UBE2H) and E3 ligases (such as UBE3A, ITCH, SMURF2, MIB1 and some F-box proteins) resulted down-regulated. Additional bioinformatic tools such as Connectivity Map and PASS analysis add supportive evidence of the involvement of the UPS in the pathogenesis of DS. Experimental data confirm a reduction of Ub-bound proteins and an increased proteasomal acitivity. Proteasome activity may be accelerated by increased damaged or misfolded proteins and/or by chronic oxidative stress, a known biochemical feature of DS resulting from either gene dosage effect of certain chr 21 genes (i.e. SOD1, CBS, APP) or mitochondrial dysfunction [36,89,98,99].

Increased proteasome activity, along with defective ubiquitination, may lead to reduction of Ub-bound proteins, including critical regulators of cellular homeostasis such as transcriptional activators or their inhibitors. Expression analysis pointed to a down-regulation of NF-*k*B, the final actor of a complex pathway of signal transduction finely modulated by ubiquitination at several levels [94]. Interestingly, definition of crosstalk between NF-*k*B signalling pathway, ubiquitin-dependent proteolysis and the critical chr 21 gene DSCR1 is still ongoing.

Because of its central role in the cell life, the proteasome has become a target for synthetic and natural drugs for the prevention and treatment of several conditions [100-102]. An example of the medical importance of its inhibition could be the stabilization of the transcription factor NF-*k*B, required to preserve cell viability in response to environmental stress or cytotoxic agents [103-105]. Furthermore, as suggested by our findings, also the DSCR1 protein levels, overexpressed in trisomic subjects, may be regulated by the proteasome inhibition.

Recent biochemical and epidemiological studies indicate that dietary minor components, such as polyphenols, may have a role in the defense against the OS in vivo [106]. Among the different phenolic compounds, epigallocatechin-3-gallate (EGCG), the major catechin of green tea, mitigates OS and inhibits the chymotrypsin-like activity of the proteasome [107-110]. Interestingly, the over-expression of DYRK1A can also be modulated by EGCG [111] and transgenic mice overexpressing this gene and presenting cognitive impairment, rescue the cognitive phenotype after a polyphenol-based diet [112]. Our functional analyses revealed an increase of the proteasome chymotrypsin-like activity in DS subjects and the Connectivity map and PASS-assisted exploration of our microarray data suggested that some compounds with proteasome inhibitor activity could revert the biological status of DS.

In conclusion, the present work offers new perspectives to better understand the pathogenesis of DS disease and suggests a rational for innovative approaches to DS treatment.

Availability of supporting data

Microarray data were deposited in the ArrayExpress database (http://www.ebi.ac.uk/arrayexpress/) (accession n. E-MTAB-1238).

Additional files

Additional file 1: A) Volcano plot of genes differentially expressed in trisomic vs control samples. B) Clustering of genes and conditions at p-value < 0.05; **C)** Clustering of genes and conditions at p-value < 0.01

(GeneTree Algorithm). The log2 of fold change between trisomic and control samples is represented on the x-axis and the negative log of p-values from the t-test is represented on the y-axis. Up-regulated genes are represented on the right side of the horizontal axis 0-value; down-regulated gene are on the left. Red dots indicate genes that are significantly up- or down-regulated at $p < 0.01$. Fold-change filter in DS vs controls ≥ 1.2. Supervised hierarchical clustering of both the 4,490 and the 406 transcripts clearly distinguish between DS and control samples.

Additional file 2: List of chr 21 transcripts, tightly regulated in both DS and control samples (CV ≤ 0.2).

Additional file 3: Average expression ratios and Pearson's correlation coefficient (r) between microarray and RT-PCR data.

Additional file 4: Selection of compounds with possible therapeutic potential in DS according to the Connectivity Map and the PASSonline software.

Abbreviations

DS: Down syndrome; chr: chromosome; LCLs: Lymphoblastoid cell lines; NFAT: Nuclear factor of activated T-cells; UPS: Ubiquitin-proteasome system; NF-*k*B: Nuclear factor-*k*B; FC: Fold change; FE: Fold enrichment; CV: Coefficient of variation; OS: Oxidative stress; EGCG: Epigallocatechin-3-gallate.

Competing interests

The authors declare that they have no competing interests.

Authors' contributions

BG carried out most of the experiments of cell cultures, western blot, functional studies and statistical analysis; IS conceived and designed the study, participated to data interpretation and drafted the manuscript; CS performed NFATc2 western blot; AV and MC participated to sample collection and carried out some of the western blot experiments; RAV participated to data interpretation and critically revised the manuscript; PDL performed microarray experiments and statistical analysis; GA was involved in the study coordination and in the critical revision of the manuscript, giving the final approval of the version to be published. All authors read and approved the final manuscript.

Acknowledgements

This work was supported by grants from the Italian Minister of Education, University and Research (MIUR) - PRIN to G.A. (2006067072, 2008FHM37R) and from Fondation Jerome Lejeune to R.V. (Vacca/1093-VR2012B).
We thank the Galliera Genetic Bank – Network of Telethon Genetic Biobanks project GTB07001 for providing fibroblast cell lines.

Author details

[1]Department of Pediatrics, Federico II University, Naples 80131, Italy. [2]Department of Biotechnological Sciences, Federico II University, Naples 80131, Italy. [3]Institute of Biomembranes and Bioenergetics, National Council of Research, Bari 70126, Italy. [4]Stazione Zoologica "A. Dohrn", c/o BioGeM, Via Camporeale, Ariano Irpino 83031, Italy.

Received: 18 February 2013 Accepted: 29 June 2013
Published: 5 July 2013

References

1. Amano K, Sago H, Uchikawa C, Suzuki T, Kotliarova SE, Nukina N, Epstein CJ, Yamakawa K: **Dosage-dependent over-expression of genes in the trisomic region of Ts1Cje mouse model for Down syndrome.** *Hum Mol Genet* 2004, **13:**1333–40.
2. Lyle R, Gehrig C, Neergaard-Henrichsen C, Deutsch S, Antonarakis SE: **Gene expression from the aneuploid chromosome in a trisomy mouse model of Down syndrome.** *Genome Res* 2004, **14:**1268–1274.
3. Kahlem P, Sultan M, Herwig R, Steinfath M, Balzereit D, Eppens B, Saran NG, Pletcher MT, South ST, Stetten G, Lehrach H, Reeves RH, Yaspo ML: **Transcript level alterations reflect gene dosage effects across multiple tissues in a mouse model of Down syndrome.** *Genome Res* 2004, **14:**1258–1267.
4. Dauphinot L, Lyle R, Rivals I, Dang MT, Moldrich RX, Golfier G, Ettwiller L, Toyama K, Rossier J, Personnaz L, Antonarakis SE, Epstein CJ, Sinet PM, Potier MC: **The cerebellar transcriptome during postnatal development of the Ts1Cje mouse, a segmental trisomy model for Down syndrome.** *Hum Mol Genet* 2005, **14:**373–384.
5. Mao R, Zielke CL, Zielke HR, Pevsner J: **Global up-regulation of chromosome 21 gene expression in the developing Down syndrome brain.** *Genomics* 2003, **81:**457–467.
6. Giannone S, Strippoli P, Vitale L, Casadei R, Canaider S, Lenzi L, D'Addabbo P, Frabetti F, Facchin F, Farina A, Carinci P, Zannotti M: **Gene expression profile analysis in human T lymphocytes from patients with Down syndrome.** *Ann Hum Genet* 2004, **68:**546–554.
7. Mao R, Wang X, Spitznagel EL Jr, Frelin LP, Ting JC, Ding H, Kim JW, Ruczinski I, Downey TJ, Pevsner J: **Primary and secondary transcriptional effects in the developing human Down syndrome brain and heart.** *Genome Biol* 2005, **6:**R107.
8. Li CM, Guo M, Salas M, Schupf N, Silverman W, Zigman WB, Husain S, Warburton D, Thaker H, Tycko B: **Cell type-specific over-expression of chromosome 21 genes in fibroblasts and fetal hearts with trisomy 21.** *BMC Med Genet* 2006, **7:**24.
9. Altug-Teber O, Bonin M, Walter M, Mau-Holzmann UA, Dufke A, Stappert H, Tekesin I, Heilbronner H, Nieselt K, Riess O: **Specific transcriptional changes in human fetuses with autosomal trisomies.** *Cytogenet Genome Res* 2007, **119:**171–84.
10. FitzPatrick DR, Ramsay J, McGill NI, Shade M, Carothers AD, Hastie ND: **Transcriptome analysis of human autosomal trisomy.** *Hum Mol Genet* 2002, **11:**3249–56.
11. Gross SJ, Ferreira JC, Morrow B, Dar P, Funke B, Khabele D, Merkatz I: **Gene expression profile of trisomy 21 placentas: a potential approach for designing noninvasive techniques of prenatal diagnosis.** *Am J Obstet Gynecol* 2002, **187:**457–462.
12. Tang Y, Schapiro MB, Franz DN, Patterson BJ, Hickey FJ, Schorry EK, Hopkin RJ, Wylie M, Narayan T, Glauser TA, Gilbert DL, Hershey AD, Sharp FR: **Blood expression profiles for tuberous sclerosis complex 2, neurofibromatosis type 1, and Down's syndrome.** *Ann Neurol* 2004, **56:**808–814.
13. Conti A, Fabbrini F, D'Agostino P, Negri R, Greco D, Genesio R, D'Armiento M, Olla C, Paladini D, Zannini M, Nitsch L: **Altered expression of mitochondrial and extracellular matrix genes in the heart of human fetuses with chromosome 21 trisomy.** *BMC Genomics* 2007, **8:**268.
14. Lockstone HE, Harris LW, Swatton JE, Wayland MT, Holland AJ, Bahn S: **Gene expression profiling in the adult Down syndrome brain.** *Genomics* 2007, **90:**647–60.
15. Rozovski U, Jonish-Grossman A, Bar-Shira A, Ochshorn Y, Goldstein M, Yaron Y: **Genome-wide expression analysis of cultured trophoblast with trisomy 21 karyotype.** *Hum Reprod* 2007, **22:**2538–45.
16. Cheung VG, Jen KY, Weber T, Morley M, Devlin JL, Ewens KG, Spielman RS: **Genetics of quantitative variation in human gene expression.** *Cold Spring Harb Symp Quant Biol* 2003, **68:**403–7.
17. Monks SA, Leonardson A, Zhu H, Cundiff P, Pietrusiak P, Edwards S, Phillips JW, Sachs A, Schadt EE: **Genetic inheritance of gene expression in human cell lines.** *Am J Hum Genet* 2004, **75:**1094–105.
18. Storey JD, Madeoy J, Strout JL, Wurfel M, Ronald J, Akey JM: **Gene-expression variation within and among human populations.** *Am J Hum Genet* 2007, **80:**502–9.
19. Stranger BE, Forrest MS, Clark AG, Minichiello MJ, Deutsch S, Lyle R, Hunt S, Kahl B, Antonarakis SE, Tavaré S, Deloukas P, Dermitzakis ET: **Genome-wide associations of gene expression variation in humans.** *PLoS Genet* 2005, **1:**e78.
20. Deutsch S, Lyle R, Dermitzakis ET, Attar H, Subrahmanyan L, Gehrig C, Parand L, Gagnebin M, Rougemont J, Jongeneel CV, Antonarakis SE: **Gene expression variation and expression quantitative trait mapping of human chromosome 21 genes.** *Hum Mol Genet* 2005, **14:**3741–3749.
21. Prandini P, Deutsch S, Lyle R, Gagnebin M, Delucinge Vivier C, Delorenzi M, Gehrig C, Descombes P, Sherman S, Dagna Bricarelli F, Baldo C, Novelli A, Dallapiccola B, Antonarakis SE: **Natural gene-expression variation in Down syndrome modulates the outcome of gene-dosage imbalance.** *Am J Hum Genet* 2007, **81:**252–263.
22. Sultan M, Piccini I, Balzereit D, Herwig R, Saran NG, Lehrach H, Reeves RH, Yaspo ML: **Gene expression variation in Down's syndrome mice allows prioritization of candidate genes.** *Genome Biol* 2007, **8:**R91.
23. Aït Yahya-Graison E, Aubert J, Dauphinot L, Rivals I, Prieur M, Golfier G, Rossier J, Personnaz L, Creau N, Bléhaut H, Robin S, Delabar JM, Potier MC: **Classification of human chromosome 21 gene-expression variations in**

Down syndrome: impact on disease phenotypes. *Am J Hum Genet* 2007, **81:**475–9.

24. Sommer CA, Pavarino-Bertelli EC, Goloni-Bertollo EM, Henrique-Silva F: **Identification of dysregulated genes in lymphocytes from children with Down syndrome.** *Genome* 2008, **51:**19–29.
25. Costa V, Sommese L, Casamassimi A, Colicchio R, Angelini C, Marchesano V, Milone L, Farzati B, Giovane A, Fiorito C, Rienzo M, Picardi M, Avallone B, Marco Corsi M, Sarubbi B, Calabrò R, Salvatore P, Ciccodicola A, Napoli C: **Impairment of circulating endothelial progenitors in Down syndrome.** *BMC Med Genomics* 2010, **3:**40.
26. De Cegli R, Romito A, Iacobacci S, Mao L, Lauria M, Fedele AO, Klose J, Borel C, Descombes P, Antonarakis SE, di Bernardo D, Banfi S, Ballabio A, Cobellis G: **A mouse embryonic stem cell bank for inducible overexpression of human chromosome 21 genes.** *Genome Biol* 2010, **1:**R64.
27. Vilardell M, Rasche A, Thormann A, Maschke-Dutz E, Pérez-Jurado LA, Lehrach H: **Meta-analysis of heterogeneous Down Syndrome data reveals consistent genome-wide dosage effects related to neurological processes.** *BMC Genomics* 2011, **12:**229.
28. Arron JR, Winslow MM, Polleri A, Chang CP, Wu H, Gao X, Neilson JR, Chen L, Heit JJ, Kim SK, Yamasaki N, Miyakawa T, Francke U, Graef IA, Crabtree GR: **NFAT dysregulation by increased dosage of DSCR1 and DYRK1A on chromosome 21.** *Nature* 2006, **441:**595–600.
29. Lee EJ, Lee JY, Seo SR, Chung KC: **Overexpression of DSCR1 blocks zinc-induced neuronal cell death through the formation of nuclear aggregates.** *Mol Cell Neurosci* 2007, **35:**585–95.
30. Kim YS, Cho KO, Lee HJ, Kim SY, Sato Y, Cho YJ: **Down syndrome candidate region 1 increases the stability of the IkappaBalpha protein: implications for its anti-inflammatory effects.** *J Biol Chem* 2006, **281:**39051–61.
31. Ryoo SR, Cho HJ, Lee HW, Jeong HK, Radnaabazar C, Kim YS, Kim MJ, Son MY, Seo H, Chung SH, Song WJ: **Dual-specificity tyrosine (Y)-phosphorylation regulated kinase 1A-mediated phosphorylation of amyloid precursor protein: evidence for a functional link between Down syndrome and Alzheimer's disease.** *J Neurochem* 2008, **104:**1333–44.
32. Canzonetta C, Mulligan C, Deutsch S, Ruf S, O'Doherty A, Lyle R, Borel C, Lin-Marq N, Delom F, Groet J, Schnappauf F, De Vita S, Averill S, Priestley JV, Martin JE, Shipley J, Denyer G, Epstein CJ, Fillat C, Estivill X, Tybulewicz VL, Fisher EM, Antonarakis SE, Nizetic D: **DYRK1A-dosage imbalance perturbs NRSF/REST levels, deregulating pluripotency and embryonic stem cell fate in Down syndrome.** *Am J Hum Genet* 2008, **83:**388–400.
33. Porta S, Serra SA, Huch M, Valverde MA, Llorens F, Estivill X, Arbonés ML, Martí E: **RCAN1 (DSCR1) increases neuronal susceptibility to oxidative stress: a potential pathogenic process in neurodegeneration.** *Hum Mol Genet* 2007, **16:**1039–50.
34. Valenti D, Tullo A, Caratozzolo MF, Merafina RS, Scartezzini P, Marra E, Vacca RA: **Impairment of F1F0-ATPase, adenine nucleotide translocator and adenylate kinase causes mitochondrial energy deficit in human skin fibroblasts with chromosome 21 trisomy.** *Biochem J* 2010, **431:**299–310.
35. Valenti D, Manente GA, Moro L, Marra E, Vacca RA: **Deficit of complex I activity in human skin fibroblasts with chromosome 21 trisomy and overproduction of reactive oxygen species by mitochondria: involvement of the cAMP/PKA signalling pathway.** *Biochem J* 2011, **435:**679–88.
36. Infantino V, Castegna A, Iacobazzi F, Spera I, Scala I, Andria G, Iacobazzi V: **Impairment of methyl cycle affects mitochondrial methyl availability and glutathione level in Down's syndrome.** *Mol Genet Metab* 2011, **102:**378–82.
37. Pallardó FV, Lloret A, Lebel M, d'Ischia M, Cogger VC, Le Couteur DG, Gadaleta MN, Castello G, Pagano G: **Mitochondrial dysfunction in some oxidative stress-related genetic diseases: Ataxia-Telangiectasia, Down Syndrome, Fanconi Anaemia and Werner Syndrome.** *Biogerontology* 2010, **11:**401–419.
38. Tlili A, Hoischen A, Ripoll C, Benabou E, Badel A, Ronan A, Touraine R, Grattau Y, Stora S, van Bon B, de Vries B, Menten B, Bockaert N, Gecz J, Antonarakis SE, Campion D, Potier MC, Bléhaut H, Delabar JM, Janel N: **BDNF and DYRK1A Are Variable and Inversely Correlated in Lymphoblastoid Cell Lines from Down Syndrome Patients.** *Mol Neurobiol* 2012, **46:**297–303.
39. Jen KY, Cheung VG: **Transcriptional response of lymphoblastoid cells to ionizing radiation.** *Genome Res* 2003, **13:**2092–100.
40. Islaih M, Li B, Kadura IA, Reid-Hubbard JL, Deahl JT, Altizer JL, Watson DE, Newton RK: **Comparison of gene expression changes induced in mouse and human cells treated with direct-acting mutagens.** *Environ Mol Mutagen* 2004, **44:**401–19.
41. Rieger KE, Chu G: **Portrait of transcriptional responses to ultraviolet and ionizing radiation in human cells.** *Nucleic Acids Res* 2004, **32:**4786–803.
42. Tsai HF, Lin SJ, Li C, Hsieh M: **Decreased expression of Hsp27 and Hsp70 in transformed lymphoblastoid cells from patients with spinocerebellar ataxia type 7.** *Biochem Biophys Res Commun* 2005, **334:**1279–86.
43. Ballestar E, Ropero S, Alaminos M, Armstrong J, Setien F, Agrelo R, Fraga MF, Herranz M, Avila S, Pineda M, Monros E, Esteller M: **The impact of MECP2 mutations in the expression patterns of Rett syndrome patients.** *Hum Genet* 2005, **116:**91–104.
44. Lee EJ, Seo SR, Um JW, Park J, Oh Y, Chung KC: **NF-kappaB-inducing kinase phosphorylates and blocks the degradation of Down syndrome candidate region 1.** *J Biol Chem* 2008, **283:**3392–400.
45. Liu H, Wang P, Song W, Sun X: **Degradation of regulator of calcineurin 1 (RCAN1) is mediated by both chaperone-mediated autophagy and ubiquitin proteasome pathways.** *FASEB J* 2009, **23:**3383–92.
46. Sugimoto M, Tahara H, Ide S, Furuichi Y: **Steps Involved in Immortalization and Tumorigenesis in Human B-Lymphoblastoid Cell Lines Transformed by Epstein-Barr Virus.** *Cancer Res* 2004, **64:**3361–3364.
47. Chen Z, Hagler J, Palombella VJ, Melandri F, Scherer D, Ballard D, Maniatis T: **Signal-induced site-specific phosphorylation targets I kappa B alpha to the ubiquitin-proteasome pathway.** *Genes Dev* 1995, **9:**1586–97.
48. Wu CJ, Fu Y, Murali TM, Kasif S: **Gene expression module discovery using gibbs sampling.** *Genome Inform* 2004, **5:**239–48.
49. Bassett DE Jr, Eisen MB, Boguski MS: **Gene expression informatics–it's all in your mine.** *Nat Genet* 1999, **1**(Suppl 1):51–5.
50. Dennis G Jr, Sherman BT, Hosack DA, Yang J, Gao W, Lane HC, Lempicki RA: **DAVID: Database for Annotation, Visualization, and Integrated Discovery.** *Genome Biol* 2003, **4:**P3.
51. Zhang B, Schmoyer D, Kirov S, Snoddy J: **GOTree Machine (GOTM): a web-based platform for interpreting sets of interesting genes using Gene Ontology hierarchies.** *BMC Bioinforma* 2004, **5:**16.
52. Lamb J, Crawford ED, Peck D, Modell JW, Blat IC, Wrobel MJ, Lerner J, Brunet JP, Subramanian A, Ross KN, Reich M, Hieronymus H, Wei G, Armstrong SA, Haggarty SJ, Clemons PA, Wei R, Carr SA, Lander ES, Golub TR: **The Connectivity Map: using gene-expression signatures to connect small molecules, genes, and disease.** *Science* 2006, **313:**1929–35.
53. Filimonov DA, Poroikov VV: **Probabilistic approach in activity prediction**. In *Chemoinformatics Approaches to Virtual Screening*. Edited by Alexandre V, Alexander T. Cambridge (UK): RSC Publishing; 2008:182–216.
54. Lagunin A, Filimonov D, Poroikov V: **Multi-targeted natural products evaluation based on biological activity prediction with PASS.** *Curr Pharm Des* 2010, **16:**1703–17.
55. Radonić A, Thulke S, Mackay IM, Landt O, Siegert W, Nitsche A: **Guideline to reference gene selection for quantitative real-time PCR.** *Biochem Biophys Res Commun* 2004, **313:**856–62.
56. de Brouwer AP, van Bokhoven H, Kremer H: **Comparison of 12 reference genes for normalization of gene expression levels in Epstein-Barr virus-transformed lymphoblastoid cell lines and fibroblasts.** *Mol Diagn Ther* 2006, **10:**197–204.
57. Mimnaugh and Neckers: **Immunoblotting Methods for the Study of Protein Ubiquitination**. In *Posttranslational Modifications of Proteins: Tools for Functional Proteomics. Volume 194.* Edited by Kannicht C. Totowa, NJ: Humana Press Inc; 2002:179–203.
58. Galletti P, De Bonis ML, Sorrentino A, Raimo M, D'Angelo S, Scala I, Andria G, D'Aniello A, Ingrosso D, Zappia V: **Accumulation of altered aspartyl residues in erythrocyte proteins from patients with Down's syndrome.** *FEBS J* 2007, **274:**5263–77.
59. Sie L, Loong S, Tan EK: **Utility of lymphoblastoid cell lines.** *J Neurosci Res* 2009, **87:**1953–9.
60. Tan EK, Sie L, Loong S: **Growth rate from patient-derived lymphoblastoid cells with LRRK2 mutations.** *Mol Genet Metab* 2008, **95:**113.
61. Lin CH, Tzen KY, Yu CY, Tai CH, Farrer MJ, Wu RM: **LRRK2 mutation in familial Parkinson's disease in a Taiwanese population: clinical, PET, and functional studies.** *J Biomed Sci* 2008, **5:**661–666.
62. Abe K, St George-Hyslop PH, Tanzi RE, Kogure K: **Induction of amyloid precursor protein mRNA after heat shock in cultured human lymphoblastoid cells.** *Neurosci Lett* 1991, **125:**169–171.
63. Cao Y, Espinola JA, Fossale E, Massey AC, Cuervo AM, MacDonald ME, Cotman SL: **Autophagy is disrupted in a knock-in mouse model of juvenile neuronal ceroid lipofuscinosis.** *J Biol Chem* 2006, **281:**20483–93.
64. Merla G, Howald C, Henrichsen CN, Lyle R, Wyss C, Zabot MT, Antonarakis SE, Reymond A: **Submicroscopic deletion in patients with Williams-Beuren**

syndrome influences expression levels of the nonhemizygous flanking genes. *Am J Hum Genet* 2006, **79:**332–41.
65. Patterson D: **Genetic mechanisms involved in the phenotype of Down syndrome.** *Ment Retard Dev Disabil Res Rev* 2007, **13:**199–206.
66. Kim SH, Vlkolinsky R, Cairns N, Lubec G: **Decreased levels of complex III core protein 1 and complex V beta chain in brains from patients with Alzheimer's disease and Down syndrome.** *Cell Mol Life Sci* 2000, **57:**1810–6.
67. Kim SH, Fountoulakis M, Dierssen M, Lubec G: **Decreased protein levels of complex I 30-kDa subunit in fetal Down syndrome brains.** *J Neural Transm Suppl* 2001, **61:**109–16.
68. Lee SH, Lee S, Jun HS, Jeong HJ, Cha WT, Cho YS, Kim JH, Ku SY, Cha KY: **Expression of the mitochondrial ATPase6 gene and Tfam in Down syndrome.** *Mol Cells* 2003, **15:**181–5.
69. Bajo M, Fruehauf J, Kim SH, Fountoulakis M, Lubec G: **Proteomic evaluation of intermediary metabolism enzyme proteins in fetal Down's syndrome cerebral cortex.** *Proteomics* 2002, **2:**1539–46.
70. Druzhyna N, Nair RG, LeDoux SP, Wilson GL: **Defective repair of oxidative damage in mitochondrial DNA in Down's syndrome.** *Mutat Res* 1998, **409:**81–9.
71. Bambrick LL, Fiskum G: **Mitochondrial dysfunction in mouse trisomy 16 brain.** *Brain Res* 2008, **1188:**9–16.
72. Busciglio J, Pelsman A, Wong C, Pigino G, Yuan M, Mori H, Yankner BA: **Altered metabolism of the amyloid beta precursor protein is associated with mitochondrial dysfunction in Down's syndrome.** *Neuron* 2002, **28:**677–88.
73. Raha S, Robinson BH: **Mitochondria, oxygen free radicals, disease and ageing.** *Trends Biochem Sci* 2000, **25:**502–8.
74. Schon EA, Manfredi G: **Neuronal degeneration and mitochondrial dysfunction.** *J Clin Invest* 2003, **111:**303–12.
75. Ames BN, Liu: **Delaying the mitochondrial decay of aging with acetylcarnitine.** *Ann N Y Acad Sci* 2004, **1033:**108–116.
76. Kidd PM: **Neurodegeneration from mitochondrial insufficiency: nutrients, stem cells, growth factors, and prospects for brain rebuilding using integrative management.** *Altern Med Rev* 2005, **10:**268–93.
77. Gandhi S, Wood NW: **Molecular pathogenesis of Parkinson's disease.** *Hum Mol Genet* 2005, **14:**2749–2755.
78. Slonim DK, Koide K, Johnson KL, Tantravahi U, Cowan JM, Jarrah Z, Bianchi DW: **Functional genomic analysis of amniotic fluid cell-free mRNA suggests that oxidative stress is significant in Down syndrome fetuses.** *Proc Natl Acad Sci USA* 2009, **106:**9425–9.
79. Costa V, Angelini C, D'Apice L, Mutarelli M, Casamassimi A, Sommese L, Gallo MA, Aprile M, Esposito R, Leone L, Donizetti A, Crispi S, Rienzo M, Sarubbi B, Calabrò R, Picardi M, Salvatore P, Infante T, De Berardinis P, Napoli C, Ciccodicola A: **Massive-scale RNA-Seq analysis of non ribosomal transcriptome in human trisomy 21.** *PLoS One* 2011, **6:**e18493.
80. Ciechanover A: **Intracellular protein degradation: from a vague idea thru the lysosome and the ubiquitin-proteasome system and onto human diseases and drug targeting.** *Cell Death Differ* 2005, **12:**1178–90.
81. Ding Q, Dimayuga E, Markesbery WR, Keller JN: **Proteasome inhibition induces reversible impairments in protein synthesis.** *FASEB J* 2006, **20:**1055–63.
82. Van Tijn P, Hol EM, van Leeuwen FW, Fischer DF: **The neuronal ubiquitin-proteasome system: murine models and their neurological phenotype.** *Prog Neurobiol* 2008, **85:**176–93.
83. Huang Q, Figueiredo-Pereira ME: **Ubiquitin/proteasome pathway impairment in neurodegeneration: therapeutic implications.** *Apoptosis* 2010, **15:**1292–311.
84. Lehman NL: **The ubiquitin proteasome system in neuropathology.** *Acta Neuropathol* 2009, **118:**329–47.
85. Rogers N, Paine S, Bedford L, Layfield R: **Review: the ubiquitin-proteasome system: contributions to cell death or survival in neurodegeneration.** *Neuropathol Appl Neurobiol* 2010, **36:**113–24.
86. Engidawork E, Juranville JF, Fountoulakis M, Dierssen M, Lubec G: **Selective upregulation of the ubiquitin-proteasome proteolytic pathway proteins, proteasome zeta chain and isopeptidase T in fetal Down syndrome.** *J Neural Transm Suppl* 2001, **61:**117–30.
87. Necchi D, Lomoio S, Scherini E: **Dysfunction of the ubiquitin-proteasome system in the cerebellum of aging Ts65Dn mice.** *Exp Neurol* 2011, **232:**114–8.
88. Choi JH, Berger JD, Mazzella MJ, Morales-Corraliza J, Cataldo AM, Nixon RA, Ginsberg SD, Levy E, Mathews PM: **Age-dependent dysregulation of brain amyloid precursor protein in the Ts65Dn Down syndromemouse model.** *J Neurochem* 2009, **110:**1818–27.
89. Busciglio J, Yankner BA: **Apoptosis and increased generation of reactive oxygen species in Down's syndrome neurons in vitro.** *Nature* 1995, **378:**776–9.
90. Pagano G, Castello G: **Oxidative stress and mitochondrial dysfunction in Down syndrome.** *Adv Exp Med Biol* 2012, **724:**291–9.
91. Zana M, Janka Z, Kálmán J: **Oxidative stress: a bridge between Down's syndrome and Alzheimer's disease.** *Neurobiol Aging* 2007, **28:**648–76.
92. Peled-Kamar M, Lotem J, Okon E, Sachs L, Groner Y: **Thymic abnormalities and enhanced apoptosis of thymocytes and bone marrow cells in transgenic mice overexpressing Cu/Zn-superoxide dismutase: implications for Down syndrome.** *EMBO J* 1995, **14:**4985–93.
93. Liu LJ, Liu TT, Ran Y, Li Y, Zhang XD, Shu HB, Wang YY: **The E3 ubiquitin ligase MIB1 negatively regulates basal IκBα level and modulates NF-κB activation.** *Cell Res* 2012, **22:**603–6.
94. Kanarek N, Ben-Neriah Y: **Regulation of NF-κB by ubiquitination and degradation of the IκBs.** *Immunol Rev* 2012, **246:**77–94.
95. Oeckinghaus A, Hayden MS, Ghosh S: **Crosstalk in NF-κB signaling pathways.** *Nat Immunol* 2011, **12:**695–708.
96. Stankunas K, Graef IA, Neilson JR, Park SH, Crabtree GR: **Signaling through calcium, calcineurin, and NF-AT in lymphocyte activation and development.** *Cold Spring Harb Symp Quant Biol* 1999, **64:**505–16.
97. Beals CR, Clipstone NA, Ho SN, Crabtree GR: **Nuclear localization of NF-ATc by a calcineurin-dependent, cyclosporin-sensitive intramolecular interaction.** *Genes Dev* 1997, **11:**824–34.
98. Butterfield DA, Drake J, Pocernich C, Castegna A: **Evidence of oxidative damage in Alzheimer's disease brain: central role for amyloid beta-peptide.** *Trends Mol Med* 2001, **7:**548–54.
99. Lott IT, Head E, Doran E, Busciglio J: **Beta-amyloid, oxidative stress and Down syndrome.** *Curr Alzheimer Res* 2006, **3:**521–528.
100. Yang H, Zonder JA, Dou QP: **Clinical development of novel proteasome inhibitors for cancer treatment.** *Expert Opin Investig Drugs* 2009, **18:**957–e971.
101. Adams J: **Potential for proteasome inhibition in the treatment of cancer.** *Drug Discov Today* 2003, **8:**307–15.
102. Zavrski I, Naujokat C, Niemöller K, Jakob C, Heider U, Langelotz C, Fleissner C, Eucker J, Possinger K, Sezer O: **Proteasome inhibitors induce growth inhibition and apoptosis in myeloma cell lines and in human bone marrow myeloma cells irrespective of chromosome 13 deletion.** *J Cancer Res Clin Oncol* 2003, **129:**383–91.
103. Beg AA, Baltimore D: **An essential role for NF-κB in preventing TNF-α-induced cell death.** *Science* 1996, **274:**782–784.
104. Van Antwerp DJ, Martin SJ, Kafri T, Green DR, Verma IM: **Suppression of TNF-α-induced apoptosis by NF-κB.** *Science* 1996, **274:**787–789.
105. Wang CY, Mayo MW, Baldwin AS: **TNF- and cancer therapy-induced apoptosis: potentiation by inhibition of NF-κB.** *Science* 1996, **274:**784–787.
106. Bogani P, Galli C, Villa M, Visioli F: **Postprandial anti-inflammatory and antioxidant effects of extra virgin olive oil.** *Atherosclerosis* 2007, **190:**181–6.
107. Koh SH, Kwon H, Kim KS, Kim J, Kim MH, Yu HJ, Kim M, Lee KW, Do BR, Jung HK, Yang KW, Appel SH, Kim SH: **Epigallocatechin gallate prevents oxidative-stress-induced death of mutant Cu/Zn-superoxide dismutase (G93A) motoneuron cells by alteration of cell survival and death signals.** *Toxicology* 2004, **202:**213–25.
108. Schroeder EK, Kelsey NA, Doyle J, Breed E, Bouchard RJ, Loucks FA, Harbison RA, Linseman DA: **Green tea epigallocatechin 3-gallate accumulates in mitochondria and displays a selective antiapoptotic effect against inducers of mitochondrial oxidative stress in neurons.** *Antioxid Redox Signal* 2009, **11:**469–80.
109. Nam S, Smith DM, Dou QP: **Ester bond-containing tea polyphenols potently inhibit proteasome activity in vitro and in vivo.** *J Biol Chem* 2001, **276:**13322–30.
110. Khan N, Adhami VM, Mukhtar H: **Apoptosis by dietary agents for prevention and treatment of prostate cancer.** *Endocr Relat Cancer* 2010, **17:**R39–52.
111. Bain J, McLauchlan H, Elliott M, Cohen P: **The specificities of protein kinase inhibitors: an update.** *Biochem J* 2003, **371:**199–204.
112. Guedj F, Sébrié C, Rivals I, Ledru A, Paly E, Bizot JC, Smith D, Rubin E, Gillet B, Arbones M, Delabar JM: **Green Tea Polyphenols Rescue of Brain Defects Induced by Overexpression of DYRK1A.** *PLoS One* 2009, **4:**e4606.

doi:10.1186/1755-8794-6-24
Cite this article as: Granese *et al.*: Validation of microarray data in human lymphoblasts shows a role of the ubiquitin-proteasome system and NF-*k*B in the pathogenesis of Down syndrome. *BMC Medical Genomics* 2013 **6**:24.